NUREG/CP-0162
Vol. 1
CONF-9710101--Vol.1

Proceedings of the U.S. Nuclear Regulatory Commission

Twenty-Fifth Water Reactor Safety Information Meeting

Volume 1
- Plenary Sessions
- Pressure Vessel Research
- BWR Strainer Blockage and Other Generic Safety Issues
- Environmentally Assisted Degradation of LWR Components
- Update on Severe Accident Code Improvements and Applications

Held at
Bethesda Marriott Hotel
Bethesda, Maryland
October 20-22, 1997

U.S. Nuclear Regulatory Commission

Office of Nuclear Regulatory Research

Proceedings prepared by
Brookhaven National Laboratory

AVAILABILITY NOTICE

Availability of Reference Materials Cited in NRC Publications

Most documents cited in NRC publications will be available from one of the following sources:

1. The NRC Public Document Room, 2120 L Street, NW., Lower Level, Washington, DC 20555-0001

2. The Superintendent of Documents, U.S. Government Printing Office, P. O. Box 37082, Washington, DC 20402-9328

3. The National Technical Information Service, Springfield, VA 22161-0002

Although the listing that follows represents the majority of documents cited in NRC publications, it is not intended to be exhaustive.

Referenced documents available for inspection and copying for a fee from the NRC Public Document Room include NRC correspondence and internal NRC memoranda; NRC bulletins, circulars, information notices, inspection and investigation notices; licensee event reports; vendor reports and correspondence; Commission papers; and applicant and licensee documents and correspondence.

The following documents in the NUREG series are available for purchase from the Government Printing Office: formal NRC staff and contractor reports, NRC-sponsored conference proceedings, international agreement reports, grantee reports, and NRC booklets and brochures. Also available are regulatory guides, NRC regulations in the *Code of Federal Regulations,* and *Nuclear Regulatory Commission Issuances*.

Documents available from the National Technical Information Service include NUREG-series reports and technical reports prepared by other Federal agencies and reports prepared by the Atomic Energy Commission, forerunner agency to the Nuclear Regulatory Commission.

Documents available from public and special technical libraries include all open literature items, such as books, journal articles, and transactions. *Federal Register* notices, Federal and State legislation, and congressional reports can usually be obtained from these libraries.

Documents such as theses, dissertations, foreign reports and translations, and non-NRC conference proceedings are available for purchase from the organization sponsoring the publication cited.

Single copies of NRC draft reports are available free, to the extent of supply, upon written request to the Office of Administration, Distribution and Mail Services Section, U.S. Nuclear Regulatory Commission, Washington, DC 20555-0001.

Copies of industry codes and standards used in a substantive manner in the NRC regulatory process are maintained at the NRC Library, Two White Flint North, 11545 Rockville Pike, Rockville, MD 20852-2738, for use by the public. Codes and standards are usually copyrighted and may be purchased from the originating organization or, if they are American National Standards, from the American National Standards Institute, 1430 Broadway, New York, NY 10018-3308.

DISCLAIMER NOTICE

DISCLAIMER

NUREG/CP-0162
Vol. 1

Proceedings of the U.S. Nuclear Regulatory Commission

Twenty-Fifth Water Reactor Safety Information Meeting

Volume 1
– Plenary Sessions
– Pressure Vessel Research
– BWR Strainer Blockage and Other Generic Safety Issues
– Environmentally Assisted Degradation of LWR Components
– Update on Severe Accident Code Improvements and Applications

Held at
Bethesda Marriott Hotel
Bethesda, Maryland
October 20-22, 1997

Manuscript Completed: March 1998
Date Published: March 1998

Compiled by: Susan Monteleone

C. Bonsby, NRC Project Manager

Office of Nuclear Regulatory Research
U.S. Nuclear Regulatory Commission
Washington, DC 20555-0001

Proceedings prepared by
Brookhaven National Laboratory

ABSTRACT

This three-volume report contains papers presented at the Twenty-Fifth Water Reactor Safety Information Meeting held at the Bethesda Marriott Hotel, Bethesda, Maryland, October 20-22, 1997. The papers are printed in the order of their presentation in each session and describe progress and results of programs in nuclear safety research conducted in this country and abroad. Foreign participation in the meeting included papers presented by researchers from France, Japan, Norway, Russia, Spain and Switzerland. The titles of the papers and the names of the authors have been updated and may differ from those that appeared in the final program of the meeting.

PROCEEDINGS OF THE
25TH WATER REACTOR SAFETY INFORMATION MEETING

OCTOBER 20-22, 1997

Published in Three Volumes

GENERAL INDEX

Volume 1

Volume 2

Volume 3

REGISTERED ATTENDEES (NON-NRC)
25TH WATER REACTOR SAFETY INFORMATION MEETING

K. ALMENAS
UNIVERSITY OF MARYLAND
COLLEGE PARK, MD 20792 USA
301-405-5213

A. ALONSO
CONSEJO DE SEGURIDAD NUCLEAR
JUSTO DORADO, 11
MADRID, 28040 SPAIN
341-346-0334 341-346-0378
aas@csn.es

R. ANDERSEN
NUCLEAR ENERGY INSTITUTE
1776 I ST., NW
WASHINGTON, DC 20006 USA
202-739-8000 202-785-1898

R. ANDERSON
NORTHERN STATES POWER CO.
414 NICOLLET MALL, RSQ8
MINNEAPOLIS, MN 55401 USA
612-337-2050 612-330-7888

P. ANDRESEN
GE CORP R&D CENTER
1 RIVER RD., K1-3A39
SCHENECTADY, NY 12301 USA
518-387-5929 518-387-7007

T. ANDREYCHEK
WESTINGHOUSE NUCLEAR SERVICES DIVISION
P.O. BOX 355
PITTSBURGH, PA 15230 USA
412-374-6246 412-374-5099
andreyts@wec.com

A. ANKRUM
BATTELLE / ENVIRONMENTAL TECHNOLOGY
PO BOX 999, K8-28
RICHLAND, WA 99352 USA
509-372-4095 509-372-6242
ar-ankrum@pnl.gov

Y. ANODA
JAPAN ATOMIC ENERGY RESEARCH INST.
2-4 SHIRAKATA-SHIRANE, TOKAI-MURA
NAKA-GUN, IBARAKI-KEN, 319-11 JAPAN
81-29-282-5263 81-29-282-6728
anoda@lstf3.tokai.jaeri.go

R. ASHLEY
AIB-VINCOTTE NUCLEAR
AVENUE DU ROI 157
BRUSSELS, B-1190 BELGIUM
32-2-5368342
ray.ashley@ava

G. ASMOLOV
RUSSIAN RESEARCH CENTRE - KURCHATOV INSTIT
MOSCOW, 123182 RUSSIA
7-095-196-93-20 7-095-196-17-02
asmolov@nsi.kige.ru

D. AUMILLER
BETTIS ATOMIC POWER LABORATORY
PO BOX 79
WEST MIFFLIN, PA 15122 USA
412-476-6687 412-476-5151

S. AZUMI
KANSAI ELECTRIC POWER CO., INC.
2001 L ST., NW, STE 801
WASHINGTON, DC 20036 USA
202-659-1138 202-457-0272
sazumi.wdc@kansai.com

T. BALDWIN
PACIFIC GAS & ELECTRIC CO/DIABLO CANYON
PO BOX 56
AVILA BEACH, CA 93424 USA
805-545-4789 805-545-6992
dav1@pge.com

M. BALE
FRAMATOME COGEMA FUELS
3315 OLD FOREST RD.
LYNCHBURG, VA 24506-0935 USA
804-832-2488 804-832-3663
mbale@framatech.com

W. BAMFORD
WESTINGHOUSE ELECTRIC
PO BOX 355
PITTSBURGH, PA 15230 USA
412-374-6515 412-374-6515
bamforwh@westinghouse. com

Y.S. BANG
KOREA INSTITUTE OF NUCLEAR SAFETY
19 GUSUNG-DONG, YUSUNG-GU
TAEJON, 305-600 KOREA
82-62-868-0140 82-42-861-1700
kl64bys@pinpoint.kins.re.kr

R. BARI
BROOKHAVEN NATIONAL LABORATORY
DAT, BLDG, 197C
UPTON, NY 11973-5000 USA
516-344-2629 516-344-5266
Bari@bnl.gov

J. BARON
CUYO UNIV., NRC ARGENTINA
BUENOS AIRES, ARGENTINA

cediac@raiz.uncu.edu.ar

D. BATES
PENN STATE, DEPT. OF NUCLEAR ENGINEERING
231 SACKETT BLDG.
UNIVERSITY PARK, PA 16802 USA
814-863-3251 814-865-8499
dwb136@email.psu.edu

G. BAVA
AGENZIA NAZIONALE PER LA PROFESCIONE DELL'A
VIA VITALIANO BRANCATI 48
ROMA, 00144 ITALY
39-6-5007-2052 39-6-5007-2044
bava@educt4.anpa

R. BEEDLE
NUCLEAR ENERGY INSTITUTE
1776 I ST., NW
WASHINGTON, DC 20006 USA
202-739-8000 202-785-1898

R. BELL
NUCLEAR ENERGY INSTITUTE
1776 I ST., NW
WASHINGTON, DC 20006 USA
202-739-8000 202-785-1898

K. BERGERON
SANDIA NATIONAL LABORATORIES
PO BOX 5800, DEPT. 6421/MS0739
ALBUQUERQUE, NM 87185-0739 USA
505-844-2507 505-844-8719
kdberge@sandia.gov

C. BEYER
PACIFIC NORTHWEST NATIONAL LAB.
PO BOX 999
RICHLAND , WA 99352 USA
509-372-4605 509-372-4439
ce.beyer@pnl.gov

N. BIXLER
SANDIA NATIONAL LABORATORIES
PO BOX 5800
ALBUQUERQUE, NM 87185 USA
505-845-3144 505-844-6466
nbixler@sandia.gov

J. BOCCIO
BROOKHAVEN NATIONAL LABORATORY
BLDG. 197C
UPTON, NY 11973-5000 USA
516-344-7690 516-344-5266
boccio@bnl.gov

B. BOYACK
LOS ALAMOS NATIONAL LABORATORY
P.O. BOX 1663, M/S K575
LOS ALAMOS, NM 87545 USA
505-667-2023 505-665-2897
bboyack@lanl.gov

B. BRADLEY
NUCLEAR ENERGY INSTITUTE
1776 I ST., NW
WASHINGTON, DC 20006 USA
202-739-8000 202-785-1898

J. BRAUN
ARGONNE NATIONAL LABORATORY
9700 SO CASS AVE, BLDG. 208
ARGONNE, IL 60439-4838 USA
630-252-5574 630-252-6690

G. BROWN
AEA TECHNOLOGY
THOMSON HOUSE
RISLEY, WARRINGTON, WA3 1HW ENGLAND
44-1925254473 44-1925254536
geoff.brown@aeot.co.u

W. BRUNSON
FRAMATOME COGEMA FUELS
3315 OLD FOREST RD.
LYNCHBURG, VA 24506-0935 USA
804-832-2687 804-832-3663
wbrunson@framatech.com

R. BRYAN
TENNESSEE VALLEY AUTHORITY
1101 MARKET ST, LP 4J-C
CHATTANOOGA, TN 37402-2801 USA

J. BUTLER
NUCLEAR ENERGY INSTITUTE
1776 I ST., NW
WASHINGTON, DC 20006 USA
202-739-8000 202-785-1898

S. BYRNE
ABB COMBUSTION ENGINEERING
2000 DAY HILL RD.
WINDSOR, CT 06095 USA
860-285-3469 860-285-4232

D. CARUGE
INSTITUT DE PROTECTION ET DE SURETE NUCLEAIR
CE FONTENAY AUX ROSES DPEA/SEAC
FONTENAY AUX ROSES, BP 6, 92265 FRANCE
33146548199 33146548559
caruge.daniel@ipsn.jr

N. CAVLINA
FACULTY OF ELECTRICAL ENG. & COMPUTING
UNSKA 3
ZAGREB, 10000 CROATIA
38516129881 6129880
nikola.cavlina@fer.hr

S. CHAKRABORTY
SWISS NUCLEAR SAFETY INSPECTORATE
PO BOX 5232
VILLIGEN, 5232 SWITZERLAND
4153103936 41563103855
chakraborty@hsk.psi.com

W-W CHAO
ATOMIC ENERGY COUNCIL TAIWAN
67 LANE 144 KEELUNG RD SECT. 4
TAIPEI, 10600 TAIWAN ROC
886-2-3634180-335 886-2-3635377
wwchao@aec.gov.tw

J. CHERRY
SANDIA NATIONAL LABORATORIES
PO BOX 5800, MS0747
ALBUQUERQUE, NM 87185-0747 USA
505-844-0090 505-844-1648
jcherr@sandia.gov

C. CHO
KOREA NUCLEAR FUEL CO.
150, DEOGJIN-DONG, YUSONG-GU
TAEJON, 305-353 KOREA
82-42-868-1840 82-42-862-4790
escho@rdns.knfc.co.kr

W. CHOE
TU ELECTRIC
1601 BRYAN ST., FP15
DALLAS, TX 75201-3411 USA
214-812-4371 214-812-8687

C.K. CHOU
LAWRENCE LIVERMORE NATIONAL LABORATORY
PO BOX 808, MS/L-638
LIVERMORE, CA 94551 USA
510-422-4950 510-423-2157
choul@llnl.gov

B. CHRISTIE
PERFORMANCE TECHNOLOGY
PO BOX 51663
KNOXVILLE, TN 37950-1663 USA
423-588-1444 423-584-3043
103007,3517@compuserve.com

B.D. CHUNG
KOREA ATOMIC ENERGY RESEARCH INST.
DUKJIN-DONG 150, YUSONG-GU
TAEJON, 305-353 KOREA
82-42-868-8312 81-42-868-8990
bdchung@nanum.kaeri.re.kr

H.M. CHUNG
ARGONNE NATIONAL LABORATORY
9700 SO CASS AVE, BLDG. 208
ARGONNE, IL 60439-4838 USA
630-252-5111 630-252-3604
hee-chung@qmgate.anl.gov

G. CLAPISSON
COUNCIL FOR NUCLEAR SAFETY
CENTURION PO BOX 7106
CENTURION, 0046 SO AFRICA
2712663550
gaclapis@cns.co.za

A. COHEN
ARGONNE NATIONAL LABORATORY
9700 SO CASS AVE, BLDG. 208
ARGONNE, IL 60439-4838 USA
630-252-5179 630-252-9232
adam.cohen@anl.gov

R. COPELAND
SIEMENS POWER CORPORATION/NUCLEAR DIV.
2101 HORN RAPIDS RD.
RICHLAND, WA 99352 USA
509-375-8290

K. COZENS
NUCLEAR ENERGY INSTITUTE
1776 I ST., NW
WASHINGTON, DC 20006 USA
202-739-8000 202-785-1898

M. CUNNINGHAM
PACIFIC NORTHWEST NATIONAL LAB.
PO BOX 999
RICHLAND, WA 99352 USA
509-372-4987 509-372-4989
me.cunningham@pnl.gov

G. DAHLL
OEC HALDEN REACTOR PROJECT
PO BOX 173
HALDEN, N1751 NORWAY
476921220 4769212960
dahll@hrp.

A. DANILOV
ATOMIC ENERGY CONTROL BOARD
PO BOX 1046, STA. B, 280 SLATER ST.
OTTAWA, ONTARIO K1P5S9 CANADA
613-992-7227

G. DAVANT
ENTERGY OPERATIONS, INC.
1340 ECHELON PARKWAY
JACKSON, MS 39213 USA
601-368-5756 601-368-5768
davant@entergy.com

L.W. DEITRICH
ARGONNE NATIONAL LABORATORY
9700 SO CASS AVE, BLDG. 208
ARGONNE, IL 60439-4838 USA
630-252-4571 630-252-4780
deitrich@anl.gov

D. DIAMOND
BROOKHAVEN NATIONAL LABORATORY
BLDG. 130
UPTON, NY 11973-5000 USA
516-344-2604 516-344-5730
diamond@bnl.gov

S. DOROFEEV
RUSSIAN RESEARCH CENTRE - KURCHATOV INSTIT
MOSCOW, 123182 RUSSIA
70951969840 70958825801
dorofeev@iaeph.kiae.ru

J. DUNKLEBERGER
NYS HEALTH DEPT.
II UNIVERSITY PLACE, RM. 375
ALBANY, NY 12203 USA
518-458-6461 518-458-6434
jdd08@health.state.ny

B. DUNN
FRAMATOME TECHNOLOGIES, INC.
3315 OLD FOREST RD.
LYNCHBURG, VA 24506-0935 USA
804-832-2427 804-832-3663

J. DUSPIVA
NUCLEAR RESEARCH INSTITUTE - REZ
REZ
NEAR PRAGUE, 25068 CZECH REPUBLIC
420-2-6617-3657 420-2-685-7960
dsp@nri.cz

Z. ELAWAR
PALO VERDE NUCLEAR PLANT
PO BOX 52034, STA. 7527
PHOENIX, AZ 85072-2034 USA
602-393-5328 602-393-5467
zelawar@apsc.com

A. ELKADY
NAT'L CTR FOR NUCLEAR SAFETY-HELIOPOLICE
8 ISMAIL KAMAL ST.
CAIRO, 11351 EGYPT
202-243-0384 202-243-0384

F. EMERSON
NUCLEAR ENERGY INSTITUTE
1776 I ST., NW
WASHINGTON, DC 20006 USA
202-739-8000 202-785-1898

P.O. ERICSSON
SWEDISH NUCLEAR POWER INSPECTORATE
S-10658
STOCKHOLM, SWEDEN
4686988400 4686619086
perolote@ski.se

H. ERIKSON
SWEDISH NUCLEAR POWER INSPECTORATE
S-10658
STOCKHOLM, SWEDEN
4686988424 4686612086
hanse@vkt.se

R. EVANS
NUCLEAR ENERGY INSTITUTE
1776 I ST., NW
WASHINGTON, DC 20006 USA
202-739-8000 202-785-1898

M. EYRE
PECO ENERGY/FUEL & SERVICES DIV.
965 CHESTERBROOK BLVD. (M/C 62a-5)
WAYNE, PA 19087 USA
610-640-6829 610-640-6797

G. FALO
HENRY JACKSON FOUNDATION - USACHPPM
MCHP DC 0, 5158 BLACKHAWK RD
APG, MD 21010-5422 USA
410-671-2670 410-671-5411
gerald.falo@chppm.ccmail.apgea.arwy.mic

I. FIERO
ABB COMBUSTION ENGINEERING
2000 DAYHILL RD.
WINDSOR, CT 06095 USA
860-687-8052 860-687-8051

S. FLOYD
NUCLEAR ENERGY INSTITUTE
1776 I ST., NW
WASHINGTON, DC 20006 USA
202-739-8000 202-785-1898

E. FORD
OAK RIDGE NATIONAL LABORATORY
PO BOX 2008, BLD.G 4500-N, MS 6238
OAK RIDGE, TN 37831 USA
423-574-5272 423-574-9646
wef@ornl.gov

W. FRID
SWEDISH NUCLEAR POWER INSPECTORATE
STOCKHOLM, SE-10658 SWEDEN
4686988460 4686619086
wiktor.frid@ski.se

FRANK FU
TECRO/SCIENCE DIVISION
4201 WISCONSIN AVENUE
WASHINGTON, DC 20016 USA
202-895-1932 202-895-1939

T. FUKETA
JAPAN ATOMIC ENERGY RESEARCH INST.
2-4 SHIRAKATA-SHIRANE, TOKAI-MURA
NAKA-GUN, IBARAKI-KEN, 319-11 JAPAN
81292826386 81292826160
toyo@nsrrsun1.tokai.jaeri.go.jp

J. GALLAGHER
CONSULTANT: NPP 8&C SYSTEMS
1450 NAVAHOE DR.
PEN, PA 15228 USA
412-343-0370 412-343-0370
jang11@tdt.net

G. GARNER
FRAMATOME COGEMA FUELS
3315 OLD FOREST RD.
LYNCHBURG, VA 24506-0935 USA
804-832-5274 804-832-5167
ggarner@framatech.com

R. GAUNTT
SANDIA NATIONAL LABORATORIES
13501 GRAMADA HILLS DR.
ALBUQUERQUE, NM 87123 USA
505-284-3989
rogaunt@sandia.gov

G. GIGGER
WESTINGHOUSE ELECTRIC
P.O. BOX 79
WEST MIFFLIN, PA 15122 USA
412-476-7365 412-476-6924

V. GILBERT
NUCLEAR ENERGY INSTITUTE
1776 I ST., NW
WASHINGTON, DC 20006 USA
202-739-8000 202-785-1898

J. GILMAN
ELECTRIC POWER RESEARCH INSTITUTE
3412 HILLVIEW AVE.
PALO ALTO, CA 94304-1395 USA
650-855-8911 650-855-2774
jgilman@epri.com

B. GITNICK
SCIENTECH, INC.
11140 ROCKVILLE PIKE, STE 500
ROCKVILLE, MD 20852 USA
301-468-6425 301-468-0883
bgitnick@scientech.com

M. GOMOLINSKI
INSTITUT DE PROTECTION ET DE SURETA NUCLEAIR
B.P. 6
FONTENAY AUX ROSES CEDEX, 92265 FRANCE

maurice.gomolinski@ipsn.fr

V. GONZALEZ
COMISION NACIONAL DE SEGURIDAD NUCLEAR
DR. BARRAGAN NUM. 779 COL. NARVARTE
MEXICO, 03020 MEXICO
525-5-90-81-13 525-590-61-03
cnsnsl@servidor.unam.mx

D. GRAY
LOCKHEED MARTIN/KNOLLS ATOMIC POWER LAB
PO BOX 1072
SCHENECTADY, NY 12301 USA
518-395-4763 518-395-6171

G. HACHE
INSTITUT DE PROTECTION ET DE SURETE NUCLEAIR
C.E. CADARACHE - DAT 702
ST PAUL LEZ DURANCE, 13108 FRANCE
33442254657 33442256143
didier.jacquemaim@ipsn.fr

K. HALAC
WESTINGHOUSE ELECTRIC
525 BRINTON AVE. #1
TRAFFORD, PA 15085 USA
412-374-5047 412-374-4011
halack@cecil.pgh.wec.1

A. HALL
HEALTH & SAFETY EXECUTIVE, NII
ST. PETER'S HOUSE, BALLIOL ROAD
BOOTLE, L20 3LZ UNITED KINGDOM
0151-951-4165 0151-951-3942
andy.hall@hse.gov.uk

R. HALL
BROOKHAVEN NATIONAL LABORATORY
ET DIV., BLDG. 130
UPTON, NY 11973-5000 USA
516-344-2144 516-344-3957
rehall@bnl.gov

G. HART
PERFORMANCE CONTRACTING INC.
4025 BONNER IND. DR.
SHAWNEE, KS 66226 USA
913-441-0100 913-441-0953
ghhart@aol.com

J. HART
NETHERLANDS ENERGY RESEARCH FOUNDATION
WESTERDUINWEG 3
PETTEN, NL 1755 LE THE NETHERLANDS
31-22456-4282 31-22456-3490
hart@ecn.nl

E. HARVEGO
LOCKHEED MARTIN IDAHO TECHNOLOGIES CO.
PO BOX 1625
IDAHO FALLS, ID 83415 USA
208-526-9544 208-526-2930
hae@inel.gov

C. HARWOOD
ATOMIC ENERGY CONTROL BOARD
PO BOX 1046, STA. B, 280 SLATER ST.
OTTAWA, ONTARIO K1P5S9 CANADA
613-996-2547 613-943-1292
harwood.c@atomcon.gc.ca

S. HASMAN
CHUBU ELECTRIC POWER CO.
900 17TH ST, NW SUITE 1220
WASHINGTON, DC 20006 USA
202-775-1960 202-331-9256

M. HECHT
SOHAR INC.
8421 WILSHIRE SUITE 201
BEVERLY HILLS, CA 90211 USA
213-653-4717 213-653-3624
myron@sohar.com

R. HENRY
FAUSKE & ASSOCIATE INC.
16W070 W. 83RD ST.
BURR RIDGE, IL 60521 USA
630-323-8750 630-986-5481
henry@fauske.com

L. HERNANDEZ
NATIONAL POLYTECHNIC INSTITUTE, DEPT. OF MEC
EDIFICIO 5, 3RD PISO COL LINDAVISTA UNIDAD PROF
ZACATONCO, MEXICO
5-729-6000 ext. 54586 5-567-0751
luishect@iris.esimez.ipn.mx

K. HIGAR
NORTHERN STATES POWER/NUCLEAR ANALYSIS &
414 NICOLLET MALL (RS-10)
MINNEAPOLIS, MN 55401 USA
612-337-2001 612-330-7671
keith.e.higar@nspco.com

T. HILL
COUNCIL FOR NUCLEAR SAFETY
CENTURION PO BOX 7106
CENTURION, 0046 SO AFRICA
27-12-6835500 27-12-6835513
thill@cns.co.za

K. HO
ATOMIC ENERGY CONTROL BOARD
PO BOX 1046, STA. B, 280 SLATER ST.
OTTAWA, ONTARIO K1P5S9 CANADA
613-995-2908 613-943-8954
ho.k@atomcon.ca

L. HOCHREITER
PENN STATE, DEPT. OF ENERGY
231 SACKETT BLDG.
UNIVERSITY PARK, PA 16801 USA
814-865-0044 814-865-8499
dav1@pge.com

J. HODGES
PACIFIC GAS & ELECTRIC CO/DIABLO CANYON
PO BOX 56
AVILA BEACH, CA 93424 USA
805-545-4622 805-545-6992
dav1@pgd.com

P. HOFMANN
FZK KARLSRUHE
P. O. BOX 3640
KARLSRUHE, 76021 GERMANY
49-7247-82-2517 49-7247-82-4567
peter.hofmann@imf.fzk.de

J. HOLM
SIEMENS POWER CORPORATION/NUCLEAR DIV.
2101 HORN RAPIDS RD.
RICHLAND, WA 99352 USA
509-375-8142

H. HOLMSTROM
VTT ENERGY, NUCLEAR ENERGY
PO BOX 1604 (TEKNIIKANTIE 4C)
ESPOO, FIN-02044 VTT FINLAND
358-9-456-5050 358-9-4565000
heikki.holmstrom@vtt.f

W. HOUSTON
SEQUOIA CONSULTING GROUP, INC.
5285 ATLANTIC VIEW
ST. AUGUSTINE, FL 32084 USA
904-461-8774 904-461-8794
whouston@sequoia-cg

D. HOWE
LOCKHEED MARTIN/KNOLLS ATOMIC POWER LAB
PO BOX 1072
SCHENECTADY, NY 12301 USA
518-395-4624

N. HOY
NEW YORK POWER AUTHORITY
PO BOX 41
LYCOMING, NY 13027 USA
315-349-6203 315-349-6148
hoy.n@nypa.gov

J. IRELAND
LOS ALAMOS NATIONAL LABORATORY
PO BOX 1663, MSF606
LOS ALAMOS, NM 87545 USA
505-667-8777 505-665-5204
john.ireland@lanl.gov

M. ISHII
PURDUE UNIVERSITY
1290 NUCLEAR ENGINEERING
WEST LAFAYETTE, IN 47906 USA
765-494-4587 765-494-9570

K. ISHIJIMA
JAPAN ATOMIC ENERGY RESEARCH INST.
2-4 SHIRAKATA-SHIRANE, TOKAI-MURA
NAKA-GUN, IBARAKI-KEN, 319-11 JAPAN
81-292-82-5277

R. ISLAMOV
IBRAE RAN
USACHEVA 29-3-186
MOSCOW, 113191 RUSSIA
7-095-9552655 7-095-9557095
isl@ibrae.ae.ru

B. JACOBS
SOUTHWEST RESEARCH INSTITUTE
6220 CULEBRA RD.
SAN ANTONIO, TX 78238 USA
210-522-2032 210-684-4822
bjacobs@SwRI.edu

K. JACOBS
NEW YORK POWER AUTHORITY
123 MAIN STREET
WHITE PLAINS, NY 10566 USA
914-681-6262 914-287-3710
jacobs.k@nypa

B. JOHNSON
UNIV. OF VIRGINIA
THORNTON HALL
CHARLOTTESVILLE, VA 22903-2442 USA

R. JOHNSON
PACIFIC GAS & ELECTRIC CO.
PO BOX 770000, MC N9B
SAN FRANCISCO, CA 94177 USA
415-973-1784 415-973-0074
rlj3@pge.com

W. JOHNSON
UNIVERSITY OF VIRGINIA
REACTOR BLDG.
CHARLOTTESVILLE, VA 22901 USA
804-982-5464 804-982-5473
wrj@virginia.edu

F. KASAHARA
NUCLEAR POWER ENGINEERING CORP.
4F 17-1, 3-CHOME TORANOMON MINATOKU
TOKYO, 105 JAPAN
81 3 5470 5470 81 3 5470 5454
kasahara@nupec.or.jp

K. KAUKONEN
TEOLLISUUDEN VOIMA OY
OLKILUOTO, 27160 FINLAND
358-2-83813222 358-2-83813209
kari.kaukonen@tuo.tuo.elisz.fi

M. KENNARD
NAC INTERNAT'L-STOLLER NUCLEAR FUEL
485 WASHINGTON AVE
PLEASANTVILLE, NY 10570 USA
914-741-1200 914-741-2093
stollerp@computer.net

H. KHALIL
ARGONNE NATIONAL LABORATORY
9700 SO CASS AVE, BLDG. 208
ARGONNE, IL 60439-4838 USA
630-252-7266 639-252-4500
khalil@ra.anl.gov

M. KHATIB-RAHBAR
ENERGY RESEARCH, INC.
P.O. BOX 2034
ROCKVILLE, MD 20847-2034 USA
301-881-0866 301-881-0867
mkr-eri@radix.net

H. KIM
COMMONWEALTH EDISON
1400 OPUS PL, SUITE 500
DOWNERS GROVE, IL 60517 USA
630-663-3072 630-663-7181
nfshk@ccmail.ceco.com

H. KIM
KOREA INSTITUTE OF NUCLEAR SAFETY
P.O. BOX 114, YUSONG
TAEJON, KOREA
82 42 868 0230 82 42 861 9945
ko98khj@pinpoint.kins.re.kr

H.D. KIM
KOREA ATOMIC ENERGY RESEARCH INST.
DUKJIN-DONG 150, YUSONG-GU
TAEJON, 305-600 KOREA
82-42-868-2664 82-42-868-8256
hdkim@kaeri.re.ler

W. KIM
KOREA INSTITUTE OF NUCLEAR SAFETY
PO BOX 114, YUSUNG
TAEJON, 305-600 KOREA
82-42-868-0327 82-42-861-9945
k095kws@pimpoimt.kims.re.kt

M. KIRK
WESTINGHOUSE ELECTRIC
1310 BEULAH RD.
PITTSBURGH, PA 15235 USA
412-256-1066 412-256-1007
kirkmt@westinghouse.com

R. KIRK
COUNCIL FOR NUCLEAR SAFETY
CENTURION PO BOX 7106
CENTURION, 0046 SO AFRICA
2712663550 27126635513
dkirk@cns.co.za

A. KISSELEV
NUCLEAR SAFETY INST., RUSSIAN ACADEMY OF SCI.
BOLSHAYA TULSKAYA STR. 52
MOSCOW, 113191 RUSSIA
095-955-28-73 095-952-57-01
kso@ibrae.gc.ru

R. KNOLL
FLORIDA POWER CORP.
15760 WEST POWERLINE ST.
CRYSTAL RIVER, FL. 34428 USA
352-563-4543 352-563-4575

D. KOKKINOS
LOCKHEED MARTIN/KNOLLS ATOMIC POWER LAB
PO BOX 1072
SCHENECTADY, NY 12301 USA
518-395-7039

K. KOLLATH
GESELLSCHAFT FUR ANLAGEN UND REAKTORSICH
SCHWERTNERGASSE 1
COLOGNE, 50667 GERMANY
004922a2068-6a9 004922a2068-888

D. KOSS
PENN STATE, DEPT. OF NUCLEAR ENGINEERING
231 SACKETT BLDG.
UNIVERSITY PARK, PA 16802 USA
814-865-5447 814-865-2917
koss@ems.psu.ed

P. KRAL
NUCLEAR RESEARCH INSTITUTE - REZ
REZ
NEAR PRAGUE, 25068 CZECH REPUBLIC
00420-2-66172447 00420-2-6857954
kra@nri.cz

P. KRISHNASWAMY
BATTELLE
505 KING AVE.
COLUMBUS, OH 43201 USA
614-424-5998 614-424-3457
kswamy@battelle.org

W. KUPFERSCHMIDT
ATOMIC ENERGY OF CANADA, LTD.
WHITESHELL LABORATORIES
PINAWA, MANITOBA R0E 1L0 CANADA
204-753-8424 204-753-2455

S. KURATA
CHUBU ELECTRIC POWER CO.
900 17TH ST, NW SUITE 1220
WASHINGTON, DC 20006 USA
202-775-1960 202-331-9256
kurata@chubudc.com

R. KUSHNER
BETTIS ATOMIC POWER LABORATORY
PO BOX 79
WEST MIFFLIN, PA 15632-0079 USA
412-476-5395 412-476-5700

K. KUSSMAUL
UNIVERSITY OF STUTTGART
PFAFFENWALDRING 32
STUTTGART, D-70569 GERMANY
49-711-685-3582 49-711-685-2635
kussmaul@mpa.uni-stuttgart.de

P. LACY
UTILITY RESOURCE ASSOCIATES
SUITE 1600, 51 MONROE ST.
ROCKVILLE, MD 20850 USA
301-294-1941 301-294-7879

J. LAKE
LOCKHEED MARTIN IDAHO TECHNOLOGIES CO.
PO BOX 1625
IDAHO FALLS, ID 83415-3860 USA
208-526-7670 208-526-2930
lakeja@inel.gov

C. LECOMTE
INSTITUT DE PROTECTION ET DE SURETA NUCLEAIR
B.P. 6
FONTENAY AUX ROSES CEDEX, 92265 FRANCE
146547736 014654g5.11
catherine.lecomte@ipsn.fr

G. LEE
KOREA NUCLEAR FUEL CO.
150 DEOGJIN-DONG, YUSONG-GU
TAEJON, 305353 S. KOREA
82 42 868 1832 82 42 862 4790
gwlee@rdns.knfc.co.kr

J-I. LEE
KOREA INSTITUTE OF NUCLEAR SAFETY
19 KUSUNG-DONG, YOUSUNG-KU
TAEJON, KOREA
82 42 868 0143 82 42 861 1700

S. LEE
KOREA ELECTRIC POWER CORP.
150 DUGJIN-DONG, YUSUNG-KU
TAEJON, KOREA
82 42 868 2795

W-J. LEE
KOREAN ATOMIC ENERGY RESEARCH INSTITUTE
DUKJIN-DONG 150, YUSONG-GU
TAEJON, 305-353 KOREA
82-42-868-2895 82-42-868-8990
wjlee@nanum.kaeri.re.kr

Y-W. LEE
KOREA INSTITUTE OF NUCLEAR SAFETY
WANGGUNG APT 4-308
ICHONDONG, YONGSAN, SEOUL, KOREA

S. LEVINSON
FRAMATOME TECHNOLOGIES, INC.
3315 OLD FOREST RD.OF54
LYNCHBURG, VA 24501 USA
804-832-2768 804-832-2683
slevinson@framatech.com

T. LINK
PENN STATE, DEPT. OF NUCLEAR ENGINEERING
231 SACKETT BLDG.
UNIVERSITY PARK, PA 16802 USA
814-863-3251 814-865-8499
tm1110@psu.edu

M. LIVOLANT
INSTITUT DE PROTECTION ET DE SURETA NUCLEAIR
B.P. 6
FONTENAY AUX ROSES CEDEX, 92265 FRANCE
146567179 146549511
michel.livolant@ipsn.fr

A. MARION
NUCLEAR ENERGY INSTITUTE
1776 I ST., NW
WASHINGTON, DC 20006 USA
202-739-8000 202-785-1898

P. MARSILI
AGENZIA NAZIONALE PER LA PROFESCIONE DELL'A
VIA VITALIANO BRANCATI 48
ROMA, 00144 ITALY
39-6-5007-2128 39-6-5007-2044
marsili@edultg.anpant

L. MARTIN
SOUTH TEXAS PROJECT NUCLEAR OPERATING CO.
PO BOX 289
WADSWORTH, TX 77483 USA
512-972-8686 512-972-8577
lemartin@stpegs.com

M. MASSOUD
BALTIMORE GAS & ELECTRIC
1650 CALVERT CLIFFS PARKWAY
LUSBY, MD 20657 USA
410-495-6522 410-495-4498
mahmoud.massoud@bje.com

M. MATSUURA
HITACHI, LTD.
175 CURTNER AVE., MC 725
SAN JOSE, CA 95125 USA
408-925-6151 408-925-4459
matsuuraM@sjcpo5.ne.ge.com

B. MAVKO
JOSEF STEFAN INSTITUTE
JAMOVA 39
LJUBLJANA, 1001 SLOVENIA
386-61-1885330 386-61-188538661
borot.mavko@Js.si

G. MAYS
OAK RIDGE NATIONAL LABORATORY
P.O. BOX 2009, BLDG. 9201-3
OAK RIDGE, TN 37831 USA
423-574-0394 423-574-0382
gtm@ornl.gov

H. McHENRY
NATIONAL INSTITUTE OF STANDARDS & TECHNOLOG
325 BROADWAY
BOULDER, CO 80303 USA
303-497-3268 303-497-5030
harry.mchenry@nist.gov

B. MCINTYRE
WESTINGHOUSE ELECTRIC
P.O. BOX 355
PITTSBURGH, PA 15230
412-374-4334
mcintybh@wesmail.com

J. MEYER
SCIENTECH, INC.
4814 LELAND STREET
CHEVY CHASE, MD 20815 USA
301-468-6425 301-468-0883
jmeyer@scientech.com

D. MITCHELL
FRAMATOME COGEMA FUELS
3315 OLD FOREST RD.
LYNCHBURG, VA 24506-0935 USA
804-832-3438 804-832-3663
dmitchell@framatech.com

S. MIXON
NUS INFORMATION SERVICES
910 CLOPPER RD.
GAITHERSBURG, MD 20878 USA
301-258-2442 301-258-2589
smixon@scientech.com

D. MODEEN
NUCLEAR ENERGY INSTITUTE
1776 I ST., NW
WASHINGTON, DC 20006 USA
202-739-8000 202-785-1898

M. MODRO
IDAHO NATIONAL ENGINEERING & ENVIRONMENTAL
P.O. BOX 1525
IDAHO FALLS, ID 83415 USA
208-526-7402

S MONTELEONE
BROOKHAVEN NATIONAL LABORATORY
BUILDING 130
UPTON, NY 11973 USA
516-344-7235 516-344-3957
smontele@bnl.gov

R. MONTGOMERY
ANATECH CORP.
5435 OBERLIN DR.
SAN DIEGO, CA 92121 USA
619-455-6350 619-455-1094

B. MORRIS
WESTINGHOUSE NSD
PO BOX 355
PITTSBURGH, PA 15601 USA
412-374-4205 412-374-5099
morrisbc@westinghouse.com

D. MORRISON
101 LION'S MOUTH COURT
CARY, NC 27511 USA
919-363-3034

A. MOTTA
PENN STATE, DEPT. OF NUCLEAR ENGINEERING
231 SACKETT BLDG.
UNIVERSITY PARK, PA 16802 USA
814-865-0030 814-865-8499
atm2@pso.edu

M. MULHEIM
LOCKHEED MARTIN ENERGY RESEARCH CORP.
PO BOX 2008
OAK RIDGE, TN 37831 USA
423-574-0386 423-574-0382
m8m@ornl.gov

K. MURATA
SANDIA NATIONAL LABORATORIES
PO BOX 5800
ALBUQUERQUE, NM 87109 USA
505-844-3552

S. NAKAMURA
OBAYASHI CORPORATION
SHINJUKU PARK TOWER, 3-7-1
SHINJUKU-KU, TOKYO 163-10 JAPAN
81-3-5323-3519 81-5323-3550
s.naka@o-net.obayashi.co.jp

R. NANSTAD
OAK RIDGE NATIONAL LABORATORY
PO BOX 2008, 4500S, MS-6151
OAK RIDGE, TN 37831-6151 USA
423-574-4471 423-574-5118
nanstadrk@ornl.gov

A. NELSON
NUCLEAR ENERGY INSTITUTE
1776 I ST., NW
WASHINGTON, DC 20006 USA
202-739-8000 202-785-1898

J. NELSON
ELECTRIC POWER RESEARCH INSTITUTE
3412 HILLVIEW AVE.
PALO ALTO, CA 94303 USA
415-855-2825 415-855-8515
jlnelson@epri.com

M. NISSLEY
WESTINGHOUSE ELECTRIC
P.O. BOX 355
PITTSBURGH, PA 15230 USA
412-374-4303 412-374-4011
nisslem@westinghouse.com

J. O'HARA
BROOKHAVEN NATIONAL LABORATORY
ET DIV., DAT, BLDG. 130
UPTON, NY 11973-5000 USA
516-344-3638 516-344-3957
ohara@bnl.gov

A. ODA
NUCLEAR POWER ENGINEERING CORP.
FUJITAKANKO TROANOMON BLDG. 6F, 17-1
MINATO-KU, TOKYO 105 JAPAN
81-3-5470-5525 81-3-5470-5544

S-H. OH
KOREA INSTITUTE OF NUCLEAR SAFETY
P.O. BOX 114
YUSUNG, TAEJEON 305-600 KOREA
82 42 868 0239 82 42 868 0943
ko67osh@pinpoint.kins.re.kr

A. OHTA
MITSUBISHI HEAVY INDUSTRIES
3-1, MINATOMIRAI 3-CHOME, NISHI-KU
YOKOHAMA, 220-84 JAPAN
81-45-224-9637 81-45-224-9970
ohta@atom.hg.mhi.co.jp

N. ORTIZ
SANDIA NATIONAL LABORATORIES
PO BOX 5800, MAIL STOP 0736
ALBUQUERQUE, NM 87185-0736 USA
505-844-0577 505-844-0955
nrortiz@sandia.gov

D. OSETEK
LOS ALAMOS TECHNICAL ASSOCIATES
BLDG 1, STE 400, 2400 LOUISIANA BLVD NE
ALBUQUERQUE, NM 87110 USA
505-880-3407 505-880-3560
djosetek@lata.com

O. OZER
ELECTRIC POWER RESEARCH INSTITUTE
3412 HILLVIEW AVE.
PALO ALTO, CA 94303 USA
650-855-2089 650-855-2774
oozer@epri.com

J. PAPIN
INSTITUT DE PROTECTION ET DE SURETE NUCLEAIR
C.E. CADARACHE - DAT 702
ST PAUL LEZ DURANCE, 13108 FRANCE
33-4-42253463 33442256143
joelle.papin@ipsn.fr

S-D. PARK
KOREA INSTITUTE OF NUCLEAR SAFETY
19 KUSUNG-DONG, YOUSUNG-KU
TAEJON, KOREA
82 42 868 0003 82 42 861 2653

A. PEREZ-NAVARRO
UNESA/LAESA
PLAZA ROMA, F1,1
ZARAGOZA, 50010 SPAIN
34-976-532614 34-976322956

K. PEVELER
IES UTILITIES/DUANE ARNOLD ENERGY CENTER
3277 DAEC RD.
PALO, IA 52324 USA
319-857-7801 319-857-7678

T. PIETRANGELO
NUCLEAR ENERGY INSTITUTE
1776 I ST., NW
WASHINGTON, DC 20006 USA
202-739-8000 202-785-1898

V. POKROVSKY
INSTITUTE FOR PROBLEMS OF STRENGTH NAN
2 TIMIRYAZEVSKAYA STR.
KIEV, UKRAINE
044-296-25-57 044-296-25-57

A. POOLE
OAK RIDGE NATIONAL LABORATORY
Y-12 PLANT, BEAR CREEK RD.
OAK RIDGE, TN 37831-8038 USA
423-574-0734 423-576-0493
aop@ornl.gov

G. POTTS
GENERAL ELECTRIC NUCLEAR FUEL
CASTLE HAYNE RD
WILMINGTON, NC 28403 USA
910-675-5708 910-675-6966

D. POWELL
PUBLIC SERVICE ELECTRIC & GAS CO.
PO BOX 236, MAIL CODE N21
HANCOCKSBRIDGE, NJ 08038 USA
609-339-2002 609-339-1448

T. PRATT
BROOKHAVEN NATIONAL LABORATORY
BLDG. 130
UPTON, NY 11973-5000 USA
516-344-2630 516-344-5730
pratt@bnl.gov

D. PRELEWICZ
SCIENTECH, INC.
11140 ROCKVILLE PIKE, STE 500
ROCKVILLE, MD 20852 USA
301-468-6425 301-468-0883
damp@scientech.com

J. PUGA
UNESA
FRANCISCO GERVAS 3
MADRID, SPAIN 28020 SPAIN
34-1-5674807 34-1-5674988
unesamuc@dial.eunet.es

C. PUGH
OAK RIDGE NATIONAL LABORATORY
P.O. BOX 2009
OAK RIDGE, TN 37831 USA
423-574-0422 423-241-5005
pug@ornl.gov

R. RANIERI
AGENZIA NAZIONALE PER LA PROFEZIONE DELL' AM
VIA VITALIANO BRANCATI 48
ROMA, 00144 ITALY
39-6-5007-2150 39-6-5007-2941

D. RAO
SCIENCE AND ENGR. ASSOCIATES, INC.
6100 UPTOWN BLVD. NE
ALBUQUERQUE, NM 87110 USA
505-884-2300 505-884-2991
dvrac@seaborse.com

J. RASH
G E NUCLEAR ENERGY
BOX 780
WILMINGTON, NC 28402 USA
910-675-5812 910-675-5879
rashjewlmpo3.wilm.ge.com

J. RASHID
ANATECH CORP.
5435 OBERLIN DR.
SAN DIEGO, CA 92121 USA
619-455-6350 619-455-1094
joe@anatech.com

T. RAUSCH
COM ED NUCLEAR FUEL SERVICES
1400 OPUS PL, STE 400
DOWNERS GROVE, IL 60515 USA
630-663-3020 630-663-7118
nfstr@ccmail.ceco.com

S. RAY
WESTINGHOUSE CNFD
NORTHERN PIKE
MONROEVILLE, PA 15146 USA
412-374-2101 412-374-2045
rays@westinghouse.com

R. REHACEK
STATE OFFICE FOR NUCLEAR SAFETY
SENOVAZNE NAM. 9
PRAGUE, 110 00 CZECH REPUBLIC
420-2-21624729 420-2-21624202
radomir.rehacek@sujb.cz

J. REYES
OREGON STATE UNIVERSITY
116 RADIATION CENTER
CORVALLIS, OR 97331-5902 USA
541-737-4677 541-737-4678
reyesj@cemail.orst.edu

I. RICKARD
ABB COMBUSTION ENGINEERING
2000 DAYHILL RD.
WINDSOR, CT 06095 USA
860-285-9678 860-285-3253

T. RIEKERT
GESELLSCHAFT FUR ANLAGEN UND REAKTORSICH
SCHWERTNERGASSE 1
COLOGNE, 50667 GERMANY
49-224-2068-758 49-224-2068-888
rik@grs.de

J. RIZNIC
ATOMIC ENERGY CONTROL BOARD
PO BOX 1046, STA. B, 280 SLATER ST.
OTTAWA, ONTARIO K1P5S9 CANADA
613-943-0132 613-943-8954
Riznic.j@atomcon.ac.ca

U. ROHATGI
BROOKHAVEN NATIONAL LABORATORY
BUILDING 475B
UPTON, NY 11973 USA
516-344-2475 516-344-1430
rohatgi@bnl.gov

A. ROMANO
BROOKHAVEN NATIONAL LABORATORY
BLDG. 197C
UPTON, NY 11973-5000 USA
516-344-4024 516-344-5266
ramano@bnl.gov

T. ROSSEEL
LOCKHEED MARTIN ENERGY RESEARCH CORP.
PO BOX 2008
OAK RIDGE, TN 37831-6158 USA
423-574-5380 423-574-5118
rosseeltm@oml.gov

R. ROSTEN
DUKE ENGINEERING & SERVICES
215 SHUMAN BLVD. SUITE 172
NAPERVILLE, IL 60563-8458 USA
630-778-4329 630-778-4444
nwrosten@duke-power.com

J. ROYEN
OECD NUCLEAR ENERGY AGENCY
12 BLVD DES ILES
ISSY LES MOULINEAUX, F 92130 FRANCE
33-1-4524-1052 33-1-4524-1129
jacques.royen@oecd.org

B. RYBAK
COMMONWEALTH EDISON
1400 OPUS PL, SUITE 500
DOWNERS GROVE, IL 60515 USA
630-663-7286 630-663-7155

Y-H. RYU
KOREA INSTITUTE OF NUCLEAR SAFETY
YUSONG-DONG 19
TAEJON, 305-338 KOREA
82 42 868 0228 82 42 861 0943
ko53ryh@pinpoint.kins.re.kr

D. SACCOMANDO
COMMONWEALTH EDISON
1400 OPUS PL, SUITE 500
DOWNERS GROVE, IL 60515 USA
630-663-7283 630-663-7155

M. SAKAMOTO
NUCLEAR POWER ENGINEERING CORP.
4F 17-1, 3-CHOME TORANOMON MINATOKU
TOKYO, 105 JAPAN
81 3 3438 3066 81 3 5470 5544
msakamoto@nupec.or.jp

O. SANDERVAG
SWEDISH NUCLEAR POWER INSPECTORATE
INSPECTORATE
STOCKHOLM, 10658 SWEDEN
4686988463 4686619086
oddbjorn@ski.se

M. SATTISON
IDAHO NATIONAL ENGINEERING & ENVIRONMENTAL
PO BOX 1625, MS 3850
IDAHO FALLS, ID 83415-3850 USA
208-526-9626 208-526-2930
sbm@inel.gov

G. SAUER
TOV ENERGIE UND SYSTEMTECHNIK GmbH
WESTENDSTRESSE 199
MUNICH, D-80686 GERMANY
49-89-5791-1267 49-89-5791-2157
gerhard.sauer@et.tueysued.de

C. SCHLASEMAN
MPR ASSOCIATES INC.
320 KING ST.
ALEXANDRIA, VA 22314 USA
703-519-0200 703-519-0224
cschlaseman@mpra.com

F. SCHMITZ
INSTITUT DE PROTECTION ET DE SURETE NUCLEAIR
CE CADARACHE
ST PAUL LEZ D., 13108 FRANCE
33-442257035 33-442252977
frauz.schmitz@ipsn.fr

S. SCHULTZ
YANKEE ATOMIC
580 MAIN STREET
BOLTON, MA 01740 USA
508-568-2131 508-568-3703
schultze@yankee.com

B.R. SEHGAL
ROYAL INSTITUTE OF TECHNOLOGY
60 BRINELVAGEN
STOCKHOLM, 10044 SWEDEN
011-46-8-790-6541 011-46-8-790-7678
sehgal@ne.kth.se

W. SHACK
ARGONNE NATIONAL LABORATORY
9700 S. CASS AVE. BLDG. 212
ARGONNE, IL 60439-4838 USA
630-252-5137 630-252-4798
wjshack@anl.gov

E. SIMPSON
PUBLIC SERVICE ELECTRIC & GAS CO.
PO BOX 236, MAIL CODE N21
HANCOCKSBRIDGE, NJ 08038 USA
609-339-1700 609-339-5070

B. SINGH
JUPITER CORPORATION
STE 900, WHEATON PLAZA NO.
WHEATON, MD 20902 USA
301-946-8088 301-946-6539
singh@jupitercorp.com

W. SLAGLE
WESTINGHOUSE ELECTRIC / CNFD
161 SAXONBURY ROAD
PITTSBURGH, PA 15238 USA
412-374-2088 412-374-2045
slaglewh@westinghouse.com

A. SMIRNOV
RESEARCH INSTITUTE OF ATOMIC REACTORS
DIMITROVGRAD 10
URYANOVSKI REGION, 433510 RUSSIA
84235-32350 84235-64163
gns@niiar.simbirsk.su

V. SMIRNOV
RESEARCH INSTITUTE OF ATOMIC REACTORS
DIMITROVGRAD 10
URYANOVSKI REGION, 433510 RUSSIA
78923532350 78423564163
gns@niiar.simbirsk.su

M. SOBAJIMA
JAPAN ATOMIC ENERGY RESEARCH INST.
2-4 SHIRAKATA-SHIRANE, TOKAI-MURA
NAKA-GUN, IBARAKI-KEN, 319-11 JAPAN
81 29 282 5815 81 29 282 6147
job916@popsvr.tokai.jaeri.go.jp

J-H. SONG
KOREA INSTITUTE OF NUCLEAR SAFETY
19 KUSUNG-DONG, YOUSUNG-KU
TAEJON, KOREA
82 42 868 0117 82 42 861 2653

K. ST. JOHN
YANKEE ATOMIC ELECTRIC CO.
580 MAIN ST.
BOLTON, MA 01740 USA
978-568-2133 978-568-3700
stjohn@yankee.com

J. STONE
MPR ASSOCIATES INC.
320 KING ST.
ALEXANDRIA, VA 22314 USA
703-519-0200

V. STRIZHOV
NUCLEAR SAFETY INST., RUSSIAN ACADEMY OF SCI.
BOLSHAYA TULSKAYA STR. 52
MOSCOW, 113191 RUSSIA
095-955-28-73 095-952-37-01
vfs@ibrae.ac.ru

K. SUDO
JAPAN ATOMIC ENERGY RESEARCH INST.
2-4 SHIRAKATA-SHIRANE, TOKAI-MURA
NAKA-GUN, IBARAKI-KEN, 319-11 JAPAN
81 29 282 5699 81 29 282 5923

R. SUNDARAM
YANKEE ATOMIC ELECTRIC CO.
580 MAIN ST.
BOLTON, MA 01740 USA
508-568-2125 508-568-3700
sundaram@yankee.com

T. TAIWO
ARGONNE NATIONAL LABORATORY
9700 SO CASS AVE, BLDG. 208
ARGONNE, IL 60439-4838 USA
630-252-7182 630-252-4500
b40364@salt.ra.anl.gov

H. TAMURA
NUCLEAR POWER ENGINEERING CORP.
4F 17-1, 3-CHOME TORANOMON
MINATOKU, TOKYO 105 JAPAN
81 3 5470 5486 81 3 5470 5487
tamura@nupec.or.jp

T. TANAKA
SANDIA NATIONAL LABORATORIES
PO BOX 5800, MS 0747
ALBUQUERQUE, NM 87185-0747 USA
505-844-2981 505-844-3321
tjtanka@sandia.gov

K. TERADA
NUCLEAR POWER ENGINEERING CORP.
SHUWA-KAMIYACHO BLDG, 2F, 4-3-13, TORANOMON
MINATO-KU, TOKYO 105 JAPAN
81 3 3434 4551 871 3 3434 9487

C. THIBAULT
WYLE LABORATORIES
7800 HIGHWY 20 WEST
HUNTSVILLE, AL 35806 USA
205-837-4411 205-837-3363

O. THOMSEN
SOUTHERN CALIFORNIA EDISON
PO BOX 128
SAN CLAMENTE, CA 92674 USA
714-368-8087 714-368-8188
thomscoj@sow65.soe.com

H. THORNBURG
901 S. WARFIELD DR.
MT. AIRY, MD 21771 USA
301-831-7328 301-829-0874
mattt@erols.com

R. TOUZET
AUTORIDAD REGULATORIA NUCLEAR
AV. LIBERTADOR 8250
BUENOS AIRES, 1428 ARGENTINA
541-704-1228 514-704-1188
rtouzet@sede.arn.gov.ar

R. TREGONING
NAVAL SURFACE WARFARE CENTER
9500 MACARTHER BLVD.
WEST BETHESDA, MD 20817 USA
301-227-5145 301-227-5548
tregon.n@metals.dt.navy.mil

H. TUOMISTO
IVO POWER ENGINEERING LTD.
RAJATORPANTIE 8
VANTAA, FIN-01019 FINLAND
358-9-8561-2464 358-9-8561-3403
harri.tuomisto@ivo.fi

R. UHRIG
UNIVERSITY OF TENNESSEE (ACRS MEMBER)
306 PASQUA ENGINEERING BLDG.
KNOXVILLE, TN 37996-2300 USA
423-974-3110 423-974-0668
ruhrig@utk.edu

G. URRIOLAGOITIA
ESIME-I.P.N.
EDIF.5, LINDAVISTA
MEXICO, MEXICO
729-6000 ext. 54586 729-6000 ext. 54588

R. VALENTIN
ARGONNE NATIONAL LABORATORY
9700 S. CASS AVE., BLDG. 308
ARGONNE, IL 60439-4838 USA
630-252-4483 630-252-3250
richv@anl.gov

K. VALTONEN
RADIATION & NUC. SAFETY AUTH, STUK
HELSINKI, FINLAND
358-09-75988331 358-09-75988382
keijo.Valtonen@stuk.fi

W. VAN DOESBURG
SWISS NUCLEAR SAFETY INSPECTORATE
PO BOX 5232
VILLIGEN, 5232 SWITZERLAND
41-56-3103862 41-56-3103854
vandoesburg@hsk.psi.ch

W. VESELY
SCIENCE APPLICATIONS
655 METRO PLACE SOUTH #745
DUBLIN, OH 43017 USA
614-793-7600 614-793-7626

M. VESHCHUNOV
NUCLEAR SAFETY INST., RUSSIAN ACADEMY OF SCI.
BOLSHAYA TULSKAYA STR. 52
MOSCOW, 113191 RUSSIA
095-955-26-18 095-952-5701
vms@ibrae.ac.ru

J. VILLADONIGA
CONSEJO DE SEGURIDAD NUCLEAR
JUSTO DORADO, 11
MADRID, 28040 SPAIN
34-1-3460240 34-1-3460588
jivt@csn.es

K. VINZENS
TOV ENERGIE UND SYSTEMTECHNIK GmbH
WESTENDSTRESSE 199
MUNICH, D-80686 GERMANY
49-89-5791-2317 49-89-5791-2157
kurt.vinzene@et.tuevsued.de

D. VOJNOVIC
SLOVENIAN NUCLEAR SAFETY ADMINISTRATION
VOJKOVA 53
LJUBLJANA, SLOVENIA
386611721147 386611721199
djordje.vojnoric@rujv.sigor.mail.si

K.C. WAGNER
SCIENTECH, INC.
8708 GREENARBOR ROAD
ALBUQUERQUE, NM 87122 USA
505-262-1800

R. WALKER
TU ELECTRIC
PO BOX 1002
GLEN ROSE, TX 76042 USA
254-897-8233 254-897-6573
rwalker5@tuelectric.com

D. WALTERS
NUCLEAR ENERGY INSTITUTE
1776 I ST., NW
WASHINGTON, DC 20006 USA
202-739-8000 202-785-1898

F. WALTHER
BAVARIAN STATE MINISTRY FOR STATE DEV. & ENV.
PO BOX 810140
MUNICH, D-81901 GERMANY
49-89-92142325 49-89-92142286

L. WARD
SCIENTECH, INC.
11140 ROCKVILLE PIKE SUITE 500
ROCKVILLE, MD 20852 USA
301-468-6425

W. WENDLAND
AMERICAN NUCLEAR INSURERS
29 SO. MAIN ST., SUITE 3005
WEST HARTFORD, CT 06107 USA
860-561-3433 860-561-4655
bwendland@amnucins.com

D. WHITEHEAD
SANDIA NATIONAL LABORATORIES
PO BOX 5800, MS0747
ALBUQUERQUE, NM 87185-0747 USA

K. WHITT
SOUTHERN NUCLEAR
40 INVERNESS CENTER PKWY.
BIRMINGHAM, AL 35242 USA
205-922-6396 205-922-6108
kermit.w.whitt@snc.com

F. WINTER
TOV ANLEGEN UND UMWELTTECHNIK GmbH
WESTENDSTRESSE 199
MUNICH, D-80686 GERMANY
49-89-5791-1126 49-89-5791-2070
friedrich.winter@aw.tuevsued.de

R. WOOD
OAK RIDGE NATIONAL LABORATORY
PO BOX 2008, BLDG. 3500 MS 6010
OAK RIDGE, TN 37831-6010 USA
423-574-5578 423-576-8380
woodrt@ornl

G. YADIGAROGLU
SWISS FEDERAL INST. OF TECHNOLOGY (AND PSI)
ETH - ZENTRUM, CLT
ZURICH, CH 8092 SWITZERLAND
41-1-632-4615 41-1-632-1166
yadie@iet.ethz.ch

Y.H. YANG
INSTITUTE OF NUCLEAR ENERGY RESEARCH
PO BOX 3-3
LUNGTAN, TAOYUAN, TAIWAN 325 ROC
886-3-4711400 886-3-4711404

A. YEGOROVA
RUSSIAN RESEARCH CENTRE - KURCHATOV INSTIT
MOSCOW, 123182 RUSSIA
7-095-196-93-20 9-095-196-17-02
asmdov@nsi.kiac.ru

Y.C. YEH
ATOMIC ENERGY COUNCIL TAIWAN
67 LANE 144, KEELUNG RD., SEC 4
TAIPEI, TAIWAN ROC
011-886-2-3634180 011-886-2-3660535
yeyeh@cc22.aec.gov

T. ZAMA
TEPCO
1901 L ST., NW, SUITE 720
WASHINGTON, DC 20036 USA
202-457-0790 202-457-0810
zama@tepco.com

G. ZIGLER
ITS CORPORATION
8015 MOUNTAIN RD. PI NE SUITE 210
ALBUQUEQUE, NM 87110 USA
505-254-1005 505-254-1251
gzigler@itsc.com

PROCEEDINGS OF THE
25TH WATER REACTOR SAFETY INFORMATION MEETING
OCTOBER 20-22, 1997

Contents - Volume 1

Page

Update on Severe Accident Code Improvements and Applications
C. Tinkler, Chair

25TH WATER REACTOR SAFETY INFORMATION MEETING
October 20, 1997

Dr. Malcolm R. Knapp, Acting Director
Office of Nuclear Regulatory Research
U.S. Nuclear Regulatory Commission

Good Morning.

I am pleased to welcome you this morning to the 25th Water Reactor Safety Information Meeting. We have three days ahead of us that contain a broad spectrum of papers that address virtually all of the major safety issues facing nuclear regulators today.

Before I proceed I would like to introduce Al Burda who has a few announcements.

I am very pleased to be with you this morning at the 25th meeting, which happens to be my first. Twenty five years of the Water Reactor Safety Meeting demonstrates the continued importance of these meetings both to the Nuclear Regulatory Commission (NRC) and to those of you outside the Commission who are here today. It also demonstrates the continued commitment that those of us here share to support discussions like these that address the safety of nuclear reactors. Twenty five years ago at our first meeting, we had about 150 attendees and 37 papers at 8 sessions. In today's meeting we anticipate 400 attendees and 63 papers in 12 sessions. Thus, the Water Reactor Safety Meeting continues to be a vital part of the NRC's research program. I look forward to over the next three days meeting as many of you as I can, and I want you to know that although this is my first meeting I certainly intend that it will not be my last.

In a few minutes Chairman Jackson will share some of her thoughts on future trends in nuclear safety research. First, I would like to speak to two of the challenges facing us and some of the directions that I anticipate the NRC's research program will take to meet them.

The first challenge is budget. In Fiscal Years 1981 and 1982 the budget for Research was over 200 million dollars. In Fiscal Year 1987 it was 100 million. This year it is 50 million. Further, I think it is reasonable to expect that in the future, NRC's budget for research will come under close scrutiny. Our resulting challenges are to ensure that the issues which we pursue are indeed significant, that the research programs we conduct to address them are as cost-effective as possible, and that we are able to clearly articulate these facts to others.

The second challenge is relevance. When I became Acting Director of Research, the Chairman charged me to make Research as relevant to the NRC as possible--to bring Research into the mainstream of the NRC. At the same time the Chairman stressed the importance of doing more than simply performing "confirmatory research" to meet the technical needs of the program offices; the Chairman emphasized her support for the portion of the research program known as "anticipatory research."

For those of you who may be unfamiliar with the terms "confirmatory research" and "anticipatory research", confirmatory research is based primarily on requirements specified by NRC's program offices, NRR, NMSS, and AEOD. Anticipatory research is research involving issues which are generally more broadly based and of longer duration than those meeting program office requests. The Chairman provided a crisp perspective on anticipatory research, saying that anticipatory research is work which is derived from, but not driven by, the program offices.

To meet these challenges there are a number of aspects of the NRC's research program that I expect to emphasize. First, our future research must focus on those areas in which we can make the largest contribution to resolving NRC's safety concerns. I anticipate that our planning will reflect both the probability and consequences of proposed research. By consequences, I mean how significant a particular issue is to the safe operation of reactors, or more broadly, to the protection of the health and safety of the American people. I will also ask, if a proposed research program to address such an issue is successful, to what extent will it resolve the issue? Third, how likely is it that the research will be successful?

Thus issues of major safety significance where successful research will have a significant impact and where the research itself is likely to be successful will receive priority. By contrast, areas of less safety significance to the agency or where successful research is less likely to resolve the issue or where a research program has a lower probability of success will receive lower emphasis.

For those programs which we support, the relevance of the products must be stressed. I will continue to ask of each of our programs what specifically will be produced and how each product will be used within the agency. It is important that our research continues to focus on the end point, which is the resolution of safety issues or development of products which can be used to resolve safety issues. I view this direction as entirely consistent with strong support for anticipatory research. It is simply that we must recognize that in the same way that confirmatory research is responsive to the needs of a program office, anticipatory research must clearly contribute to the resolution of safety issues. Research which advances understanding but which does not demonstrate a path toward resolution of a safety issue must be given lower priority.

These challenges are significant. With fewer resources we must focus on what is the safety significance of our work, how likely is it that the work will succeed, whether we are continuing to look at the end point and how useful that end point will be to the agency. Another group might find some of these challenges daunting, but in my work with Research over the last two months, I find a capable, energetic staff. I find contractors with a true wealth of talent and commitment and I have every confidence that we can rise to these challenges.

I would now like to introduce the Chairman of the NRC, Dr. Shirley Ann Jackson. Dr. Jackson has been Chairman of the NRC since July 1, 1995. Dr. Jackson earned a Bachelor of Science degree in Physics and a Doctorate in

Theoretical Elementary Particle Physics both from the Massachusetts Institute of Technology (MIT) in Cambridge, Massachusetts. Among the many firsts which Dr. Jackson has achieved, she is the first African-American woman to receive a Doctorate from MIT in any subject.

Prior to her becoming Chairman of the NRC, she conducted research at Bell Laboratories and was a Professor of Physics at Rutgers. Since joining the NRC, she has brought energy and a sense of commitment to the agency. Among her achievements here have been her emphasis on the pursuit of risk-informed, performance-based regulation; her initiative of a strategic assessment and rebaselining effort which has given new direction to the agency; and her international efforts which resulted this May in the formation of the International Nuclear Regulators Association of which she has been elected the group's first Chairman. We are privileged to have her with us today to share her thoughts on future trends in nuclear safety research.

UNITED STATES
NUCLEAR REGULATORY COMMISSION
Office of Public Affairs
Washington, D.C. 20555

No. S-97-20

Future Trends in Nuclear Safety Research

by

Dr. Shirley Ann Jackson, Chairman
U.S. Nuclear Regulatory Commission

25th Annual Water Reactor Safety Meeting
Bethesda, Maryland
October 20, 1997

Good morning, ladies and gentlemen. I am pleased to join you at this opening session of the 25th Annual Water Reactor Safety Meeting. By the large number of attendees here--including those from around the world--I can see that nuclear safety research still commands global interest.

I. INTRODUCTION

This morning I want to discuss with you the challenges, directions and opportunities facing both the nuclear safety research program at the U.S. Nuclear Regulatory Commission (NRC) and, by implication, the research programs of other countries.

We are in a time of rapid change, including changes that many of us have not faced before, and that have direct effects on our research programs. These changes primarily fall into two categories: changes within the nuclear power industry, and reductions in research budgets.

- Changes in the Nuclear Power Industry: The issues facing the nuclear power industry are different than they were 10 or 15 years ago. In part, this is attributable to the problem-solving contributions made in past years by nuclear safety research programs. In addition, the focus of many nuclear power programs today has changed--from introducing new nuclear plants--to safely and economically generating power from

existing plants over their remaining lifetimes. Related issues, such as the aging phenomena associated with extending nuclear plant lifetimes, decommissioning, and waste disposal are now upon us and no longer just on the horizon.

Along with the technical challenges, the nuclear power industry also faces economic challenges. Chief among these is the deregulation of the electrical generation market, which allows and encourages competition for customers, and increases the pressure to control and to reduce facility operating and maintenance costs. This environment may engender new ownership arrangements and/or new models by which to judge the economics of a facility which, in turn, could lead to new operational entities, the sale of some plants, and the early decommissioning of others. These economic and technical challenges could have unforeseen safety impacts, and research has a role in assessing those impacts.

- Reductions in research budgets: The increasing pressure to reduce expenditures, as you may well know, is being felt throughout both government and industry. The traditional dominant role of the government in funding research is evolving. Since industry is frequently the beneficiary of the research, industrial entities are playing a greater role. In the U.S., the nuclear safety research budgets of both the NRC and the U.S. Department of Energy (DOE) have declined substantially over the past several years. Currently, nearly the entire NRC budget is recovered through annual fees paid by our licensees. In this environment, how can we ensure that sufficient research expertise and capability is maintained to address current and future issues?

II. DISCUSSION

The nuclear power industry is not the first industry to face such challenges, and certainly will not be the last. In the U.S. alone, the aerospace, communications, and defense industries have dramatically changed the ways they conduct business. Certain themes can be gleaned from their experiences:

- First, these industries had to adapt to a different set of rules--and in many cases--to the use of fewer rules as a result of deregulation. This, in turn, produced new market opportunities, the chance to offer new services, but required new ways of doing business. Those companies which recognized and acted on those opportunities did well, and those which did not are, in many cases, no longer in existence.

- Secondly, competition required vision, new business strategies and new management approaches--rather than simply using the old "cost plus fixed fee" methods.

- Thirdly, these industries had to learn to do things in a less costly fashion. This included better planning and budgeting, re-engineering old processes to improve efficiency, and utilizing new technology--including improved information management.

The nuclear power industry faces many of these same challenges. At least on the generation side, nuclear utilities are facing competition from coal, gas, and other power producers. As deregulation of the electric utility industry proceeds, nuclear utilities may face increased competition among themselves. These trends increase the importance of holding down costs, improving efficiency, and searching for new opportunities.

At the NRC, we face many of these same challenges. Internally, we are motivated by the desire to improve continually. Externally, as I have partially described, our licensees face a new world. Our other stakeholders are holding us to higher standards. We are being asked to fulfill our health and safety mission with fewer resources. Increasingly, the Congress and our other stakeholders, more than ever, are demanding that we demonstrate value for the money we spend through annual performance reports that focus on outcomes. Our methods of regulation are under constant scrutiny to ensure that we are properly focused on safety-significant issues and on functions that truly are matters of NRC responsibility. They also are demanding that we enforce our regulations more consistently and more fairly.

As many of you are aware, during the past 2 years we painstakingly have conducted an agency-wide Strategic Assessment and Rebaselining, methodically analyzing what we do, how we do it, and what we can do to improve our overall efficiency and effectiveness. Within this Strategic Assessment, one of the Commission focus areas was Direction-Setting Issue (DSI) 22, which dealt with nuclear safety research. The review of this issue identified several areas for improvement in order to meet expected future challenges: (1) we must delineate our research goals for the future, and understand what capabilities must be maintained at the NRC to ensure that these goals are met; (2) we must find ways to use NRC research funds more efficiently and effectively, to share costs and to avoid duplication; and (3) we must ensure that NRC research programs focus on the most risk-significant issues and result in products that are important to issue resolution. I would like to expand briefly on each of these three areas, and to discuss what we are doing to prepare for the future.

A. Research Goals

Simply put, our research goals for the future are:

- To anticipate and explore problems proactively, rather than reactively,
- To identify and focus on the most risk-significant issues, and
- To maintain sufficient expertise and capability to respond to our future needs.

Relative to the changes occurring within the nuclear power industry, meeting these goals will be a complex and constantly evolving endeavor. Consider several elements that will shape this undertaking:

- Plants are aging and new technical issues continue to emerge (such as the recent concern over cracking in BWR internals);
- Licensees continue to push for improved plant economic performance (including longer refueling cycles, higher fuel burnups, and higher power levels);
- Some licensees would like to extend the lives of their plants;
- Older plants are being decommissioned; and
- Spent fuel storage is becoming a significant problem for some licensees.

Considering these industry directions and considering the relative risk significance of various issues, the NRC is attempting to define its core research needs. This entails identifying what expertise and facilities should be maintained, and whether they should be maintained in-house, or by using NRC contractors. Maintaining expertise in any given area requires several ingredients.

First, there must be meaningful, useful work to be done--practical research of real importance that will produce either information or a product which, in turn, will help to resolve important and longstanding safety issues, or will be used to advance beyond the current state of knowledge or practice. The approach should treat the issues comprehensively, and may involve a mix of experimental and analytical activities--that is, more than simply running an experiment or developing a computer code. Secondly, the program must be stable. If researchers are constantly uncertain of their own futures, their research is less likely to be focused and productive. In addition, programs that are continually reduced eventually reach a point where termination is preferable to maintaining a pretense of viability.

Thirdly, a "critical mass" of individuals must exist, with the right mix of skills, to promote interaction and the development of ideas. Finally, the work should allow for professional recognition, and participation in conferences and professional societies.

B. Cost Sharing and Cooperation

As resources diminish, sharing costs becomes increasingly essential. Cooperative research programs that serve regulatory needs must be sought out, information and experience shared, and common solutions to common problems identified. At the NRC, we are actively seeking ways to expand our cooperative research with other government agencies, other countries, and industry. Organizations like the Electric Power Research Institute (EPRI) (domestically) and the Nuclear Energy Agency (NEA) (internationally) play an important role. They have been and can continue to be leaders in proposing and facilitating the establishment of cooperative research programs.

In fact, the NRC is nearing the completion of a memorandum of understanding (MOU) with EPRI to better coordinate and to increase our cooperative research. Under this MOU, EPRI will act as a point of contact for our cooperative research with the U.S. nuclear power industry. We also are promoting the use of consensus standards, where practical, as a way of standardizing approaches and solutions to common problems. Some of you are aware of a number of international cooperative activities that are being held in conjunction with this Water Reactor Safety Meeting (WRSM). These include the semi-annual meetings of the NRC Code Applications and Maintenance Program (CAMP), the Cooperative Severe Accident Research Program (CSARP), and the first meeting of a cooperative research program on probabilistic risk assessment (PRA). In addition, two NEA-organized meetings are being held this week--the bureau meeting of the Committee for the Safety of Nuclear Installations (CSNI) and the RASPLAV Management Board meeting. I am pleased to see that, in addition to sharing research results, the WRSM also facilitates expanded and enhanced cooperation in a number of areas.

C. Risk-Informed Research

One of my early initiatives as the NRC Chairman was to push for greater use of risk information and, where appropriate, a performance-based

approach in our regulatory activities--risk-informed, performance-based regulation. I believed then, and continue to believe, that a risk-informed, performance-based approach to regulation benefits the agency, the industries we regulate, and the public--through better decision-making, more judicious use of resources, and the reduction of unnecessary burdens.

In developing a proposed strategy for the reassessment of regulatory requirements, and for moving to risk-informed, performance-based regulation, our fundamental objective is to incorporate more risk-informed thinking into regulations and activities which are directed at controlling contributors to risk, so that requirements and actions are consistent with the actual risk importance of the contributors. The most severe requirements and the highest resource commitments should be directed at the highest risk contributors. Less severe requirements and lesser amounts of resources should be directed at less important contributors. I believe it is important for us to have a common understanding on the meaning of the term "risk-informed, performance-based regulation." A "risk-informed" approach means that, in the decision-making process, risk information is considered along with other factors such as the need for defense-in-depth and good engineering practice. Risk information does not become the sole basis for a decision, but rather provides a systematic way of identifying what is important and where uncertainties exist.

Recently, increased attention has been focused on performance-based regulation. Performance-based initiatives should be selected where objective performance criteria can be established for performance monitoring, and where failure to meet the performance criteria results in tolerable conditions for which appropriate corrective action will be taken. Of course, if failure to meet performance criteria could result in intolerable conditions, we will continue to pursue a more prescriptive approach.

An essential component of the risk-informed, performance-based initiative is the feedback of actual experience into the risk-informed activities. As data from performance monitoring of structures, systems, and components are accumulated, the NRC expects licensees to evaluate the impact of the performance data on activities.

As part of its efforts to develop guidance on risk-informed, performance-based decision-making, the NRC staff is developing criteria to judge the contributions to risk of licensees' proposed regulatory

changes. These criteria may reference various elements of the Commission's safety goals or their subsidiary numerical objectives, and thus become, in effect, plant-specific applications of the goals and subsidiary objectives.

The development of Regulatory Guides and Standard Review Plans will enable the staff to establish and to standardize industry applications and staff reviews--in anticipation of the increased use of risk-informed, and, where appropriate, performance-based regulatory approaches.

I am pleased to see that a panel discussion is scheduled for tomorrow on risk-informed regulation. This panel discussion will provide an opportunity to exchange views on this important topic.

I believe that assembling leaders from the regulatory, industry, and risk arenas to share their views and experiences with risk-informed regulation will stimulate some lively discussion, and will help to give focus to risk-informed and performance-based regulatory approaches.

The Commission intends to use risk analysis in all relevant regulatory matters, to the extent supported by the state of the art in risk analysis methods and data, and the law. This philosophy was articulated in the 1995 Commission Policy Statement on the use of PRA methods, and is being implemented in NRC functions ranging from inspection to rulemaking. Likewise, risk considerations also must be taken into account in research, as well.

First, as operating experience or the results of other research identifies new issues, each such issue must be evaluated in terms of its relative importance. Risk analysis provides a consistent, systematic framework for this evaluation, since it provides an integrated look at plant systems and potential accidents. Secondly, in planning research on a specific issue, the systematic use of risk information can help to identify what is needed to answer the open question or to reduce uncertainties associated with it. For example, shutdown operations involve a wide range of activities. Which of these pose the greatest risk? What is the level of risk? What could and should be done to reduce this risk? Risk assessment is a useful tool in answering such questions--and, in fact, the NRC staff is proposing to initiate such a study to improve the assessment of shutdown safety issues. Thirdly, risk assessment work itself can identify areas in which research is needed to improve the quality of data or analysis methods. Finally,

assessment of risk can be useful in prioritizing research programs. As resources and issues change, difficult choices have to be made as to which programs to continue, and which to reduce or terminate. On a very practical note, recent Congressional action on the NRC FY98 budget may affect some of our research programs, and if any such changes are necessary, we will endeavor to make them in a risk-informed fashion.

III. INTERNATIONAL COORDINATION AND COOPERATION

As you know, the safe generation and effective regulation of nuclear energy and reactor byproduct materials are topics that transcend national boundaries. Changes to a particular aspect of how business is conducted in one country--such as the current trend in electric power industry competition and restructuring--can have a direct impact on the world electricity market, and, by implication, on the nuclear power industry around the globe. Emergent issues related to nuclear regulation--for example, the effects of exposure to low-level radiation, challenges associated with decommissioning standards and costs, or waste disposal methods and developments--command attention throughout the world. Therefore, we each must understand our own domestic issues, but, at the same time, we must work within the larger sphere of international energy demands and regulatory activities. This requires sharing knowledge to broaden international perspectives on nuclear issues, and to enhance a global nuclear safety culture.

In the Fall of 1996, a group of regulators from various countries reached consensus on the need for a working group to meet and to discuss the possible formulation of a free-standing, independent international organization specifically focused on the needs of national nuclear regulatory bodies. The most senior nuclear regulators from eight countries--from Canada, France, Germany, Japan, Spain, Sweden, the U.K. and the U.S.--met in Washington in January of this year, and met again in May, in Paris, to negotiate and to constitute formally the International Nuclear Regulators Association (INRA). Emphasizing that nuclear safety must remain the responsibility of the nation states in which the technology is utilized, but believing in the value of sharing regulatory perspectives at the highest policy levels, the Association determined that its aims and objectives would be as follows:

- To establish a forum for the most senior nuclear regulatory officials to exchange views on broad regulatory policy issues (including technical, legal, economic, and administrative issues);
- To build a global nuclear safety culture;

- To encourage the most efficient use of resources in areas of common interest;
- To work to enhance the stature of nuclear regulatory organizations worldwide;
- To seek consensus on how nuclear regulatory issues can be approached and implemented;
- To facilitate international cooperation in regulation;

- To work to advance nuclear safety through cooperation among its members, cooperation with relevant existing intergovernmental organizations (such as the IAEA, or the OECD/NEA), with other national nuclear regulatory organizations, and other groups and organizations, as appropriate; and
- To identify emerging nuclear regulatory challenges.

The INRA will act by consensus to meet these objectives, and will make recommendations to international and national bodies on nuclear safety issues. At the constituting meeting in Paris, the founding members of INRA elected me to serve a 2-year term as the Association's first chairman. Within this role--as well as within my role as Chairman of the U.S. Nuclear Regulatory Commission--I intend to bring forward, for discussion, policy matters related to increasing research cooperation, sharing of research results, and maintaining research capability. Such policy discussions could prove to be useful to organizations such as the NEA which are involved in establishing cooperative research programs and in attempts to address the maintenance of research capabilities and facilities.

IV. CONCLUSION

To conclude, let me summarize what I see for the future for nuclear safety research. Clearly, increased cooperation is essential. This includes the increased sharing of costs, information, and issue resolution. It includes both cooperation between industry and government, and cooperation among countries. The role of organizations like EPRI, and the NEA, in facilitating such cooperation will become increasingly important. The development of common solutions to common problems not only will reduce duplication, but also will lead to better solutions through the increased interaction and stimulation that results from the sharing of ideas. We must ensure that adequate expertise and capabilities are maintained, working together within the global nuclear community. Research priorities must be established, based on risk analyses of the issues in question, as well as on the need for information and tools to ensure safe operation in the future. These considerations should guide us in meeting the challenges and opportunities that lie ahead.

In closing, let me again express my appreciation for your interest in our work and to invite your active participation in this important meeting. Thank you for your attention.

Risk Informed Regulation

Agustin Alonso, Counsellor
Nuclear Regulatory Council of Spain

Good morning, ladies and gentlemen. It is for me a real pleasure to talk to you today on risk-informed regulation in Spain, the way we see that concept and the philosophy behind it.

I believe that the transition from the deterministic to the probabilistic approach to nuclear safety cannot be stopped now and probably it will never be complete. The rate of introduction of the probabilistic methodology in a given country depends on its scientific and technical development and also on the magnitude and on the nature of national nuclear power program.

Spain can be defined as a qualified importer of nuclear technology and there are in that contest many countries like Spain. The nine operating nuclear power plants that we have include Westinghouse PWRs, General Electric BWRs of different vintages and different families, as well as one KWU-PWR. This nuclear power program has been developed with an increasing participation of the country's industry and institutions who are, of course, now fully responsible for the safe operation of its nuclear units and the corresponding fuel cycle. And also Spain has a long-standing and independent nuclear regulatory organization, what we call the Nuclear Safety Council. This set of circumstances, of course, do apply to many other countries.

Qualified importers like Spain are forced by their own nature to incorporate risk-informed regulation by mirroring into the most advance countries from where the nuclear power plants have been imported, in the case of Spain, the United States of America and Germany. And this explains the path that we have followed in Spain in introducing this interesting concept of risk-informed regulation.

In 1986 the new methodology of risk analysis was considered mature enough for the Nuclear Safety Council which is, as you know, the Spanish regulatory agency. In that year this body established formally an Integrated Program for the Conduct and Utilization of Probabilistic Safety Studies in Spain. This document may be considered the Spanish policy statement and it has set the pace for this type of studies in the country.

This first version of this Integrated Program adopted the principle that the probabilistic safety studies should be performed for each one of the Spanish nuclear power plants, but shifting for about a year the starting time of each study with reference to the previous one, so that the maximum utilization of the then scanty human resources of the country will not be precluded. It was also decided that the coverage of each study will increase from one to the next with the idea of incorporating the developments which were taking place in the most advanced countries. The starting date and the complexity of each study was determined on a case-by-case basis by the Nuclear Safety Council and in all cases by making references to the U.S. NRC and international standards of the moment. The German practice was also incorporated when the study for the KWU-PWR started.

One important aspect of the policy referred to the creation of an indigenous data bank including both reliability of components and operating incidents. Today, such data bank has been satisfactorily developed, although, of course, improvements are always identified. Another important decision in those days was to involve experts from the regulatory body for evaluation purposes into the actual conduct of the study by the plant owner/operator. This interactive evaluation process may have produced delays and cost increases in the projects, but it is estimated that it has generated better products. So we do agree with the statement by Commissioner McGaffigan saying that the quality of the PSA is a very important issue and we have tried to get that high quality.

At present, all power stations have practically completed at least level of one PSA including external and internal initiating events. And all plants, but the German plant, have almost finished a level two PSA and two pilot plants have almost completed a PSA for other modes of operation including shut-down. The total program, which will cover up to PSA level two with internal and external initiating events and other modes of operation for each one of the nuclear power plants in operation it is expected it will be completely evaluated by the regulatory body and possible accepted in 1999.

The Nuclear Safety Council has recently decided also that the operating plants should perform a periodic safety review every ten years. The terms and conditions for these reviews are specified in the corresponding individual operating license. And within the documents that have been identified for that review the probabilistic safety analysis has been included. This decision clearly indicates that the regulatory authority in the country and indeed also the nuclear industry considers probabilistic risk analysis as ideal tools to measure the safety level of the operating plants and is also an ideal tool in defining adequate protection when backed by the defense in depth principle.

The second version of the Integrated Program has been also worked out and is now out for comments and it puts emphasis on applications. These applications have been subdivided in the document into 17 groups or categories including aspects such as: optimization of technical specifications and maintenance, backfitting decisions in operating plants, severe accident management and training of operating personnel, among other aspects. The document also contemplates how risk studies may help the regulatory body itself in discharging its responsibilities in aspects such as: the prioritization of inspection and enforcement, emergency planning and evaluation of operating experience.

In fact, the Nuclear Safety Council has already received 50 applications from the Spanish plant owner/operators. Most of these applications refer to the optimization of technical specifications, the implementations of Appendix J, on containment leakage testing, and Appendix R, on fire protection, to 10 CFR Part 50, the training of operating personnel in full scope simulators and the testing of motor operated valves, to name only the most salient examples. About one-third of these 50 applications have been approved basing the results on the risk information provided in the application. The second third of these 50 applications have been discharged or considered non-applicable and the rest are in the process of being evaluated. For the moment, the evaluation of such applications is not, of course, completely based on probabilistic considerations, the deterministic approach is also used in a complementary basis to the first or vice versa, I don't know what of the two approaches is the most important or is the leading one.

This new Integrated Program declares that enough experience has already been gained in the industry and in the regulatory body on the realization and evaluation of probabilistic studies and in the formulation of applications. Therefore, it announces the publication of regulatory guides and standard

review plans covering the activities to be conducted from now on. Of course, the recent documents published by the U.S. NRC on safety guides and the standard review plans are already serving as guides and references for such work.

The new Spanish document concedes also a great deal of attention to research and development pointing out specific problems such as: seismic risks, human reliability, common mode failures, expert judgment and other advanced probabilistic methods. The Council has recently signed an agreement with the plant owner/operators through an organization that they have to engage in research activities of common interest some of which have already been mentioned and others will be included. And also I want to say that the new international PRA cooperative program proposed by the U.S. NRC which is going to be discussed next week is also of great significance in this context.

The new PSA Spanish policy statement also contemplates the living PSA as a concept to be developed in the future. The document recognizes that the living PSA is the basic information tool to the full development of risk-informed regulation. For that reason, the document is very prudent on pushing its full development at this time, recognizing the intrinsic difficulties and the distortion that a complete displacement of the deterministic approach might produce in the way to approach and evaluate safety.

Thank you very much for your attention.

Risk Informed Regulation

Ralph Beedle, Sr. Vice President and Chief Nuclear Officer
Nuclear Generation, Nuclear Engineering Institute

I appreciate the opportunity to be a member of this panel. Last night when considering how I would travel here today, I did a brief deterministic assessment. I concluded that I would take the Metro to the Bethesda Medical Center Station and then walk to the Marriott. On advice from a member of my staff we concluded that it would be feasible because it is a relatively short walk and it is going to definitely be a nice day. So that is what we did this morning.

Now, after sitting here and thinking about that I did a quick probabilistic risk assessment and would like to emphasize the fact that I am truly glad that I am here today, after walking down Rockville Pike.

It is an opportunity to share thoughts on risk assessment. It is a topic of significant interest to not only the NRC, but also to the licensees. We are entering a competitive environment for nuclear generating facilities, and I am sure that this topic is going to take on increased importance as we deal with the competitive nature of our business.

As you have heard from other panel members, we truly are at a crossroad. It is a crossroad that represents the intersection of the deterministic and the probabilistic. Some people might say that it is an opportunity to take one road or the other, but I think in fact what it means is we are going to deal with this problem in a parallel manner. Some of our rules and regulations will continue to be deterministic while others will be probabilistic.

So it is not an either-or situation with which we are dealing. Some aspects of regulation are clearly deterministic in nature, and I do not believe that the licensees are balking at that. The licensees do not believe that it is a case of one or the other.

But the problem we are going to be challenged with is trying to decide where to apply the probabilistic process to our rules and regulations. More importantly, how do we derive cost benefit from that. I think that is going to be the crux of the argument in going one way or the other -- what does it cost the industry as you deal with the competitive environment. If we maintain the status quo, we know the process that we have to live with, we know the cost associated with it as we change. As Larry pointed out, if you invest $10 million into a program, will there be some benefit derived from that?

Now, as a matter of policy the Commissioners have established safety goals that answer the question of how safe is safe enough, yet we are looking at compliance with the body of regulations to provide adequate protection. Now, these two standards are in fact somewhat inconsistent, although the quantitative risk assessment provides a way to determine if the quantitative health objectives have been achieved. They are based in part on a body of regulation that is deterministic in nature.

Risk insights have taught us that some of these deterministic requirements, such as the double-ended guillotine rupture and some fire scenarios required by Appendix R, are not likely to occur. At the same time, other more likely scenarios may not be adequately covered by regulation. For example, some non-safety-related valves that are safety significant are not covered in an IST program. The bottom line is that until regulations, where appropriate, are adjusted to become risk-informed, adequate protection, and how safe is safe enough will remain questions to be pondered. The relationship of the industry's programs will be questioned.

The industry has proposed a pilot project with the objective of using risk insights to determine the level of attention required to plant system and processes. The pilot project is in its early phase and will examine the relationship between the current regulations and current implementation practices against what is important from a risk and operating experience perspective. Regulations, implementation guidance, and license commitment changes need to align risk with the requirements that will be identified. The NRC has agreed to support this pilot effort.

In looking at the role of risk analysis in operational safety we find that plants are designed to be able to withstand the extreme events. This approach has resulted in a robust generation of plants with considerable equipment capability to respond to the extraordinary events.

One of the problems with the current regulatory framework of operating plants is that regulations largely deal with plant design. Carrying over this design approach into operations is not always appropriate, a lesson the industry learned from the accident at Three Mile Island.

The design features of the plant should be maintained to ensure that the plants can respond to the extraordinary event. However, operational safety can be best achieved by ensuring that the plant will respond appropriately to the expected operational events. For example, training should have a strong operational focus. Risk assessments can help to identify scenarios and combinations of faults that are likely to occur. Training should focus on these scenarios, not just the highly-improbable, design-basis scenarios for which the plant was designed.

Equipment testing can also be better focused through risk analysis. It does not make sense to put equipment through harsh design basis testing regimes for events that are highly improbable. For example, an emergency diesel generator testing to meet 10-second start and load time requirements in response to the double-ended guillotine loss of coolant accident generally results in degradation of the diesel engines.

Technical specifications should be rewritten to consider risk insights particularly in the area of configuration management. Many allowed outage times do not have a sound technical basis. Some LCOs caused the plant to undergo transients that pose more risks than the initial condition. A good example is having to shut the plant down in response to a loss of RHR train. This places the plant in the condition where the unavailable equipment is in fact needed.

There are many positive actions taken based on risk insights within the industry. An early success story is in the emergency operating procedures. The EOPs today are significantly better than the deterministic design-basis procedures in place at the time of the TMI accident. Today's EOPs are based on generic, vendor-specific risk analysis that prepare the operator for a wide range of events.

Many plants have had success by making changes to their facility based on insights gleaned from the plant-specific IPE studies. Many of these insights would not have been evident or supported without the use of the risk analysis tools.

A third success story is in shut-down risk management. Through risk models developed by EPRI and the risk management guidelines developed by NUMARC the industry has greatly decreased the frequency and severity of shut-down events. This in turn has produced real increases in plant safety during shut-down.

Then a fourth area of success is evident in the plants making extensive use of risk analysis in planning on-line maintenance activities. This has resulted in significant improvement in outage times because of the maintenance conducted while the plant is on line.

Unfortunately there have been some negative implications and applications of risk insights. The NRC's recent change to the enforcement policy allows high severity level and civil penalties to be assigned to items that have greater risk significance, but explicitly does not allow a reduction in severity level and civil penalty for an issue determined to be of low significance. This one-way application of risk insights is fundamentally wrong. We have noted an increasing list of violations and civil penalties notices with the phrase, "This issue has low safety significance, but high regulatory interest."

Since issuing civil penalties with violations of low safety significance sends a confusing message to the public, it is hard to determine how we, in operating the plants, can adequately use the PRA insights to establish good operating practices.

The NRC's recently-issued draft regulatory guide and standard review plan on risk applications focused far too much on the uncertainties in risk analysis. What is lost is that many of these uncertainties existed under the deterministic approach as well, but were not quantified. The rigor asked for in these documents and the associated costs may have the effect of minimizing risk analysis applications by making the process too burdensome.

So what do we do differently? We need to find ways to encourage the use of risk analysis by showing the positive benefits that can be realized. It is interesting to note that the real improvements in safety such as those described above have been achieved without prescriptive or rigorous NRC review and approval processes. The regulatory approvals need to be processed faster than they are today. For example, the industry has several ASME risk application code cases and several pilot plant risk applications that have been awaiting NRC approval for years.

The BWR owners' group has developed a graded regulatory approach, outlined in the regulatory review group report completed in 1993. The benefit of its approach is that questions that are not germane to the application need not be addressed thus maximizing the potential benefit while conserving resources.

It is necessary for plant safety to obtain top priority and there is no question about that. However, as we move toward deregulation of the electric generation industry how we achieve safety must be based on sound business principals. Our resource expenditures must provide a tangible safety and operating benefit. If PRAs can help in this, we should use them.

Risk Informed Regulation

Lawrence E. Martin, Vice President
Nuclear Assurance and Licensing
South Texas Project

Having yesterday sat through some of the presentations I think it's very important for me to make a statement. You're not going to see any graphs, you're not going to see any calculations in this presentation. Yesterday I was amazed at the technical presentations that I sat through.

I am not a PRA expert. I'm a PRA advocate. I think that's very important to distinguish. I have a number of PRA experts that work for me and we're increasing that number. One of the things I'd like to share with you is the perspective that we have at South Texas and where we're going with risk-informed insights in our operation maintenance and engineering of our plant.

In 1982 we started our first PSA and PSA initiatives. The reason we started is we were having some questions coming out of our Public Utility Commission and out of our four owners with regard to the way we were designing and building the plant. Our plant is a three-train plant. But I don't want to confuse you, it's a 2.97 train plant.

If South Texas were truly a three-train plant we would have found ourselves in a very enviable position. We could have developed and implemented the two-train tech specs and had an installed spare in every case. However, in a couple of our ventilation systems and in our feedwater system and a couple of other places, we are not truly three 100 percent trains. And that was part of what was going on with the questions in the PUC on whether or not we were being prudent with the way we were designing the plant, and out of the owners on whether or not they wanted to continue on with some of the three-train installations.

What developed was a very, very robust design in our plant. So in 1982 in answering those questions we also recognized that we were dealing with a plant that was designed different than a number of others. Now, that was the catalyst to continue to do some things.

When we licensed the plant we licensed it in an era and under pressures that made us license the plant as a true two-train plant. Our AOTs, LCOs are based on two-train numbers.

As we started to evaluate that in PSA space we recognized that we really needed relief in some areas if we were going to truly take advantage of the design that we had in our plant. So we started looking at it.

Now, Commissioner McGaffigan talked about some cost figures that he was given. He's real close to it. We've estimated that in developing our PRA we have about $10 million invested in our PRA and in the maintenance of it over the time period that we're talking about. We

started out with two, we now have seven people working in that group. We just recently hired two new PRA analysts because we see that risk-informed decision making processes in operating and maintaining our plant are very important to us.

Let me explain just a little bit to you about the South Texas Project, it's a two-unit, (1250 MW each) site about 80 miles south-west of Houston. We have our own cooling reservoir, not open to the public; we have a separate cooling water pond; we have seven lines coming in for off-site power; we have main transformers, generator breakers, aux transformers, emergency transformers; we have more diesels than probably any other plant in the country. So it really is a robust-design.

Now, a lot of utilities today are looking at the work that they put in the PSA and the IPE, and the IPEEEs and making decisions that it is probably not prudent to continue that level of expenditure. There are a number of utilities in this country right now today that are downsizing their PSA staffs. Why in the world would South Texas be increasing their staff size in a time when we're talking about deregulated electric power in this country, competition? We feel that risk insights into how we operate and maintain our plants are essential if we're going to operate in a competitive era. That gives us a driver, it makes us willing to spend that money. We think that as we spend that money and we put these initiatives in place that we're also blazing trails, if you want to call it that.

We want to make a contribution to the industry, but we also have our financial drivers that make it worthwhile for us to do that. So we're looking and we're heading in that direction. We are working as a pilot with the NRC in a number of different areas. We have been a graded QA pilot for quite some time. We are, I hope the Commissioner was giving me a little insight, getting close to completion. I know our submittal is at the Commission review level now. We are proud of that program. It has both deterministic and probabilistic insights in it. We factor that into everything that we do in risk-informed space.

We do not allow the PRA to be the only driver. We have an expert panel that's made up of our senior design engineer, our senior system engineer, our maintenance manager, our plant manager, our quality assurance manager, and our licensing manager to go through all of the decisions coming out of PRA to classify equipment and how we're going to do maintenance on it . They go through those and put deterministic insights back into how we rank our systems.

At South Texas we have what we think is a very robust design, but we also believe we have a very robust PRA. We have had a level one and a level two PRA with external events including seismic and fire. We have a shut-down risk model being developed. We are also developing a balance-of-plant model dealing with secondary systems because we think there are some insights in risk-informed space for us on the secondary side of the plant in the way we're maintaining and operating it.

As a matter of fact, as we've gone through this we found a number of individual components in the plant in our safety-related systems and subsystems where we found that in risk-informed space they had no contribution in core damage frequency or large early area release frequency. I told you we had an emergency cooling water pond that was totally independent of our other pond, and it's seismic and qualified for everything. We have a screen wash pump on that. We have been operating with it in tech spec space, safety-related maintenance, and all.

When we look at that particular pump in that system, we find out there's no advantage to it whatsoever. For the particular accidents it was brought into consideration for, we could go out and manually clean that screen if we needed to. But we have come close on a couple of different occasions of actually having to shut our plant down because we couldn't get through the action item or the LCO for that particular pump. That's a shame because it has nothing to add to the plant in risk space. At some plants it does. It depends on the way the plant is designed and where it's located. At our particular plant it doesn't, except for the regulations and the way our tech specs are set up, that's the driver.

The reason we're interested in participating in PSA initiatives, is that we want to make sure as owners and operators of the plant that we're spending our money in the right place, we're putting our resources in the right place and we're maintaining our plant in a manner that assures safety and reliability. If we are expending resources in areas that add nothing to the plant reliability and add nothing to the plant safety or the health and safety of the public, then we are misusing our resources

So that's the reason we are in this. We are trying to make sure that we are putting our resources in the right place. We want to make sure that we have the right drivers for what we are doing. Not just to save money, we think we can use risk-informed decision making processes in every area of our plant. And, by the way, we're also looking at it for how we buy our insurance. We've been in a pilot study with EPRI concerning insurance and how much we ought to be carrying because we think that gives us some insight into where we are and what we ought to be spending in that area. But, as we look at it, we're wanting to make sure that we're putting our resources in the right place.

I think that risk-informed regulation will help us do that. Now, if the regulations are the driver for risk information, we probably have it backwards. We need to be using the risk information to make the regulations the way we need to.

Now, I agree that we need to look at our PRAs and we need to make sure that they are robust and that they meet certain standards. There should be some standards for that. We need to grade them, because whether or not we're using them for certain insights takes a different level and a different quality PRA. I believe the ASME is looking at developing a grading process for the PRAs so that you can use them in the right way, and we need to have that, there is no doubt about it.

One of the things that we find today as we're going through the regulations, some of the definitions that we've had in the past and that we have used seem to be the driver in the direction on how far we can go. I don't think we need to throw the gates wide open. I think we need to do it cautiously and we need to do it prudently. But in the particular area of safety-related, the definition of safety-related has permeated throughout the regulations. But one of the things that does is, if you've ever once declared it safety-related and there was some rationale for that, then you have to go back and either say that rationale was incorrect and downgrade it, or you still have to apply the Appendix B programs and the standards in that direction. We have been working with the NRC to try to get some relief in that. One of the areas that we've worked in our graded QA program is we are basically going with what we call three classifications of components. For high risk components or those that are determined to be high risk through engineering insights also, not just risk, we are applying the QA program we have always had in place. For those that are low, we are going to what we call a basic -- basic Appendix B program.

For those that are in our BOP or balance of plant where we think they have some risk levels associated with them, we are going to a targeted program where we will apply certain aspects of our QA program -- targeted aspects -- to those balance of plant activities and components.

We think that risk-informed insights and risk-informed regulation are the only way to go, if we are going to operate and maintain our plants the way we need to.

Thank you very much.

Risk Informed Regulation

Ashok C. Thadani
U.S. Nuclear Regulatory Commission

One of my responsibilities at the agency is to coordinate and direct our efforts in this area. I'll make a very few remarks and raise a few issues for our distinguished panel to comment on. We do have very accomplished panel members. Commissioner McGaffigan from NRC, Commissioner Alonso from CSN in Spain, Mr. Lawrence Martin from South Texas Project, Mr. Ralph Beedle from Nuclear Energy Institute.

Well, what is "risk informed regulation"? What do we mean? At least at the NRC we use that term to describe a philosophy that encourages the use of both the qualitative and the quantitative information to focus our as well as licensee's attention to what is believed to be more important to safety.

The insights, and I underline the term "insights" provided by risk information are used to supplement our traditional engineering defense in-depth approach and improving our decisions, but not replacing the traditional approach. This is in contrast to risk-based regulation where actual risk criteria are included in regulations and where compliance with these criteria must be demonstrated.

The NRC's philosophy on the use of risk information and regulatory activities was in fact stated in a 1995 policy statement which encouraged the use of such information in all regulatory matters to improve our decision making, make better use of agency resources as well as reduce unnecessary burden on the industry.

Qualification in terms of use of all this information was to be sure that in fact the methods and data would support such application of these techniques.

As many of you are aware, several months ago NRC issued for comment a set of draft documents. These are guidance documents for industry as well as NRC staff that provide a framework for incorporating risk information into the process for making changes to any license amendments. We believe this was a very significant step forward in terms of the use of risk-informed approaches in our regulatory decisions.

At this panel we have invited several leaders and I think it will be very worthwhile to hear their thoughts on at least some of the issues we need to deal with in the coming months, or perhaps longer time period. And the questions that I have challenged this panel to address, if possible, on this chart.

It's very clear that there is significant discussion going on in terms of "how safe is safe enough?" That is, could quantitative measures be used to define that? How would these techniques be used in terms of defining, at least in this country, a minimum set of requirements which we call adequate protection. And do these techniques have a part to play in definition of adequate protection?

Risk information has been used in improving operations. Some examples would be configuration control, training, and there are many more examples. Finally, it's very clear that some things have gone well in terms of use of these techniques, and perhaps we haven't done as well in other areas. It would be very useful to identify what we could do better and how we might go about that.

Each panel member will make some introductory remarks in terms of their views and facts on these and many other issues. It's our intention to allow some time period, perhaps 20 minutes or so, at the end of this session for questions and answers. I encourage you to please come forward and raise any questions that you might have.

CONSIDERATIONS IN THE USE OF NDE AND REVISED FRACTURE TOUGHNESS CURVES IN REACTOR PRESSURE VESSEL INTEGRITY ANALYSIS

by

E.M. Hackett, S.N. Malik, C.J. Fairbanks, D.A. Jackson, M.G. Vassilaros and M.E. Mayfield, U. S. Nuclear Regulatory Commission, Washington, DC

Abstract

The NRC Office of Nuclear Regulatory Research (RES) maintains a broad research program in the area of reactor pressure vessel (RPV) integrity. Three areas of importance and recent interest in this program are: (1) use of revised (master curve) fracture toughness curves in RPV integrity analyses, (2) use of NDE to determine RPV flaw distributions, and (3) use of NDE for evaluation of RPV embrittlement. NRC research activities in these areas and technical and regulatory issues will be discussed briefly.

Introduction

Structural integrity analyses are used to assure the safe operation of nuclear reactor pressure vessels (RPVs). These structural integrity analyses are used in setting allowable operating pressure and temperature limits, in demonstrating that pressure vessels can survive pressurized thermal shock (PTS) conditions, and in determining whether flaws that might be detected during an inservice inspection can remain in the vessel during subsequent operation or if they must be repaired. These applications of structural integrity analysis methods differ in some of the specifics of the application -- flaw sizes considered, rigor in the fracture mechanics models, and explicit margins, for example -- but they are all similar in general approach.

The NRC Office of Nuclear Regulatory Research (RES) maintains a broad research program in the area of RPV integrity. Two areas that are of particular importance in regard to RPV structural integrity analyses are: (1) use of standardized fracture toughness curves and; (2) use of NDE to determine RPV flaw distributions. With respect to (1), a traditional approach, endorsed by NRC regulations, involves the use of ASME Code fracture toughness curves which are indexed for specific levels of embrittlement by impact toughness test results for the materials of interest. This methodology can be subject to significant uncertainties which relate to material and test method variability. The uncertainties, in turn, require the application of additional margin terms in the regulatory approach. In certain cases this can result in overly conservative conclusions with respect to RPV integrity.

A more recently proposed approach involves the use of smaller specimens to directly measure the fracture toughness of the material of interest and the assumption of a universal or "master" curve to define the fracture behavior of the material in the transition

in transition toughness due to irradiation, size effects, etc. This is the basis for the current NRC RPV integrity regulatory framework. There are several weaknesses in this approach, starting with the use of the dynamic Charpy V-Notch (CVN) impact test results in determining an index parameter for static fracture toughness. Another weakness is the lack of a comprehensive analytical framework for assessing large section behavior from small surveillance specimens. Recent technical and standardization efforts have focused on an alternative approach that could provide a more direct assessment of the fracture toughness, potentially eliminating some of the implicit margins in the analysis. The methodology referred to as the master curve (MC) approach provides such an alternative, but by necessity for nuclear pressure vessel applications, the MC approach still relies on small specimen data.

Dr. Wallin at VTT in Finland has pioneered research to devise a more direct method of predicting the fracture toughness transition behavior of a steel from a small set of specimens. His work has created what is called the MC approach to predicting fracture toughness in the transition temperature region [3]. The MC approach has several important assumptions:

1) Fracture toughness behavior is controlled by a weakest link mechanism.
2) The weakest link mechanism can be described by a three-parameter Weibull function with a Weibull slope value of four.
3) The shape of the curve of mean Weibull fracture toughness values versus temperature is similar for all pressure vessel steels.
4) A single master curve can describe the fracture toughness transition behavior of all pressure vessel steels with a simple temperature scale adjustment of the reference temperature (T_0), which is calculated for toughness specimens which have a Weibull mean value of 100 Mpa$\sqrt{m}$.
5) A T_0 value can be calculated from as few a six fracture toughness specimens.

In addition to the above, the full implementation of this technology for nuclear pressure vessel applications involves the use of small (CVN-sized) specimens. The development and verification of the MC approach for pressure vessel steels has been performed with valid fracture toughness data which required a size of at least ½T [4]. In order for the MC approach to be applicable for reactor pressure vessel surveillance programs which currently use CVN specimens, the T_0 would need to be calculated using precracked CVN specimens. The fracture toughness value calculated using CVN specimens is often invalid due to the size requirements currently published in ASTM E1737. The Master Curve is being considered by ASTM to be included as a standard procedure with the provision to accept some fracture values from invalid fracture toughness specimens with a cautionary declaration. The use of invalid fracture toughness data for the calculation of transition toughness behavior which may be used in a possible regulatory issue will be difficult to support without other valid material specific toughness data. The ASTM standard regarding use of the MC approach, and based on the elements described above, is being ballotted for approval in November, 1997. The cautionary language regards the ability of

materials with low strain hardening capacities (typical of RPV materials) to be adequately described by a single fracture parameter in terms of the crack tip deformation state. This cautionary statement provides insufficient guidance as to whether the crack tip constraint level in the small scale specimens is sufficient to describe large scale behavior.

Other NRC concerns with the MC approach, which are discussed in more detail in [2], include:

(1) Fracture toughness characterization performed on the actual material in question or an appropriately qualified "surrogate."

(2) Fracture toughness characterization performed on specimens at appropriate loading rates.

(3) Quantification of the effects of irradiation on the shape of the master curve.

(4) Development and finalization of consensus Codes and Standards (ASTM, PVRC and ASME).

The NRC has encouraged interested licensees and Owners Groups to seek resolution of the technical issues related to application of the MC technology with Codes and Standards Committees on a consensus basis. NRC and its' contractors are also involved with supporting these processes. In this regard it is appropriate to note the following:

(1) The NRC Office of Nuclear Regulatory Research (RES) has a user's request from the Office of Nuclear Reactor Regulation (NRR) regarding the MC approach. RES research efforts with respect to MC approach issues are contained in the Heavy Section Steel Irradiation and Technology (HSSI/HSST) efforts at the Oak Ridge National Laboratory (ORNL) and in the NRC research effort at the Naval Surface Warfare Center (NSWC).

(2) Through the HSST program, NRC is supporting development of a technical basis document for standardization of the MC approach which includes collaboration with Dr. Wallin.

(3) The NRC staff participates regularly in meetings of the appropriate ASTM, PVRC and ASME committees regarding MC issues.

The MC approach provides an alternative that could provide a more direct assessment of the fracture toughness, potentially eliminating some of the implicit margins in the analysis for RPV integrity. The NRC staff considers the MC approach to be promising in this regard, however significant technical, process and regulatory issues remain to be adequately addressed before full implementation of such an approach can be endorsed by NRC.

RPV Weld Flaw Density and Size Distributions

Probabilistic fracture mechanics analyses for vessel failure under PTS conditions have typically involved the use of an assumed flaw distribution such as that attributed to Marshall [1]. Recent NRC-sponsored work at the Pacific Northwest National Laboratory (PNNL) work in this area has non-destructively evaluated actual unirradiated reactor vessel welds to determine the specific flaw size distributions and densities. The NRC staff recently (August, 1997) completed an assessment [5] of a BWR/VIP report concerning the proposed elimination of the inspection of circumferential welds in BWR RPV beltlines. This evaluation was based on a probabilistic fracture mechanics assessment which contains the RPV weld flaw size distribution and density as key inputs. The BWR/VIP used the Marshall flaw distribution for their baseline assessment. In it's evaluation of the BWR/VIP report, the staff used a modified distribution, based on the PNNL evaluation of the circumferential welds in the Pressure Vessel Research Users Facility (PVRUF) vessel [6] which was fabricated by Combustion Engineering (CE). Weld material from the Midland vessel had also been previously examined by PNNL. However, the database from the PVRUF examinations was judged to be more statistically rigorous for application to the BWR/VIP inspection issue.

The PVRUF vessel was examined using advanced ultrasonic testing (UT) procedures and the results indicated a very high density (995 flaws/cubic meter) of flaws near the surface. This is in contrast to the density assumed when using a Marshall distribution (0.4 to 40 flaws/meter cubed). The mitigating factor here, is that although the PVRUF data indicated a very high density of surface indications, these indications were very shallow and were found not to contribute significantly to the overall vessel failure probability for a BWR cold overpressurization transient. The flaw size distribution beyond the near surface region, was found to follow the Marshall distribution closely.

Although the resulting impact of a revised flaw distribution and density on the BWR/VIP assessment was found not to be highly significant, assessments of PTS scenarios have not been performed and might yield different results. An important issue that remains to be resolved is whether a "generic" flaw size distribution and density can be reasonably assumed for PTS analyses or whether such analyses need to consider vessel-specific distributions.

Ongoing work at PNNL will provide destructive verification of the indications from the PVRUF UT exams in the near future. Fifty feet of circumferential weld from the River Bend Unit 2 vessel will also be examined in the coming year. In addition, NRC, PNNL and EPRI are currently conducting cooperative research on welds removed from the unirradiated Shoreham vessel. This work will yield comparisons from two different UT examination approaches and destructive verification of the findings will be performed.

NDE for Evaluation of RPV Embrittlement

The prediction of RPV embrittlement due to neutron irradiation is a key element of RPV integrity evaluations. The current approach, described in NRC regulatory guide 1.99, revision 2, relies on an empirical methodology which is supported by statistical evaluation of available data and by physical and mechanistic insights. A recent effort by NRC contractors at Modeling and Computing Services (M&CS) and the University of California at Santa Barbara (UCSB) has produced a much more rigorous empirical correlation based on a greatly expanded and qualified data set and consistency with recent research on modeling of radiation damage mechanisms. However, due to the largely empirical nature of the correlations that are used, the methodology is still subject to uncertainties which require compensation by additional margin terms. It would ultimately be desirable to use a non destructive methodology that could yield a direct measurement of vessel embrittlement. The NRC has therefore undertaken a research initiative in this area with the initial goal of evaluating non-destructive measurement technologies which have the capability for discerning and quantifying fine scale microstructural damage in RPV steels.

Prior to undertaking this research initiative, the NRC convened a panel of experts from industry and academia to provide recommendations regarding techniques and approaches. The consensus of the panel was that ultrasonic and magnetic methods showed the greatest potential promise, but that the research would be high-risk and would require a dedicated and lengthy (approximately 10 years) research effort to ultimately validate promising candidate approaches. In this regard it is important to emphasize that ongoing and planned industry initiatives in this area will be critical to any successful outcome since the NRC has neither the focused mission or resources to bring this technology to fruition.

For this reason, NRC has planned a phased approach to the initiative with the first phase focused on evaluation of promising NDE measurement techniques. This work is currently ongoing with the National Institute of Standards and Technology (NIST) at the Boulder, CO laboratories. The NIST program is initially focusing on: (1) ductile-to-brittle transition studies; (2) correlations with precipitation hardening; and (3) measurements through cladding.

In addition to and to complement the NIST work, NRC plans to develop and produce a metallurgical surrogate material to initially minimize the resource impact with testing and evaluation of irradiated materials while in the development phase. The NRC has also made available irradiated and unirradiated samples of RPV plate and weldment materials for a part-blind study in the hot cells at the University of Michigan. Interested researchers are welcome to use this facility to evaluate their NDE techniques. Extensive documentation of the actual material properties for these samples is maintained by ORNL.

SUMMARY

The NRC maintains a broad research program in RPV integrity. Within that program, three areas of importance and recent interest are highlighted:

(1) The master curve approach to fracture toughness provides an alternative that could provide a more direct assessment of the fracture toughness, potentially eliminating some of the implicit margins in the analysis for RPV integrity. The NRC staff considers the MC approach to be promising in this regard, however significant technical, process and regulatory issues remain to be adequately addressed before full implementation of such an approach can be endorsed by NRC.

(2) Flaw distribution data has been obtained from the PVRUF vessel and portions of the Midland vessel. This data along with future data from Shoreham, River Bend and other sources of information, will be used in future work directed towards the longer term goal of establishing improved flaw distribution input for probabilistic fracture mechanics calculations and possible generic flaw size distribution and density. Evaluation of flaw size distribution and density data from Midland and PVRUF welds has yielded information that conflicts in certain aspects with previous assumed distributions such as that from the Marshall study. These evaluations raise the issue of whether or not a "generic" distribution can be assumed for purposes of RPV integrity analyses.

(3) The NRC has undertaken a research initiative in the area of NDE for quantification of RPV embrittlement with the initial goal of evaluating non-destructive measurement technologies which have the capability for discerning and quantifying fine scale microstructural damage in RPV steels. Ongoing and planned industry initiatives in this area will also be critical to any successful outcome since the NRC has neither the focused mission or resources to bring this technology to fruition.

REFERENCES

[1] Marshall Committee, "An Assessment of the Integrity of PWR Pressure Vessels," United Kingdom Atomic Energy Authority, October 1, 1976.

[2] "Considerations in the Use of Revised Fracture Toughness Curves in Pressure Vessel Integrity Analysis," M.E. Mayfield, et al, 17th Structural Mechanics in Reactor Technology (SMiRT) Meeting, Lyon, France, August, 1997.

[3] Wallin, K., "The Scatter in K_{IC} - Results," Engineering Fracture Mechanics, Vol. 22, No. 1, pp. 149-163, 1985

[4] McCabe, D.E., R.K. Nanstad, S.K. Iskander and R.L. Swain, "Unirradiated Material Properties of Midland Weld WF-70," NUREG/CR-6264, USNRC, October, 1994.

[5] Letter from Brian W. Sheron, USNRC to Carl Terry, BWR/VIP, "Transmittal of the NRC Staff's Independent Assessment of the Boiling Water Reactor Vessel and Internals Project BWRVIP-05 Report and Proprietary Request for Additional Information," August 14, 1997.

[6] Schuster, G.J., S.R. Doctor, P.G. Heasler, "Characterization of Flaws in U.S. Reactor Pressure Vessels," NUREG/CR-6471, PNNL-11143.

Resolving Reactor Vessel Embrittlement Issues -- An Industry Perspective

Robert O. Hardies
Baltimore Gas and Electric Company

John R. Harrell
Virginia Power Corporation

James R. Pfefferle
Wisconsin Electric Power Company

ABSTRACT

Brittle fracture of reactor vessel materials during Pressurized Thermal Shock (PTS) events must always remain incredible. Toward that end, utilities and the NRC have devoted considerable resources over the past twenty years in evaluating reductions in resistance to brittle fracture due to interactions between steel and neutrons. Historically, new programs to address embrittlement have been established in response to acute perceived shortcomings in vessel embrittlement safety analyses. Such programs tend to have short term objectives that do not comprehensively address longer term or broader issues. In an effort to achieve greater stability in the evaluation of embrittlement issues, the industry (individual utilities, Owner's Groups, EPRI and NEI) has transitioned to a proactive and coordinated approach for managing embrittlement issues. The approach involves identification of new or improvable technology areas and subsequent planning and development work to establish the viability of the new or improved methods. Selection of areas for focus was based on the goal of significantly improving the accuracy of determination of vessel material embrittlement state. The two technology areas that were targeted for development were: direct measurement of fracture toughness; and improvement of embrittlement correlations. These programs were supported as ASTM and ASME activities.

In 1979, the Rancho Seco nuclear power plant experienced an operational transient that subjected the reactor vessel to normal operating pressure following a significant coolant cooldown. The event had been unanticipated during design of the plant, and superimposed a vessel inside diameter thermal tensile stress on the pressure stress. It was subsequently hypothesized that a similar event in the presence of a vessel flaw could lead to cleavage fracture of the vessel if the vessel material lacked sufficient toughness to withstand the stresses. The event was given a name: Pressurized Thermal Shock; an acronym: PTS; and was designated an unreviewed safety question. Initial attempts to deterministically solve the problem proved fruitless; subsequent probabilistic assessments provided assurance that imminent vessel failure was extremely unlikely. In the ensuing years a significant industry developed to study PTS events, their effects, and neutron embrittlement. Nearly twenty years later the only currently developed process for totally solving PTS continues to be probabilistic. Aggressive flux reduction remains the

most common and effective method of postponing the possibility of vessel failure by PTS until after plant retirement.

Pressurized Thermal Shock has been a relatively complex and difficult technical issue, and has occasionally been a difficult political and regulatory issue as well. For example, in 1991 Yankee Rowe nuclear power plant shut down to resolve protracted technical argument about whether its reactor coolant pumps, which had already operated reliably for three decades, would operate an additional twenty minutes during PTS type transient conditions. The chain of argument that culminated in discussions of pump reliability started with discussions of the state of embrittlement of the reactor vessel. As has been common in PTS issue assessment over the past fifteen years, the plant owner prepared an initial assessment using best estimate data, and unable to satisfactorily defend its initial assumptions, capitulated to use of conservative assumptions that ultimately predicted imminent failure. Six years later we know the Yankee Rowe vessel was extremely tough, and vessel failure due to PTS was never credible. The data necessary for proof was not indisputably available until recently. This illustrates the difficulty in addressing emergent PTS problems. The specific data necessary to address immediate issues often take time to develop -- more time than either the NRC or the utilities are always willing or able to withstand.

Following the demise of the Yankee Rowe facility, the NRC issued a revision to the PTS Rule (10CFR 50.61) and, shortly thereafter, Generic Letter 92-01. These actions required licensees to verify they had sufficient vessel material information, and to indicate when they would expect to exceed the PTS screening criteria. The plant that provided the earliest estimated date for exceeding the screening criteria was Palisades. The next several years saw Palisades nearly postpone startup following a completion of a refueling outage, agree to anneal, and finally obtain sufficient information to prove PTS was not a near term (3-5 years) safety concern. While Palisades was performing their analyses they performed chemistry measurements of certain steam generator welds and discovered a wider range of copper content than either they or the NRC had anticipated. Bounding analyses subsequently indicated no immediate safety issue due to copper variability. In 1995, the NRC issued Supplement 1 to GL-92-01, which requested licensee validation that all available data were considered in analyses of PTS.

PTS management has followed a pattern of crises followed by calm, followed by crises, followed by calm, for the past two decades. Funding to develop long term solutions followed the level of crisis. For example, while Palisades pursued annealing, both the Nuclear Industry and the Government invested heavily in annealing technology, analysis and demonstration. Coincident with the Palisades decision not to anneal all funding for development of annealing has disappeared, despite the fact the technological and regulatory aspects have not been brought to closure. A similar fate was faced by Regulatory Guide 1.154, the analytical tool Yankee Rowe attempted to use to demonstrate adequate margin against PTS. A tremendous amount of funding, both commercial and governmental was devoted to honing the R. G. 1.154 type analysis. Now the analytical tool is defunct, at least partly because the crisis that fueled research funding disappeared along with Yankee Rowe's operating license.

Against this backdrop of recurrent PTS crises and incompletely developed mitigative technology, a group of Utility, NSSS vendor, and EPRI representatives met in 1995 to try to identify a potentially more productive path. Out of a series of small meetings grew the kernel of a long term solution. Through interaction between Owners Groups and EPRI, and by choice of a few potentially high-benefit initiatives, PTS could be solved. By devoting resources to just a few areas, by spreading the

costs over several funding bodies, and by committing resources through completion of the activities, it was believed significant advances in the measurement or prediction of the vessel material embrittlement state could be developed. Finally, for the first efforts at least, initiatives were restricted to activities that could be performed in public. Specifically, activities were chosen that were already underway or were to be started shortly in ASTM. The consensus process used by ASTM permitted unlimited public participation with a high level of technical review. This not only facilitated a high quality product, but permitted in-progress review by a diverse group of interests. Too often in past work, representatives of the nuclear industry had developed products for evaluation of PTS in the intellectual isolation of the their point of view. Work through ASTM forces much earlier, broader participation in thedevelopment and review of the product, with concomitant increased applicability of the results.

The group that convened to develop a plan, produced a list of potential activities. Two broad technology areas were chosen as having the highest likelihood of shortest term, lowest cost, and highest payback in terms of increased accuracy in embrittlement knowledge. These areas were Direct Measurement of Fracture Toughness and Improved Embrittlement Correlations. Two other areas were identified for potential future work: Improved Flaw Distributions; and Quantification of Event Frequencies. One technology, annealing (which at the time was enjoying a funding boom), was identified as being sufficiently mature that no additional support was necessary

Original analyses of PTS relied on probabilistic fracture mechanics analyses. The fracture mechanics technology at the time did not support measurement of toughness on actual vessels. Instead, toughness was measured on a few laboratory materials. The measurements were applied to other materials by correlation to measurements of Charpy impact transition temperature or drop weight test results. The correlations necessarily needed large safety margin terms to account for the uncertainty. Fracture toughness technology has advanced significantly since the early 1970s. It is now be possible to measure the fracture toughness of reactor vessel materials directly on surveillance specimens irradiated in power reactor vessels. Use of this approach requires more development, as well as abandonment of the technology used in the past. Use of the approach provides a direct measurement of fracture toughness, vice use of the product and sum of estimations, correlations, and repeated margin applications to account for uncertainties, all based solely on toughness tests performed on three plates and two welds in the 1970s.

The program to develop a method for Direct Measurement of Fracture Toughness started with a draft ASTM standard that described a method for analyzing fracture toughness data. The method has come to be known as the "Master Curve Approach." The method permits analysis of K_{JC} data produced from three point bend specimens. It was believed the technology for measurement and analysis of such data had progressed to the point that Charpy specimens from surveillance programs could be pre-cracked and tested in three point bend. By using six or eight Charpy specimens a toughness master curve could be developed directly for the vessel surveillance material at a fluence that exceeded the beltline fluence. The resulting toughness curve could be used directly for analysis of PTS and for development of heatup and cooldown curves. The Master Curve Approach provided not only a method to analyze data to determine a toughness curve, but also the statistical tools to quantify the uncertainty in the measurement. It was believed the approach would permit the determination of mean values previously unobtainable. It willalso permit the determination of bounding values that would provide quantification of the margins between physical reality and hypothetical trouble. Representatives from the Owners Groups, Vendors and EPRI met to devise a plan.

Implementation of Direct Measurement of Fracture Toughness required, first and foremost, an ASTM standard that codified the test and analytical methods. With a standard in hand, implementing standards that would codify methods of interpreting and applying the information developed from data analyzed using the ASTM standard could be acquired. It was envisioned that changes to the ASME code would alternatively define RT_{NDT} in terms of toughness, or the concept of RT_{NDT} would be abandoned entirely for measured values of toughness. In terms of usefulness to utilities, NRC rulemaking to ratify the ASTM and ASME methodology will be necessary.

The Owners Groups provided funding to key NSSS personnel to contribute towards the progress of the draft standard and attend ASTM meetings. A task group of experts was convened under the Committee on Failure Modes of Components of the Pressure Vessel Research Council (PVRC) to identify the data needs and implementation strategy for recommendation to ASME for appropriate code changes. The NSSS representatives are also serving PVRC in this capacity. An ASME task group drafted a code case describing how to apply the approach. As with all standards and Code activities, committee work is prioritized via the 'squeaky wheel' method. The committees tend to work most diligently on issues that committee members raise and are willing to work on. If committee members do not raise an issue, or are unwilling to work on it, an issue can languish, unaddressed, for long periods. By providing personnel specifically funded to work on the Master Curve Approach it was expected that work could proceed on a faster, more focused path. The Owners Groups essentially provided the various committees a pool of engineering and metallurgical expertise to draw upon to expeditiously produce work.

In parallel with assisting in standards and Code development, the Owners Groups identified testing needs to provide data that could be analyzed using the new techniques. A significant number of different reactor vessel weld and plate materials were located and tested. Various draft Master Curve Standards were used to analyze data developed from 3pb and CT specimens, as well as from reconstituted precracked Charpys. Some irradiated materials were tested in addition to a significant body of unirradiated materials. To date, approximately 16 Linde 1092 welds, six Linde 80 welds and three plates have been tested. Since the Master Curve Approach describes an analysis, not a testing method, the data produced will be useful regardless of the ultimate description of the ratified analysis standard. In addition to generation of specifically applicable data, the Owners Groups have funded efforts to participate in a Materials Property Council (MPC)/PVRC round robin. In this task, a number of laboratories from around the world are performing testing on CTs and precracked Charpys. The objective of the task is to establish Weibull statistics for precracked Charpy size specimens and to verify size corrections (1/2t CT-to-Charpy).

The initial activities have yielded significant insights. For Linde 1092 welds tested and analyzed to date, an RTNDT based on a toughness master curve indicates much higher material toughness than previously attributed to these materials (equivalent RT_{NDT} greater than 100° F lower than RT_{NDT} measured by Charpy impact testing). Since toughness shifts due to irradiation are not likely to duplicate Charpy shifts due to irradiation, usefulness of the Master Curve Approach for unirradiated material will probably be limited to improving accuracy of initial toughness estimates. Since a shift of some sort would still need to be added to the measured value, high margins to account for uncertainties in the estimate of shift would still need to be applied.

The profound improvements the Master Curve Approach will provide for PTS analysis will occur by directly measuring irradiated material from the vessel surveillance programs. The unirradiated value of toughness, the shift due to irradiation, and the copper, nickel, and phosphorus content of the material will be irrelevant. Their effects will not need to be estimated and summed. They will be measured, not separately, but in an integral manner. By eliminating the necessity of accounting for uncertainties in the estimation of these parameters, their contribution to a margin term will be null. Additionally, since the surveillance program significantly leads the vessel in fluence, the measurements will represent vessel behavior many years in the future in terms of irradiation. For probabilistic PTS analyses the complexity involved in verifying the adequacy of numerous assumptions that must be made in order to begin the analysis render the output sufficiently uncertain that very large "margin terms" are added to the results to ensure conservatism. The validity of the assumptions that form the basis of the analysis is, in some cases, so difficult to quantify that the actual margin between analysis and vessel failure are not rigorously quantifiable. When vessel material toughness is measured instead of being estimated from a family of correlations, rules of thumb, and empirical relationships between other material properties and toughness, it is expected that a deterministic analysis of PTS will be possible. Quite simply, the vessel material could be proven to be tough, not brittle when subjected to PTS loading. In addition, the "safety margin" between brittle behavior and ductile behavior could be quantified statistically.

The Owners Groups support has not been central, or even critical, to development of the capability to directly measure fracture toughness. This technology would have been developed whether or not the Owners Groups had ever become involved, and was fairly mature when the Owners Groups initially became involved. What industry has provided, however, is a customer for the technology and talented resources to further its development. With continued diligence, this much more accurate technique for assessing vessel integrity should be used by an operating nuclear power plant by the year 2000.

The second major initiative being supported by the Owners Groups involves development of more accurate embrittlement correlations. Direct measurement of Fracture Toughness can only be performed for materials that are currently contained in surveillance programs. For other materials, toughness changes due to embrittlement must be estimated. In current rules the basis for adjustment of material properties due to irradiation is performed by using a correlation between irradiation exposure and Charpy measurement changes. The existing correlation was developed in the mid 1980s based on surveillance data available at the time. The available data has since increased approximately threefold.

ASTM has a standard, E900, Guide for Predicting Neutron Radiation Damage to Reactor Vessel Materials, that is due for revision in 1999. In preparation for the revision, ASTM Subcommittee E10.02.02 on Behavior and Use of Nuclear Structural Materials commissioned a task group to review the bases for the existing standard and develop recommended changes. A major activity was to validate existing surveillance databases. Owners Groups funded activities to research each data point and verify its uniqueness and accuracy. In particular, material copper and nickel content, fluence, and identity were evaluated. Missing chemistry or flux information was provided, when available. Repeat or erroneous entries were documented and eliminated.

During evaluation of the database it was determined that the irradiation temperature measurements were based on melt wire temperatures. The Owners Group representatives commissioned

activities to determine vessel inlet temperatures as a vastly more accurate method of estimation of irradiation temperature. The inlet temperatures were added to the database.

Subsequent to verification of data, E10.02.02 released the database to the task group and any other interested parties for development of embrittlement correlations. After nearly a year of work, task group members have produced a variety of correlations and are nearing selection of a final version. The Owners Groups funded activities in support of task group work similar to the activities in support of development of the Master Curve Approach. By providing funding for key personnel to perform the task group work, the revision to E900 has been expedited.

In addition to validation of the database and assistance in development and review of improved correlations, the Task Group has generated draft language regarding application of the new correlations. A draft standard has been prepared and may be balloted in the winter of 1998. Implementation of the new correlation required some changes to current methods. The new correlation represents mean behavior of more than 600 surveillance results from a broad variety of materials and irradiation conditions. As is done in the existing standard, it is envisioned that two sigma uncertainty bands would be added to the mean behavior prediction to ensure a bounding analysis. Since the new correlation is drawn from, and validated across, such a large database, the results of plant specific surveillance are probably less accurate than use of the correlation. It is expected that the revised version of E900 may suggest that plant specific data be used only to validate approximately normal irradiation embrittlement behavior for the vessel. Current practice includes provisions to adjust plant specific data from the surveillance material to the vessel material using a "Ratio Procedure." Since plant specific data may not be considered applicable in the new method, the ratio procedure could not be applied (there would be nothing from which to ratio). While the use of the mean behavior plus an uncertainty term is apparently technically superior to plant specific data application, such an approach is a radical departure from traditional methods.

The ASTM E10.02.02 task group has nearly completed definition of the new application language. According to current schedule estimates, a draft will be issue for ASTM Subcommittee E10.02.02 consideration in January 1997. Resolution of comments and balloting at subsequent levels should permit establishment of a completed standard by the ASTM 1999 deadline. The refinements produced by development of an improved correlation are modest in comparison to the benefits provided by direct measurement of toughness. Measurement would revolutionize PTS analyses. New correlations will provide an incremental improvement in prediction accuracy. Since relatively few materials are available for direct measurement of toughness, however, the improved correlations will offer the most widely applied improvement The new correlations suggest average RT_{PTS} values should decline approximately 20°F, demonstrating substantially greater fracture toughness than the current predictions. For vessels with accumulated fluence greater than 10^{19} n/cm^2 this seemingly small improvement can equate to dozens of operating years.

These two broad programs (Direct Measurement of Fracture Toughness and Development of Improved Embrittlement Correlations) form the core of the Owners Group activities to address PTS in the long term. Several shorter term, high effort activities have been recently completed. In particular, significant work has been expended over the past two years identifying, cataloguing and analyzing weld chemistry data. Those efforts have now been completed and the Industry has substantially complete

knowledge about weld chemistry and weld chemistry variability. The results of those efforts have been transmitted to EPRI for incorporation into the EPRI RPVDATA material database.

Besides the broad technology initiatives and the short term work on weld chemistry, the Owners Groups did not forget the list of items developed during brainstorming at the initial joint Owners Group meeting. Event Frequencies and Flaw Distributions were aspects of PTS analysis that contributed significant uncertainty to the analyses and had not been updated in the previous 15 years.

The risk of vessel failure due to PTS must be below $5x10^6$ per reactor year and will preferably be zero. To assess this risk, the probability of an event is multiplied by the probability the event will cause vessel failure. The products are summed for all credible events. Judicious analysis has been performed to show that the probability of vessel failure will be below $5x10^6$ for any combinations of analysis input variables provided the vessel material reference toughness is below 270° F. In determining this screening value, the probability of a PTS event was chosen at one event per reactor year of operation. There have been eight events: none since 1982.

Figure 1 reproduced from SECY 82-465 illustrates the event frequency distribution used for development of the screening criteria. Since that figure was developed an additional approximately 1500 reactor years of operation have accumulated. Figure 2 illustrates Figure 1 updated with the most recent 15 years of experience. The original screening criterion was developed using an assumed event frequency that was recognized as a significant conservatism. Updated event frequency information reveals additional hidden conservatism in the original analysis totaling approximately one order of magnitude. Applying a more accurate and modern event frequency would increase the screening criteria by approximately 40 degrees. Recognizing a potential opportunity to quantify safety margin against vessel failure during a PTS event the Owners Groups have begun to explore methods of gathering and validating the operating experience data in preparation for the time when the NRC revisits the basis of the screening criteria.

A final area for technological advancement is in the identification of the vessel flaws that PTS events change into cracks. Current analyses derive their basis from the Marshall Distribution. This distribution of flaws was developed by expert solicitation of ultrasonics examiners in Europe in the 1960s. While fracture mechanics technology has improved and the number of surveillance data points has increased significantly since the 1960s, their improvements pale in comparison to advances in electronics and ultrasonics. The ultrasonics examiner in the 1960s needed to use his or her slide rule to interpret the signature on his vacuum tube oscilloscope in order to evaluate indications. Modern inspectors employ transducer arrays and time of flight data analysis to provide pictures of indications. Besides being based on the opinion of experts who used primitive technology, the Marshall Distribution was not validated by destructive analysis. In other words, the flaws were completely hypothetical. Not surprisingly, the flaw distribution is the major contributor to uncertainty in PTS analysis, overwhelming the nearest contributors by more than an order of magnitude.

Attempts over the years to use modern ultrasonic data from actual vessels to develop distributions instead of the antique hypothetical data from the 1960s have been unsuccessful. Basically, the ultrasonic data has been deemed unacceptable because of a characteristic inherent to the Marshal Distribution also: the examination data have not been validated by destructive analysis. Lacking a

comprehensive destructive examination, purely imaginary and very conservative distributions will continue to be applied in PTS analysis.

Prior attempts to perform concerted ultrasonic, radiographic, and destructive examinations of vessel materials have yielded indications that modern ultrasonics provide conservative estimates of flaw distribution. The Owners Groups have not yet sponsored research to extend prior work in this area.

Opportunities for increasing the accuracy of understanding of vessel resistance to PTS can be developed through revisiting the frequency of events and by better representing the location, size and number of flaws in a vessel. Activities to address these areas have not been initiated, but if they ever are, the results would offer alternative methods of demonstrating that vessels will not fail.

The coming years will see evolutionary and revolutionary advances in the evaluation of PTS that should permit final resolution. Improved correlations will enhance accuracy of embrittlement predictions, which will result in improved understanding of the margin to vessel failure. The incremental benefits in PTS analysis would be small but would support continued operation of all vessels through the end of their licenses. For vessels whose materials are available to be measured, direct measurement of toughness offers the opportunity to address PTS deterministically. For these vessels, the potential for a PTS event to cause failure could be determined with nearly exact precision. The Owners Groups activities have been paramount to the recent advances in each of these areas.

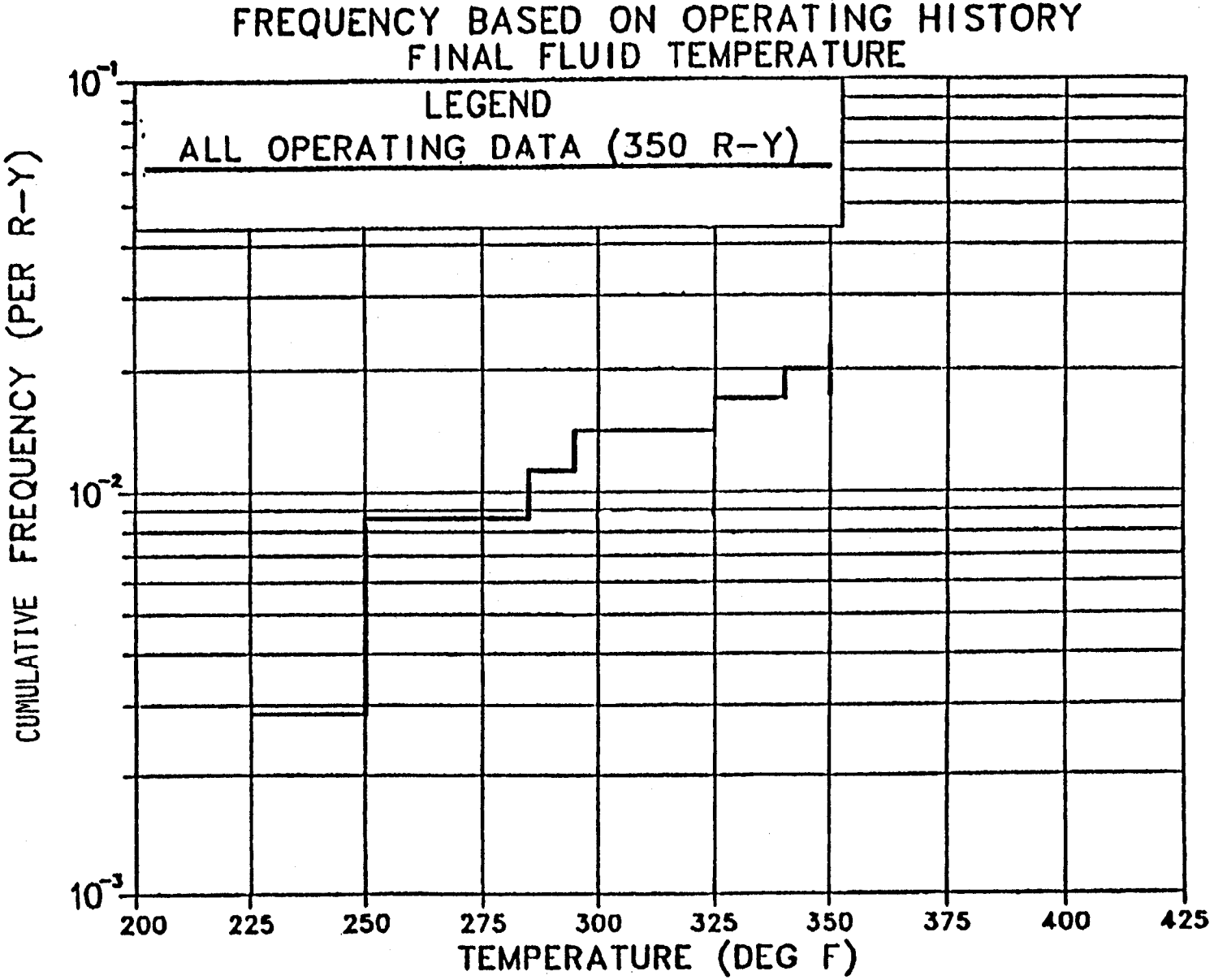
FREQUENCY BASED ON OPERATING HISTORY
FINAL FLUID TEMPERATURE
LEGEND
ALL OPERATING DATA (350 R-Y)
CUMULATIVE FREQUENCY (PER R-Y)
10^{-1}
10^{-2}
10^{-3}
200
225
250
275
300
325
350
375
400
425
TEMPERATURE (DEG F)

FIGURE 1

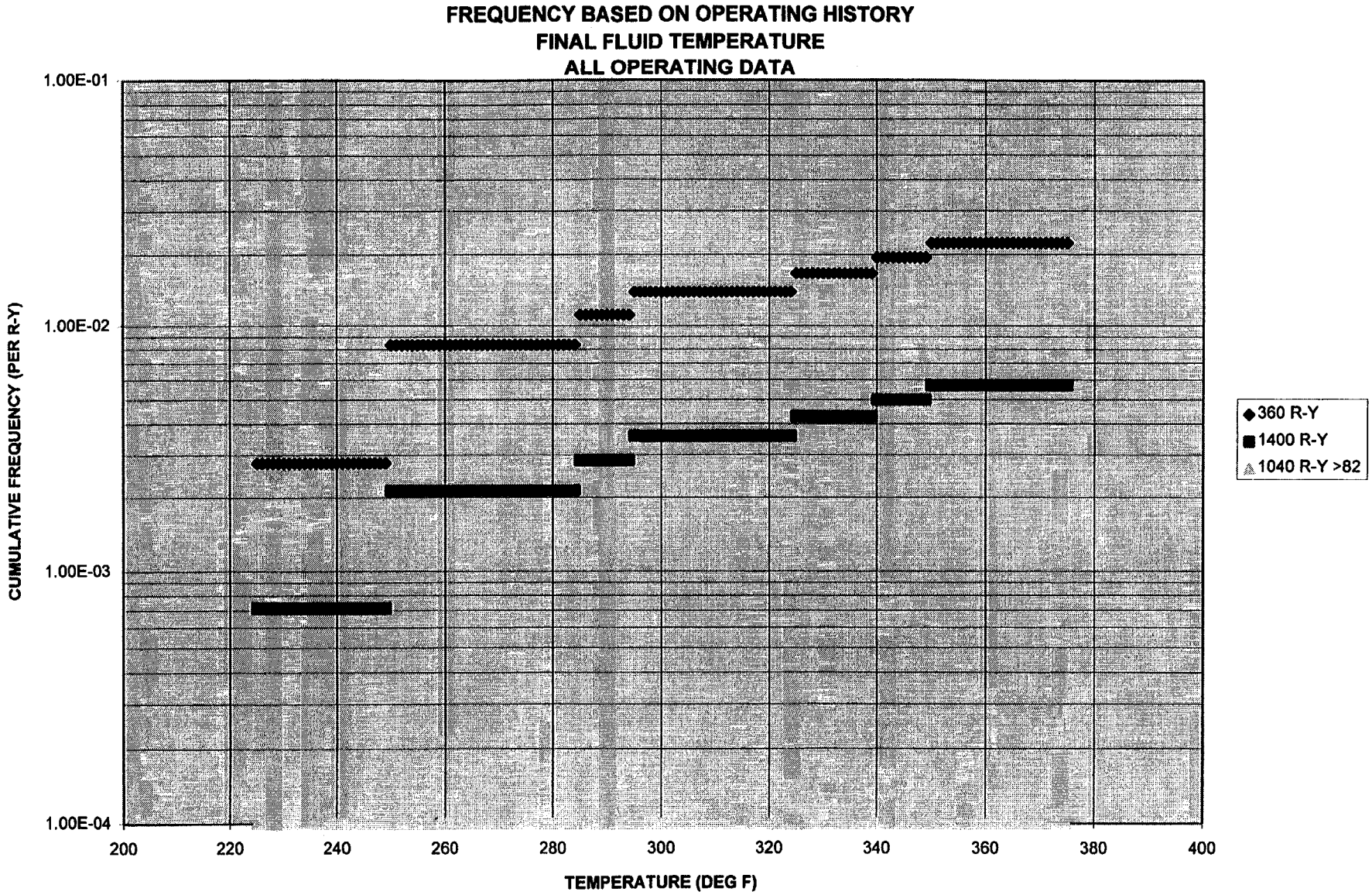
FREQUENCY BASED ON OPERATING HISTORY
FINAL FLUID TEMPERATURE
ALL OPERATING DATA
CUMULATIVE FREQUENCY (PER R-Y)
1.00E-01
1.00E-02
1.00E-03
1.00E-04
200
220
240
260
280
300
320
340
360
380
400
TEMPERATURE (DEG F)
360 R-Y
1400 R-Y
1040 R-Y >82

Figure 2

EPRI Activities to Address Reactor Pressure Vessel Integrity Issues

Stan T. Rosinski
Robert G. Carter
Electric Power Research Institute
1300 Harris Boulevard
Charlotte, NC 28262

Abstract

The demonstration of reactor pressure vessel (RPV) structural integrity is an essential element in ensuring the continued safe and reliable operation of U.S. nuclear power plants. The Electric Power Research Institute (EPRI), through its domestic and international member utilities, continues to pursue an aggressive research program to develop technologies and capabilities that will address issues associated with reactor pressure vessel integrity. Ongoing research in the EPRI Nuclear Power Group Materials Performance Program covers a broad range of technical areas associated with RPVs. The program is structured under the following product groups; (1) Management and Mitigation, (2) Material Performance Databases, (3) Material Condition Assessment, and (4) Operability Assessment. Specific activities under each of theses product groups are described in this paper.

Introduction

The demonstration of reactor pressure vessel (RPV) structural integrity is essential to ensure the continued safe and reliable operation of US nuclear power plants. The primary concern with the RPV is the degradation of material properties due to radiation embrittlement. Approaches to RPV integrity assessment (including NRC regulations and industry standards such as the ASME Boiler and Pressure Vessel Code) were originally developed with a high degree of conservatism to account for various uncertainties associated with material condition assessment. However, as plants age, operation of the RPV is often becoming restricted due to the inherent conservative nature of existing regulations and assessment procedures. A realistic determination of RPV integrity, utilizing advancements in material characterization and integrity assessment technologies, can provide the flexibility needed by utilities to operate plants efficiently while maintaining adequate levels of safety.

The Electric Power Research Institute (EPRI) has been conducting research in many areas of vessel integrity for the last two decades. During that time significant advancements have been made in predicting the behavior and expected life of the vessel materials that are exposed to radiation. Today, new technologies are emerging which hold promise for improving current life prediction models.

Nuclear utilities are experiencing added pressures of remaining economically competitive as the industry moves toward deregulation. Decisions with regard to how they operate and monitor the plant, including the RPV, need to be based on technically defensible information and tools to maximize its useful life while maintaining proper safety margins.

In view of these emerging changes in the industry, EPRI is restructuring its R&D program to reflect the anticipating needs of nuclear utilities. This paper presents an overview of EPRI's R&D program for 1998 and beyond.

EPRI R&D Program for RPV Integrity

The RPV Integrity Program at EPRI is comprised of four main areas. These are called 1) Management and Mitigation; 2) Material Performance Databases, 3) Material Condition Assessment and 4) Operability Assessment. Figure 1 illustrates the structure and organization of activities in the program.

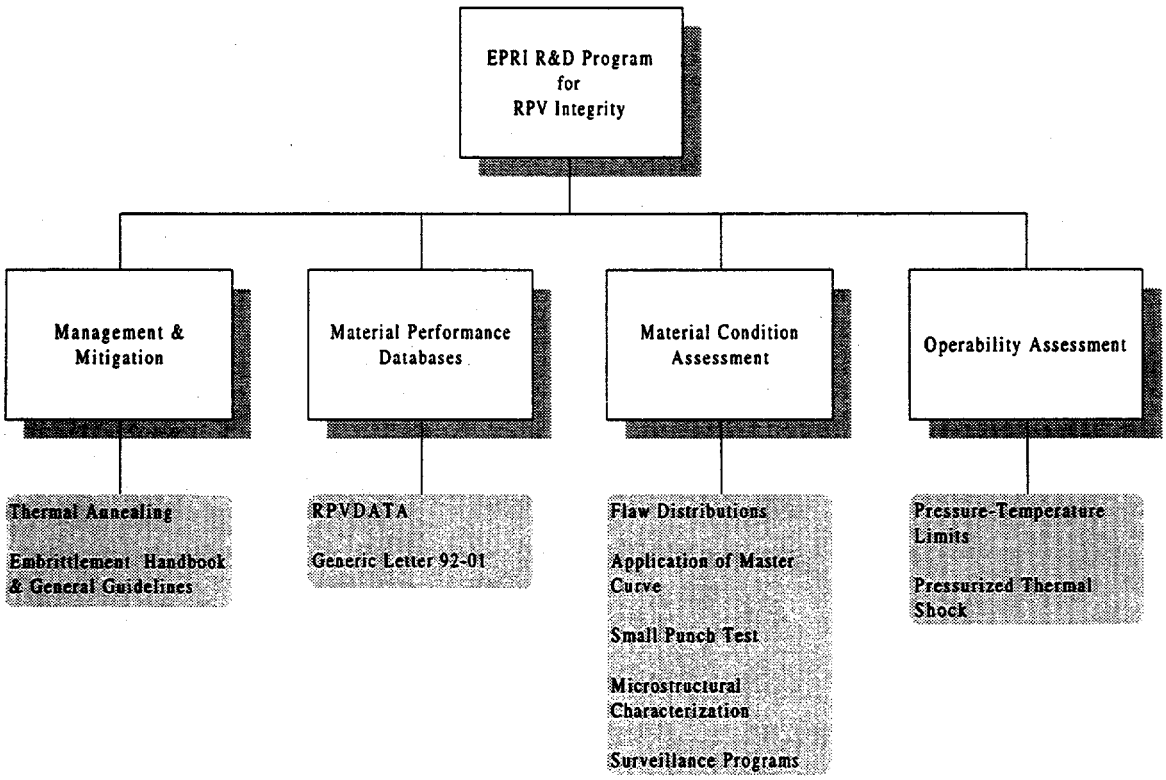

Figure 1. EPRI R&D Program for RPV Integrity

The discussion that follows presents a brief description of each major element of the RPV integrity program along with a summary of the associated projects.

Management and Mitigation

Reactor vessel embrittlement management and mitigation can be viewed as part of a nuclear plant maintenance program. To preserve and possibly extend the life of operating plants, utilities must have

various options and decision analysis tools for choosing the most cost-effective strategies to deal with embrittlement. Some of the projects currently underway are discussed below.

Reactor Vessel Thermal Annealing

Conceived in 1993, EPRI helped to develop and participated in an industry program to demonstrate the feasibility of thermal annealing a RPV. This annealing treatment was performed at the canceled Marble Hill plant in 1996. EPRI is working with its collaborators to document the results in a technical report [1].

In order for utilities to apply thermal annealing it is important to understand the material property recovery and future re-embrittlement of the beltline materials following thermal annealing. EPRI is developing an irradiation-anneal-reirradiation database to evaluate material property behavior. It is envisioned that this database will be useful to determine the optimum annealing process time and temperature as well as to predict the recovery and reembrittlement trends for various steels.

EPRI Embrittlement Management Handbook

There are many aspects to managing embrittlement in reactor pressure vessels that must be considered. An overall approach is described in the EPRI Reactor Vessel Embrittlement Management Handbook [2]. This handbook is designed so that utilities can develop plant-specific embrittlement management programs. It encompasses all of the analysis methods, databases and decision support tools necessary for developing a strategic plan for the vessel. EPRI intends to publish updates to this handbook in the future in order to incorporate new EPRI products and advances in technology.

Material Performance Databases

RPV material property databases are necessary tools to monitor and predict embrittlement. Renewed concerns related to variability in RPV material properties led the NRC to issue Generic Letter 92 01 [3,4]. This letter requested additional plant-specific data for assurance that all data has been considered to determine embrittlement of the vessel materials. EPRI has addressed this issue through development of a materials database.

RPVDATA and Generic Letter 92-01

In response to Generic Letter 92-01, EPRI developed a comprehensive database called RPVDATA [5]. This database contains all of the licensing information of the NRC RVID database [6] plus all available measured chemistries and initial RT_{NDT} data for welds, plates and forgings. It also contains a summary of vessel surveillance data from a database called PREP4 [7], also developed by EPRI. The RPVDATA database has led to a major step forward in understanding and resolving reactor vessel material variability. EPRI has made this database available to all nuclear utilities and intends to make periodic updates and enhancement to this database.

Material Condition Assessment

Life prediction of the RPV is possible only through a comprehensive understanding of the behavior of irradiated materials. This process begins with a characterization of metallurgical mechanisms that cause damage to materials. This information provides a framework for a mechanistic basis for embrittlement. Improvements in fracture mechanics technology yield greater accuracy in predicting crack initiation, growth and arrest or failure. Finally a characterization of material properties (e.g., toughness, hardness,

etc. as a function of fluence) using a variety of specimens and testing methods provides the necessary inputs for determining component lifetimes. EPRI's role is to accelerate development and application of these technologies, where necessary, and develop appropriate tools for application. Some of the projects currently under development are discussed below.

Flaw Distributions in RPV Beltline Materials

A continuing area of uncertainty regarding probabilistic fracture mechanics is the assumed distribution of flaws that is postulated to exist in an RPV. PTS analyses that have been performed in accordance with Regulatory Guide 1.154 [8] have assumed a flaw distribution that is not based on, or well supported by actual inservice inspection experience. The flaw distribution is a key input to predicting vessel failure probabilities. Consequently, EPRI is collaborating with its members and the USNRC to develop more realistic flaw distribution models and to assess how the models may be affected by inspection reliability.

Small Punch Test for Assessing Radiation Embrittlement

To provide utilities with improved capabilities for assessing toughness loss, EPRI is evaluating the use of the small punch (SP) testing technique for radiation-embrittled materials. This project is part of a long-term EPRI R&D program begun in 1990 to develop and introduce SP technology, an essentially nondestructive evaluation (NDE) approach that provides direct, accurate measurement of material toughness properties using single miniature samples about the size of a dime (6.35 mm diameter, 0.5 mm thickness). Findings to date [9,10] demonstrate the fundamental applicability of SP testing for direct toughness assessment of pressure vessel materials. Also, because numerous SP specimens can be obtained from individual surveillance samples, the technique maximizes the condition assessment and life optimization information that can be obtained from this limited material. Presently, the feasibility of using the SP technique to directly measure fracture toughness is being investigated. US and international materials will be tested to demonstrate its applicability. Ultimately, SP testing may allow in-service assessment of radiation embrittlement in pressure vessels through nondestructive sampling of a vessel itself.

Application of the Master Curve Approach

The ASME Code reference toughness curves are based upon an approach which utilizes a material indexing parameter called RT_{NDT}. This parameter is derived from Charpy V-notch and drop-weight nil-ductility transition temperature tests. In many cases, this indexing parameter is overly conservative relative to the real toughness of ferritic pressure vessel steels, and a more direct index and measure of true fracture toughness is needed. The ASTM Master Curve approach [11] is considered to be a better indicator of fracture toughness behavior in terms of a directly measured toughness index, T_o. EPRI is leading an effort to develop the technical basis for applying the Master Curve approach to RPV integrity assessment. Prior applications of this technology have demonstrated that it can substantially improve the accuracy of determining the transition temperature of specific RPV weld materials steels. A future EPRI report [12] will serve as a white paper for consideration by the ASME Code for incorporating fracture toughness testing into Section XI. Future work will concentrate on applying this methodology to irradiated materials.

Irradiation-Induced Changes in RPV Steels

EPRI and the Central Research Institute of Electric Power Industry (CRIEPI) in Japan have jointly developed a 5-year program to identify and study the mechanisms that cause radiation embrittlement. The goal of the program is to develop a quantitative link between microstructure and mechanical properties in order to significantly improve predictive capabilities. The program is structured to examine

the effects of chemistry, flux, fluence and product form (plate, weld, and forging) on irradiation damage of typical RPV steels. The first report [13] documented the behavior of low and high copper steels irradiated in a test reactor environment. Future reports will document the effects of identical material irradiated in PWR and BWR environments.

Surveillance Programs

USNRC regulations require that all utilities monitor the embrittlement of the RPV through a surveillance program. Since the late 1980's EPRI has been compiling surveillance results (including the raw data from each surveillance capsule evaluation) for all US reactor vessels. This information has been included in a database called the Power Reactor Embrittlement Program (PREP). The latest version , PREP4, incorporates all available surveillance data through 1995. The databases program includes a customized menu-driven interface, special search capabilities for data navigation and review, and built-in report generation. It is being used to support future nuclear plant aging research and management of embrittlement. EPRI and utilities have used the information from this database to identify and evaluate the irradiation response of various steels. EPRI intends to make period updates and enhancements to the PREP4 database.

Operability Assessment

As components age, plant operation may become somewhat restricted in order to meet established operating limits and criteria. Consequently it is usually necessary to adjust the operation of the component to account for this restriction. Adjustments are usually based on well-founded experimental data or information obtained from actual tests of the component. Utilities are continually quantifying operating limits to ensure compliance with NRC regulations. They are also evaluating operating limits to optimize plant availability and reduce costs of operations. Some of the projects EPRI is developing to address operability assessments are discussed below.

RPV P-T Limit Optimization

10CFR50 Appendix G requires that plant heatup and cooldown limits be determined in accordance with the rules of the ASME Code. To assist utilities in determining pressure and temperature limits for the RPV, EPRI is responding by developing a software tool to automate the calculation process. The software will incorporate various improvements in fracture mechanics analyses and will also include the latest approved revisions to the ASME Code. The software will be developed under a quality assurance program so that utilities can use it for all safety-related applications.

Resolution of PTS Issues

This work focuses on reevaluation of the fracture mechanics modeling assumptions and acceptance criteria for the pressurized thermal shock (PTS) analyses. The primary goals include development of an alternate approach to evaluate the risk of RPV failure due to PTS events, and providing means by which utilities evaluate corrective measures effectively (such as flux reduction, plant modifications, changes in plant operating procedures, etc.). EPRI has developed a simplified process for evaluating the overall risk associated with PTS [14]. A plant-specific pilot application of the PTS methodology is planned for 1998.

Summary

The RPV is arguably the most important single safety-related component in a nuclear plant. Demonstration of RPV integrity (referenced principally via its resistance to brittle fracture) is critical to ensure continued, safe plant operation. As such, approaches to RPV integrity assessment (including NRC regulations and standards organizations methodologies) were originally developed with a high degree of conservatism to account for various uncertainties associated with material condition assessment. As plants age, operation of the RPV is often becoming unnecessarily restricted due to the inherent conservative nature of existing regulations and assessment procedures. A realistic determination of RPV integrity, utilizing advancements in material characterization and integrity assessment technologies, can provide the flexibility required by licensees in plant operation and still maintain adequate levels of safety against vessel failure.

In response to this changing environment in the nuclear industry EPRI is restructuring its R&D program for RPV Integrity to better complement the needs of member utilities. The R&D program is structured under the following product groups; 1) Management and Mitigation, 2) Material Performance Databases, 3) Material Condition Assessment and 4) Operability Assessment.

EPRI's role in this regard is to integrate the various aspects of aging into cost-effective and technically sound solutions for managing the embrittlement of the reactor pressure vessel.

References

1. EPRI TR-108316, "Marble Hill Reactor Vessel Thermal Annealing Demonstration", to be published.
2. EPRI TR-101975, V1-V9, "Reactor Vessel Embrittlement Management Handbook," December 1993.
3. Generic Letter 92-01, Revision 1, "Reactor Vessel Structural Integrity, 10CFR50.54(f)," US Nuclear Regulatory Commission, March 6, 1992.
4 Generic Letter 92-01, Revision 1, Supplement 1, "Reactor Vessel Structural Integrity," US Nuclear Regulatory Commission, May 19, 1995.
5. EPRI Software SW-106390, "Reactor Vessel Materials Database Version 1.3," January 1996.
6. NRC Administrative Letter 95-03, Revision 1, "Availability of the Reactor Vessel Integrity Database, July 10, 1996.
7. EPRI Software SW-106726, "PREP4: Power Reactor Embrittlement Program, Version 1.0, October 1996.
8. Regulatory Guide 1.154, "Format and Content of Plant-Specific Pressurized Thermal Shock Safety Analysis Reports for Pressurized Thermal Shock," US Nuclear Regulatory Commission, January 1987.
9. EPRI TR-105130, "Small Punch Testing for Fracture Toughness Measurement," June 1995.
10. EPRI TR-105131, "Small Punch Testing for Irradiation Embrittlement," August 1995.
11 "Test Method for the Determination of Reference Temperature, T_o, for Ferritic Steels in the Transition Range," American Society for Testing and Materials, Draft 14.
12. TR-108390, "Technical Basis for Application of Master Curve Fracture Toughness Methodology for Ferritic Steels," to be published.
13. EPRI TR-107535, "Microstructural Characterization of RPV Steels - Phase 1," December 1996.
14. EPRI TR-107128, "Alternative Method for Performing Regulatory Guide 1.154 Pressurized Thermal Shock Analysis," December 1996.

Nondestructive Characterization of Embrittlement in Reactor Pressure Vessel Steels A Feasibility Study

Harry I. McHenry and George A. Alers
National Institute of Standards and Technology
Materials Reliability Division
Boulder, Colorado 80303

ABSTRACT

The Nuclear Regulatory Commission recently initiated a study by NIST to assess the feasibility of using physical-property measurements for evaluating radiation embrittlement in reactor pressure vessel (RPV) steels. Ultrasonic and magnetic measurements provide the most promising approaches for nondestructive characterization of RPV steels because elastic waves and magnetic fields can sense the microstructural changes that embrittle materials. The microstructural changes of particular interest are copper precipitation hardening, which is the likely cause of radiation embrittlement in RPV steels, and the loss of dislocation mobility that is an attribute of the ductile-to-brittle transition. Measurements were made on a 1% copper steel, ASTM grade A710, in the annealed, peak-aged and overaged conditions, and on an RPV steel, ASTM grade A533B. Nonlinear ultrasonic and micromagnetic techniques were the most promising measures of precipitation hardening. Ultrasonic velocity measurements and the magnetic properties associated with hysteresis-loop measurements were not particularly sensitive to either precipitation hardening or the ductile-to-brittle transition. Measurements of internal friction using trapped ultrasonic resonance modes detected energy losses due to the motion of pinned dislocations; however, the ultrasonic attenuation associated with these measurements was small compared to the attenuation caused by beam spreading that would occur in conventional ultrasonic testing of RPVs.

INTRODUCTION

The NRC Chairman has challenged the Office of Nuclear Regulatory Research to develop a nondestructive methodology for the direct measurement of radiation embrittlement of reactor pressure vessels (RPVs). In response, NRC initiated the present study to assess the feasibility of using physical-property measurements for evaluating embrittlement in RPV steels.

Radiation embrittlement is attributed [1] to copper in the Mn-Mo-Ni steel, ASTM A533B, used for RPVs. Radiation damage enhances the diffusion rate of copper, leading to the formation of copper-rich precipitates. The small (~1 nm), coherent precipitates increase the yield strength and decrease the toughness of the steel, particularly in the welds because of their higher concentrations of copper. The extent of embrittlement is evaluated by periodically testing surveillance specimens made from steels that are representative of the RPV. An empirical method, described in NRC Regulatory Guide 1.99, Revision 2 [2], is used to convert the Charpy impact test results on surveillance specimens to fracture toughness values suitable for assessing reactor safety.

The purpose of this study is to assess the feasibility of using physical-property measurements for the nondestructive characterization of radiation embrittlement in RPV steels. The specific objectives are

(1) to correlate selected ultrasonic and magnetic measurements with precipitation hardening in a copper-strengthened steel, and

(2) to explore the sensitivity of ultrasonic and magnetic measurements to the ductile-to-brittle transition in A533B steel and in the copper-stregthened steel.

Ultrasonic and magnetic measurements provide the most promising approaches for nondestructive characterization of RPV steels because elastic waves and magnetic fields can sense microstructural characteristics of materials. Our approach is to find discriminants that uniquely characterize microstructural changes that affect toughness, particularly precipitation hardening and dislocation mobility. The feasibility study was an eight month project to demonstrate the technical basis for a more ambitious program to develop measurements and standards for the nondestructive characterization of RPV steels.

MATERIALS

Copper-precipitation-hardened steel plates, ASTM grade A710, were used as the experimental materials to develop correlations between physical-property measurements and hardening. The steel was given the following heat treatments to control the precipitation hardening and to change the mechanical properties: solution treated at 885 °C, solution treated and peak aged at 525 °C, and solution treated and overaged at 700 °C. The tensile properties are summarized in Table 1.

The most common RPV steel, ASTM Grade A533B, was used as the experimental material to explore the sensitivity of ultrasonic and magnetic measurements to the ductile-to-brittle transition. Sections of A533B steel plate were taken from the SNUPPS reactor by Oak Ridge National Laboratory and sent to NIST for this study. Specimens were taken from near the quarter-thickness level of the plates. The mechanical properties are summarized Table 1. The SNUPPS vessel has not been exposed to radiation. The test materials removed from the vessel were not heat treated nor otherwise processed to modify their properties. Measurements on A533B were taken as a function of temperature, and thus, the microstructure was constant, but the mechanical properties varied as a function of test temperature.

Elastic Properties

The complete elastic stiffness tensors of the A710 and A533B steels were measured by resonant ultrasound spectroscopy (RUS). These are considered baseline measurements that would reveal any sensitivity of ultrasonic measurements to precipitation hardening or to the ductile-to-brittle transition. Note that simultaneous measurements on internal friction are discussed later in this paper.

The RUS technique [3] is shown schematically in Figure 1. Piezoelectric transducers are used to excite and detect a continuous rf wave produced by a signal generator. The amplitude of the received signal is recorded as a function of the frequency of the excitation signal. About fifty resonant modes are detected in the frequency range from 50 kHz to 2 MHZ. The resonant frequencies are converted to elastic constants using an algorithm developed by Heyliger and Ledbetter [4]. The RUS measurements of velocity have an accuracy of 0.05 %. The results for A710, summarized in Table 2, show a 1 % increase in shear modulus as precipitation increases. However, it should be noted that the measurements are sensitive to copper precipitation, but not to precipitation hardening. The peak-aged steel has modulus values that lie between the values for the solution treated and the overaged conditions. Apparently, the velocity measurements are sensing the stiffening of the iron lattice that occurs when copper is precipitated from solid solution.

Young's modulus of A710 steel was measured as a function of temperature using a Marx-oscillator resonance procedure. At temperatures between room temperature and -85°C, the modulus increased linearly with decreasing temperature (3.4% over 110°C); there was no apparent effect of the ductile-to-brittle transition. The results are shown in Figure 2, along with the temperature dependence of Young's modulus for pure iron [5].

Magnetic Properties

The magnetic properties of A710 and A533B steels were measured using a vibrating sample magnetometer (VSM) [6]. We consider this a baseline measurement that would reveal the sensitivity of static magnetic measurements to precipitation hardening or to the ductile-to-brittle transition.

The VSM concept is shown in Figure 3. The steel sample is vibrated in an applied magnetic field and the moment induced by the field is detected by a set of pickup coils next to the sample. The samples were in the form of rods, 2 mm in diameter by 20 mm long. For each of the steels, two types of measurements were made: the first is a hysteresis loop, from -240 kA/m to +240 kA/m , used to measure coercivity. The second measurement starts at zero field with a demagnetized sample, and the field is taken to 368 kA/m. The latter curve is used to determine the saturation magnetization.

The results, summarized in Table 2, show significant variations in coercivity and small variations in saturation magnetization among the samples. The coercivity variations do not correlate with precipitation hardening. We attributed this to a lack of sensitivity of domain wall motion to the small copper precipitates (~10 nm) in the A710 steel. Domain walls, which are on the order of 100 nm thick, tend to interact with defects of comparable or larger sizes. We did not expect variations in saturation magnetization because of the small composition variations among the A710 samples and between the A533B plate and weld.

NONDESTRUCTIVE CHARACTERIZATION OF PRECIPITATION HARDENING

The Fe-Cu alloy A710 was used as the model material to explore the question, "Can physical-property measurements be correlated with precipitation hardening?" This is a difficult question because copper precipitates in A710 are typically 5 to 10 nm in diameter, and thus, the precipitates are too small to interact with ultrasonic waves or magnetic domain walls. The problem is even worse for radiation embrittlement, which is caused by even finer precipitates, about 1 nm in diameter. Ultrasonic measurements of elastic-stiffness coefficients confirmed that ultrasonic wave velocities are not simply related to hardening caused by copper precipitation. Similarly, measurements of the magnetic hysteresis loops in the A710 samples were not sensitive to precipitation hardening.

The internal strain fields associated with precipitation hardening extend over greater lengths than the particle diameter and may interact with ultrasonic waves and magnetic fields. The magnitude of the internal strain was measured by X-ray diffraction for the A710 steel in each heat treatment. Measurements were made by the line-broadening technique described by Balzar [7]. The average strain in the iron lattice caused by precipitation hardening and other lattice defects was determined by measuring the width of the α-Fe diffraction peak and correcting for instrumental effects. The magnitude of this strain was on the order of 7×10^{-4} and varied with hardness, as shown in Figure 4.

Nonlinear Ultrasonics

The elastic response of a material is adequately described by Hooke's law at the low strains typically used in ultrasonic testing. Nonlinear ultrasonic methods, however, employ strains sufficiently large that higher-order terms are necessary to completely describe the elastic response. The strain fields caused by precipitation hardening affect these higher-order terms;

therefore, nonlinear ultrasonic properties are sensitive to the degree of strain associated with precipitates.

Experimentally, nonlinear ultrasonic properties are determined using harmonic generation techniques. When an ultrasonic wave of frequency f propagates through a material, nonlinearities in the interatomic forces produce a small wave at frequency 2f that grows with propagation distance. The amplitude of this second-harmonic wave at a given distance from the source is proportional to the square of the amplitude of the fundamental wave through a proportionality constant called β. The parameter β is a measure of nonlinearity, and hence, β is potentially a measure of the internal strains caused by precipitation hardening. Hurley and Fortunko [8] use high-power, low-distortion electronics and an infrared Michelson interferometer to enable the measurement of absolute ultrasonic-wave displacements, including the harmonics arising from nonlinear elastic behavior. The measurement concept is shown in Figure 5. A tone burst of amplitude A_0 and angular frequency ω_0 is applied to a piezoelectric transducer coupled to one surface of the sample. A Michelson interferometer detects the ultrasonic vibrations reaching the opposite face of the sample and measures the amplitude A_1 of the fundamental wave and the amplitude A_2 of the second harmonic. β is proportional to the ratio of $A_2/(A_1)^2$.

Measurements of β for A710 in three heat treatments were related to the lattice strains caused by precipitation hardening, as shown in Figure 6. The linear relationship between β and internal strain demonstrates the feasibility that β could be related to the extent of copper-precipitation hardening.

Micromagnetics

At applied fields higher than the coercivity, domain walls play a diminishing role in magnetization, and the magnetic response is dominated by rotation of magnetic dipoles away from specific crystallographic directions within each grain toward the direction of the applied field. Two magnetic properties that reflect these atomic scale rotations are transverse incremental permeability and magnetostriction. The former is related to the local slope of the hysteresis curve, while the latter measures the change in dimensions of the material as the applied field changes. When the applied field is a small alternating field superimposed on a larger static value, the incremental permeability can be deduced from measurements of the inductance of the coil that is applying the alternating field. The magnetostriction is related to the amplitude of ultrasonic waves generated at the surface of the ferromagnetic material under the coil.

Measurements of magnetostriction were made on the A710 steel samples using the experimental technique shown in Figure 7. Here, the coil that applies the alternating magnetic field is in the shape of a meander line held close to the surface of the sample. The magnetic field around each wire subjects the surface to alternating strains through the magnetostriction of the material. When the applied biasing field is parallel to the wires in the meander coil and the

coil carries an alternating current whose frequency is the value of the shear wave velocity divided by twice the spacing between the wires, then there is a shear ultrasonic wave produced that can be detected by a transducer located at some distance from the meander coil [9]. Figure 7B shows how the shear wave amplitude varies with the magnitude of the bias, and the highest amplitude can be related to the heat treatment. The amplitude of this shear wave is a measure of the magnetostrictive coefficient of the material under the coil at the value chosen for the applied biasing field [10]. Figure 8 shows that the magnetostriction in A710 correlates with the internal strain in the sample.

Incremental permeability can be determined by measuring the inductance of an oval spiral coil as a function of the applied bias field. This magnetic property, when plotted as a function of the bias field, also exhibits a maximum that is different for the three heat treatments of the A710 steel. Figure 9 shows that the maximum incremental permeability can be correlated with the internal strain linearly, much the same as the magnetostriction correlation shown in Figure 8. These correlations demonstrate the feasibility that micro magnetic measurements are potentially suitable for characterizing the extent of copper-precipitation hardening.

NONDESTRUCTIVE CHARACTERIZATION OF THE DUCTILE-TO-BRITTLE TRANSITION

Both the A533B steel and the Fe-Cu alloy, A710, were used as test materials to explore the question, "Are physical-property measurements sensitive to the ductile-to-brittle transition?" The main idea guiding the experimental program is that internal friction measurements can sense dislocation mobility and a measure of reduced dislocation mobility should correlate with the D.T. temperature.

Ultrasonic measurements of the elastic-stiffness coefficients of A710 steel as a function of temperature, Figure 2, revealed a linear increase in modulus as temperature was lowered from room temperature to -90 °C. No deviations from linearity were detected as the materials passed through their D.T. temperatures. Similarly, magnetic measurement of the hysteresis loop did not change appreciably at six temperatures between room temperature and -116 °C. Thus, conventional ultrasonic and magnetic methods of nondestructive testing are not expected to be useful for estimating the DBT temperature.

The Internal Friction Tensor

The complete internal friction tensor Q_{ij}^{-1} for A710 and A533B samples was measured by the RUS method [11]. The ultrasonic amplitude is measured as a function of frequency, and over the range 50 kHz to 2MHz about fifty resonance peaks were detected. The resonant frequencies were used to calculate the nine elastic constants as discussed previously. For internal friction, the width of each normal mode resonance curve at half the maximum power is measured and the damping capacity of the materials vibrating in that mode was calculated. The results for A710 steel are shown in Figure 10. Internal friction decreased as yield strength increased as could be expected if the primary cause of internal friction was the motion of dislocations

responding to the oscillating force of the sound wave. Increasing the amplitude of vibration during the internal friction measurements increased the damping, presumably due to dislocation depinning and longer dislocation-loop lengths.

The percentage changes in internal friction as shown in Figure 10 are quite large. However, the absolute values of the log decrement are on the order of 10^{-4}. Thus, ultrasonic attenuation due to internal friction is small relative to attenuation that occurs in conventional ultrasonic testing, such as that caused by beam spreading.

Stress Induced Internal Friction

Johnson [12,13] recently developed a resonance technique, called stress-induced internal friction, that traps ultrasonic resonant modes in a local region of a cylinder. The cylindrical specimen can be loaded in a tensile machine to allow measurement of internal friction, in terms of log decrement δ, due to dislocation motion caused by the static stress plus the oscillating force of the sound wave. In the initial experiments, the measurements were conducted under a sustained static stress. The results were time dependent and difficult to interpret. However, upon unloading, there was a rapid change in δ that could reproducibly be measured. The revised approach was to preload the specimen and measure δ immediately upon unloading. δ was measured as a function of prior stress to determine the level of static stress needed to unpin the dislocations, and then additional measurements were done as a function of temperature to determine the temperature dependence of δ. The temperature where stress-induced changes in δ drop below a critical level, yet to be defined, is expected to correlate with the DBT temperature. The experimental facility is shown schematically in Figure 11. Note that the ultrasonic excitation is done with a noncontact electromagnetic acoustic transducer (EMAT). The electromagnets are used to approach magnetic saturation of the specimen, and thus, reduce magnetic contributions to damping.

Experiments to develop the test procedure were conducted on A710 steel in a peak aged condition. A cylindrical specimen was monotonically loaded to a stress of 600 MPa with load interruptions at about 10 MPa increments to measure internal friction. A stress slightly above the yield strength was needed to get a 10 % increase in the log decrement δ . The specimen was subjected to a plastic strain of 0.15 % in the test section during the initial test. The same specimen was then used to evaluate the effect of temperature on dislocation mobility. In the temperature dependence tests, the specimen was loaded to 76 % of yield strength for 10 s. The specimen was unloaded to a level of 5 MPa and δ was measured as a function of time for radial resonances at a frequency of 2.12 MHz. The results, shown in Figure 12, show that recovery processes occurred at 27°C and -20°C. At -90°C, δ did not change much with time indicating that a marked decrease of dislocation mobility occurs between -20°C and -90°C. This test suggests that a temperature indicative of the DBT can be measured where recovery drops below a defined level. However, subsequent tests on A533B, discussed below, revealed that the prior plastic strain was a critical part of the experiment.

The intention in the A533B tests was to conduct temperature dependence tests similar to those shown in Figure 12 for A710 steel. The initial tests were done at room temperature where it was observed that 100 s static preloads at stresses up to the yield strength did not induce any dislocation motion, i.e., δ was the same before and after the preload as shown in Figure 13. It was then postulated that plastic prestrain was a necessary precursor to the stress induced internal friction experiments. Indeed, the A533B sample was prestrained to 0.39 % and the internal friction experiment repeated. As shown in Figure 13, a modest preload of 163 MPa for 100 s was followed by extensive damping. However, plastic prestrain is not a viable option for nondestructive characterization of radiation embrittlement in RPVs. Thus, the temperature dependence study was abandoned.

Further studies of internal friction in A533B were conducted to ascertain the sensitivity of attenuation measurements. The results, Figure 14, show the frequency dependence of internal friction measurements. More importantly, the results show that δ values are on the order of 2×10^{-4}, which is a level of attenuation that is negligible compared to the ultrasonic attenuation that would occur in propagating-wave ultrasonic testing of RPVs. For propagating waves, attenuation due to bean spreading and scattering is two orders of magnitude greater than attenuation caused by internal friction. Thus, it is likely to be difficult to extract the losses caused by internal friction from ultrasonic attenuation measurements.

SUMMARY AND CONCLUSIONS

Nondestructive Characterization of Precipitation Hardening

Internal strain is the principal attribute of precipitation hardening in A710 steel that could be sensed by physical measurements. Nonlinear ultrasonic measurements of the relative amplitude of the second harmonic and micromagnetic measurements of magnetostriction and incremental permeability correlated with internal strains measured by x-ray diffraction. **Thus, these techniques offer promise for nondestructive characterization of precipitation hardening.**

Ultrasonic velocity measurements are sensitive to precipitation in A710 steel, but not to precipitation hardening. Static magnetic properties derived from hysteresis loop measurements are not sensitive to precipitation hardening. **Thus, conventional ultrasonic and magnetic testing methods are not suitable for nondestructive characterization of precipitation hardening in A710 steel.**

Internal friction measurements by RUS are sensitive to precipitation hardening in A710 steel. However, ultrasonic attenuation caused by internal friction is small compared to the attenuation that occurs in propagating-wave ultrasonic testing. **Thus, ultrasonic attenuation is a potential measure of embrittlement, but it may not be adaptable to periodic inspections of RPVs.**

Nondestructive Characterization of the Ductile-to-Brittle Transition

Sress-induced internal friction can monitor dislocation mobility as a function of temperature, and thus, it offers potential for correlating with the DBT temperature. However, plastic strain prior to the internal friction measurements is a necessary condition for creating mobile dislocations in A533B steel. **Thus, this technique is not suitable for periodic inspection of RPVs.**

Ultrasonic velocity and magnetic hysteresis loop measurements as a function of temperature did not reveal any sensitivity to the ductile-to-brittle transition. **Thus, conventional ultrasonic and magnetic testing methods are not suitable for nondestructive characterization of the DBT temperature in A533B steel.**

RECOMMENDATIONS

The present study was limited to laboratory measurements on unirradiated samples of A710 and A533B steel, however, it did reveal clear directions for further research. Specifically

1. Confirm the results of this study on a surrogate material that more closely simulates radiation embrittlement in A533B steel.

2. Evaluate nonlinear ultrasonic and micromagnetic techniques for nondestructive characterization of radiation embrittlement in irradiated A533B samples.

3. Assess the feasibility of adapting nonlinear ultrasonic and micromagnetic techniques to the nondestructive characterization of clad A533B plates representative of RPVs.

ACKNOWLEDGMENTS

The feasibility study was a joint program of NIST and the Nuclear Regulatory Commission. The NRC contract monitor was Carolyn Fairbanks of the Office of Regulatory Research. The authors are particularly indebted to the staff of the Materials Reliability Division for their expertise and dedication in making the measurement described in this paper. Particularly vital to the program were: D. Balzar (x-ray diffraction), F.R. Fickett (magnetic properties), B. Igarashi (micro- magnetic properties), D.C. Hurley (nonlinear ultrasonics), W. Johnson (internal friction), H. Ledbetter and S.A. Kim (elastic properties), J.D. McColskey (sample preparation), P.T. Purtscher (microstructure control), and C.M. Fortunko for his critical reviews of all the work.

REFERENCES

1. G.R. Odette, "Radiation Induced Microstructural Evolution in Reactor Pressure Vessel Steels", Microstructure of Irradiated Materials, Mat. Res. Soc. Symp. Proc. Vol. 373, I. Robertson, L. Rehn, S. Zinkle and W. Phythian (Eds.) p. 137 (1995).

2. United States Nuclear Regulatory Commission, Regulatory Guide 1.99: Radiation Embrittlement of Reactor Vessel Materials, U.S. Government Printing Office, Washington, D.C. (1988).

3. H. Ledbetter, C.M. Fortunko and P. Heyliger, "Orthotropic Elastic Constants of a Boron-Aluminum Fiber-reinforced Composite: An Acoustic-Resonance-Spectroscopy Study " J. Appl. Phys., vol. 78, p. 1542 (1995).

4. P. Heyliger, A. Jilani, H. Ledbetter, R.G. Leisure and C.-L. Wang, "Elastic Constants of Isotropic Cylinders Using Resonant Ultrasound " J. Acoust. Soc. Am., vol. 94, p. 1482 (1993).

5. J. A. Rayne and B. Chandrasekhar , "Elastic Constants of Iron from 4.2 to 300 K", Phys. Rev. vol. 122, p. 1714 (1961).

6. S. Foner, "The Vibrating Sample Magnetometer: Experiences of a Volunteer," J. Appl. Phys. vol. 79, p. 4740 (1996).

7. D. Balzar, "Voigt-Function Model in Diffraction Line-Broadening Analysis," To appear in Microstructure Analysis from Diffraction, R.L. Snyder, H. J. Bunge, and J. Fiala (Eds.), International Union of Crystallography (1998).

8. D. C. Hurley and C.M. Fortunko, "Determination of the Nonlinear Ultrasonic Parameter Beta Using a Michelson Interferometer," Meas. Sci. Technol. vol. 8, p. 634 (1997).

9. R.B. Thompson, "Generation of Horizontally Polarized Shear Waves in Ferromagnetic Materials Using Magnetostrictively Coupled Meander Coil Electromagnetic Transducers," Appl. Phys. Lett. vol. 34, p. 175 (1979).

10. B. Igarashi, G.A. Alers and P.T. Purtscher, "An Ultrasonic Measurement of Magnetostriction," To appear in Proc. IEEE Ultrasonics Symposium, October (1997).

11. P. Heyliger, H. Ledbetter and S. Kim, "The Internal-Friction Tensor Q^{-1}_{ij}". To appear in Mechanical Spectroscopy, L. Magalas (Ed.) Elsevier, Amsterdam (1998).

12. W. Johnson, B.A. Auld and E. Segal, "Trapped Torsional Modes in Solid Cylinders," J. Acous. Soc. Am., vol. 100(1), p. 285 (1996).

13. W. Johnson and G.A. Alers, "Force Measurement Using Vibrational Spectroscopy," Rev. Sci. Instrum. vol. 68(1) p. 102 (1997).

Table 1 Mechanical Properties of the Test Materials

STEEL	CONDITION	YIELD STRENGTH MPa	ULTIMATE STRENGTH MPa	ELONGATION %	HARDNESS ROCKWELL A HRA	DBT (41J)* TEMPERATURE °C
A710	Solution Treated	415	650	28	55.5	-33
A710	Peak Aged	551	718	25	58.5	-10
A710	Overaged	471	558	29	53	-60
A533B	Plate 1-1	465	610	38	55	-20
A533B	Plate 1-2	452	574	43	53	-60
A533B	Plate 2-1	475	600	40	55	-25
A533B	Plate 2-2	507	640	35	56	-20
A533B	Weld	—	—	—	57	-30

* DBT (41J) Temperature is the DBT temperature measured at a Charpy impact energy level of 41J.

Table 2 Physical Properties of the Test Materials

Steel	Condition	Elastic Constants			Internal Friction			Magnetic		Internal Strain %
		E GPa	G GPa	B GPa	Q_E^{-1} $X10^{-5}$	Q_G^{-1} $X10^{-5}$	Q_B^{-1} $X10^{-5}$	H_C A/m	B_s Tesla	
A710	Soln. Treated	211.9	79.6	163.4	14.4	13.3	20.9	668	2.03	0.070
A710	Peak Aged	212.6	79.6	163.7	7.5	8.0	4.3	642	2.07	0.074
A710	Over Aged	212.8	80.4	164.4	8.5	8.5	8.9	485	2.06	0.054
A533B	Plate 1-2	211.0	82.0	165.1	7.1	8.6	9.4	544	2.06	0.074
A533B	Weld	211.1	82.2	164.4	7.8	6.7	3.4	712	2.05	0.080

where E is Young's modulus
G is shear modulus
B is bulk modulus
H_c is coercive force
B_s is saturation magnetization

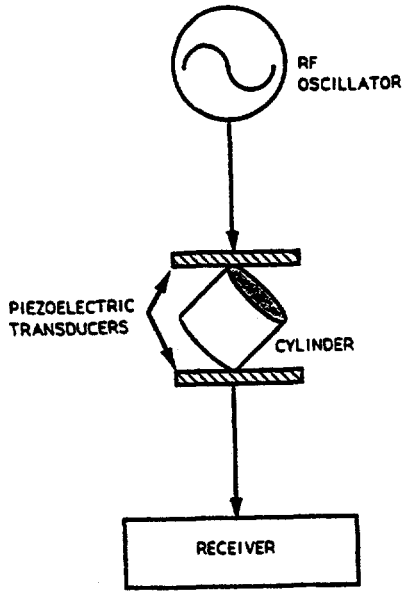

Figure 1. Experimental arrangement for using resonant ultrasound spectroscopy to determine a material's elastic-stiffness tensor C_{ij} and internal-friction tensor Q_{ij}^{-1} from a regular-shaped specimen.

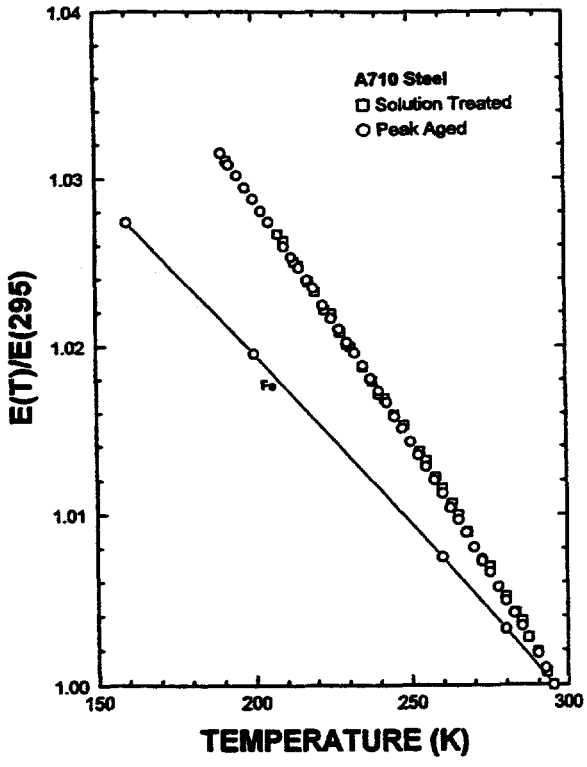

Figure 2. Young's modulus measured as a function of temperature for A710 steel and iron.

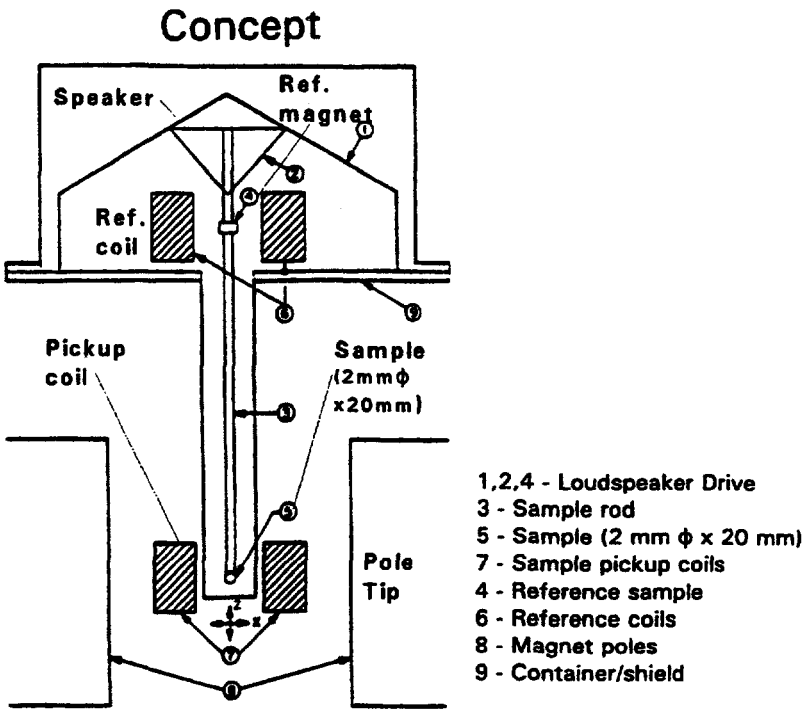

Figure 3. Experimental concept for using a vibrating sample magnetometer to determine the magnetic properties of steel samples.

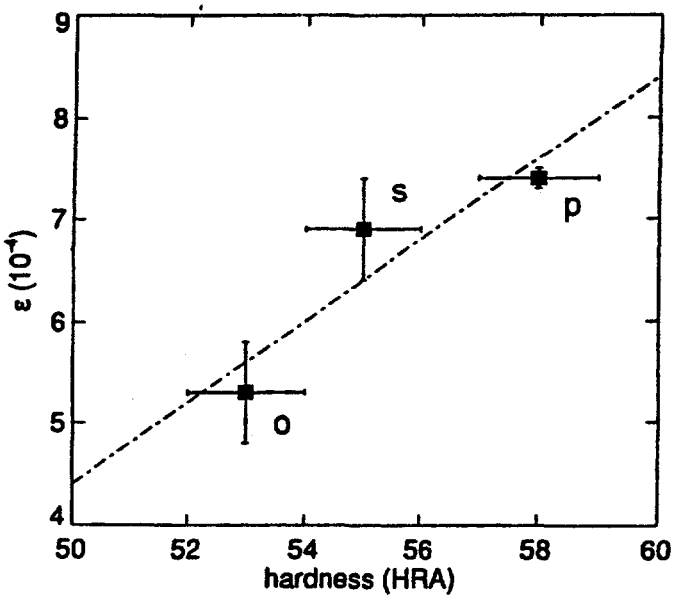

Figure 4. Internal strains measured by x-ray line broadening, steel in the solution treated (s), peak aged (p) and overaged conditions (o).

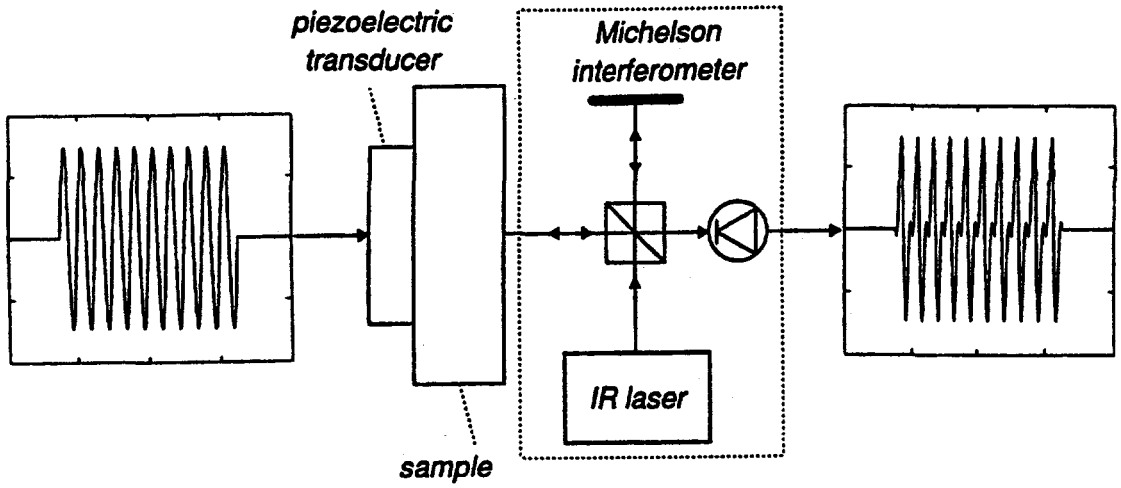

Figure 5. Experimental arrangement for conducting harmonic generation experiments to determine the nonlinear ultrasonic parameter β.

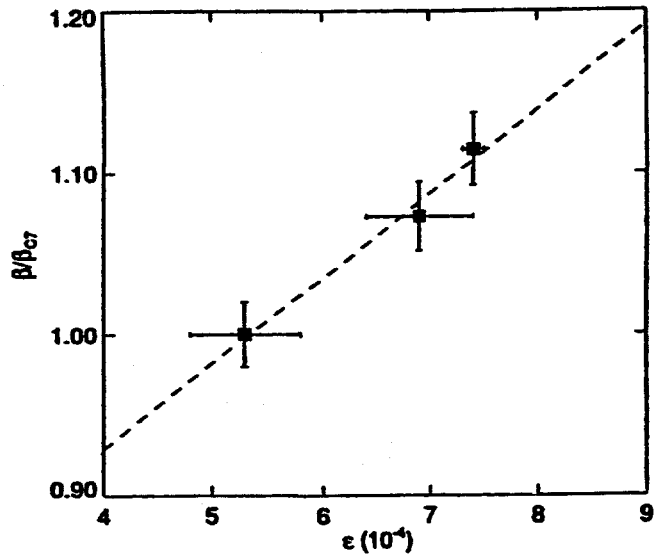

Figure 6. The nonlinear ultrasonic parameter β, correlated with internal ϵ strain in A710 steel. β_{C7} is the value of β in the solution treated condition.

(a)

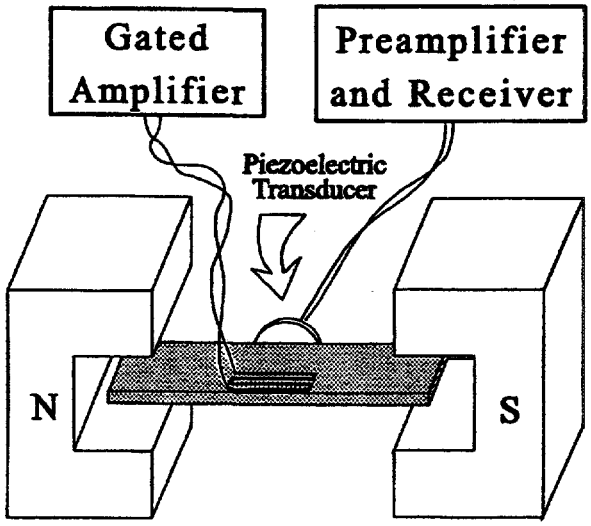

(b)

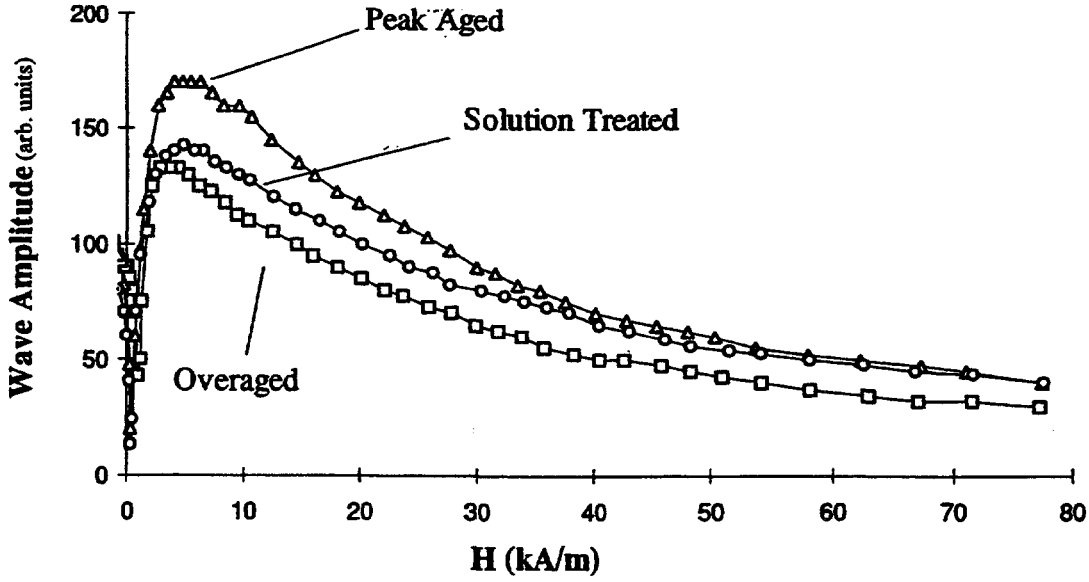

Figure 7. (a) Experimental arrangement for using ultrasonic coupling of an electromagnetic acoustic transducer (the meander coil mounted in the specimen) to measure the magnetostriction of steel samples, (b) Experimental results of wave amplitude as a function of magnetic field for A710 steel.

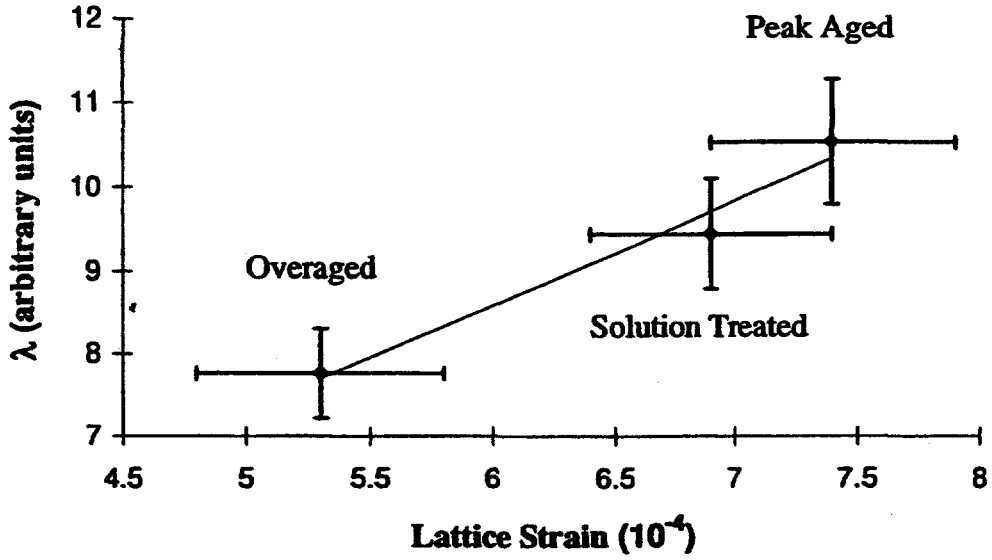

Figure 8. Magnetostriction λ, correlated with internal strain for A710 steel in three heat treatments.

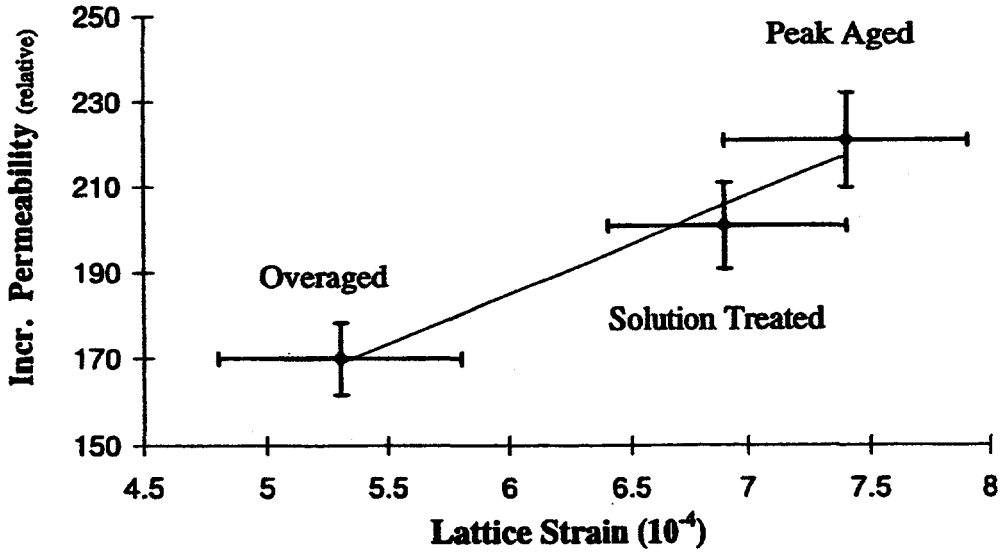

Figure 9. Incremental permeability correlated with internal strain for A710 steel in three heat treatments.

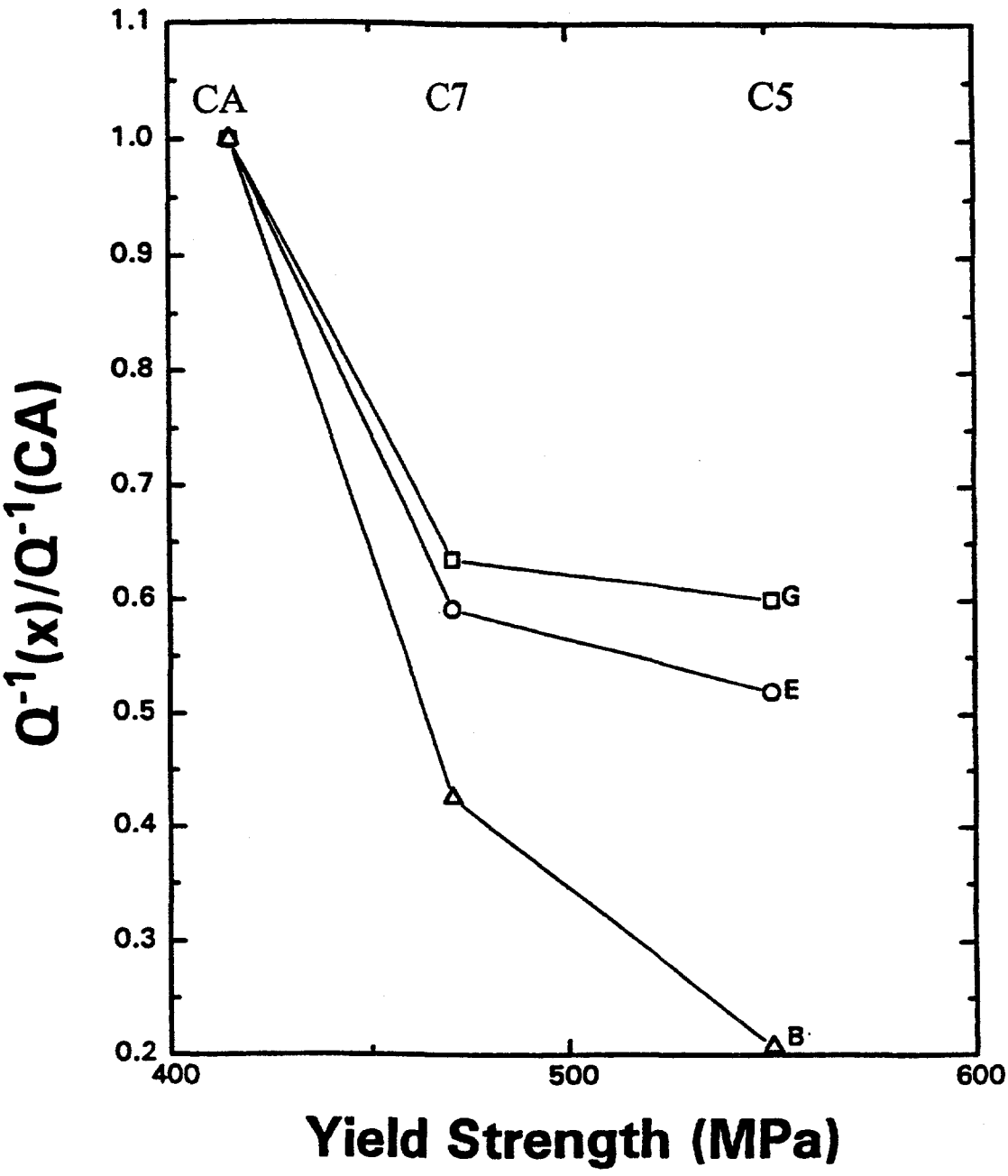

Figure 10. Internal friction Q^{-1}, measured by resonant ultrasound spectroscopy as a function of yield strength for A710 steel in three heat treatments. The CA condition is solution treated, C7 condition is overaged, and the C5 condition is peak aged.

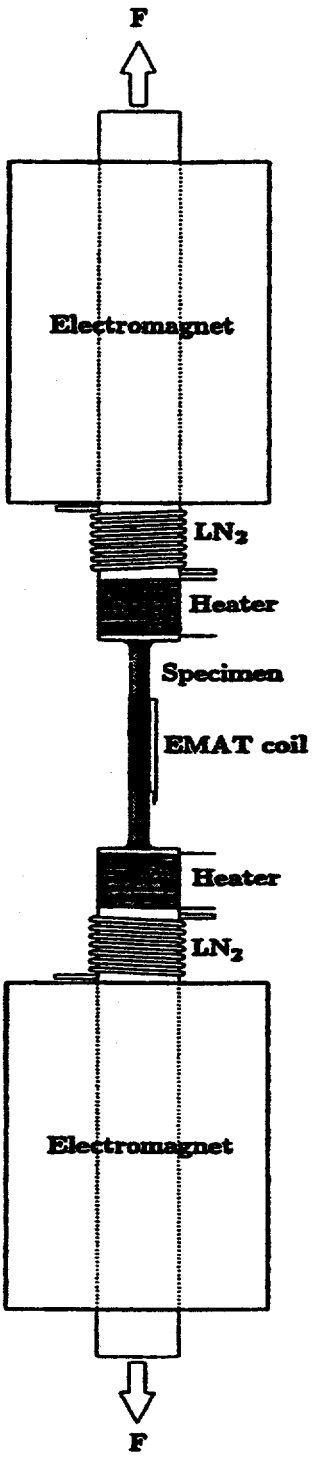

Figure 11. Experimental arrangement for using trapped resonant modes to measure the internal friction as a function of temperature for specimens subjected to prior loading.

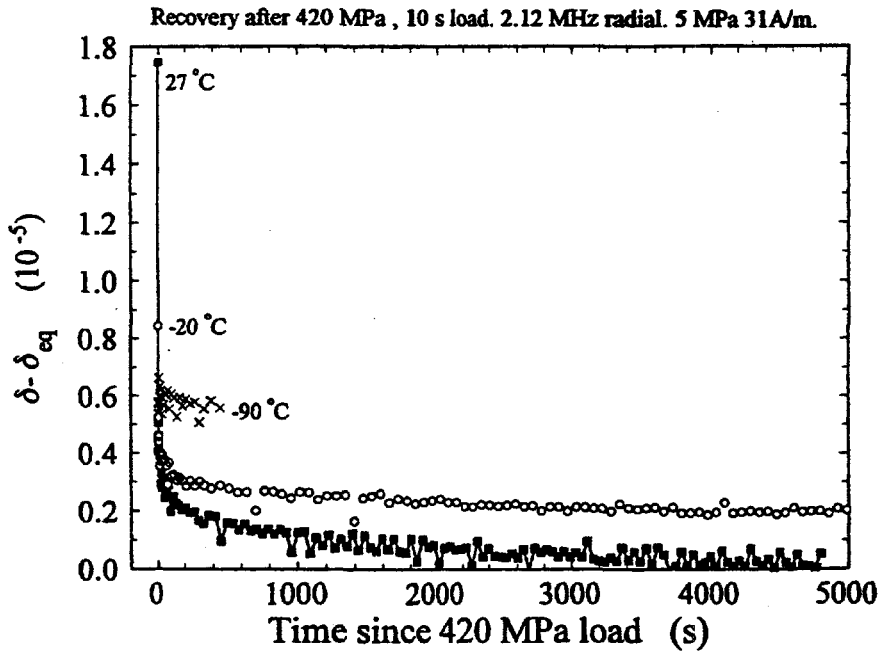

Figure 12. Internal friction of A710 steel in the peak aged condition expressed as log decrement ($\delta - \delta_{eq}$) measured at 27, -20 and -90°C. δ eq is the log decrement δ measured prior to application of the prestress of 420 MPa for 10s.

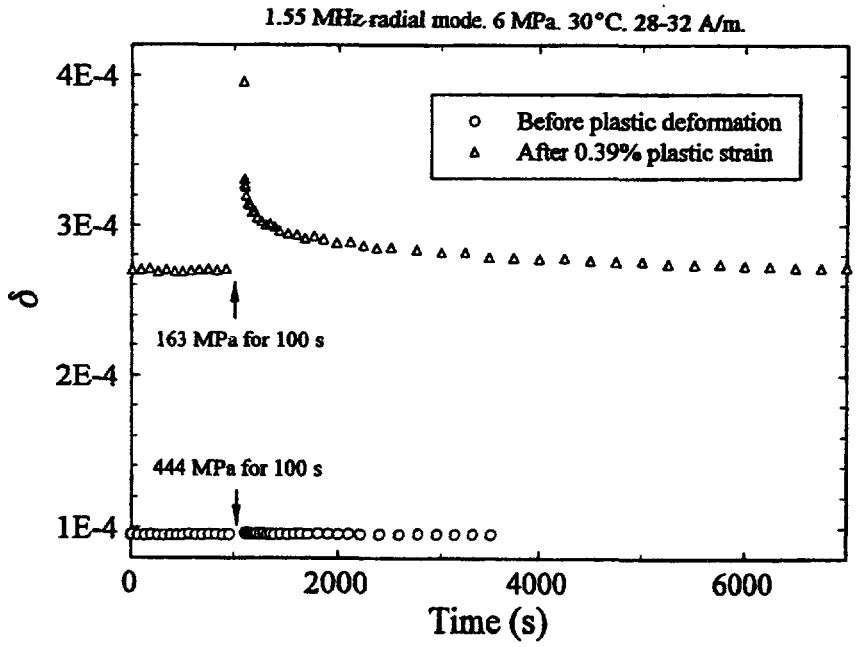

Figure 13. Internal friction (expressed as log decrement δ) of A533B steel (plate 1-1) measured before and after a prestrain of 0.39%. Note that energy losses due to internal friction occurred only if plastic prestrain was applied.

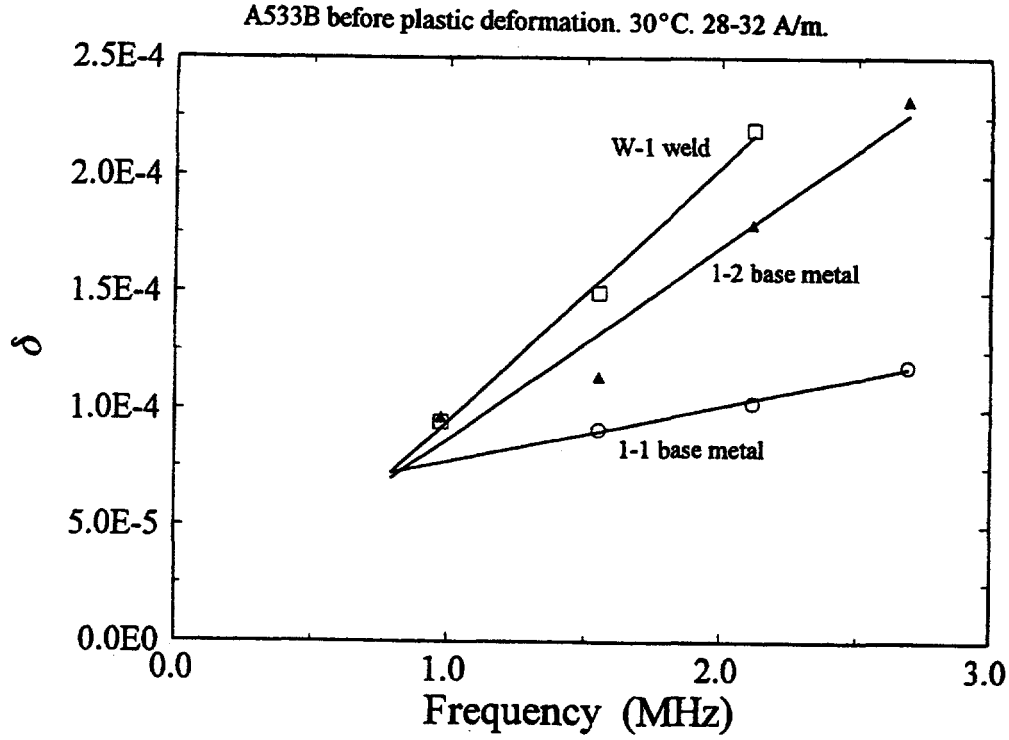

Figure 14. Internal friction δ, measured by trapped resonant modes as a function of frequency for A533B plates and weld.

ASPECTS OF THE BOILING WATER REACTOR STRAINER DEBRIS BLOCKAGE STUDY

Michael L. Marshall, Jr.
U.S. Nuclear Regulatory Commission
Office of Nuclear Regulatory Research
Division of Engineering Technology
Generic Safety Issues Branch
(301) 415-5895

October 20, 1997
25th Water Reactor Safety Meeting
Rockville, Maryland

BACKGROUND

- **SAFETY CONCERN**
  - ♦ 10 CFR 50.46 Requires Each Operating Nuclear Power Plant to Have an ECCS That Provides Long-Term Cooling.
  - ♦ Operational Events/Incidents and Analysis Has Shown That the Blockage of (pre 96-03) BWR Suction Strainers by Debris Can Prevent the ECCS from Providing Long-term Cooling.

- **PURPOSE OF SUCTION STRAINERS**
  - ♦ Prevent Debris That May Block Restrictions in the Systems Served by the ECCS Pumps or Damage Components from Entering the ECCS Pump Suction.

BACKGROUND (continued)

- **PROGRAM RATIONALE**
  - ♦ Concern About the Adequacy of USI A-43 Resolution and Implementation
  - ♦ Revise RG 1.82, Rev. 1, "Water Sources for Long-Term Recirculation Cooling Following a Loss-of-Coolant Accident"

- **CONTRACTORS**
  - ♦ Science and Engineering Associates, Inc. (Primary Contractor)
  - ♦ Alden Research Laboratory, Inc. (Subcontractor)
  - ♦ Siemens AG Power Generation Group (Subcontractor)
  - ♦ Software Edge, Inc. (Subcontractor)
  - ♦ Colorado Engineering and Experimentation Station, Inc. (Subcontractor)

LIST OF STUDIES

- **NRC-SPONSORED STUDIES**

  I. Potential of BWR ECCS Strainer Blockage Due to LOCA Generated Debris Study
  II. Blockage Code Development
  III. Assessment of Reflective Metallic Insulation Debris
  IV. Debris Drywell Transport Study

- **RELATED AND SUPPORTING STUDIES**

  V. ECCS Pump Debris Ingestion Study
  VI. Phenomena Identification Ranking Table Panel

BWR ECCS STRAINER DEBRIS BLOCKAGE STUDY

- **PURPOSES:**

  I. Estimate Likelihood (ORIGINAL).
  II. Develop Debris Generation, Debris Transport, and Debris Head Loss Models (ORIGINAL).
  III. Develop Criteria for Long Term Resolution.

- **FINDINGS:**

  I. Very High Conditional Probability of Loss of ECCS with Pre 96-03 Strainers.
  II. Most MLOCAs and All LLOCAs Can Generate Enough Debris to Pose Threat Too Pre 96-03 Strainers.
  III. Significant Head Loss Across Conical and Truncated Cone Perforated Plate Pre 96-03 Strainers Occurs Quickly.
  IV. Increasing Strainer Surface Area is the most Effective Fix.

BWR ECCS STRAINER DEBRIS BLOCKAGE STUDY

- **DOCUMENTATION:**

I. Zigler, G., et. al., "Parametric Study of the Potential for BWR ECCS Strainer Blockage Due to LOCA Generated Debris," NUREG/CR-6224 (SEA No. 93-554-06-A:1), U.S. Nuclear Regulatory Commission (Science and Engineering Associates, Inc.), Washington, DC (Albuquerque, NM), October 1995.

II. Souto, F. and Rao, D., "Experimental Investigation of Sedimentation of LOCA-Generated Fibrous Debris and Sludge in BWR Suppression Pools, "NUREG/CR-6368 (SEA No. 95-554-06-A:9), U.S. Nuclear Regulatory Commission (Science and Engineering Associates, Inc.), Washington, DC (Albuquerque, NM), December 1995.

III. Rao, D. and Souto, F., "Experimental Study of Head Loss and Filtration for LOCA Debris," NUREG/CR-6367 (SEA No. 95-554-06-A:8), U.S. Nuclear Regulatory Commission (Science and Engineering Associates, Inc.), Washington, DC (Albuquerque, NM), February 1996.

BLOCKAGE v2.5 CODE DEVELOPMENT

- **PURPOSE:**

  I. Develop "User Friendly" Code That Can Be Used by the NRC Staff to Independently Verify Plant Specific Debris Blockage Analysis.

- **CAPABILITIES:**

  I. Generic Form for Other Head Loss Correlations.
  II. Track Multiple Debris Types.
  III. Selected Parameters Can Be Varied with Time.
  IV. Handle Various Strainer Configuration.
  V. Extensive Online Help.
  VI. Sample Problems.

BLOCKAGE v2.5 CODE DEVELOPMENT

- **DOCUMENTATION:**

  I. Rao, D., et. al., "BLOCKAGE 2.5 User's Manual," NUREG/CR-6370 (SEA No. 96-3104-010-A:3), U.S. Nuclear Regulatory Commission (Science and Engineering Associates, Inc.), Washington, DC (Albuquerque, NM), December 1996.

  II. Shaffer, C., et. al., "BLOCKAGE 2.5 Reference Manual," NUREG/CR-6371 (SEA No. 96-3104-010-A:4), U.S. Nuclear Regulatory Commission (Science and Engineering Associates, Inc.), Washington, DC (Albuquerque, NM), December 1996.

- **AVAILABILITY:**

  - Code Is Available Through the Energy Science and Technology Software Center.

ASSESSMENT OF RMI DEBRIS

- **PURPOSES:**

  I. Determine if Metallic Debris is Benign

- **FINDINGS:**

  I. Reflective Metallic Insulation Can Be Fragmented During a LOCA
  II. Reflective Metallic Insulation Debris Is Transportable
  III. Reflective Metallic Insulation Debris Does Increase Head Loss Across Strainers

ASSESSMENT OF RMI DEBRIS

- **DOCUMENTATION:**

  I. Zigler, G., (Editor), "Experimental Investigation of Head Loss and Sedimentation Characteristics of Reflective Metallic Insulation Debris," SEA No. 95-970-01-A:2, Science and Engineering Associates, Inc., Albuquerque, NM, May 1996. (Accession Number:

DEBRIS DRYWELL TRANSPORT STUDY

- **PURPOSES:**

  I. Provide the NRC Staff with a Reasonable Basis for Making an Informed Engineering Decision on the Magnitude of Debris Transport from the Drywell to the Wetwell.

  II. Determine Which Phenomena or Plant Features Dominate or Control Debris Transport from the Drywell to the Wetwell.

- **FINDINGS:**

  I. The Key Plant Features Affecting Fibrous Debris Transport are (1) Number and Arrangements of Floor Gratings, (2) Duration of ECCS Flow, and (3) Drywell Floor Layout.

  II. The Key Phenomena Affecting Fibrous Debris Transport are (1) Short-Term Transport of Small Fibrous Debris, (2) Short-Term Transport of Large Fibrous Debris Below the Lowest Floor Grating, (3) Erosion of Large Fibrous Debris, and (4) Settling of Fibrous Debris in Water Pool on Floor of Drywell.

DEBRIS DRYWELL TRANSPORT STUDY

- **DOCUMENTATION:**
  - Rao, D., Shaffer, C., and Haskin, E., "Drywell Debris Transport Study," NUREG/CR-6369 (SEA No. 97-3106-A:14), U.S. Nuclear Regulatory Commission (Science and Engineering Associates, Inc.), Washington, DC (Albuquerque, NM), August 1997. (DRAFT)

LIST OF EXPERIMENTS

- **EXPERIMENTAL WORK**

I. Fibrous Debris Head Loss Experiments
II. Fibrous Debris and Sludge Sedimentation Experiments
III. Fibrous Debris Filtration Experiments
IV. Reflective Metal Insulation Debris Generation Test
V. RMI Sedimentation Experiments
VI. RMI Debris Head Loss Experiments
VII. Separate Effects Fibrous Debris Transport Experiments
VIII. Integrated Fibrous Debris Transport Experiments
IX. Fibrous Debris Washdown-Erosion Experiments

LOCA GENERATED DEBRIS TRANSPORT IN A BWR DRYWELL

Dasari V. Rao and Clinton J. Shaffer
Science and Engineering Associates, Inc.
Albuquerque, NM

George E. Hecker
Alden Research Laboratory, Inc.
Holden, MA

The drywell debris transport study (DDTS) was performed by Science and Engineering Associates, Inc. (SEA) for the United States Nuclear Regulatory Commission (NRC) to support resolution of the BWR ECCS strainer blockage issue. The objectives of this research were to: 1) estimate drywell transport factors associated with the transport of LOCA generated fibrous insulation debris and 2) identify important LOCA thermal-hydraulics phenomena (or mechanisms) and plant features that control drywell transport. The drywell transport factor is defined as the fraction of the volume of fibrous insulation contained in the zone of influence (ZOI)[1] that is transported to the suppression pool as a result of steam and water flows that occur during either blowdown or long-term ECCS recirculation phases. The focus of the DDTS is the transport of fibrous debris by double-ended guillotine break in a main steam line or a recirculation line in the mid-region of a BWR drywell. This paper describes the DDTS and presents significant findings.

1. Introduction

A loss of coolant accident (LOCA) in BWR would destroy fibrous insulation blankets, generating fibrous debris in a region close to the break referred to as the zone of influence. This debris would be carried away from the ZOI by high velocity steam flow, in the case of a main steam line break (MSLB), and by steam-water mixtures, in the case of a recirculation line break (RLB). The debris entrained by the vapor flow will be transported across the drywell volume through floor gratings to the drywell floor where it enters the downcomer vent pipes. However, the drywell presents numerous impediments to such a transport in the form of I-beams, floor gratings, pipes, instrument panels etc., where the debris may become attached or trapped. The remaining debris would be transported to the suppression pool during blowdown phase, within minutes after a LOCA.

Following blowdown, water would be introduced into the drywell by break overflow or containment sprays. Water from the containment sprays would wet all of the drywell structures located underneath the sprays, whereas water from break flow would spread out over a limited cross-section of the drywell located directly beneath the break. In both cases, as the water cascades down from the location of its introduction, it would washdown (i.e., re-entrain or erode) some of the debris captured on (or trapped by) the drywell structures during blowdown. The washed down debris would be brought to the drywell floor where water accumulates to form a pool until the water level rises above the entrance to the downcomer vents. The pool height and the pool flow dynamics, including turbulence levels are highly plant-specific controlled by such features as the water flow rate, height from which water falls into the pool, vent pipe

[1] Zone of Influence is the region surrounding the break where impingement pressures are sufficiently large to inflict damage on the insulation blankets.

offset and type of structures located close to the floor. Depending on the pool dynamics, the debris brought to the floor may remain in suspension or form a sediment. The fraction that remains in suspension would ultimately be transported with the water into the vents.

Insulation debris transport is a complex process occurring over two distinct phases: designated blowdown and washdown, as shown in Figure 1. The objective of the drywell debris transport study (DDTS) was to investigate debris transport using a bounding analysis approach to estimate the fraction of the debris transported by blowdown and washdown processes and to identify important phenomena and plant features that control or dominate debris transport. The results of the DDTS provide a basis by which the NRC can judge the appropriateness of the debris transport factors used in the utility strainer blockage analyses. The DDTS is documented in NUREG/CR-6369.

2. Program Overview

Due to the complexity of the DDTS study, initiated in September 1996, the problem was decomposed into several individual steps [Ref. 1]. Each step was then studied either experimentally [Ref. 2] or analytically [Ref. 3]. Engineering judgment was applied where applicable data were not available. The results of the individual steps were quantified using logic charts to determine transport factors for each debris size classification, for both upper bound and central estimates, and for each accident scenario studied. The overall study is shown schematically in Figure 2. Upper bound estimates provide transport factors that are extremely unlikely to be exceeded. Each upper bound estimate represents the compounding of upper bound estimates for each individual step. The central estimates were developed using a more realistic representation of each individual step.

Early in the study, the thermal and hydraulic conditions that would govern debris transport were assessed analytically by performing calculations, referred to as end-to-end scoping calculations, that encompassed the possible debris transport and capture processes. These calculations included both a series of hand computations and system level computer code calculations (i.e., MELCOR, RELAP, and CFD). Each calculation, including the code calculations, was designed to examine selected specific aspects of the overall problem. The understanding gained as a results of these calculations was then used to decomposed the problem into several components that were amenable to resolution by the knowledge base that would be developed from separate effects experiments, analytical modeling and engineering calculations. The calculations also identified vital database elements necessary to quantify transport.

Experiments and further analytical studies were undertaken to compile the necessary knowledge base on debris transport during blowdown, washdown of debris by ECCS water flow, and debris sedimentation on the drywell floor. In particular, three experiments were designed and conducted as part of this study. The first two experiments studied inertial capture of fibrous insulation fragments during air-borne transport on typical drywell structures. The third experiment studied washdown of debris previously deposited on various drywell structures by break overflow and containment sprays. Detailed CFD simulations were used to determine likely flow patterns that would exist on the drywell floor during ECCS recirculation and the likelihood of debris sedimentation under these conditions.

3. Plant Features

The results of the study were used to delineate plant features and transport phenomena that dominate debris transport in the BWR drywell. Three such plant features were identified: (1) number and

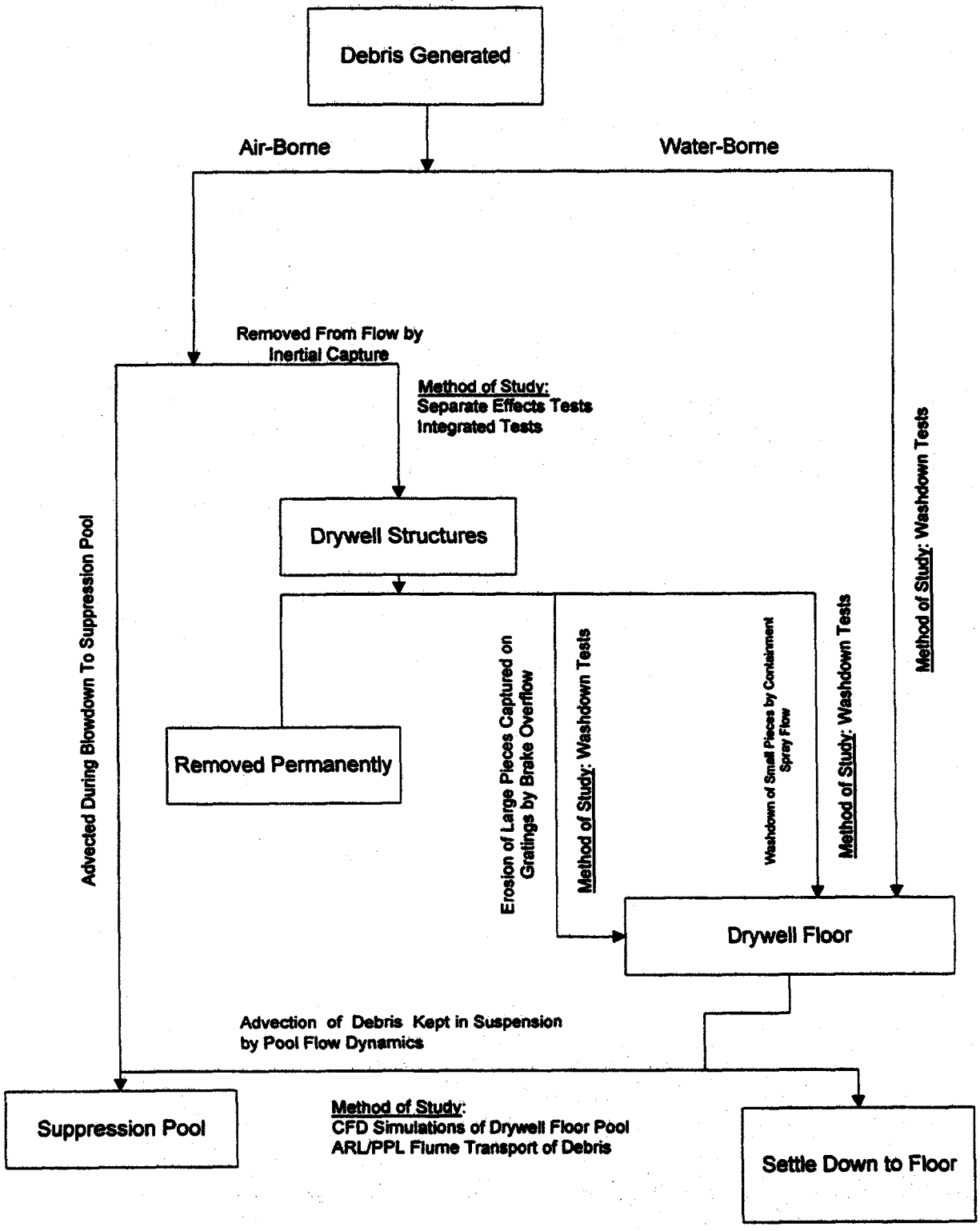

Figure 1. Postulated Debris Transport Pathways and Experiments/Analyses Conducted to Compile the Necessary Knowledge Base

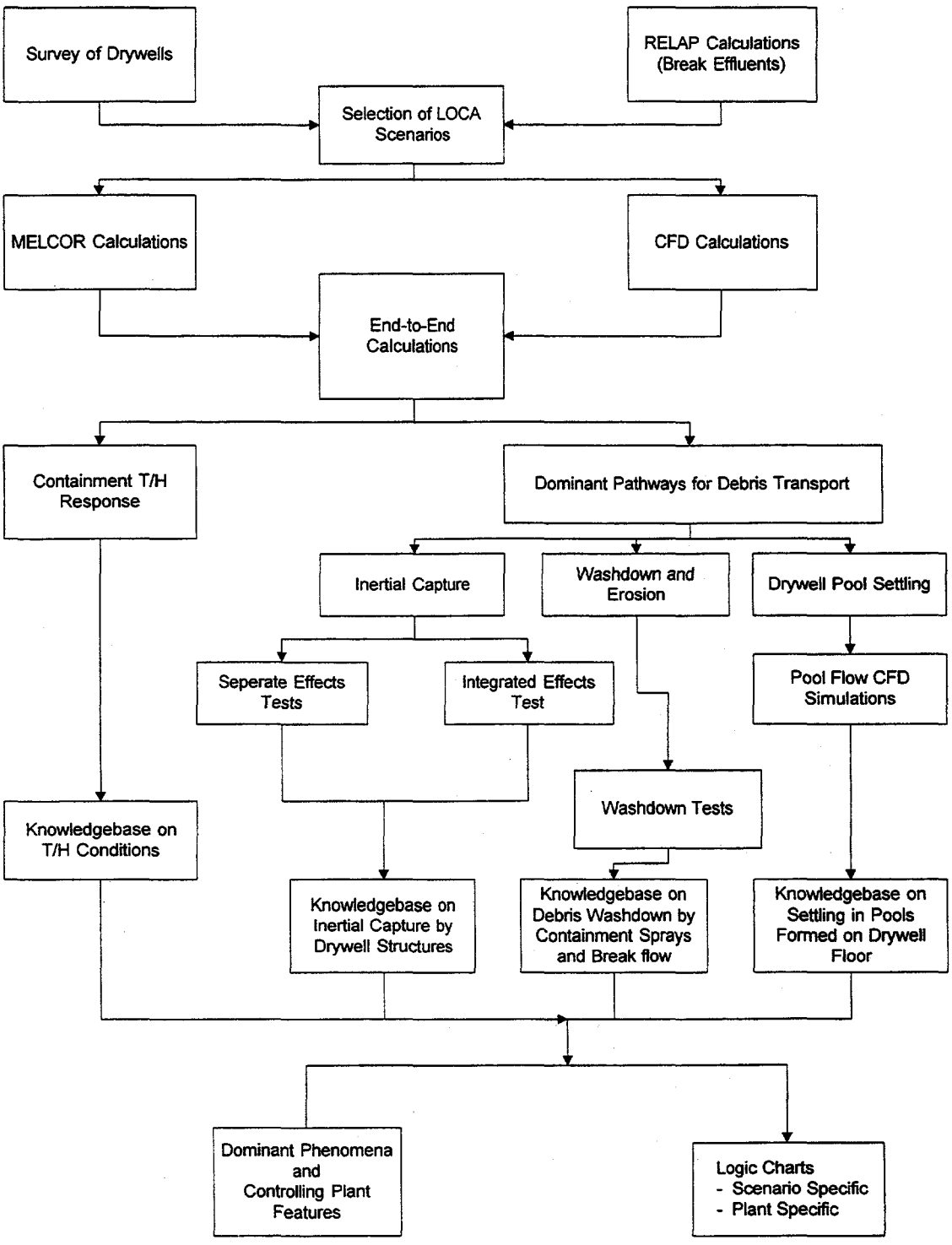

Figure 2. Programatic Overview of the Drywell Debris Transport Study

arrangement of gratings with respect to the break, (2) duration of unthrottled ECCS flow, and (3) vent and drywell floor design. The debris transport pathways for the Mark I design are illustrated in Figure 3.

Experimental data clearly illustrate that during blowdown, the drywell floor gratings provided the largest potential for capture of both small and large debris, with capture efficiency between 15% and 30% for small debris and 100% for large debris. The small pieces captured on gratings could be easily re-entrained by ECCS water flow during washdown. The only mechanism available for washdown of large pieces is erosion, which was found to be a constant rate process. Therefore, the time assumed for unthrottled operation of ECCS plays a key role in determining the fraction of large pieces that would be washed down. Although vents may provide an effective location for capture during blowdown, the captured debris may become re-entrained depending on the drywell pool flow dynamics. Typically, higher flow velocities and turbulence levels characterize pools formed as a result of break over flow. Sedimentation of small or large debris in such pools is unlikely. On the other hand, sedimentation is likely in the pools formed by containment sprays.

4. Debris Size Classifications

Insulation debris can be broadly divided into three size classes: small, large, and large-canvassed. Since each of these debris classifications followed different transport pathways, the analyses considered each classification separately. Small pieces of debris were small enough to easily pass through gratings. Fine particles such as individual fibers or groups of fibers were also considered small debris. Large and large-canvassed pieces of debris were too large to pass through a grating. The large-canvassed debris consisted of sections of relatively intact canvas covered insulation or even an intact insulation blanket within the ZOI, whereas the large pieces were pieces of relatively intact insulation that were not protected in any way by canvas. A medium category was originally considered but there was so little debris generated in this category that it was dropped from further analyses. A few pieces of debris, referred to as agglomerated debris, consisted of small pieces of insulation entangled in a web of canvas fibers, such that the piece transported as a large piece of debris. Samplings of small, medium, large, and agglomerated debris are shown in Figure 4.

5. Supporting Experiments

The DDTS included three small-scale experiments design to gain a basic understanding of debris transport and capture processes. Two of these experiments known as the separate effects tests and the integrated effects tests both examined debris transport and capture during blowdown; the third experiment, known as the washdown and erosion tests, studied debris erosion and re-entrainment during washdown.

Separate Effect Tests. The separate effects tests focused on measuring removal efficiency of isolated structural elements placed in a test channel and subjected to constant velocity air flow intermixed with debris particles of known size. Water sprays were used to wet the structures to the desired surface wetness covering the range of conditions anticipated in the drywell. The debris was injected uniformly into the flow steam by a debris injection gun. The structures examined included a variety of pipes, I-beams, floor gratings, and a Mark II vent pipe arranged singularly and in combinations with a variety of orientations. The experiments also studied the potential for degradation of large insulation pieces that are trapped on structures, such as the floor and gratings, when subjected to remaining blowdown flow at a velocity of 150 ft/sec. A schematic of the experimental apparatus is shown in Figure 5. The cross-section

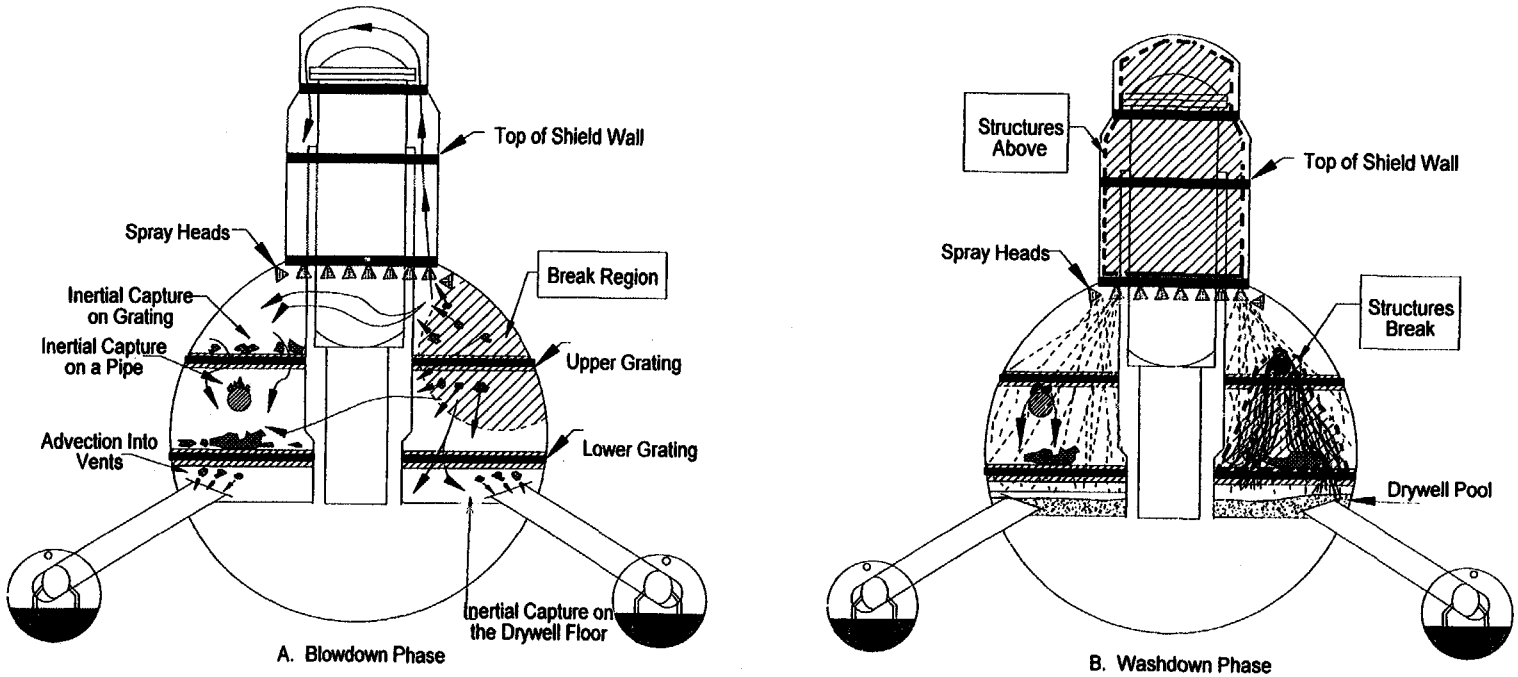

Figure 3. Postulated Debris Transport Pathways in a Mark I BWR

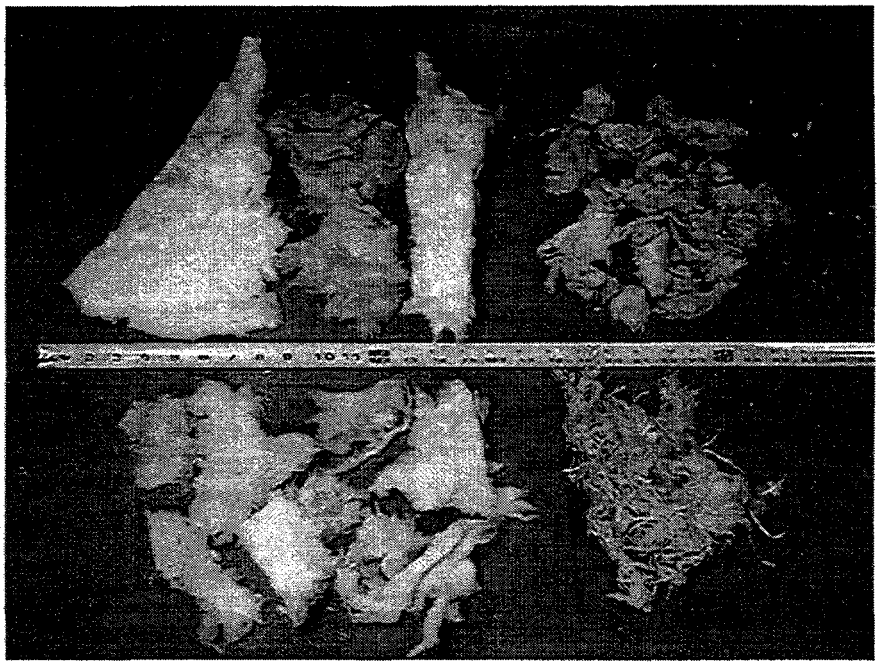

Figure 4: Sampling of Insulation Debris

of the test section was 4 ft by 4 ft for tests with flow velocities up to 50 ft/sec and 2 ft by 2 ft for tests with velocities up to 150 ft/sec. The tests produced debris capture fractions specified as the percent of the debris in the path of the structure captured by that structure. These capture fractions were correlated with fractions obtained from the integrated effects tests.

Integrated Effects Tests. The integrated effects tests, conducted at the Colorado Engineering Experimental Station, Inc. (CEESI), combined debris generation with debris transport and capture in an experimental apparatus more prototypical of a BWR drywell. The CEESI experimental apparatus is shown in Figure 6. Prototypical operating conditions considered included flow velocities, surface wetness, debris transport path lengths, and congestion and type of structures along the debris transport pathway. Bulk flow velocities entering the area containing the congestion of structural components generally ranged from 25 to 50 ft/sec. The CEESI debris transport tests were artificially wetted with a misting system prior to initiating each test because surfaces within a BWR drywell following a LOCA would be expected to become rapidly wet with steam condensate, and structural surface wetness was found to strongly influence debris capture. Insulation blankets were mounted and restrained to maximize the destruction of the blanket, i.e., generate the largest possible concentrations of debris passing through the congestion of structures. The principal test results were the overall fraction of debris transported to the far end of the test chamber and debris capture fractions for the various structural components.

Debris transport and capture in these tests conducted at CEESI focused on the small debris which consisted of debris generally smaller than the cell size of a grating. The first grating always stopped relatively intact sections of blanket, large sections of canvas, and large pieces of insulation. A substantial fraction of the medium debris, which was generally larger than a grating cell size, was forced through the

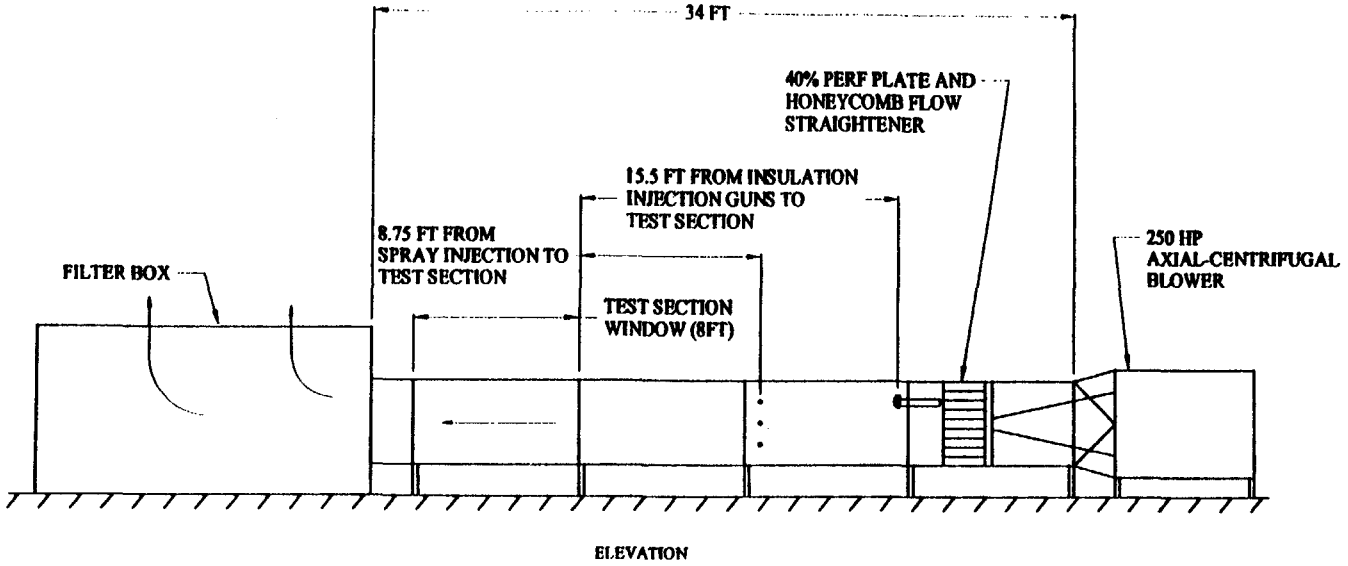

Test Chamber

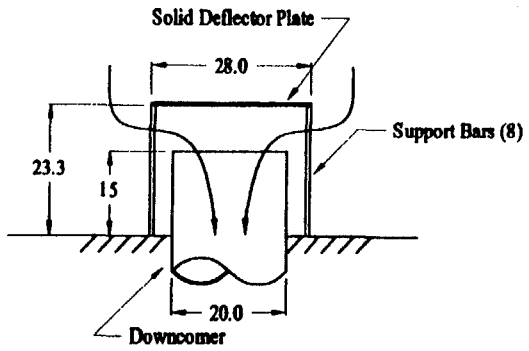

A) DIMENSIONED SKETCH OF VENT
(INCHES PROTOTYPE)

Mark II Vent

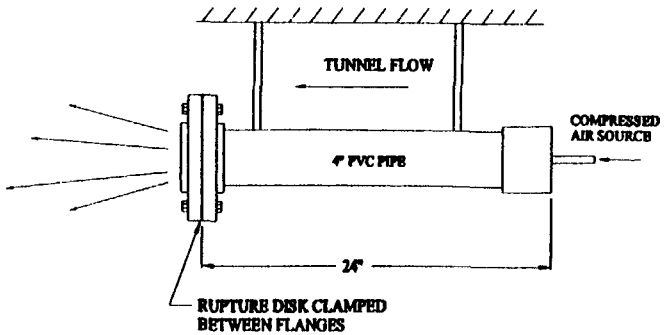

Debris Injection Gun

Figure 5. Separate Effects Test Program Experimental Apparatus

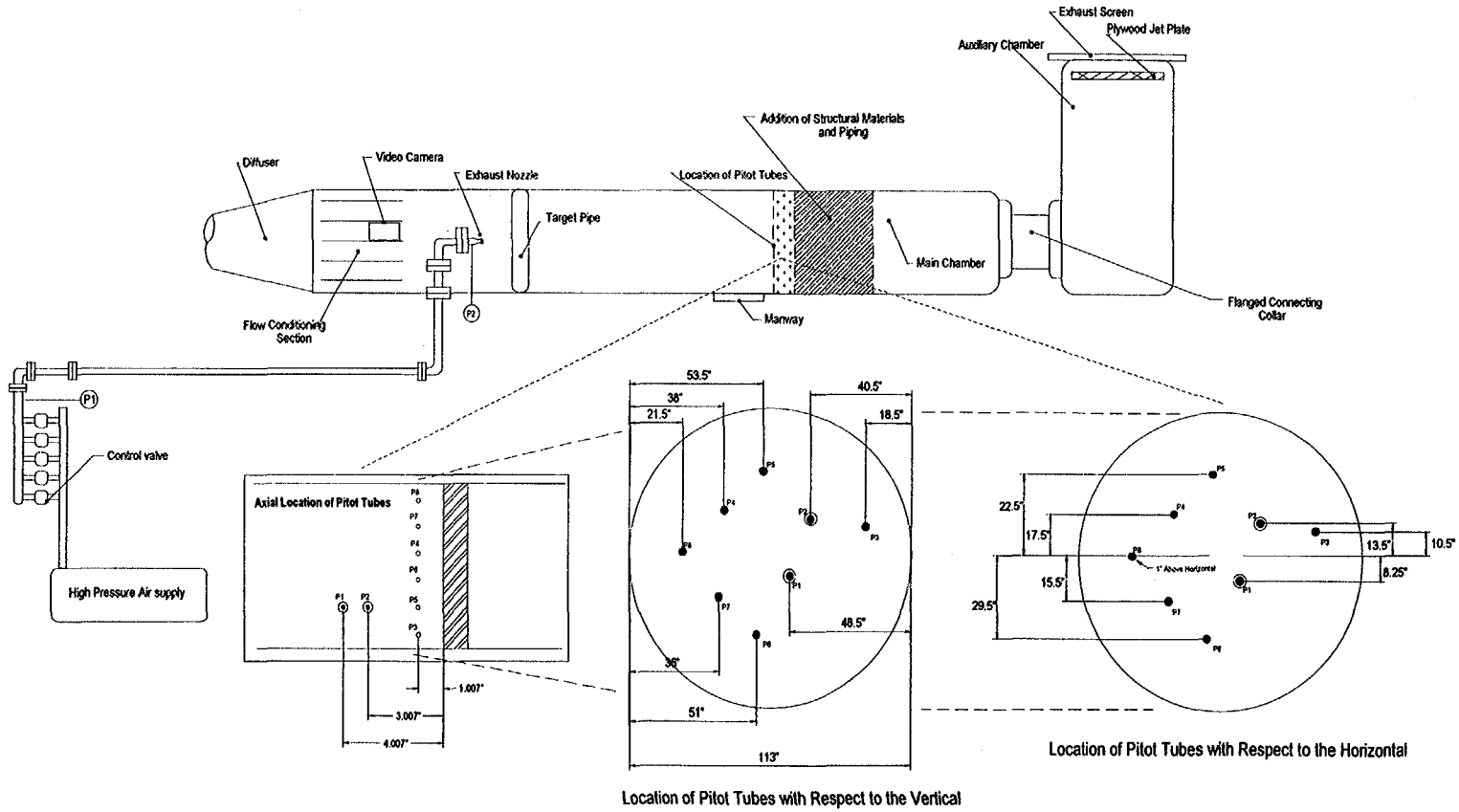

Figure 6. Test Setup Used in the Integrated Experimental Program

first grating encountered but was then subsequently stopped by the next grating encountered. Only small debris reached the exhaust screen at the chamber exit.

Small debris was found to readily transport at the CEESI test flow velocities. Flow turbulence kept debris churning until completion of the air blast, thus significant gravitational settling was not observed. Inertial deposition was clearly the dominant debris capture mechanism and was strongly influenced by surface wetness. Figure 7 shows photos of small debris captured by gratings. The photo on the left shows a large section of grating while the photo on the right shows very fine debris captured on individual bars.

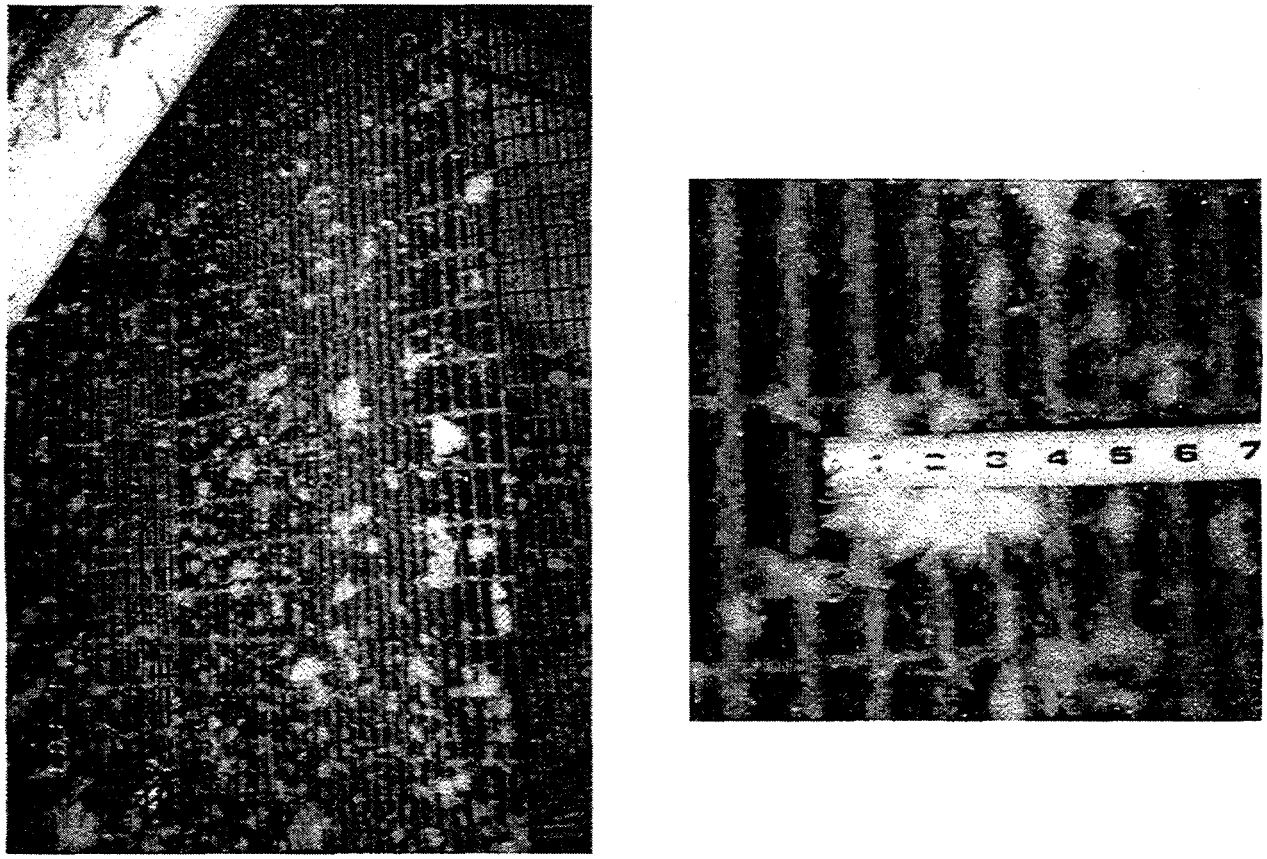

Figure 7: Photos of Small Debris Captured on a Grating

The ability of structural components, particularly a grating, to capture debris was demonstrated. The average overall transport of small debris in the CEESI facility through the structural test assemblies to the test chamber exhaust screen was 33%. Gratings were found to be effective at removing small debris from the flow stream. I-beams and pipes were considerably less effective. Substantial debris deposited onto a wet surface whenever the flow went through a sharp bend. The average fraction of debris captured by each of the structural components tested is shown in Table 1.

The ability of a structure to capture debris was relatively independent of the mass flux impacting the structure, at least within the range of debris loadings tested. The CEESI debris capture data compared

well with the corresponding debris capture data from the separate effect test conducted by ARL. The data for capture of small debris on one of the gratings is shown in Figure 8. Test repeatability was clearly demonstrated.

Table 1: Small Debris Capture Fractions

Structure Type	Debris Capture
I-Beams and Pipes (Prototypical Assembly)	9%
Gratings	
V Shaped Grating	28%
Split Grating	24%
90° Bend in Flow	17%

Washdown and Erosion Tests. A test series was conducted to determine if pieces of debris of various sizes located on drywell structures could be washed down or eroded away when subjected to water flow. Debris of known size and mass was placed on a grating and subjected to water flows at specified rates for a pre-determined duration. Erosion as measured by weighing the mass of debris remaining on the grating after terminating the water flow. The test apparatus, illustrated in Figure 9, consisted of a 2 ft by 2 ft section of clear viewing glass where insulation was located on mock-up grating and pipes. Water flow rates ranged from 20 to 175 GPM, providing flow velocities typical of BWR drywell containment spray and recirculation break flows. The debris used was generated in air jet experiments using aged fiberglass insulation and consisted of small, medium, and large pieces, including insulation protected by canvas cover.

The erosion of large debris was found to be time-dependent that was apparently linear with time, as shown in Figure 10. Photos of typical debris, before and after exposure to water, are shown in Figure 11.

The implications of these test data were that:

- substantial fractions of small and medium pieces of debris on gratings would be washed down by break and/or containment spray flows,
- erosion of large pieces is time dependent for break flow and negligible for sprays,
- secondary debris generated by erosion are very small and float at residual turbulence, and
- insulation protected by canvas did not erode.

6. Supporting Analyses

Analyses supporting the DDTS included a variety of calculations designed to examine selected specific aspects of the overall problem. These included hand calculations, system level code calculations, and CFD calculations.

MELCOR Code Calculations. The MELCOR code was used to examine thermal-hydraulic conditions within the drywell following a postulated LOCA, including:

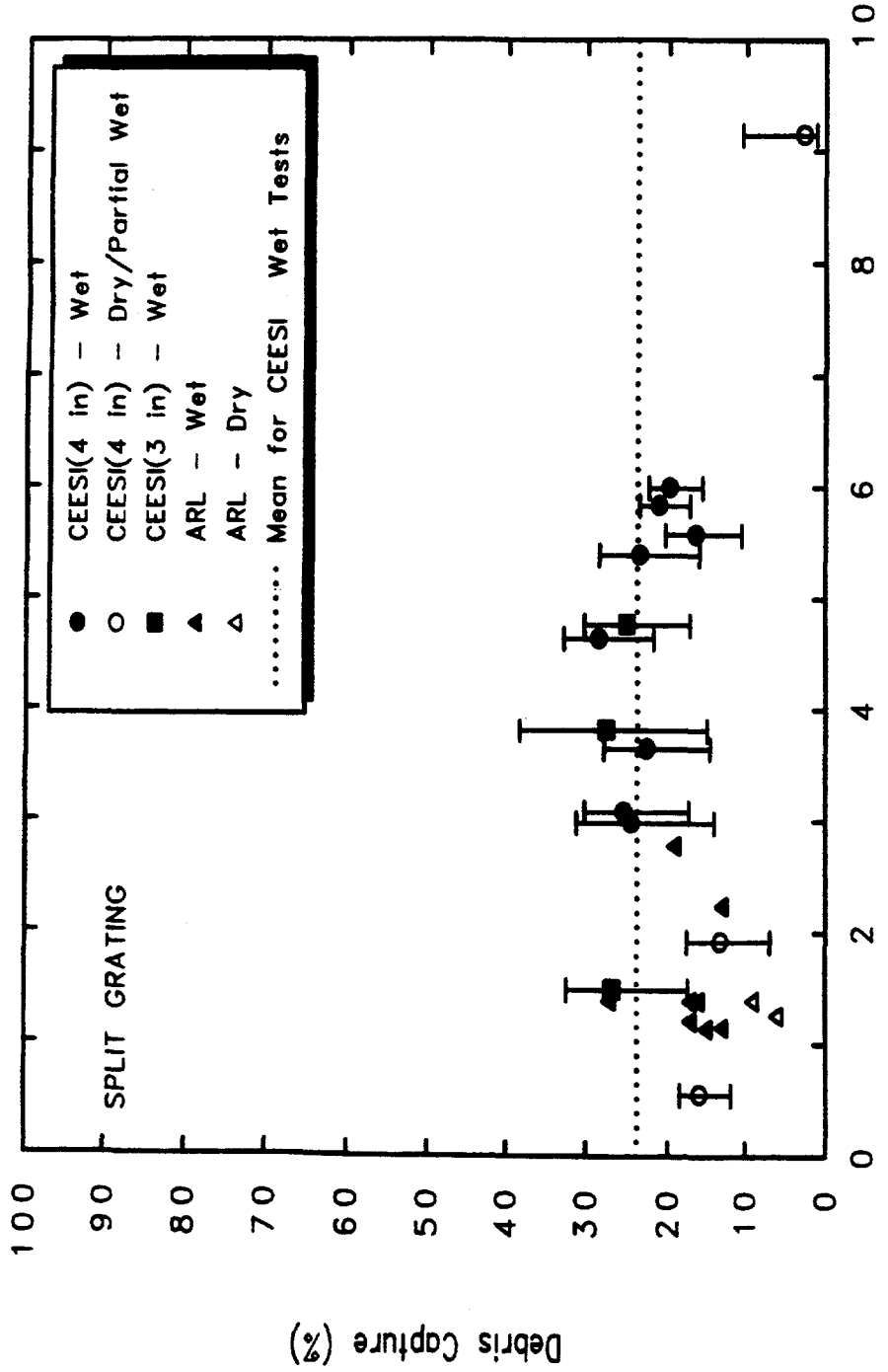

Figure 8. Grating Capture Efficiency for Small debris

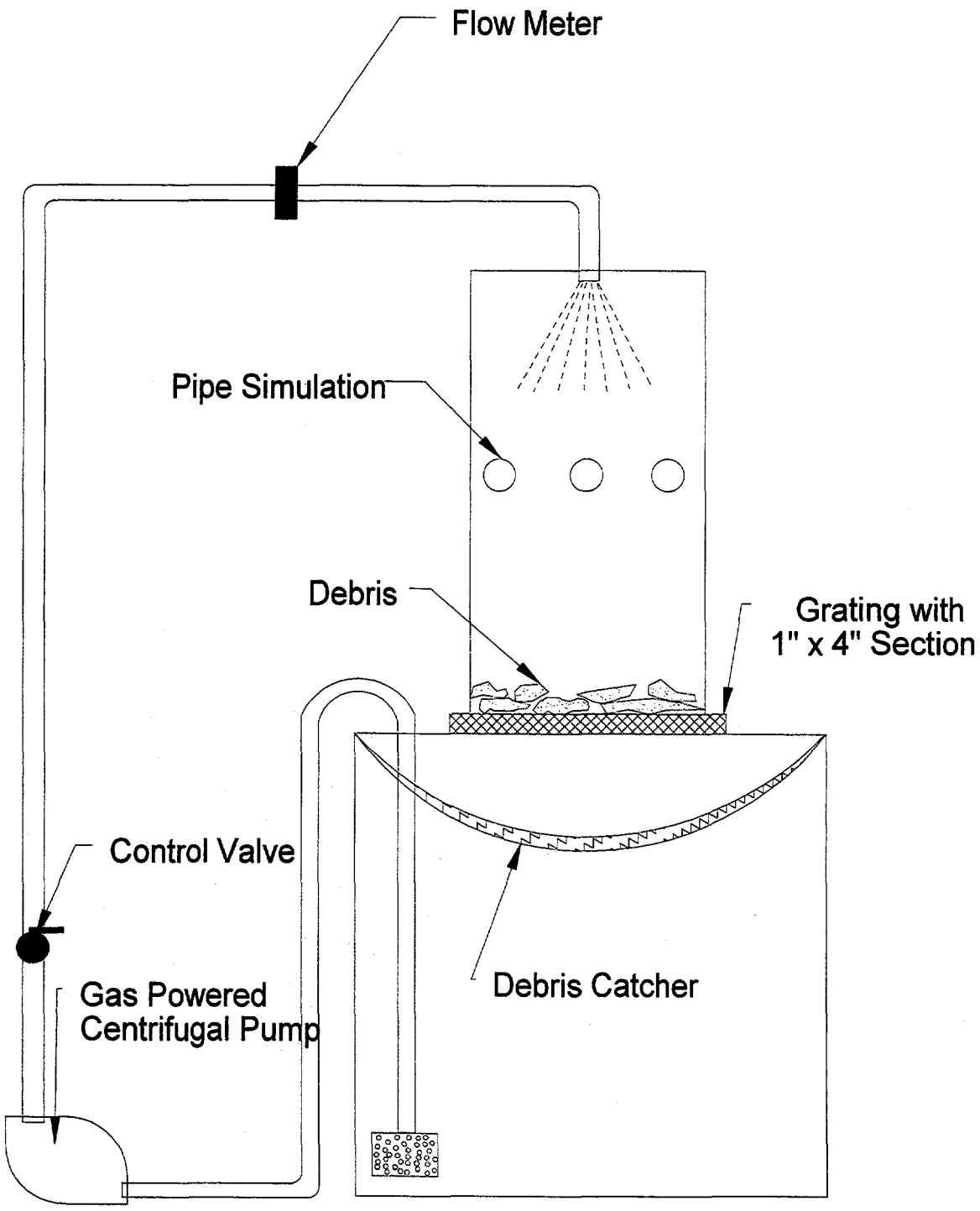

Figure 9. Setup used for the Washdown Experiments

- containment pressures and temperatures,
- bulk flow velocities,
- time required to clear the vent downcomer of water,
- rate of steam condensation on drywell structures and subsequent film thicknesses,
- rate of accumulation of water on the drywell floor,
- transport of noncondensible gases to the wetwell.

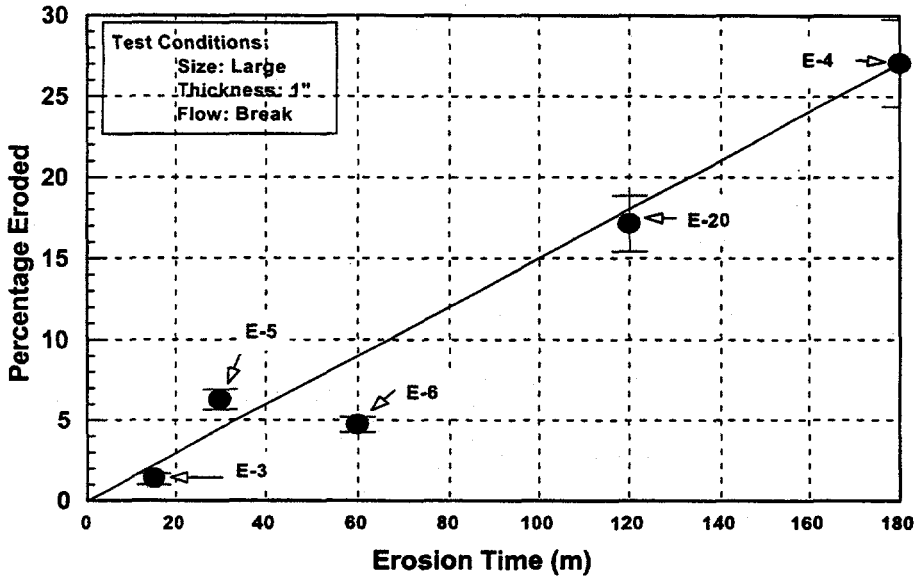

Figure 10: Effects of Duration of Erosion on the Percentage of Initial Blanket Eroded

Key observations of these MELCOR calculations included:

- The containment pressures rapidly increased to about 3 atmospheres in about 1 second, corresponding to the clearing of the downcomer vents. Further pressurization was then prevented by the pressure suppression system. After a relatively short period of 5 to 10 seconds, the pressures decreased again.

- The water in the downcomer vent pipes was purged from the pipes in about one second.

- Steam immediately condensed upon contact with surface structures until the temperature of the surface equilibrated with the steam environment. The total rate of condensation within the drywell for the high MSL break, for example, peaked at 530 kg/sec at about 2.5 seconds.

- Water films with a thickness of 200 to 400 microns accumulated on the structures in as little time as one second, depending upon the location of the surface relative to the pipe break.

- Peak flow velocities as high as 250 m/sec were found near the break and flow velocities through the vent downcomer pipes exceeded 200 m/sec. Elsewhere in the drywell the velocities varied considerably from one location to another. (Velocity distributions at 5 sec are provided in Section 7.)

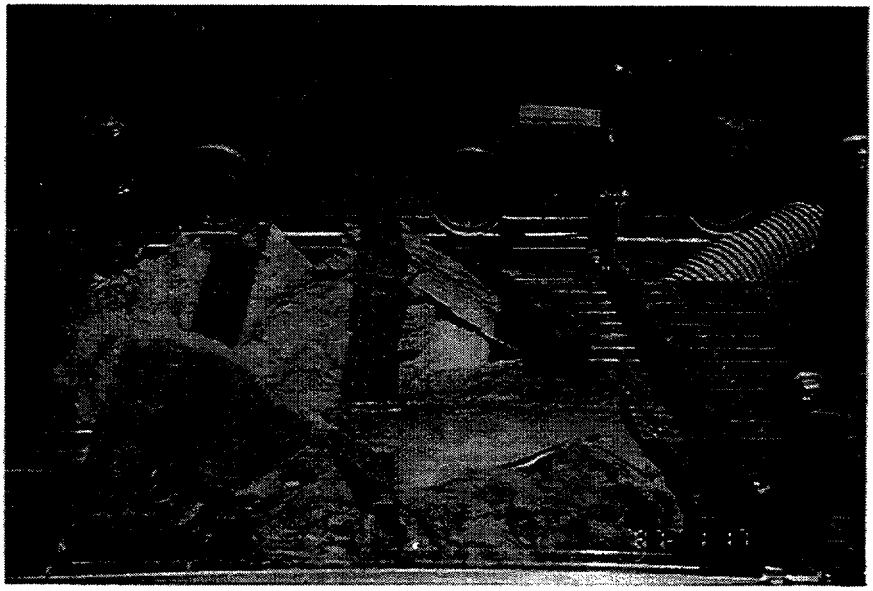

A. Before Exposure to Water

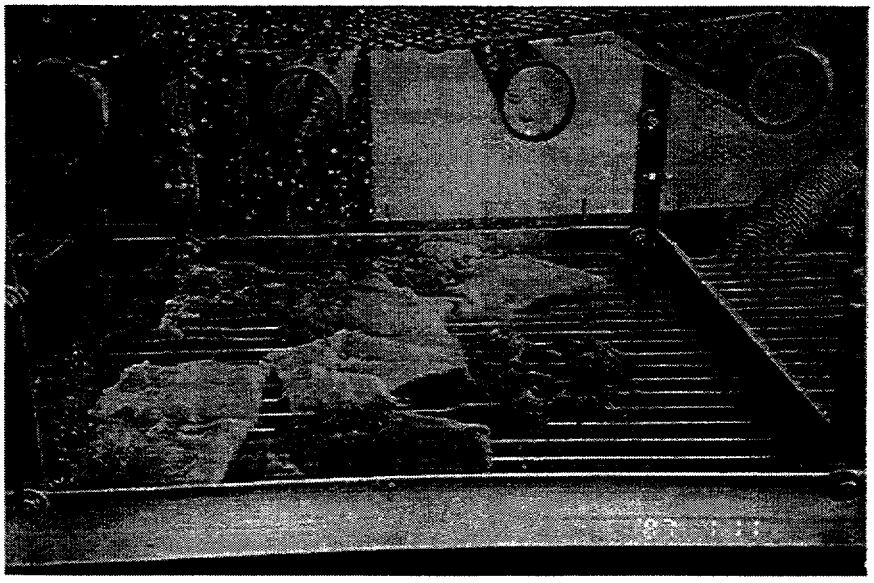

B. After Exposure to Water

Figure 11. Erosion of Large Debris Trapped on Floor Grating by Water Flow

- The majority of the nitrogen gas initially located in the drywell was forced into the wetwell in about three seconds. The residence time for a tracer gas injected into the drywell along with the break source was generally less than two seconds.

- A pool of water accumulated on the drywell floor and in the reactor cavity sumps as was expected. In the MSL breaks, the pool was much too shallow to overflow into the downcomer vent pipes, i.e., the depth of the water was only about a quarter of the depth required to overflow. In the RLB, the results were considerably different where the overflow began at five seconds for the low RLB. The asymmetrical pressures acting on the drywell floor pool pushed the accumulated water to the back side of the pedestal from the break and after the drywell pressures peaked, the pool became two-phased. The swollen water level caused the water to overflow into the vents at the back side. The drywell pool, of course, leveled out again after the primary system was depressurized.

RELAP Code Calculations. Calculations were performed with the RELAP code to characterize the break flow, i.e., rate of flow and thermodynamic state as a function of time. Following a MSLB, essentially dry steam expands into the containment. The steam mass flow rate falls from an initial value of close to 6,000 lbm/s (assuming blowdown from both ends of the broken pipe) to about 1,000 lbm/s within a period of 50 seconds, while the steam velocity remains essentially at the sonic velocity of about 700 ft/s. Water enters the drywell in the form of fine droplets ($\approx$5 μm) of entrained water but the water content is not likely to be large enough to completely wet the debris during their generation.

Following a RLB, the initial flow would be mainly water, but after a period of five to ten seconds, a mixture of water and steam is discharged at high velocities. During this phase, the dynamic pressures far outweigh the corresponding pressures during the initial five seconds after the break. Since the debris generation is proportional to the dynamic pressure, these results suggest that for a RLB most of the fibrous insulation debris will be produced in the later stages of the accident. The total mass flow rate remains fairly high ($\approx$ 20,000 lbm/s) throughout the blowdown phase of a RLB compared to a similar size MSLB; however, the water content of the exit flow is very large. In these conditions, it is expected that all of the structures located in the path of the jet will be drenched with water and the insulation materials in the vicinity of the break are likely to be thoroughly wet prior to the time when the break jet would produce significant debris. Additionally, it is likely that the majority of the debris generated will follow the steam component of the break flow rather than following the liquid component. The DDTS assumed that 80% of the debris would be transported with the steam and 20% with the water.

CFD Calculations. Substantial quantities of insulation debris could either be deposited on the drywell floor during the period of primary system depressurization or washed down to the drywell floor from drywell structures where the debris was captured during depressurization. This debris could then subsequently be transported from the floor into the vent downcomers. Therefore, determining the potential for debris to remain captured on the floor was a necessary step in the overall debris transport study. This determination was made based on analysis performed by simulating the drywell floor pool for a variety of conditions using the CFD2000 code. The primary objective of this analysis was to examine the potential for debris to settle in drywell pools and to estimate debris transport fractions (both central and upper bound estimates). The transport fraction was defined as the fraction of debris entering a drywell pool that would transport into the downcomer vents. The study considered Mark I, II, and III designs and it examined some variations in the pool depth and the entrance conditions to the pools.

The process of applying this methodology is illustrated graphically in Figure 12. The available knowledge base, shown at the top of the figure, included data from one applicable series of tests as well as theoretical CFD knowledge, plant data, and the characteristics of fibrous insulation debris. The experimental data came from a series of tests performed by Alden Research Laboratories (ARL) under the sponsorship of Pennsylvania Power and Light Company (PPL) to determine the transport and entrainment characteristics of different kinds of insulation materials in a small laboratory flume [Ref. 4]. Considerable knowledge exists regarding the quantification of turbulence levels in water pools using CFD tools. Existing safety analysis reports document the plant designs and thermal-hydraulic conditions in a BWR drywell following a LOCA

Anchoring the analytical results to prototypical experimental data was needed to correlate pool turbulence levels with conditions that allowed debris to settle. This was accomplished by simulating the ARL PP&L flume tests with the CFD code and then correlating the code predicted turbulence level for a given test with the test results showing whether or not debris actually settled in that test. Maximum levels of turbulence whereby debris could settle were determined and applied to the drywell floor pool simulation results. Two maximum levels were determined; one for small debris and one for large debris. This step is shown in the figure as the calibration of the CFD code.

The results of each of the drywell floor pool simulations consisted of graphical pictures showing pool flow behavior such as two and three-dimensional pictures of flow velocities and flow turbulence in the form of specific kinetic energy. These turbulence levels were then compared to the maximum levels for debris settling determined by the code calibration. If the pool turbulence was higher than a maximum level, then debris would not likely settle. An example flow simulation is shown in Figure 13 which shows velocity contours, i.e., line of equal velocity, for one-half of a Mark I drywell floor pool. In the figure, each contour is actually a different color allowing the analyst the ability to view the pool velocities in three dimensions. Figures showing specific kinetic (turbulence) look similar to the velocity profiles.
With all of this graphical data in hand, engineering judgment was applied to determine the likelihood for debris settling for each pool configuration. The drywell floor pool configurations simulated are shown in Table 2.

Table 2: Drywell Pool Configurations Simulated

Plant Design	Water Source	Pool Depth	Entrance Area	Inlet Turbulence	Inlet Flow
Mark I	Break Overflow	17 inches	Focused	100%	25000 GPM
			Dispersed	2%	
	Containment Sprays	17 inches	Uniform	2%	4800 GPM
		6 inches			
Mark II	Break Overflow	6 inches	Focused	100%	28600 GPM
			Dispersed	2%	
	Containment Sprays	6 inches	Uniform	2%	7400 GPM
		17 inches			
Mark III	Break Overflow	15.5 ft	Focused	100%	27410 GPM
			Dispersed	2%	

The study resulted in a complete set of transport fractions. Generally speaking, drywell floor pools formed by recirculation break flows are likely to transport the majority of insulation debris into the vent downcomers and pools formed by the containment sprays are likely to retain debris. The study did take

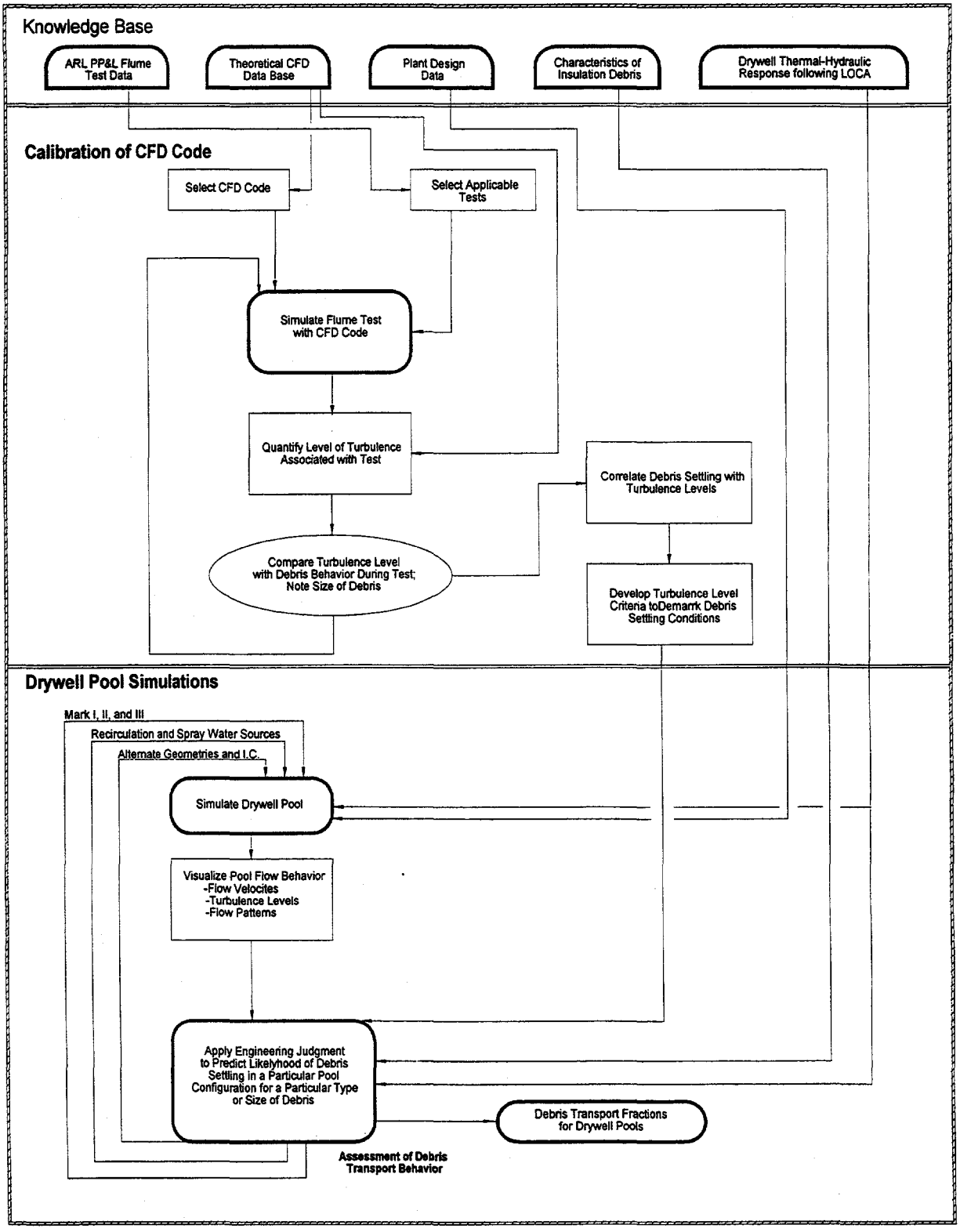

Figure 12. Drywell Floor Pool Debris Transport Methodology

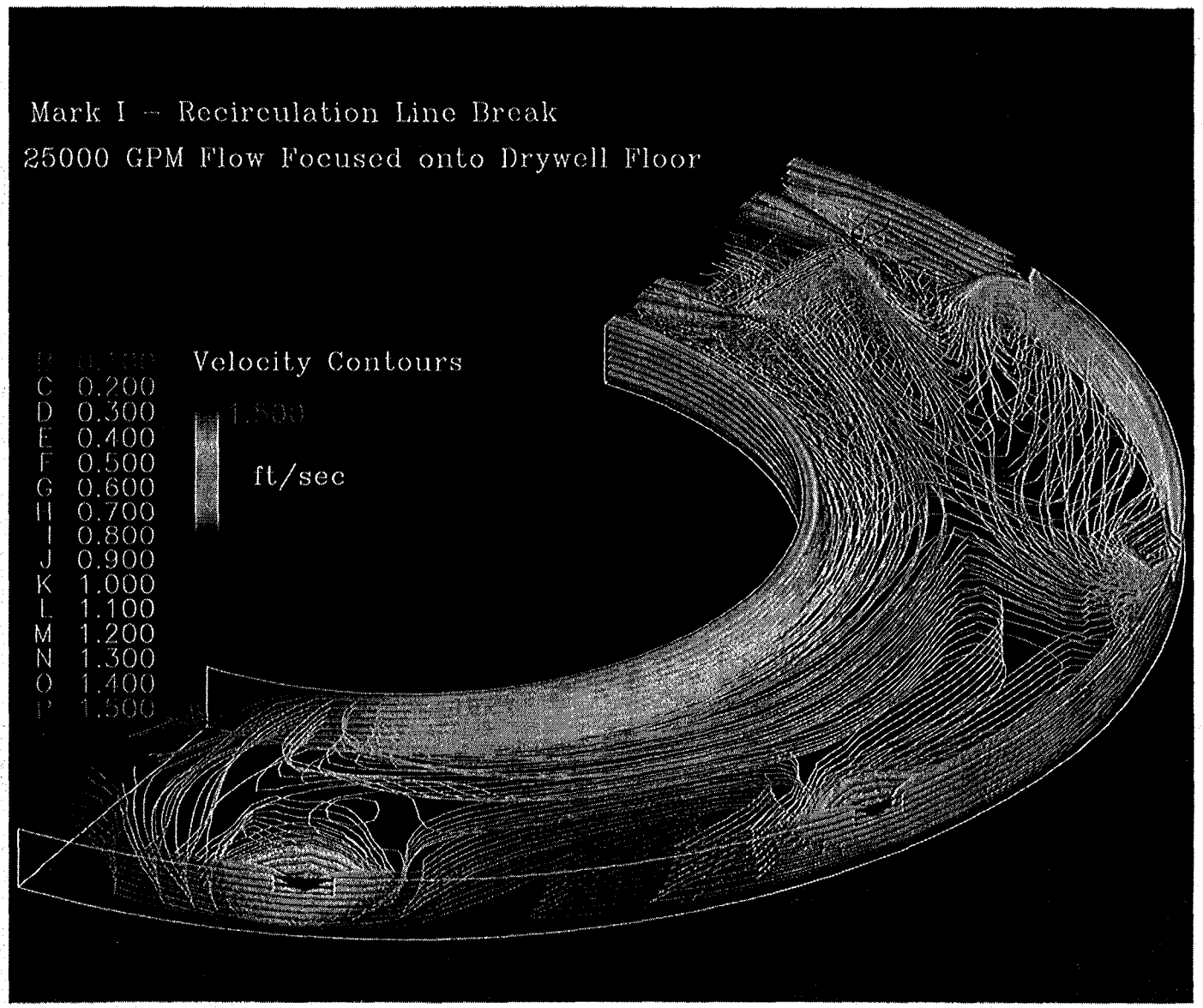

Figure 13. CFD Simulation of Mark I Flow Patterns

some exception to these generalities for the much larger pools associated with the Mark III design and break flows and in regards to the Mark II design and spray flows. Detailed results can be found in NUREG/CR-6369.

7. Logic Charts

The transport of fibrous debris is a complex process involving several competing phenomena, as evident from the previous discussions. Development of a comprehensive "best-estimate" predictive tool that accounts for each phenomenon mechanistically was beyond the scope of this study. Instead, the study decomposed the problem and studied each transport pathway independently. To further complicate the study, a total of twenty accident scenarios were studied, as illustrated in Figure 14, and debris transport factors were deduced for both the upper bound and the central estimates. The scenarios included the following:

- Mark I, II, and III BWR designs,
- Main steam line and recirculation line breaks,
- ECCS flow throttled or not throttled, and
- Containment sprays operated or not operated.

The conditions of ECCS throttling was whether or not the operators reduced ECCS flow when full flow was not needed. The specifications for throttled and not throttled were different for MSLB and RLB as shown in Table 3. The ECSS throttling condition primarily affected the length of time water flows eroded large debris deposited onto gratings below the break and the turbulence levels in the drywell floor pool.

Table 3: Definition of ECCS Throttling

Break Type	Throttled	Not Throttled
MSLB	Steaming	Full ECCS Flow < 1 Hour
RLB	Full ECCS Flow < 1 Hour	Full ECCS Flow < 3 Hour

A simplified logic chart method was chosen to link both experimental and analytical results along with engineering judgment, thereby integrating the individual steps into a comprehensive study. (The logic charts are similar to PRA event trees except distribution fractions are multiplied through the trees rather than probabilities.) A separate chart was prepared for each scenario and each estimate. An example of a logic chart is shown in Figure 15.

The logic chart decomposes the problem into five independent steps: (1) LOCA type, (2) debris classification, (3) debris distribution after blowdown, (4) erosion and washdown, and (5) sedimentation in the drywell floor pool. The accident scenario is specified in the first column. The second column specifies a size distribution for the debris, i.e., each debris classification is then subsequently treated individually. Since the debris size distribution was not within the scope of this study, a size distribution from another study (BWR Owners' Group Utility Resolution Guidance for ECCS Suction Strainer Guidance) [Ref. 5] was used in the DDTS in order to illustrate the computation of overall debris transport

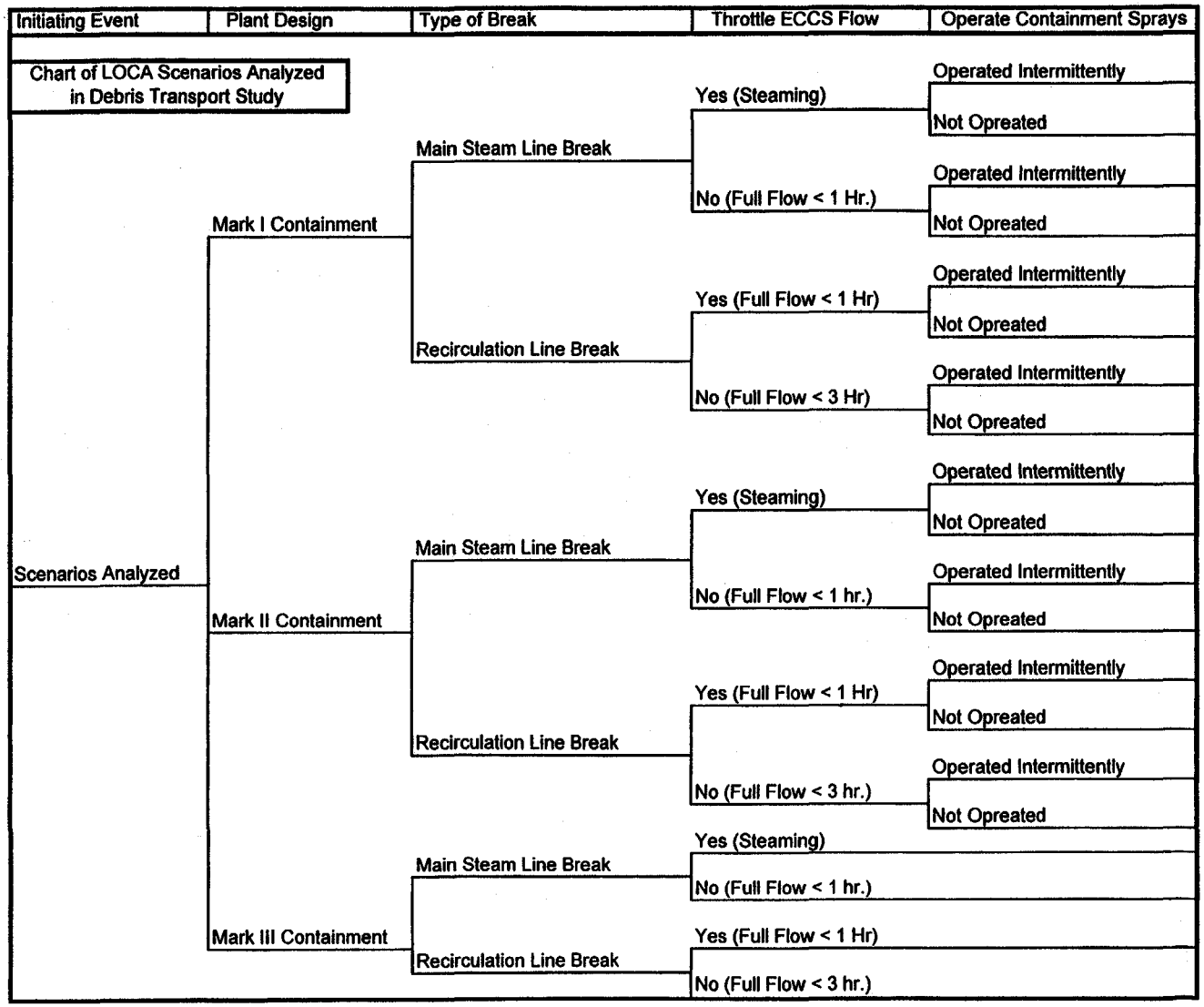

Figure 14. Accident Scenarios Analyzed in the Study

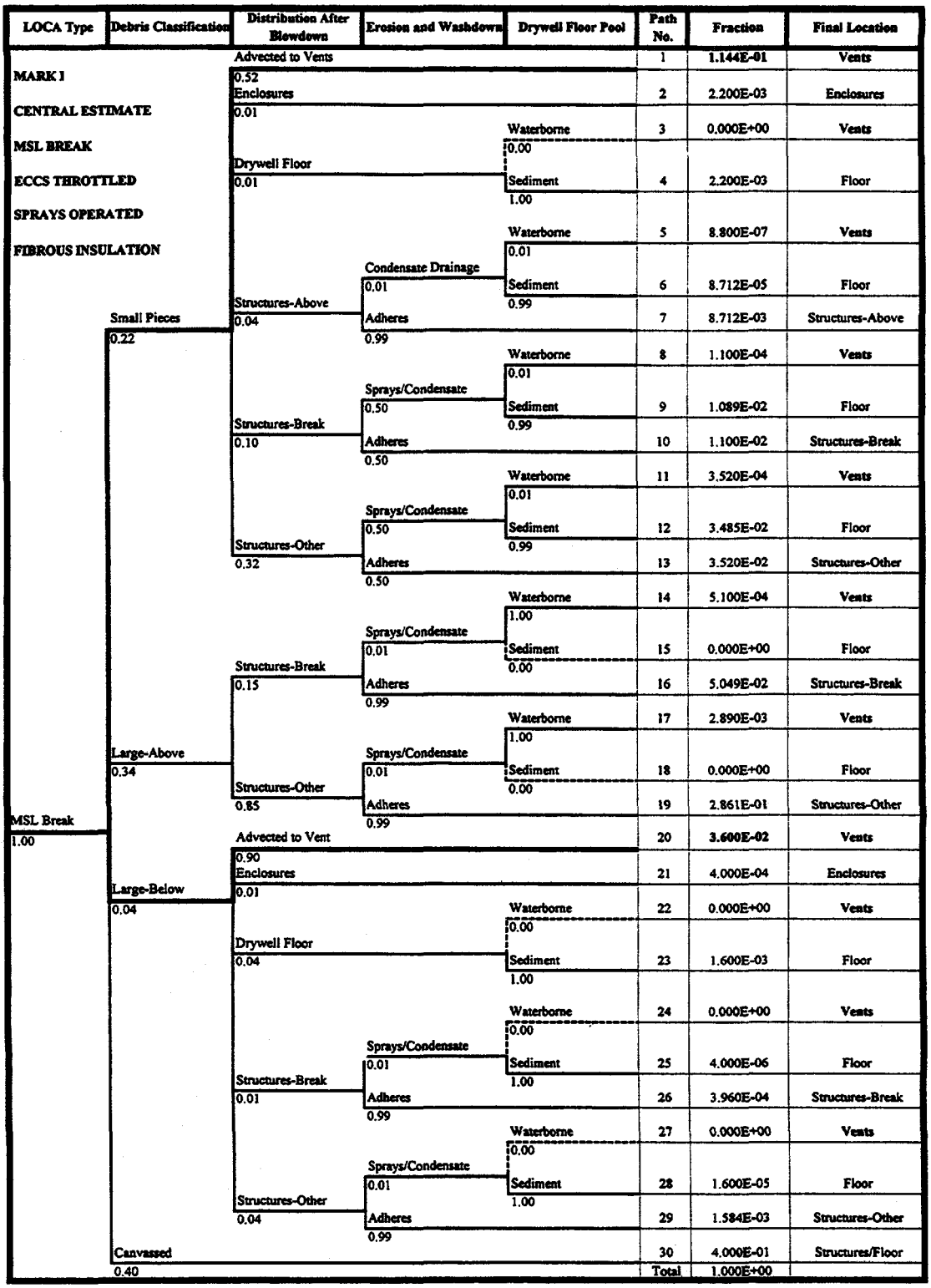

LOCA Type	Debris Classification	Distribution After Blowdown	Erosion and Washdown	Drywell Floor Pool	Path No.	Fraction	Final Location
MARK I CENTRAL ESTIMATE MSL BREAK ECCS THROTTLED SPRAYS OPERATED FIBROUS INSULATION	Small Pieces 0.22	Advected to Vents			1	1.144E-01	Vents
		Enclosures 0.52			2	2.200E-03	Enclosures
		Drywell Floor 0.01		Waterborne 0.00	3	0.000E+00	Vents
				Sediment 1.00	4	2.200E-03	Floor
		Structures-Above 0.04		Waterborne 0.01	5	8.800E-07	Vents
			Condensate Drainage 0.01	Sediment 0.99	6	8.712E-05	Floor
			Adheres 0.99		7	8.712E-03	Structures-Above
		Structures-Break 0.10		Waterborne 0.01	8	1.100E-04	Vents
			Sprays/Condensate 0.50	Sediment 0.99	9	1.089E-02	Floor
			Adheres 0.50		10	1.100E-02	Structures-Break
		Structures-Other 0.32		Waterborne 0.01	11	3.520E-04	Vents
			Sprays/Condensate 0.50	Sediment 0.99	12	3.485E-02	Floor
			Adheres 0.50		13	3.520E-02	Structures-Other
	Large-Above 0.34	Structures-Break 0.15		Waterborne 1.00	14	5.100E-04	Vents
			Sprays/Condensate 0.01	Sediment 0.00	15	0.000E+00	Floor
			Adheres 0.99		16	5.049E-02	Structures-Break
		Structures-Other 0.85		Waterborne 1.00	17	2.890E-03	Vents
			Sprays/Condensate 0.01	Sediment 0.00	18	0.000E+00	Floor
			Adheres 0.99		19	2.861E-01	Structures-Other
MSL Break 1.00		Advected to Vent			20	3.600E-02	Vents
	Large-Below 0.04	Enclosures 0.90			21	4.000E-04	Enclosures
		Drywell Floor 0.01		Waterborne 0.00	22	0.000E+00	Vents
				Sediment 1.00	23	1.600E-03	Floor
		Structures-Break 0.04		Waterborne 0.00	24	0.000E+00	Vents
			Sprays/Condensate 0.01	Sediment 1.00	25	4.000E-06	Floor
			Adheres 0.99		26	3.960E-04	Structures-Break
		Structures-Other 0.04		Waterborne 0.00	27	0.000E+00	Vents
			Sprays/Condensate 0.01	Sediment 1.00	28	1.600E-05	Floor
			Adheres 0.99		29	1.584E-03	Structures-Other
	Canvassed 0.40				30	4.000E-01	Structures/Floor
					Total	1.000E+00	

Figure 15. Central Estimate Logic Chart with BWROG Size Distribution Data

fractions. Note that if each size classification branch of the chart is normalized to one, the transport factors for that size classification can be readily computed. The logic charts were programmed into a spreadsheet so the quantification could be performed automatically.

Four size classifications are shown in the chart, i.e., small, large-above, large-below, and canvassed. Because the large debris does not pass through grating like small debris does, the large debris classification was subdivided into debris formed above any grating and debris formed below all gratings. Obviously, these two sub-classifications follow different transport pathways. The canvassed debris consists of large blanket sections where the insulation is protected by the canvas cover. Since the overall transport factors are applied to all insulation within the ZOI, the canvassed classification must necessarily include intact blankets located within the ZOI. No credible pathways were identified for canvassed debris to transport to the wetwell.

The third column shows where the debris is expected to reside following the end of blowdown. Debris will either be captured by a structure or be transported directly into the downcomer vents. Small debris capture was subdivided into five locations. The structures were divided according to location in the drywell: structures located above the containment spray heads, since the sprays cannot reach these structures; structures located directly below the break which can be subjected to recirculation break flows; and all other structures subjected to sprays but not break flows. Additionally, small debris can be deposited directly onto the floor by mechanisms such as vent capture or the debris may become trapped within an enclosure such as the reactor cavity. Large debris generated above any grating was assumed to reside on a grating either below the break or not below the break, i.e., large debris deposited above the spray heads or in enclosures was not considered credible. The study generally estimated that a large fraction of small debris and large debris produced below the lowest grating would be transported to the vents; however, in the central estimates, a small fraction of this large debris was credited as retained.

Each branch in the erosion and washdown column simply asked how much of the captured debris remained on the structures after being subjected to the appropriate washdown flows, i.e., recirculation break flow, containment spray flow, and condensate drainage. Similarly, each branch in the drywell floor pool column asks how much of the debris settles to the floor.

The last three columns provide a number for each of the 30 total pathways, the fractions that propagated through the tree, and a description of the outcome for each pathway. Only the eleven pathways labeled vents result in debris being transported to the suppression pool. Note that the sum of all of the fractions adds to one.

8. Findings

A summary of the upper bound and central estimate transport factors for a postulated LOCA in the mid-region of the drywell are presented in Tables 4 and 5 for the main steam line breaks and the recirculation line breaks, respectively. A complete set of results can be found in NUREG/CR-6369.

The central estimate transport factors shown in Table 4 are the factors for the MSLB scenarios where the ECCS is throttled back to the steaming mode by the operators and the containment sprays are operated intermittently. This scenario was chosen for summary purposes because it is the most likely scenario that operators would follow. Conversely, the upper bound estimate transport factors in Table 4 are the factors for the MSLB scenarios where the ECCS is not throttled back to the steaming mode but the sprays are operated. This scenario was chosen for the upper bound estimate because it represents the worst case

scenario in terms of debris transport. Similarly, the transport factors shown in the Table 5 summary for RLB scenarios are those for ECCS throttling and spray operation for the central estimates and no throttling and spray operation for the upper bound.

Table 4: Study Transport Factors for Main Steam Line Breaks

Plant Design	Central Estimate			Upper Bound Estimate		
	Small Debris	Large Debris		Small Debris	Large Debris	
		Above	Below		Above	Below
Mark I	0.52	0.01	0.90	1.0	0.05	1.0
Mark II	0.74	0.01	0.90	1.0	0.05	1.0
Mark III	0.55	0	0.90	0.93	0.03	1.0

Table 5: Study Transport Factors for Recirculation Line Breaks

Plant Design	Central Estimate			Upper Bound Estimate		
	Small Debris	Large Debris		Small Debris	Large Debris	
		Above	Below		Above	Below
Mark I	0.86	0.02	0.94	1.0	0.30	1.0
Mark II	0.89	0.02	0.95	1.0	0.30	1.0
Mark III	0.72	0.01	0.90	1.0	0.30	1.0

Transport factors corresponding to Tables 4 and 5 for all of the insulation initially located within the ZOI was provided in Table 6. These transport factors were determined using the BWROG debris size distribution of 0.22, 0.38, and 0.40 for small, large, and canvassed debris. The large debris was then further subdivided into large-above and large-below using engineering judgment. These subdivisions were 80% and 90% above for the central and upper bound estimates, respectively.

Table 6: Study Transport Factors for All Insulation Located in ZOI

Plant Design	Main Steam Line Break		Recirculation Line Break	
	Central	Upper Bound	Central	Upper Bound
Mark I	0.15	0.31	0.23	0.39
Mark II	0.20	0.31	0.24	0.39
Mark III	0.16	0.29	0.20	0.39

Several general conclusions can be drawn from these results:

- The total fraction of debris transported depends strongly on the assumed size distribution of the debris and the location of the break,
- Small debris readily transport towards the vents entrances with a substantial amount captured primarily by the gratings,
- A majority of the large debris generated above any grating is not likely to transport to the vents,
- A majority of the large debris generated below all gratings will likely transport into the vents.

The study concluded that the URG-recommended transport factors for Mark II containments underestimate debris transport. For Mark I and Mark III drywells, URG appears to provide reasonable estimates, provided the plant contains a continuous lower grating with no large holes. On the other hand, Regulatory Guide (RG) 1.82, Rev. 2, recommended 100% transport of transportable debris was found to provide a reasonable upper bound for breaks located below the lowest grating. RG (RG) 1.82, Rev. 2 overestimates debris transport for breaks located above the lowest grating. Finally, licensees should pay close attention to plant features that are unique to their plant and how they were modeled in this study. If necessary, the logic charts provided in this study can be easily modified to account for plant-specific features, such as number and arrangement of floor gratings. Also, they are flexible enough to accommodate new evidence and assumptions related to debris size and distribution.

9. References

1. D. V. Rao, C. Shaffer, and E. Haskin, "Drywell Debris Transport Study," Science and Engineering Associates, Inc., Draft Final Report, NUREG/CR-6369, August 1997.

2. D. V. Rao, C. Shaffer, B. Carpenter, D. Cremer, and J. Brideau, "Drywell Debris Transport Study: Experimental Work," Science and Engineering Associates, Inc., Draft Final Report, NUREG/CR-6369, Supplement 1, August 1997.

•

3. C. J. Shaffer, D. V. Rao, and J. Brideau, "Drywell Debris Transport Study: Computational Work," Science and Engineering Associates, Inc., Draft Final Report, NUREG/CR-6369, Supplement 2, August 1997.

4. K. W. Brinkman and P. W. Brady, "Results of Hydraulic Tests on ECCS Strainer Blockage and Material Transport in a BWR Suppression Pool," Pennsylvania Power and Light Company, EC-059-1006, Rev. 0, May 1994.

5. NEDO-32686, "Utility Resolution Guidance for ECCS Suction Strainer Blockage," Boiling Water Reactor Owners' Group, 1996.

WATER REACTOR SAFETY MEETING PRESENTATION ON

REGULATORY STATUS OF THE ECCS

SUCTION STRAINER/SUMP SCREEN BLOCKAGE ISSUE

OCTOBER 20, 1997

Presented By:
Robert Elliott

RBE 10/19/97

BACKGROUND

- **SAFETY CONCERN**
  - ♦ 10 CFR 50.46 Requires Each Operating Nuclear Power Plant to Have an ECCS That Provides Long-Term Cooling.
  - ♦ Operational Events/Incidents and Analysis Has Shown That the Blockage of BWR Suction Strainers by Debris Can Prevent the ECCS from Providing Long-term Cooling.
- **PURPOSE OF SUCTION STRAINERS**
  - ♦ Prevent Debris That May Block Restrictions in the Systems Served by the ECCS Pumps or Damage Components from Entering the ECCS Pump Suction.

RBE 10/19/97

BACKGROUND (continued)

- **SIGNIFICANT OPERATIONAL EVENTS**

  I. PERRY [May 1992]

  - ♦ During an Inspection with a Remote Controlled Video Camera, Fouled RHR Strainers Were Discovered.

  II. PERRY [January 1993]

  - ♦ After Strainers were Cleaned, Deformation of Strainers Discovered, Strainers Replaced.
  - ♦ "Cleaned" Suppression Pool.
  - ♦ Fouling Material Identified as Corrosion Products, Hair, and Tape.

  III. PERRY [March 1993]

  - ♦ Used ECCS During a Rapid Plant Shutdown.
  - ♦ Fouling Strainers Discovered, and One Strainer Deformed.
  - ♦ Fouling Material Identified as Fibrous Material and Corrosion Products.

RBE 10/19/97

SIGNIFICANT OPERATIONAL EVENTS (continued)

IV. BARSEBÄCK [July 1992]

- Accidental Srv Discharge into Drywell, That Dislodged Thermal Insulation.
- Dislodged Insulation Washed Into Wetwell by Containment Sprays.
- High Differential Pressure Noticed Across Suction Strainers.

V. LIMERICK 1 [September 1995]

- Suppression Pool Cooling Started to Remove Heat Introduced by Leaking SRVs.
- About 30 Minutes Fluctuating Flow and Motor Current.
- Thin Mat of Fibrous Material and Sludge Found on Strainers.

BACKGROUND (continued)

- **RECENT REGULATORY HISTORY**

  I. NRCB 93-02, Supp. 1 "Debris Plugging of Emergency Core Cooling Suction Strainers" [February 1994]

  - ♦ Requested BWR Licensees to (1) Provide Training and Briefing to Operators, (2) Ensure EOPs Address Indications and Mitigation, and (3) Institute Measures to Provide Compensatory Actions to Prevent, Delay, or Mitigate Loss of Available NPSH.

  II. NRCB 95-02, "Unexpected Clogging of a Residual Heat Removal Pump Strainer While Operating in the Suppression Pool Mode" [October 17, 1995]

  - ♦ Requested BWR Licensees to (1) Perform Operability Evaluation of ECCS Pumps, (2) Schedule Suppression Pool Cleaning, and (3) Review FME Procedures.

BACKGROUND (continued)

- **RECENT REGULATORY HISTORY** (continued)

III. NRCB 96-03, "Potential Plugging of Emergency Core Cooling Suction Strainers by Debris in Boiling Water Reactors" [May 1996]

- ♦ Requested BWR Licensees to Implement Appropriate Measures to Ensure That ECCS is Capable of Performing its Functions.
- ♦ Three Suggested Options: (1) Large Passive Strainers, (2) Self Cleaning Strainers, and (3) Installation of Backflush System.
- ♦ BWR Licensees Requested to Implement Actions by the End of the First Refueling Outage Starting After January 1, 1997.
  - Plants With a Spring 1997 Refueling Outage were allowed to defer implementation.

IV. RG 1.82, Rev. 2, "Water Sources for Long-Term Recirculation Cooling Following a Loss-of-Coolant Accident" [May 1996]

- ♦ More Comprehensive Guidance for BWRs.

CURRENT RESOLUTION STATUS

- **NRC Bulletin 96-03 Implementation**
  - ◆ All BWRs have selected Option 1 (large capacity passive strainers) and are proceeding with installion of the new strainers
  - ◆ Four Strainer Designs

    1- Performance Contracting, Inc.

    2- General Electric

    3- Mark III Design by Centerior Energy and Entergy

    4- ABB
  - ◆ Plants with Spring 1997 Refueling Outages granted deferrals due to inadequate lead time for strainer procurement
  - ◆ Four of nine Spring Outage Plants successfully installed new strainers on time.

RBE 10/20/97

CURRENT RESOLUTION STATUS (continued)

- **NRC Bulletin 96-03 Implementation (continued)**
  - One plant voluntarily shut down to install new strainers over the summer
  - LaSalle will install new strainers in both units before restarting from their current dual unit extended outage
  - Only one plant with a Fall 1997 refueling outage will be unable to install on schedule
  - Utility Resolution Guidance SER expected to be issued in November 1997
- **Emerging Regulatory Issues during 96-03 Implementation**
  - 10 CFR 50.59 Issues
    - I. Containment Overpressure Credit
    - II. Hydrodynamic Load Calculations

RBE 10/20/97

RELATED REGULATORY ISSUE/GENERIC COMMUNICATIONS

- **PWRs**
  - Staff evaluating need for further action relative to PWRs based on lessons learned from the BWRs
- **COATINGS GENERIC LETTER**
  - Research Effort underway
  - EPRI developing guidelines for coating programs
  - ASTM D33
  - December 1997
- **NET POSITIVE SUCTION HEAD GENERIC LETTER**
  - Staff concerns over consistency in calculating ECCS NPSH

RBE 10/20/97

GENERIC SAFETY ISSUE (GSI) 171 - ENGINEERED SAFETY FEATURE (ESF) FAILURE FROM A LOOP SUBSEQUENT TO LOCA: ASSESSMENT OF PLANT VULNERABILITY AND CDF CONTRIBUTIONS*

G. Martinez-Guridi, P. Samanta, L. Chu, and J. Yang
Brookhaven National Laboratory
Upton, New York 11973-5000

ABSTRACT

Generic Safety Issue 171 (GSI-171), Engineered Safety Feature (ESF) from a Loss Of Offsite Power (LOOP) subsequent to a Loss Of Coolant Accident (LOCA), deals with an accident sequence in which a LOCA is followed by a LOOP. This issue was later broadened to include a LOOP followed by a LOCA. Plants are designed to handle a simultaneous LOCA and LOOP. In this paper, we address the unique issues that are involved in LOCA with delayed LOOP (LOCA/LOOP) and LOOP with delayed LOCA (LOOP/LOCA) accident sequences. LOCA/LOOP accidents are analyzed further by developing event-tree/fault-tree models to quantify their contributions to core-damage frequency (CDF) in a pressurized water reactor and a boiling water reactor (PWR and a BWR). Engineering evaluation and judgements are used during quantification to estimate the unique conditions that arise in a LOCA/LOOP accident. The results show that the CDF contribution of such an accident can be a dominant contributor to plant risk, although BWRs are less vulnerable than PWRs.

1 INTRODUCTION

Background

Generic Safety Issue 171 (GSI-171), Engineered Safety Feature (ESF) Failure from a Loss Of Offsite Power (LOOP) subsequent to a Loss Of Coolant Accident (LOCA), primarily addresses an accident sequence in which a LOCA is followed by a delayed LOOP. This issue was initially identified by the United States Nuclear Regulatory Commission's (NRC's) Office of Nuclear Reactor Regulation (NRR) in NRC Information Notice (IN) 93-17, "Safety System Response to Loss of Coolant and Loss of Offsite Power" issued March 8, 1993 (NRC Info Notice 93-17). This IN was partly based on an identified deficiency in the loading logic of the Surry Power Station Emergency Diesel Generator (EDG) that could have overloaded the EDGs if a LOCA had occurred followed by a LOOP before the Safety Injection Signal (SIS) was reset. The NRC subsequently learned from the Nuclear Steam Supply System (NSSS) owners' group that other plants were not necessarily designed to respond properly to a LOCA followed by a delayed LOOP if the SIS was not reset. The IN 93-17 did not request any specific action by (nor information from) the licensee.

In response to the Nuclear Utility Backfitting and Reform Group's (NUBARG) request, NRC's Committee to Review Generic Requirements (CRGR) considered IN 93-17 and noted that "...the staff is considering the need for further generic action to determine if all power reactor licensees should be required to demonstrate the capability to withstand the LOCA/delayed LOOP sequence of concern..." (Letter from E.L. Jordan to D.F. Stenger and R.E. Helfrich, April 12, 1994). NRC IN 93-17, Rev. 1 was issued March 25, 1994.

A prioritization analysis was carried out by NRC's Office of Research (RES) and a HIGH priority ranking was given to the GSI-171 (Attachment to D.L. Morrison to L.C. Shao's Memorandum, June 16, 1995). This prioritization was further reviewed (Memorandum from M.A. Cunningham to C.Z. Serpan, October 18, 1995) and questions raised about some assumptions made in the analysis. The GSI-171 Task Action Plan was developed. A technical evaluation of the GSI-171 accident sequences was conducted for operating power reactors to obtain insights for addressing the concerns raised as part of this generic issue and was published in NUREG/CR-6538 (Martinez-Guridi, et al., 1997); this paper summarizes the technical evaluation.

GSI-171 encompasses two scenarios in which a LOCA and a LOOP are not independent events, but the occurrence of one triggers some events that cause the other to happen; those events usually take some time to occur, and thus, there is usually a delay between the LOCA and the LOOP. The scenario in which the LOCA causes the LOOP is called either LOCA with consequential LOOP or LOCA with delayed LOOP; here we refer to it by the notation LOCA/LOOP. The other scenario in which the LOOP causes the LOCA is called LOOP with consequential LOCA or LOOP with delayed LOCA; we refer to it as LOOP/LOCA.

Objectives

The objective of this study was to evaluate the LOCA with delayed LOOP (LOCA/LOOP) sequences in pressurized- and boiling-water reactors (PWRs and BWRs), addressing the issues raised as part of GSI-171 and the assumptions made in earlier evaluations. The following were the specific objectives of the study:

a) To analyze the LOCA/LOOP accidents in power reactors considering the loading sequences in response to accidents involving LOCA and LOOP, and the electrical distribution systems along with their applicable protective features;

b) To evaluate the Individual Plant Examinations (IPEs) conducted as part of NRC's Generic Letter 88-20, and determine whether LOCA/LOOP and LOOP/LOCA accidents, as postulated in GSI-171, have been addressed;

c) To develop frequency estimates of LOCA/LOOP accidents considering the dependency of a subsequent LOOP on the preceding LOCA;

d) To develop models (event trees) to delineate accident sequences leading to core damage in a LOCA/LOOP, identifying the progression of events;

e) To develop approaches to estimate the probabilities of events identified as part of the event trees, particularly those involving unique failure conditions and mechanisms that may occur during a LOCA/LOOP accident but have not been considered in a conventional probabilistic risk assessment (PRA);

f) To quantify the core damage frequency (CDF) contributions for LOCA/LOOP accidents considering the different, relevant design features in a plant, and assess the sensitivity of the results to the assumptions influencing the evaluations.

In addition, since the GSI-171 also discusses a LOOP/LOCA scenario, i.e, a LOOP followed by a delayed LOCA, we discuss these types of sequences, the adequacy of their modeling in IPEs, and estimate their frequencies.

Scope

The scope of this study was to analyze LOCA/LOOP and LOOP/LOCA accidents addressed in GSI-171 and the vulnerabilities of nuclear power plants to such accidents:

a. To review selected IPEs to determine whether these accident scenarios have been addressed;

b. To estimate the likelihood of LOOP given LOCA, using the events that occurred at operating nuclear power plants, and similarly, the likelihood of LOCA given a LOOP, based on reviewing LOOP events; and

c. To develop models to quantify the contributions to core-damage frequency associated with LOCA/LOOP accident scenarios.

The evaluations considered both a pressurized water reactor (PWR) and a boiling-water reactor (BWR).

We recognized that because of differences in design characteristics the risk contribution of such accidents may vary from plant to plant, and an evaluation of a single plant might not reveal the resulting variations in risk impact. Accordingly, the scenario was modeled in a manner that would facilitate evaluation for different designs. Because of the significant differences between PWRs and BWRs, they were considered separately. Quantitative analysis was conducted using data and other modeling features, as needed, from the following plants: Sequoyah (a PWR), and Peach Bottom (a BWR). These particular plants were chosen because their PRA models were available in the SAPHIRE computer code (Russell et al., 1994), not because of their vulnerability to GSI-171 issues.

The risk contribution was calculated at the level of core-damage frequency (CDF), i.e., an evaluation corresponding to a Level 1 PRA. During a LOCA/LOOP accident, the containment systems also can be adversely affected (NRC Info Notice 96-95), thus affecting the Level 2 and 3 results, but an evaluation beyond CDF was not within the scope.

In quantifying the CDF contributions, probability estimates are given for different conditions in a LOCA/LOOP accident. The estimates ideally are based on detailed plant-specific information which, however, was not available for all cases during this study. In many cases, past operating-experience data either was not available or its compilation would have taken large resources, if at all possible. Thus, the scope of the evaluation involved the following:

a) using the information available in Final Safety Analysis Reports (FSARs), NRC Information Notices, Licensee Event Reports (LERs), and Individual Plant Examinations (IPEs) dealing with similar conditions; and

b) using engineering judgments to estimate the probabilities, based on the above information.

2 LOCA/LOOP AND LOOP/LOCA ACCIDENT SEQUENCES, ELECTRICAL DISTRIBUTION SYSTEMS, AND PROTECTIVE FEATURES

2.1 Description of GSI-171

GSI-171, "ESF failure from LOOP subsequent to LOCA", primarily deals with a LOOP *caused* by the LOCA event and Engineered Safety Features Actuation System (ESFAS) sequencing. Thus, the LOCA and subsequent LOOP would not be *independent* events. The loss of a large amount of electric-power generation, as might be precipitated by the trip of the unit with the LOCA, can cause instability in the transmission system grid, resulting in a total LOOP. The loss of generation from the LOCA-affected unit can also degrade voltage at the unit switchyard, so actuating degraded voltage protection and subsequent total LOOP. Plants that have no Technical Specifications (TS) upper setpoint limit on degraded voltage sensing, and have little margin between the setpoint and minimum operating grid voltage may be susceptible to this problem.

Besides problems with the transmission system grid, a LOOP may also occur because of problems with the plant's electrical-distribution system. In many plants, the main generator normally feeds the plant loads through a unit auxiliary transformer. When the reactor trips, the main generator often remains connected to the plant's electrical systems and high voltage switchyard until protective relaying transfers the power source from the main generator to an offsite source. If the transfer fails during ESFAS sequencing, the buses which provide power to ESF systems would become isolated from offsite power sources, and then the EDGs would be required to provide power.

When a LOCA occurs at a PWR, the ESFAS are actuated by one of four automatic signals, or manually if the plant operators detect the LOCA before the automatic signals respond. These are the four automatic signals:

1) Low Pressurizer Pressure

2) High Containment Pressure

3) High Steam Line Flow Rate Coincident with either Low Steam Line Pressure or Low-Low Average Temperature (T_{avg})

4) Steam Line High Differential Pressure.

The ESFAS will typically cause the following system responses:

1) Reactor trip initiated

2) Safety Injection Sequence initiated, i.e., emergency core-cooling system (ECCS) pumps started and aligned for cooling the core

3) Phase "A" containment isolation

4) Auxiliary feedwater initiated

5) Main feedwater isolated

6) EDG Startup

7) Auxiliary Cooling System Line-up (pumps started in essential service water and Component Cooling Water systems)

8) Control Room and Containment Ventilation Isolation.

The EDGs at most plants probably cannot handle simultaneous starting of all of the pumps and motors actuated by the ESFAS and, thus, it is necessary to sequence the startup of all ESFAS-actuated systems to prevent overloading the EDGs. There are similar system responses for LOCAs at BWRs.

2.2 LOCA With Delayed LOOP (LOCA/LOOP)

This section expands on the issues and concerns associated with a LOCA/LOOP accident.

Overload of EDGs

The Surry report (Virginia Electric and Power Company, May 1989), referenced in NRC IN 93-17 (March 8, 1993), describes a deficiency in the diesel generator's loading logic for the LOCA/-LOOP scenario that results in the generator attempting to pick up, simultaneously, the permanently connected loads plus any safety loads that were sequenced onto the offsite power system before the delayed LOOP signal. Such a problem might occur because a designer did not provide for a load-shed signal to previously sequenced loads following a LOCA because a simultaneous LOCA/LOOP would not require that capability. The safety significance of this deficiency depends on the amount of safety load that was energized before the LOOP signal. If the LOOP signal comes in just a few seconds after the LOCA signal and before the first sequenced load-step is energized there is no significance because the diesel generator will pick up only the permanently connected loads that are normally energized when the diesel generator's breaker closes. If the LOOP signal comes in substantially later (e.g., more than 30 seconds after the LOCA signal), the diesel generator would have to pick up a large block of load, and could potentially trip off on overload or be damaged with no immediate possibility of recovery.

Block-load

For plants that start all LOCA loads simultaneously (one large load-block versus load-sequence) on offsite power, the worst-case scenario would occur any time the LOCA signal follows the LOOP signal. Block-loading to offsite power may also increase the likelihood of a consequential LOOP.

Non-Recoverable Damage to EDGs and ECCS Pump Motors

EDGs are generally designed to start automatically on a LOCA signal and remain running in standby if offsite power is available during a LOCA. Following a subsequent loss of offsite power, systems that are designed to respond automatically to a LOCA/LOOP will use a time-delay or voltage-sensing relay to delay the closing of the diesel generator's output circuit breakers if the generators are up and running. This feature allows the residual voltages of motors that had been running on the safety buses to decay to a sufficient value (approximately less than 25%) of their nominal voltage to avoid an out-of-phase transfer of the motors with the already running diesel generators. If systems are not specifically designed to respond to the LOCA/LOOP scenario they may not have this feature, and the diesel generator's circuit breakers will likely close immediately upon receiving the LOOP signal, creating the potential for an out-of-phase transfer. Damage to the motor and diesel generator may result from this.

Lockout Energization of Safety Loads (Anti-pump Circuits)

Two utility reports (Clinton Power Station Unit 1, November 19, 1993, and Indian Point 3 Nuclear Power Plant, April 4, 1994) and NRC IN 88-75 (September 16, 1988) identify a problem involving the anti-pump circuits in circuit breakers that could result in the inability to automatically or manually reclose safety-related load breakers in designs that attempt to load-shed and reclose these circuit breakers given a LOCA/LOOP. The anti-pump circuits are intended to prevent the close/open pumping of a circuit breaker when both a close signal and open signal are

simultaneously presented, such as might occur if an operator attempts to close a breaker against a fault. Because of the time delays and permissives involved in resetting anti-pump circuits, the circuits can also lockout closing of circuit breakers in some anti-pump designs if a breaker is rapidly closed-opened-closed or opened-closed, even though the signals do not overlap. Such a series of close/open signals could occur in designs that attempt to load-shed and reclose circuit breakers given a LOCA/LOOP. Whether or not a breaker is locked out depends on the design of the particular anti-pump circuit and the timing of the LOOP signal. Because load-sequencing times on redundant trains of safety equipment usually are identical, there is the potential that redundant loads, such as safety injection pumps, could be locked out by their breakers in a LOCA/LOOP. Before reclosing a circuit breaker that has been locked out by an anti-pump circuit, the circuit must be reset by either removing the automatic close signal to the breaker, or de-energizing the control power to the anti-pump circuit. Neither of the required actions are likely to be known by the operator.

Lockup of the Load Sequencers

An additional potential vulnerability associated with the LOCA/LOOP event involves the timers used in the load-sequencing logic. Typically, the timers must be reset at some point to reinitialize the timing circuits to restore the circuits to their original pre-event status. In plants that were not designed to accommodate a LOCA/LOOP event, these timers may require resetting by the operator at some point after load-sequencing, or may be automatically reset following load-sequencing. In either case, the inability to reset the timers in the middle of an interrupted load-sequencer operation, such as one occurring during a LOCA/LOOP in plants that load sequence on both offsite and onsite power, could lockup the load sequencers, and lose all subsequent accident-loading capability.

Double Sequencing

The Palo Verde plant (January 5, 1995) discovered the potential for double-sequencing of safety-related equipment following a LOCA, which could delay injection. Following a LOCA and a successful fast bus transfer, the following sequence of events potentially could occur:

1) start of sequencing safety-related equipment onto the preferred offsite power,

2) load-shed due to the class 1E 4.16 kV undervoltage relays dropping out during sequencing onto offsite power, and failing to reset during the time delay (less than 90 percent for approximately 35 seconds),

3) isolation of the class 1E 4.16 kV bus from the offsite source,

4) closure of the EDG breaker, and

5) resequence of the equipment onto the EDG.

This double-sequencing has the net effect of delaying water-makeup injection into the reactor coolant system by more than half a minute after the safety injection signal.

Water Hammer

Water hammer is a concern because of the potential drainback associated with a pumped system when the system is de-energized and then re-energized with voids in the outlet piping. The resulting water hammer may damage the piping and its supports.

Pumps Tripping on Overload

Pumps may also require larger and more prolonged accelerating torques when re-energized with the outlet valves in the open versus closed position. This could result in a stalled pump motor or a more prolonged accelerating current, and potential tripping of the pump on overload. Tripping on overload also is possible in large air-conditioning chiller-pump motors that are re-energized before the system's pressures are equalized. In both cases, the large, prolonged motor currents could degrade the electrical system beyond only tripping the associated motors.

2.3 LOOP With Delayed LOCA (LOOP/LOCA)

This section expands on the issues and concerns associated with a LOOP/LOCA accident.

EDG Overload

If the LOOP loads have all completed loading on the diesel generators when the LOCA signal comes in, and the loading logic simply load-sequences the additional LOCA loads, the diesel generators may or may not be able to satisfactorily handle the additional loads on top of the already existing ones if this capability was not considered in the original design.

Failure of Logic Associated with the Load Sequencing

If the LOCA loads begin sequencing onto the diesel generators in the middle of the LOOP sequence, the load-sequencing steps may overlap, and the diesel may stall or the generator's voltage collapse in attempting to pick up the excessively large, simultaneous starting load. The logic associated with the load sequencing may fail to actuate, or may lockup if it was not specifically designed to handle a LOOP/LOCA.

Accident Loads Not Automatically Sequenced onto the EDGs

NRC IN 84-69 (August 29, 1984) and its supplement (February 24, 1986) also identify the potential that, in some designs, accident loads may not be automatically sequenced onto the diesel generators if they are already providing power to the safety buses, which would be the case in a LOOP/LOCA event.

2.4 Electrical Distribution System

This section describes the different schemes used to energize the ECCS pump motors, and gives an overview of the response of the EDS to three situations: LOOP, LOCA, and LOCA with a delayed LOOP.

Energization of ECCS Loads

There are two main schemes of energization of ECCS loads. In the first, the ECCS loads are energized sequentially by a sequencer that closes the circuit breakers of the ECCS loads in a certain sequence. In the second scheme, all ECCS loads are energized at once; this is called block-load.

When offsite power is available, the ECCS loads are either sequentially loaded or block-loaded, depending on the particular design of a plant. When offsite power is not available, i.e., there is a LOOP, the ECCS loads are energized by the EDGs; usually, this energization scheme is sequential. In BWRs 5 & 6, a diesel generator is dedicated for the High Pressure Core Spray system.

Response to LOOP

In the event of a LOOP, the EDG1 will be started, and, once it has reached its rated frequency and voltage, UV relays will signal the circuit breaker CBDG1 to close. The circuit breakers of the ECCS loads connected to the 1E bus also will receive a signal to close.

Response to LOCA

In a LOCA, an SI signal will be generated some time after its onset, depending on its size. For a small LOCA, it may take up to 2 minutes until it is detected, and, therefore, for the SI signal to be generated. Medium and large LOCAs are detected almost immediately and, therefore, the SI signal is generated immediately after their onset.

In a LOCA, primary coolant is being lost through the break, the level of coolant is decreasing in the pressure vessel, and water makeup must be provided to the vessel; injection is carried out by the ECCS pumps. If there is no injection to the pressure vessel, the core will eventually uncover, overheat, and be damaged.

The larger the size of the LOCA, the faster the pressure vessel will lose water inventory, and the shorter the time to uncover the core. Usually, three sizes of LOCA are analyzed: Large, Medium, and Small.

The SI signal will cause the EDG1 to start automatically, but its circuit breaker will remain open. The ECCS loads are energized either using a sequencer or the block-load scheme. In particular, if offsite power is available when the LOCA occurs, some plants energize all ECCS loads (from offsite power) using the block-load scheme.

If offsite power is not available when the LOCA occurs, the ECCS loads are usually energized sequentially.

Response to LOCA and a Delayed LOOP

A LOCA will generate a SI signal, that, in turn, will cause a reactor trip. The loss of generation from the LOCA-affected unit can also degrade voltage at the unit switchyard, so actuating degraded voltage protection and subsequently, a total LOOP. Any of the three types of offsite power sources mentioned before may be affected in this scenario, but the first two are expected to be more susceptible since there is no electrically independent offsite power source to the plant.

Besides problems with the transmission system grid, a LOOP may also occur because of problems within the plant's electrical distribution system. In many plants, the main generator normally feeds the plant loads through a unit auxiliary transformer. When the reactor trips, protective relaying transfers the power source from the main generator to an offsite power source. If the transfer fails during the ESFAS sequencing, the 1E buses become isolated from sources of offsite power, and then, a transfer to the EDGs would be required.

2.5 Protective Features

Protective devices are used throughout the electrical distribution system. The different devices that protect EDGs and the ECCS pump motors from damage include synchronizing relay or in-phase monitor, undervoltage relay, overcurrent relay, and underfrequency relay. Martinez-Guridi, et al., (1997) have a detailed discussion of these protective devices.

3 EVALUATIONS AND RESULTS

The work carried out to address the issues associated with LOCA/LOOP and LOOP/LOCA can be summarized as follows:

a. Selected IPE submittals were reviewed to determine whether they modeled or addressed the accident sequences (LOCA/LOOP and LOOP/LOCA) postulated in GSI-171.

b. Operating experience data were evaluated to estimate the probability of LOOP given a LOCA, and of LOCA given a LOOP, using surrogate events and data.

c. Event tree models were developed defining the progression of events leading to core damage for LOCA/LOOP accidents.

d. Core-damage frequency (CDF) contributions were quantified for LOCA/LOOP accidents at a PWR and a BWR plant using engineering analyses and judgment to estimate the required parameters for quantification.

e. Sensitivity and uncertainty analyses were conducted to address plant-specific vulnerabilities, variabilities in data, and assumptions in modeling, and to obtain insights on dominant contributors to CDF for a LOCA/LOOP accident.

The details of the technical evaluation methods, analyses conducted, and the results are given in Martinez-Guridi, et al. (1997); the following is a summary of the results.

Treatment of LOCA/LOOP and LOOP/LOCA Accidents in IPE Submittals

Individual Plant Examination (IPE) submittals for 20 plants were reviewed to understand the extent to which GSI-171 accident scenarios and the associated issues were addressed in them. The technical findings from these reviews can be summarized as follows:

1) The IPEs do not model, nor do they discuss LOCA/LOOP, i.e., LOCA with consequential or delayed LOOP, along with the GSI-171 concerns about damage to EDGs and ECCS pumps, the loss of this equipment due to overloading, lockup of the load sequencer, and lockout energization of circuit breakers due to their anti-pump circuits. Some IPEs model random occurrence of LOOP following LOCA in the LOCA analysis, but these analyses do not address nor provide any insights into the plant's response in the GSI-171 postulated scenario.

2) The IPEs model LOOP/LOCA sequences and the associated core-damage frequency (CDF) contribution can be greater than 1.0×10^{-5}/yr. Fifteen PWRs have sequences with a CDF contribution greater than 1.0×10^{-6}/yr, with the highest being 4.7×10^{-5}/yr. However, these models do not address GSI-171 concerns.

3) The IPEs have limited information about the protective devices that may be present in a plant to adequately respond to LOCA/LOOP and LOOP/LOCA sequences. Such information shows that some plants may have protection against damage to the EDGs and ECCS pumps. Plant-specific information is needed to develop a complete understanding about whether plants have or lack such protective features.

Frequency of LOCA/LOOP and LOOP/LOCA Accidents

Operating experience data were used to estimate the initiating-event frequencies associated with GSI-171 accident scenarios: LOCA/LOOP and LOOP/LOCA. Since the initiating-event frequencies associated with LOCA and LOOP have been studied separately in PRAs, this work focussed on estimating the probability of LOOP given a LOCA, and the probability of LOCA given a LOOP.

The probability of LOOP given a LOCA, as postulated in GSI-171, was estimated using automatic reactor scram and ECCS actuations as surrogate events for a LOCA (Table 1). Operating experience data relating to reactor trips, ECCS actuations, and LOOP events over ten years (1984 to 1993) were reviewed to obtain the estimates for PWRs and BWRs; they are averages over the population of each type of reactor. The average estimates can be significantly different for a plant which has a specific vulnerability to such an event. An example was the Palo Verde plant (Palo Verde Nuclear Power Plant, Dec. 1994) before an administrative control was implemented. Also, although ten years of data were evaluated, relatively few conditional LOOP events were observed which were used to obtain the estimates. The conclusions from this assessment can be summarized as follows:

1) The point estimates for the probability of LOOP given LOCA for BWRs and PWRs are, respectively, 6.0×10^{-2} and 1.4×10^{-2}, while the comparable probability of random occurrence of a LOOP given a LOCA is of the order of 10^{-4} or less.

2) There is an increased likelihood of LOOP given a LOCA compared to a random occurrence of LOOP; the estimates obtained for PWRs and BWRs are higher than a random occurrence probability by factors of approximately 70 and 300, respectively, but the range is comparable to, or less than, some previous estimates used for prioritization in GSI-171.

LOOP/LOCA scenarios are modeled in almost all IPEs, though concerns associated with GSI-171 are not addressed. Some IPEs, and some PRAs completed as part of the NUREG-1150 study were reviewed to obtain their frequency estimates. LERs were examined to obtain estimates for the probability of PORVs or SRVs to open subsequent to a LOOP. These estimates then were multiplied by the probability that the valve will be stuck or fail to close, to obtain an assessment for the stuck-open PORV or SRV, i.e., a small LOCA. The findings can be summarized as follows:

1) The estimates for stuck-open PORV or SRV subsequent to a LOOP, based on operating experience, are lower than those used in IPEs or other PRAs reviewed for this study.

2) The LOOP/LOCA frequency used in the IPEs or PRAs reviewed appear to be conservative.

Modeling and Quantification of LOCA/LOOP Accident Sequences

In this paper, a LOCA/LOOP accident, i.e., LOCA with delayed LOOP, in a nuclear power plant was analyzed and its risk impact estimated in terms of its contribution to core-damage frequency (CDF). Because a LOCA/LOOP accident, as postulated in GSI-171, involves several issues and unique combinations of failure mechanisms not routinely analyzed in a probabilistic risk assessment (PRA), new event-tree models were developed to analyze the progression of events leading to core damage. Quantification of the event tree to obtain CDF contributions involved assessing the probability of some parameters that are not quantified in PRAs, nor available elsewhere. As practical, in some cases (e.g., conditional probability of LOOP given LOCA, timing of LOOP given LOCA), available data were evaluated to obtain the probability estimates, whereas in other cases, (e.g., EDG overloading, lockout energization of circuit breakers due to their anti-pump circuits, pump overloading), the estimates were based on engineering judgments. These judgments were made from information given in NRC Info Notices, FSARs, and insights from reviewing LERs related to selected, relevant incidents that have occurred. A more detailed model was established of the electrical characteristics of EDGs and ECCS pumps to estimate their probability of damage due to an out-of-phase bus transfer. In general, because of the unique situation and conditions that were modeled for which operating experience data are not available nor expected, the evaluation involved engineering analyses, judgments, and several assumptions.

Table 1 Point estimate of LOOP probability given LOCA

A. Probability of LOOP given reactor trip

Plant Type	# Trip-Loop Events	# Trips	Conditional Probability of LOOP (A) (Grid Disturbance, Failure during bus transfer)
BWR	3	813	3.7×10^{-3}
PWR	7	1804	3.9×10^{-3}
Total	10	2617	3.8×10^{-3}

B. Probability of LOOP given ECCS actuations

Plant Type	# ECCS-LOOP Events	# ECCS Actuations	Conditional Probability of LOOP (B) (Safety-Bus undervoltage)
BWR	1	18	5.6×10^{-2}
PWR	1	100	1.0×10^{-2}
Total	2	118	1.7×10^{-2}

C. Probability of LOOP given LOCA

Plant Type	A	B	Probability of LOOP Given LOCA (A+B)
BWR	3.7×10^{-3}	5.6×10^{-2}	6.0×10^{-2}
PWR	3.9×10^{-3}	1.0×10^{-2}	1.4×10^{-2}
Total	3.8×10^{-3}	1.7×10^{-2}	2.1×10^{-2}

The evaluation was carried out for a PWR and a BWR plant based on their general characteristics, but using information from reference plants Sequoyah, and Peach Bottom, respectively. For both, various design characteristics were considered relating to loading the ECCS loads to offsite power, load-shedding, and reloading to EDGs; this allowed us to develop different plant groups since such characteristics significantly influence the CDF contribution in such an accident. In addition, we conducted sensitivity analyses to elucidate the dominating influence(s) to the CDF contribution in a particular plant group, and to observe the influence of the assumptions in estimating the parameters used in the quantification.

LOCA/LOOP Accident at a PWR Plant

The evaluation of PWR plants showed that the CDF contribution of a LOCA/LOOP accident can vary by two orders of magnitude (2.8×10^{-6}/yr to 1.2×10^{-4}/yr), depending on the design characteristics relating to the load-shedding/load-energization features in such an accident scenario (Table 2). The major conclusions relating to the PWR plants are summarized as follows:

Table 2 Sequoyah-like PWR: CDF contribution for different plant groups.

Plant Group	Energization Scheme From Offsite Power	Load Shed	Time Delay	Energization From EDG	CDF (/yr)			Dominant Contributor to CDF
					5th Percentile	Mean	95th Percentile	
1	Sequential	Implemented	Implemented or not	Inadequate sequence	4.3×10^{-7}	1.1×10^{-5}	4.4×10^{-5}	EDG overload
2	Sequential	Implemented	Implemented or not	Sequential	1.1×10^{-7}	2.8×10^{-6}	9.0×10^{-6}	Lockup of sequencers and/or lockup of circuit breakers of safety loads due to anti-pump circuits
3	Sequential	Not implemented	Implemented	(Non-intentional) Block-loading*	5.8×10^{-7}	1.8×10^{-5}	6.0×10^{-5}	EDG overload and/or lockup of sequencers
4	Sequential	Not implemented	Not implemented	(Non-intentional) Block-loading*	1.0×10^{-6}	2.5×10^{-5}	9.4×10^{-5}	EDG overload and/or damage of pump motors and/or lockup of sequencers
5	Block-loading	Implemented	Implemented or not	Inadequate sequence	1.6×10^{-6}	4.3×10^{-5}	1.8×10^{-4}	EDG overload
6	Block-loading	Implemented	Implemented or not	Sequential	4.1×10^{-7}	1.4×10^{-5}	5.6×10^{-5}	Lockup of circuit breakers of safety loads due to anti-pump circuits
7	Block-loading	Not implemented	Implemented	(Non-intentional) Block-loading*	3.4×10^{-6}	9.1×10^{-5}	3.3×10^{-4}	EDG overload
8	Block-loading	Not implemented	Not implemented	(Non-intentional) Block-loading*	5.0×10^{-6}	1.1×10^{-4}	3.9×10^{-4}	EDG overload and/or damage of pump motors

* Block-loading because load-shed is not implemented

1) For some combination of design characteristics, the CDF contribution can be of the order 1.0×10^{-4}/yr., particularly in plants using block-loading to the offsite power and block-loading to the EDG following a LOOP without a load shed. Identifying specific plants with these features was not within the scope of this project.

2) Plants where sequential loading to offsite power and the EDG is used along with load-shedding appear better equipped to handle this accident; their CDF contribution is about 3×10^{-6}/yr.

3) Plants which use a combination of block- and sequential-loading schemes have CDF contributions about 2×10^{-5}/yr.

4) Sensitivity analyses show that the dominant contributors to risk from a LOCA/LOOP accident are EDG overloading and lockout of circuit breakers due to their anti-pump circuits. Design features which avoid failures from those concerns will significantly reduce the CDF contribution. These aspects may be further explored to identify and eliminate conservatism associated with their evaluation.

5) Some plants may have specific vulnerabilities. Examples relate to operating with switchyard undervoltage that may increase the probability of a delayed LOOP and overloading of pumps, the specific design of load sequencers making lockup in such a scenario highly likely, and the setting in anti-pump circuits causing increased likelihood of lockout of circuit breakers of safety loads. Such vulnerabilities further increase the CDF contributions of LOCA/LOOP accidents.

6) A comparison of our results with those obtained in earlier studies shows that, similar to previous evaluations, for some plants the risk contribution for such an accident remains high, but our calculated contributions are generally lower than, or comparable to, previous ones. Earlier studies only considered the damage to EDG and ECCS pumps. Present modeling and analyses evaluated the relative impacts of different issues identified as part of GSI-171 which showed that EDG overloading and lockout of circuit breakers due to their anti-pump circuits dominate the risk contribution, and focussing on them can reduce the impact of such an accident.

LOCA/LOOP Accident at a BWR Plant

The evaluation of a BWR plant showed that, similar to the PWR plants, the CDF contribution of a LOCA/LOOP accident can vary by orders of magnitude and depends on similar design characteristics, i.e., load shedding, and load energization features (Table 3). Our insights on differences and similarities can be summarized as follows:

1) The CDF impact of a LOCA/LOOP accident for most BWR plants (6.1×10^{-7}/yr to 3.1×10^{-5}/yr) is about an order of magnitude lower than PWR plants.

2) Similar to PWR plants, BWRs that block-load to offsite power in response to a LOCA, and block-load to the EDG without load-shed in response to a LOOP are the most vulnerable; the relative impact of other design features is similar to that observed for PWRs.

3) Similar to PWR plants, EDG overloading and lockout of circuit breakers due to their anti-pump circuits dominate the risk contributions; these concerns can be addressed to further reduce risk.

4) Similar plant-specific vulnerabilities may exist for BWR plants, and there, CDF contributions will be higher.

Table 3 Peach Bottom-like BWR: CDF contribution for different plant groups.

Plant Group	Energization scheme to Offsite Power	Load Shed	Time Delay	Energization to EDG	CDF (/yr)			Dominant Contributor to CDF
					5th Percentile	Mean	95th Percentile	
1	Sequential	Implemented	Implemented or not	Inadequate sequence	3.8×10^{-8}	2.8×10^{-6}	1.3×10^{-5}	EDG overload
2	Sequential	Implemented	Implemented or not	Sequential	4.5×10^{-9}	4.5×10^{-7}	1.8×10^{-6}	Lockup of sequencers and/or lockup of circuit breakers of safety loads due to anti-pump circuits
3	Sequential	Not implemented	Implemented	(Non-intentional) Block-loading*	5.8×10^{-8}	3.7×10^{-6}	1.6×10^{-5}	EDG overload and/or lockup of sequencers
4	Sequential	Not implemented	Not implemented	(Non-intentional) Block-loading*	7.5×10^{-8}	6.2×10^{-6}	2.4×10^{-5}	EDG overload and/or damage of pump motors and/or lockup of sequencers
5	Block-loading	Implemented	Implemented or not	Inadequate sequence	1.2×10^{-7}	9.9×10^{-6}	4.0×10^{-5}	EDG overload
6	Block-loading	Implemented	Implemented or not	Sequential	2.0×10^{-8}	2.0×10^{-6}	7.9×10^{-6}	Lockup of circuit breakers of safety loads due to anti-pump circuits
7	Block-loading	Not implemented	Implemented	(Non-intentional) Block-loading*	3.4×10^{-7}	2.0×10^{-5}	7.8×10^{-5}	EDG overload
8	Block-loading	Not implemented	Not implemented	(Non-intentional) Block-loading*	3.4×10^{-7}	2.1×10^{-5}	7.7×10^{-5}	EDG overload and/or damage of pump motors

* Block-loading because load-shed is not implemented

4 CONCLUSIONS

A technical evaluation was conducted for Generic Safety Issue (171) which addresses two types of accidents: LOCA with consequential or delayed LOOP (LOCA/LOOP), and LOOP with consequential or delayed LOCA (LOOP/LOCA). A review of selected IPEs shows that they do not address the unique issues associated with these accident sequences. LOOP/LOCA accidents are addressed more fully by IPEs than LOCA/LOOP ones. We analyzed LOCA/LOOP accidents further by developing event-tree/fault-tree models to quantify their contributions to core-damage frequency (CDF) in a pressurized water reactor and a boiling water reactor. Engineering evaluation and judgements are used during quantification to estimate the unique conditions that arise in a LOCA/LOOP accident. The results show that the CDF contribution of such an accident can be a dominant contributor to plant risk, although BWRs are less vulnerable than PWRs.

5 REFERENCES

1. LER No. 93-004-00, "Clinton Power Station Unit 1, Failure of Shutdown Service Water System to Automatically Restart During Emergency Diesel Generator/Emergency Core Cooling System Testing Due to Breaker Contact Sequencing," Nov. 19, 1993.

2. Letter from R. Hill to USNRC Document Control Desk, "Information Regarding 480V Safety Injection Pump Circuit Breaker Design, Indian Point 3 Nuclear Power Plant," April 4, 1994.

3. Letter from E.L. Jordan (AEOD) to D.F. Stenger and R.E. Helfrich (Winston & Straun), April 12, 1994, "NRC Information Notice 93-17."

4. Martinez-Guridi, G., P.K. Samanta, T-L. Chu and J.W. Yang, "Evaluation of LOCA with Delayed LOOP and LOOP with Delayed LOCA Accident Scenarios," NUREG/CR-6538, BNL-NUREG-52528, June 1997.

5. NRC Information Notice 84-69, "Operation of Emergency Diesel Generators," August 29, 1984.

6. NRC Information Notice 84-69, Supplement 1, "Operation of Emergency Diesel Generators," February 24, 1986.

7. NRC Information Notice No. 88-75, "Disabling of Diesel Generator Output Circuit Breakers By Anti-Pump Circuitry," Sept. 16, 1988, Supplement 1, April 17, 1989.

8. NRC Information Notice 92-53, "Potential Failure of Emergency Diesel Generators Due to Excessive Rate of Loading," July 29, 1992.

9. NRC Information Notice 93-17, "Safety Systems Response to Loss of Coolant and Loss of Offsite Power," March 8, 1993.

10. NRC Information Notice 93-17, Revision 1, "Safety Systems Response to Loss of Coolant and Loss of Offsite Power," March 25, 1994.

11. NRC Memorandum from B. Sheron to L.C. Shao, "Proposed Generic Issue on Safety Systems' Response to the Sequential Occurrence of LOCA and Loss of Offsite Power Events," February 17, 1995.

12. NRC Memorandum from D.L. Morrison to L.C. Shao, Attachment 1, "Prioritization Evaluation - Issue 171: ESF Failure from LOOP Subsequent to LOCA," June 16, 1995.

13. NRC Memorandum from M. Cunningham to C. Serpan, "Evaluation of Assumptions Used in Generic Issue 171 Prioritization," October 18, 1995.

14. NRC Information Notice 96-45, "Potential Common-Mode Post-Accident Failure of Containment Coolers," August 12, 1996.

15. Palo Verde Nuclear Power Plant, "Statistical Analysis of the 525 kV Line Undervoltage Probability, Rev. 1," December 16, 1994.

16. Palo Verde Nuclear Power Plant, Event Number 28210, January 5, 1995.

17. Virginia Electric and Power Company, "Surry Power Station Units 1 and 2 Emergency Diesel Generator Sequencing," Final Summary Report, May 1989.

Environmentally Assisted Degradation of LWR Components: Session Overview

M. B. McNeil and A. L. Lund
Office of Nuclear Regulatory Research
U.S. Nuclear Regulatory Commission

ABSTRACT

In the area of environmentally assisted cracking (EAC) of piping and vessel steels, much information exists on environmental effects on materials used in light water reactors (LWR). Current research in EAC is primarily directed at addressing how these data can best be used to evaluate realistic stress histories in real reactor situations. For example, collection of crack growth data on nickel alloys in simulated reactor environments has begun, but there are currently insufficient data, and an inadequate understanding of mechanisms, to satisfy regulatory needs. Work on analyzing, benchmarking, and validating existing industrial crack growth computer programs is just beginning. Most importantly, while a considerable body of data on irradiation assisted stress corrosion cracking exists, the fundamental mechanistics are not well understood and it is not yet possible to predict susceptibility to irradiation assisted stress corrosion cracking (IASCC) or residual life in reactor components subject to IASCC.

Historically, the study of EAC phenomena which might degrade safety systems has been focused primarily on boiling water reactor (BWR) primary system piping and reactor vessel internals. EAC of BWR recirculation piping was significant enough to warrant either replacements or substantial repairs of piping in many plants during the middle 1980's. More recently, EAC in reactor internals has raised moderate concerns with regard to maintaining adequate safety margins. When EAC is detected, repairs are often possible and have been implemented in many cases. Future research activities are focused on improvements in predictive capabilities, by better understanding the fundamental mechanisms of EAC.

In order to maintain a sound technical base in the area of environmental degradation for timely rulemaking and related decisions in support of NRC regulatory/licensing/inspection activities, the NRC has a continuing formal commitment to the Electric Power Research Institute (EPRI) Cooperative IASCC Research (CIR) program and less formal involvement with another IGSCC/IASCC international collaboration and with various other American Society of Mechanical Engineers (ASME)-based international cooperative activities. One of the presentations in this session will describe the CIR program in more detail. Two other speakers will discuss the specific environmentally assisted degradation issues specific to BWRs and pressurized water reactors (PWR) in more detail. And finally, another talk will be given on NRC funded research in LWR materials and evaluation of EAC computer codes.

INTRODUCTION:

Environmentally assisted cracking (EAC) has been a problem for many classes of materials for a very long time. The most famous example is "season cracking" of copper alloys caused by reduced nitrogen species such as ammonia and thiosulfate[1]. The most famous example of the phenomenon is the crack in the liberty bell, which occurred when it was inadvertently stored in the presence of decaying organic material associated with stables. Another important practical example of environmentally assisted cracking is that fatigue lives in a chemically active environment may be much less than lives for identical specimens measured in a laboratory atmosphere. A famous example of this was an epidemic of Navy cables which fractured in seawater service after far shorter lives than had been anticipated from laboratory tests.

The prevalence of EAC in reactors has, however, always exceeded the expectations not only of the manufacturers of systems but also of the scientists involved in research and materials selection. It has become, in the words of Peter Ford, "The engineer's nightmare and the scientist's meal ticket".

There are several reasons for this. It is trivial to say that one could not know what the properties of high-fluence materials would be until one had accumulated materials with high fluence, but the point is a little subtler than that. In the 1950s, when many of what is now the older generation of materials scientists were being trained, it was generally thought that radiation damage saturated at fairly low levels and annealed fairly quickly. For example, the review of radiation damage in metals by Seitz and Koehler [2] was, at one time, a fairly standard reference, and it places heavy emphasis on the ease of annihilation of point defects. Even when it was realized that these defects were likely to produce black dots and other long-lived damage, the damage was regarded as only affecting the topology of the lattice. It was not until quite recent times that serious attention began to be paid to non-equilibrium segregation in general[3,4] and radiation-induced segregation in particular[5] Another factor is that corrosion scientists and engineers, used to working with waters of much higher ionic strength, underestimated the aggressiveness of reactor coolants and the effect of radiation on coolant chemistry. A third factor is that, when many people in this audience took nuclear engineering, it was assumed that the workmanship of nuclear reactors would be so good that no attention need be paid to flaws; the question of flaw tolerance and the effect of flaws on material degradation is a relatively new one.

As reactors age, of course, not only does the fluence in the maximum-fluence parts increase, but also the fluence in components which, in a relatively new reactor, are not high-fluence components: the core shroud and top guide of a BWR, for example. Consequently, the scope of EAC issues is continually broadening. Furthermore, the need to repair components has introduced a new variable: how does repair, especially weld repair, affect the EAC behavior of a material under reactor conditions, and what information does one need to answer the regulatory questions which arise from weld repairs?

GENERAL PLAN:

The core of the program is the ongoing research at Argonne National Laboratory, which will be described later by Dr. Shack. This is supplemented by major international interactions. One of the primary international activities is the Cooperative IASCC Research

(CIR) program managed by EPRI, which will be described by Dr. Nelson; NRC also has participated for many years in other international groups in IASCC and IGSCC, and in addition has cultivated direct informal contacts with scientific groups in other countries.

Another significant activity has been to put this research into the context of non-reactor-related research. Many of the issues which are of importance are not peculiar to the reactor world, and especially not to the LWR world. For example, IASCC is intimately connected both with grain boundary segregation [4,6,7], with irradiation-induced segregation[8], with the characteristics of grain boundary distributions [9], and with grain boundary triple line research [10]. The ability to draw on the research of groups like this to improve understanding of EAC in reactors is very important. We cannot afford duplication when we cannot afford to do the things unique to reactor applications!

The development process of the confirmatory aspect of the NRC research program is as follows. The Office of Nuclear Reactor Regulation identifies areas in which additional research is required to provide them with the basis for assessing present or anticipated licensee submittals and sends a "User need letter" to the Office of Nuclear Regulatory Research requesting that research be done in these areas. In consultation with NRR staff, RES staff then prioritize these needs in the light of budgetary considerations and contract for the research. The results of this research are then provided to NRR, and are communicated to the general scientific and engineering community through NUREG reports and journal articles. The rate-determining step is usually the actual experimentation.

In order to provide results in a timely fashion, NRR and RES attempt to "get ahead of the wave", to initiate necessary research well before the time the results are required. This has not been uniformly successful; while NRC has managed, in this area, to avoid the trap of doing research and then finding that the results are not required, there have been a number of cases (core shroud cracking being an example) when the practical problem presented NRC with the necessity to take regulatory actions before the research program was fully mature. RES management is attempting to improve its batting average on this point, but perfection is not possible. NRC is, however, addressing a number of problems in the areas of PWR IASCC and BWR core shroud support structures where there is reason to expect that problems lie ahead.

RESEARCH NEEDS:

The research program of the Nuclear Regulatory Commission can address very few issues, and so it has had to be focused carefully on those areas of EAC where the Commission is faced with major regulatory decisions involving major uncertainties. In recent years, the program has addressed the following general areas:

Environmental effects on fatigue lives and cumulative usage factors (CUFs) of steel reactor components

Crack growth rates in primary-side Ni alloys

Component degradation by IASCC

Core shroud cracking

Assessment of industry crack growth models

Evaluation of consequences of thermal processing.

Research efforts in these areas were prompted by widespread observations of cracking in LWR components, most notably in PWR steam generators and BWR in-vessel components. In very recent time the program has been expanded to cover underwater welding of irradiated structures. This, still primarily a matter of literature study and efforts to learn from research sponsored by the Department of Energy (DOE) Office of Fusion Energy, is driven by the observation that mechanical approaches such as the clamp/rod systems used for BWR core shrouds cannot be applied to all repair needs for in-vessel components. For this reason, there has been a great deal of interest in developing repair strategies for cracked high-fluence components, attachments, and weldments in situations where mechanical repairs are not feasible for reasons of configuration or economics.

EXPERIMENTAL STRATEGIES:

The general thrust of NRC's regulatory research in this area is to do confirmatory research; that is, research which provides data necessary to assess submittals by licensees. There are three major areas represented. First, it is necessary to collect data which determine the conservatism (or lack of conservatism) in existing data bases. It is critical that regulatory decisions be based on the very best available data, and the scatter in EAC data, especially in nuclear applications, is a major problem. Part of this problem is a matter of technique and part of it reflects such issues as heat-to-heat chemistry variations, grain boundary structure effects, etc. Second, it is important for NRC to be able to assess the appropriateness of models and codes being used for such purposes as estimation of residual life. Third, it is necessary for NRC in some cases to determine the implications of observed cracking for future behavior, mitigation and inspection; in other words, to maintain an independent capability for extrapolation, for getting ahead of the curve of EAC in aging reactors.

PRESENT ACTIVITIES:

The details of the research program will be covered in papers given elsewhere in this meeting, so this review will be limited to thumbnail sketches of the most important ongoing activities.

Environmental effects on fatigue lives and cumulative usage factors was listed as a research need, and has been the focus of ongoing research funded by the NRC. A significant question has been whether ASME S-N curves are adequately conservative if one uses the factors of 2 in stress/20 in cycles to account for the effects of scale, surface finish, environment, etc. These factors are conservative for the effects of the variables for which they were intended, but the environmental effects thought of in these factors were atmospheric chemistry/cleanliness factors and not water-chemistry factors. A presentation from Argonne National Laboratory elsewhere in this meeting summarizes the results up to date of this work, and how it has been used in calculating cumulative usage factors (CUFs).

A second major area of research has been in the determination of cracking characteristics of high-Ni alloys. This has been a difficult and complex issue. A goal of this program is to identify the alloy/component characteristics which lead to highly variable results for nominally similar materials.

In addition, ANL has a long-standing research program on irradiation-assisted stress corrosion cracking (IASCC); this is also the subject of the EPRI-administered Cooperative IASCC Research program, which will be described in detail later.

The fundamental problem addressed by these programs is that, while Cr depletion clearly plays a central role in IASCC, it is equally apparent that less obvious phenomena can make major differences in IASCC behavior. The research on minor impurities such as sulphur, oxygen, and fluorine, will be described in the Argonne paper. There is also evidence from recent work[11] that the geometry of the grain boundaries plays a role. Research in non-IASCC applications[9] has shown that high fractions of the so-called special grain boundaries (coherent twins, low angle tilt and twist boundaries, and other boundaries where the grain-to-grain mismatch is not great) have a major effect on cracking behavior, and grain-boundary analysis may reduce the apparent inconsistencies in IASCC data.

A major source of uncertainty in regulatory decisions has been the problem of estimating the rate of growth of cracks in in-service components. This is critical not only to decisions on residual-life questions but also on inspections. Improvements in water chemistry in recent years, and especially the availability of hydrogen-water chemistry for BWRs, has made it necessary to have better techniques for estimating these crack growth rates. There are several codes being used by licensees, and NRC's contractors are studying them carefully, trying to reach an optimum decision on new disposition curves.

There is also a major program at ANL for determining how crack growth in high-Ni alloys is affected by alloy chemistry, microstructure, and other variables in PWR and BWR environments. This is of particular importance considering the use of 690 as a substitute for 600, and some of the problems with X-750 and other alloys.

Recent attention has been focused on the feasibility of welding high-neutron-fluence materials, which presents problems not only because of helium-induced cracking, but also possibly because of other aspects of radiation damage. The problem is even more complex because much of the welding must be done remotely under water. Research by several groups (most supported by DOE Office of Fusion Energy) has indicated that at least the helium-induced cracking aspects of the problem can be mitigated by improved welding techniques involving low energy input and stress relief. A literature survey on this topic[12] has been issued, and NRC continues to study regulatory issues in this field.

FUTURE ACTIVITIES:

Work on the topics identified as the NRC research needs will continue, although the work on piping and vessel steels is gradually winding down. This is not so much because it is not important but because other problems appear to present more pressing regulatory

issues. The NRC research staff and contractors are going to be doing more research on IASCC of PWR components, on welds and heat affected zone problems, and on repair problems. The challenge in the time ahead will be to incorporate these findings into predictive capabilities that can be used to assess the effects of aging and address the issues surrounding life extension. Certainly, this predictive capability will be enhanced by the research efforts, funded by the commercial nuclear industry, to develop better EAC models and computer codes in tandem with the development of more sophisticated on-line monitoring techniques. It also appears that more attention will be paid to the effects of grain boundary structure on component degradation, residual life, and inspection issues. Having said this, it is necessary to finish on a cautionary note. The purpose of this program is to supply research results needed for regulatory purposes, so the program is at the mercy of components in operating reactors, and may have to be significantly altered if (or when) unanticipated problems arise or existing problems prove to be more threatening or immediate than they appear at present.

REFERENCES:

1. A.J. Forty, "The Initiation and Propagation of Cracks in Brass", in "The Physical Metallurgy of Stress Corrosion Fracture", ed. T. Rhodin, The Metallurgical Society, New York, 1959.

2. F. Seitz and J. F. Koehler, "Displacement of Atoms During Irradiation", in Solid State Physics vol. 2, Academic Press, New York, 1956.

3. K. T. Aust, R. E. Hanemann, P. Niessen, and J. H. Westbrook, Acta Metallurgica vol. 19 pp 291-302 (1968).

4. E. D. Hondros and M. P. Seah, "Interfacial and Surface Microchemistry" in "Physical Metallurgy (Third Edition)", R. W. Cahn and P. Haasen, eds., North-Holland, Amsterdam 1983.

5. W. Widersich, P. R. Okamoto, and N. Q. Lam, J. of Nuclear Materials vol. 83 pp 98-108 (1979).

6. E. Rabkin, Materials Letters vol. 25 pp 199-204 (1995).

7. D. Udler and D. N. Seidman, Materials Science Forum vols. 155-6 pp 189-208 (1994).

8. T. R. Allen, D. L. Damcott, G. S. Was, and E. A. Kenik, "Radiation-Induced Grain Boundary Segregation in Proton-Irradiated Austenitic Iron and Nickel-Based Alloys" in Proceedings of the Seventh International Symposium on Environmental Degradation of Materials in Nuclear Power Systems, NACE, Houston, Texas (1995).

9. K. T. Aust, "Future Trends in Grain Boundary Engineering" in Grain Boundary Engineering, U. Erb and G. Palumbo, eds., Canadian Institute of Mining, Metallurgy, and Petroleum, Montreal 1994.

10. V. Randle, Modeling and Simulation in Materials Science and Engineering vol. 5 pp 117-127 (1997).

11. Y. Pan et al., Acta Mater. vol. 44, pp. 4685 - 4695 (1996).

12. A. L. Lund, "Underwater Welding of Highly Irradiated In-Vessel Components of Boiling Water Reactors: A Literature Review," NUREG-1616, U.S. Nuclear Regulatory Commission, In publication.

Fundamental Understanding and Life Prediction of Stress Corrosion Cracking in BWRs and Energy Systems

Peter L. Andresen and F. Peter Ford
GE Corporate Research and Development Center
Schenectady, New York 12301

ABSTRACT

Numerous well documented instances of environmentally assisted cracking exist in various energy-related industries involving various subcomponents of boilers, steam turbines, piping, pressure vessels, pressurizers, steam generators, deaerators, etc. The common element in these cracking incidents is exposure in high temperature water of various materials such as austenitic stainless steels, nickel base alloys, turbine steels, low alloy and carbon steels, and their weld metals. Because of the large economic and potential safety consequences, there is a strong driving force to derive design and life prediction codes that account for the multitude of material, stress, and environmental combinations relevant to individual plants.

The proper conceptual understanding of crack advance and the crack tip system is an essential precursor to predicting and controlling environmental cracking. This conceptual framework must, of course, be confirmed by critical experiments, then the essential fundamental processes quantified to create, ideally, a deterministic model for life prediction. A fundamental framework is acknowledged as essential, because the variables that affect environmental cracking are so numerous and inter-dependent that factorial (or other designs for) experiments are hopelessly expansive. Once a solid conceptual understanding is established, its use to conceive and evaluate mitigation approaches is very powerful, and its extension to related materials and environments straightforward.

The objective of this paper is to present an approach for design and lifetime evaluation of environmental cracking based on experimental and fundamental modeling of the underlying processes operative in crack advance. In detailing this approach and its development and quantification for energy (hot water) systems, the requirements for a life prediction methodology will be highlighted and the shortcomings of the existing design and lifetime evaluation codes reviewed. Examples are identified of its use in a variety of cracking systems, such as stainless steels, low alloy steels, nickel base alloys, and irradiation assisted stress corrosion cracking in boiling water reactor (BWR) water, as well as preliminary use for low alloy steel and Alloy 600 in pressurized water reactors (PWRs) and turbine steels in steam turbines. Identification of the common aspects with environmental cracking in other hot water systems provides a secure basis for its extension to related energy systems.

INTRODUCTION

Stress corrosion crack initiation and subcritical growth in structural materials from the combined presence of tensile stress, "susceptible" material, and "aggressive" environment have been recognized for many years, and the mechanisms widely investigated [1-10]. This is particularly true in concentrated environments (e.g., chlorides, phosphates, hydroxides, etc.), either in bulk environments (e.g., in paper, chemical, petrochemical, and marine industries) or in localized environments (where boiling and potential or thermal gradients concentrate species). However, it is now recognized that environmental cracking under static or cyclic loading (i.e., stress corrosion or corrosion fatigue) can occur in high purity

water, e.g., where the total impurity level is below 10 ppb. Although the cracking susceptibility is generally lower than in concentrated environments, it is sufficient to cause concern when extended lives or high plant availability is required, as in the power generation industry, and especially for light water reactors (LWRs). This paper focuses on high temperature water environments (Figure 1) associated with energy systems, including high purity water environments relevant to boiling water reactors (BWR) and pH-buffered chemistries relevant to pressurized water reactors (PWR).

Environmental cracking in high temperature water has been documented for austenitic stainless steels, nickel base alloys, turbine steels, low alloy and carbon steels, and their weld metals in piping, pressure vessels, pressurizers, steam generators, steam turbines, boilers, deaerators, etc. (Figure 1). Consequently, there is a strong driving force to derive design and life prediction codes that address the scatter in cracking response associated with the broad range of material, stress, and environmental combinations relevant to these systems (e.g., Figures 2 - 4) rather than attempt to use mechanics-based codes that ignore the dominance in the contributions of the material and environment. Studies in high temperature have posed difficulties for the experimentalist, as it is not easy to adequately control the conditions (e.g., water purity, material / microstructure, loading, etc.) and to measure crack growth rates with sufficient sensitivity for cracking that slowly proceeds over a typical 40 year design life.

As a result, existing life prediction codes for environmental cracking in high temperature water usually represent an upper bound of the available data, and do not account for the wide range of material / environment conditions within a "nominal" system (Figures 3 and 4). This conservative "upper-bound" scenario can put unreasonable constraints on continued operation, especially of plants that operate under better conditions than those represented by the empirical design or life evaluation code. In other cases, life prediction codes do not exist either because of excessive scatter in the data (e.g., stress corrosion of low alloy pressure vessel steels, Figure 4) or because of lack of relevant data (e.g., irradiation assisted stress corrosion cracking of stainless steel).

Essential ingredients of any comprehensive life prediction methodology include:

- treatment of the continuum in material, environment, and stress;
- treatment of time dependent crack growth to encompass the continuum from static, to slow strain rate, to cyclic loading;
- unified approach for crack initiation and growth, which requires understanding of short crack behavior;
- fracture mechanics and crack chemistry similitude for relevance to varying component geometries and loading conditions;
- calculational approaches for complex service conditions which require accounting for the time and through-thickness variations in properties, and the use of distributions in properties as well as probabilistic approaches;
- integrated predictive modeling and on-line monitoring of system behavior;
- extensibility into related cracking systems.

The current design and lifetime evaluation procedures (e.g., ASME Section III and XI) for power generation components are inadequate by these standards. The approach described in this paper incorporates the elements outlined above, and has been developed by identifying the conceptual elements and fundamental mechanism of environmental crack advance, then independently evaluating the underlying parameters. On this basis, predicted subcritical crack growth rates are obtained for different combinations of environment (e.g., dissolved oxygen, hydrogen, and hydrogen peroxide; impurity concentration; radiation flux), material (e.g., thermal or radiation-induced sensitization, sulfur content), or stress, (e.g., static, monotonically increasing, and cyclic load). Short crack studies address the transition between crack initiation and growth, as well as crack tip chemistry similitude issues. The

complex variations of properties vs. time and thickness are accounted for using computer codes that incrementally integrate these effects over elapsed time and crack depth. Ranges in distributions (e.g., mean, upper, and lower limits) are easily input into the model, and a variety of approaches have been used for statistical and probabilistic treatment. Direct measurements from system monitors have been used to fine tune the model by providing improved characterization of specific system conditions, or to calibrate the overall model prediction using in-situ, on-line measurements of crack growth in reference components or specimens. Predictions have been compared with observed data to evaluate the quantitative validity of the original working hypothesis and modeling algorithms. The power and flexibility of a conceptually accurate, fundamentally based model is also shown in its extensibility to related systems, ability to treat previously unevaluated parameters, and ability to help identify novel mitigation techniques.

CONCEPTUAL SIMILARITES AMONG HOT WATER SYSTEMS

Undoubtedly the most extensive fundamental and predictive modeling work has been undertaken for BWR systems, which employ "pure" water containing radiolytically formed oxidants [8-28]. However, conceptual similarities among all hot water systems are high, and the differences associated with addressing PWR and other "non-pure water" systems from a common perspective tend to be over-stated, probably originating from early interpretations that viewed each new observation of environmental cracking in a given material, water chemistry, or temperature as an entirely unique phenomenon. Most differences are associated, not with obvious, fundamentally different crack advance mechanisms, but with considerations that must logically be factored into any predictive framework. For example, the absence of a potential gradient between crack mouth and tip in some PWR systems is merely a special case of the varying potential gradient which is consistently treated in BWR systems. While water chemistry / pH, temperature, etc., differences do exist in various hot water systems, there are many areas of commonality in the fundamental processes, parametric dependencies, cracking phenomenology, and experimental approaches for isolating and quantifying the critical parameters. The following similarities in BWRs and PWRs provide examples of the underlying linkage that exists among all hot water systems:

Effects of Corrosion Potential. The range of corrosion potentials that exist in BWRs is large, especially with the increasing use of hydrogen water chemistry, which lowers the dissolved oxygen concentration and corrosion potential. Laboratory data and predictions show a continuum in environmental cracking behavior vs. corrosion potential, even down to conditions (e.g., hydrogen deaerated water) that represent a thermodynamic minimum corrosion potential (e.g., –0.52 V_{she} for the H_2 / H_2O in neutral, 288°C water).

Further, the corrosion potential near the crack tip is always low in both BWR and PWR systems, since oxygen is always fully consumed within the crack (typically near the crack mouth, even for short cracks and under irradiated conditions, etc., Figure 5 [17,26,27]). Differences in crack tip corrosion potential do exist, primarily as a result of variations in pH and hydrogen fugacity; the corrosion potential in deaerated water is usually controlled by the H_2 / H_2O line (Figure 6 [29]), which is dependent primarily on pH and hydrogen fugacity. Thus, any claim that cracks advance by a different *mechanism* in BWRs vs. PWRs because of the high corrosion potential in BWRs (e.g., 0 to +0.3 V_{she}) may be largely based on this misconception.

Finally, the gradients in corrosion potential (from crack mouth to tip, e.g., from differential aeration, Figure 5) characteristic of cracks in BWRs do not represent a unique condition, since, e.g., thermal gradients common to PWRs can also have a similar effect on, e.g., crack chemistry as that due to potential gradients. Also, potential gradients in crevices and cracks probably exist in many hot water systems; for example, copper ion, lead ion, and oxygen in-leakage can all increase the corrosion potential in PWR steam generators.

Role of Metal Ion Solubility. The crack chemistries and associated metal ion solubilities don't differ that dramatically between BWRs and PWRs (Figure 7). In PWRs the pH is buffered and there is little opportunity for pH shifts (or any chemistry shift from the bulk value) in the absence of large potential or thermal gradients; however, even in BWRs operating under "normal water chemistry" the shift in pH is generally small [15,17,26,27] because the typical bulk impurity concentrations are low (well below than the OH^- and H^+ concentrations in 288°C pure water of $\approx 2.3 \times 10^{-6}$ M, i.e., $pH_{288C} = 5.63$).

Further, dissolved iron, chromium, and nickel species are quite insoluble in high temperature, near-neutral water [30,31] and thus corrosion and metal ion formation within the crack neither permit a thermodynamic (Nernstian) equilibrium concentration of metal ions to form (so that dissolution "stops") nor directly contribute to charge balancing (e.g., of Cl^-) in the crack (hydrolysis of low solubility metal ions does produce H^+, which can charge balance Cl^-, and produce acidification). This contrasts with, e.g., concentrated acidic or caustic environments, especially at lower temperatures, where the solubility of metal ions can be sufficiently high to permit a Nernstian equilibrium concentrations of metal ions to be achieved in some instances; subsequent dissolution requires a decrease in metal ion concentration by mass transport out of the crack. Such metal - metal ion equilibrium conditions aren't achievable for iron and chromium in typical hot water environments, and only under special circumstances for nickel.

Effects of Sensitization. The effect of sensitization in stainless steels or nickel-base alloys is often cited as a major difference between environmental cracking in BWRs and PWRs. However, as observed in both crack growth and repassivation measurements, no effect of sensitization is observed in BWR water (as in PWR water) if significant pH shifts are avoided in the crack tip environments, e.g., by lowering the corrosion potential or buffering the pH. The role of Cr at higher pH or with substantial S^{2-} present is not as clear, although the S^{2-} level at which repassivation is diminished, and crack growth rates enhanced, doesn't appear to shift that much with the Cr concentration in the alloy [32-35]. However, apart from its "chemical" (repassivation) role, Cr can have marked effects on the slip character and creep behavior. Also, the effect of carbide distribution and morphology may have significant effects on slip localization, e.g., near grain boundaries. The role of Cr, Ni, Fe, C, N, etc. on creep rates is very important, with creep rates going up dramatically for nickel base alloys (compared to stainless steels), low C alloys, increasing temperature, and in the environment [36,37].

Effects of Specific Anions. Most of the effects of specific anionic impurities on crack growth has been attributed to their ability to shift the crack tip pH, although it is also clear that S^{2-} species can directly inhibit complete repassivation [32-35], as will be discussed later. Species such as sulfate and chloride, whether present in the bulk solution as acids or salts, are able to promote acidity in the crack in the presence of a potential gradient (e.g., differential aeration cell), and thereby cause a significant increase in crack growth rate. Species such as $NaOH$ or KOH can only support an alkaline shift in the crack, because acidification (increased H^+) can only occur when an anion other than OH^- exists at an adequate concentration, because the presence of water fixes the relative concentrations of H^+ and OH^- ($pK_{25C} = 10^{-14}$, $pK_{288C} = 10^{-11.26} = [H^+] \times [OH^-]$).

Species such as CrO_4^{2-} and NO_3^- are not thermodynamically stable in the crack (although for kinetic reasons, they may persist to varying extents); thus, they should reduce to Cr_2O_3 and NH_4^+ and have a much lesser effect on environmental cracking, as is observed [26,27,38]. Nitrate is a particularly interesting species, because its anionic character causes it to be drawn into the crack by the potential gradient (Figure 5); once in the low potential crack environment, it will reduce to the ammonium cation, which is pushed out of the crack by the potential gradient [27,39]. Also, the effect on the corrosion potential of species that undergo redox reactions can't be ignored, although at typical ionic concentrations in water containing oxygen, their role in shifting corrosion potential is very limited.

These effects can be rationalized in terms of the dependence of metal oxide solubility on pH. As the crack tip pH shifts from neutral (the position of minimum metal oxide solubility) the quantity of precipitated oxides decreases and the rate-controlling liquid diffusion kinetics for oxidation, or crack advance, is increased. Other phenomena may have an additional role; for example, at neutral and higher pHs, the presence of S^{2-} (by addition, dissolution of MnS, or reduction of sulfate, sulfite, etc.) affects passive film stability and repassivation kinetics [32-35], as will be discussed later. Of course, non-ionic species (especially hydrogen for nickel alloys) can also be important, especially since hydrogen (alone) is effectively not consumed in the crack (in contrast to oxygen and hydrogen peroxide, which are rapidly consumed) and can shift the crack tip potential.

Overall Continuum in Response. Experimental data and modeling predictions show a continuum in behavior for the transitions (1) in water chemistry (e.g., from aerated to deaerated water, from nitrogen deaerated water to increasing hydrogen levels); (2) in temperature; (3) in cracking morphology (intergranular to transgranular), (4) in loading (fully constant load; constant displacement load; slow strain rate; constant load with periodic unloading; high load ratio, slow cyclic loading; high ΔK, high frequency cyclic loading); (4) in material and heat treatment; etc. This continuum in cracking response is now predicted by evaluating various cracking mechanisms.

EVALUATION OF CRACKING MECHANISMS

Environmental cracking has historically been separated into "initiation" and "propagation" phases. This distinction is almost always arbitrary, for "initiation" is invariably defined as the time at which a crack is *detected*, or when the load has relaxed a specific amount (in a strain controlled test); in these cases initiation generally corresponds to a crack depth of significant metallurgical dimensions (e.g., ≥2 mm). For the purpose of lifetime modeling it is more appropriate to assume (Figure 8) that, phenomenologically, initiation is associated with microscopic crack formation at localized corrosion or mechanical defect sites associated, e.g., with pitting, intergranular attack, scratches, weld defects or design notches. This is particularly appropriate when cracks of such small dimension behave like "deep" cracks [17], as will be discussed later. If it is further assumed that the probability that initiation sites exist or develop relatively early in the life of the component is high (generally reasonable if the population of potential sites (e.g., grain boundaries) is large), then the problem of life prediction devolves to understanding the growth of small cracks from these geometrically separated initiation sites, then the coalescence of these small cracks to form a major crack which may accelerate or arrest depending on the specific material, environment, and stress conditions. Of course, if necessary, a probabilistic or statistical approach to predicting the number of initiation sites vs. time can also be used.

Relatively little fundamental work on the growth of such microscopically short cracks has been undertaken. These efforts will not be reviewed in detail, apart from noting that most work has been done under fatigue loading [40-44], with emphasis on the microstructural interactions required for microscopic crack arrest or propagation, and modifications to linear elastic fracture mechanics to account for the observed behavior in this crack size range. In the area of environmentally assisted cracking, the coalescence of microscopically small cracks has been investigated for carbon steels in carbonate / bicarbonate solutions [45,46] and stainless steels and nickel base alloys in high temperature water [17]. In these cases it is observed that the crack growth rate increases as the small cracks coalesce, and approaches a steady state value when the mean crack depth is about 20 to 50 μm (Figure 9); thereafter the crack propagation rate may be analyzed in terms of linear elastic fracture mechanics normally applicable to "deep" cracks. Coalescence dominated the retarded growth rate early on, with no evidence of either mechanical or chemical short crack effects [17]. Thus, the focus can be on crack advance of "deep" cracks (e.g., ≥ 1 grain diameter), recognizing that the resulting life predictions may be conservative because the microscopic crack initiation and coalescence periods are not incorporated.

All of the proposed crack advance mechanisms for ductile alloys in hot water require that growth at the crack tip occurs faster than the corrosion rate on the unstrained crack sides so that the crack does not degrade into a blunt notch [47,48]. Based on this criterion, the material / environment conditions for cracking can be defined using thermodynamic criteria for the presence of a protective oxide, salt, or compound film on the crack sides. For example, cracking susceptibility of mild steel in hydroxide, carbonate / bicarbonate, nitrate, phosphate, and molybdate solutions are predicted to occur in the specific potential/pH regimes where the protective film is thermodynamically stable or metastable [49]. Very similar thermodynamic arguments may be made for other systems, (e.g., brass / ammoniacal solutions [50]), and are extended to kinetic arguments [51-53] that require the electrochemical reaction rates (e.g. dissolution or oxidation) at the strained crack tip to be significantly higher than those on the crack sides for an "electrochemical knife" [51] to propagate. Indeed, the suppression of stress corrosion and corrosion fatigue in many systems may be explained in terms of chemical blunting of cracks during their development. For example, low alloy steels do not exhibit stress corrosion in acidic or concentrated chloride solutions unless the general corrosion / blunting effect is counteracted with chromium or nickel alloying additions [49,54]. Similarly, in high purity water systems, carbon steel does not undergo stress corrosion cracking in low temperature, oxygenated environments, since the embryo crack is blunted by pitting; however, at temperatures >150°C, cracking is possible because of the protective nature of magnetite (Fe_3O_4) [55] that constitutes the inner film of the duplex surface oxide.

Where chemical blunting is not a concern, numerous crack advance mechanisms were proposed between 1965-1979 [1,3,4,6,57-63], including pre-existing active path mechanisms, strain assisted active path mechanisms, and mechanisms that depend on various adsorption / absorption phenomena (e.g., hydrogen embrittlement mechanisms). There was considerable debate concerning the dominant mechanism in a given system, promulgated in part by the fact that up to 15 years ago there were few analytical techniques to quantitatively test the various hypotheses. However, Parkins [64] noted early on that there was probably a "stress corrosion spectrum" between cracking systems that were mechanically dominated (e.g., hydrogen embrittlement of high strength steels) and those that were environmentally dominated (e.g., pre-existing active path attack in the carbon steel / nitrate system). Indeed, it was suggested that two mechanisms may operate in one alloy / environment system with a dominant mode being determined by perhaps small changes in the material, environment, or stressing condition. This was followed by the suggestion (e.g., [11,47,64-66]) that a similar spectrum of behavior occurs for constant load (stress corrosion), dynamic load (strain induced cracking), and cyclic load (corrosion fatigue).

With improvements in experimental and analytical capabilities in the last 15 years, many of the early cracking hypotheses were shown to be untenable, and the candidate mechanisms for environmental crack propagation have been narrowed down to slip dissolution, film induced cleavage, and hydrogen embrittlement. These mechanisms are briefly described below.

Slip / Film Rupture / Dissolution Mechanism

A variety of crack advance theories have been proposed to relate crack advance to oxidation rates and the stress / strain conditions at the crack tip, and these are supported by a good correlation in a number of systems [48,67] between the average oxidation current density (e.g., obtained on a straining surface) and the crack growth rate (Figure 10). There have also been various hypotheses for the atom-atom rupture process at the crack tip; for example, the effect that the environment has on the ductile fracture process (e.g., the tensile ligament theory [68]; the increase in the number of active sites for dissolution because of the strain concentration [69]; the preferential dissolution of mobile dislocations because of the inherent chemical activity of the solute segregation in the dislocation core [70]; etc.).

Aspects of these earlier hypotheses that were experimentally validated have been incorporated into the current slip dissolution model, which Faradaically relates crack advance to the metal oxidation that

occurs when the protective film at the crack tip is ruptured [71-76]. Different types of protective films have been proposed, including oxides, mixed oxides, salts, or noble metals left on the surface after selective dissolution of a more active component in the alloy.

Figures 11 and 12 schematically shows the change in oxidation current and charge densities with time following the rupture of a protective film at the crack tip. The initial oxidation rate (and, hence, crack advance rate) will be rapid, typically controlled by activation or diffusion kinetics as the exposed metal rapidly dissolves; availability of the balancing cathodic reduction current is also clearly necessary, but is generally not limiting in hot water environments. However, in most (if not all) hot water cracking systems, a protective oxide reforms at the bared surface and the rate of total oxidation (and crack tip advance) slows with time. Thus, crack advance can only be maintained if the film rupture process is repetitive. Therefore, for a given crack tip environment, corrosion potential, and material condition, the crack growth will be controlled by the change in oxidation charge density with time and the frequency of film rupture at the strained crack tip. This latter parameter will be determined by the fracture strain of the film, ε_f, and the strain rate at the crack tip, $\dot{\varepsilon}_{ct}$. By invoking Faraday's law, the average environmental crack growth rate, $\bar{V}_t$, can be related to the oxidation charge density passed between film rupture events, Q_f, and the strain rate at the crack tip, $\dot{\varepsilon}_{ct}$:

$$\bar{V}_t = \frac{M}{z\rho F}\,\frac{Q_f}{\varepsilon_f}\,(\dot{\varepsilon}_{ct}) \tag{1}$$

where: M, ρ = atomic weight and density of the crack tip metal
F = Faraday's constant
z = number of electrons involved in the oxidation of a metal atom

Repassivation current transients generally exhibit an initially high bare surface dissolution current density, i_o, for a short time, t_o; thereafter, oxide formation or precipitation leads to a decay in the oxidation current density which often follows a power law relationship:

$$i_t = i_o \left[\frac{t}{t_o}\right]^{-n} \tag{2}$$

Because of this power law relationship, Equation 1 can be reformulated as:

$$\bar{V}_t = A\,(\dot{\varepsilon}_{ct})^n \tag{3}$$

where "A" and "n" are constants taken from the *measured* repassivation response ("n" is the slope on a log-log plot from Equation 2) that depend on the material and environment compositions at the crack tip [11-16,77], as discussed below. Note that *measurements* of repassivation response are necessary because insufficient fundamental understanding and modeling exist of the repassivation process in hot water. Attempts to associate crack tip repassivation response with other factors (such as the ionic current flow in the crack from a differential aeration cell) are inappropriate because it has been shown that these factors don't directly control the local (crack tip) repassivation behavior [26], which is controlled by the local chemistry and crack tip material.

If a *bare surface* condition is maintained at the crack tip (i.e., $\varepsilon_f / \dot{\varepsilon}_{ct} < t_o$) then integration of Equation 2 leads to a predicted *maximum* environmental crack growth rate:

$$\bar{V}_{max} = \frac{M}{z\rho F}\,i_o \tag{4}$$

This expression for the maximum environmental crack growth rate is the quantitative basis for the early observations (discussed earlier in this section) relating the maximum oxidation current density on a straining surface to the maximum crack growth rate (Figure 10). However, these early correlations were

obtained primarily for alloys in concentrated environments (boiling $MgCl_2$, 9M NaOH solutions, etc.) under dynamic straining conditions. By comparison, in relatively dilute environments characteristic of LWRs it is expected that (a) the passivation rate can be high (e.g., in unaggressive chemistries or for lower susceptibility materials) and thus "n" (in Equation 2) will be high; (b) the onset of repassivation is rapid, and thus t_o will be short; and (c) under constant load or displacement conditions, the periodicity of oxide rupture, $\varepsilon_f / \dot{\varepsilon}_{ct}$, will be much greater than t_o. Under these circumstances a bare surface will not be maintained at the crack tip, and the crack propagation rate will be given by the integration of Equation 2:

$$\bar{V}_t = \frac{M}{z\rho F} \frac{i_o t_o^n}{(1-n)\varepsilon_f^n} (\dot{\varepsilon}_{ct})^n \tag{5}$$

This is an expanded version of Equation 3 and relates the parameters "A" and "n" to the specific oxidation rates (e.g., Equation 2) and the fracture strain of the oxide at the crack tip.

For constant load or constant displacement conditions, the crack tip strain rate can be related (as discussed later) to the creep processes at a moving crack tip [11,77]. Under monotonically or cyclically changing bulk strain conditions, $\dot{\varepsilon}_{ct}$ can be related to an applied strain rate $\dot{\varepsilon}_{app}$. Thus, the slip dissolution mechanism may be applied to not only stress corrosion but also to "strain induced cracking" [78] and corrosion fatigue. Under cyclic loading conditions, however, the crack is also moving forward by irreversible cyclic plastic deformation, e.g., fatigue striation formation. Since this mechanical crack advance is occurring independently of the crack advance by oxidation processes, these two crack advance mechanisms (striation formation and oxidation) are considered additive, as shown by the dotted lines in Figure 13.

Film Induced Cleavage Mechanism

For some transgranular cracking systems, it has been observed [79] that the Faradaic equivalent of the oxidation change density at a strained crack tip is insufficient to account for the observed crack advance. Moreover, the detailed cleavage-like crystallographic features on the fracture surfaces are hard to convincingly justify using a dissolution / oxidation model. Consequently, several authors [79-83] have proposed that transgranular environmental crack advance may occur by a combination of oxidation and brittle fracture mechanisms. Specifically, the crack front is envisioned to "initially" advance by an oxidation process controlled by the same processes operative in the slip dissolution model but, when the film rupture event occurs, the elastic energy of the crack in the coherent film causes penetration into the underlying ductile metal matrix by a small amount, a^* (Figure 14). Thus, Equation 1 becomes:

$$\bar{V}_t = \left[\frac{M}{z\rho F} Q_f + a^* \right] \frac{\dot{\varepsilon}_{ct}}{\varepsilon_f} \tag{6}$$

The contribution of the "film induced cleavage" component of crack advance, a^*, is governed [79] by the state of coherency between the surface film and matrix, the fracture toughness of the substrate, the film thickness, and the initial velocity of the cleavage crack emerging from the surface film. Although the surface film has been traditionally considered to be an oxide, more recent investigations [82,83] have shown that dealloyed surface films (e.g., copper rich films in Cu-Zn or nickel rich films in Fe-Cr-Ni alloys) can also form, exhibit "passive" behavior, and be very brittle. The extent of the cleavage propagation into the matrix is estimated to be of the order of 1 μm and to depend on the plasticity and microstructural factors mentioned above. Although there is evidence for this mechanism in copper base alloys and austenitic nickel base alloys and stainless steels in some low temperature environments (i.e., <115°C), it has not been extensively evaluated for other alloy systems, including hot water. Its attractiveness is, however, that it provides a rational basis for explaining the inter-relationships between the electrochemical parameters and the transgranular fractographic features in, e.g., the carbon and low

alloy steels used for nuclear reactor pressure vessels and steam generator shells, and for quantitatively predicting the transitions between intergranular and transgranular cracking in stainless steels in high temperature water [11] as a result of changes in strain rate, corrosion potential, and degree of sensitization.

Hydrogen Embrittlement Mechanisms

Thompson and Bernstein [84], Hirth [85], Nelson [86], and Birnbaum [87] have reviewed the general concepts and concerns associated with various hydrogen models. The subcritical crack propagation rate due to hydrogen embrittlement in aqueous environments depends on a sequence of events (Figure 15 [88]):

- Diffusion of a reducible hydrogen containing species (e.g., H_3O^+) to the crack tip region.
- Reduction of the hydrogen containing ions to give adsorbed hydrogen atoms.
- Absorption of the hydrogen adatoms followed by interstitial diffusion of these hydrogen atoms to a "process" zone at a distance, X, in front of the crack tip.
- Once the hydrogen concentration in a "process" zone has reached a critical level, C_{crit}, over a critical volume, d_{crit}, then localized crack (re-) initiation can occur within this zone followed by rapid propagation back to the main crack tip [89].

Setting aside the specifics of these localized fracture mechanisms in the "process" zone for the present, it is apparent that hydrogen embrittlement models predict discontinuous crack propagation at an average rate of:

$$\bar{V}_t = \frac{X}{t_c} \tag{7}$$

where X is the distance from the main crack tip to the process zone (which, in turn, is defined by the values of C_{crit} and d_{crit}) and t_c is the time for the concentration of absorbed hydrogen, $C_{x,t}$, to reach a critical value, C_{crit}, over the volume d_{crit}. To evaluate the validity of Equation 7, quantitative data for X and t_c are needed. Unfortunately, these are difficult to determine from fundamental calculations or measurements [90] and rely mechanistically on the validity of the various atom-atom rupture hypotheses (e.g., decohesion [91,92], gas rupture [93,94], enhanced plasticity [95,96], hydride formation [97], martensite formation [98], etc.) that have been made.

Hydrogen embrittlement mechanisms have traditionally been applied qualitatively to high strength alloys, although Hanninen, Torronen, and coworkers [99,100] have suggested that a hydrogen embrittlement mechanism is operating in the relatively ductile pressure vessel steels in 288°C water. The prime experimental evidence for this hypothesis is the observation of "brittle" cracks associated with elongated MnS stringers ahead of the main crack tip. The degree of environmental enhancement in fatigue crack growth rates is therefore directly correlated with the extent of these "brittle" fracture areas on the fracture surface. The following series of steps for low alloy steels in 288°C water are hypothesized [100] to occur:

- enhanced oxidation (dissolution and oxide reformation) at the strained crack tip.
- hydrolysis of the metal cations to produce H^+ (acidification) in the crack environment.
- dissolution of exposed MnS inclusions in this acidic environment, which produces H_2S and promotes incorporation of sulfur into the reforming oxide.
- creation of adsorbed hydrogen atoms due to the local hydrogen ion reduction reaction, followed by absorption. The kinetics of these reactions are believed to be accelerated both by the necessity to

balance the enhanced oxidation reactions, and by the presence of the sulphur species in the crack tip environment.

- recombination of hydrogen atoms at MnS inclusions ahead of the crack tip, leading to the formation of brittle cracks at the inclusion / matrix interface which propagate under the action of hydrogen gas pressure and triaxial tensile stress.
- linkage of these microcracks to give a discontinuous crack propagation over and above that due to "mechanical" fatigue failure.

However, little direct evidence of a unique and distinguishing role of hydrogen in environmental cracking in hot water exists. Hydrogen is always present in engineering materials exposed to hot water, and factors that should accentuate hydrogen effects (such as cathodic charging, increased dissolved hydrogen, or deposition of surface layers of noble metals) almost always retard crack growth in hot water. While sulfide ion can enhance hydrogen absorption, its effect on repassivation kinetics is also very pronounced, and this provides an adequate explanation for crack growth based solely on a slip dissolution mechanism. Finally, many hydrogen studies show that the damaging effect of dry hydrogen gas on higher strength alloys (where a dissolution component to crack advance is not possible) diminishes rapidly above about 125 - 150°C; in turn, studies on austenitic and partially martensitic stainless steels show no surprising increase in crack growth rate with increasing martensite, as expected for a hydrogen dominated mechanism. Below 150°C, hydrogen can play a pronounced role, and tests on high strength alloys such as X-750 show that the presence of hydrogen from exposure to hot water can result in very rapid crack propagation at lower temperatures [101].

PREDICTION METHODOLOGY DEVELOPMENT

Evaluation of these candidate crack advance mechanism has led to the conclusion that the film rupture / slip oxidation mechanism represents a *justifiable* model for hot water systems that is capable of being *quantatively* evaluated. This is based on wide-ranging evidence that argues against the importance of other specific mechanisms (e.g., hydrogen embrittlement) as well as the consistent importance and quantitative agreement obtained for the film rupture / slip oxidation mechanism.

The mechanism is *justifiable* because almost all engineering alloys depend on the presence of a stable oxide film to act as a kinetic barrier to rapid dissolution / oxidation, especially in hot water. It is *quantifiable*, because predictions result *directly* from measurements of repassivation kinetics, typically obtained by rapidly straining wires of base alloy or synthetic (e.g., representative of the grain boundary) composition (Figure 12). If reasonable assumptions are made regarding the typically observed characteristics of repassivation (i.e., that the repassivation current follows a power law response, Equation 2, Figure 16), the Faradaic relationship between the oxidation rate following oxide rupture and crack advance increment per time (growth rate, V), coupled with the relationship between crack tip strain rate, $\dot{\varepsilon}_{ct}$ and periodicity of oxide rupture, distills to the appealing and elegant expression shown in Equation 3.

The film rupture / slip oxidation mechanism is also applicable to direct chemical oxidation (i.e., in the absence of separated anodic and cathodic reactions), where no electrochemical reactions occur and thus neither "dissolution" nor ionic transport are necessary. Accordingly, the observation of cracking in steam at 400°C, and the smooth transition vs. temperature in growth rate between water and steam, are consistent with the slip oxidation model. Even in high temperature (liquid) water, it is hypothesized that spontaneous oxidation becomes an important reaction with increasing temperature, with transport of water to the metal/ oxide interface probably being the rate controlling step. The contribution of direct oxidation is, however, not quantifiable from measured repassivation currents.

The periodicity of film rupture is related to the strain rate in the metal matrix and this, in turn, is controlled by either creep processes under constant load or applied strain rates under monotonically increasing or cyclic load conditions. The model is thus applicable not only to stress corrosion (under constant stress or strain rate conditions) but also to corrosion fatigue over the range of stress amplitude, mean stress, frequency, etc. combinations. Indeed, the fundamental importance of (crack tip) strain rate supersedes other parameters such as stress intensity and stress intensity amplitude, stress and mean stress, percentage of yield stress, strain / deflection, etc. as the appropriate fundamental parameter for environmental cracking. In turn, it provides a common framework for interpreting / integrating diverse loading conditions, crack sizes / shapes / morphology, and crack initiation (smooth surface), short crack, and (deep) crack propagation response. As such, crack tip strain rate, while more difficult to calculate (or measure) than fracture mechanics parameters, provides an improved basis for similitude.

One limit to the validity of this relationship (Figure 13) occurs at high crack tip strain rates ($\approx 10^{-2}\ s^{-1}$), where the environmental crack growth rate saturates because a bare surface is maintained continuously at the crack tip. At low crack tip strain rates, changes in the parameters in Equation 1 can occur if, e.g., crack blunting occurs (i.e., when the corrosion rate of the crack sides approaches the oxidation rate at the crack tip), or the dynamic creep–crack growth processes which sustain crack advance under static loading are disrupted.

The model has been quantified in BWR water [11-27] by evaluating: (1) the steady state and transient compositions of the environment at the crack tip as a function of the conditions in the bulk (external) solution, with particular emphasis in this system given to the effect of the potential gradient (differential aeration cell) and the ability in a non-buffered system for the crack tip pH to vary; (2) the oxidation rates (repassivation current vs. time) for the material / environment system that exists at a strained crack tip; and (3) the oxide fracture strain and the crack tip strain rate, defined in terms of engineering parameters such as K, ΔK, R, frequency, applied strain rate, etc. These efforts will be discussed in more detail in the next section. Additionally, short crack behavior and the transition to long crack behavior [17], concerns for crack chemistry similitude [17], treatment of thickness- and time-varying properties, and treatment of distributions in properties and statistical approaches [11-23] have also been addressed.

Important conceptual elements in this model [11-17,26-28] include the differentiation of "crevice" macrocell currents (e.g., associated with potential gradients in the crack from differential aeration) from microcell metal dissolution currents that give rise to crack advance (Figure 5). Crevice macrocell currents are widely acknowledged in all crevice geometries, independent of the presence of stress or a crack, and is usually driven by cathodic reduction of oxygen on the outside and oxidation of hydrogen or metal just inside the crevice / crack, with the remainder of the crack at relatively constant potential and chemistry. The microcell currents directly associated with crack advance occur in the vicinity of the crack tip, with rupture of the protective oxide causing metal dissolution charge balanced locally by cathodic reduction of hydrogen ion. The presence of a low corrosion potential over the majority of the crack length, even in highly oxygenated water and/or high neutron / gamma fluxes, has been clearly demonstrated [27,28,102].

Evaluation of the Film Rupture / Slip Oxidation Model

Atomistic details of crack advance are difficult to directly observe and thus will be a continuing source of debate. Even with demonstrated quantitative Faradaic agreement between measured repassivation kinetics and crack growth rates, there remains the possibility that crack advance occurs by hydrogen-induced or brittle-film-rupture-induced cleavage. Of course, this requires that the Faradaic agreement with crack advance is fortuitously associated with dissolution of the freshly exposed metal, which appears unlikely.

However, quantitative agreement between repassivation kinetics and crack advance rates across a range of conditions certainly diminishes the likelihood that alternate mechanisms are responsible for crack advance. Several specific examples, e.g., effects of pH, sulfide concentration, and hydrogen fugacity, will be used to highlight this consistency and agreement. These examples of Faradaic equivalence represent a wide range of variables, all of which have a pronounced effect on crack growth rate. In some cases, their effect is observed on many materials (e.g., sulfide effects on low alloy steel, stainless steel, and nickel-base alloys); in other cases (e.g., hydrogen fugacity), a very striking effect occurs only on nickel-base alloys, for a well-defined, well-explained reason.

Effects of pH on crack growth. The first example relates primarily to BWR systems where pH buffering doesn't occur and Cr depletion can play a significant role. Here the role of species that can affect the pH within the crack is well documented [26,27,38]. Figure 17 provides an example of the dependence of repassivation kinetics on chromium content in stainless steel. These measured responses are directly (Faradaically) related to the observed crack growth rates on sensitized stainless steels, as represented in Figures 18 and 19.

Similar repassivation measurements show that the effect of chromium depletion diminishes greatly in neutral to slightly alkaline water, consistent with the general observation that chromium depletion is of much less importance in PWR systems. The effect of carbides (Nb/Ti/Cr carbide) and carbide distribution can cause differences in slip character and homogeneity, as discussed later.

Effects of sulfide on crack growth. A second example of the direct link between repassivation kinetics and crack growth rates draws on the effect of sulfide. Various investigators have shown strong effects on crack growth rate of sulfide, whether present from direct addition of H_2S or Na_2S, from formation via dissolution of MnS inclusions, or from reduction from sulfate or sulfite [32-35]. These effects have been observed on a wide variety of alloys ranging from low alloys steel [33,34], to stainless steel [35], to nickel-base alloys [32,34], and have been shown to be consistent with repassivation kinetics (Figure 20) under either rapid or slow straining conditions. Note that sulfide only *impedes* repassivation, but does not maintain a *bare surface* current density; thus, film rupture and repassivation are still important.

The vast differences in alloy composition and yield strength, and significant range in pH and temperature over which these phenomena are observed tend to diminish the likelihood that hydrogen embrittlement or film-induced cleavage are responsible for crack advance.

Effects of H_2 fugacity on crack growth. A final example is the repassivation kinetics and crack growth rate response of Alloy 600 as a function of hydrogen fugacity in 288°C water. Under neutral or slightly alkaline conditions, the Ni/NiO boundary is relatively close to the H_2 / H_2O boundary, which usually controls the corrosion potential in hot water (Figure 6). As the hydrogen fugacity is increased, the H_2 / H_2O curve shifts to lower potentials, eventually "crossing" the Ni/NiO (which itself depends on the activity of various species). If a film rupture / slip dissolution model is operating, then the addition of hydrogen and lowering of potential into the regime of Ni^o stability should reduce crack growth rates and correspondingly affect repassivation kinetics. If a hydrogen-related mechanism is responsible for crack advance, then increasing the hydrogen fugacity (and eventually removing the NiO film) should greatly enhance crack growth kinetics.

Data on the effects of hydrogen on crack growth rate at 288°C [39] and >300°C [103] clearly show similar responses, with growth rates on actively loaded, fracture mechanics specimens continuously monitored for crack length vs. time monotonically decreasing as the hydrogen fugacity was increased from ≈0 (perhaps 10^{-3} bar) to several bar (Figure 21). The thermodynamic predictions for the hydrogen fugacity required for the H_2 / H_2O line to "cross" the Ni/NiO boundary, which varies substantially with temperature (Figure 22 [104-106]), could be confirmed by the dc potential drop crack length measurements, which showed significant (e.g., 0.3 mm) "healing" of the apparent crack length

consistent with the creation of shorting paths for the dc current flow in the wake of the crack, probably from mode 2 / mode 3 motion of crack flanks which cause contact of NiO-free grain boundary facets. This "healing" phenomenon is not observed on stainless or low alloy steels because of their low nickel content and the large "distance" between the H_2 / H_2O line and the Fe^o stability region [29].

The monotonic decrease in crack growth rate with hydrogen, which drops to very low levels at the hydrogen fugacities associated with crossing into the region of Ni^o stability, is consistent with the slip dissolution model and with the thermodynamic predictions of hydrogen requirements vs. temperature.

However, the most compelling evidence of the underlying role of slip dissolution in crack advance comes from measurements of repassivation kinetics on rapidly strained wires of Alloy 600 in 288°C water of identical composition as a function of hydrogen fugacity (Figure 23) [39]. As hydrogen is increased (nominally) from 0 bar, the repassivation charge density monotonically decreases, precisely mirroring the observed crack growth rates. However, as hydrogen is increased, the contribution of hydrogen oxidation ($H_2 \rightarrow 2H^+ + 2e^-$) begins to emerge, causing an increase in the minimum current repassivation current density observed at long times after the wire is rapidly strained. At fairly high hydrogen fugacities, the metal oxidation current density is sufficiently low, and the hydrogen oxidation current density sufficiently high, that the observed "repassivation" transient is completely unaffected by the rapid straining of the wire, instead showing a continuous and constant (hydrogen) oxidation current density.

These examples provide compelling evidence that the film rupture / slip dissolution model represents the fundamental mechanism by which cracks advance in hot water. However, there are no reasonable models for predicting repassivation kinetics in hot water from (crack tip) material and water chemistry data, so the *measurement* of these kinetics remains central to modeling and prediction of environmental cracking. Indeed, the importance of (crack tip) strain rate and film rupture (inherent in the importance of repassivation kinetics) is a given in most hot water environments, since the bare surface dissolution kinetics of iron- and nickel-base alloys is exceedingly rapid. Also, the solubility of metal ion in hot water is inadequate to permit a Nernstian equilibrium to be achieved (i.e., shifting the Fe/Fe^{2+} equilibrium above the H_2 / H_2O line. Thus, with the exception of high nickel alloys in water with high hydrogen fugacity (where repassivation measurements still provide a meaningful, accurate prediction), crack growth is controlled by the repassivation kinetics of the strained metal. This is equally true in high sulfide (and other concentrated) environments, since while film repair is impaired, the observed repassivation rates or passive current densities are still orders of magnitude below the bare surface rate, indicative of an important role of "passive" films, (crack tip) strain rate, and repassivation kinetics.

Model Quantification

The initial emphasis of our modeling activity was on the quantitative prediction of cracking in austenitic type 304/316 stainless steels in 288°C high purity BWR water. This methodology was then extended to treat the effects of irradiation on the cracking of stainless steel and to address other alloys (e.g., nickel base, low alloy steels) and environments (PWR).

To develop this concept to a state of practical usefulness, Equation 5 must be redefined in terms of measurable engineering or operational parameters. This involves: (a) defining the crack tip alloy / environment composition in terms of, e.g., bulk alloy composition, anionic concentration or solution conductivity, dissolved oxygen content or corrosion potential, etc., (b) measuring the reaction rates for the crack tip alloy / environment system that corresponds to the "engineering" system, and (c) defining the crack tip strain rate in terms of continuum parameters such as stress, stress intensity, loading frequency, etc. There has been extensive work conducted in these areas, and the progress will be reviewed only briefly before illustrating how these advances have been incorporated into verified, quantitative life prediction methodologies.

Definition of Crack Tip System: Alloy/Environment. On the basis of direct measurements on stainless steel, Alloy 600, and low alloy steel in 288°C water, it is known that the corrosion potential and pH conditions at the tip of a crevice/crack can differ markedly from those at the exposed crevice / crack mouth [11,27,107-110]. These variations are understood and have been extensively reviewed [77,111-113] in terms of the thermodynamics of various metal oxidation and metal cation hydrolysis reactions, and how they are influenced by the reduction processes of, e.g., dissolved oxygen at the crack mouth and the associated differential aeration macrocell (Figure 5). From a practical viewpoint, the corrosion potential that exists at the deaerated crack tip is controlled primarily by pH, but it can be defined [11] in terms of the measurable dissolved oxygen content in the external water environment (or preferably by the measurable corrosion potential of the external system) and the purity of the external water.

The transient and steady state concentration of anions in the crack have also been experimentally measured and analytically modeled [11,27,114]. The anion level present at the crack tip is directly dependent on the external anionic activity, the dissolvable metallurgical impurities (e.g., MnS) level, the corrosion potential difference between the crack mouth and tip, and convection from fluid flow and/or significant cyclic loading. For example, the steady state sulfur anion concentration at the crack tip in low alloy steels can be defined by the MnS content, aspect ratio and orientation, the solution flow rate, and the oxygen concentration in the water [11,115,116]. Under specific conditions the dissolved sulfur concentration at the crack tip can be ≈ 3 ppm vs. <10 ppb in the bulk solution.

For stainless steel exposed under normal BWR conditions, the potential drop down the crack length leads to a concentration of (non-OH^-) anions at the crack tip such that typical crack tip anion concentrations between 0.1 and 1.0 ppm are expected; under deaerated operating conditions, where no potential drop exists along the crack length, the (non-OH^-) anion content at the crack tip will approximate that in the bulk environment (e.g., ≈15 ppb). As the anion concentration increases, there must be a corresponding concentration of cations at the crack tip to maintain electroneutrality. The anodic (crack tip) end of the differential aeration cell can involve the oxidation of hydrogen and/or metal; however, because of the low solubilities of iron, nickel, and chromium cations, hydrolysis occurs (e.g., $Ni^{2+} + H_2O \rightarrow NiO + 2H^+$), so that H^+ is the dominant cation under most circumstances, and thus a decrease in pH occurs. However, in typical BWR water, the concentration of (non-OH^-) anions at the crack tip is only sufficient to produce acidification of 1-2 pH units [27]. In the absence of non-OH^- anions, acidification cannot occur and generally a slight increase in pH is observed both in aerated [27] and deaerated [117] water. In this case, OH^- is balanced by, e.g., Na^+ or the (sparingly soluble) transition metal cations; since cations tend to be driven out of the crack by the potential gradient, alkanization tends to less favored than acidification.

The role of convection on corrosion potential and crack advance is evolving and interesting. Fluid flow velocity can significantly increase the corrosion potential on metal surfaces, particularly when oxygen is diffusion limited, and especially below ≈ 20 ppb oxygen. Under these conditions, convection decreases the thickness of the stagnant liquid boundary layer, shortening the diffusion path, and increasing the flux of oxygen to the surface. Under some conditions, an elevation in corrosion potential of >0.3 V has been observed [26]. Because of the recognized link between corrosion potential and crack growth rate, this has been widely interpreted as representing an acceleration of environmental cracking. It has been proposed [26] that any such elevation in potential should have no deleterious effect on crack growth rate.

This conceptual argument relies on the orders of magnitude higher mass transport kinetics from convection than from ordinary diffusion or potential driven ion migration. Thus, the effect of convection is merely to shift the "electrochemical crack mouth" to some interior point within the crack. The "electrochemical crack mouth" is defined as the point of (near) zero convection, because any potential gradient that exists from the external surface to this point will have no effect on mass transport - i.e., the mass flux from this gradient is completely overwhelmed by convection. At the "electrochemical crack mouth", the potential gradient acts to concentrate anions and shift pH. Thus, because of convection is

kinetically dominant, it merely shifts the "electrochemical crack mouth" to a point inside the crack; the fact that this is somewhat nearer to the crack tip is of little consequence, because the potential gradient forms over a short distance near the "electrochemical crack mouth" in any event.

In the extreme condition of convection throughout the entire crack (including crack tip), one might be concerned that the high oxidant concentration and elevated corrosion potential at the crack tip would be deleterious and dramatically enhance crack growth rates. As such, this extreme condition provides an interesting comparison of the relative roles of elevated corrosion potential vs. modified crevice/crack chemistry. However, several studies on both sensitized type 304 stainless steel and low alloy steel involving high flow rates or rapid crack tip microsampling [26] showed that crack growth rates dramatically *dropped* under these conditions.

Apart from the influence of MnS inclusions, the alloy composition at the tip of transgranular cracks is generally assumed to be that of the bulk alloy. However, the alloy composition at the tip of an intergranular crack may be considerably different from the bulk composition if metal solute segregation or denudation at the grain boundary exists; such compositional heterogeneity will be controlled by, e.g., thermal diffusion and/or irradiation assisted damage. Discussion of these metallurgical aspects is outside the scope of this paper, but adequate knowledge exists, including extensive analytical electron microscope studies, to permit definition of the grain boundary composition in terms of the bulk alloy composition and the thermal history during fabrication or irradiation history during reactor operation [118-123]. Thus, the crack tip alloy / environment system can be defined in terms of measurable or definable bulk system parameters.

Evaluation of Oxidation Rates at Crack Tip. Various techniques have been used to create a macroscopic analogy to the crack tip bare surface on which the oxidation and reduction rates can be measured. These include mechanical methods to rupture the surface oxide that involve: slowly [117,124-127] or rapidly [128,129] straining the alloy; complete fracturing of the specimen to create a bare fracture surface [130,131]; cyclic straining [117,132]; scratching the alloy surface [133-138]; and grinding [139]. Electrochemical methods have also been used to cathodically reduce the oxide [11,140-142] and pulse to the potential of interest. Most of these techniques have been applied in the study of environmental cracking. The experimental difficulties with these techniques have been reviewed [77,143,144], along with the interpretations of the atomistics of the reaction rate [77] at a strained crack tip. These topics will not be covered further in this paper.

The main conclusions with regard to dissolution and repassivation kinetics in structural materials in 288°C crack tip environments are that both the oxidation and reduction reaction rates are increased when the protective oxide is removed. The bare surface oxidation rate, i_o, is a function of the electrode potential and the dissolved anion content, as shown in Figure 24 for the effect of sulphur on the bare surface dissolution rate of low alloy steels [11,117,145]. Explanations for this behavior range from those by Ford and Andresen [11,27] who argue that the rate controlling process for bare surface dissolution is the diffusion of solvating water molecules to the oxidizing surface (and the influence of anionic activity and pH and on the solubility of impeding oxide precipitates), to those of Combrade et.al. [117] who argue that adsorbed sulfur on the surface impedes the incipient solid state passivating oxide nucleation.

Oxide formation leads to a decrease in the overall oxidation rate, according to Equation 2. The value of "n" in this equation (which is the same as in the crack propagation rate Equation 5) varies with the alloy chemistry (e.g., chromium content for a denuded grain boundary of type 304 stainless steel, or dissolved sulfur content from MnS dissolution in low alloy steels, Figure 25), electrode potential, and anionic activity, and this can be related to, e.g., solid state oxide growth, dissolution / precipitation reactions, and oxide breakdown [11,47]. Thus, all of the parameters in Equation 5 (apart from $\dot{\varepsilon}_{ct}$) can be quantified for the crack tip system, which can, in turn, be related to definable or measurable bulk system conditions.

Definition of Crack Tip Strain Rate. It has been long recognized that the oxide rupture prerequisite for crack advance leads to a relationship between cracking susceptibility and slip morphology, since coarse slip at the crack tip will more readily rupture a brittle film of given thickness [146] than fine slip. This relationship has been observed [84] for various alloys in both aqueous and gaseous environments, where the different dislocation morphologies are related to changes in stacking fault energy, short range order, precipitate / matrix coherency, and precipitate distribution.

Despite these effects of microscopic heterogeneity of plastic flow at a crack tip on the cracking susceptibility, the main emphasis in formulating expressions for the periodicity of film rupture has been on continuum parameters such as strain rate and oxide fracture strain. Reviews of the formulations for crack tip strain rate have been conducted by Parkins, et.al. [147], Lidbury [148], and Ford [77,149], among others. These reviews address the need for the crack tip strain rate formulations to account for various observed factors, including:

a. Can the strain rate formulations account for the limiting stress conditions for cracking, defined by σ_{th}, ΔK_o, or K_{Iscc}? This aspect has been covered by, e.g., Parkins et al [150] in assessing the criteria for maintaining a critical creep rate and how this might be achieved by various stressing conditions.

b. How will the crack tip strain rate vary with time dependent stressing conditions and the degree of plastic constraint? A subsidiary aspect is the examination of the belief that σ_{th} or K_{Iscc} are system constants.

c. How does the fact that the crack is propagating affect the crack tip strain rate when dislocation movement is governed by an exhaustion theory of creep? Associated with this is the definition of the criteria that determine the onset of crack arrest.

Numerous formulation approaches have been suggested and reviewed [77,147-149] but currently these questions have not been completely answered. However, given the urgent *practical* importance of evolving *usable* life prediction algorithms, preliminary crack tip strain rate algorithms have been developed for LWR systems in the following form:

$$\textit{For constant load:} \quad \dot{\varepsilon}_{ct} = A\,\dot{\varepsilon}_{creep} + B\left[\frac{\bar{V}_t}{x^*}\right] \tag{8}$$

$$\textit{For slow strain rate:} \quad \dot{\varepsilon}_{ct} = C\,\dot{\varepsilon}_{appl} + D\left[\frac{\bar{V}_t}{x^*}\right] \tag{9}$$

$$\textit{For cyclic load:} \quad \dot{\varepsilon}_{ct} = \left[\frac{\delta\varepsilon}{\delta K}\right]\dot{K} + \left[\frac{\delta\varepsilon}{\delta a}\right]\bar{V}_t \tag{10}$$

In these equations, it is recognized that the crack tip strain rate is a function, not only of the applied stress, stress intensity, or strain rate, but also of the crack growth rate, $\bar{V}_t$. That is, the movement of the crack tip stress field into the underlying metal matrix by an amount, x^*, activates new dislocation sources, thereby increasing the strain rate above that in a stationary crack. Despite the simple yet sound logic inherent in the above formulations, they have proven to be remarkably difficult to quantify in terms of crack tip plasticity and to independently verify. For instance, uniaxial creep deformation laws at low homologous temperatures are not necessarily applicable to the multiaxial stress conditions in the surface region adjacent to the crack tip, and the use of linear elastic fracture mechanics has limitations in the region of high plastic deformation near the crack tip. These difficulties are discussed in some detail elsewhere [77,147-149]. Despite these fundamental difficulties, empirical formulations between the crack tip strain rate and "engineering" parameters have evolved which have proven useful for a wide range of stressing conditions for structural alloys in 288°C water (Table 1) [11,77].

CRACKING PREDICTIONS IN LWR SYSTEMS

The methodology outlined above provides a specific framework for quantitatively predicting environmentally assisted cracking in structural alloy/water systems at 288°C. This is illustrated below for stainless steels under both unirradiated and irradiated conditions, where intergranular stress corrosion has been observed, e.g., in weld sensitized and thermally sensitized piping, and irradiated core components. The methodology is also illustrated for transgranular stress corrosion cracking of A533B and A508 low alloy steels used for pressure vessel plates and forgings, and for intergranular cracking of nickel base alloys used for safe ends, weldments, etc. Remarks are then made about the extension of these capabilities to other, e.g., PWR systems.

Sensitized or Irradiated Type 304 Stainless Steel / BWR System

Extensive investigations of the relevant fundamental reactions pertinent to crack tip systems have led to a quantification of the basic parameters in Equation 5. For stainless steels, this equation may be simplified [11] to:

$$\bar{V}_t = 7.8 \times 10^{-3} n^{3.6} (\dot{\varepsilon}_{ct})^n \tag{11}$$

As discussed previously, "n" is fundamentally related to the crack tip environment (pH, potential, anionic activity) and material (chromium denudation at grain boundaries) conditions. For practical use, "n" has been reformulated [11] in terms of measurable system parameters such as specific anionic activity (plotted in terms of solution conductivity, κ, the most commonly used measurement, although conductivity is not appropriate for all species, especially buffered chemistries), corrosion potential, ϕ_c (which, in turn, is a function of the dissolved oxygen, hydrogen peroxide, and dissolved hydrogen concentrations), and the "Electrochemical Potentiokinetic Repassivation" (EPR) parameter (which is related to the chromium denudation in the grain boundary). The formulation is of the form (Figure 26):

$$n = \left[\frac{e^{f(\kappa)}}{e^{f(\kappa)} + e^{g(\phi_c)}} \right]^{h(EPR)} \tag{12}$$

The crack tip strain rate, $\dot{\varepsilon}_{ct}$, in Equation 11 is related to the engineering stress (or stress intensity) parameters via the formulations in the Table 1.

The validity of the prediction methodology with respect to the strain rate sensitivity is indicated in Figure 27, which covers data obtained on sensitized type 304 stainless steel in 288°C water containing 8 ppm oxygen and stressed over a wide range of constant load, monotonically increasing load, and cyclic load conditions [11]. The solid line is the theoretical relationship and illustrates the applicability of the methodology to the whole stress corrosion / corrosion fatigue spectrum. The specific effects of changes in corrosion potential and solution conductivity on the propagation rate under constant load is shown in Figures 28 and 29. An example the effect of compositional changes is illustrated later in reference to irradiation induced chromium denudation at the grain boundaries.

The comparison between the theoretical and observed crack growth rate / stress intensity relationships are shown for a sensitized stainless steel in a somewhat impure BWR environment and a more modern "hydrogen water chemistry" BWR environment (Figure 2). The agreement between observation and theory is apparent, as is the inapplicability of a single life prediction law such as the "NRC disposition line" to a system which can exhibit a wide range of conditions within a "nominal" specification.

The broad agreement between observation and theory for propagation of environmentally assisted cracking in the stainless steel / water system at 288°C is shown in Figure 30. In this diagram, the data refer to a wide range of material, environment, and stressing conditions for the generic "stainless steel / water" system at 288°C. Again, the agreement between observation and theory is apparent. Indeed,

given the sensitivity of the crack propagation rate to relatively small changes in the system conditions (e.g., Figures 28 and 29), it has been proposed [11] that the scatter in Figure 30 is due primarily to relatively small unmeasured changes in the system conditions. For instance, unmonitored changes in corrosion potential of ≈100 mV in 200 ppb oxygen water — a range which is perfectly possible because of flow rate effects, etc. — would give a predictable change in crack propagation rate of about a factor of 4. It follows, therefore, that the practical use of such a prediction methodology for life prediction, codification, etc., hinges around an adequate definition of the actual system via the use of system monitors and prediction models for corrosion potential, solution conductivity, etc. [13,14,151].

Integration of the crack propagation rate algorithms leads to an appropriate crack depth / time (a/t) relationship which, for a uniform tensile stress situation, is of the form:

$$a_t = \left\{ a_i^{(1-2n)} + 7.8 \times 10^{-3}\, n^{3.6}\, (1-2n) \left[C\pi^2 (B\sigma)^4 \right]^n t \right\}^{1/(1-2n)} \qquad (13)$$

This particular form applies in the simple case when the stress intensity can be defined by:

$$K = B \cdot \sigma \sqrt{\pi a} \qquad (14)$$

These formulations can become more complicated, e.g., for complex stress fields adjacent to welds, and are treated by incremental calculations as broadly outlined in Figure 31. Examination of Equation 13 indicates that, at time zero, there is an assumed intrinsic initiating defect, a_i; in the following analyses for "smooth" stainless steel components, a value of 50 μm has been used [11-17].

Equation 13, in conjunction with the variation in stress intensity as a crack grows through a residual stress field adjacent to a weld, provides a prediction of the effects of, e.g., (a) the effect of water purity on the crack depth / operating time for stainless steel piping, and (b) the effects of a range in residual stress on the predicted range of crack depths in a piping system (Figure 32). A range in actual system conditions inherently leads to a predicted range in cracking response, as illustrated in Figure 33 for the theoretical relationships between the coolant purity and the operating time required for a crack to penetrate 25% of the wall thickness in a welded type 304 stainless steel pipe. These theoretical relationships are shown for typical ranges in carbon contents (i.e., EPR values) and in residual stress profiles. Figure 33 shows that the observed data lie within the theoretical bounds. Thus, with this proven prediction capability, quantitative decisions can be made about the future behavior for proposed modifications in environment, material, or stress (Figure 34).

Similar predictions can be made for the effect of irradiation on the intergranular cracking susceptibility of stainless steel components in the reactor core [18,102,152]. The prediction methodology developed for unirradiated conditions was modified to account for the effect of fast neutron and gamma irradiation on (a) irradiation hardening and its effect on crack tip strain rates, (b) irradiation induced relaxation of residual stresses, (c) irradiation induced depletion / enrichment of species at the grain boundary, and (d) the effect of irradiation on the corrosion potential via the radiolysis of water.

Once these individual effects have been qualified and verified, it is relatively easy to extend the existing prediction methodology for IGSCC of unirradiated stainless steels to cover the effects of fast neutron fluence on the time to failure of stainless steels in oxygenated water (Figure 35). Figure 36 shows the predicted variation of a *"threshold"* fluence (below which cracking is not observed in, e.g., 10 operating years) for different combinations of stress and solution purity. Moreover, specific remedial actions can be defined to arrest cracking which is detected in a reactor component. For example, Figure 37 shows the effect of reducing corrosion potential (e.g., by noble metal coating [152-154]) as a function of crack size in a BWR core shroud.

Low Alloy Steel / BWR System

It is assumed that the slip dissolution model is applicable to transgranular environmentally assisted cracking in the A533B/A508 low alloy steel / water system at 288°C [11]. It is recognized that this assumption may introduce a systematic error due to undefined components of crack advance associated with film induced cleavage or hydrogen embrittlement, but this is regarded as a small error at this stage of the life prediction methodology development [11,149]. Thus, Equation 5 is retained as the primary basis for prediction, and its quantification has been accomplished [11,115,149] in a similar manner to that described for stainless steel. A primary difference, however, has been the unique role played by the dissolution of MnS inclusions and the associated definition of the crack tip environment [11,115,116]. This is addressed in detail elsewhere [11,115,116,155-159], and it should merely be recognized that MnS inclusions do dissolve in high temperature water. The dissolution rate is sufficiently rapid to increase the concentration of dissolved sulfur species in the crack and, thereby, to significantly increase the crack growth rate. Other influential factors, such as anion enhancement in the crack due to a gradient in potential down the crack, and anion dilution due to flushing of the crack at high bulk solution flow rates, are also important, as in stainless steel.

The agreement between theory and observation of cracking under laboratory conditions is encouraging (Figure 38) [11,115], as is the agreement between the observed and theoretical crack depth / operating time relationships for cracks in the limited number of incidences of cracking in A508 feedwater nozzles of BWR reactors (Figure 39). In this latter case, cracks were observed to initiate on the surface due to thermal fatigue caused by mixing of hot water coolant and the cooler feed water, and the theoretical analysis [115] addressed the subsequent propagation of these cracks due to stress corrosion from pressurization stresses alone.

As with stainless steels, the stress corrosion predictions can be logically expanded to cover corrosion fatigue. Corrosion fatigue of low alloy steels in LWR environments and the impact on ASME XI life evaluation analyses has been exhaustively reported [155-159]. In summary, the current ASME XI code for corrosion fatigue crack propagation of low alloy steels can be overly conservative under certain operating conditions; however, under specific conditions of low cyclic frequencies, high oxygen content environments, and high sulphur steels, it is predicted and observed that $(da/dN)_{\Delta K}$ values greater than the ASME XI code curve are possible [158].

The validity of the current ASME III code for corrosion fatigue crack *initiation* in low alloy and carbon steels in LWR environments is under current review [159]. Although review actions are still in a preliminary stage, it is apparent that the cycles to crack initiation (N_i) are predictable and that the conditions under which the ASME III design curve is non-conservative can be defined (Figure 40).

The laboratory and field experience base for environmentally assisted cracking low alloy steel is far smaller than for sensitized stainless steel, and more development and validation work is required before the prediction methodology can responsibly be reduced to practice.

Nickel Base Alloys / BWR System

The development of prediction models for environmentally assisted cracking of nickel base alloys in BWR systems is made difficult by the fact that the data base against which the prediction models can be validated exhibits extreme scatter (Figure 3) and/or was obtained under conditions which are not directly applicable to BWR operation (e.g., high conductivity). Establishing a link between crack growth rates in stainless steels and ductile nickel base alloys helps to resolve this problem, since it permits the much broader base of data and modeling for stainless steels to provide guidance on the expected response of nickel base alloys in BWR systems [27,160]. This mechanistic link is reasonable since:

- Intergranular cracking is the dominant failure mode and is associated with chromium depletion at the grain boundary in both types of alloys. For stainless steels, EPR is used to quantify sensitization, as described above. However, the EPR technique cannot be used without significant modification on nickel alloys; thus, an "equivalent EPR" is used to represent equivalent chromium depletion profiles in nickel alloys.

  For Alloy 182 weld metal, an equivalent EPR in the range 10 to 20 C/cm^2 is used. For fully solutionized (or fully healed, i.e., no Cr depletion) Alloy 600, an equivalent EPR of 0 to 5 C/cm^2 is appropriate, while for sensitized Alloy 600 a value of 10 to 20 C/cm^2 is used. Alloy 82 is higher in chromium than Alloys 600 or 182 and has less tendency to sensitize; thus an equivalent EPR of 0 to 5 C/cm^2 is justified for the as-welded condition, and 5 to 10 C/cm^2 is appropriate for the post-weld heat treated condition. Clearly more work is needed to evolve a test to quantify the grain boundary compositional effects in nickel alloys.
- Both alloy systems involve ductile FCC structures with similar mechanical properties. Thus, it is reasonable, in preliminary model derivations, to use the same crack tip strain rate algorithms for ductile nickel base alloys as for stainless steels.
- The solubility of the (NiCr) oxides and (FeCr) oxides are similar in BWR water at 288°C, and thus from an electrochemical viewpoint the rate determining steps in the bare surface oxidation kinetics are likely to be comparable for the nickel base and austenitic stainless steel systems. Thus, it is to be expected that the i_o, t_o, and "n" values in Equation 5 will be similar in the two systems and, hence, the general propagation Equation 11 can be used for nickel base alloys.
- Recent studies show that the cracking response of sensitized Alloy 600/182 and sensitized stainless steel is very similar as a function of temperature [161] and water chemistry [24].

Despite these assumptions, the prediction capabilities are in remarkably good agreement with the observations of stress corrosion and corrosion fatigue in the nickel base alloy / BWR systems. For instance, the observed crack propagation rate / stress intensity data for Alloys 182 and 600 are in reasonable agreement with the theoretical predictions for a variety of conductivities in 288°C water containing 200 ppb oxygen (Figure 41). Similarly, the dependency of the crack propagation rate on the BWR water conductivity is accurately predicted for 1T CT specimens of Alloy 182 exposed to BWR recirculation water (Figure 42). Finally, the incidence of cracking of Alloy 600 shroud head bolts as a function of average plant conductivity is also predicted with good accuracy (Figure 43).

Nickel Base Alloys / PWR System

In contrast to the high purity water in BWRs, PWR primary water contains chemical buffers (≈1000 ppm H_3BO_3 and several ppm $LiOH$, values which decrease during the fuel cycle) and about 3.2 ppm of hydrogen (≈35 cc H_2/kg of water). The buffers fix the high temperature pH at ≈6.8, whereas the pH of pure, 288°C water is ≈5.6. This buffered chemistry, and the absence of large potential gradients, helps minimize the aggressiveness of the environment. However, this advantage is partially compensated for by the higher temperatures, ranging up to ≈340°C in the pressurizer.

Unfortunately, little crack growth rate data has been generated in PWR systems against which to compare modeling predictions; experimental focus has traditionally been placed on various types of U-bend specimens. Preliminary efforts based on estimating [104-106] or measuring [39] an appropriate "n" value (Figure 44) indicate that the range in crack growth data in PWR environments are reasonably predicted using the same modeling methodology (Figure 45), especially given the range in temperature, environment, and alloy / microstructure conditions represented by the data. Given the similarity in alloys, temperature, (crack tip) environments, etc., this is not surprising, unless one insists that cracks propagate by fundamentally different mechanisms.

APPLICATION TO SCC MITIGATION AND LIFE EXTENSION

Predictive modeling has numerous applications. Evaluation of optimum plant operation conditions can be made, e.g., by calculating the cost / benefit of reducing corrosion potential and/or conductivity to insure a specific, low growth rate (Figure 46). The benefit of specific mitigation actions, whether hydrogen water chemistry (Figure 34), weld residual stress improvements, or noble metal coatings (Figure 37) can be quantified for generalized or specific components.

Qualification and quantification of mitigation actions are always performed in the accelerated laboratory tests, and predictive modeling can validate the accelerated conditions and interpret the test data to determine the actual factor of improvement (FOI) that is expected in-plant. For example, the diverging curves in Figures 2 and 13 at lower stress intensities or crack tip strain rates mean that the FOI from a remedial action varies with mechanical loading. Thus, a moderate FOI, e.g., from hydrogen water chemistry (Figure 47) that is observed in a slow strain rate test translates to a much greater improvement under plant conditions (lower crack tip strain rate). Similarly, the benefit from a large decrease in corrosion potential from, e.g., noble metal coatings, varies markedly with loading, solution conductivity, and other parameters (Figure 48). The ability to quantitatively predict the complex inter-relationships among all influential variables is critical to these analyses.

Detailed insight into the conceptual elements and underlying dependencies can also lead to the discovery of novel mitigation techniques. This has been the case in the development of noble metal alloys and coatings [153,154], which reduce the corrosion potential to its thermodynamic minimum value (of $\approx -520\ mV_{she}$ in pure, 288°C water) even in the presence of high concentrations of dissolved oxygen and hydrogen peroxide. This technique only requires that stoichiometric excess hydrogen is always present, a condition that is much easier to achieve in BWRs than the large reduction of the oxidant concentrations required by hydrogen water chemistry. Similarly, the discovery of protective insulating oxides [162] provides an opportunity for same low corrosion potentials at high oxidant levels and in the absence of hydrogen (or other reductants). The development of these and other techniques were possible because of the conceptual insight that resulted from the development of predictive modeling.

Finally, the longer term goal of plant life extension is facilitated by mechanistic modeling by providing insight into the long-term repercussions of improved operation and mitigation actions which are always most effective if undertaken earlier in plant operation. Because cracking is quite sensitive to specific environmental parameters (e.g., Figures 28 and 29), real time predictions on operating plants are best accomplished by coupling these factors with system "definers", such as crack monitors and environmental sensors (Figure 49) [13,14,151]. These monitors and sensors can act as calibration devices for the modeling algorithms, and also as clear indications to the operator that the cracking susceptibility of a specific monitored component or system has changed.

CONCLUSIONS

A review has been presented of the unique characteristics of environmental cracking of structural materials in hot water, with an emphasis on high temperature, dilute aqueous environments associated with LWR operation. Candidate mechanisms of environmental crack advance were discussed, and justification was given for the use of the slip dissolution model. The quantitative development of the predictive model was reviewed, and it was shown to be quantitatively accurate for the stainless steel / BWR water system. Extensions to address the special characteristics of irradiation, nickel-base alloys, low alloy and carbon steels, and PWR environments were also presented. The advantages of quantitative, fundamental environmental crack advance models for addressing the design and life evaluation issues were highlighted by comparison with existing, mechanics-based codes.

ACKNOWLEDGEMENTS

The authors would like to acknowledge the innumerable discussions and contributions of our colleagues at the GE Corporate Research and Development Center and GE Nuclear Energy, as well as international colleagues associated with the International Cooperative Groups on Environmentally Assisted Cracking and Irradiation Assisted Stress Corrosion Cracking. The support, spanning nearly 20 years, in the form of enthusiasm and funding from GE Corporate Research and Development Center, GE Nuclear Energy, Electric Power Research Institute, Japan Engineering and Inspection Corporation, and Technische Vereinigung der Grosskraftwerksbetreiber (VGB, Germany) has clearly been critical to this work, and is deeply appreciated.

REFERENCES

1. Proc., *Fundamental Aspects of Stress Corrosion Cracking*, Eds. RW Staehle, AJ Forty & D van Rooyen, NACE, 1969.
2. Proc., *Corrosion Fatigue, Chemistry, Mechanics and Microstructure*, Eds., AJ McEvily & RW Staehle, NACE, 1971.
3. Proc., *Mechanisms of Environment Sensitive Cracking of Materials*, Eds., PR Swann, FP Ford & ARC Westwood, The Metals Society, London, 1977.
4. Proc., *Stress Corrosion Cracking and Hydrogen Embrittlement of Iron-Base Alloys*, Eds., R Staehle, J Hochmann, R McCright & J Slater, NACE, 1977.
5. Proc., *Corrosion Fatigue: Mechanics, Metallurgy, Electrochemistry and Engineering, STP 801*, Eds., TW Crooker & BN Leis, ASTM, 1984.
6. Proc., *Environment Induced Cracking of Metals*, NACE, October 1988.
7. Proc., *Embrittlement by the Localized Crack Environment*, Ed., RP Gangloff, AIME, 1984.
8. Proc. Fifth Int. Symp. on *Environmental Degradation of Materials in Nuclear Power Systems - Water Reactors*, ANS, 1992.
9. Proc., Sixth Int. Symp. on *Environmental Degradation of Materials in Nuclear Power Systems - Water Reactors*, AIME, 1993.
10. Proc., Seventh Int. Symp. on *Environmental Degradation of Materials in Nuclear Power Systems - Water Reactors*, NACE, 1995.
11. F.P. Ford, D.F. Taylor, P.L. Andresen and R.G. Ballinger, "Corrosion Assisted Cracking of Stainless and Low Alloy Steels in LWR Environments", EPRI Contract RP2006-6, Report NP5064M, February 1987.
12. F.P. Ford and P.L. Andresen, "Development and Use of a Predictive Model of Crack Propagation in 304/316L, A533B/A508 and Inconel 600/182 in 288°C Water", *Third Int. Symp. on Degradation of Materials in Nuclear Power Systems - Water Reactors*, AIME, p.789-800, 1988.
13. P.L. Andresen and F.P. Ford, "Life Prediction by Mechanistic Modelling and System Monitoring of Environmental Cracking of Fe and Ni Alloys in Aqueous Systems", *Materials Sci. and Eng.*, A103, p.167-183, 1988.
14. F.P. Ford, P.L. Andresen, H.D. Solomon, G.M. Gordon, S. Ranganath, D. Weinstein, and R. Pathania, "Application of Water Chemistry Control, On-Line Monitoring and Crack Growth Rate Models for Improved BWR Materials Performance", *Fourth Int. Symp. on Environmental Degradation of Materials in Nuclear Power Systems - Water Reactors*, NACE, pp.4-26 to 4-51, 1990.
15. F.P. Ford and P.L. Andresen, "Corrosion in Nuclear Systems: Environmentally Assisted Cracking in Light Water Reactors", in "Corrosion Mechanisms", Ed. P. Marcus and J. Ouder, Marcel Dekker, p.501-546, 1994.
16. P.L. Andresen and F.P. Ford, "Fundamental Modeling of Environmental Cracking For Improved Design and Lifetime Evaluation in BWRs", *Int. J. of Pressure Vessel and Piping* 59, 1994.
17. P.L. Andresen, I.P. Vasatis & F.P. Ford, "Behavior of Short Cracks in Stainless Steel at 288°C", Paper #495, Corrosion/90, NACE, 1990.
18. P.L. Andresen, "Irradiation Assisted Stress Corrosion Cracking", in *Stress Corrosion Cracking: Materials Performance and Evaluation*, Ed. R.H. Jones, ASM, Materials Park, p.181-210, 1992.
19. P.L. Andresen, "Fracture Mechanics Data and Modeling of Environmental Cracking of Nickel Alloys in High Temperature Water", VGB Conference on Corrosion and Corrosion Protection in Power Plants, Germany, 1995.
20. F.P. Ford and P.W. Emigh, *Corrosion Science* 2, 8/9, 673-692, 1985.
21. F.P. Ford, P.L. Andresen, D. Weinstein & S. Ranganath, "SCC of Low Alloy Steels in High Temperature Water", *Proc. Fifth Int. Symp. on Environmental Degradation of Materials in Nuclear Power Systems - Water Reactors*, ANS, pp.561-570, 1991.
22. F.P. Ford and P.L. Andresen, "Corrosion Fatigue of A533B/A508 Pressure Vessel Steels in Water at 288°C", *Proc. Third Intl. Atomic Energy Agency Specialists Mtg on Subcritical Crack Growth*, Moscow, NRC NUREG/CP-0112 (ANL-90/22), Vol. 1, p.105-124, 1990.

23. F.P. Ford and P.L. Andresen, "Stress Corrosion Cracking of A533B/Pressure Vessel Steels in Water at 288°C", *Third Inter. Atomic Energy Agency Specialists Mtg on Subcritical Crack Growth*, Moscow, NRC NUREG/CP-0112 (ANL-90/22), Vol. 2, p.37-54, 1990.
24. P.L. Andresen, "Fracture Mechanics Data & Modeling of Environmental Cracking of Nickel-Base Alloys in High Temperature Water", Corrosion 47, p.917-938, 1991.
25. P.L. Andresen, "Development of Data and Predictive Models for Environmental Cracking of Nickel Alloys in 288°C Water", Final Report on EPRI Contract RP2006-17, May 1991.
26. P.L. Andresen and L.M. Young, "Characterization of the Roles of Electrochemistry, Convection and Crack Chemistry in Stress Corrosion Cracking", *Proc. Seventh Int. Symp. on Environmental Degradation of Materials in Nuclear Power Systems - Water Reactors*, NACE, p.579-596, 1995.
27. P.L. Andresen, "Modelling of Water and Material Chemistry Effect on Crack Tip Chemistry and Resulting Crack Growth Rate Kinetics", *Proc. Third Int. Symp. on Environmental Degradation of Materials in Nuclear Power Systems - Water Reactors*, AIME, p.301-312, 1988.
28. P.L. Andresen, "Conceptual Similarities and Common Predictive Approaches for SCC in High Temperature Water Systems", Paper 96258, Corrosion/96, NACE, 1996.
29. C.M. Chen, K. Aral and G.J. Theus, "Computer Calculated Potential pH Diagrams to 300°C", EPRI NP-3137 Vol.2 (1167-2), June 1983.
30. P.R. Tremaine and J.C. LeBlanc, "The Solubility of Magnetite and the Hydrolysis and Oxidation of Fe^{2+} in Water to 300°C", *J Soln Chem* 9, 6, p.415-442, 1980.
31. P.R. Tremaine and J.C. LeBlanc, "The Solubility of Nickel Oxide and Hydrolysis and Oxidation of Ni^{2+} in Water to 573°K", *J Chem Thermodynamics* 12, 16, p.521-538, 1980.
32. P. Combrade, M. Foucault, P. Marcus, J.-M. Grimal, and A. Gelpi, "Effect of Sulfur on the Protective Layers of Alloys 600 and 690 in Low and High Temperature Environments", *Proc. Fourth Int. Symp. on Environmental Degradation of Materials in Nuclear Power Systems - Water Reactors*, NACE, p.5-79 to 5-95, 1990.
33. P. Combrade, M. Foucault, P. Marcus, G. Slama, "On the Role of Sulfur on the Dissolution of Pressure Vessel Steels at the Tip of a Propagating Crack in PWR Environment", *Proc. Fourth Int. Symp. on Environmental Degradation of Materials in Nuclear Power Systems - Water Reactors*, NACE, p.8-48 to 8-63, 1990.
34. T. Shoji, S. Moriya and M. Tada, "Computer Simulation of Environmentally Assisted Cracking of RPV Steels in LWR Environments", *Proc. Fourth Int. Symp. on Environmental Degradation of Materials in Nuclear Power Systems - Water Reactors*, NACE, p.8-28 to 8-47, 1990.
35. B.W. Bussert, I. Goldberg, R.F. Keefer, and N. Lewis, "An Integrated Approach to Investigating SCC", Workshop on PWSCC of Alloy 600 in PWRs, EPRI, April 1993.
36. T.M. Angeliu and G.S. Was, "Creep and Intergranular Cracking of Ni-Cr-Fe Alloys in Argon at 360°C", *Met. Trans*, 25A, p.1169-1184, 1994.
37. T.M. Angeliu, D.J. Paraventi, and G.S. Was, "Creep and Intergranular Cracking of Ni-Cr-Fe-C Alloys in 360°C Water", *Corrosion*, 51, p.837-848, 1996.
38. P.L. Andresen, "The Effects of Nitrate on the Stress Corrosion Cracking of Sensitized Stainless Steel in High Temperature Water", *Proc. Seventh Int. Symp. on Environmental Degradation of Materials in Nuclear Power Systems - Water Reactors*, NACE, p.609-620, 1995.
39. T.M. Angeliu, P.L. Andresen, and M.L. Pollick "Repassivation and Crack Propagation of Alloy 600 in 288°C Water", Paper 96086, Corrosion/96, NACE, 1996.
40. S. Suresh and R. Ritchie, "The Propagation of Short Fatigue Cracks", U. of California Berkeley Report UCB/RP/83/1014, June 1983.
41. J. Lankford, *Fat. Eng. Mat'ls and Str.* 6, 15, 1983.
42. S. Pearson, *Eng. Fracture Mech.* 7, 235, 1975.
43. W.L. Morris, O. Buck and H.L. Marcus, *Met. Trans.* A74, 1161, 1976.
44. M.H. El Haddad, T.H.. Topper and B. Mukherjee, *J. Test Eval.* 9, 65, 1981.
45. R.N. Parkins, *Corrosion* 43, 130, 1987.
46. R.N. Parkins and P.M. Singh, *Corrosion*, 46, 485-498, 1990.
47. F.P. Ford, "Mechanisms of Environmental Cracking Peculiar to the Power Generation Industry", Report NP2589, EPRI, Palo Alto, September 1982.
48. F.P. Ford, "Stress Corrosion Cracking", in *Corrosion Processes*, Ed. RN Parkins, Applied Science, 1982.
49. R.N. Parkins, N.J.H. Holroyd and R.R. Fessler, *Corrosion* 34, 253, 1978.
50. T.P. Hoar and G.P. Rothwell, *Electrochem. Acta* 15, 1037, 1976.
51. T.R. Beck, *Corrosion* 30, 408, 1974.
52. C. Manfred, I. Maier and J.R. Galvale, *Corr. Sci.* 27, 887, 1987.
53. J.M. Sutcliff, R.R. Fessler, W.K. Boyd and R.N. Parkins, *Corrosion* 28, 313, 1972.
54. B. Poulson and R. Robinson, *Corr. Sci.* 20, 707, 1980.
55. F.P. Ford, "BWR Environmental Cracking Margins in Carbon Steel Piping", Final Report, Contract RP1248-1, EPRI, Palo Alto, 1981.

56. "Environmental Sensitive Mechanical Behavior", Eds., ARC Westwood and NS Stoloff, Gordon and Branch, 1965.
57. "Theory of Stress Corrosion Cracking", Ed., JC Scully, NATO, Brussels, March 1971.
58. "Corrosion Fatigue Chemistry, Mechanics and Microstructure", Eds., O Devereaux, AJ McEvily and RW Staehle, NACE, 1972.
59. "L'Hydrogene dans les Metaux", Paris, Ed. MP Bastein, Science et Industrie, 1972.
60. "Hydrogen in Metals", Eds., IM Bernstein and AW Thompson, ASM, 1973.
61. "Effect of Hydrogen on Behavior of Materials", Eds., AW Thompson and IM Bernstein, AIME, 1975.
62. "Surface Effects on Crystal Plasticity", Eds., RM Latanision and JT Fourie, Noordhof-Leyden, 1977.
63. "Corrosion Fatigue", University of Newcastle, Met. Sci. 13, 1979.
64. R.N. Parkins, *British Corr. J.* 7, 15, 1972.
65. R.N. Parkins and B.S. Greenwell, *Met. Sci.* 405, 1977.
66. C. Laird and D.J. Duquette, in *Surface Effects on Crystal Plasticity*, Eds., RM Latanision and JT Fourie, Noordhof-Leyden, p.88, 1977.
67. R.N. Parkins, "Environment Sensitive Fracture - Controlling Parameters", Proc. of Third Int. Conf. on *Mechanical Behavior of Materials*, Cambridge, Eds., KJ Miller and RF Smith, Pergamon, Vol. 1, p.139-164, 1980.
68. J.M. Kraft and J.H. Mulherin, *Trans. ASM* 62, 64, 1969.
69. T.P. Hoar, *Corrosion* 19, 331, 1963.
70. P.R. Swann, *Corrosion* 19, 102, 1963.
71. T.R. Beck, *Corrosion* 30, 408, 1974.
72. H.L. Logan, *J. Natl. Bur. Stand.* 48, 99, 1952.
73. R.W. Staehle, *Theory of Stress Corrosion Cracking*, Ed., JC Scully, NATO Brussels, p.223, March 1971.
74. J.C. Scully, *Corros. Sci.* 8, 771, 1968.
75. T.P. Hoar, *Theory of Stress Corrosion Cracking*, Ed., JC Scully, NATO Brussels, p.106, March 1971.
76. D.A. Vermilyea, *J. Electrochem. Soc.* 119, 405, 1972.
77. F.P. Ford, "The Crack Tip System and its Relevance to the Prediction of Environmentally assisted Cracking", Proc., First Int. Conf. on *Environment Induced Cracking of Metals*, NACE, p.139-166, 1988.
78. J. Hickling, "Strain Induced Corrosion Cracking; Relationship to Stress Corrosion Cracking/Corrosion Fatigue and Importance for Nuclear Plant Service Life", *Third IAEA Specialists Meeting on Subcritical Crack Growth*, Moscow, May 1990.
79. K. Sieradzki and R.C. Newman, *Phil. Mag.* A51, 95-132, 1985.
80. C. Edeleanu and A.J. Forty, *Philos. Mag.* 5, 1029, 1960.
81. J.A. Beavers and E.N. Pugh, *Met. Trans.* 11A, 809, 1980.
82. K. Sieradzki, "Atomistic and Micromechanical Aspects of Environment Induced Cracking of Metals", Proc., First Int. Conf. on *Environment Induced Cracking of Metals*, NACE, p.125-138, 1988.
83. R.C. Newman, "Stress Corrosion of Austenitic Steels", Proc., First Int. Conf. on *Environment Induced Cracking of Metals*, NACE, p.489-510 1988.
84. A.W. Thompson and I.M. Bernstein, "The Role of Metallurgical Variables in Hydrogen Assisted Environmental Fracture", Rockwell Science Center Report SCPP-75-63, 1975.
85. J.P. Hirth, *Met. Trans.* 11A, 861-890, 1980.
86. H.G. Nelson, "Hydrogen Embrittlement", *Treatise on Material Science and Technology* Vol. 25, Eds., CL Briant & SK Banerji, Academic Press, p.275-359, 1983.
87. H.K. Birnbaum, "Hydrogen Embrittlement", Proc., First Int. Conf. on *Environment Induced Cracking of Metals*, NACE, p.21-29, 1988.
88. F.P. Ford, *Metal Sci.*, p.326-334, July 1978.
89. R. Raj and V.K. Varadan, "The Kinetics of Hydrogen Assisted Crack Growth", *Mechanisms of Environment Sensitive Cracking of Materials*, Eds., PR Swann, FP Ford & ARC Westwood, The Metals Society, p.426, April 1977.
90. R.A. Oriani, "Hydrogen Effects in High Strength Steels", Proc., First Int. Conf. on *Environment Induced Cracking of Metals*, NACE, p.439-448, 1988.
91. R.A. Oriani, *Bertichte der Bunsenges for Phys. Chem.* 76, 848, 1972.
92. W.W. Gerberich, Y.T. Chen, C. St. John, *Met. Trans.* 6, 1485, 1975.
93. F. de Kazinski, *J. Iron Steel Inst.* 177, 85, 1954.
94. C.A. Zapffe and C.E. Sims, *Trans. AIME* 145, 225, 1941.
95. C.D. Beachem, *Met. Trans.* 3, 437, 1972.
96. S.P. Lynch, *Met. Forum* 2, 189, 1979.
97. R.A. Gilman, "The Role of Surface Hydrides in Stress Corrosion Cracking", *Stress Corrosion Cracking and Hydrogen Embrittlement of Iron-Base Alloys*, Eds., RW Staehle, J Hochmann, RD McCright & JE Salter, NACE, p.326, 1977.
98. C.L. Briant, *Met. Trans.* 10A, 181, 1979.
99. H. Hanninen, K. Torronen, M. Kempainen, and S. Salonen, *Corr. Sci.* 23, 663, 1983.
100. K. Torronen, M. Kemppainen, and H. Hanninen, "Fractrographic Evaluation of Specimens of A533B Pressure Vessel Steel", Final Report of EPRI Contract RP1325-7, Report NP 3483, May 1984.

101. C.A. Grove and L.D. Petzold, "Mechanism of SCC of Alloy X750 in High Purity Water", *J. of Materials for Energy Systems* 7, 2, p.147-162, 1985.
102. P.L. Andresen, F.P. Ford, J.P. Higgins, I. Suzuki, M. Koyama, M. Akiyama, T. Okubo, Y. Mishima, "Life Prediction Of Boiling Water Reactor Internals", Proc. *ICONE-4 Conference*, ASME, 1996.
103. T.B. Cassagne A. Gelpi, "The Influence of Loading on the IGSCC Crack Growth Rate of Alloy 600 Steam Generator Tubing", *Proc. Int. Symp. on Plant Aging and Life Prediction of Corrodible Structures*, NACE, 1996.
104. C.D. Thompson, N. Lewis, and H.T. Krasodomski, "Analysis of A600 and X-750 SCC Cracks", Proc., *Alloy 600 Experts Meeting*, Arlie, VA, EPRI, Palo Alto, April 6-9, 1993.
105. C.D. Thompson, H.T. Krasodomski, N. Lewis, and G.L. Makar, "Prediction of PWSCC in Nickel Base Alloys Using Crack Growth Models", *Proc. Seventh Int. Symp. on Environmental Degradation of Materials in Nuclear Power Systems - Water Reactors*, NACE, p.867-880, 1995.
106. D.M. Carey, D.J. Perry, T.R. Miller and C.D. Thompson, "Alloy 600 SCC Growth Measurements in Primary Coolant", Proc., *Workshop on PWSCC of Alloy 600 in PWRs*, EPRI, November 1994.
107. D.F. Taylor and C.A. Caramihas, "High Temperature Aqueous Crevice Corrosion in Alloy 600 and 304L Stainless Steel", Proc., *Embrittlement by Localized Crack Environment*, Ed., RP Gangloff, AIME, p.105-114, 1983.
108. D.F. Taylor and C.C. Foust, *Corrosion* 44, pp.204-208, 1988.
109. G. Gabetta and G. Buzzanaca, "Measurement of Corrosion Potential Inside and Outside Growing Crack During Environmental Fatigue Tests", Proc., *Second Int. IAEA Specialists Meeting on Subcritical Crack Growth*, NUREG CP0067, Vol. 2, Sendai, Japan, p.219-230, May 1985.
110. P. Combrade, M. Foucault and G. Slama, "About the Crack Tip Environment Chemistry in Pressure Vessel Steel Exposed to Primary PWR Coolant", Proc., *Second Int. IAEA Specialists Meeting on Subcritical Crack Growth*, NUREG CP0067, Vol. 2, Sendai, Japan, pp.201-218, May 1985.
111. A. Turnbull, *Reviews on Coatings and Corrosion* 5, 43-171, 1982.
112. A. Turnbull, *Corr. Sci.* 23, 833-870, 1983.
113. A. Turnbull, "Progress in the Understanding of the Electrochemistry in Cracks", Proc., *Embrittlement by Localized Crack Environment*, Ed., RP Gangloff, AIME, p.3-31, 1983.
114. P.L. Andresen, "Transition and Delay Time Behavior of High Temperature Crack Propagation Rates Resulting from Water Chemistry Changes", Proc., *Second Int. Symp. on Environmental Degradation of Materials in Nuclear Power Systems - Water Reactors*, ANS, p.84-92, 1986.
115. F.P. Ford and P.L. Andresen, "Stress Corrosion Cracking of Low Alloy Steels in 288 C Water", Paper 89498, Corrosion/89, NACE, 1989.
116. P.L. Andresen & L.M. Young, "Crack Tip Microsampling and Growth Rate Measurements in Low Alloy Steel in High Temperature Water", *Corrosion* 51, p.223-233, 1995.
117. P. Combrade, "Prediction of Environmental Crack Growth on Reactor Pressure Vessels", EPRI Contract RP2006-8, UNIREC Report #1667, February 1985.
118. S.M. Bruemmer, L.A. Charlot and B.W. Arey, *Corrosion* 44, 328-333, 1988.
119. S.M. Bruemmer, L.A. Charlot and D.G. Atteridge, *Corrosion* 44, 427-434, 1988.
120. K.L. Luthra and C.L. Briant, *Met. Trans. A*, 19A, 1091-2108, 1988.
121. G.S. Was and V.B. Rajan, *Corrosion* 43, 576, 1987.
122. T.M. Devine, *Acta Met.* 36, 1491, 1988.
123. Proc., Symp. on *Radiation Induced Sensitization of Stainless Steels*, Ed., DIR Norris, CEGB, Berkeley Nuclear Laboratories, September 1986.
124. T.P. Hoar and F.P. Ford, *J. Electrochemical Soc.* 120, 1013, 1973.
125. D. Engseth and J.C. Scully, *Corr. Sci.* 15, 505, 1975.
126. T. Zakroczmski and R.N. Parkins, *Corr. Sci.* 20, 723, 1980.
127. Y.S. Park, J.R. Galvele, A.K. Agrawal and R.W. Staehle, *Corrosion* 34, 413, 1978.
128. R.B. Diegle and D.A. Vermilyea, *J. Electrochem. Soc.* 122, 180, 1975.
129. F.P. Ford and M. Silverman, *Corrosion* 36, p.558-565, 1980.
130. T.R. Beck, *Corrosion* 30, p.408, 1974.
131. R.P. Wei and A. Alavi, *Scripta Met.* 22, p.969-974, 1988.
132. C. Patel, *Corr. Sci.* 21, p.145, 1981.
133. F.P. Ford, G.T. Burstein and T.P. Hoar, *J. Electrochem. Soc. 127, 6, 1980.*
134. T. Hagyard and W.B. Earl, J. Electrochem. Soc. 115, 623, 1968.
135. J. Pagetti, D. Lees, F.P. Ford and T. Hoar, *Comp. R. Acad. Sci. Paris*, 273, 1121, 1971.
136. D.J. Lees and T.P. Hoar, *Corr. Sci.* 20, 723, 1980.
137. R.C. Newman and G.T. Burstein, *Corr. Sci.* 21, 119, 1981.
138. R.B. Diegle and D.M. Lineman, *J. Electrochem. Soc.* 131, 106, 1984.
139. J.R. Ambrose and J. Kruger, *Corrosion* 28, 30, 1972.
140. Z. Szklarski-Smialowska and W. Kozlowski, *J. Electrochem. Soc. 131, 234, 1984.*
141. B. McDougall, J. Electrochem. Soc. 130, 114, 1983.

142. G.M. Bulman and A.C.C. Tseung, *Corr. Sci.* 12, 415, 1972.
143. A.T. Cole and R.C. Newman, *Corr. Sci.* 28, 109-118, 1988.
144. M. Cid, M. Puiggali, H. Fatmaoui and M. Petit, *Corr. Sci.* 28, 61-68, 1988.
145. P. Hurst (UKAEA Risley), private communication, Vasteras, Sweden, June 1988.
146. R.W. Staehle, J.J. Royuela, T.L. Raredon, E. Serrate, C.R. Morin and R.V. Ferrar, *Corrosion* 26, 451, 1970.
147. R.N. Parkins, G.P. Marsh and J.T. Evans, "Strain Rate Effects in Environment Sensitive Fracture", Proc., EPRI Conf. on *Predictive Methods for Assessing Corrosion Damage to BWR Piping and PWR Steam Generators*, Mt. Fuji, Eds., H Okada & RW Staehle, NACE, 1982.
148. D.P.G. Lidbury, "The Estimation of Crack Tip Strain Rate Parameters Characterizing Environment Assisted Crack Data", Proc., *Embrittlement by Localized Crack Environment*, Ed., RP Gangloff, AIME, p.149-172, 1983.
149. F.P. Ford, *J. Pressure Vessel Technology* 1, 113, 1988.
150. W.R. Wearmouth, G.P. Dean and R.N. Parkins, *Corrosion* 29, 251, 1973.
151. P.L. Andresen, F.P. Ford, H.D. Solomon and D.F. Taylor, "A Monitoring and Modelling Approach for Predicting Stress Corrosion and Corrosion Fatigue Damage", *J. of Metals*, 42, p.7-12, 1990.
152. P.L. Andresen & F.P. Ford, "Modeling & Prediction of Irradiation Assisted Stress Corrosion Cracking", Proc., *Seventh Int. Symp. on Environmental Degradation of Materials in Nuclear Power Systems - Water Reactors*, NACE, p.893-908, 1995.
153. P.L. Andresen, "Application of Noble Metal Technology for Mitigation of SCC in BWRs, *Seventh Int. Symp. on Environmental Degradation of Materials in Nuclear Power Systems - Water Reactors*, NACE, p.563-578, 1995.
154. S. Hettiarachchi, G.P. Wozadlo, T.P. Diaz, P.L. Andresen and R.L Cowan, "The Concept of Noble Metal Addition Technology for IGSCC Mitigation of Nuclear Materials", *Seventh Int. Symp. on Environmental Degradation of Materials in Nuclear Power Systems - Water Reactors*, NACE, p.735-746, 1995.
155. Proc., *First Int. Atomic Energy Agency Specialists Meeting on Subcritical Crack Growth*, Vol.1,2, Freiberg, Germany, NUREG CP-0044, May 13-15, 1981.
156. Proc., *Second Int. Atomic Energy Agency Specialists Meeting on Subcritical Crack Growth*, Vol.1,2, Sendai, Japan NUREG CP-0067, May 15-17, 1985.
157. Proc., *Third Int. Atomic Energy Agency Specialists Meeting on Subcritical Crack Growth*, Moscow, USSR, NUREG/CP 0112, May 1990.
158. F.P. Ford and P.L. Andresen, "Corrosion Fatigue of Pressure Boundary Materials", Manuscript 1571, Proc., *Seventh Int. Conf. on Fracture*, Eds., K Salama et al., ISBN 0-08-034343-0, Vol. 2, p. 1571-1583, March 1989.
159. F.P. Ford, "Prediction of Corrosion Fatigue Initiation in Low Alloy and Carbon Steel/Water Systems at 288C", *Sixth Int. Symp. on Environmental Degradation of Materials in Nuclear Power Systems - Water Reactors*, TMS, p.9-18, 1993.
160. P.L. Andresen, *Corrosion* 44, 376, 1988.
161. P.L. Andresen, "Effects of Temperature on Crack Growth Rates of Stainless Steel and Alloy 600", *Corrosion* 49, p.714-725, 1993.
162. P.L. Andresen and Y.J. Kim, "Insulated Protective Coating for Mitigation of SCC in Metal Components in High Temperature Water", U.S. Patent 5,465,281, Issued November 7, 1995.
163. WS Hazelton, "Technical Report on Material Selection and Processing Guidelines for BWR Coolant Pressure Boundary Piping", Draft Report NUREG 0313, Rev. 2, U.S. Nuclear Regulatory Commission.
164. M. Higuchi and K. Iida, Nuclear Engineering and Design 129, pp. 293-306, 1991.
165. W. Shack et al. "Environmentally Assisted Cracking in LWR", NUREG/CR 4667 Vol. 14, Semi Annual Report October 1991-March 1992, pp. 4-13.
166. W. Shack, Presentation to ASME PVRC Meeting, New York, October 13, 1992.

TABLE 1

Crack Tip Strain Rate (s^{-1}) Formulations for Unirradiated Steels in 288°C Water

	Type 304 Stainless Steel	A533B Low Alloy Steel
Constant Load	$4.1 \times 10^{-14} K^4$	$3.3 \times 10^{-13} K^4$
Slow Strain Rate	$5 \dot{\varepsilon}_{app}$	$10 \dot{\varepsilon}_{app}$
Cyclic Load	$68.3 \dot{\nu} A_R \Delta K^4$	$547 \dot{\nu} A_R \Delta K^4$

K (ΔK) = stress intensity (amplitude) in $MPa\sqrt{m}$
$\dot{\varepsilon}_{app}$ = applied strain rate in s^{-1}
$\dot{\nu}$ = frequency of (symmetrical) load cycle in s^{-1}
R = minimum load / maximum load

A_R = constant in "dry" Paris Law
$= 2.44 \times 10^{-11}$ (for $R \leq 0.42$)
$= -2.79 \times 10^{-11} + 1.115 \times 10^{-10} R + 5.5 \times 10^{-11} R^2$ (for $R > 0.42$)

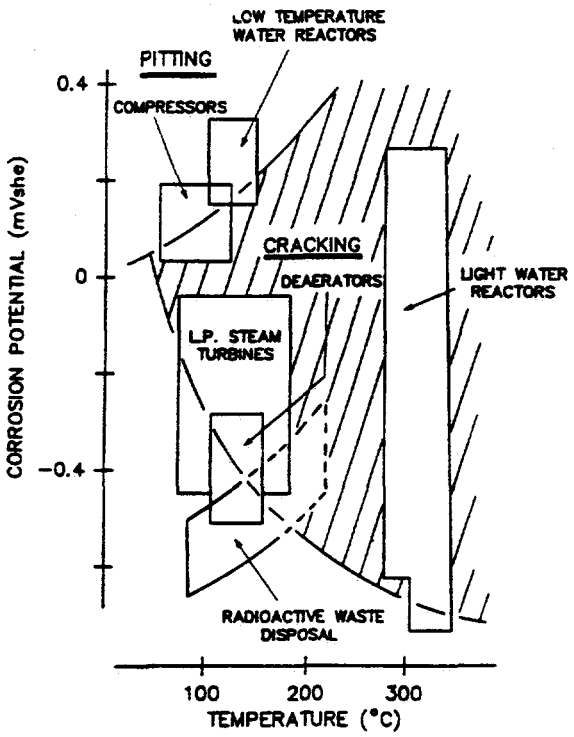

Figure 1 - Schematic of corrosion potential vs. temperature showing the range and commonality of hot water systems associated with various technologies.

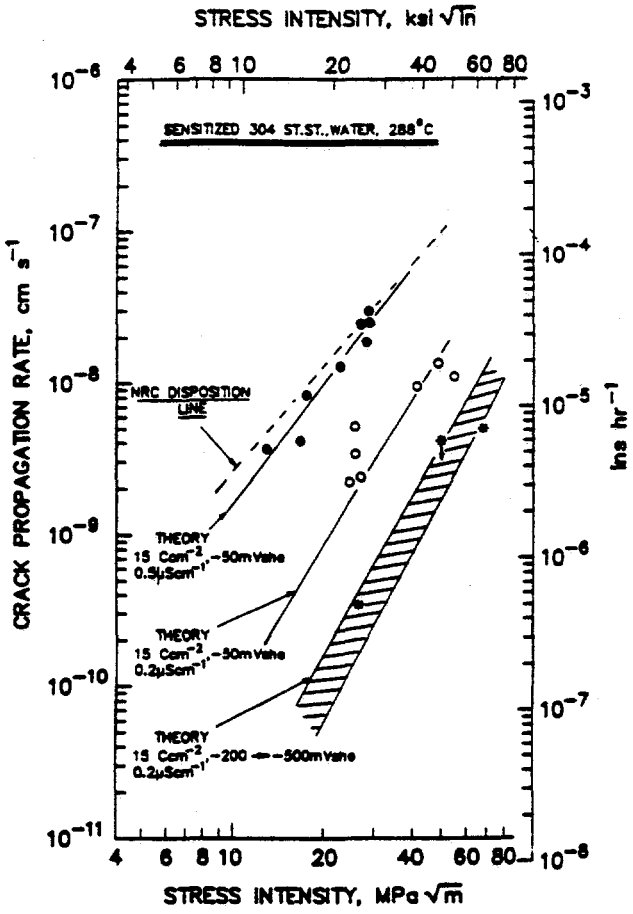

Figure 2 - Predicted crack velocity vs. stress intensity for different water chemistries or degrees of sensitization for sensitized type 304 stainless steel in oxygenated 288°C water or nominally high purity. The relationship to the empirically derived NRC disposition line [163], which is based on a single material and water chemistry condition, is also shown.

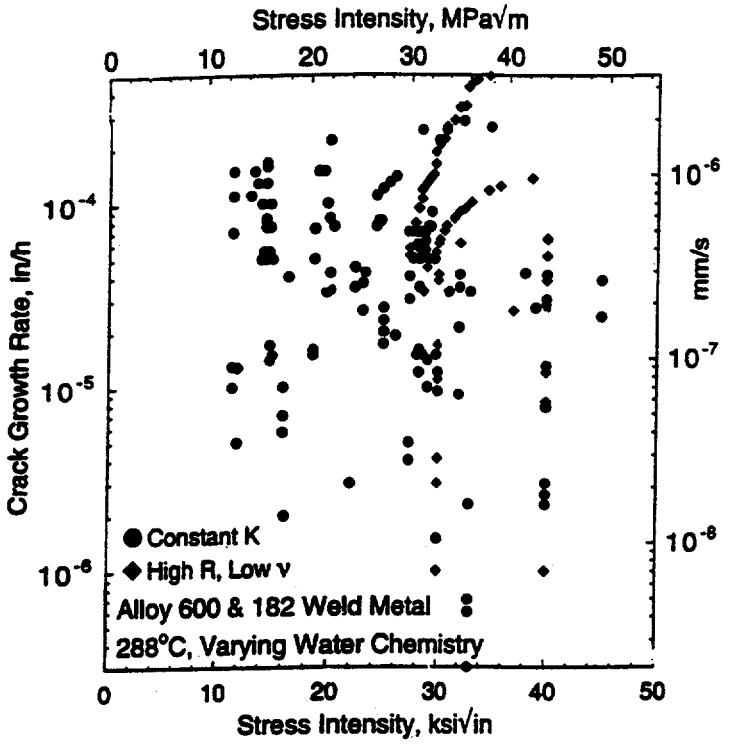

Figure 3 - Crack growth rate vs. stress intensity in 288°C water for Alloy 600 and Alloy 182 weld metal. The inadequate definition of a nominal water and/or material chemistry condition results in orders of magnitude spread in crack growth rate that can be mistakenly interpreted, e.g., for a very high dependence on stress intensity.

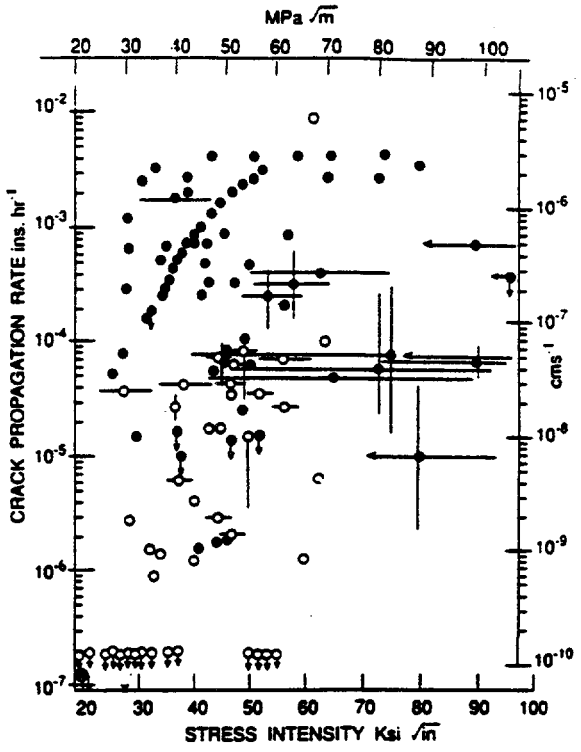

Figure 4 - Summary of stress corrosion data for A533B, A508, SA333, and SA106 low alloy and carbon steels in oxygenated, 288°C water. The closed symbols represents tests in 8 ppm O_2; open symbols, 200 ppb O_2.

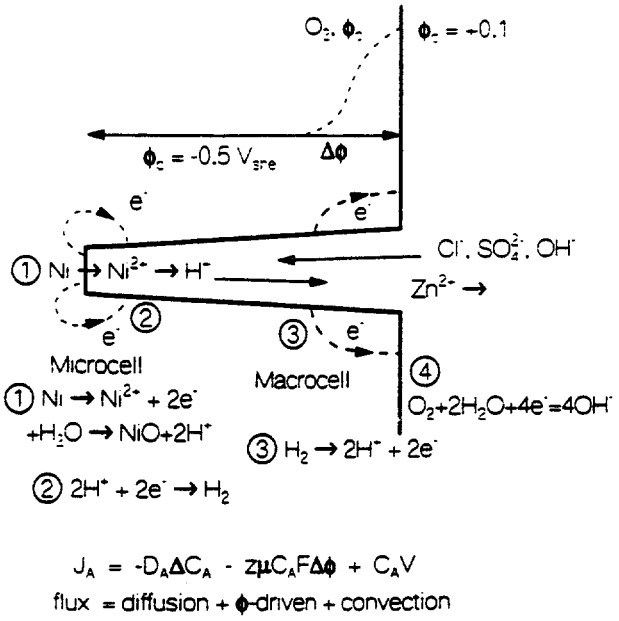

Figure 5 - Schematic of crack showing the differential aeration macrocell that establishes the crack tip chemistry and the local microcell associated with metal dissolution and crack advance. O_2 depletion typically occurs near the mouth of the crack. While it strongly influences crack chemistry, the differential aeration macrocell is not essential to the crack advance process.

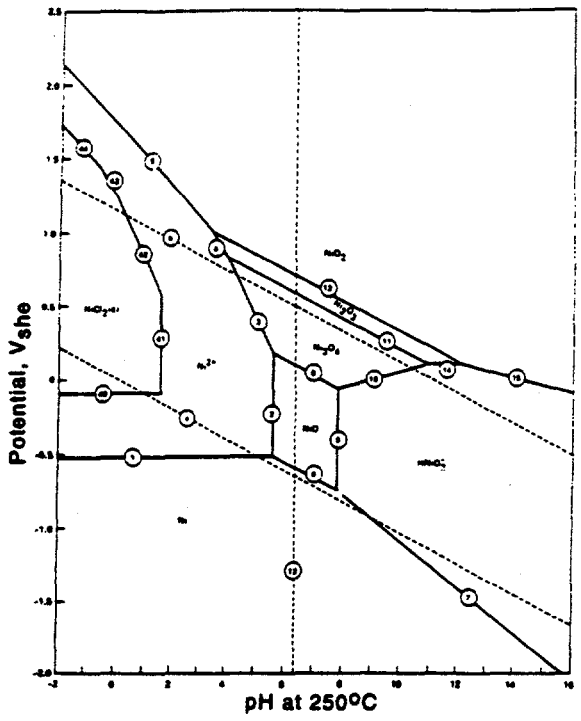

Figure 6 - Pourbaix (potential vs. pH) diagram for the Ni - water system at 250°C [29].

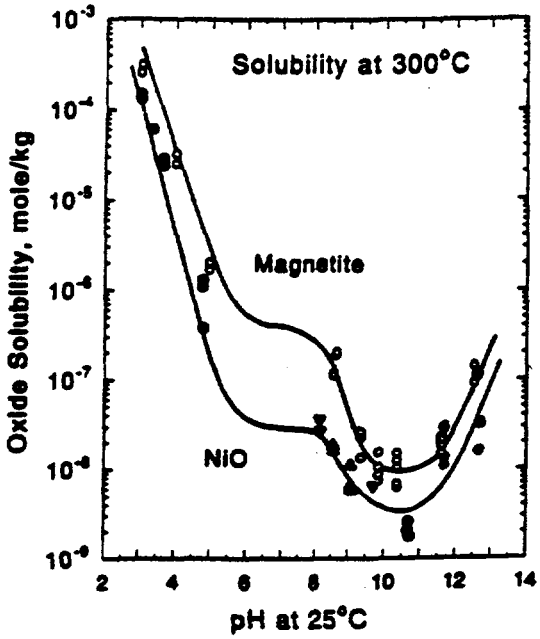

Figure 7 - Experimental solubilities of iron and nickel oxides at 300°C and 780 mole/kg H_2 with least squares fit plotted against $pH_{25°C}$. Compared to chromium oxide, the solubilities of iron and nickel oxides are similar [30,31].

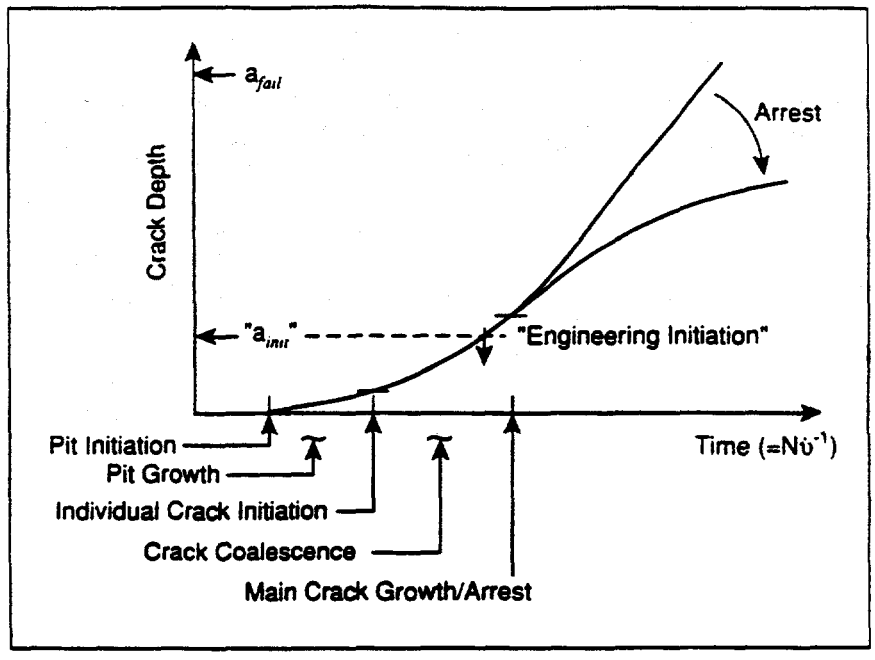

Figure 8 - Schematic sequence of crack initiation, coalescence and growth for environmental cracking of steels in aqueous environments.

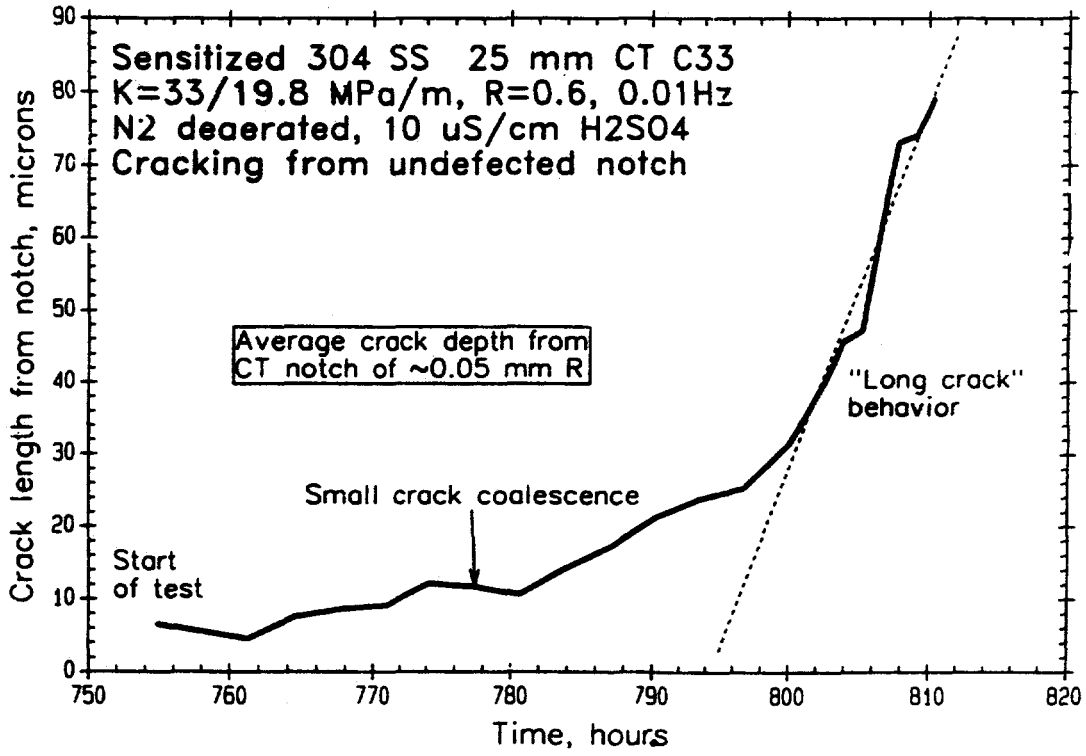

Figure 9 *- Crack depth vs. time for initiation, coalescence and growth of small intergranular cracks in a blunt notch, 1T CT specimen of sensitized stainless steel in 288°C water.*

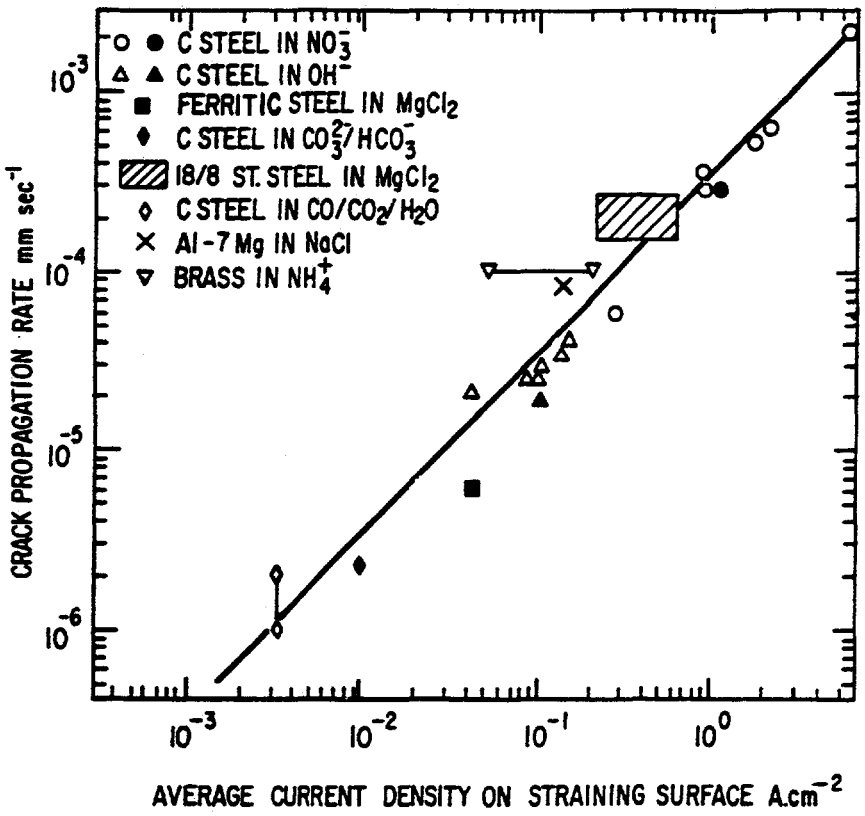

Figure 10 *- The relationship between the average crack growth rate and oxidation kinetics on a strained surface for various ductile alloys in aqueous environments.*

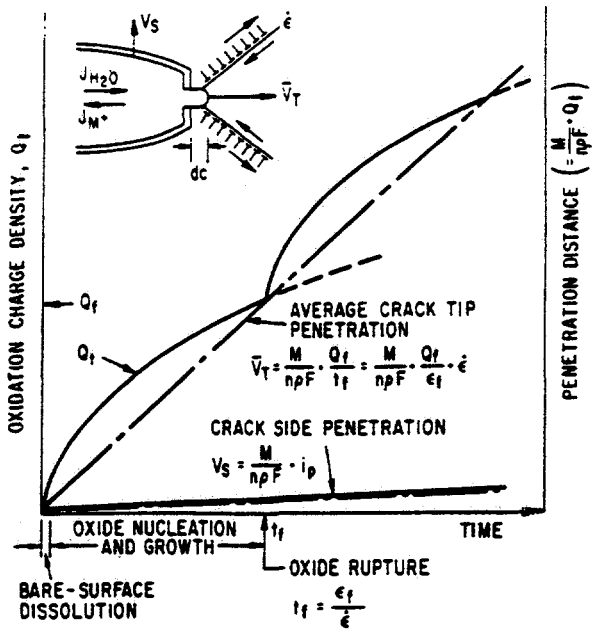

Figure 11 *- Schematic oxidation charge density vs. time for a strained crack tip and unstrained crack sides in the slip dissolution mechanism.*

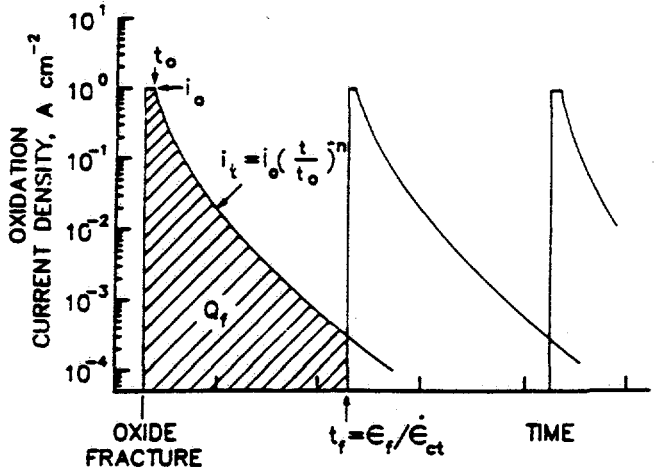

$$V = \frac{dq}{dt}\ ;\ \bar{V}_{av} = \frac{M}{ZF}\cdot\frac{Q_f}{t_f}$$

FOR HIGH $\dot{\epsilon}_{ct}$ AND/OR LONG t_o :

$$\bar{V}_{av} = \frac{M}{ZF}\cdot i_o$$

FOR LOW $\dot{\epsilon}_{ct}$ AND/OR SHORT t_o :

$$\bar{V}_{av} = \frac{M}{ZF}\,\frac{i_o t_o^n}{(1-n)\epsilon_f^n}\,\dot{\epsilon}_{ct}^n = f(n)\,\dot{\epsilon}_{ct}^n$$

Figure 12 *- Schematic of oxidation current density vs. time following repeated oxide rupture events. Since repassivation typically follows a power law response of* $i = i_o \cdot (t/t_o)^{-n}$*, the mathematics distills to an appealing and elegant expression:* $V = A\,(\dot{\epsilon}_{ct})^n$.

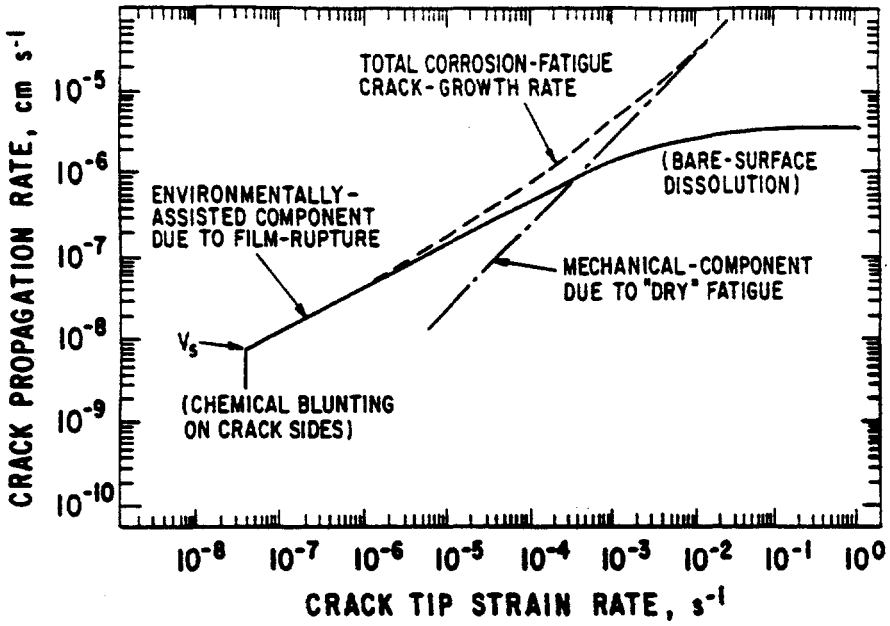

***Figure 13** - Illustration of the strain rate dependence of the crack growth rate due to the slip dissolution model, the additive nature of the mechanical and environmental components of crack advance during corrosion fatigue, and the saturation in the environmental component of crack advance at high strain rates.*

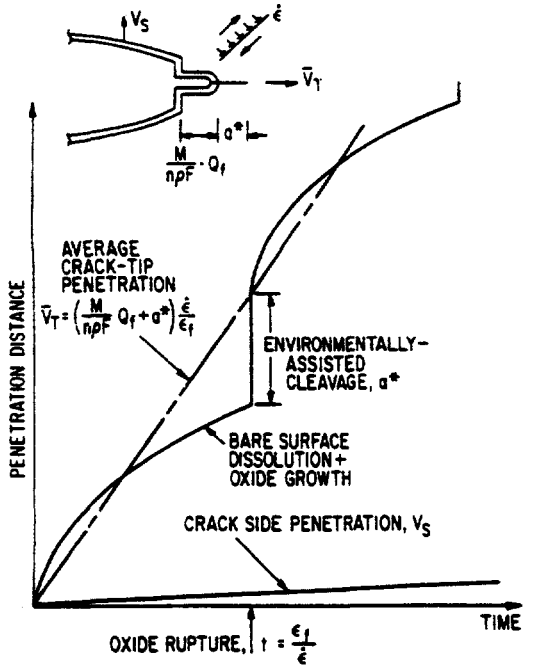

***Figure 14** - Schematic oxidation charge density vs. time showing the elements of the film induced cleavage mechanism of crack advance. Note the contribution of the slip dissolution model to total crack advance.*

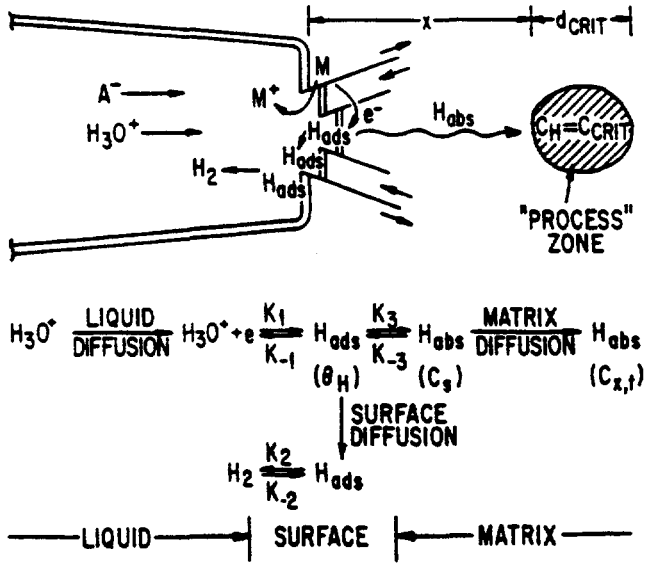

***Figure 15** - Schematic of various crack tip reactions associated with hydrogen embrittlement mechanisms in aqueous environments.*

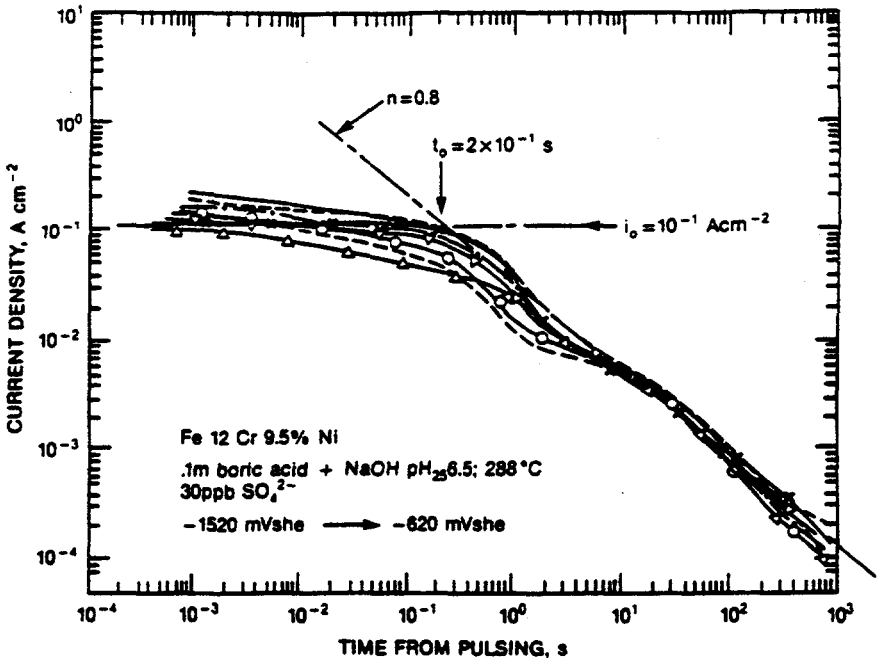

Figure 16 - Oxidation current density vs. time following rupture of the protective oxide on a wire by rapid straining.

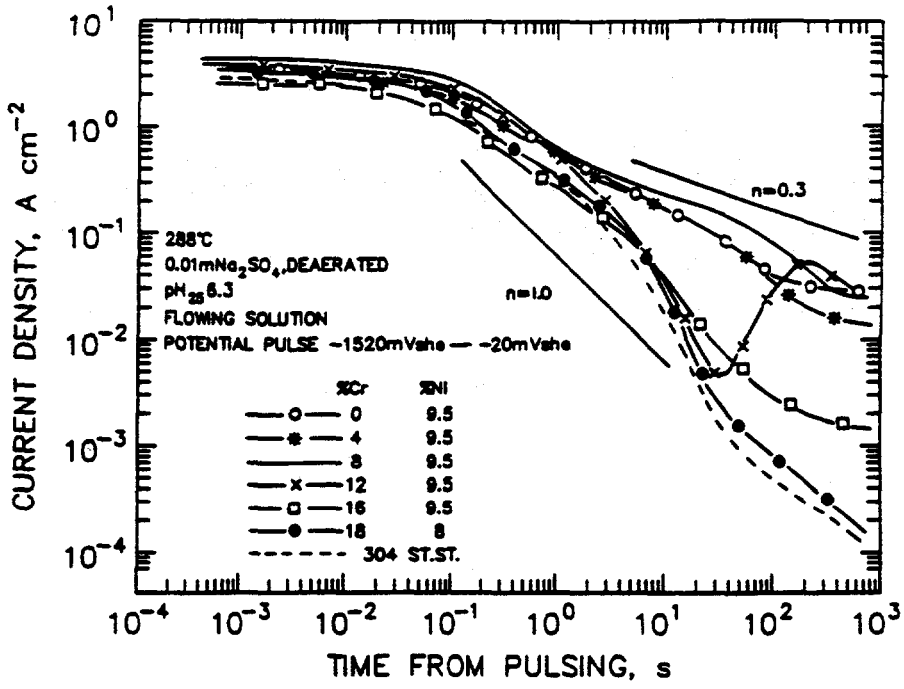

Figure 17 - Example of the dependence of chromium content in stainless steel on repassivation kinetics (oxidation current density vs. time) following rupture of the protective oxide on a wire by rapid straining.

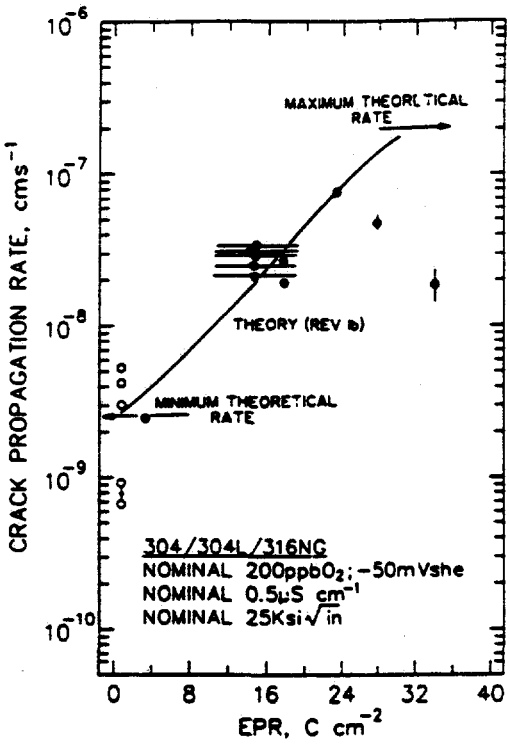

***Figure 18** - Comparison of the observed (points) and predicted (solid curve) crack growth rate vs. degree of sensitization (as measured by EPR) for stainless steel in 288°C water.*

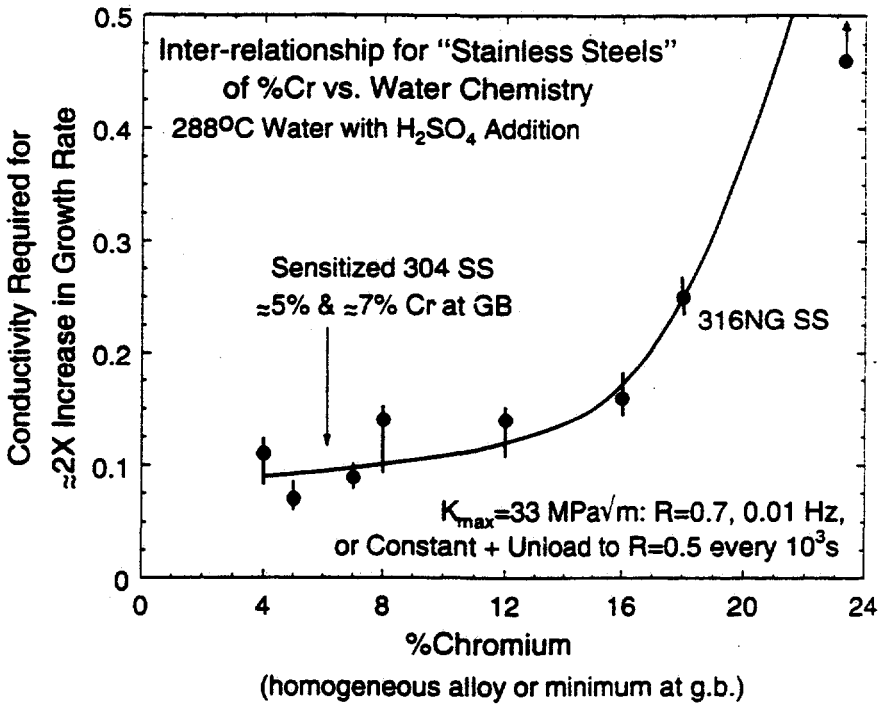

***Figure 19** - The relationship between the chromium content in "stainless steel" and the solution conductivity (as H_2SO_4) required to cause a 2X increase in crack growth rate above that observed in high purity water. Grain boundary chromium was varied by using custom melted, homogeneous alloys and by thermally sensitizing type 304 stainless steel.*

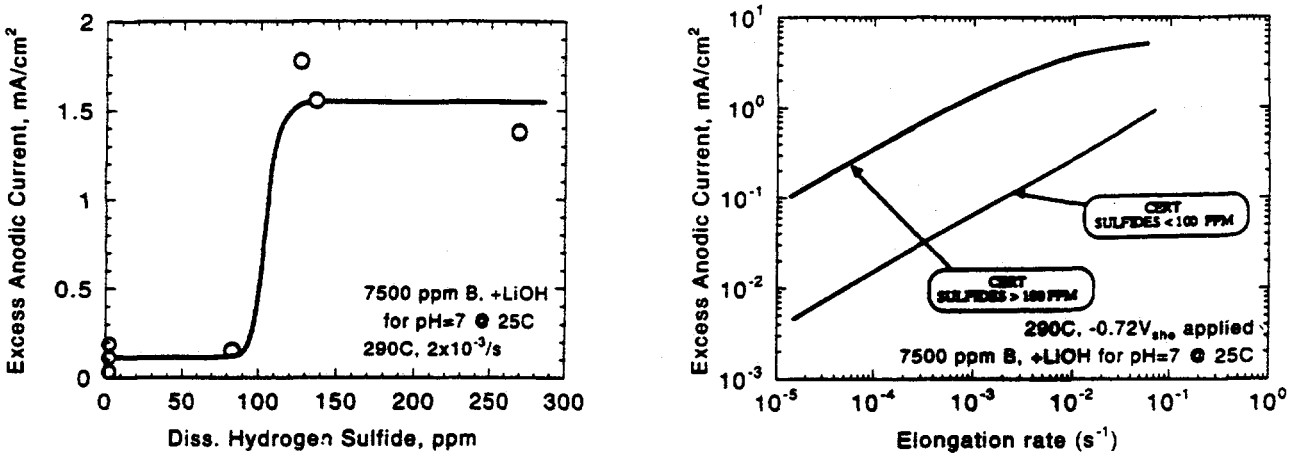

Figure 20 *- The effects of sulfide concentration on the excess anodic current density (metal dissolution rate) and slow strain rate behavior of Alloy 600 showing a steep threshold at ≈100 ppm sulfide [32].*

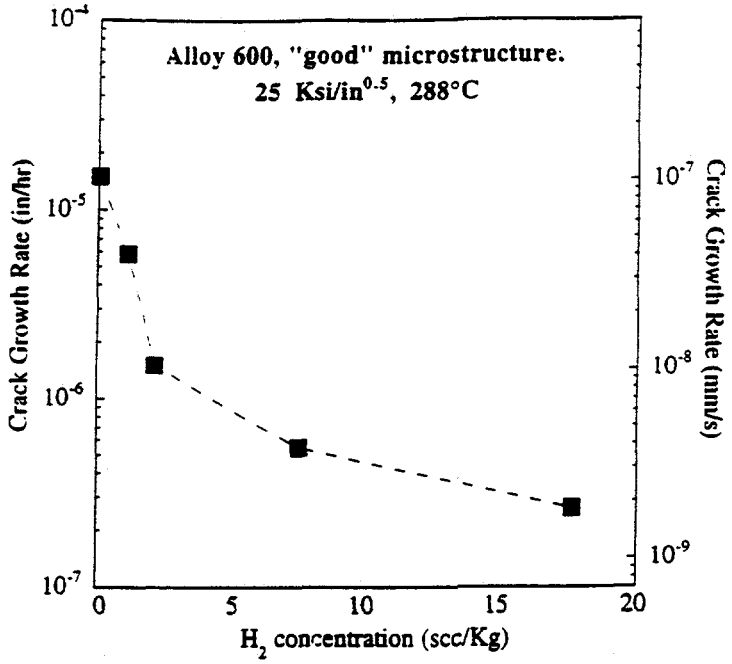

Figure 21 *- The effects of H_2 on crack growth rate at 288°C [39] on continuously monitored, actively loaded, fracture mechanics specimens. Data show a monotonically decreasing crack growth rate as the H_2 fugacity was increased from ≈0 (perhaps 10^{-3} bar) to several bar.*

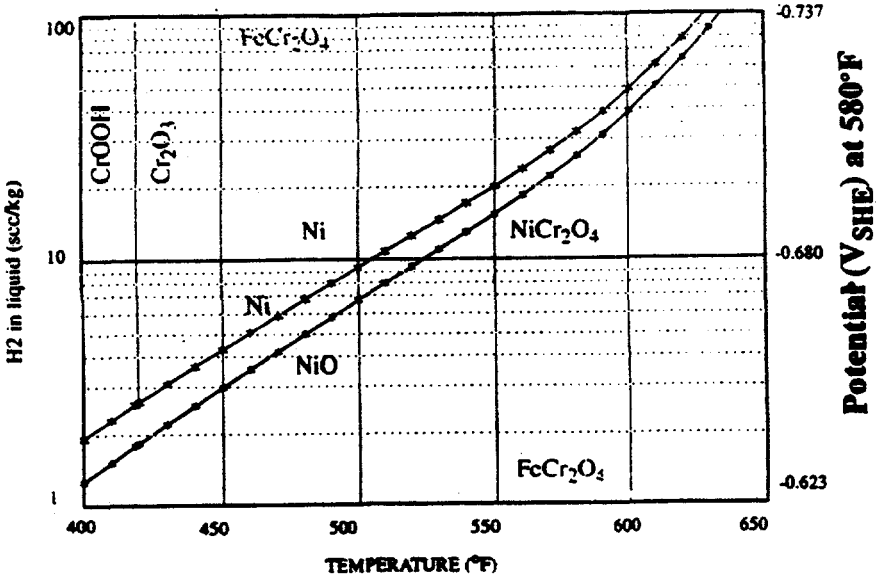

Figure 22 - The thermodynamic predictions for the H_2 fugacity required for the H_2 / H_2O line to "cross" the Ni/NiO boundary, which varies substantially with temperature [104-106].

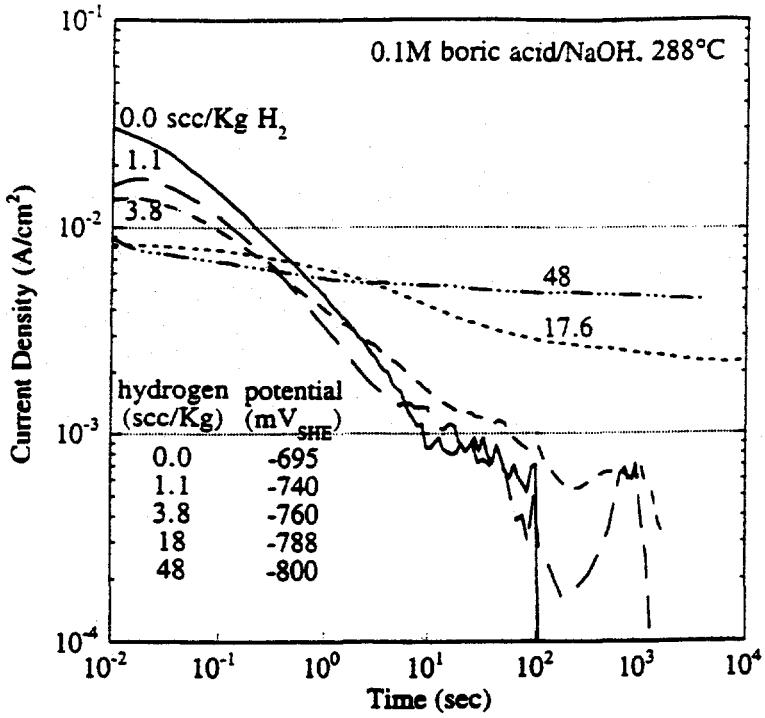

Figure 23 - Oxidation current vs. time (repassivation kinetics) vs. H_2 fugacity following rupture of the protective oxide on Alloy 600 wires by rapid straining in 288°C water. With increasing H_2, Ni^o becomes stable, leading to a decrease in the oxidation kinetics at shorter times. The higher H_2 level also promotes H_2 oxidation, which increases the "background" oxidation current density.

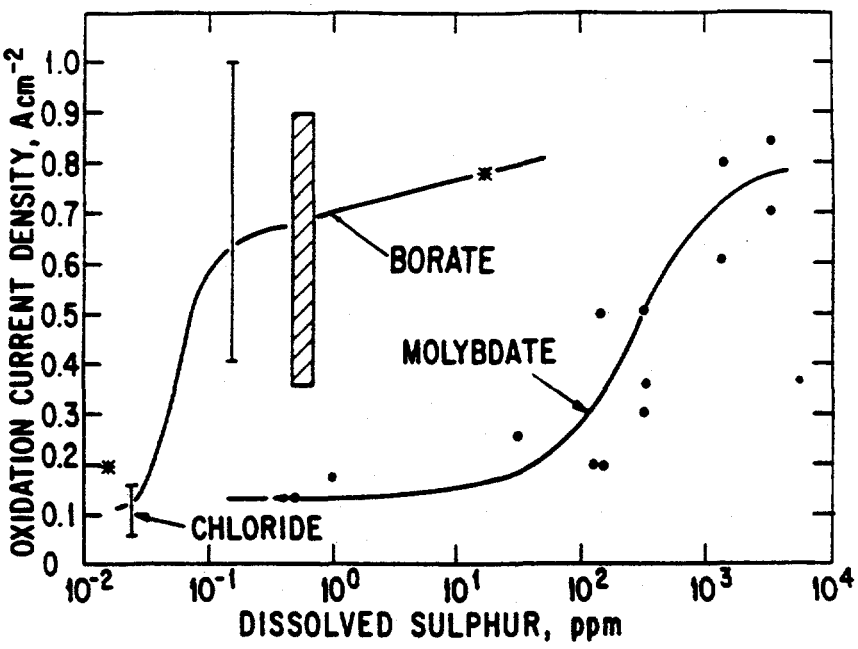

Figure 24 *- Relationship between the bare surface dissolution rate, i_o, on low alloy steel at –620 mV_{she} and the dissolved sulfur activity.*

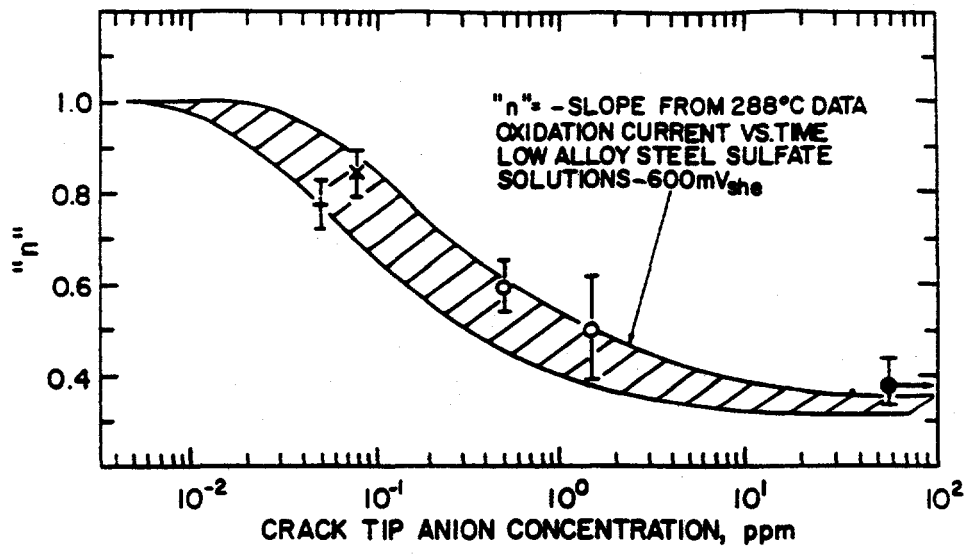

Figure 25 *- Relationship between "n" in Equations 2 and 3 and the crack tip sulfur activity for low alloy steels in high temperature water.*

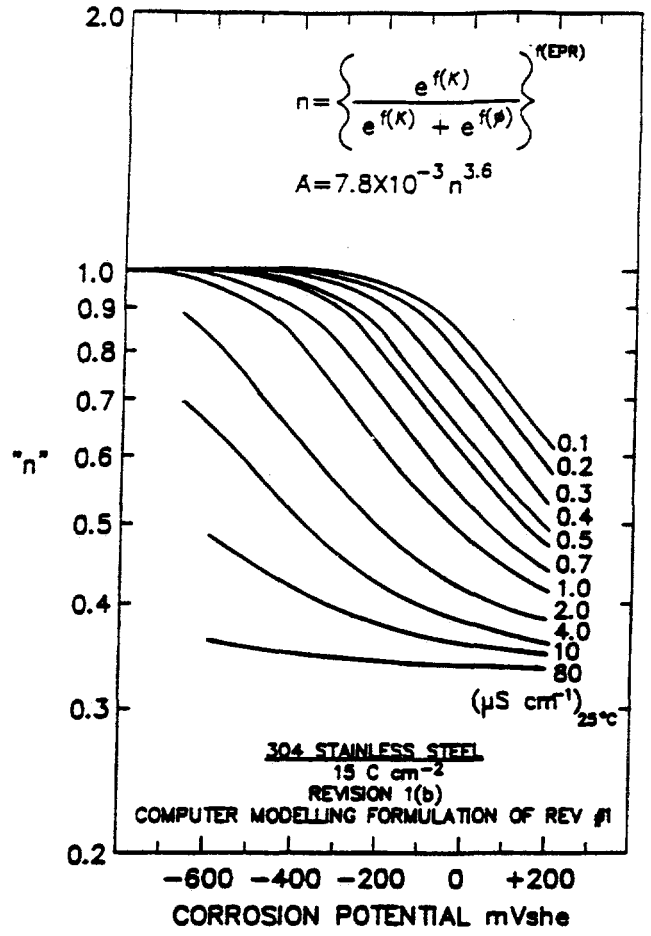

Figure 26 - Relationships between "n" in Equations 2, 3, 5, and 12 and the corrosion potential and bulk solution conductivity for sensitized (EPR = 15 C/cm^2) type 304 stainless steel in 288°C water.

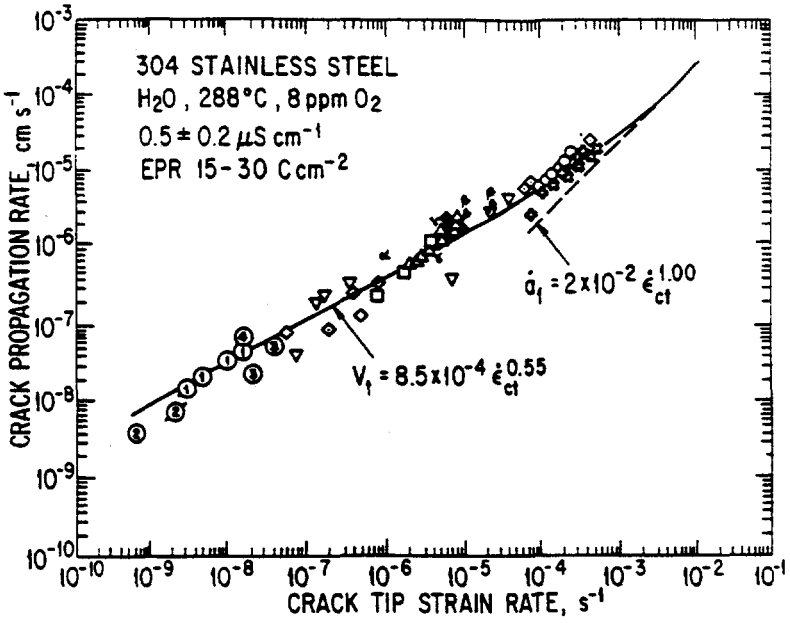

Figure 27 - Observed and predicted crack growth rate vs. crack tip strain rate for sensitized type 304 stainless steel in oxygenated 288°C water.

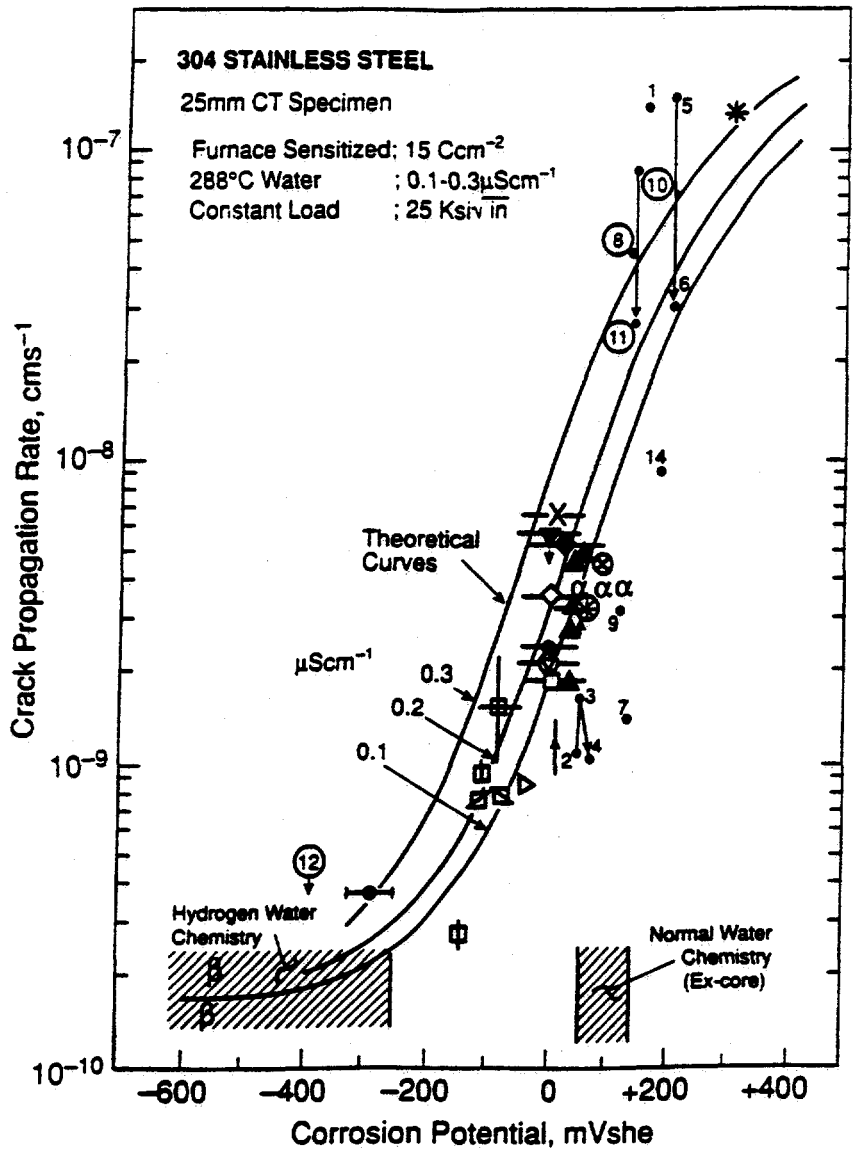

Figure 28 - Observed and predicted crack growth rate vs. corrosion potential for sensitized type 304 stainless steel in 288°C water at constant load.

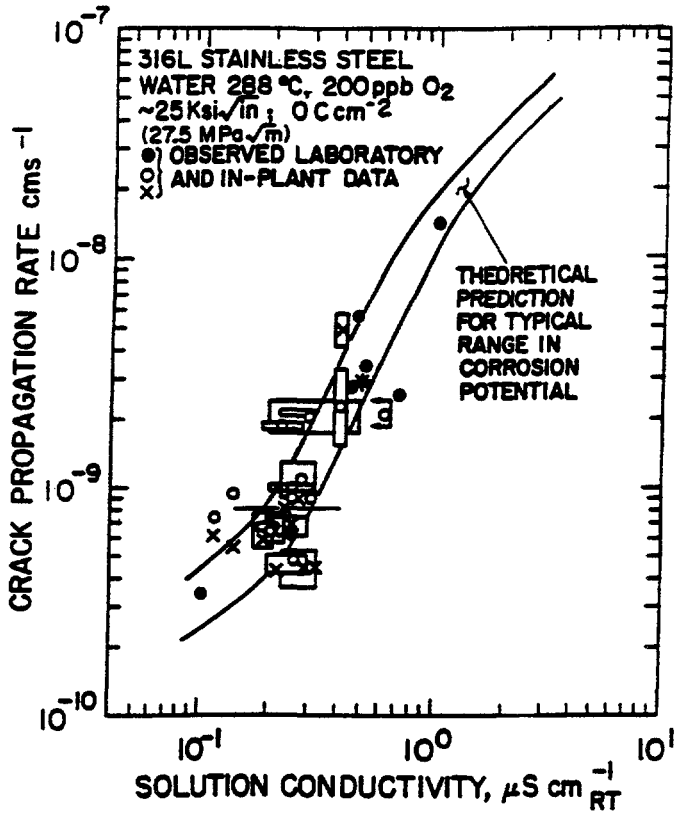

Figure 29 - Observed and predicted crack growth rate vs. solution conductivity for type 316L stainless steel at constant load (25 ksi$\sqrt{in}$) in 288°C water containing 200 ppb O_2.

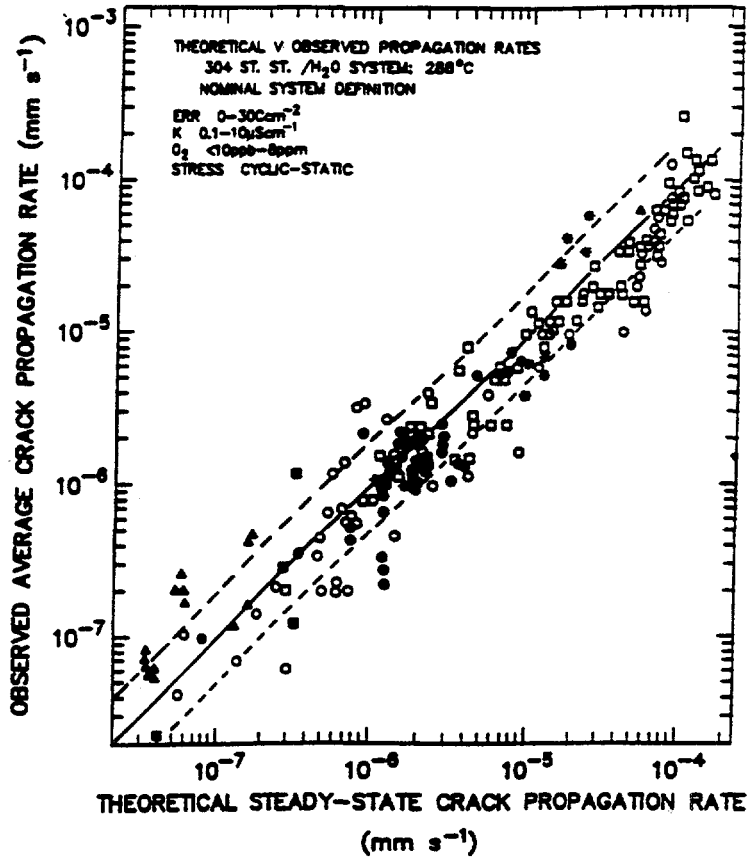

Figure 30 - Comparison of observed and predicted steady state crack growth rates for stainless steel in 288°C water representing a wide range of materials, stresses, and environments.

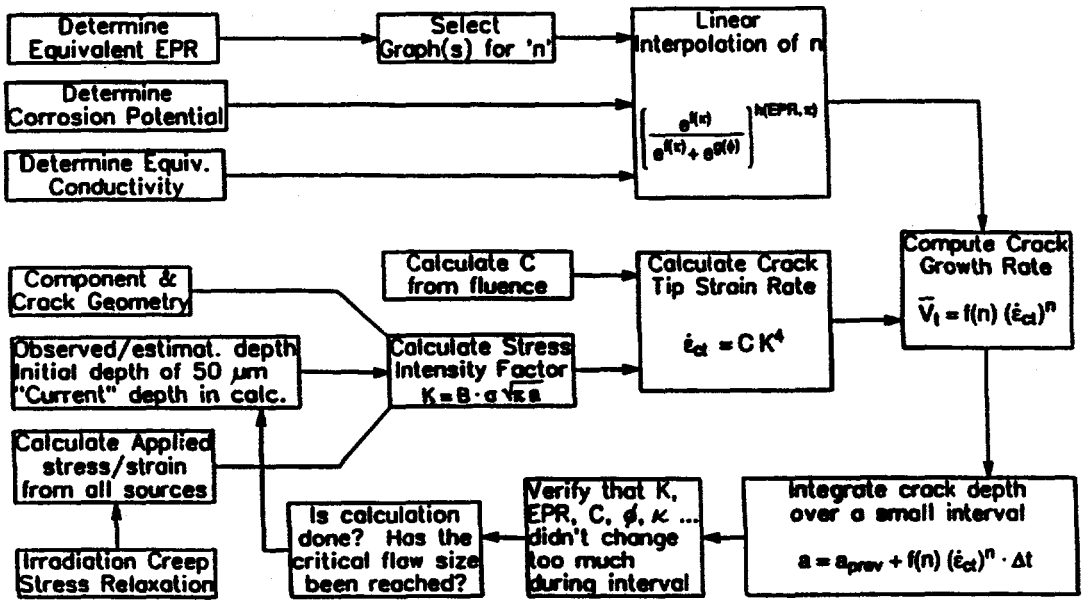

Figure 31 - Schematic of the procedure employed to predict the crack length vs. time for irradiation assisted stress corrosion cracking of stainless steels.

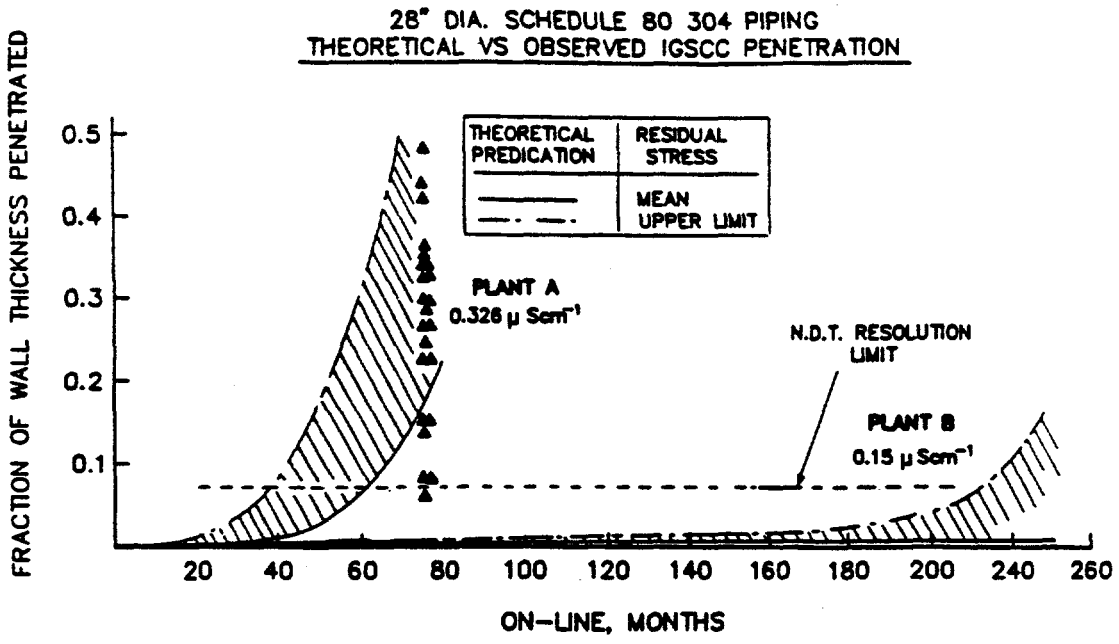

Figure 32 - Predicted and observed crack depth vs. operational time in 28 inch diameter, schedule 80 type 304 stainless steel piping for BWRs operating with different mean coolant conductivities. The range in predicted response results from the use of the mean and maximum residual stress profiles.

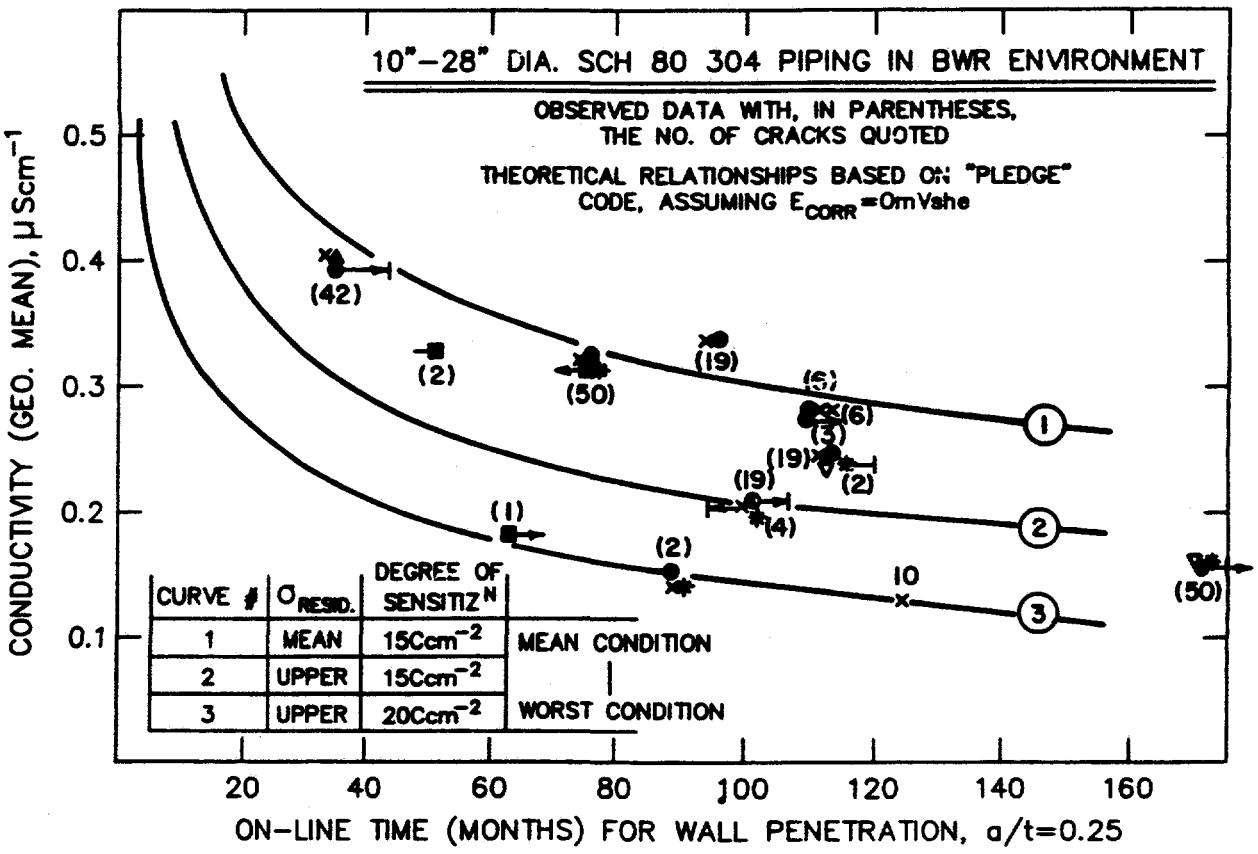

Figure 33 - Predicted and observed relationships between average BWR coolant conductivity and the operational time to achieve quarter wall penetration by SCC. The number of cracks detected is shown in parenthesis.

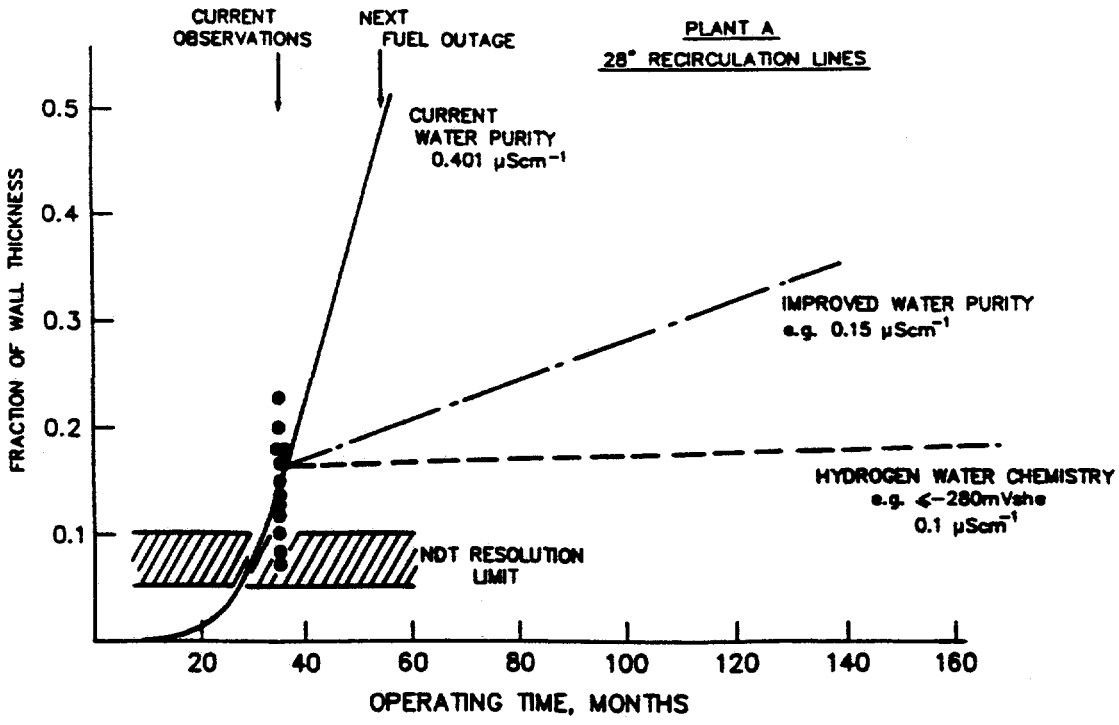

Figure 34 - Predicted response of a pipe crack for specific changes in water chemistry.

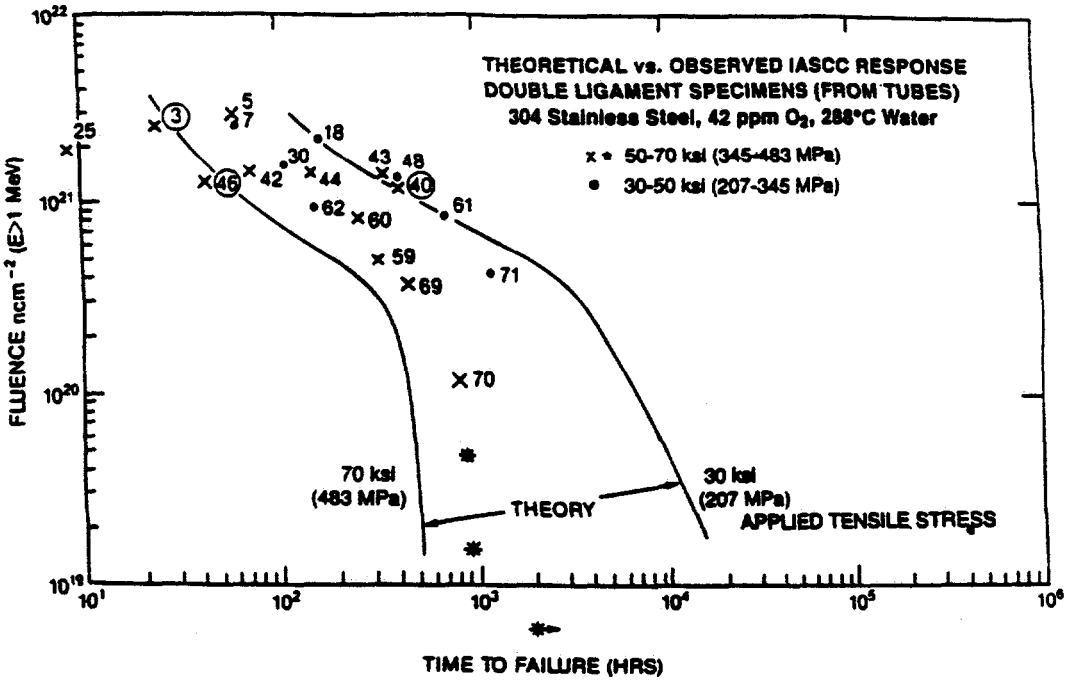

Figure 35 - Comparison between observed and predicted cracking behavior for irradiated type 304 stainless steel tested at constant load in 32 ppm oxygenated, 288°C water.

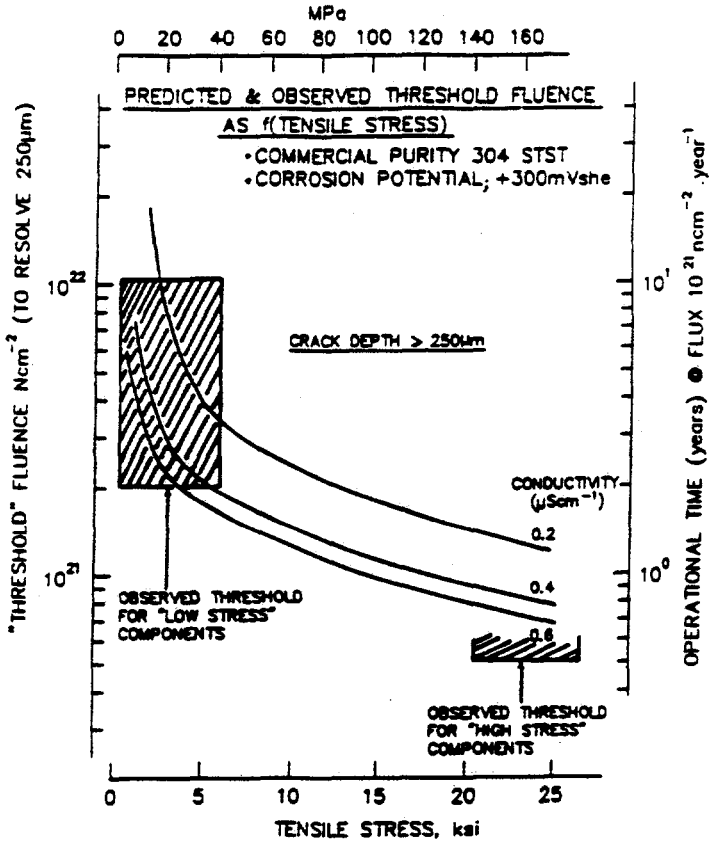

Figure 36 - Predicted and observed variation in the "threshold" fluence for observed cracking in irradiated BWR components as a function of the tensile stress and solution conductivity.

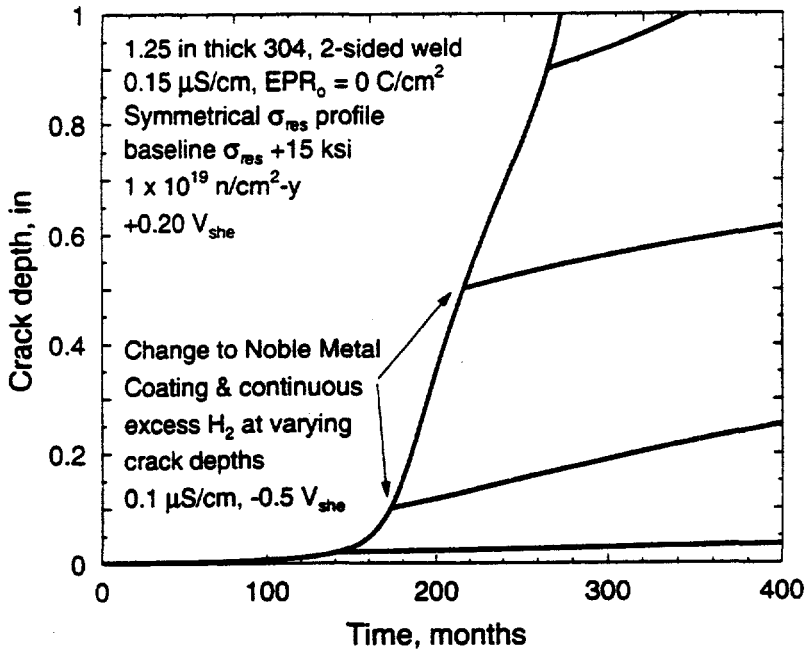

Figure 37 - Example of the predicted crack depth vs. time in a BWR core shroud, showing the effect of changes in corrosion potential on subsequent crack advance.

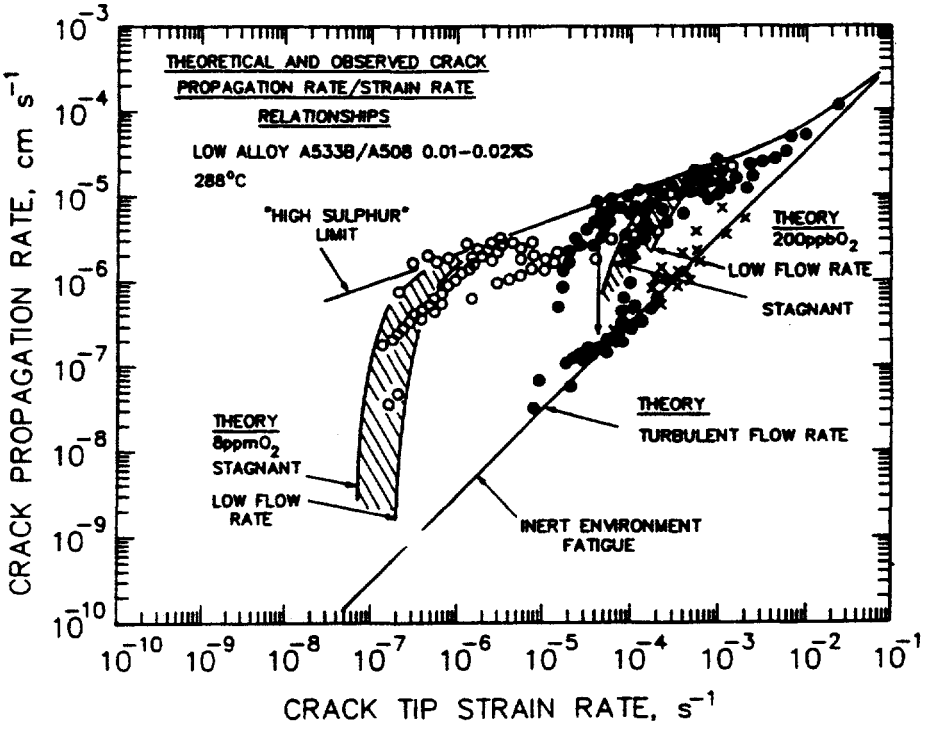

Figure 38 - Predicted and observed crack growth rate vs. crack tip strain rate for low alloy steels in 288°C water.

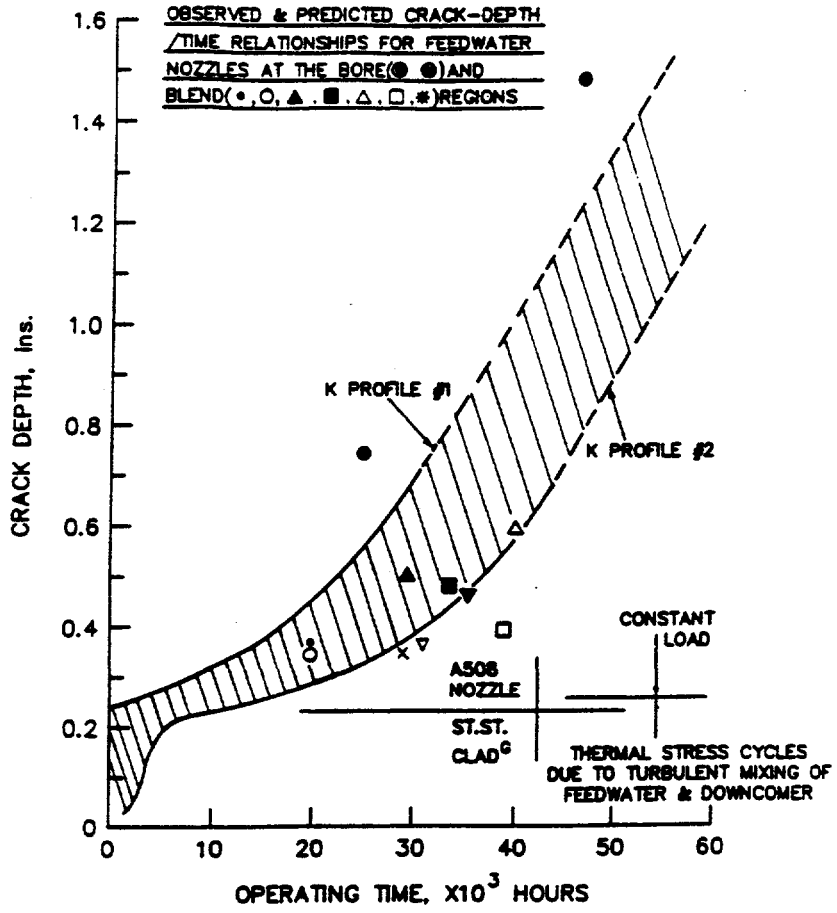

Figure 39 - Predicted and observed crack depth vs. operating time for BWR feed water nozzles.

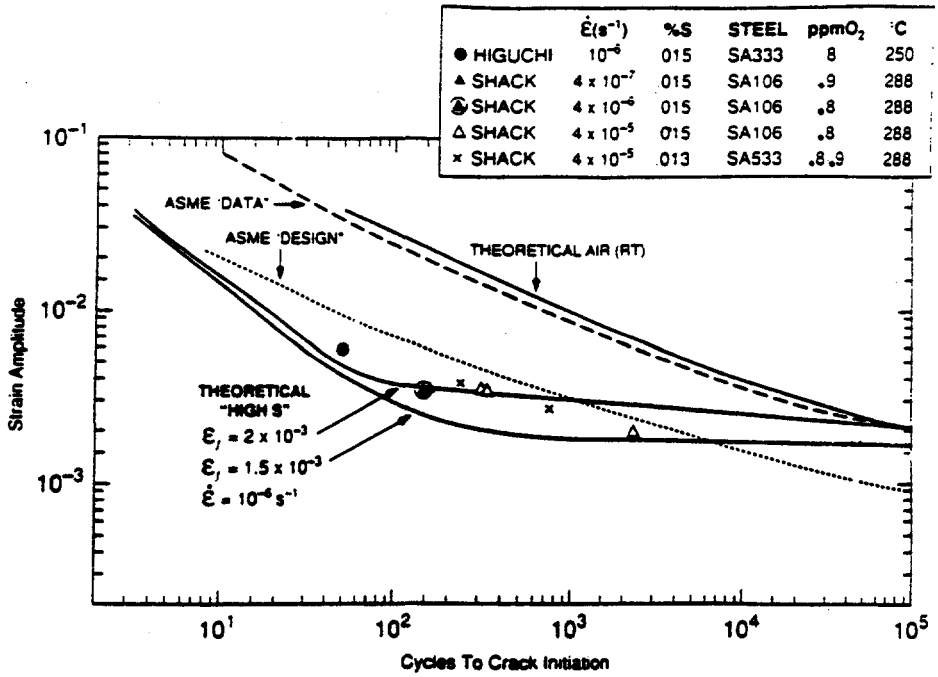

Figure 40 - Predicted and observed [164-166] strain amplitude vs. cycles to initiation for (unnotched) carbon and low alloy steels in high temperature water tested under the worst combinations of material and environment. Carbon and low alloy steels behave very similarly, with a $N_i / \Delta\varepsilon_T$ response in high O_2, 250 / 288°C water which is dictated by the sulfur content of the steel.

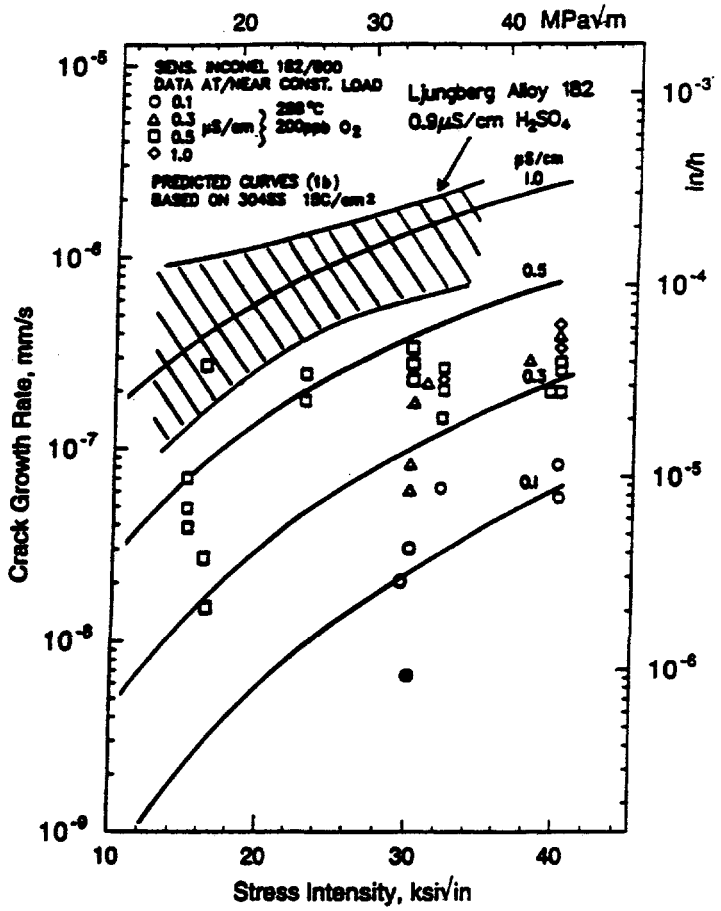

Figure 41 - Crack growth rate vs. stress intensity comparison of the predicted and observed crack growth rates for Alloy 600 and Alloy 182 weld metal tested at or near constant load in 288°C water containing 200 ppb O_2.

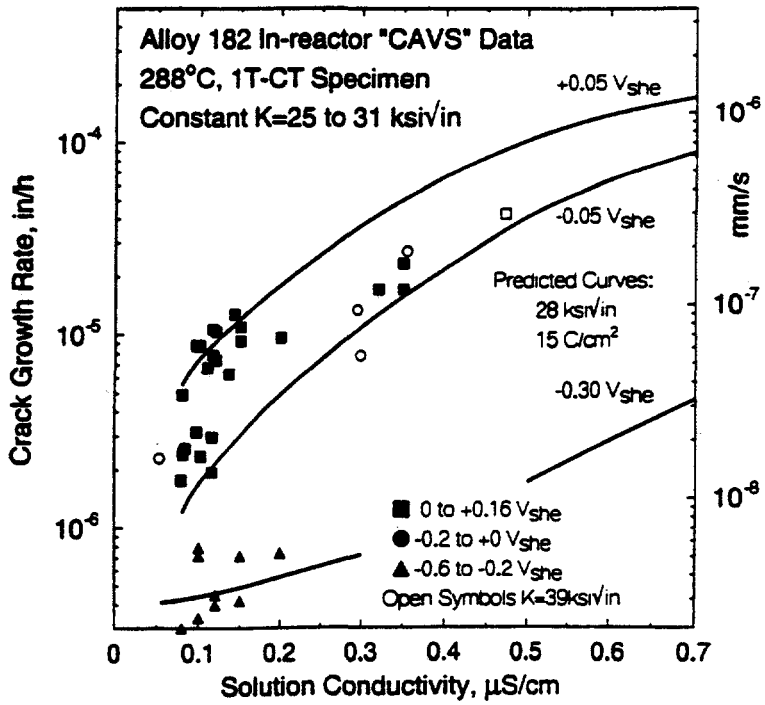

Figure 42 - Comparison of the predicted and observed crack growth rates vs. solution conductivity for in-plant GE "CAVS" data on Alloy 182 weld metal tested at constant load in BWR water of varying chemistry (corrosion potential).

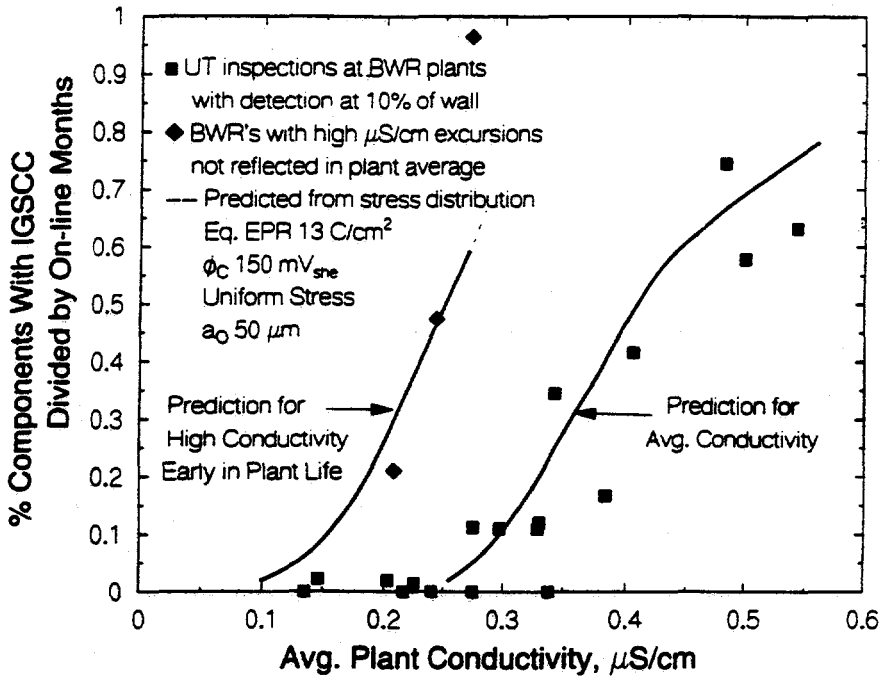

Figure 43 - The predicted and observed effects of average plant water purity on the crack incidence of creviced Alloy 600 BWR shroud head bolts.

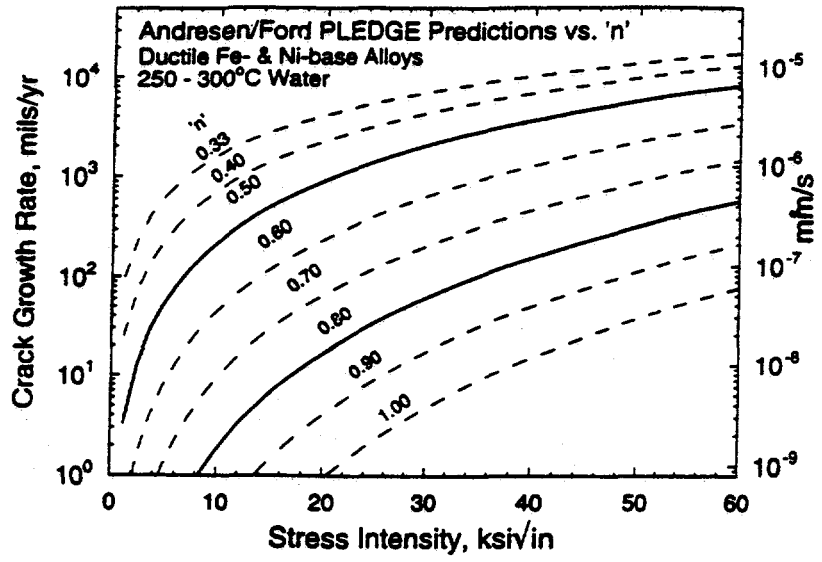

Figure 44 - The effect of "n" on predicted crack growth rate over the range of "n" values considered applicable to high temperature water.

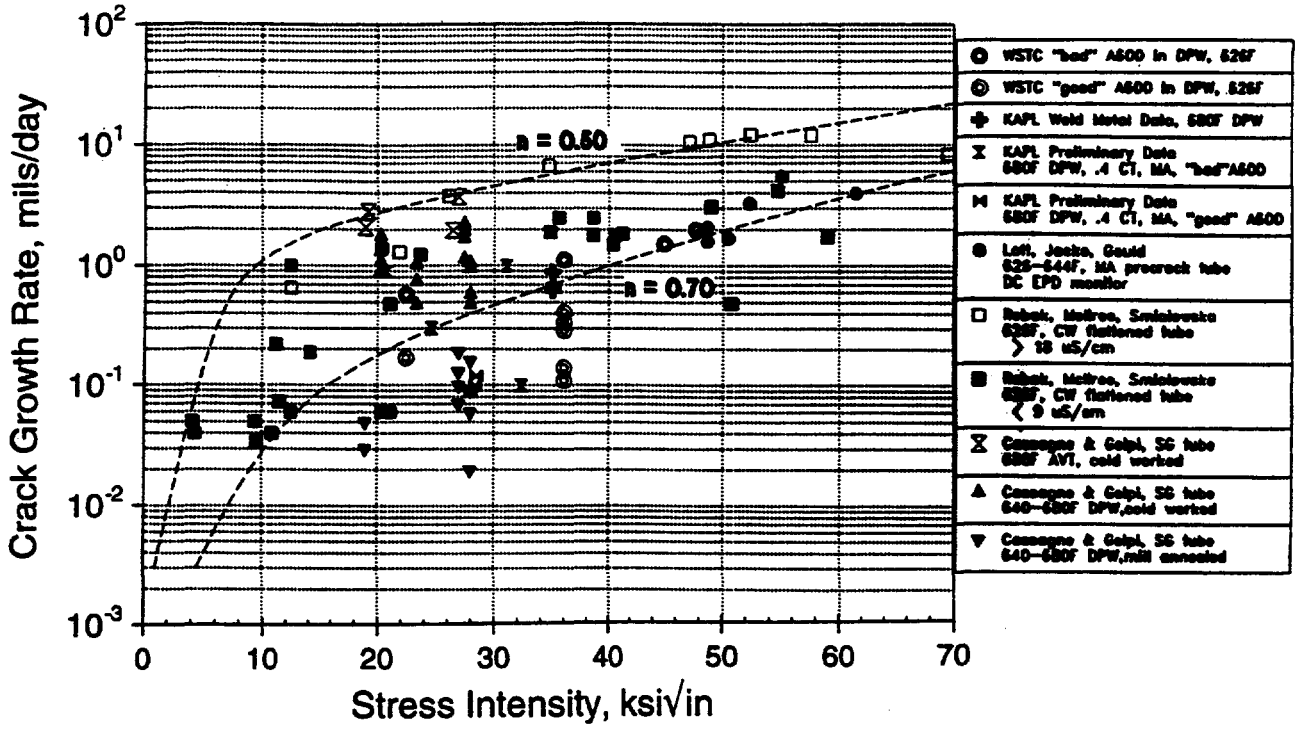

Figure 45 - Compilation of Alloy 600 crack growth rate data vs. stress intensity in high temperature deaerated pure water. Model predictions are shown for "n" values of 0.5 and 0.7.

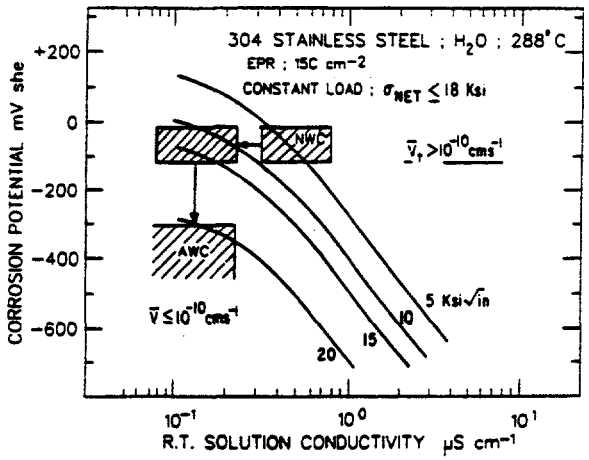

Figure 46 - Predicted combinations of corrosion potential, solution conductivity, and stress intensity that give rise to crack growth iso-velocity curves (10^{-10} cm/s) on sensitized Type 304 stainless steel.

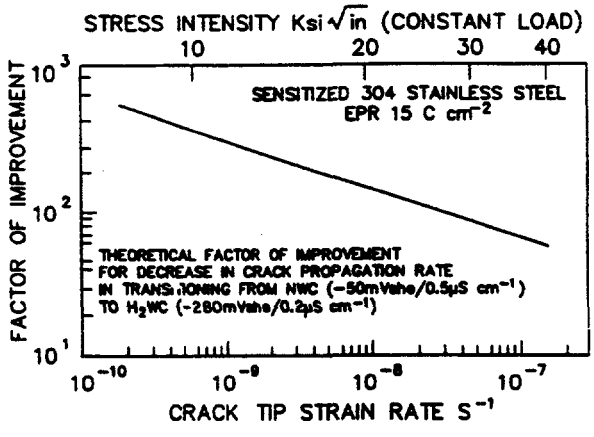

Figure 47 - Factor of improvement (ratio of crack growth rates in "normal" to hydrogen water chemistry) for sensitized type 304 stainless steel as a function of the stress intensity and corresponding crack tip strain rate.

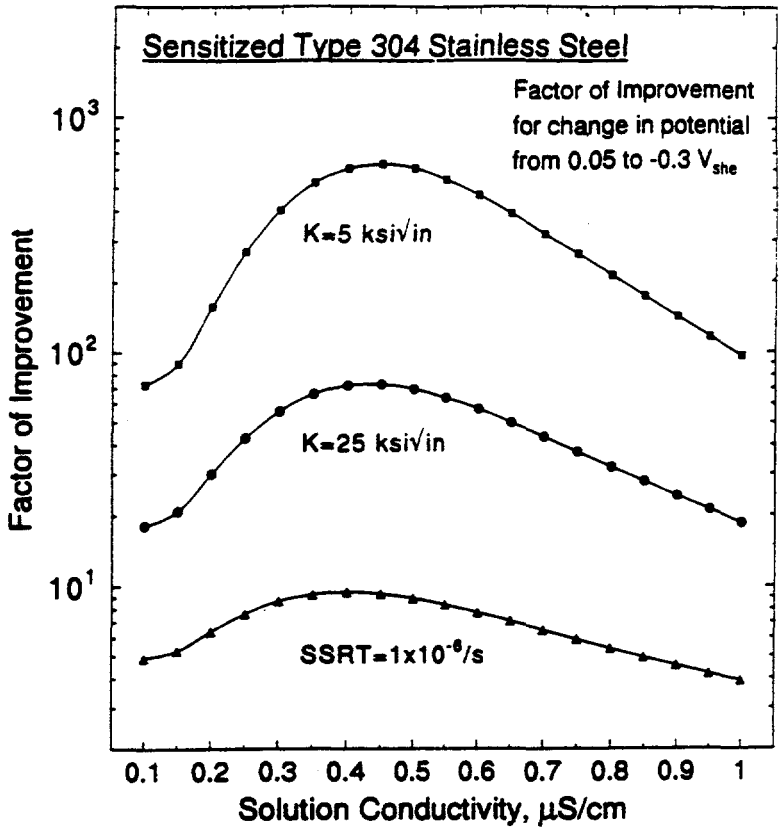

Figure 48 - Factor of improvement (FOI) for sensitized type 304 stainless steel associated with decreasing the corrosion potential from 0.05 to –0.3 V_{she}. The FOI varies substantially with specific solution conductivity and loading conditions.

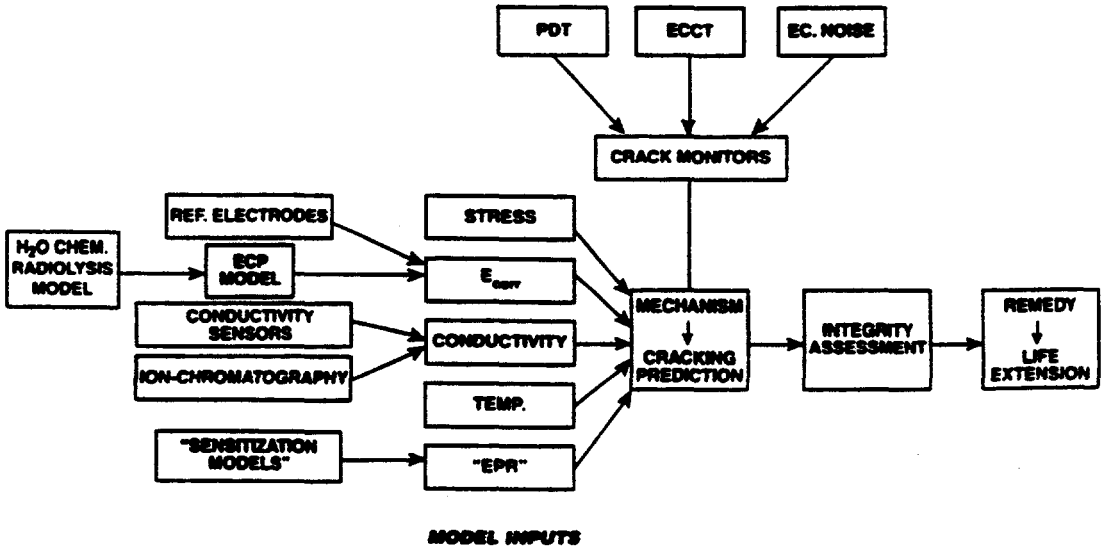

Figure 49 - The integration of crack monitoring devices and environmental sensors with a mechanistically based model of crack advance can provide an accurate assessment of structural integrity and plant life extension.

ENVIRONMENTALLY ASSISTED CRACKING ISSUES IN PRESSURIZED WATER REACTORS

W. BAMFORD
WESTINGHOUSE ENERGY SYSTEMS

ENVIRONMENTALLY ASSISTED CRACKING ISSUES IN PWR'S

- Introduction/Background
- Fatigue Crack Growth
- Stress Corrosion Cracking
- International Cooperation
- Conclusions

ENVIRONMENTALLY ASSISTED FATIGUE CRACK GROWTH ISSUES

- Feedwater Line Counterbore Cracking (Ferrite Steel)

- Inservice Inspection Findings - Section XI

- Other Stratification Locations (Stainless Steel)

    - Auxiliary Lines
    - Surge Line

FEEDWATER LINE COUNTERBORE CRACKING

- First discovered in 1979.
- Results from stratification at low flows in the feedwater line.
- Counterbore and weld discontinuities on pipe ID provide preferred sites.
- Large plant-to-plant differences in operation lead to large differences in the degree of cracking.

FEEDWATER FLOW STRATIFICATION

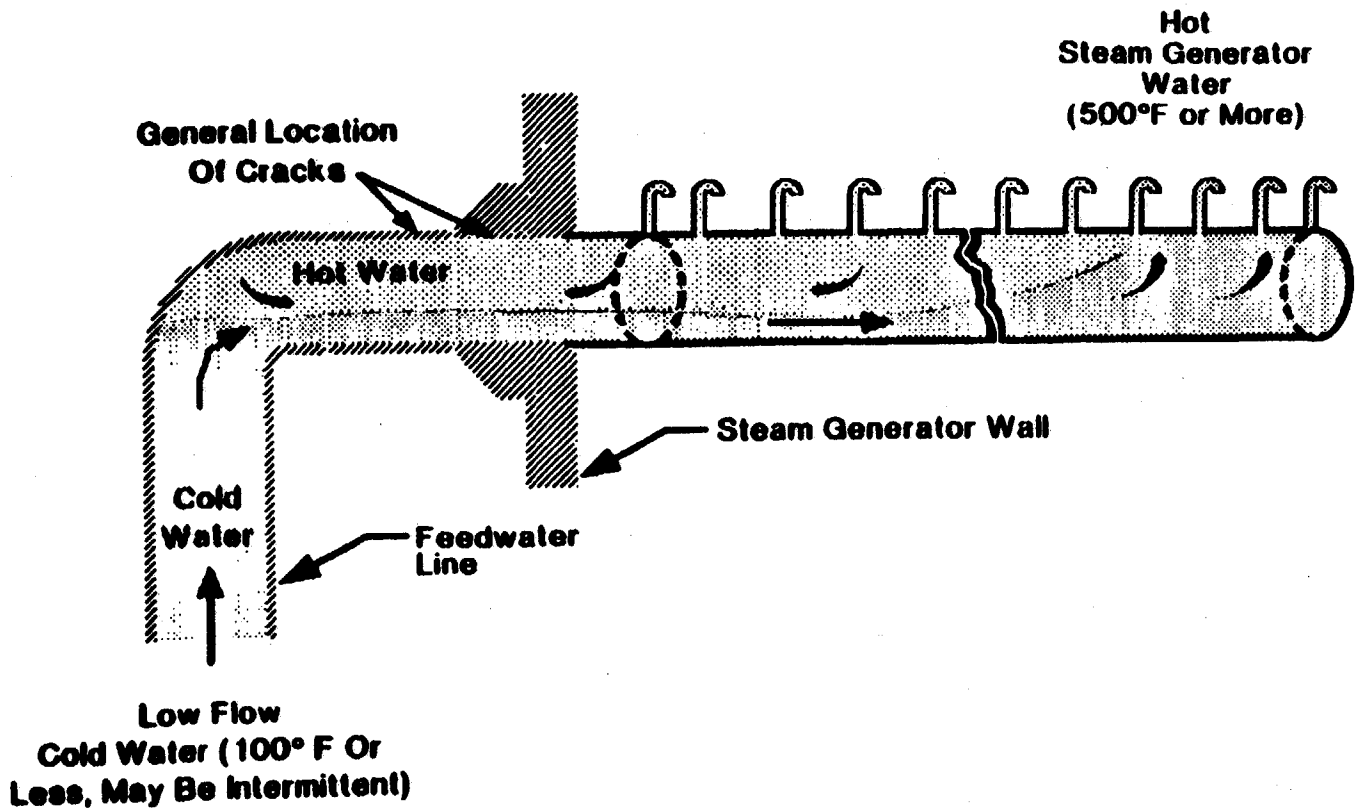

CRACK GROWTH PREDICTIONS: FEEDWATER LINES

- Based on measured stratification cycles-monitoring.

- Predictions based on Section XI reference crack growth law compared well with actual cracking.

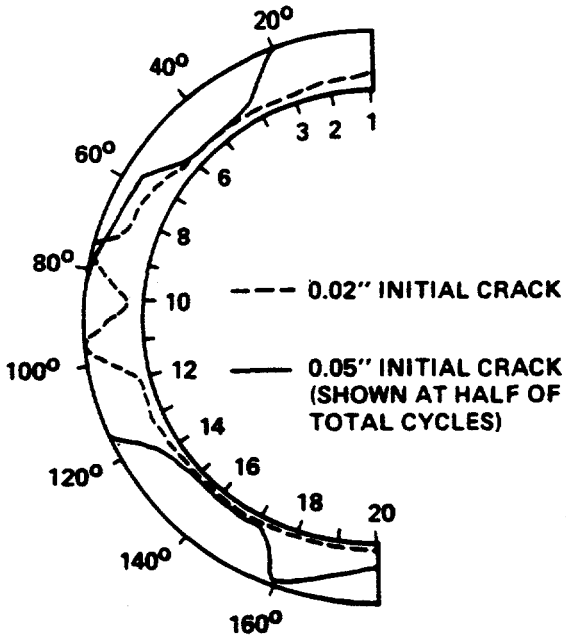

CRACK SIZE PREDICTION ASSUMING INITIATION OCCURS IMMEDIATELY

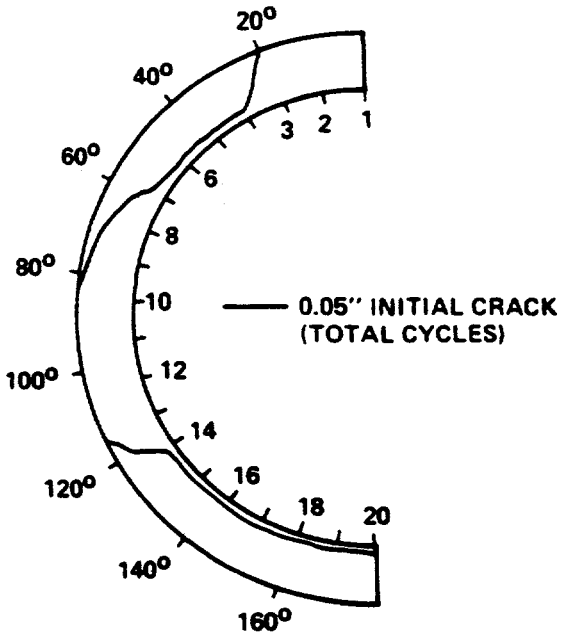

CRACK SIZE PREDICTION ASSUMING INITIATION OCCURS WHEN USAGE FACTOR = 1

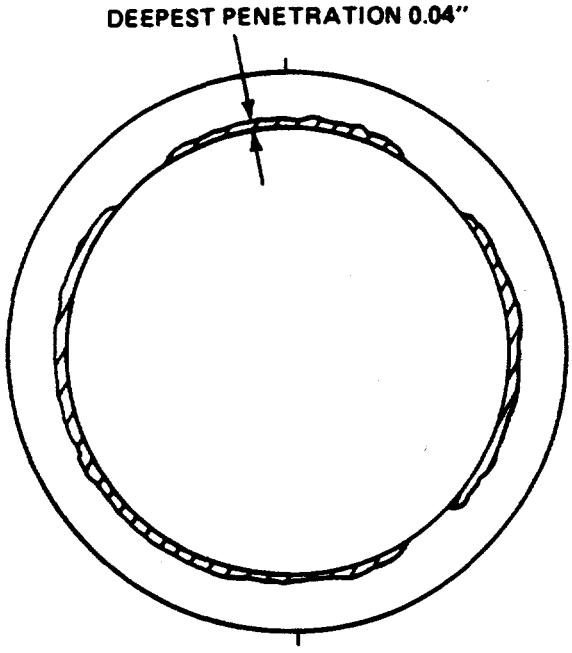

ACTUAL CRACK PROFILE - UNIT 1 - LOOP 2

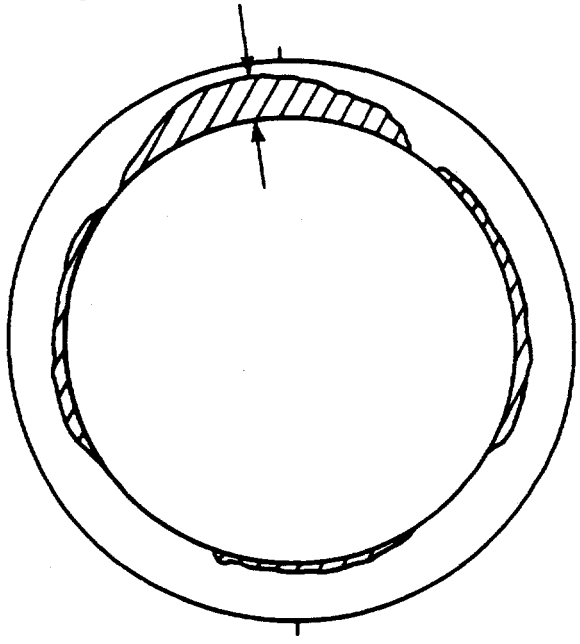

ACTUAL CRACK PROFILE - UNIT 2 - LOOP 3

Results of Fatigue Crack Growth Analysis -

GOOD NEWS!

ENVIRONMENTAL EFFECTS ON CRACK GROWTH OF FERRITIC STEELS ARE LOWER THAN EXPECTED

- Mechanisms of Environmental Enhancement
- Development of the Hypothesis
- Experimental Validation
- Implementation of the Approach

Mass Transfer Inside a Growing Crack - Combrade

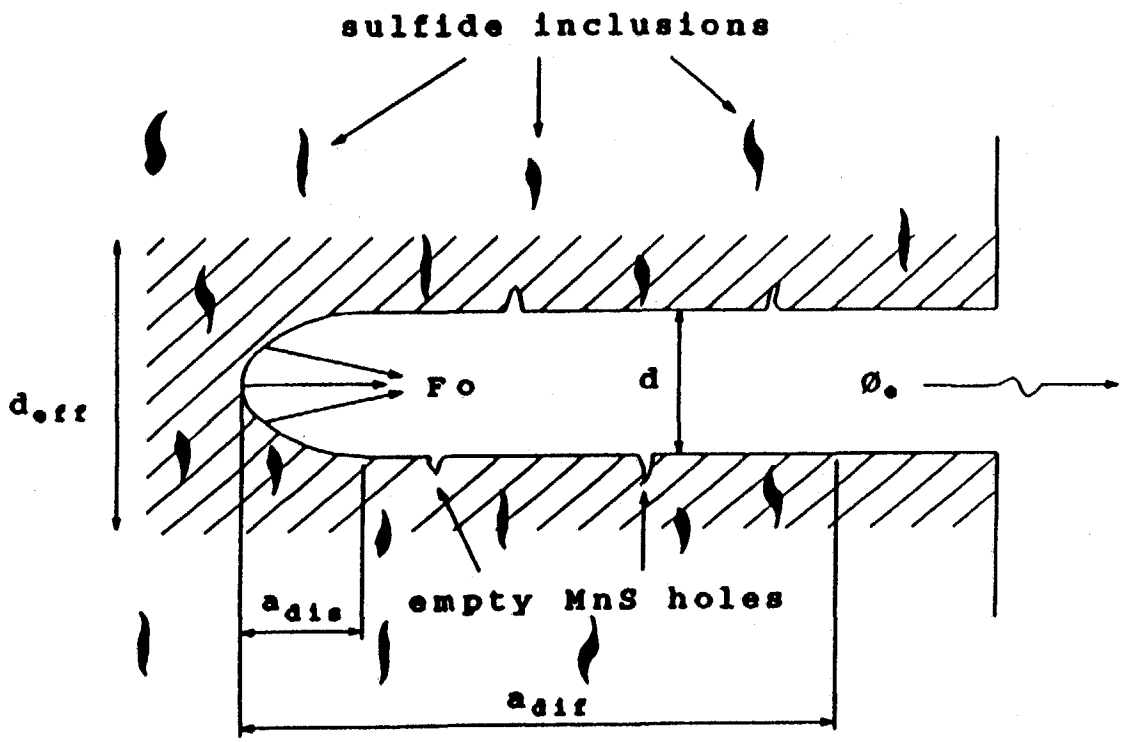

Fo input flux of sulfide ions by dissolution of MnS inclusions

ϕ_e output flux of sulfide ions by diffusion and advection

ENVIRONMENTALLY ASSISTED STRESS CORROSION CRACKING

ALLOY 600 R.V. HEAD PENETRATIONS

- First Observed in Steam Generator Tubes
- 1991 - Observed in Reactor Vessel Head Penetrations
- PWSCC Occurs in Pure Deoxygenated Water, Driven by Attachment Weld Residual Stresses
- Affects 1-2 Percent of Head Penetrations in Service

REACTOR VESSEL HEAD PENETRATIONS

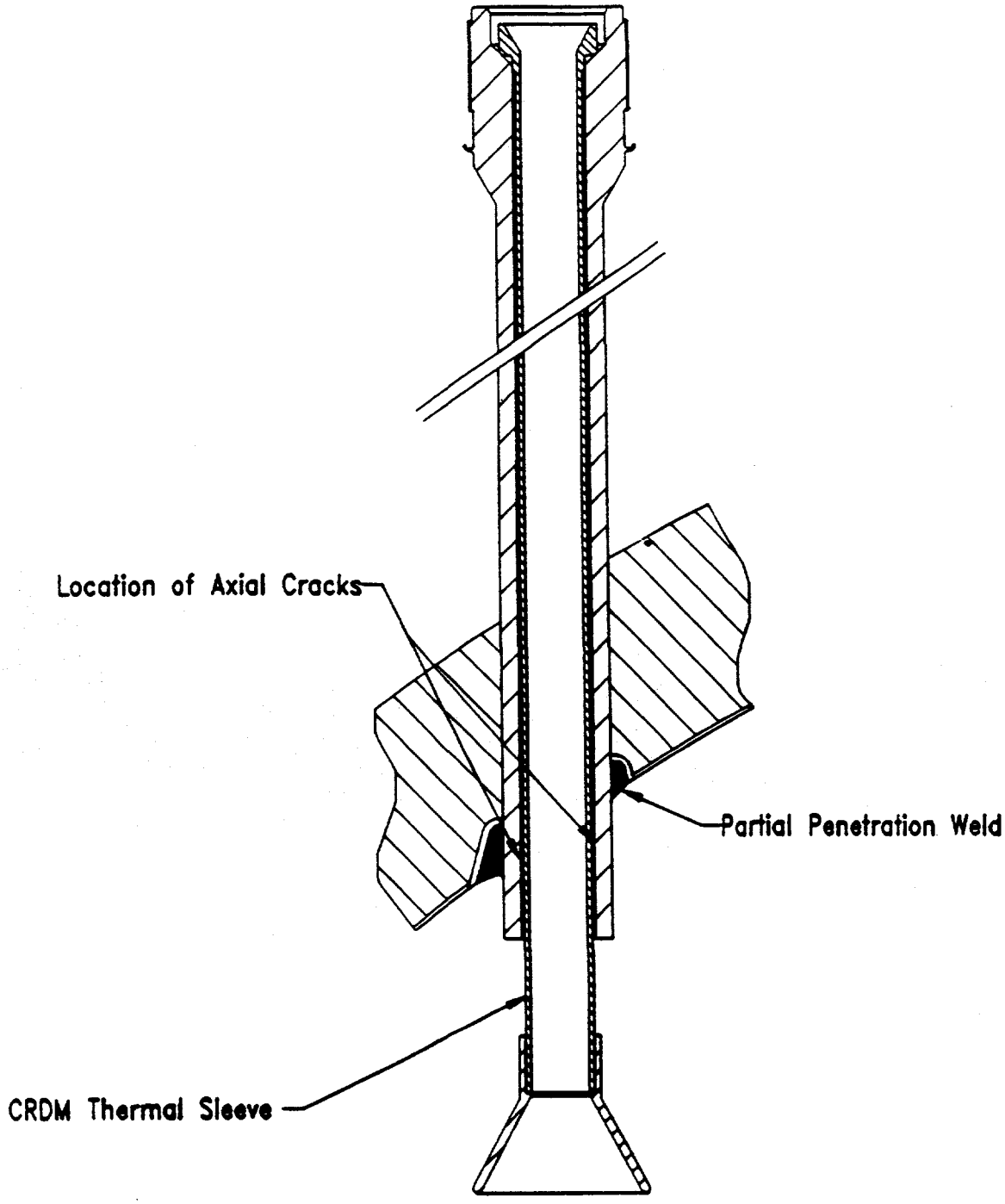

ALLOY 600 PWSCC

- Strongly Dependent on Applied Stress Intensity Factor and Temperature
- Weakly Dependent on Water Chemistry
- Significant Material Variability (Heat-to-Heat)
- Modified Scott Model Works Well to Bound the Crack Growth Rates Observed

INTERNATIONAL COOPERATION ON ENVIRONMENTAL CRACKING

- In the early 70's it became evident that environmental cracking was a very complex process.
- NRC concluded that the best way to tackle the issue was international cooperation.
- The ICCGR Group was formed in 1976 - first meeting was at the WRSIM.
- The group still exists, under a new name, ICGEAC "International Cooperative Group on Environmentally Assisted Cracking".

ACCOMPLISHMENTS OF ICCGR/ICGEAC

- Sharing of technical data on crack growth.
- Development of environmental characterization tools - electrochemical potential measurement.
- Development and debate of mechanisms of environmental cracking.
- Cooperation in testing programs - common materials, environments and loadings - round robins.
- Discussion of reference crack growth laws.

CONCLUSIONS

- **Service-induced cracking has resulted from unanticipated loadings, or unknown cracking mechanisms.**

- **No cracks have resulted from designs where the loadings were known and properly analyzed.**

- **Cooperative efforts provide significant benefits, saving both time and money.**

- **We must be on guard for new types of age-related environmental cracking.**

Cooperative IASCC Research (CIR) Program

J. Lawrence Nelson
Manager, Corrosion Research
Nuclear Power Group
Electric Power Research Institute

Irradiation assisted stress corrosion cracking (IASCC) describes intergranular environmental cracking of material exposed to ionizing radiation. The term IASCC is generally applied to environmental cracking that has been accelerated by radiation whether it acts alone or in combination to change water chemistry, material microchemistry, material microstructure, etc. Laboratory and field data show that intergranular stress corrosion cracking of stainless steels and nickel-base alloys can result from long-term exposure to high energy neutron radiation that exists in the core of light water reactors. To date, IASCC in reactor internals has been discovered during routine inspections and thus has not been a cause of unplanned shutdowns. However, concerns for IASCC are increasing.

The implications of IASCC are significant, both in terms of repair and outage costs as well as the potential for cracking in components that may be extremely difficult to repair or replace. Significant advancements have been made in the understanding of IASCC. However, it is clear that major unknowns persist and must be understood and quantified before the life of a reactor component at risk from IASCC can be predicted or significantly extended.

Although individual organizations are continuing to effectively address IASCC, it became apparent that a more direct form of cooperation would be more timely and efficient in addressing the technical issues. Thus in 1995 EPRI formed the Cooperative IASCC Research (CIR) Program. This is a cooperative, jointly funded effort with participants from eight countries providing financial support and technical oversight.

The efforts of the CIR Program are directed at the highest priority questions in the areas of material susceptibility, water chemistry and material stress. Major research areas of the Program are: 1) evaluation of IASCC mechanisms, 2) development of methodology for predicting IASCC, and 3) quantification of irradiation effects on metallurgy, mechanics and electrochemistry. Studies to evaluate various IASCC mechanisms include work to better understand the possible roles of radiation-induced segregation (RIS), radiation microstructure, bulk and localized deformation effects, overall effects on strength and ductility, hydrogen and helium effects, and others. Experiments are being conducted to isolate individual effects and determine the relative importance of each in the overall IASCC mechanism. Screening tests will be followed by detailed testing to identify the contribution of each effect over a range of conditions.

The development of a methodology for predicting IASCC will focus on the dominant elements identified from the mechanistic work described above. The development process would identify variables that are measurable on a component and devise a practical predictive methodology to start. Identification and planning of experiments needed to enhance development of the methodology will be conducted. This experimental planning includes ongoing critical reviews of available data with emphasis on filling gaps in the existing data, as necessary.

Research investigating irradiation effects on material properties is examining defect microstructural development, RIS including grain boundary orientation effects, radiation hardening, and the influence of bulk material composition and temperature. Efforts in the area of irradiation effects on crack-tip mechanics will evaluate the influence of defect type, defect density and dislocation loop size on deformation characteristics. Other mechanics-related areas to be examined include irradiation creep, mechanical cracking and the role of stress/strain during irradiation.

Identification of possible countermeasures to IASCC will be undertaken when sufficient mechanistic understanding of IASCC is obtained and when predictive capabilities are sufficiently developed to provide conclusive direction for work on potential countermeasures. The work in this area is expected to include identification of: potential remedial actions for existing components; new materials; stress reduction techniques; and environmental modifications.

The paper to be presented will describe the completed and ongoing work being sponsored by the CIR Program in the above areas.

Cooperative IASCC Research (CIR) Program

Larry Nelson
Manager, Corrosion Research
EPRI

EPRI/NPG

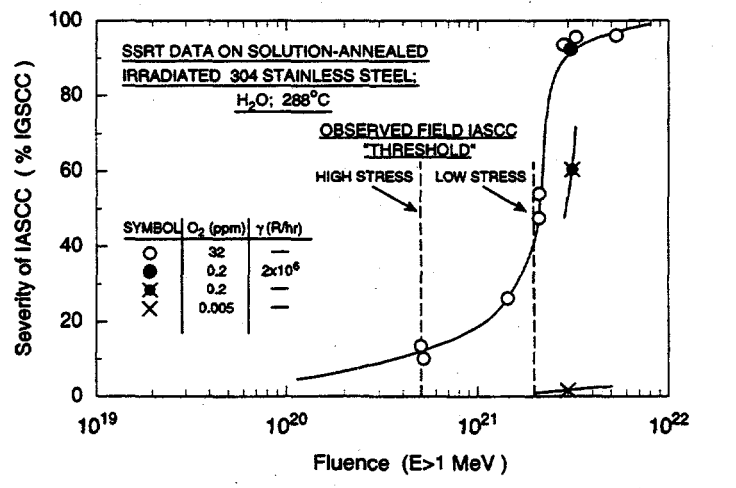

From: A. Jacobs

CIR Program

NRC-CIR-10/97-2

EPRI/NPG

IASCC Mechanistic Issues

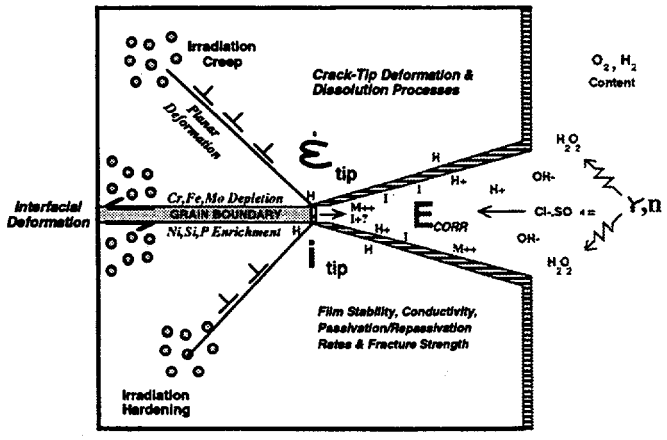

From: S. Bruemmer

CIR Program

NRC-CIR-10/97-3

EPRI/NPG

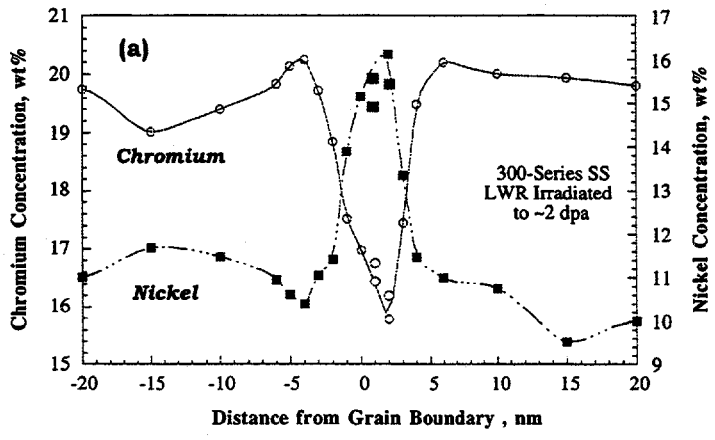

CIR Program

NRC-CIR-10/97-4

EPRI/NPG

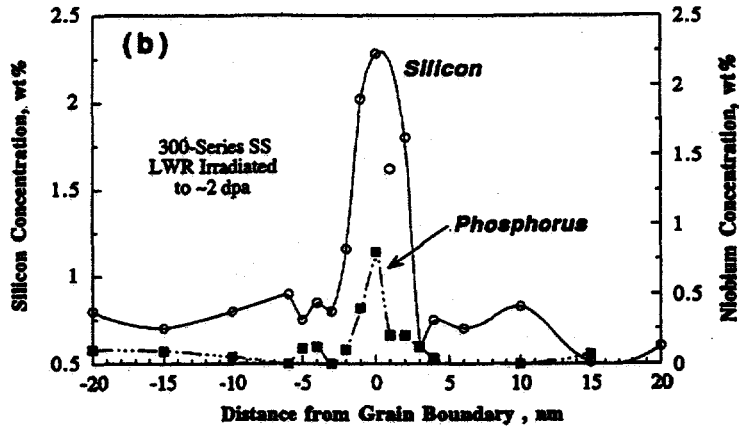

CIR Program

NRC-CIR-10/97-5

EPRI/NPG

Typical Westinghouse Baffle/Former Plate Arrangement

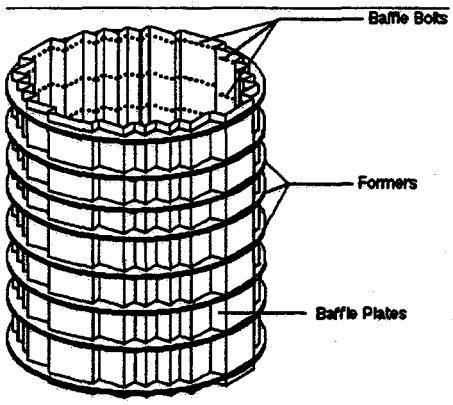

CIR Program

NRC-CIR-10/97-6

EPRI/NPG

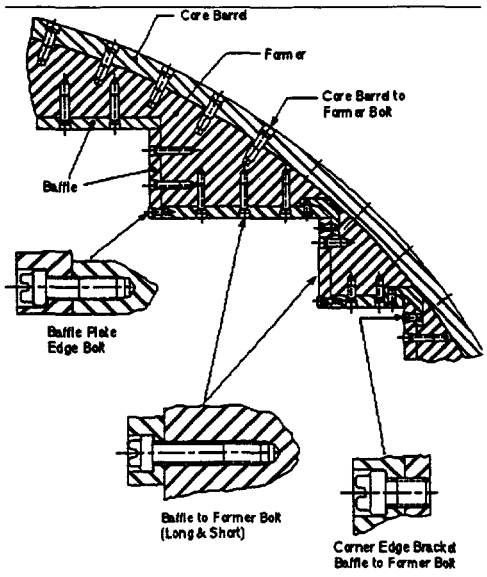

CIR Program

NRC-CIR-10/97-7

EPRI/NPG

BWR Internal Components

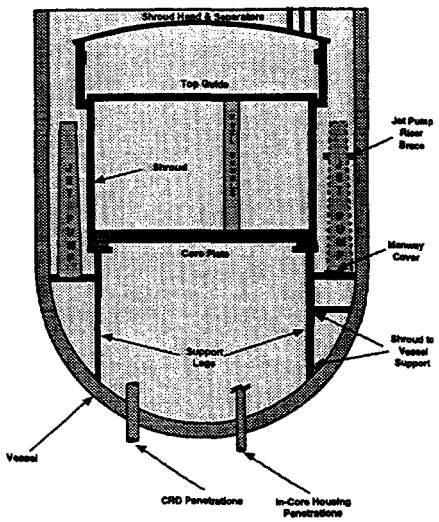

CIR Program

NRC-CIR-10/97-8

EPRI/NPG

Cooperative IASCC Research Program

Objectives:

1. Develop a mechanistic understanding of IASCC
2. Develop a methodology to predict a component's behavior
   - -- Mechanistic guidance required
   - -- Empirical fitting parameters?
3. Identify possible countermeasures to IASCC

CIR Program

NRC-CIR-10/97-9

EPRI/NPG

Cooperative IASCC Research Program Committee Structure

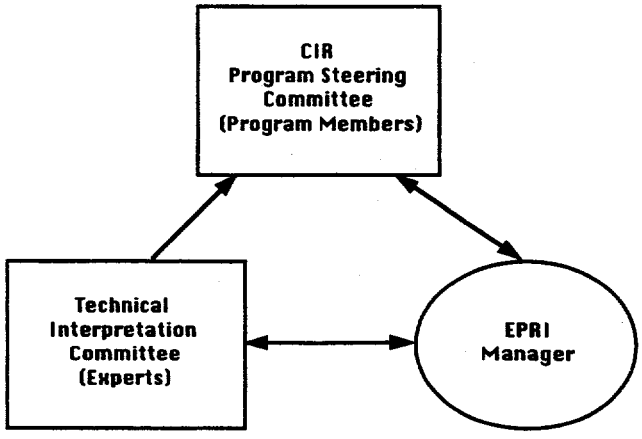

CIR Program

NRC-CIR-10/97-10

EPRI/NPG

Cooperative IASCC Research Program

Technical Interpretation Committee

Dr. Peter Andresen	General Electric R&D
Dr. Steve Bruemmer	Battelle Northwest Laboratories
Dr. Ernie Eason	Modeling & Computing Services
Dr. Frank Garner	Battelle PNL
Dr. Fredrich Garzarolli	Siemens AG (KWU)
Professor Kjell Pettersson	Royal Institute of Technology
Dr. Peter Scott	Framatome
Professor Tetsuo Shoji	Tohoku University
Dr. Jean-Claude Van Duysen	Electricite de France

CIR Program

NRC-CIR-10/97-11

EPRI/NPG

IASCC Database

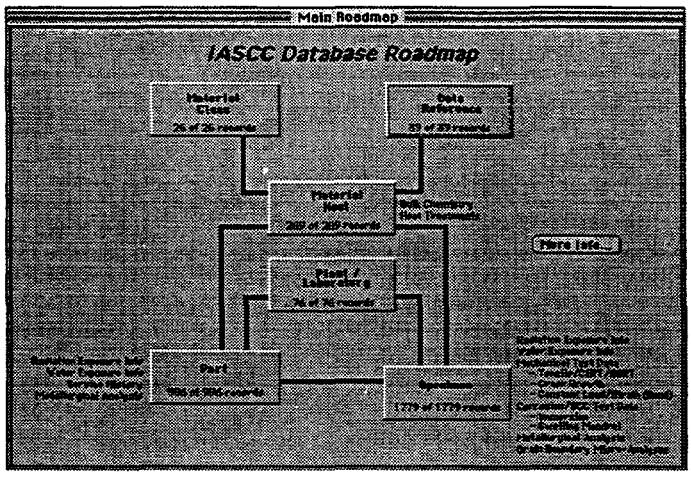

CIR Program

NRC-CIR-10/97-12

EPRI/NPG

CIR Program White Papers

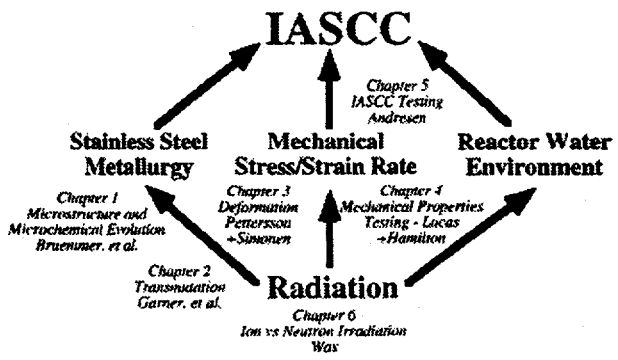

CIR Program

NRC-CIR-10/97-13

EPRI/NPG

Change in Yield Strength with Irradiation for SS

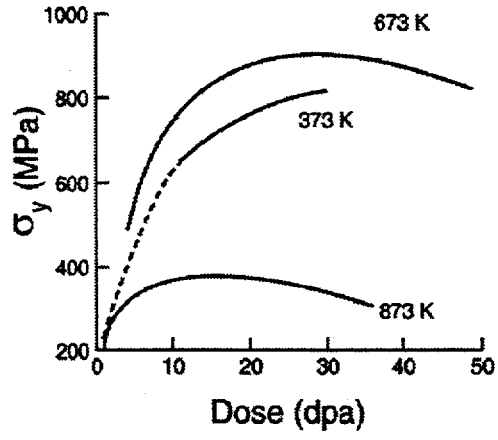

CIR Program

NRC-CIR-10/97-14

EPRI/NPG

Change in Uniform Elongation with Irradiation for SS

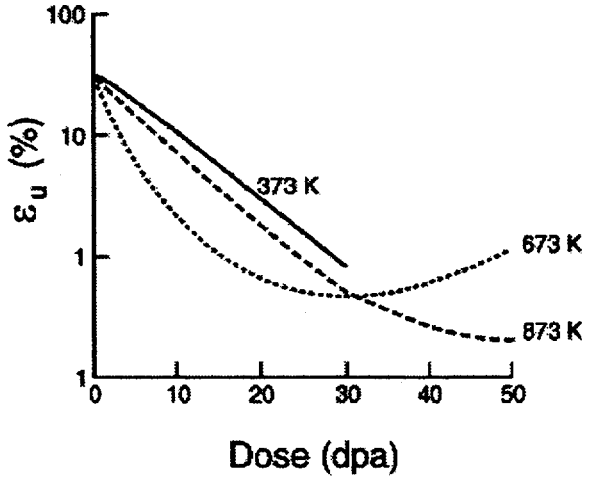

CIR Program

NRC-CIR-10/97-15

EPRI/NPG

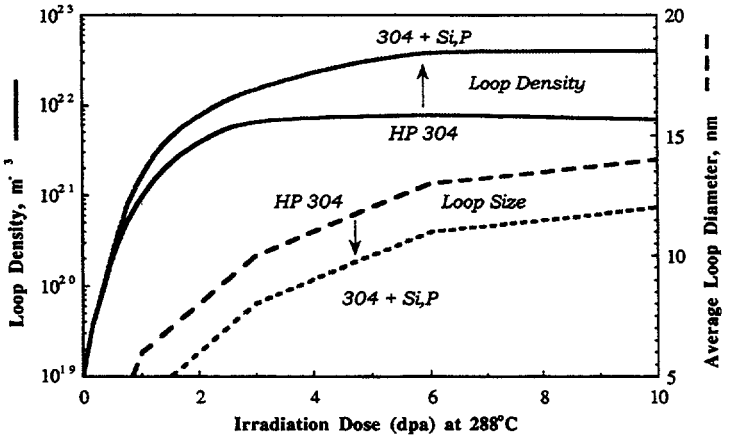

CIR Program

NRC-CIR-10/97-16

EPRI/NPG

BWR Neutron Spectra

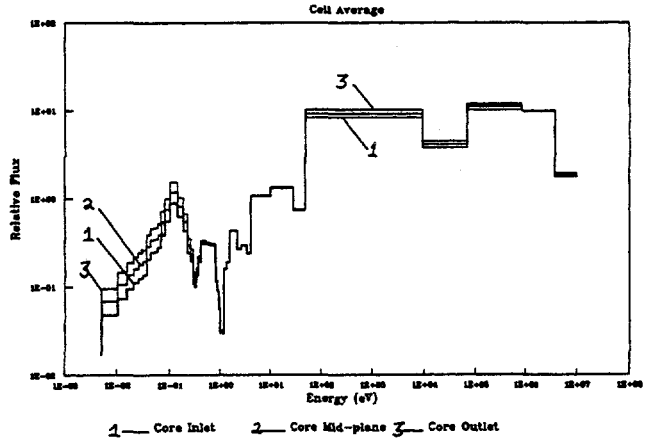

CIR Program

NRC-CIR-10/97-17

EPRI/NPG

Manganese Burnup in a PWR Due to Transmutation to Iron

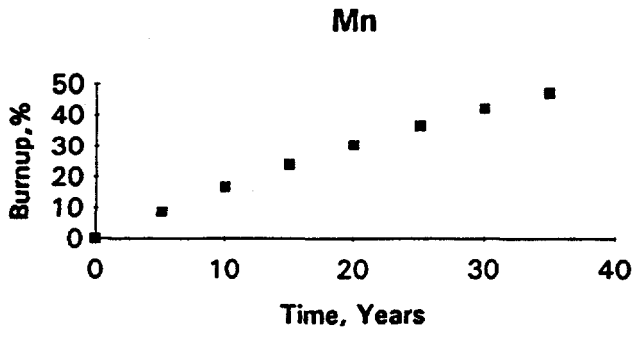

CIR Program

NRC-CIR-10/97-18

EPRI/NPG

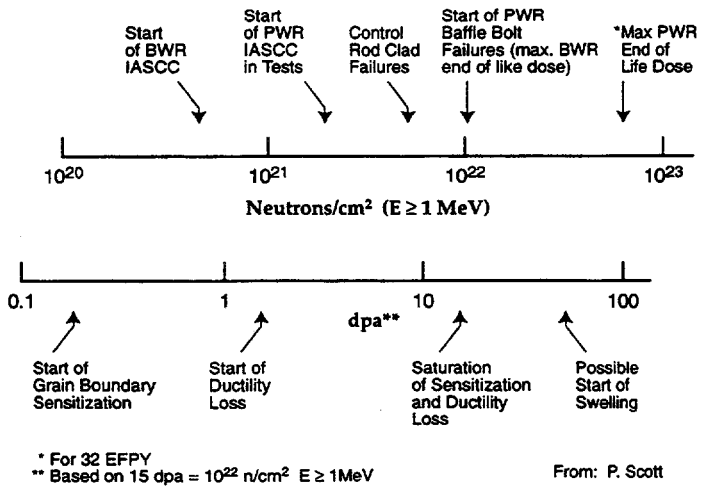

CIR Program

NRC-CIR-10/97-19

EPRI/NPG

Characterization of Neutron-Irradiated Stainless Steels

Objectives:

- To fully characterize critical changes in 300-series SS following neutron irradiations relevant to both PWR and BWR core components
- To thoroughly characterize examples of in-service cracking of irradiated 300-series SS in LWRs which are believed to have been caused by IASCC

CIR Program

NRC-CIR-10/97-20

EPRI/NPG

Evaluation of Fundamental Linkage Among SCC Phenomena

Objectives:

- Evaluate the extent of linkage or continuum in response among SCC and IASCC phenomena
  - IASCC in PWRs and BWRs
  - High fluence
- Evaluate common dependencies in irradiated and unirradiated SS
  - Water chemistry, temperature

CIR Program

NRC-CIR-10/97-21

EPRI/NPG

Evaluation of Fundamental Linkage Among SCC Phenomena

Test matrix for Task 1 SSRT testing. Test temperature is 288C.
All tests performed in duplicate.

Test	Fluence (n/cm²) [E> 1 MeV]	Oxygen	Hydrogen	Additions
Test 1-1	"low fluence"	42 ppm	0 ppb	
Test 1-2	"low fluence"	0 ppb	3.2 ppm	
Test 1-3	4.2×10^{21}	42 ppm	0 ppb	
Test 1-4	4.2×10^{21}	0 ppb	3.2 ppm	
Test 1-5	4.2×10^{21}	0 ppb	3.2 ppm	500 ppm B + 1.2 ppm Li
Test 1-6	4.2×10^{21}	----	----	(Gettered Argon)

- "low fluence" ...fluence levels of ~0.6×10^{21} or ~1.6×10^{21} n/cm²

CIR Program

NRC-CIR-10/97-22

EPRI/NPG

Evaluation of Fundamental Linkage Among SCC Phenomena

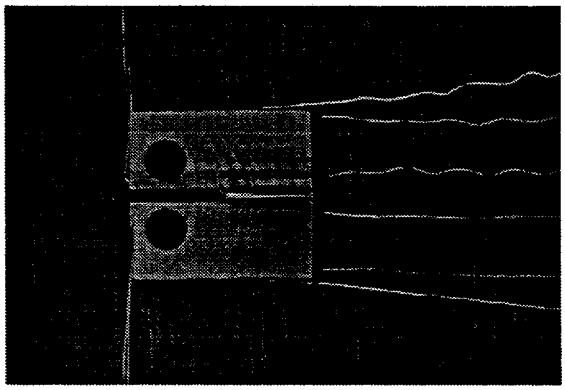

[1.25 inch wide by 1.20 inch high]

CIR Program

NRC-CIR-10/97-23

EPRI/NPG

Evaluation of Fundamental Linkage Among SCC Phenomena

Crack growth test environments for Task 2 testing

Specimen Number	Environment	pH (288C)	Sulfide (ppm)	Other Additions	Temperature (deg C)
2-1	A	9	300	Vary Li and B levels to achieve desired pH	315
2-1	C	9	30	Vary Li and B levels to achieve desired pH	315
2-1	B	5.5	30	Vary Li and B levels to achieve desired pH	315
2-1*	D	5.5	300	Vary Li and B levels to achieve desired pH	315
2-1*	E	~6.8	—	500 ppm B + 1.2 ppm Li	288
2-1*	F	~6.8	—	500 ppm B + 1.2 ppm Li	315
2-1*	G	~6.8	—	500 ppm B + 1.2 ppm Li	340

CIR Program

NRC-CIR-10/97-24

EPRI/NPG

Influence of Radiolysis & Hydrogen Embrittlement on In-Service Cracking

Objective:

- To determine the role of radiolysis on IASCC in a PWR
- To determine the role of hydrogen on IASCC

CIR Program

NRC-CIR-10/97-25

EPRI/NPG

Influence of Radiolysis & Hydrogen Embrittlement on In-Service Cracking

Task 1

Environment	Influence of			
	temperature	preirradiation	coolant	n /γ
Argon	✔	✔		
PWR - out of pile	✔	✔	✔	
PWR - in pile	✔	✔	✔	✔

Task 2

Environment	irradiated	unirradiated	hydrogen charged	hydrogen uncharged	T=320°C	T=100°C
Ar		✔	✔		✔	
Ar		✔		✔	✔	
Ar	✔			✔	✔	
Ar	✔		✔		✔	
PWR		✔		✔	✔	✔
PWR	✔			✔	✔	✔
PWR	✔		✔		✔	✔
PWR		✔	✔		✔	✔
PWR	✔		charging/annealing		✔	

CIR Program

NRC-CIR-10/97-26

EPRI/NPG

Use of Proton Irradiation to Understand IASCC in LWR Cores

Background:

- Testing of neutron irradiated material is expensive
- Proton irradiation has desirable characteristics
  - Deep penetration
  - Lower activity
- Displacement damage process is different
  - Grain boundary composition profiles and microstructural evolution is similar for both proton and neutron irradiated material

CIR Program

NRC-CIR-10/97-27

EPRI/NPG

Use of Proton Irradiation to Understand IASCC in LWR Cores WO4068-26

Background:(continued)

- May be able to use proton irradiation for screening
  - New materials, compositions and water chemistries

Objective:

- To compare proton and neutron irradiation effects on IASCC response and relate to material microstructure and microchemistry

CIR Program

NRC-CIR-10/97-28

EPRI/NPG

Cooperative IASCC Research Program

Summary:

- Primary objective is to develop a mechanistic understanding of IASCC
- Five year program ending in 2000
- Cooperatively sponsored - currently 18 member organizations
- $8-10 M workscope + in-kind program and resource sharing
- Program workscope defined by sponsors and managed by EPRI

CIR Program

NRC-CIR-10/97-29

Environmentally Assisted Cracking of LWR Materials*

O. K. Chopra, H. M. Chung, T. F. Kassner, J. H. Park, and W. J. Shack
Argonne National Laboratory
Argonne, Illinois

J. Zhang, F. W. Brust, and P. Dong
Battelle Columbus Laboratories
Columbus, Ohio

Abstract

The effect of dissolved oxygen level on fatigue life of austenitic stainless steels is discussed and the results of a detailed study of the effect of the environment on the growth of cracks during fatigue initiation are presented. Initial test results are given for specimens irradiated in the Halden reactor. Impurities introduced by shielded metal arc welding that may affect susceptibility to stress corrosion cracking are described. Results of calculations of residual stresses in core shroud weldments are summarized. Crack growth rates of high–nickel alloys under cyclic loading with R ratios from 0.2–0.95 in water that contains a wide range of dissolved oxygen and hydrogen concentrations at 289 and 320°C are summarized.

The program on Environmentally Assisted Cracking of Light Water Reactor (LWR) Materials is currently focused on five areas: fatigue initiation in pressure vessel and piping steels, irradiation–assisted stress corrosion cracking of austenitic SSs and cracking in BWR core shrouds, residual stresses in core–shroud welds, environmentally assisted crack growth in high–nickel alloys, and an assessment of industry–developed proprietary codes for prediction of crack growth rates.

Fatigue of LWR Structural Materials

The ASME Boiler and Pressure Vessel Code provides fatigue design curves for the structural materials used for nuclear power plant components. The effects of reactor coolant environments are not explicitly addressed by these design curves, although test data illustrate potentially significant effects of LWR environments on the fatigue resistance of pressure boundary structural materials.[1] Interim fatigue design curves that account for environmental effects have been developed.[2,3] Additional studies have been undertaken to better assess the effect of PWR environments on the fatigue life of austenitic and aged cast stainless steels and to better understand the actual mechanisms of degradation in carbon and low alloy steels.

During fatigue loading of smooth test specimens, cracks form immediately at surface irregularities/discontinuities already in existence or produced by slip bands, grain boundaries, second–phase particles, etc. Growth of these surface cracks may be divided into three regimes: (a) an initial period, which involves growth of microstructurally small cracks (MSCs) that are characterized by decelerating crack growth, as

*Job Code W-6610; NRC Program Manager: Dr. M. McNeil

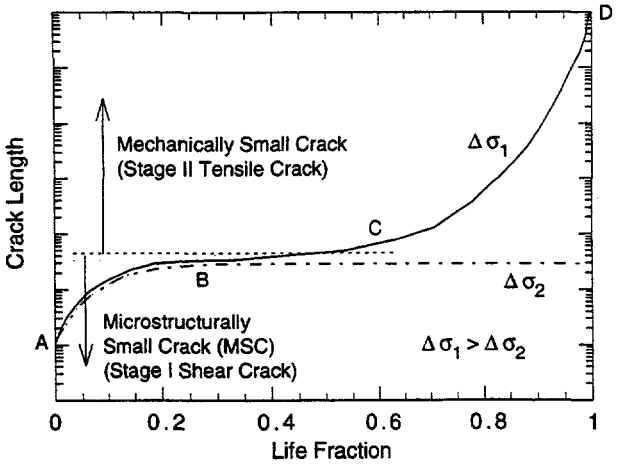

Figure 1.
Growth of cracks in smooth fatigue specimens

shown in region AB of Fig. 1; (b) a final period of growth characterized by accelerating crack growth, region CD; and (c) a transition period controlled by a combination of the two regimes, region BC.

The growth of MSCs is very sensitive to microstructure.[4–7] In air, the MSCs grow along slip planes as shear cracks in the early stage of growth. Grain boundaries, triple points, and phase boundaries markedly decrease growth rates. In ferritic–pearlitic steels, the ferrite–pearlite phase boundaries act as strong barriers to crack propagation, and growth rates decrease significantly when small cracks grow into the pearlite from the ferrite.[6]

Fatigue cracks greater than the critical length of MSCs show little or no influence of microstructure and are called mechanically small cracks.[5] For a stress ratio of –1, the transition from an MSC to a mechanically small crack for several materials has been estimated to be approximately eight times the unit size of the microstructure.[5] Mechanically small cracks are characterized by striated crack growth with a fracture surface normal to the maximum principal stress. Their growth rates tend to decrease as the cracks grow because crack closure becomes significant for larger cracks.

At low stress levels, e.g., $\Delta\sigma_2$ in Fig. 1, the transition from MSC growth to accelerating crack growth does not occur and the cracks are nonpropagating, i.e., a fatigue limit exists. Although cracks can form below the fatigue limit, they do not grow to engineering size. Of course, preexisting large cracks in the material, e.g., defects in welded samples, or those created by growth of microcracks at high stresses, can grow at stress levels below the fatigue limit.

The reduction in fatigue life in LWR coolant environments could arise from easier formation of surface microcracks and/or an increase in growth rates of cracks, during either the initial stage of MSC and shear crack growth or the transition and final stages of tensile crack growth. The environmental enhancement of fatigue crack growth in pressure vessel steels in high–temperature water and the effects of dissolved oxygen, sulfur content, loading rate, and flow velocities are well known.[8–12] Carbon steel (CS) and low alloy steel (LAS) specimens tested in water show surface micropitting and cavities that were produced by either corrosion or dissolution of MnS inclusions.[13] These micropits could act as sites for the formation of fatigue cracks. However, testing and detailed metallographic studies[13,14] suggest that the reduction in fatigue life in high–dissolved–oxygen (high–DO) water is due primarily to environmental effects on crack propagation. Although all specimens tested in water show surface micropitting, there is no indication that these micropits enhance cracking. Irrespective of environment, fatigue

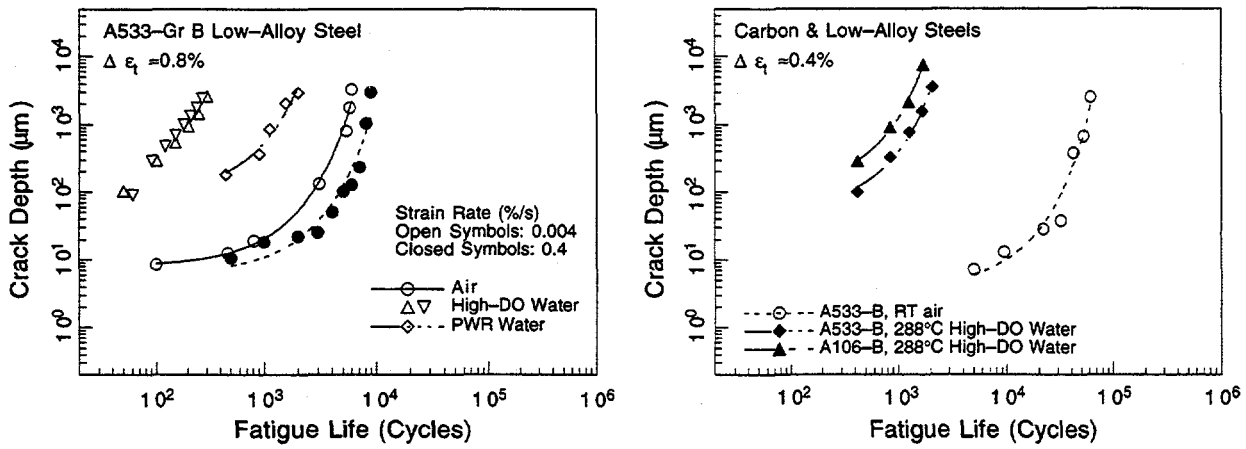

Figure 2. Depth of largest crack as a function of fatigue cycles for A533–Gr B LAS and A106–Gr B CS in air and water environments

cracks in CS and LAS nucleate along slip bands, sulfide inclusions, carbide particles, or at the ferrite/pearlite phase boundaries.

The depth of the largest crack is plotted as a function of fatigue cycles in Fig. 2, and as a function of fractional life in Fig. 3. The results indicate that in room-temperature air, ≈10-μm cracks form at <10% of fatigue life. Under these conditions, the depth of the largest crack is <100 μm at half–life. For the same life fraction, crack depth is greater in high– or low–DO water than in air. At ≈0.8% strain range, only 30–50 cycles are needed to form a 100–μm crack in high–DO water (average growth rate of 2–3 μm/cycle), whereas more than 3000 cycles are needed to form a 100-μm crack in air (average growth rate of 0.033 μm/cycle). In a low–DO PWR environment, the growth of cracks is faster than it is in air but slower than in high–DO water. The results in high–DO water show that the decrease in fatigue life of both A106–Gr B CS and A533–Gr B LAS is caused primarily by the effects of environment during early stages of fatigue damage, i.e., growth of cracks <100 μm in depth (Stage I crack growth).

Figure 4, which includes data from earlier studies,[4,6,15] shows that in both air and water environments, fatigue crack size at different life fractions is independent of strain range, strain rate, and DO content of the water. The depth of the largest crack at different life fractions is approximately the same at 0.75 and 0.4% strain ranges. These results imply that for strain or stress ranges above the fatigue limit, linear damage summation (Miner's rule) is valid for CS and LAS in both air and water environments.

In both A533–Gr B and A106–Gr B steels, the formation and growth of surface cracks appear to be different in high–DO water than in air or simulated PWR water.[16] In air and low–DO PWR environments, surface cracks grow as Mode II (shear) cracks in Stage I growth along planes that were usually at 45° to the stress axis. The Stage I crack extends across several grains until the increasing stress intensity of the crack promotes slip on systems other than the primary slip, and the crack begins to propagate as a Mode I (tensile) crack normal to the stress axis. Furthermore, in A106–Gr B CS, Stage I crack growth occurs entirely along the soft ferrite grains, avoiding the relatively hard pearlite regions. In high–DO water, the surface cracks appear to grow entirely as Mode I tensile cracks normal to the stress axis. In A106–Gr B CS, cracks propagate across both ferrite and pearlite regions.[16]

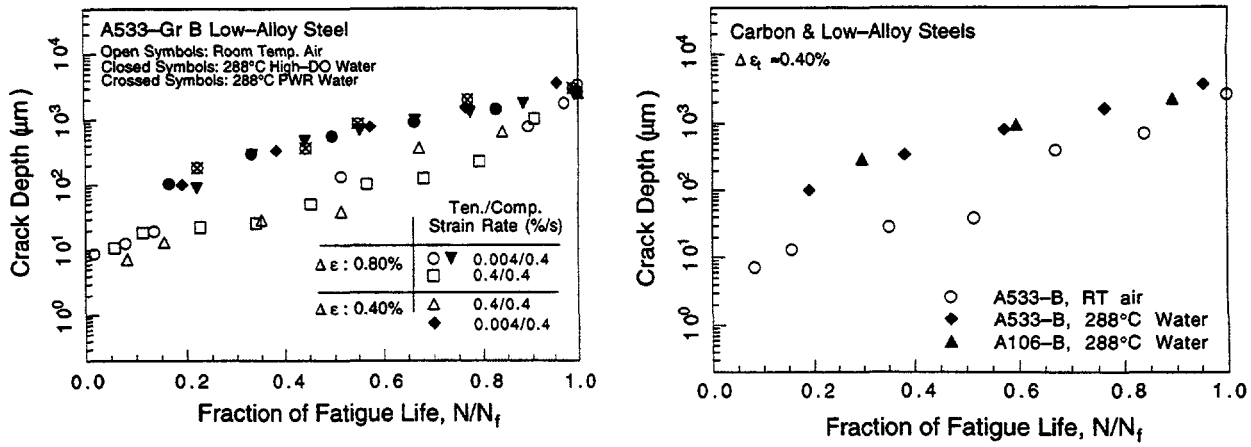

Figure 3. Depth of largest crack as a function of fractional life for A533–Gr B LAS and A106–Gr B CS in air and water environments

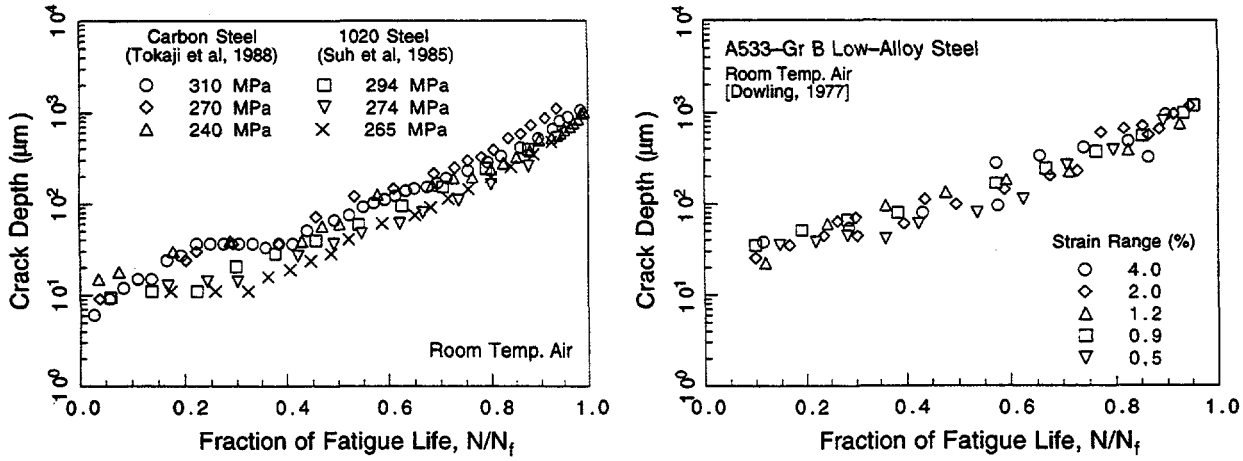

Figure 4. Crack depth as a function of fractional life for CSs and LASs tested in room–temperature air

The CGRs determined from the crack-depth-versus-cycles data shown in Fig. 2 are plotted as a function of crack depth in Fig. 5. For crack depths >100 μm, the CGRs in high–DO water are an order of magnitude higher than in air; the CGRs in the low–DO PWR environment are a factor of 2 to 3 higher than in air. For crack lengths <100 μm), the CGRs are nearly two orders of magnitude higher in high–DO water than in air. In high–DO water, surface cracks grow entirely as tensile cracks normal to the stress.

In Fig. 6, the measured CGRs are compared with the current and proposed[17] ASME Section XI reference crack growth curves for CSs and LASs. The degree of environmental enhancement observed in the fatigue initiation tests appears comparable to that determined in the fracture mechanics tests, although no evidence of a lower threshold below which EAC effects are unimportant can be seen.

The available data on the fatigue life of austenitic SSs were reviewed and statistical models were developed to estimate the effects of material and loading conditions on the fatigue lives of austenitic SSs.[3] In air, there is good agreement between the results of the present statistical analysis and the correlation developed by Jaske and O'Donnell[18] as shown in Fig. 7. Figure 7 also shows that the mean curve used to develop the ASME fatigue design curve for these materials is not consistent with the existing fatigue S–N data for austenitic SSs. When the Code

fatigue S–N curve for austenitic SSs was extended to 10^8 cycles, this discrepancy was taken into account, but no change was made to the design curve for $<10^6$ cycles.

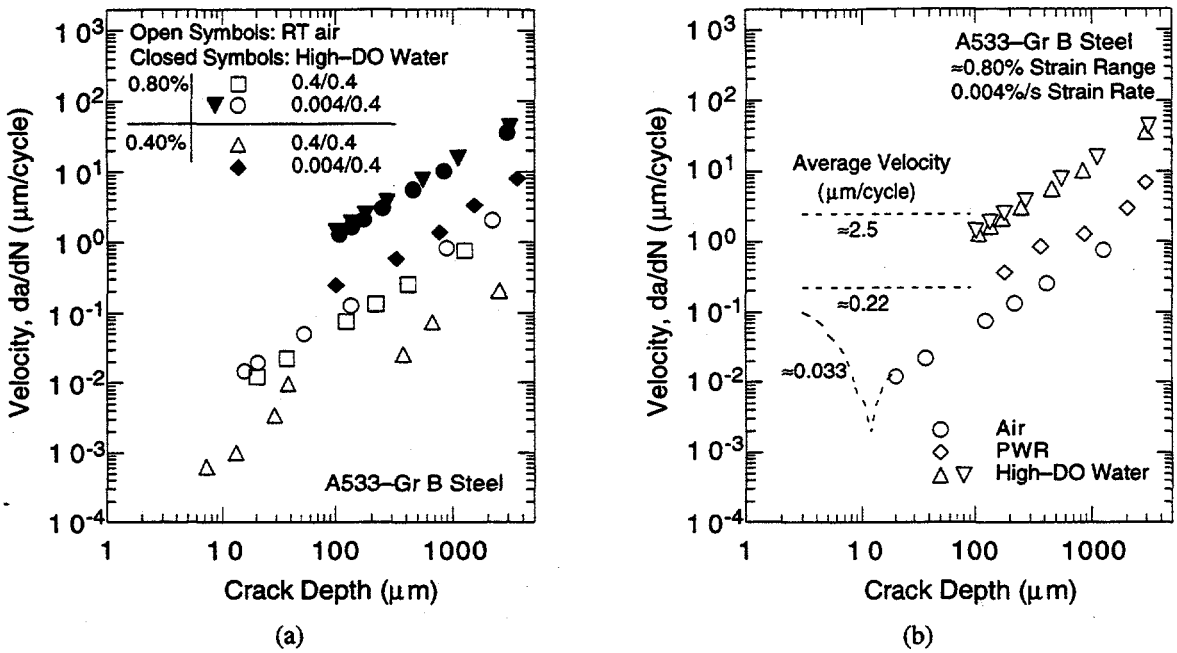

Figure 5. Crack growth rates as a function of crack depth for A533–Gr B LAS tested in air and water environments. Dotted lines show the probable growth rates during the early stage of fatigue damage in air and low– and high–DO.

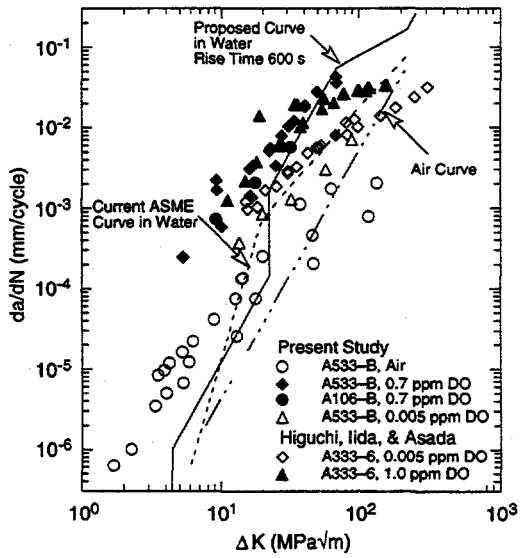

Figure 6.
Crack growth rates determined from smooth cylindrical fatigue test specimens and ASME Section XI reference curves for CSs and LASs in air and water environments

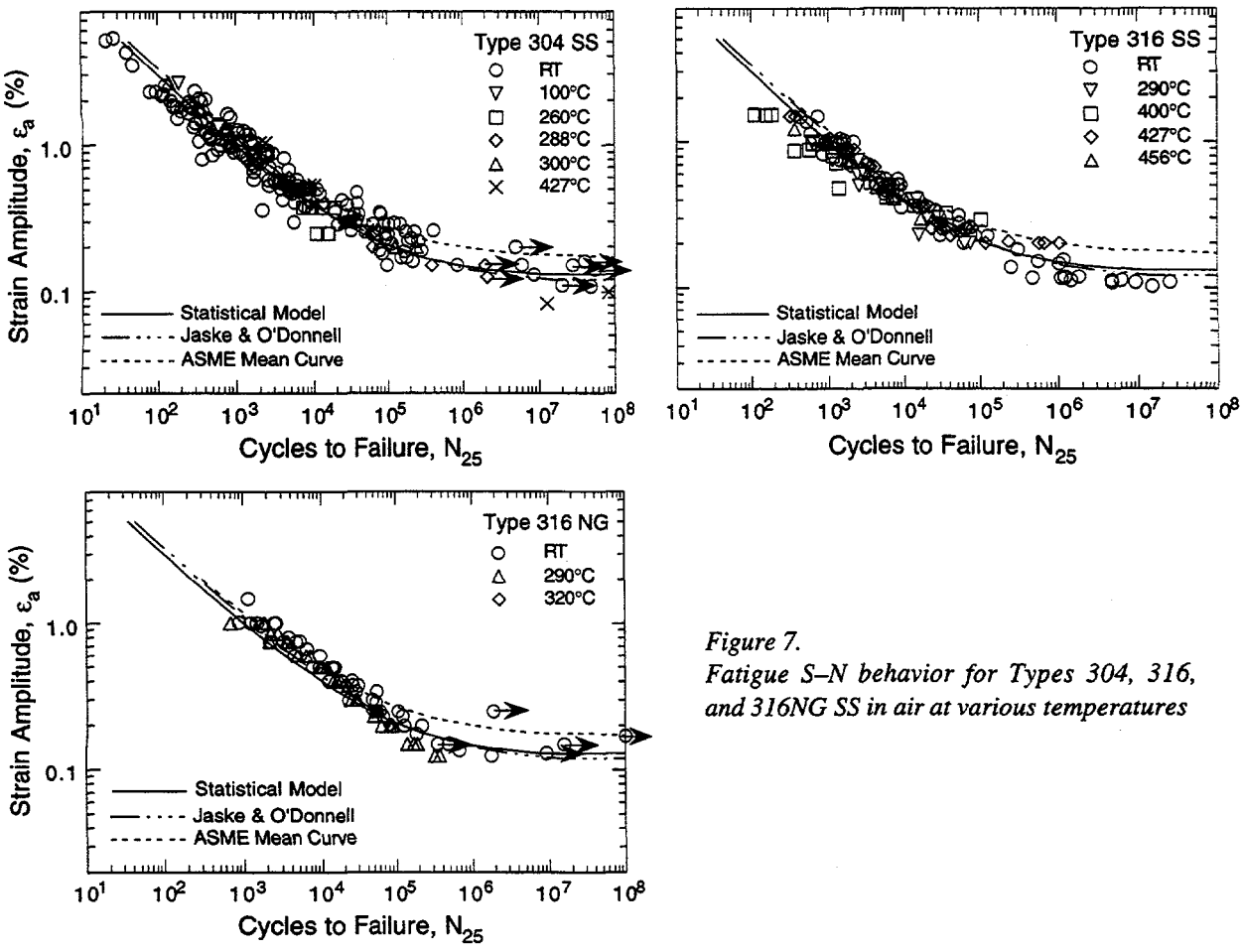

Figure 7.
Fatigue S–N behavior for Types 304, 316, and 316NG SS in air at various temperatures

Fatigue S–N data for Types 316NG and 304 SS in water at 288°C are shown in Fig. 8, along with the ASME Code fatigue design curve. There is a decrease in fatigue life in water relative to that in air. The reduction in life depends on strain range, strain rate, and DO level. For these steels, environmental effects on fatigue life are more pronounced in low–DO than in high–DO water. This is quite different from the behavior or ferritic steels. In Fig. 9, fatigue life is shown as a function of strain rate. In all environments, the fatigue lives of these steels decrease with decreasing strain rate. The effect of strain rate is smallest in air and largest in a low–DO PWR environment.

Irradiation Assisted Stress Corrosion Cracking and Core Shroud Cracking

Irradiation–induced grain–boundary depletion of chromium has been considered as the primary metallurgical process that causes IASCC. Recent results[19,20] suggest that fabrication–related variables, i.e., grain–boundary segregation and depletion of alloying and impurity elements by thermal processes, thermomechanical treatment, hardening by cold work, use of recycled scrap metals, and uptake of minor impurities during iron– and steelmaking can have significant effects on susceptibility to SCC. Core shrouds are subject to relatively low fluence and would not usually be considered susceptible to IASCC, and most cases of core shroud cracking have been attributed to classical intergranular stress corrosion cracking (IGSCC) of thermally sensitized SS. However, cracking has been

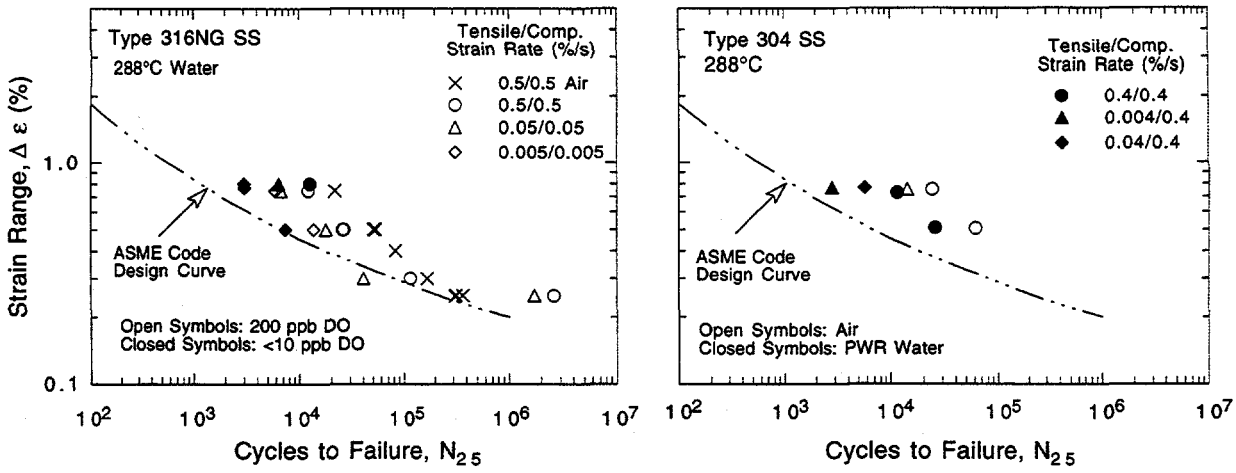

Figure 8. Total-strain-range-versus-fatigue–life data for Types 316NG and 304 SS in air and water

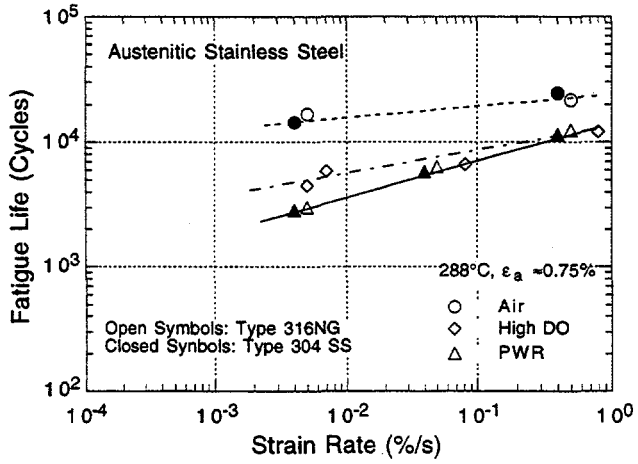

Figure 9.Effect of strain rate on fatigue lives of austenitic SSs in air and in simulated PWR and high–DO water environments

observed in core shrouds fabricated from Type 304L SS, an alloy in which sensitization would not be expected to occur and in which the absence of grain boundary carbides has been confirmed.

To obtain a better understanding of the failure mechanism(s) that may be involved in IASCC and cores shroud cracking, the stress corrosion cracking behavior and microstructural characteristics of austenitic stainless steels have been investigated by slow–strain–rate tensile (SSRT) testing, scanning electron microscopy, Auger electron spectroscopy, secondary-ion mass spectroscopy, and field-emission-gun advanced analytical electron microscopy. The effects of several metallurgical and electrochemical processes are being considered, i.e., neutron fluence, irradiation hardening, irradiation-induced grain-boundary Cr depletion and impurity segregation, non-equilibrium thermal segregation, fabrication-related impurity contamination, and water chemistry. Much of this work focuses on the analysis of specimens irradiated in the Halden reactor. The composition of the model alloys were specially designed to systematically investigate the effects of Cr, Ni, Mn, Si, P, S, C, N, O, and B. SSRT tests are currently underway on these materials and J_R and fracture–mechanics CGR tests will be performed in the coming year.

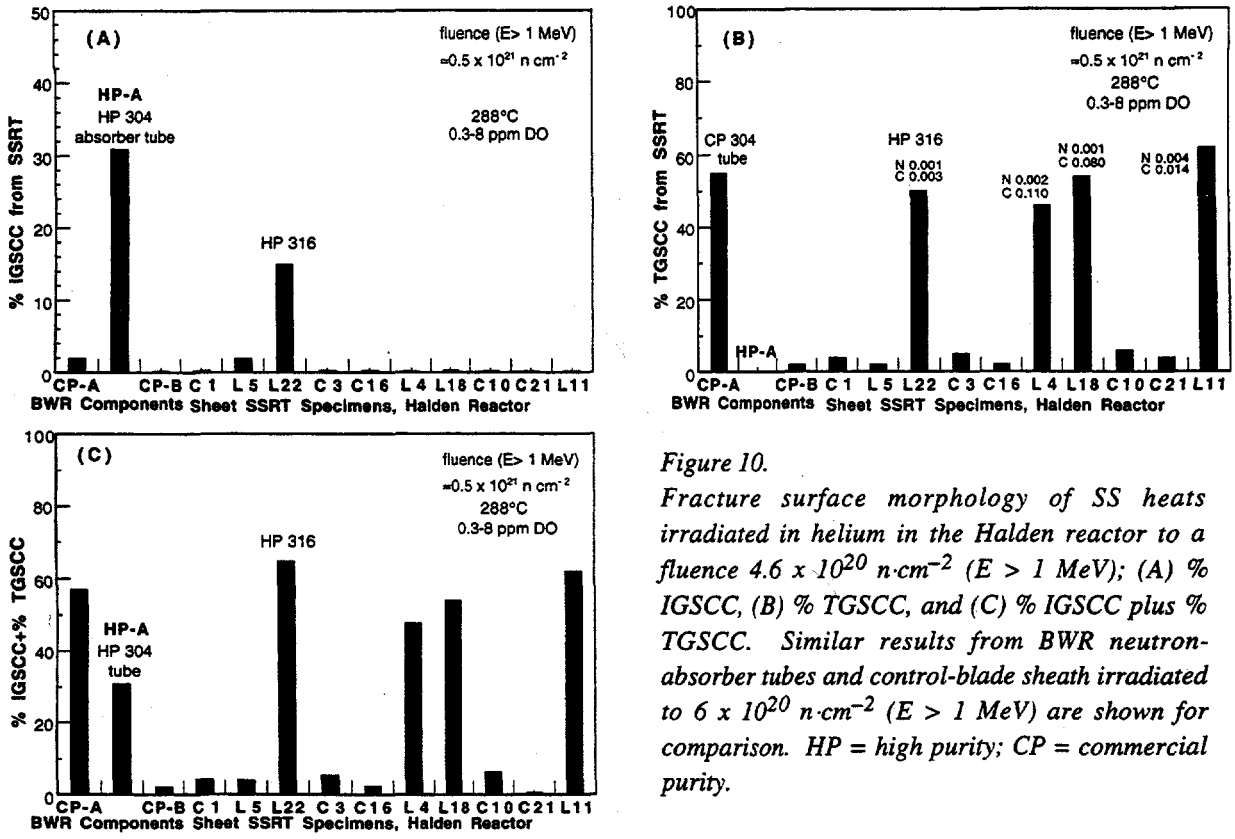

Figure 10.
Fracture surface morphology of SS heats irradiated in helium in the Halden reactor to a fluence 4.6 x 10^{20} n·cm^{-2} (E > 1 MeV); (A) % IGSCC, (B) % TGSCC, and (C) % IGSCC plus % TGSCC. Similar results from BWR neutron-absorber tubes and control-blade sheath irradiated to 6 x 10^{20} n·cm^{-2} (E > 1 MeV) are shown for comparison. HP = high purity; CP = commercial purity.

Preliminary results from SSRT tests on model austenitic SS alloys irradiated to a fluence of 4.6 x 10^{20} n·cm^{-2} (E > 1 MeV) at ≈289°C in helium environment in the Halden reactor are shown in Fig. 10. The SSRT tests were conducted at 288°C in simulated BWR water that contains ≈8 ppm DO. Percent intergranular stress corrosion cracking (IGSCC) determined by SEM fractography of the SSRT specimens is plotted in Figs. 10a. Similar comparisons are also shown in the figure in terms of percent transgranular SCC (TGSCC) and combined percent of IGSCC and TGSCC in Figs. 10b and 10c, respectively. Some previous results on high purity and commercial purity materials irradiated in a commercial BWR are included for comparison.

For these heats and test conditions, only the high-purity Type 316 SS (Heat L22) showed any susceptibility to IGSCC after irradiation. This heat and three other heats exhibited susceptibility to TGSCC after irradiation. All the heats that showed susceptibility to TGSCC contain very low levels of nitrogen [<0.004%, Fig. 10(B)]. However, it is not clear if nitrogen content is the primary factor that promotes susceptibility to TGSCC; further tests on specimens irradiated to higher fluences should provide a better understanding. The other six heats that were tested exhibit low or negligible susceptibility to IGSCC or TGSCC at this relatively low fluence. Future tests will include higher–fluence materials.

Most large components, such as BWR core shrouds, are welded in the field by either shielded metal arc (SMA) or submerged-arc (SA) procedures. These procedures require the use of welding electrodes coated with a welding flux. Consequently, the welding flux is a potential source of impurities that can contaminate the fusion zone and heat–affected zones (HAZs), and the microchemistry and microstructure of these regions will differ from those of the base metal. Because this contamination could conceivably influence IGSCC and IASCC behavior, the structure and properties of weld HAZs of Types 304, 304L, and 316 are being investigated.

Table 1. Composition of SMA weld HAZ and base metal of commercial heat C1 of Type 304 SS

	HAZ	Base Metal
	wt.%	
Cr	19.91	18.11
Ni	9.36	8.12
Mn	1.18	1.00
Mo	**0.27**	**<0.05**
Cu	0.07	0.05
Si	0.56	0.50
	wppm	
C	600	600
O	**640**	**80**
P	310	380
S	50	20
	appm	
F	**20-240**	**negligible**

Table 2. Composition of SMA weld HAZ and base metal of commercial heat C21 of Type 316 SS

	HAZ	Base Metal
	wt.%	
Cr	**19.19**	**16.28**
Ni	10.10	10.24
Mn	1.21	1.19
Mo	**0.81**	**2.08**
Si	0.56	0.51
	wppm	
C	600	600
O	**420**	**70**
P	**280**	**340**
S	**60**	**10**

Table 3. Composition of GTA weld HAZ and base metal of commercial heat C1 of Type 304 SS

	HAZ	Base Metal
	wt.%	
Cr	18.88	18.11
Ni	9.60	8.12
Mn	1.30	1.00
Mo	0.06	<0.05
Cu	0.05	0.05
Si	0.47	0.50
	wppm	
C	600	600
O	97	80
P	330	380
S	20	20

Table 4. Composition of GTA weld HAZ and base metal of commercial heat C21 of Type 316 SS

	HAZ	Base Metal
	wt.%	
Cr	17.74	16.28
Ni	10.24	10.24
Mn	1.42	1.19
Mo	**1.45**	**2.08**
Si	0.53	0.51
	wppm	
C	500	600
O	51	70
P	310	340
S	20	10

Weldments of 12.7-mm-thick plates of commercial-grade heats of Types 304, 304L, and 316 were prepared by SMA and gas-tungsten-arc (GTA) procedures. The compositions of the HAZ of the SMA weld and base metal of Type 304 SS Heat C1 and Type 316 SS Heat C21, determined by bulk chemical analysis, are summarized in Tables 1 and 2, respectively. Similar results for GTA welds of the same heats are given in Tables 3 and 4. Significant increases or decreases in concentration in the HAZ relative to those in base metal is denoted in the tables by bold type.

The fluorine content was analyzed only for the SMA weld of Heat C1. Based on the results in Tables 1–4, welding by the SMA procedure appears to lead to significant contamination of the HAZ by oxygen, fluorine, and

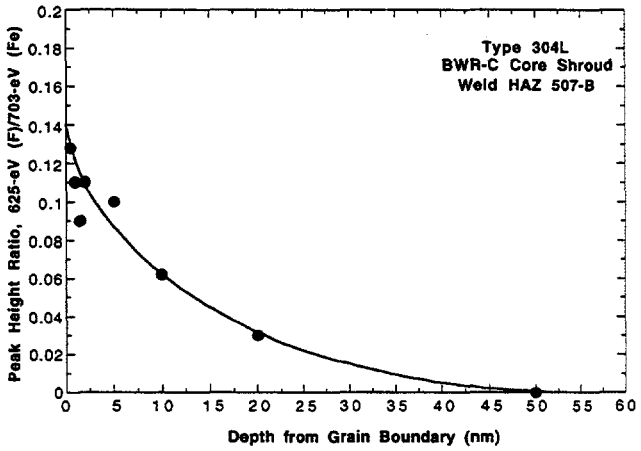

Figure 11.
Intensity of fluorine AES signal as function of sputter distance from grain boundary surface in Type 304L core-shroud weld HAZ, Specimen 507-B

sulfur. The major sources of contamination are the weld electrode coating and air. The chemical composition of the HAZ in the GTA weld is similar to that of the base metal.

The detection limit of fluorine by the wet-chemistry method is <≈30 wppm if several grams of material are available for analysis, but only ≈120 wppm (≈360 appm) if the sample mass is <1 mg. Therefore, it is difficult to determine the distribution of these elements by this technique. To do this, fluorine and oxygen contamination in the specimen was analyzed by secondary-ion mass spectroscopy (SIMS).[21] Secondary ions of fluorine that were ejected from the weld fusion zone and the HAZ were analyzed by using cesium primary ions in one case and oxygen ions in another.

Examination of the distribution maps of fluorine and oxygen suggests that local regions high in oxygen concentration are also high in fluorine concentration. This observation is consistent with the results of AES analyses of BWR core shroud, which showed a high fluorine content in oxide or spinel precipitates.[22]

Auger electron spectroscopy analysis of grain-boundary distribution of fluorine was also conducted on a specimen from a Type 304L SS BWR core shroud weld. The HAZ of the weld specimen was fractured in–situ in the scanning auger microscope, and one of the grain boundaries was selected and analyzed by a depth-profiling technique. The fluorine signal (at 625 eV) as a function of distance beneath the grain boundary is shown in Fig. 11. The fluorine content is significantly higher on grain boundaries than in grain matrices, probably as a result of thermal segregation during cooling of the HAZ. Because of its very low solubility in SSs, fluorine will segregate by a thermal process to local sites such as matrix/precipitate interfaces, grain boundaries, and stacking faults; however, irradiation-induced segregation cannot be ruled out and further investigation will be needed to clarify this point.

Residual Stresses Distributions in Core Shroud Weldments

Under a subcontract with Argonne National Laboratory (ANL), Battelle Columbus Laboratories has used numerical models to characterize weld residual stresses and the associated stress intensity factors at BWR core shroud welds. A detailed description of the weld residual stresses has been obtained for the H4 and H8 welds of core shrouds with a cone–type support. The core shroud structure and the geometry of the H4 weld is shown in Fig. 12. The H4 weld is a multipass submerged-arc weld that joins two Type 304 SS cylinders. The H8 weld geometry is more complex since it joins the conical lower support to a forged ring structure that supports the shroud. The geometry of the H8 weld and the finite–element grid used to model it are shown in Fig. 13. For both weld geometries, the multipass welding process was simulated with by axisymmetrical solid–elements. A thermal

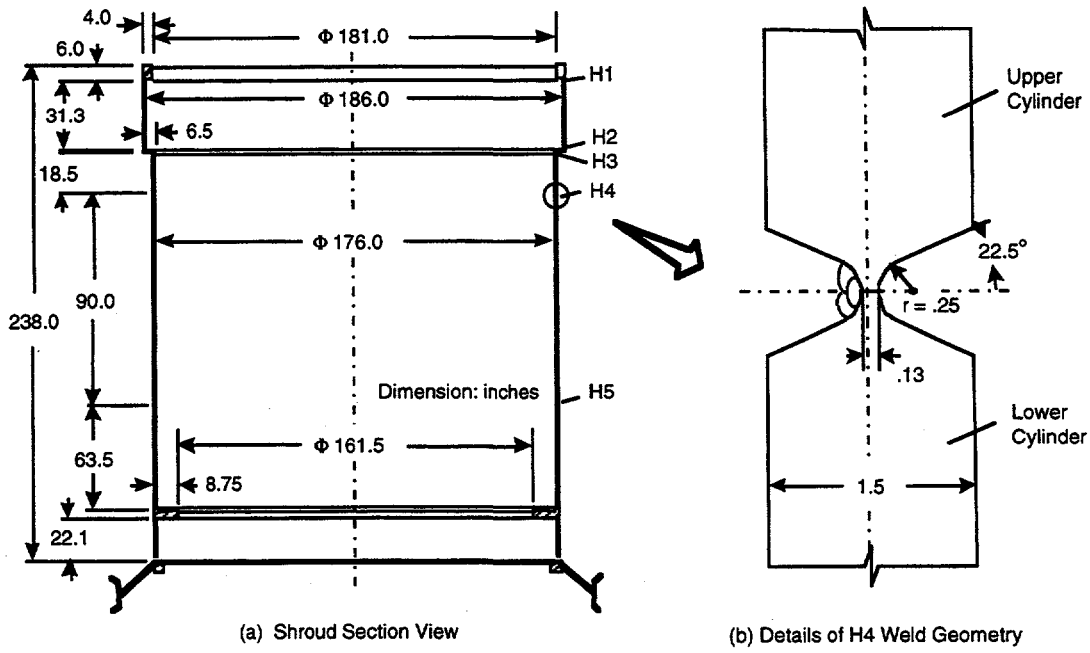

Figure 12. Core shroud structure and H4 weld geometry

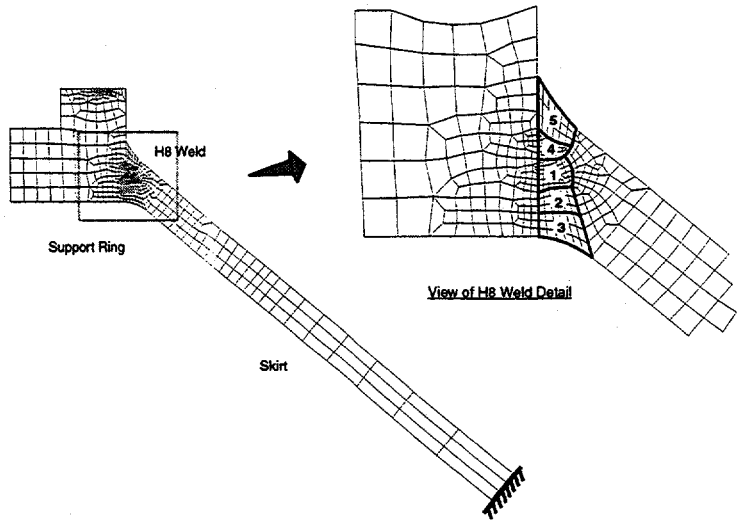

Figure 13. Axisymmetric finite element model for H8 weld joining the core shroud support ring to the conical support skirt

analysis was performed with the TEMPER code developed at BCL, and the temperature solutions obtained from the thermal analysis were then used as input for the structural analysis, which was performed with the ABAQUS finite–element code.[23] Currently, almost all general-purpose commercial finite–element codes, including ABAQUS, are incapable of directly modeling welding phenomena such as material melting and metal deposition. A special user–material subroutine developed at BCL was used to model material behavior during welding.[24]

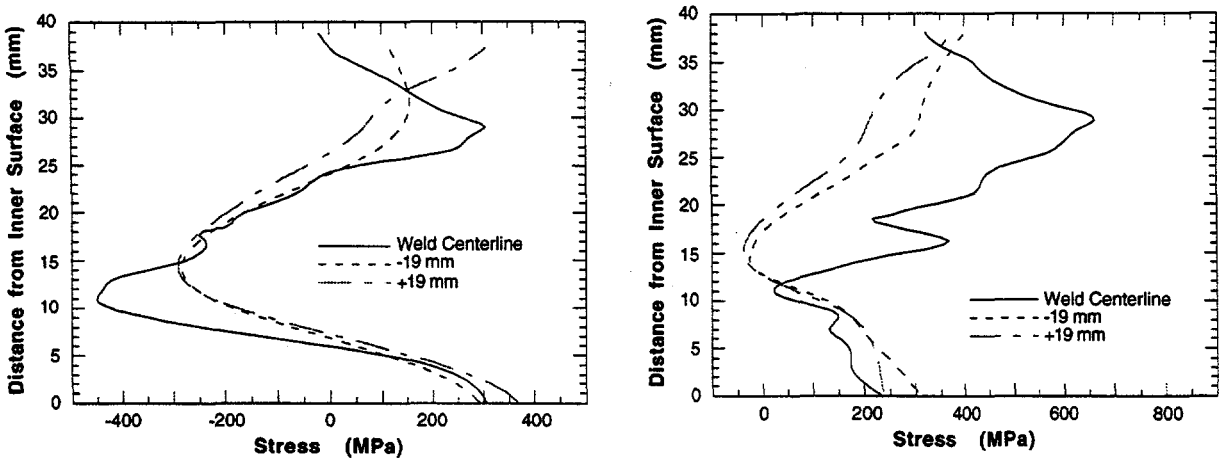

Figure 14. Distribution of (a) axial and (b) circumferential residual stresses through the wall at the weld centerline and HAZ for the H4 weld

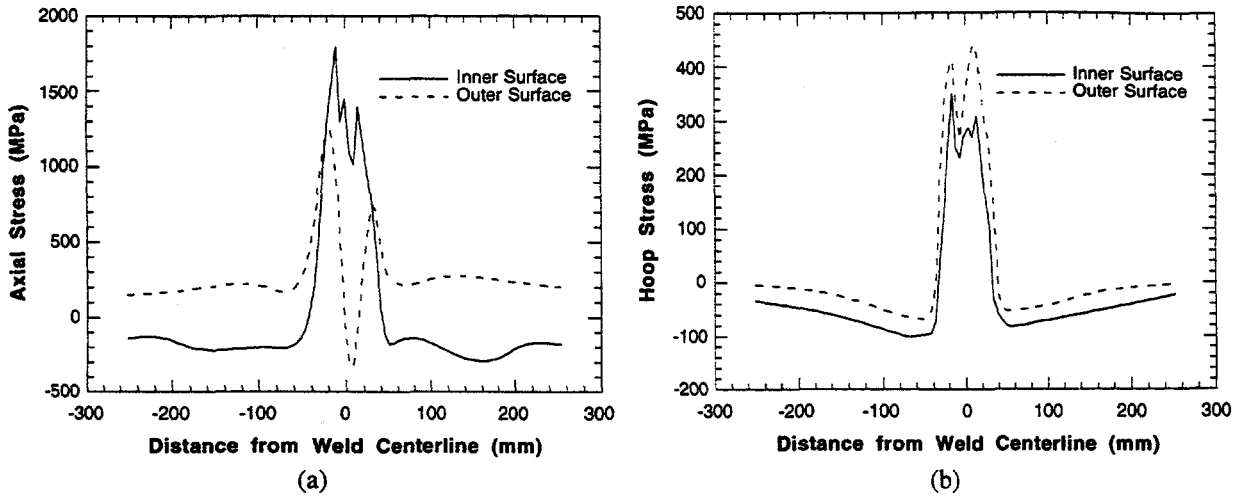

Figure 15. Distribution of (a) axial and (b) circumferential residual stresses along the inner and outer surfaces of the H4 weld

The axial residual stresses for the H4 weld show a "thick-shell" type of distribution as shown in Fig. 14. In the middle of the wall, the axial residual stresses are compressive, whereas tensile stresses were present at both inner and outer surfaces of the pipe except at the weld centerline, where a small-amplitude compressive stress is present on the outer surface. This compressive axial stress was primarily due to axial bending of the wall caused by radial shrinkage of the weld and the presence of a weld cap. The axial stresses are tensile in the HAZs on the inner and outer surfaces. At these cross sections, the maximum tensile axial stresses are at the inner surface of the shroud wall. The hoop stresses are tensile almost throughout these cross sections. The maximum tensile hoop stress occurs at the weld centerline between the mid–thickness and outer surfaces, as shown in Fig. 15. At the HAZs, the tensile stresses peak at the inner and outer surfaces. However, their magnitudes are much smaller than the peak value at the weld centerline.

After the residual stress distributions in the uncracked weldment were determined, stress intensity factors K for weldments that contained flaws were determined by the finite–element alternating method (FEAM).[25,26]

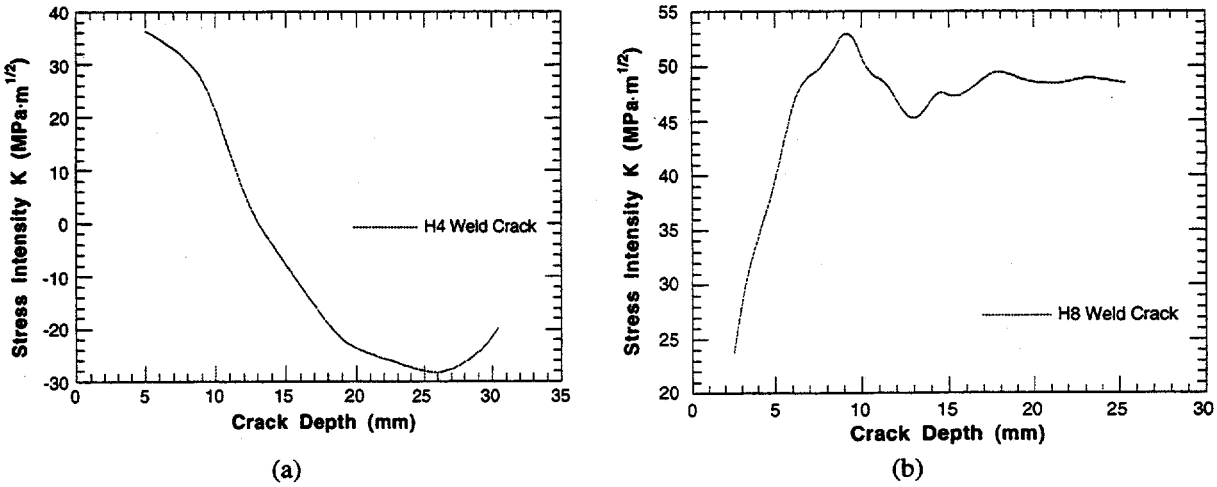

Figure 16. (a) Variation of stress intensity factor K with crack depth for 360° cracks starting from the inside surface in the H4 weld; (b) Variation of stress intensity factor K with crack depth for 360° cracks starting from the inside surface in the H8 weld

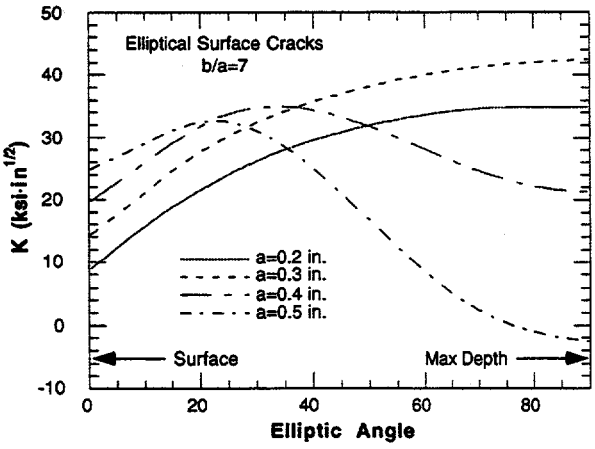

Figure 17.
Variation of stress intensity factor K along crack front for elliptical cracks with a half-length to depth ratio of 7 for depths of 0.2, 0.3, 0.4, and 0.5 in.

Complete 360° cracks and a surface crack that extends over only a portion of the circumference of the cylinder were considered. For the axisymmetrical case with a complete 360° crack shown in Figure 16(a), the results indicate that a crack growing from the inside to the outside of the vessel surface, or vice versa, would be likely to stop growing at approximately midwall, because K becomes negative for deeper cracks. The stress intensity factor K along the crack front for an elliptical surface crack with a half-length-to-depth ratio of 7 is shown in Fig. 17. The K value at the deepest point of the crack decreases as the crack depth increases. However, the K values along the crack front near the surface remain positive, and in fact, increase as the crack grows deeper. These results suggest that cracks, if driven by corrosion mechanisms that depend on K, will tend to increase in length in the angular direction much more rapidly than they will grow throughwall. Indeed, there will be a tendency for full 360° cracks to develop; the average depth of the cracks is expected to be ≈50% of the wall thickness, although local perturbations in the stress distributions could produce localized regions of deeper cracking. Although the throughwall stress distribution inhibits crack growth throughwall for the H4 weld, other weld geometries can have less favorable residual stress distributions. Figure 16(b) shows the throughwall distribution of K for the H8 weld. In this case, K increases with depth for the first 10 mm or so and then remains at a high positive value even for deep cracks.

Environmentally Assisted Cracking of Alloy 600 and SSs in Simulated LWR Water

Cracking has occurred in Alloy 600 in applications such as instrument nozzles and heater thermal sleeves in the pressurizer and the penetrations for control–rod drive mechanisms in reactor vessel closure heads in the primary system of PWRs and in shroud–support–access–hole covers in BWRs. Experience with EAC in other systems strongly suggests that materials that are susceptible to SCC are also susceptible to environmental enhancement of fatigue–crack growth and that studying environmental enhancement under cyclic loading conditions provides an understanding of the effect of environmental variables that is also applicable to the constant loading case and has some experimental advantages.

The results from our CGR tests in oxygenated and deoxygenated HP water are summarized in Figs. 18–20. In general, the present results do not reveal large differences in CGR behavior of Alloys 600 and 690 in HP deoxygenated water or in air under the conditions in these experiments. Similarly, temperatures in the range of 240-320°C in water and 35-289°C in air do not appear to have a large effect on the rates. It is possible that other heats of material with different heat-treatment conditions could produce a wider variation in the results. Although the data are plotted in terms of ΔK, it should be noted that the low ΔK values correspond to high R loading, i.e., as ΔK approaches zero, the loading approaches the constant load SCC situation. The comparison is presented in terms of the ratio of the CGR's in water and air as a function of ΔK. The ratio is based on "best-fit" correlations for the CGR versus ΔK data in air and water, respectively. The best comparison would be for rates determined at the same temperature on specimens from the same heat of material with the same heat treatment, but not enough data are available in every case to make such comparisons. However, because of the relatively small effect of differing material conditions (heat and heat treatment) and temperature on the CGRs, comparisons have been made on the basis of the combined results for different heat treatments and temperatures when insufficient data are available for a particular set of conditions.

Figure 18a and 18b shows the dependence of the ratio of the CGRs of Alloys 690 and 600 at 289°C in HP deoxygenated water to that in air at 289°C on ΔK , and the ratio of the CGRs from the combined data at the three temperatures in water to that in air at 289°C. The ratios of the CGRs of Alloys 600 and 690 in water and air at 289°C (Fig. 18a) indicate that the rates for Alloy 600 are higher in water than in air (ratio >1) at ΔK values <6 MPa·m$^{1/2}$ and are lower in water than in air (ratio <1) at higher values of ΔK. In contrast, the CGRs of Alloy 690 are only slightly higher in water than in air over the entire range of ΔK. Thus, environmental enhancement of the CGR even for Alloy 600 occurs only at R ratios close to 1.

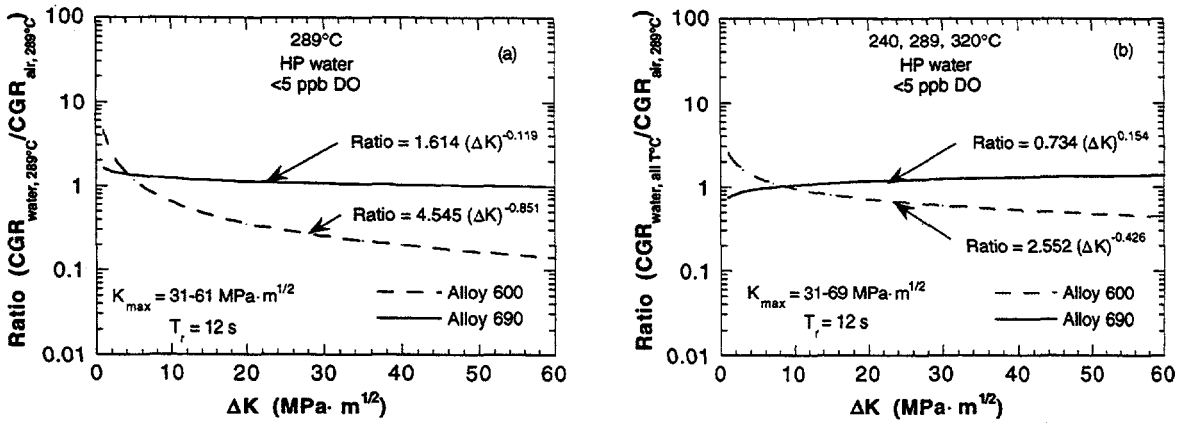

Figure 18. Dependence on ΔK of (a) ratio of CGRs of Alloys 600 and 690 at 289°C, (b) combined data at 240–320°C in HP deoxygenated water to CGRs in air at 289°C

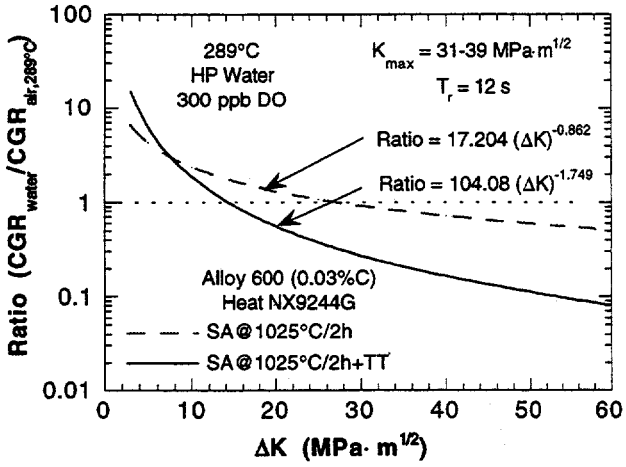

Figure 19.
Dependence on ΔK of ratio of CGRs of solution-annealed (1025°C) and thermally treated Alloy 600 in HP oxygenated water to CGRs of mill-annealed Alloy 600 in air at 289°C

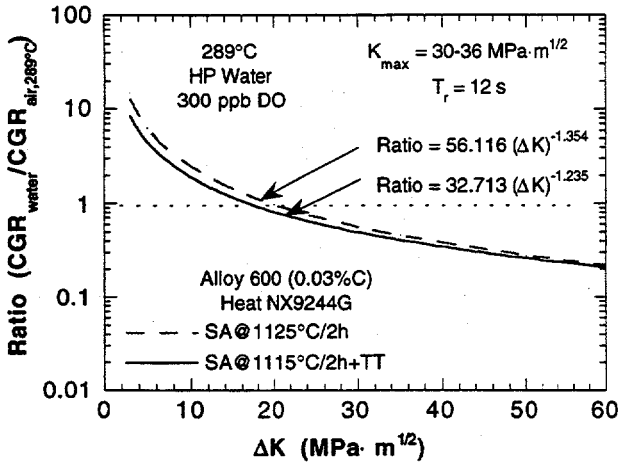

Figure 20.
Dependence on ΔK of ratio of CGRs of solution-annealed (1115°C) and thermally treated Alloy 600 in HP oxygenated water to CGRs of mill-annealed Alloy 600 in air at 289°C

The results in Fig. 18b , which are based on the combined data obtained in water at 240, 289, and 320°C, are consistent with behavior shown in Fig. 18a. These results suggest that larger differences in the CGRs of the two materials in water and of the materials in water versus air may occur under constant load, i.e., at R = 1.0.

CGRs in HP oxygenated water of specimens with different heat-treatment conditions are shown in Figs. 19 and 20. The best comparison to determine environmental effects would be with data in air determined from the same heat of material with the same heat treatment. Such data are not available, and instead, the comparison is made with data in air from another heat of Alloy 600. Our previous work[27] suggests that differences in fatigue CGRs in air due to heat–to–heat and heat treatment conditions are fairly small.

The ratios of the CGRs for Alloy 600 in water and air at 289°C (Figs. 19,20) indicate that the rates are higher in water than in air (ratio >1) at ΔK values <18 MPa·m$^{1/2}$ and are lower in water than in air (ratio <1) at higher values of ΔK. Again, small ΔK values correspond to high R loading. For R ≥ 0.95 and a K_{max} of ≈40 MPa·m$^{1/2}$, which corresponds to ΔK values of ≤2 MPa·m$^{1/2}$, the rates in water are higher than in air by a factor of ≈10. Tests are being conducted in HP oxygenated water under constant load at K_{max} of <40 MPa·m$^{1/2}$ to verify the CGRs extrapolated from the high R loading. In Fig. 20, as ΔK increases from ≈18 MPa·m$^{1/2}$, the ratio of the CGRs in water and air is <1, and at a ΔK of 40 MPa·m$^{1/2}$, the rate in water is lower than in air by a factor of ≈3, based on the combined data from the four specimens.

The results in Figs. 18–20 show the interdependence of loading conditions and DO in HP water and CGRs of Alloy 600 and that generalization of CGR results from a single loading condition and DO level in water to other loading and/or DO conditions can be misleading. For example, at a ΔK of 18 Mpa·$m^{1/2}$ ($R \approx 0.5$), the CGRs of Alloy 600 are the same in air as in water that contains 300 ppb DO at 289°C, whereas at this ΔK (R), the rate is higher by a factor of 2 in air than in water that contains <5 ppb DO. Similarly, at a ΔK of 6 MPa·$m^{1/2}$ ($R \approx 0.8$), the CGRs are the same in air and in water that contains ≈5 ppb DO at 289°C, although the rate in water that contains ≈300 ppb DO is higher by a factor of 5 than in air at this ΔK.

Assessment of Crack-Growth Models Proposed by the Industry

Two industry–developed proprietary codes for predicting SCC CGRs for austenitic stainless steels in BWR environments have been benchmarked against representative experimental data obtained from laboratory tests and from tests in autoclaves attached to operating reactor coolant boundary systems. One code was developed by the BWR Vessel Internals Program (BWRVIP) and the other, Pledge, was developed at General Electric (GE.* A total of 252 tests, some of which are proprietary, were selected for comparison with the models. The tests cover a wide range of sensitization conditions, conductivities, electrochemical potentials, and stress intensity factors. However, the comparison was limited to tests with $K \leq 40$ MPa·$m^{1/2}$ to ensure validity of the CGR measurements from a fracture mechanics standpoint. About one half of the data are from constant load tests; the other half are from cyclic load tests with load ratios R between 0.9 and 0.95 and frequencies of 0.08 Hz or less. Only tests in which the ECP and conductivity were reported were included in the data base for the comparison.

Unlike Pledge, which is intended to predict CGRs under both constant load and cyclic loading conditions, the BWRVIP model was developed only for the constant load case. Much of the available data base consists of data with high R ($R \geq 0.9$) loading. Even if the intended application of the model is only for constant load situations, it would be useful to extend the BWRVIP model to include cyclic loading to develop increased confidence in its predictions of the effects of material and environmental variables. This was done by an approach similar to that described by Ford.[28] The mechanical loading parameter K was considered to be a surrogate for the more fundamental parameter, i.e., the crack tip strain rate, $\dot{\varepsilon}_{ct}$.

For cyclic loading, there is an additional contribution to the crack tip strain rate. Shoji[29] has argued that the crack tip strain due to the cyclic loading is proportional to the CGR due to the cyclic loading in an inert environment (air). That is,

$$\dot{\varepsilon}_{ct} \propto \dot{a}_{air} = \frac{1}{t_R}\frac{da}{dN},$$

where it is assumed that all the crack growth during the cycle occurs during the rising–load portion of the cycle of duration t_R. The correlation used for da/dN is that developed by James and Jones.[30]

Comparisons of the predictions of the BWRVIP model (modified to account for cyclic loads) and the Pledge model with the experimental data are shown in Fig. 21. The predictions of the modified BWRVIP model seem to be in better agreement with these experimental data than the predictions of the Pledge model. There is a major

*The cooperation of EPRI and BWRVIP, which provided technical information on the BWRVIP proprietary model and an electronic data base containing proprietary data, and the cooperation of General Electric, which provided technical information on the Pledge model, is acknowledged.

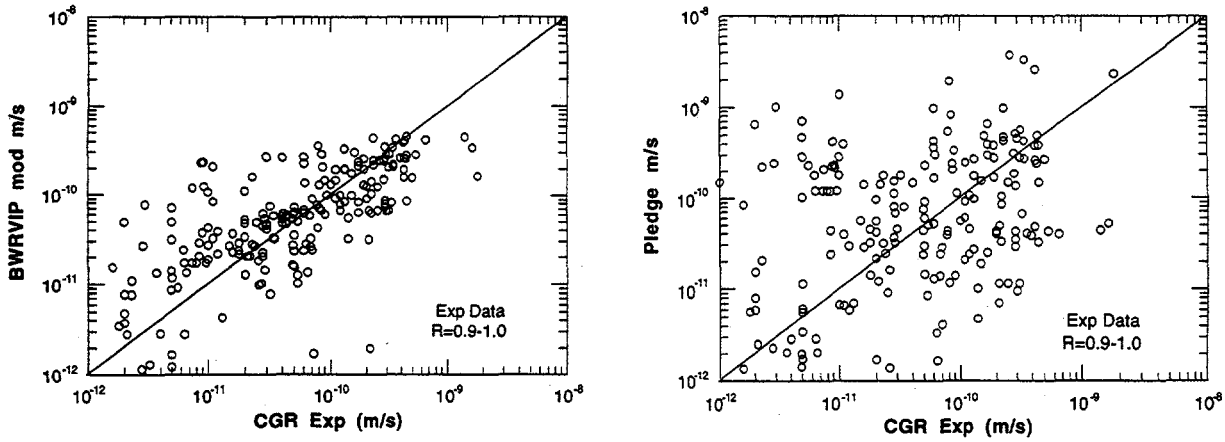

(a) (b)

Figure 21. (a) Comparison of predictions of the BWRVIP model modified to account for cyclic loading with experimental data; (b) Comparison of the predictions of the Pledge model with the same experimental data set.

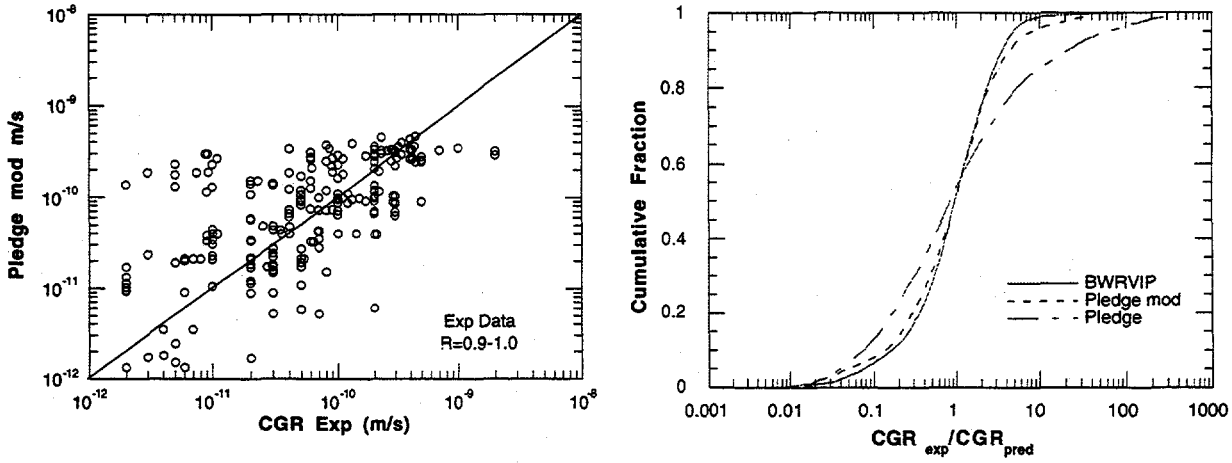

(a) (b)

Figure 22. (a) Comparison of predictions of the Pledge model modified to eliminate dependence on EPR with experimental data; (b) Cumulative distributions of the ratio of the experimental data to the predicted CGRs for the modified BWRVIP, Pledge, and modified Pledge models.

difference between the two models in the importance given to the sensitization level of the material as characterized by the electrochemical potentiokinetic reactivation (EPR) test. The BWRVIP model ignores variations in EPR, whereas in Pledge the CGR is a fairly strong function of EPR. A modified version of Pledge, in which the effect of variations in EPR on CGR were ignored, was considered. The predictions of this modified version of Pledge are shown in Fig. 22a. The agreement with the experimental data is significantly improved and is almost as good as that achieved by the BWRVIP model, as can be seen by comparing the cumulative distributions of the ratio of the experimental data to the predicted CGRs shown in Fig. 22b.

References

1. M. Higuchi and K. Iida, *Fatigue Strength Correction Factors for Carbon and Low–Alloy Steels in Oxygen–Containing High–Temperature Water,* Nucl. Eng. Des. **129**, 293–306 (1991).

2. S. Majumdar, O. K. Chopra, and W. J. Shack, *Interim Fatigue Design Curves for Carbon, Low-Alloy, and Austenitic Stainless Steels in LWR Environments,* NUREG/CR-5999, ANL-93/3 (April 1993).

3. J. Keisler, O. K. Chopra, and W. J. Shack, *Fatigue Strain-Life Behavior of Carbon and Low-Alloy Steels, Austenitic Stainless Steels, and Alloy 600 in LWR Environments,* NUREG/CR-6335, ANL-95/15 (Aug. 1995); also in Nucl. Eng. Des. **167**, 129-154 (1996).

4. C. M. Suh, R. Yuuki, and H. Kitagawa, *Fatigue Microcracks in a Low Carbon Steel,* Fatigue Fract. Eng. Mater. Struct. **8**, 193-203 (1985).

5. K. Tokaji and T. Ogawa, *The Growth of Microstructurally Small Fatigue Cracks in Metals,* in Short Fatigue Cracks, ESIS 13, M. J. Miller and E. R. de los Rios, eds., Mechanical Engineering Publication, London, pp. 85-99 (1992).

6. K. Tokaji, T. Ogawa, and S. Osako, *The Growth of Microstructurally Small Fatigue Cracks in a Ferritic-Pearlitic Steel,* Fatigue Fract. Eng. Mater. Struct. **11**, 331-342 (1988).

7. E. R. de los Rios, A. Navarro, and K. Hussain, *Microstructural Variations in Short Fatigue Crack Propagation of a C-Mn Steel,* in Short Fatigue Cracks, ESIS 13, M. J. Miller and E. R. de los Rios, eds., Mechanical Engineering Publication, London, pp. 115-132 (1992).

8. W. H. Cullen, M. Kemppainen, H. Hänninen, and K. Törrönen, *The Effects of Sulfur Chemistry and Flow Rate on Fatigue Crack Growth Rates in LWR Environments,* NUREG/CR-4121 (1985).

9. J. H. Bulloch, *A Review of the Fatigue Crack Extension Behaviour of Ferritic Reactor Pressure Vessels Materials in Pressurized Water Reactor Environments*, Res Mech. **26**, 95-172 (1989).

10. W. A. Van Der Sluys and R. H. Emanuelson, *Environmental Acceleration of Fatigue Crack Growth in Reactor Pressure Vessel Materials and Environments,* in Environmentally Assisted Cracking: Science and Engineering, ASTM STP 1049, W. B. Lisagor, T. W. Crooker, and B. N. Leis, eds., American Society for Testing and Materials, Philadelphia, PA, pp. 117-135 (1990).

11. J. D. Atkinson, J. Yu, and Z.-Y. Chen, *An Analysis of the Effects of Sulfur Content and Potential on Corrosion Fatigue Crack Growth in Reactor Pressure Vessel Steels*, Corros. Sci. **38** (5), 755-765 (1996).

12. G. L. Wire and Y. Y. Li, *Initiation of Environmentally-Assisted Cracking in Low-Alloy Steels*, in Fatigue and Fracture – 1996 – Volume 1, PVP Vol. 323, H. S. Mehta, ed., American Society of Mechanical Engineers, New York, pp. 269-289 (1996).

13. O. K. Chopra, W. F. Michaud, W. J. Shack, and W. K. Soppet, *Fatigue of Ferritic Steels*, in Environmentally Assisted Cracking in Light Water Reactors, Semiannual Report, April-September 1993, NUREG/CR-4667 Vol. 17, ANL-94/16, pp. 1-22 (June 1994).

14. O. K. Chopra and W. J. Shack, *Effects of LWR Environments on Fatigue Life of Carbon and Low–Alloy Steels, in Fatigue and Crack Growth: Environmental Effects, Modeling Studies, and Design Considerations,* PVP Vol. 306, S. Yukawa, ed., American Society of Mechanical Engineers, New York, pp. 95–109 (1995).

15. N. E. Dowling, *Crack Growth During Low–Cycle Fatigue of Smooth Axial Specimens, in Cyclic Stress–Strain and Plastic Deformation Aspects of Fatigue Crack Growth,* ASTM STP 637, American Society for Testing and Materials, Philadelphia, PA, pp. 97–121 (1977).

16. D. J. Gavenda, P. R. Luebbers, and O. K. Choprea, *Initiation and Crack Growth Behavior of Carbon and Low–Alloy Steelss*, in Fatigue and Fracture 1, PVP–Vol. 350, S. Rahman, et al., eds., American Society of Mechanical Engineers, New York, 243–255, 1997.

17. E. D. Eason, E. E. Nelson, and J. D. Gilman, *Modeling of Fatigue Crack Growth Rate for Ferritic Steels in Light Water Reactor Environments*, PVP–Vol. 286, Changing Priorities of Code and Standards, American Society of Mechanical Engineers, New York, pp. 131–142 (1994).

18. C. E. Jaske and W. J. O'Donnell, *Fatigue Design Criteria for Pressure Vessel Alloys*, Trans. ASME J. Pressure Vessel Technol. **99**, 584–592 (1977).

19. H. M. Chung, W. E. Ruther, and R. V. Strain, *Slow-Strain-Rate-Tensile Tests of Austenitic Stainless Steels Irradiated in the Halden Reactor*, Environmentally Assisted Cracking in Light Water Reactors Semiannual Report January 1996—June 1996, NUREG/CR–4667 Vol. 22, ANL–97/9 (June 1997).

20. J.-H. Park and H. M. Chung, *Properties of Stainless Steel Welds,* in Environmentally Assisted Cracking in Light Water Reactors, Semiannual Report, January 1996-June 1996, NUREG/CR–4667 Vol. 22, ANL–97/9, pp. 44-48 (June 1997).

21. J.-H. Park and H. M. Chung, *Properties of Stainless Steel Welds*, Environmentally Assisted Cracking in Light Water Reactors Semiannual Report July 1996—December 1996, NUREG/CR–4667 Vol. 23, ANL–97/10 (September 1997).

22. H. M. Chung, W. E. Ruther, J. E. Sanecki, A. G. Hins, N. J. Zaluzec, and T. F. Kassner, *Irradiation-Assisted Stress Corrosion Cracking of Austenitic Stainless Steels: Recent Progress and New Approaches*, J. Nucl. Mater. **239** 61 (1996).

23. J. Zhang, P. Dong and F. W. Brust, *Analysis of Residual Stresses in a Girth Weld of a BWR Core Shroud,* Approximate Methods in the Design and Analysis of Pressure Vessels and Piping Components, W. J. Bees, Ed., PVP-Vol. 347, pp. 141-156 (1997a).

24. Brust, F. W., P. Dong and J. Zhang, *A Constitutive Model for Welding Process Simulation using Finite Element Methods*, Advances in Computational Engineering Science, S. N. Atluri and G. Yagawa, Eds., pp. 51-56 (1997a).

25. T. Nishioka and S. N. Atluri, *Analysis of Surface Flaw in Pressure Vessels by a New3 Dimensional Alternating Method,* J. Pressure Vessel Technol., **104**, pp. 299-307 (Nov. 1992).

26. Brust, F. W., P. Dong and J. Zhang, *Crack Growth Behavior in Residual Stress Fields of a Core Shroud Girth Weld,* Fracture and Fatigue, H. S. Mehta, Ed., PVP-Vol. 350, pp. 391-406 (1997b).

27. W. E. Ruther, W. K. Soppet, and T. F. Kassner, *Corrosion Fatigue of Alloys 600 and 690 in Simulated LWR Environments*, NUREG/CR–6383, ANL–95/37 (April 1996).

28. F. P. Ford, *Quantitative Prediction of Environmentally Assisted Cracking*, Corrosion, **52**, pp. 375–395 (1997).

29. T. Shoji, *Quantitative Prediction of Environmentally Assisted Cracking Based on Crack Tip Strain Rate*, Proc. Conf. on Predictive Capabilities in Environmentally–Assisted Cracking, R. Rungta, ed., PVP Vol. 99, American Society of Mechanical Engineers, NY, pp.127-142 (1985).

30. L. A. James and D. P. Jones, *Fatigue Crack Growth Correlation for Austenitic Stainless Steels in Air,* Proc. Conf. on Predictive Capabilities in Environmentally–Assisted Cracking, R. Rungta, ed., PVP Vol. 99, American Society of Mechanical Engineers, NY, pp. 363–414 (1985).

RECENT SCDAP/RELAP5 CODE APPLICATIONS AND IMPROVEMENTS[a]

E. A. Harvego, L. S. Ghan, D. L. Knudson, and L. J. Siefken
(Idaho National Engineering and Environmental Laboratory)

ABSTRACT

This paper summarizes (1) a recent application of the severe accident analysis code SCDAP/RELAP5/MOD3.1, and (2) development and assessment activities associated with the release of SCDAP/RELAP5/MOD3.2. The Nuclear Regulatory Commission (NRC) has been evaluating the integrity of steam generator tubes during severe accidents. MOD3.1 has been used to support that evaluation. Studies indicate that the pressurizer surge line will fail before any steam generator tubes are damaged. Thus, core decay energy would be released as steam through the surge line and the tube wall would be spared from exposure to prolonged flow of high temperature steam. The latest code version. MOD3.2, contains several improvements to models that address both the early phase and late phase of a severe accident. The impact of these improvement to the overall code capabilities has been assessed. Results of the assessment are summarized in this paper.

1. INTRODUCTION

The SCDAP/RELAP5 code is being developed for best-estimate simulations of severe accidents in light water reactors. The code is capable of representing the reactor coolant system, the core, fission product release, the secondary system, and control system. A wide range of transients may be simulated including large-break and small-break loss-of-coolant accidents, operational transients such as anticipated transient without SCRAM, loss of offsite power, loss of feedwater, and loss of main coolant flow. The code allows the user flexibility with nodalization of input models. The model may be finely nodalized where it is necessary for accurately representing the problem, and coarsely nodalized elsewhere. Thus, computer resources are economically used.

The focus of this paper is two-fold: (1) to discuss the recent application of SCDAP/RELAP5/MOD3.1 for evaluating the potential of steam generator (SG) tube failure, and (2) to summarize the models that have been improved for SCDAP/RELAP5/MOD3.2 and to discuss assessment of these models. This paper is therefore divided into two main sections. The first section discusses the application of SCDAP/RELAP5/MOD3.1 toward evaluating the potential of SG tube failure during a station blackout (TMLB'). The second section discusses recent development of SCDAP/RELAP5/MOD3.2, namely the improved models and corresponding assessments.

a. Work supported by the U. S. Nuclear Regulatory Commission, Office of Nuclear Regulatory Research, under DOE Idaho Field Office Contract DE-AC07-94ID13223.

2. APPLICATION OF SCDAP/RELAP5/MOD3.1

During a severe accident, SG tubes are vulnerable to failure by creep damage due to heating caused by natural circulation flow of steam in the reactor coolant system (RCS). As shown in Figure 1, two modes of natural circulation flow may develop within the coolant loops: (1) full-loop flow, and (2) hot leg countercurrent flow. These flows may heat the tubes substantially, causing the metal to weaken so that, when combined with sufficient pressure differential across the tube wall, the tube will fail. Other components, such as the pressurizer surge line nozzle and the hot leg nozzles are also vulnerable to creep damage. However, damage to the SG tubes is of particular concern due to the potential for releasing fission products to the atmosphere. Therefore, the analyses presented in this section focus on the parameters that contribute toward potential failure of the SG tubes.

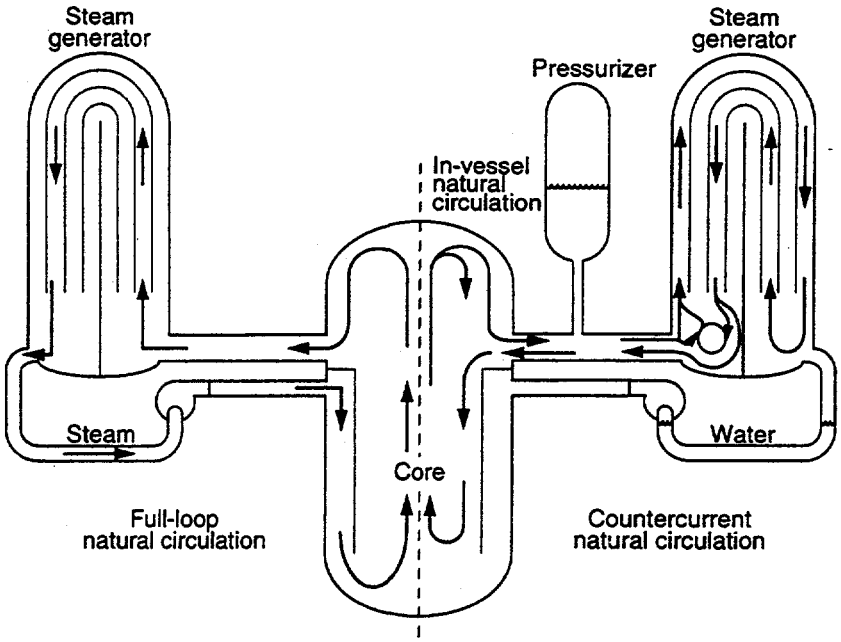

Figure 1. Natural circulation flow patterns that could develop during severe accidents in pressurized water reactors with U-tube steam generators.

One proposed method of mitigating tube damage during a severe accident is to open the power operated relief valve (PORV) on the pressurizer. The pressure differential across the tube wall is thereby reduced. Depressurizing the RCS, however, increases the potential for clearing liquid from the pump suction piping (loop seal). With a cleared loop seal, full-loop natural circulation flow may develop, which could increase the flow of hot stream through the tubes, and therefore increase the potential for failing the tubes due to creep damage.

Four different types of plants were assessed for the likelihood of tube failure under the proposed mitigation scheme: (1) 3-loop Westinghouse, (2) 4-loop Westinghouse, (3) Combustion Engineering, and (4) Babcock and Wilcox. Results of the analyses of the other plant types are given in a table at the end of this paper but no comment is offered.

The parameters studied were: (1) varying leak rates through the seals of the reactor coolant pumps (RCPs), (2) varying downcomer-to-hot leg bypass flow rates, and (3) sludge buildup on the SG tubesheet. Leaks through RCP seals or a blocked downcomer-to-hot leg bypass could increase the potential for loop seal clearing, which would allow full-loop natural circulation to develop. Sludge buildup on the tubesheet reduces the heat transfer capability in the entrance region, that is, the hottest region of the tubes.

2.1 Model Description

A station blackout (TMLB') was assumed to initiate the accident scenario. AC power and all feedwater was immediately lost, and it was assumed that the emergency core cooling system (ECCS) was unavailable. Since it was desired to assess the impact of the proposed mitigation scheme for preventing tube damage, it was assumed that, upon detection of 922 K steam at the core exit, the operator would intentionally depressurize the RCS by opening the PORV at the top of the pressurizer. No other operator intervention was simulated.

To maximize the pressure differential across the tube wall, it was assumed that the first SG PORV to be challenged would fail open. Thus, the secondary side of that SG would depressurize faster than the RCS and the tube wall would experience a greater pressure differential. It should be noted that these analyses are primarily concerned with tube tensile stress, which means that only positive pressure differential (high pressure inside the tube the low pressure outside the tube) is of concern. Negative pressure differential induces compressive stresses in the tube wall, but the tube wall can withstand substantial compressive stress without incurring creep damage.

Nodalization of the reactor vessel is shown in Figure 2. The core was modeled with SCDAP components while the remainder of the vessel was composed of RELAP5 thermal-hydraulic components.

To enable the code to simulate the natural circulation of steam in the primary coolant loops, two different nodalization schemes were used. For the early part of the transient when the hot legs were full of water, the nodalization shown in Figure 3 was used. (Only one of the three loops is shown in Figure 3. The other two loops are similarly nodalized except for the exclusion of the pressurizer.) After the hot legs were drained, the potential for natural circulation of steam in either the full-loop mode, or the hot leg countercurrent mode was allowed by using the nodalization shown in Figure 4. In that nodalization each hot leg and SG tube bundle was split into two parts. Hot steam can flow from the vessel towards the SG in the upper half of the hot leg while cooler steam may flow from the SG to the vessel through the lower half of the hot leg. Similarly, hot steam may flow in the forward direction through one part of the tube bundle while cooler steam may flow in the reverse direction through the other part. During countercurrent flow, flows from the tube bundle and the hot leg may mix in the SG inlet plenum. The model was benchmarks against Westinghouse data[1] by adjusting the loss coefficient of junctions in the SG inlet and outlet plenums. In full-loop circulation, both parts of the hot leg and tube bundle carry flow in the normal direction.

The base model described above was modified to accommodate the sensitivity parameters. To study the effects of RCP seal leaks, a leak path was added between the RCP outlet and the containment. The leak flow rate was specified for nominal operating conditions. For a TMLB' scenario, the seals are expected to degrade when two-phase flow enters the pump casing. Therefore, when saturated liquid was detected in an RCP, the leak flow rate was increased. The maximum simulated leak flow rate was selected according to the consensus of a panel of experts.[2]

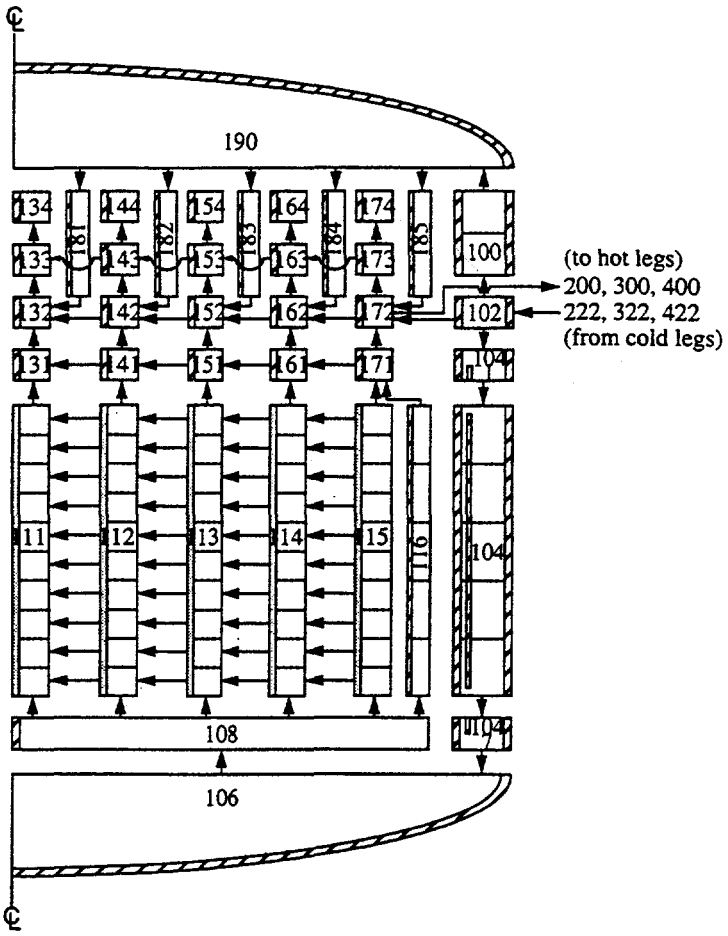

Figure 2. Nodalization for the reactor vessel of a 3-loop Westinghouse plant.

It has been postulated that during a severe accident, the core barrel could heat and expand faster than other internal structures. As a result, the small gap that normally exists between the hot leg nozzle and the core barrel (the downcomer-to-hot leg bypass) would be closed off. Consequently, circulation patterns in the vessel and coolant loops may be affected, which could then affect the potential for creep damage for the SG tubes. To assess the influence of this flow path, the flow path was removed from the base model.

Finally, the influence of a one foot thick layer of sludge on top of the tubesheet was assessed. To accommodate the sludge layer, it was necessary to renodalize the tube bundle. Additional hydrodynamic cells and heat structures were added near the bottom of the boiler region in order to better capture the temperature response of the tubes in that region. Since the new nodalization represented a change to the base model in addition to the sludge layer, two newly nodalized models were created - one with sludge present, and one without, so that the influence of nodalization could be eliminated from consideration.

2.2 Calculations Results

All of the cases described in this paper are discussed in more detail in Reference 3 through Reference 6. The following discussion highlights the results of those studies.

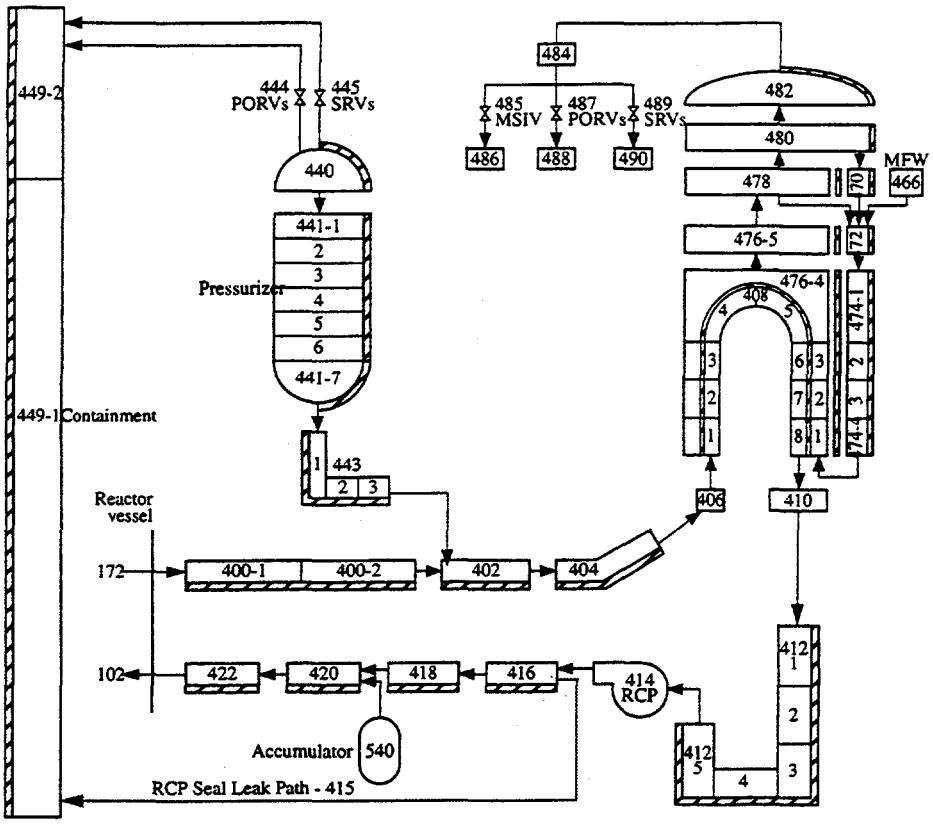

Figure 3. Nodalization for a 3-loop Westinghouse plant without provisions for hot leg countercurrent flow.

In all cases studied, the overall plant response was similar. the following describes specifically the response of the Surry plant to the base case; that is, with nominal leakage through the RCP seals, nominal hot-leg-to-downcomer bypass flow, and no sludge on top of the SG tubesheet.

The loss of ac power resulted in reactor scram and RCP trips at transient initiation. In addition, SG isolation valves closed and feedwater pumps tripped, effectively isolating the SG secondaries. The resulting primary pressure is shown in Figure 5. The RCS pressure initially decreased from the nominal 15.5 to about 14.4 MPa because core power dropped rapidly after scram while RCP coasting was relatively gradual. A small pressure increase (to about 14.8 MPa) then occurred while full-loop natural circulation of primary liquid was established. Thereafter, the RCS pressure gradually decreased to about 13.6 MPa (by 1,140 s) because full-loop natural circulation of liquid was effective in cooling the core by rejecting decay heat to SG secondary water.

SG secondary pressures began to increase as a result of heat transferred by full-loop natural circulation of primary liquid. The first SG PORV challenge occurred at 23.4 s when the secondary pressure in the SG attached to the pressurizer loop increased to the opening pressure of 7.2 MPa. The PORV of that SG was assumed to fail open at that time. SG PORVs in the remaining (non-pressurizer) loops were assumed to function as designed; that is, to control secondary pressures between 6.9 and 7.2 MPa.

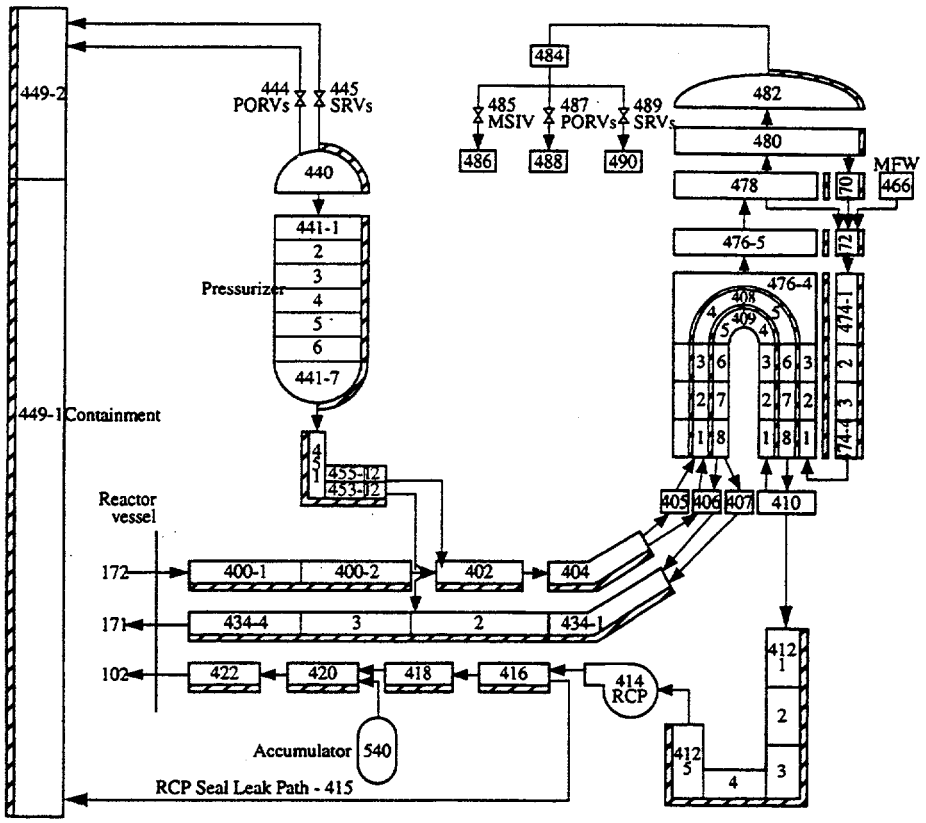

Figure 4. Nodalization for a 3-loop Westinghouse plant with provisions for hot leg countercurrent flow.

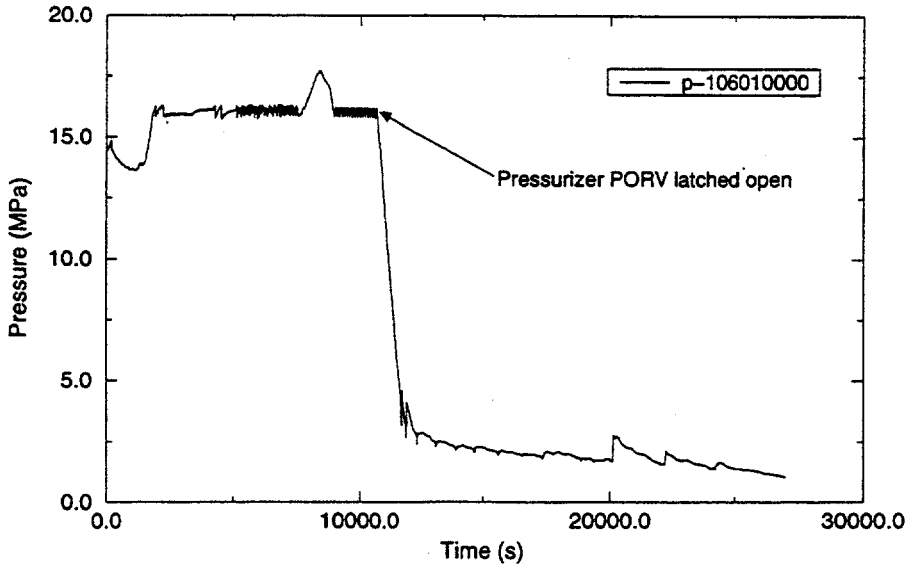

Figure 5. Primary pressure (typical)

Water in the SGs was boiled off; the SG with the stuck open PORV was the first to dry out at about 2,300 s. The other two SGs boiled dry by about 5,300 s. With reduced heat transfer capability to the secondary system following dryout, the primary liquid began to saturate and boil. The RCS liquid was heated to a saturated state by about 7,500 s, and thereafter liquid boiled in the core. As boiling progressed, vapor collected in the top of the SG U-tubes, ending full-loop natural circulation of primary liquid.

Boiling in the core and venting through the pressurizer PORV led to depletion of the RCS inventory. As indicated in Figure 6, the collapsed liquid level fell below the top of the fuel rods by 8,920 s. Shortly thereafter, the hot legs voided and vapor in the core exit began to superheat, presenting conditions that could support hot leg countercurrent natural circulation. Accordingly, the calculation was stopped and the loop was renodalized as was previously discussed. Core uncovery was complete by 10,520 s, as indicated in Figure 6. Shortly thereafter, vapor leaving the core reached a temperature of 922 K. At that time (10,690 s) the pressurizer PORV was latched open, resulting in a rapid depressurization of the RCS as shown in Figure 5.

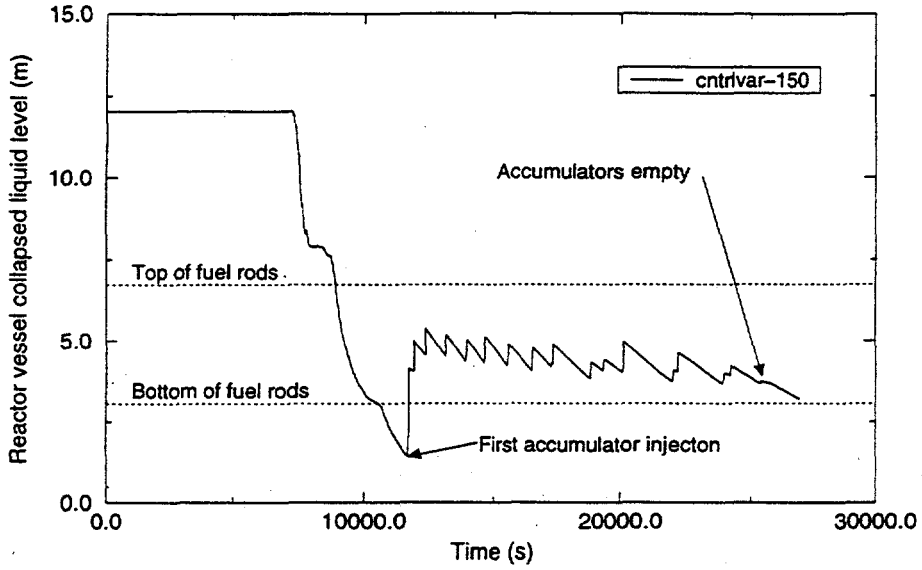

Figure 6. Primary collapsed liquid level (typical).

Within a few seconds after the accumulators began injecting, at least one loop seal cleared in every case. This is evident from Table 1. With at least one loop seal cleared, conditions were right in the RCS for full-loop natural circulation of steam (i.e., the hot legs, cold legs, and loop seals were full of steam). Thus, a path was available for steam to travel from the vessel, through the loop seals, and back to the vessel. This mode of circulation is of concern because it could lead to an increase in SG tube heating. In all cases studied, however, the increase in SG tube temperature as a result of the onset of full-loop natural circulation was small. SG tube temperatures are shown in Figure 7 for the base case and for the case that exhibited the highest tube temperatures (the case which simulated sludge on top of the tubesheet). Full-loop natural circulation of steam began at about 11,700 s for each case. The largest temperature increase was only 80 K and the temperature after full-loop flow was established was still well below that which was required to cause creep damage. Therefore the transition to full-loop flow had but a small effect on tube wall temperatures.

Table 1. Sequence of transient events in the SCDAP/RELAP5 calculations.

Event	Time (s) for					
	Base case	125 gpm per RCP	250 gpm per RCP	With sludge	Without sludge	Without DC-HL bypass
TMLB' initiation	0	0	0	0	0	0
Pressurizer loop SG PORV/SRV opens and fails open	23.40	27	27	23.40	23.40	23.40
Pressurizer PORV cycling begins	1,960	7,140	7,140	1,960	1,960	1,960
SGs dryout (pressurizer/non-pressurizer loops)	2,293/ 5,284	3,000/ 5,335	3,000/ 5,335	2,293/ 5,284	2,293/ 5,284	2,293/ 5,284
Collapsed liquid level falls below top of fuel rods	8,916	8,836	8,941	8,916	8,916	8,916
Vapor in the core exit begins to superheat; hot leg countercurrent circulation begins	9,091	9,005	8,961	9,091	9,091	9,091
Collapsed liquid level falls below top of fuel rods	10,510	10,530	10,740	10,510	10,510	10,720
Core outlet temperature reaches 922 K; pressurizer PORV latched open ending PORV cycling	10,690	10,810	10,690	10,670	10,700	10,690
Onset of fuel rod oxidation	11,030	11,100	11,100	11,440	11,440	11,070
Pressurizer drains (and remains empty)	11,110	11,220	11,440	11,110	11,110	11,080
First accumulator/core flood tank injection	11,660	11,610	11,470	11,660	11,660	11,640
First RCP loop seal clears; onset of full loop natural circulation	11,700	11,610	11,470	11,690	11,690	11,650
Pressurizer surge line fails by creep rupture	18,350	24,390	22,950	19,460	19,550	22,600
Upper plenum stainless steel begins to melt and relocate to lower head	23,380	29,590	29,480	21,010	24,910	24,660
Pressurizer loop hot leg nozzle fails by creep rupture	25,200	not predicted	not predicted	24,070	not predicted	not predicted
Steam generator tubes fail due to creep rupture	not predicted	not predicted	not predicted	24,790	not predicted	not predicted
Accumulators empty	25,430	22,360	21,400	25,870	24,180	23,090
First relocation of core materials into the lower head	not predicted	31,130	30,070	not predicted	not predicted	not predicted
End of calculation	26,980	31,130	35,480	26,000	26,000	26,530

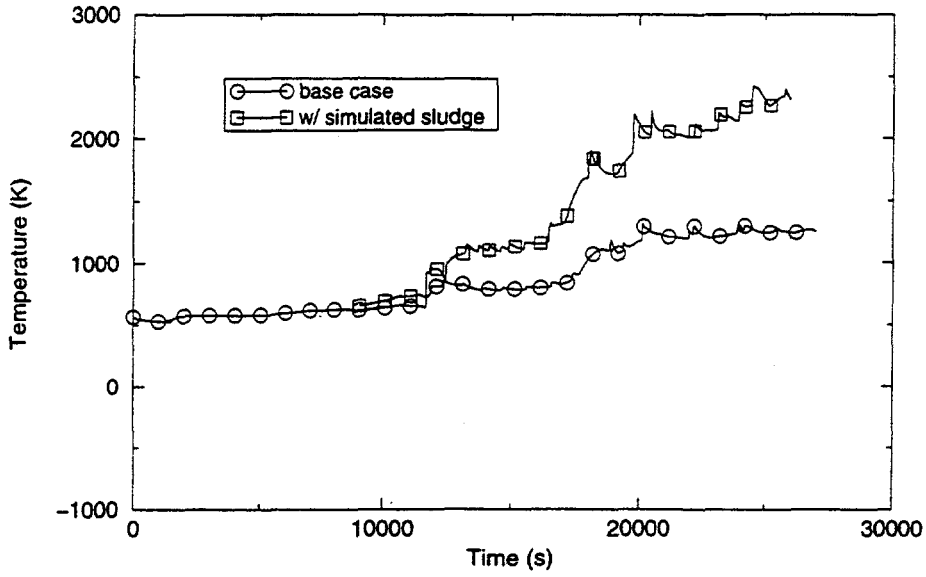

Figure 7. Steam generator tube temperature for the base case and the case with sludge simulated on top of the tubesheet.

The pressurizer surge line to fail in every case as is indicated in Table 1. Failure occurred due to relatively large flow rate of hot steam passing through the surge line as it travelled toward the pressurizer PORV. The time of surge line failure listed in Table 1 is the time at which the creep damage model predicted failure of the structure. However, the modeled RCS pressure boundary remained intact even when the structure was predicted to fail; that is, a break of the surge line was not modeled. This was believed to be a conservative approach with respect to increasing the likelihood of failure of the SG tubes. With this approach, hot steam that would have otherwise exited through the ruptured surge line travelled through the tubes instead.

Steam temperature at the core exit continued to increase as a result of the oxidation of fuel cladding. Some of this hot steam was carried through the SG tubes as a result of full-loop natural circulation. Consequently, the tube wall temperature increased. In all but one of the cases studied, the tube wall temperature never became high enough to cause creep damage. Therefore, even though full-loop flow caused the tubes to heat, creep damage did not occur. The only occurrence of creep damage was for the case which simulated sludge on top of the tubesheet.

Even with the conservative approach of not rupturing the RCS pressure boundary when a structure failed, only one of the cases predicted failed SG tubes. Tube failures were predicted when a one-foot thick layer of sludge on top of the tubesheet was modeled. But even then, tube failure occurred long after the surge line had failed (the SG tubes failed 5,330 s after the surge line failed). This indicates that, in reality, the RCS pressure boundary would be ruptured before the tubes failed. If the RCS pressure boundary were to rupture, then the potential for SG tube failure would decrease because steam would be more likely to flow out the break rather than through the SG tubes.

The calculations were terminated some time after 26,000 s when possibility of further tube damage was unlikely. Surge line failure had occurred earlier in all cases, already limiting the possibility of tube rupture. For all cases, except for that which simulated sludge on top of the tube sheet, the SG tubes had not

incurred creep damage and tube temperatures had stopped increasing. In addition, the accumulators had emptied, thus eliminating the possibility of pressure increases, due to boiling, that could be detrimental to SG tube integrity.

Results of the calculations performed for the other plant types are summarized in Table 2. In general, SG tube failure was predicted only when the accumulation of sludge in the SG was simulated. SG tube failure was not predicted for Calvert Cliffs in that case; however, the SG tubes did incur significant tube damage before the end of the calculation at 50,000 s. Although tube failure was predicted when SG sludge was accounted for, the tube failures occurred long after the surge line had failed.

Table 2. Summary of SCDAP/RELAP results for all cases studied.

	Plant	Failure time (s)			Timing difference between tube failure and first RCS failure (s)
		Surge line	Hot leg	SG tube	
Without RCP seal leaks	Surry	18,350	25,200	-	-
	Zion	13,440	20,330	-	-
	C. Cliffs	22,000	27,430	-	-
	Oconee	8,240	10,340	-	-
With small RCP seal leaks	Surry	24,390	-	-	-
	Zion	22,170	-	-	-
	C. Cliffs	18,650	28,100	-	-
	oconee	11,000	16,880	-	-
With large RCP seal leaks	Surry	22,590	-	-	-
	Zion	20,600	25,480	-	-
	C. Cliffs	17,130	32,930	-	-
	Oconee	11,980	20,040	-	-
With blocked downcomer hot leg bypass	Surry	22,600	-	-	-
	Zion	16,060	19,760	-	-
	C. Cliffs	35,110	32,950	-	-
	Oconee	8,800	10,710	-	-
With SG sludge accumulation	Surry	19,460	24,070	24,790	5,330
	Zion	17,460	20,810	20,930	3,470
	C. Cliffs	17,280	26,370	-	-

In summary, full-loop natural circulation of steam generally did not result in SG tube failure. Tube failure was predicted only with a simulated one-foot thick layer of sludge on top of the tube sheet. Even then, tube failure was predicted to occur long after the surge line had failed. Considering the conservative approach used for this evaluation (namely that the RCS pressure boundary was assumed to remain intact), the long time interval between the surge line failure and the tube failure indicates that, in reality, the RCS pressure boundary would be likely to rupture before the SG tubes incurred significant creep damage. Primary steam would then exit through the break rather than travel through the tubes and tube damage would be mitigated.

3. SCDAP/RELAP5/MOD3.2 ASSESSMENT RESULTS

The development of SCDAP/RELAP5/MOD3.2 began in the spring of 1994, and contains a number of added code capabilities and modeling improvements since the last version of the code, SCDAP/RELAP5/MOD3.1, was released. These improvements include the completion of several late-phase models identified in the NRC independent review group report issued in January 1993. Completion of these latest models is a major step toward completion of the SCDAP/RELAP5 code resolution plan, developed by the NRC in response to the January 1993 report.

Specific modeling changes in the latest code version include improvements in: (a) molten pool formation and growth, including transient natural circulation heat transfer, (b) in-core molten pool thermal-mechanical crust failure criteria, (c) the melting and relocation of upper plenum structures, (d) interactions between the in-core melt and shroud, (e) BWR control blade/channel box enhancements, (f) ex-vessel CHF heat transfer correlations, and (g) lower plenum debris behavior. The BWR control blade model developed by Oak Ridge National Laboratory has been linked to SCDAP/RELAP5 late phase models to allow relocating control blade materials to participate in the formation and growth of in-core or lower plenum molten pools and debris beds. The MATPRO material properties library was also updated to include material interactions not previously considered. To eliminate abrupt transitions between core damage states and provide more realistic predictions of accident progression phenomena, a transition smoothing methodology was implemented that results in the calculation of a gradual transition from an intact core geometry through different core damage states. Finally, two changes were made in SCDAP/RELAP5 to provide consistency between SCDAP and RELAP5 calculation methods. The first was to update the SCDAP heat transfer correlation package to be consistent with that used in the current RELAP5 code version, and the second was to implement the same implicit coupling of convective heat transfer and hydrodynamics in SCDAP that is currently used in RELAP5.

The assessment of SCDAP/RELAP5/MOD3.2 encompassed a wide range of severe accident experiments, plant analyses and independent calculations. The assessment matrix used to evaluate the code is shown in Table 3. The matrix consisted of 64 separate assessment cases, with each case intended to evaluate specific modeling features or improvements to the code. A more detailed discussion of the specific modeling features and code improvements addressed by each of the assessment cases is provided in Reference 7. The following paragraphs summarize results of the experiment assessment cases, assessment calculations using independent models, and an integral plant calculation of the TMI-2 accident. The experimental calculations primarily address models for predicting the early phase of a severe accident, while independent calculations were used to evaluate late phase models.

Table 3. Summary of selected test problems and cases to be analyzed.

Problem no. and title		Behavior evaluated by various cases	Case 1	Case 2	Case 3	Case 4	Case 5	Case 6	Case 7	Case 8	Case 9
1.	Bundle boiloff	HT, NUM[a]	X	X	X	X					
2.	FLHT-5	HTC, TOX, SOX, DIF, NUM	X	X	X	X	X	X			
3.	PBF SFD 1-1	HTC, TOX, SOX, DIF, NUM	X	X	X	X	X				
4.	PBF SFD-1-4	TOX, DIF	X	X							
5.	PBF SFD ST	HTC, TOX, DIF	X	X							

Table 3. Summary of selected test problems and cases to be analyzed. (Continued)

Problem no. and title		Behavior evaluated by various cases	Case 1	Case 2	Case 3	Case 4	Case 5	Case 6	Case 7	Case 8	Case 9
6.	CORA-13	TOX, SOX, DIF, NUM	X	X	X	X	X	X			
7.	CORA-7	TOX, DIF, SOX	X	X	X						
8.	CORA-5	TOX, DIF	X	X	X						
9.	CORA-17	TOX, DIF, SOX	X	X	X						
10.	PHEBUS B9+	TOX, SOX	X	X							
11.	PHEBUS FPT0	TOX	X	X							
12.	Heatup of externally cooled lower head filled with molten core material	NC	X	X							
13.	Heat transfer at interface of flowing molten material and cold wall; SCDAP vs. theoretical solution	NC, NUM	X	X							
14.	Heat transfer in lower head filled with molten core material; SCDAP vs. FIDAP	NC	X	X							
15.	Structural analysis of crust around in-core molten pool; SCDAP vs. ABAQUS	CR	X	X	X	X	X	X	X	X	
16.	TMI-2 accident	DAM, TOX, SOX, CR	X	X							
17.	Surry PWR severe accident	DAM, NUM, SOX	X	X	X	X	X	X	X	X	X
18.	Browns Ferry LOCA without ECCS	DAM	X								

a. Letter code designate areas of modeling assessed:
HTC: Coolant boiloff and convective heat transfer
TOX: Heatup during rapid oxidation, hydrogen production, meltdown of fuel rods
SOX: Strength of ZrO_2 layer on outside surface of fuel rod cladding (failure temperature, durability threshold, and potential for shattering)
DIF: Mass diffusion of water vapor near surface of fuel rod cladding
NC: Heat transfer from molten pool to lower head
CR: Structural analysis of crust supporting molten pool, crust configuration and temperature
NUM: Method of numerical solution, time step and nodalization sensitivity
DAM: Core damage progression in full-scale plant.

3.1 Assessment of Early Phase Models

The early phase of a severe accident is generally defined as the period during which initial heating and melting of the reactor core structures occurs, but the original rod like geometry of the core is still identifiable. Table 4 provides a summary of measured and calculated results from the ten experiments used

in the SCDAP/RELAP5/MOD3.2 developmental assessment of the early phase modeling capabilities of the code. The table includes a qualitative evaluation of the calculated versus measured test bundle heat up for each of the experiments, and comparisons of measured and calculated cumulative hydrogen production and elevation of primary blockage. These selected parameters provide the best indication of the overall capability of the SCDAP code models to predict early phase core degradation, and are also most readily measured during the experiment or as part of the post experiment examinations of the test bundles.

Table 4. Summary of assessment of SCDAP/RELAP5/MOD3.2 to calculate fuel rod heatup and cladding oxidation during early phase of severe accident.

Experiment	Quality of MOD3.2 calculated rate of heatup[a]	Cumulative hydrogen production (g)			Elevation of maximum blockage (m)	
		Calculated MOD3.1	Calculated MOD3.2	Measured	Calculated MOD3.2	Measured
FLHT-5	Good	267	265	300 ± 30	0.90	1.64
PBF SFD 1-1	Good	94	94	64 ± 7	0.15	0.10
PBF SFD 1-4	Good	60	88	86 ± 12	0.20	0.08
PBF SFD ST	Good	105	121	150 ± 35	0.20	0.18
KfK CORA-13 (pre-reflood)	Good	83	145	126	-	-
KfK CORA-13 (post-reflood)	-	110	175	210	0.75	0.50
KfK CORA-7	Fair[b]	105	124	114	0.75	0.42
KfK CORA-5	Good	-	150	-	0.20	0.55
KfK CORA-17	Good	-	155	150	-	-
PHEBUS B9+	Fair[c]	33	49	39 ± 8	0.20	0.25
PHEBUS FPT0	Good	-	70% of measured[d]	-	0.40	e

a. Definitions of level quality: 1. good = average difference between calculated and measured temperatures in test bundle in temperature range of 1,000 to 2,000 K is less than 100 K, fair = average difference between calculated and measured temperatures is less than 200 K, poor = average difference between calculated and measured temperatures is greater than 200 K.

b. Significant underprediction of temperatures at 0.55 m elevation in period of 4,200 to 4,800 s.

c. Significant overprediction of temperature in elevation interval of 0.2 to 0.6 m during period of He flow (8,000 to 15,000 s).

d. Experimentally measured hydrogen production is proprietary.

e. Extensive ceramic melting of test bundle obfuscated for PIE the configuration of test bundle at end of early phase damage progression.

The qualitative assessment of the measured versus calculated initial bundle heat up rate shown in the second column of Table 4 was necessary because there was no single experiment measurement that could be used to characterize this behavior. Therefore, a qualitative assessment of "good" was given when there was agreement between calculated and measured temperatures in all parts of the test bundle, and a "fair" was assigned when a discrepancy between calculated and measured was observed in part of the test bundle for a significant period of time. As indicated in Table 4 only two experiments showed "fair" agreement between measured and predicted results. These were the CORA-7 experiment which showed an under

prediction in the heat up of the upper portion of the test bundle, and the PHEBUS B9+ experiment which showed an overprediction of temperature in the middle elevation interval during the period of time in which steam flow through the test bundle was replaced with helium flow. The remaining eight experimental comparisons showed "good" agreement between calculated and measured test bundle heat up rates at all locations of the bundle.

An example of a "good" assessment result is shown in Figure 8, which compares calculated and measured cladding temperatures at the 0.75-m and 0.35-m elevations of the test bundle for the CORA-13 experiment, which was a PWR experiment with reflood. As indicated in the figure, calculated and measured temperatures in both the top and bottom portions of the bundle were in close agreement up until the time of thermocouple failure. Figure 8 also shows the code calculated the expected oxidation induced rapid temperature rise in the upper part of the bundle at approximately 4,900 s when reflood of the test bundle occurred. These results are an improvement over earlier results obtained with SCDAP/RELAP5/ MOD3.1, which showed greater variability between calculated and measured test bundle heat up rates. Figure 9, which compares MOD3.2 and MOD3.1 calculated temperature response with measured results from the PBF SFD 1-4 experiment at the 0.74-m elevation, is an example of the improved predictive capabilities of MOD3.2. For this experiment, the length of the test bundle was also 1.0 m.

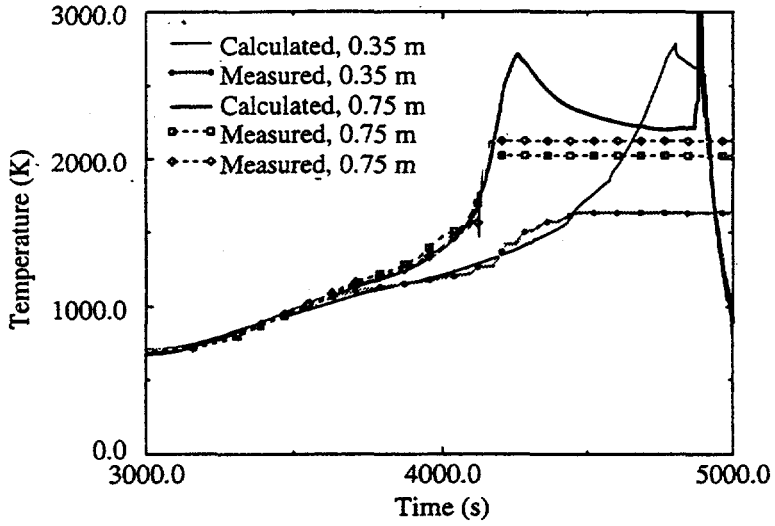

Figure 8. Calculated and measured temperatures at 0.35 m and 0.75 m elevations for KfK CORA-13 experiment.

The comparisons of cumulative hydrogen production and elevation of primary blockage in Table 4 show good agreement between measured and calculated results for these parameters. In most cases, the predicted hydrogen production is within the experimental uncertainty of the measured results. The MOD3.2 calculations of cumulative hydrogen production also show that the bias or tendency to under predict hydrogen production, which was observed in earlier MOD3.1 calculations, has been eliminated in MOD3.2. The comparison of MOD3.2 calculations with measured results now shows about an equal tendency to over predict or under predict hydrogen production. The MOD3.2 modeling improvements are also apparent in the comparison of measured and calculated elevation of primary blockage in Table 4,

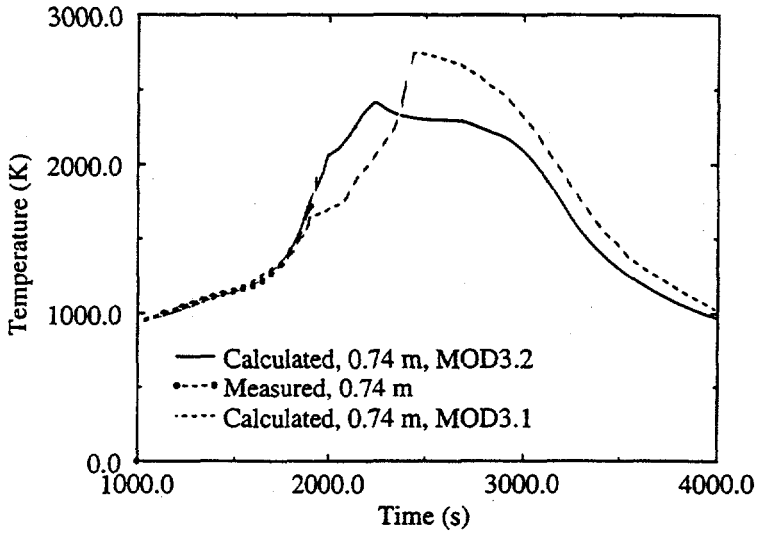

Figure 9. Calculated and measured temperatures at 0.74 m elevation for PBF SFD 1-4 experiment.

which shows good agreement between measured and calculated results. If there is a tendency, it is to slightly over predict the elevation of primary blockage as indicated by the comparison of calculated and measured results for the CORA-7 and PBF experiments.

3.2 Assessment of Late Phase Models

The assessment of the capabilities of SCDAP/RELAP5/MOD3.2 to calculate the late phase of a severe accident relied on comparisons with independent calculations using other recognized general purpose codes to compare with SCDAP/RELAP5 calculated results. This approach was necessary because very little experimental information is available for assessing the late phase of a severe accident. In this context, late phase is defined to begin with onset of ceramic melting of fuel rods and continue through the progression to damage that includes heat up and spreading of molten material, slumping of molten material from the core region to the lower head, and the heat up and ultimate damage of the lower head. Two of these assessments described in this paper were (1) investigation of heat transfer in a lower head filled with molten materials, and (2) assessment of the failure of a crust surrounding an in-core molten pool. The results of these assessment test problems are summarized below.

3.2.1 Assessment of Lower Head Heat Transfer

This assessment problem required the solution of the heat transfer taking place in the lower head of a reactor vessel that is filled with molten material and cooled externally by a pool of water. This situation is representative of conditions that might occur if the external cavity of a reactor vessel was flooded as an accident management strategy to prevent lower head failure. The problem, described in greater detail in Reference 7, was analyzed using SCDAP/RELAP5/MOD3.2 and a general purpose fluid dynamics and heat transfer code, FIDAP.[8] The FIDAP code modeled the lower head and molten material as shown in Figure 10. The finite element model consisted of 6,500 connected finite elements. The external pool of

water was assumed to be at a constant temperature of 325 K and a constant heat transfer coefficient of 15,000 W/m^2 was applied to the external surface of the vessel. The initial temperature of the internal molten pool was assumed to be at 2,995 K, and the internal molten pool heat generation rate was assumed constant at 12 MW.

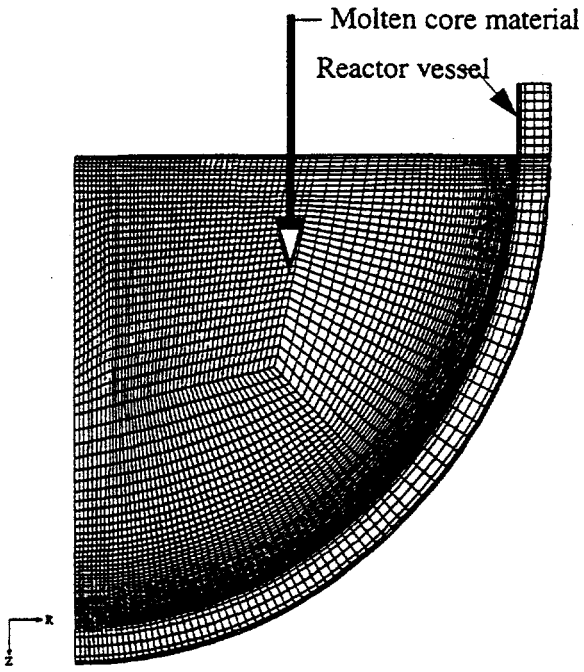

Figure 10. Finite element mesh used for FIDAP analysis of molten pool and lower head.

Using the above initial conditions, each of the codes was used to calculate the transient response of the molten pool to steady-state conditions. The results of the FIDAP and SCDAP/RELAP5/MOD3.2 calculations are compared in Table 5. The FIDAP code calculated the transient velocity field in the molten pool. On the basis of this calculated velocity field, it calculated the rate of heat transfer from the molten material to the external pool of water. The SCDAP/RELAP5/MOD3.2 code calculated the heat transfer from the molten pool based on either steady-state or transient correlations for natural convection heat transfer. The most important variable in the calculations was the heat flux at the exterior surface of the lower head. The value of this variable determines whether CHF occurs and whether the lower head remains intact following contact with molten core material. The comparison of SCDAP and FIDAP showed that the maximum heat flux on the exterior surface at conditions approaching steady-state as calculated by the two codes were within 8% of each other. Both codes also calculated that the maximum heat flux occurs at almost the same position in the lower head. As shown in Figure 11 for the angular position of 75 degrees, the transient heat flux as calculated by SCDAP was consistent with that calculated by FIDAP. The angular position of 0.0 degrees corresponds with the bottom center of the lower head and 90 degrees corresponds with the elevation of the top of the lower head. The time of 0.0 s in this figure corresponds with the instant that the lower head was filled with molten material. As shown in Figure 11, the SCDAP/RELAP5/MOD3.2 calculated heat flux histories were similar for the steady-state and transient correlations for natural convection heat transfer. The greatest difference in calculations of heat flux occurred for the bottom center position of the lower head. At this location, as steady-state was approached the SCDAP/RELAP5/MOD3.2 calculated heat flux was 58% of that calculated by FIDAP.

Table 5. Summary of results of test problem "SCDAP vs. FIDAP."

Parameter describing heatup of lower head by molten pool it supports	FIDAP value	SCDAP value
Maximum heat flux at steady-state on external surface of lower head supporting molten pool (MW/m^2).	0.52	0.48
Location of maximum heat flux at steady-state on external surface (degrees) (0^o = bottom center, 90^o = upper ring of hemisphere).	85	75
Heat flux at bottom center of lower head at steady-state (MW/m^2).	0.31	0.18
Average temperature of molten pool at steady-state (K).	2,940	3,260

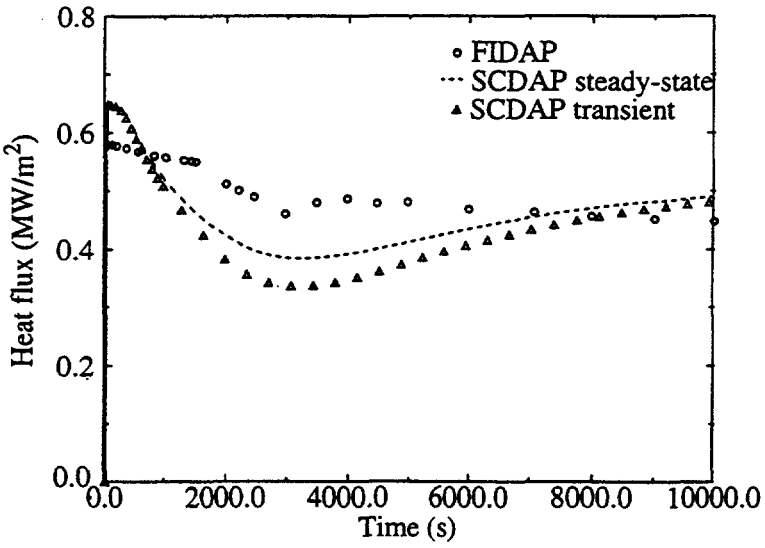

Figure 11. Comparison of SCDAP and FIDAP calculations of heat flux histories at external surface of lower head at angular position of 75^o.

The greatest difference in the SCDAP and FIDAP calculations was that of the temperature of the molten pool as it approached steady-state heat transfer. The molten pool temperatures calculated by SCDAP and FIDAP were 3,260 K and 2,940 K, respectively. This difference indicates that FIDAP calculated a significantly larger heat transfer coefficient at the interface of molten material with solidified material than that calculated by SCDAP. The difference in calculated heat transfer coefficient at the liquid-solid interface resulted in significant differences in calculated molten pool temperature but not in significant differences in the heat flux at the external surface of the lower head.

The rates of heat transfer to the external pool was similar for the two models because this heat transfer was driven by a similar temperature gradient for the two models in the region extending from the inner surface of the crust of frozen previously molten material to the outer surface of the lower head. For both models, this region at one side had a temperature equal to the liquidus temperature of the molten pool and on the other side a temperature approximately equal to the external pool of water. The only difference in temperature gradient for the two models was due to the difference in the thickness of the crust of solidified molten material for the two models, which did not have a large impact on the temperature gradient. The difference in the heat transfer coefficient at the liquid-solid interface caused a difference in the manner in which heat was removed from the molten material. In the case of the FIDAP model, a large amount of sensible heat was removed and a relatively small amount of latent heat was removed, which resulted in a relatively low temperature of the molten pool. In the case of the SCDAP model, a lesser amount of sensible heat was removed and a greater amount of latent heat was removed, which resulted in a relatively high temperature of the molten pool. Thus, for both models, the overall rate of heat transfer from the molten material to the external pool of water was about the same.

3.2.2 Assessment of Molten Pool Crust Failure

The assessment of the crust failure model in SCDAP/RELAP5/MOD3.2 was evaluated by comparing the SCDAP structural analysis of a ceramic crust surrounding a molten pool with the analysis performed by the ABAQUS structural analysis code.[9] Figure 12 shows the problem analyzed by the two codes. The ceramic crust surrounded 1.5 m in diameter hemispherically shaped a molten pool with internal heat generation. The bottom portion of the crust was supported vertically by intact fuel rods, but was free to move in the lateral direction. The top of the crust supported a 1-m layer of rubble debris with an assumed porosity of 50%. The analyses of this crust configuration, described in more detail in Reference 7, investigated the effects of crust dome height and external heat transfer on the load carrying capability of the crust and on the location at which crust failure occurred.

In general, the SCDAP model for failure of a crust surrounding a pool of molten material is in qualitative but not quantitative agreement with that calculated by the ABAQUS code. The test problem, requiring the solution of the transient stresses in the bottom and top crusts encasing a hemispherical shaped molten pool that is covered with water are summarized in Table 6. The situation for which the crust stresses were solved is representative of that in the TMI-2 reactor after sustained High Pressure Injection (HPI) System flooding of the reactor core. The results in Table 6 show that both SCDAP and ABAQUS calculated that the stresses in the crust are primarily driven by a pressure differential between the inner and outer surfaces of the crust and not by the weight of the molten pool or by the weight of debris on top of the crust above the molten pool. Both SCDAP and ABAQUS calculated that the maximum stresses in the crust occur at the juncture of the top crust with the side crust. The two codes are in fairly good agreement on the pressure differentials that can be withstood by crusts with post-CHF heat transfer (film boiling) at the outer surface of crust. However, the two codes calculated significantly different capabilities of the pressure differential withstood by a crust with a dome height of 0.5 m and pre-CHF heat transfer (nucleate boiling) at the top surface of top crust. For this case, SCDAP calculated that the crust could withstand a factor of three greater pressure differential than that calculated by ABAQUS. This difference in calculations was in part because SCDAP modeled the crust as having unlimited ductility while ABAQUS modeled the crust as being brittle. Another important result of this test problem was that it indicated that a flat top crust around a molten pool that is not covered with water has a negligible amount of strength and cannot support any debris on top of it. A solution of the test problem with another model available in the literature, similar in form to the SCDAP model, indicated that implementation of this model into the code would result in an upper bound calculation of the crust stresses. Both this model and the SCDAP model calculate the crust stresses with a closed form set of equations and thus calculate the stresses in a rapid and robust manner. As

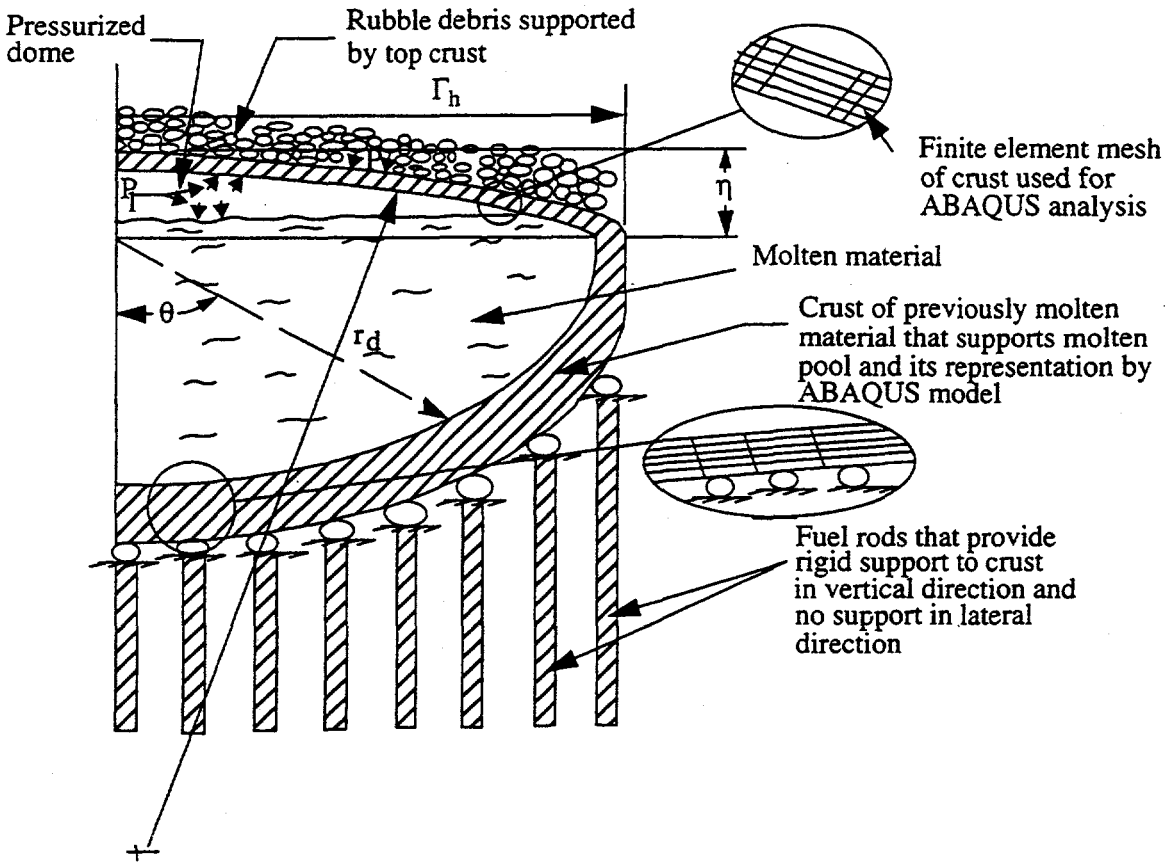

Figure 12. Configuration of crust surrounding molten pool for test problem comparing ABAQUS and SCDAP models for crust failure.

a result of the comparison of SCDAP calculations with ABAQUS calculations, the SCDAP model for the structural integrity of a crust has been adjusted to calculate the timing of the loss of structural integrity of a crust that corresponds with the timing calculated by the ABAQUS code.

Table 6. Summary of results of test problem "SCDAP vs. ABAQUS."

Parameter in stress calculation	ABAQUS	SCDAP
Source of load on crust that causes maximum stresses.	Pressure differential	Pressure differential
Location of maximum stresses in crust.	Juncture of top crust with side crust	Juncture of top crust with side crust
Maximum pressure differential withstood by flat crust with post-CHF heat transfer (MPa).	0.050	0.058

Table 6. Summary of results of test problem "SCDAP vs. ABAQUS." (Continued)

Parameter in stress calculation	ABAQUS	SCDAP
Maximum pressure differential withstood by crust with dome height of 0.075 m and post-CHF heat transfer (MPa).	0.080	0.100
Maximum pressure differential withstood by crust with dome height of 0.5 m and post-CHF heat transfer (MPa).	0.200	0.320
Maximum pressure differential withstood by crust with dome height of 0.5 m and pre-CHF heat transfer (MPa).	0.340	1.090

3.2.3 TMI-2 Analysis

The TMI-2 accident was calculated by SCDAP/RELAP5/MOD3.2 as part of the code developmental assessment because this accident scenario provided a thorough and challenging assessment of the full range of modeling capabilities of the code. The accident involved a wide range of damage progression; (1) ballooning of fuel rods following core uncovery, (2) intense oxidation and rapid heatup of the core, (3) reflood of a hot partially oxidized core, (4) formation of a molten region across the entire diameter of the core, (5) flooding of a molten pool, and (6) slumping of a significant amount of molten material to the lower head.[10] During and following the TMI-2 accident, measurements and analyses based on measurements have provided a basis for a quantitative assessment of some of the important variables calculated by a severe accident computer code. These variables include the increase in primary coolant system pressure following reflood of the hot core, hydrogen production before and after reflood of a hot and partially oxidized core, maximum mass and location of molten material, and timing of the slumping of molten material from the core region to the lower head. Since most of the damage progression models in a severe accident computer code are interdependent, these limited number of measurements and values inferred from measurements nevertheless provide a basis for assessing most of the damage progression models in the SCDAP/RELAP5/MOD3.2 code.

The results of the TMI-2 test problem indicate that the early and late phase damage progression models in SCDAP/RELAP5/MOD3.2 are performing adequately. Table 7 summarizes the comparisons of SCDAP/RELAP5/MOD3.1 and MOD3.2 calculations with measurements and results inferred from measurements. The calculations that are compared with measured values include; (1) hydrogen production before and after start-up of the 2-b pump, (2) increase in primary coolant system pressure before and after start-up of the 2-b pump, (3) mass and location of molten material, and (4) time of slumping of molten material to the lower head. Two MOD3.2 cases are presented in Table 7. The first case had default values for all modeling parameters. The second case had default values for all modeling parameters except for the percentage of oxidation of the fuel rod cladding oxide shell that results in a durable oxide shell. For case 2, this modeling parameter was set to a value of 20% instead of 60%. The value of 20% is appropriate for severe accident sequences in which the primary coolant system pressure is relatively high (> 7 MPa) during the period in which the fuel rod cladding is increasing in temperature from 1,000 K to 2,500 K, as was the case for the TMI-2 accident. The value of 60% is appropriate for the analysis of severe accident experiments conducted in small test facilities. The results in Table 7 show that hydrogen production was accurately calculated by MOD3.2. The calculations of hydrogen production after start-up of the 2b-pump were significantly improved over the values calculated by MOD3.1. The calculated mass of molten material and the calculated timing of slumping of molten material to the lower head were in good agreement with the measured values for Case 1 of MOD3.2.

Table 7. Summary of results of TMI-2 test problem.

Damage progression parameter	Measured or inferred	MOD3.2 Case 1	MOD3.2 Case 2
Cumulative hydrogen production at time of 2-b pump activation (kg).	300	268	275
Final cumulative hydrogen production (kg).	460	436	453
Primary system pressure just before 2-b pump activation (MPa).	8.20	4.98	5.03
Increase in primary coolant system pressure after start-up of 2-b pump.	6.30	7.09	5.21
Total mass of molten core material (kg).	40,800	17,500	37,400
Mass of molten material that slumped to lower head (kg).	15,800	0.0	37,400
Fraction of total mass of molten material that slumped to lower head (%).	39	0.0	100.
Time at which bulk of material in core slumped to lower head (s).	13,500	-	13,379

The results in Table 7 show that the important late phase damage progression parameter of the amount of molten material that slumps to the lower head is sensitive to the modeling parameters in the early phase damage progression models that defines the durability threshold of the cladding oxide shell. The two MOD3.2 cases presented in this table had different values for durability threshold. Even though the difference in these modeling parameters was small relative to the level of uncertainty in this modeling parameter, nevertheless this difference caused significant difference in late phase damage progression. The MOD3.2 case with a durability threshold of 20% calculated an amount of molten material that was in good agreement with the measured value, while the MOD3.2 case with a durability threshold of 60% underpredicted the amount of molten material and did not calculate material slumping to the lower head. This impact of an early phase modeling parameter on the calculated level of late phase damage progression points to the benefits of research to put the evaluation of this early phase damage progression modeling parameter on a more complete and mechanistic basis.

There are discrepancies between calculated and measured results in Table 7 that show the early and late phase damage progression models in MOD3.2 are open to improvements. Significant discrepancies also exist in the calculated and measured values of primary coolant system pressure at the time of start-up of the 2-b pump shown in Figure 13 and in the amount of material that slumps to the lower head (Table 7). The causes and resolutions of these two discrepancies are discussed in more detail below.

Although the first discrepancy, namely the underprediction of the primary system pressure before the 2-b pump transient, may be due to incorrect assumed boundary conditions that are not known, there is also the possibility that it is due to deficiencies in modeling. One possible deficiency may be that in modeling counter-current flow through the surge line, which is a model that has a strong influence on the amount of

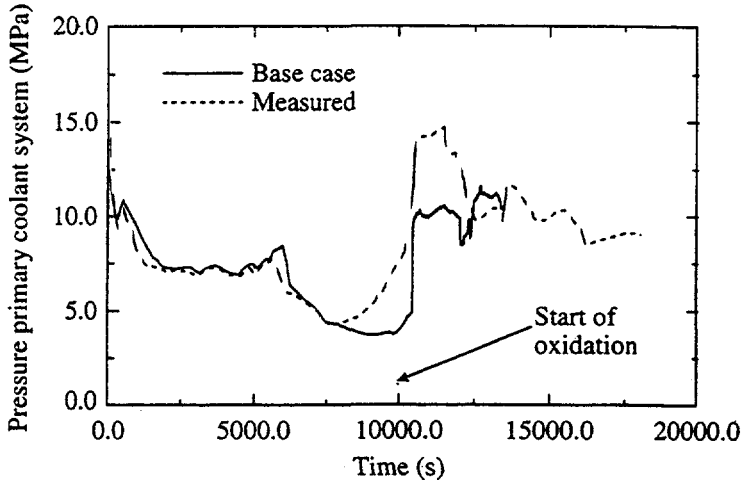

Figure 13. Calculated and measured pressures of the primary coolant system of the TMI-2 test problem.

water that is calculated to drain from the pressurizer and thus on the time at which intense oxidation of the core begins. Since the calculated pressure appears to parallel but be offset in time from the measured pressure, there is the possibility that an improvement in the calculation of pressurizer draining would also correct the calculated time for beginning of intense oxidation of the reactor core and thus also correct the calculated pressure history.

The second discrepancy, namely that in the calculated amount of material that slumps to the lower head, may be due to a lack of a model for the axial relocation of embrittled fuel rods above a molten pool that disintegrated during the reflood of the reactor. The amount of material that slumps to the lower head is a function of the axial relocation of these disintegrated fuel rods. As the molten pool in the TMI-2 accident was reflooded with HPI, the cooling water caused the crust on top of the molten pool to thicken and gain strength and at the same time caused embrittled fuel rods suspended above the molten pool to disintegrate and slump downward. The relative timing of these two events determines whether the disintegrating fuel rods enter the molten pool or are supported by the crust on top of the molten pool. The amount of material that slumps to the lower head is in turn a function of which of these two possibilities for behavior of the fuel rods occurs. If a structural failure occurred to the crust on top of the molten pool, the disintegrated fuel rods supported by the crust would plunge into the molten pool and displace molten material from the molten pool. For the TMI-2 accident, the displaced molten material may have been the sum of the material that slumped toward the lower head. The measured results indicate that about 40% of the molten material drained from the molten pool at the time of crust failure. Since the code currently lacks a model for the axial relocation of disintegrated fuel rods, the code assumes that all the molten material drains from the molten pool in the event of failure of the crust. In addition to a model for the axial relocation of disintegrated fuel rods, there is also the possibility that extensions to one early phase modeling parameter, namely oxide durability threshold may resolve some of the discrepancies in the calculated amount of molten material that slumps. The basis for this possibility is the difference in the calculated damage progression between the two MOD3.2 cases shown in Table 7, which differs only in the value of oxide durability threshold. In summary, resolution of the outstanding deficiencies in calculated late phase damage progression may best be done on a step by step basis with resolution of deficiencies in the early phase modeling being resolved first and those in the less well understood late phase modeling of the structural behavior of crusts and damaged fuel rods being resolved later.

The MOD3.2 calculations of the TMI-2 accident were significantly improved over those of MOD3.1 due to a cumulation of extensions and corrections made to the damage progression models in the code. The extensions in modeling that contributed the most to improvements in the calculated results were the model for transition smoothing of the change in fuel rod geometry that begins with the onset of ceramic melting and the model for structural failure of the crust at the top and side of the molten pool. The transition smoothing model allows the calculation of fuel rod oxidation at locations with partially melted fuel. This model also allows the modeling of flow of coolant through these locations during this period of time. MOD3.1 flagged any location at which the onset of fuel melting had occurred to be completely blocked of coolant flow, which resulted in an underprediction of the hydrogen production at that location and an overprediction of the cooling of the region of the reactor core into which coolant was diverted by the blockage. The crust failure model results in the timing of slumping of molten material from the core region to the lower head being coordinated with events that influence the capability of the crust to support a molten pool, such as reflood of the core and changes in pressure of the primary coolant system. Other extensions and corrections that had some effect on improving the MOD3.2 calculations were; (1) addition of a model for transition smoothing of the metallic meltdown of cladding, (2) correction of the model for oxidation of porous debris, such as that resulting from fragmentation of embrittled fuel rod cladding following the 2b-pump activation, and (3) convective cooling of porous debris.

4. CONCLUSIONS

SCDAP/RELAP5 calculations haves shown that SG tube rupture is unlikely to occur during a TMLB' transient when the RCS is depressurized via the pressurizer PORV. The calculations have shown that surge line failure is the first RCS pressure boundary failure in all calculations for all operating PWRs. G tube rupture occurred only in Westinghouse PWRs with SG sludge accumulation (although significant tube damage developed with sludge in the Calvert Cliffs SGs). The time period between surge line failure and SG tube rupture was relatively long. However, because of conservatism in the analyses (the RCS was not allowed to depressurize when surge line failure was predicted), SG tube rupture may not occur in reality because RCS depressurization through the surge line break would have flow through the SGs, hence reducing the possibility of creep damage. Consequently, the potential for a SG tube rupture in the plants analyzed is considered to be low for conditions that have been considered.

Recent updates and improvements made to SCDAP/RELAP5/MOD3.2 have enhanced code predictive capabilities and improved overall code performance. These improvements have been particularly significant in modeling molten pool behavior, and in the transitions from intact core geometry to debris blockages and molten pools. These improvements, as well as improvements in early phase modeling have been demonstrated in this paper through comparisons with measured experimental results, independent analytical solutions, and previous MOD3.1 calculations. Those areas requiring further improvement are currently under development at the INEEL, and will be reported on in future publications.

4.0.1 References

1. W. A. Stewart et al., *Natural Circulation Experiments for PWR High Pressure Accidents, EPRI Project No. RP2177-5 Final Report,* Westinghouse Electric Corporation, July 1992.

2. T. A. Wheeler et al., *Analysis of Core Damage Frequency from Internal Events: Expert Judgment Elicitation,* NUREG/CR-4550, April 1989.

3. D. L. Knudson, INEEL letter to Dr. R. Lee, USNRC, "Transmittal of JCN W6242 Task 6.1 and 6.2,

Letter Reports - DLK-4-97," May 23, 1997.

4. D. L. Knudson, INEEL letter to Dr. R. Lee, USNRC, "Transmittal of JCN W6242 6.2 Letter Reports - DLK-4-97," June 13, 1997.

5. D. L. Knudson, INEEL letter to Dr. R. Lee, USNRC, "Transmittal of JCN W6242 6.4 Letter Reports - DLK-4-97," September 25, 1997.

6. D. L. Knudson, INEEL letter to Dr. R. Lee, USNRC, "Transmittal of JCN W6242 6.5 Letter Reports - DLK-4-97," August 4, 1997.

7. The SCDAP/RELAP5 Development Team, *SCDAP/RELAP5/MOD3.2 Code Manual, Volume V: Developmental Assessment Draft,* NUREG/CR-6150, INEL-96/0422, Revision 1, October 1997.

8. Fluid Dynamics International, Inc., *FIDAP (FLuid Dynamics Analysis Package) 7.0 User's Manual,* 1993.

9. *ABAQUS User's Manual, Version 4.6,* Hibbitt, Karlsson & Sorensen, Inc., Providence, RI, 1987.

10. J. K. Hohorst et al., *TMI-2 Analysis Using SCDAP/RELAP5/MOD3.1,* INEL-94/0157, November 1994.

Overview of MELCOR 1.8.4: Modeling Advances and Assessments

Randall O. Gauntt, Randall K. Cole, Salvador B. Rodriguez,
Michael F. Young, Ronald D. Gasser, Mark T. Leonard[✧], and Scott Ashbaugh[✧]
Modeling and Analysis Department
Sandia National Laboratories
Albuquerque, New Mexico 87185

ABSTRACT

The newly released MELCOR 1.8.4 reactor accident analysis code contains many new modeling features as well as improvements to existing models. New model additions to the MELCOR code include a model for predicting enhanced depletion rates for hygroscopic aerosols and a model for predicting the chemisorption of Cesium to the surfaces of piping. Improvements to existing models include: upgrading the core module (COR) to handle flow redistribution resulting from the formation of core blockages, improving the thermalhydraulics (CVH) coupling with COR to handle flow reversal situations, and upgrading the fission product scrubbing model to incorporate the SPARC90 code. Significant upgrading of the COR package core degradation modeling was also included in the new code release version. New and improved models are described in the following paper. In addition, a number of assessment analyses were recently performed, focusing on demonstrating the new and improved capabilities in the code. Results of assessment calculations demonstrating code performance for aerosol (pool) scrubbing, hygroscopic aerosol behavior, and core degradation and hydrogen production are presented. Finally, ongoing code development activities beyond MELCOR 1.8.4 are described. These include models for treating iodine behavior in containment sumps, pools, and atmosphere, and plans for implementing reflood models and the attendant effects on accident progression. Further improvements and additions to the core degradation modeling in MELCOR are described, including the implementation of enhanced clad failure models to treat clad ballooning and eutectic interaction with grid spacers, and expansion of the COR package to allow for improved representation of UO_2-Zr eutectic behavior, improved melt relocation treatment, greater detail in describing aspects of BWR core degradation (fuel channel, bypass, and lower plenum), and more flexibility in modeling "other structures" in the core such as core plate structures (supporting) and PWR control elements (non-supporting).

OVERVIEW OF IMPROVEMENTS IN MELCOR 1.8.4

The MELCOR code development project passed an important milestone in 1997 with the release of MELCOR version 1.8.4 [1]. The new version contains many new modeling features as well as improvements to existing models.

Significant upgrading of the COR package core degradation modeling is a major feature of the new code release version. The changes include correcting the implementation of the model that retains oxidizing molten Zircaloy in place behind the outer oxide shell until a user-specified (2400 K default) temperature is attained, and allowing the outer cladding oxide shell itself to preserve fuel rod integrity until an oxide failure temperature is attained (2800 K default). Also, some improvements and corrections were made to the debris relocation modeling. This corrects the tendency of previous versions of MELCOR to predict premature fuel collapse following melting of the metallic Zircaloy cladding, resulting in low peak fuel temperatures in certain calculations..

Modeling of the vessel lower head in the COR package was upgraded to include a creep rupture failure model and heat transfer from the outside of the head. The code was also modified to allow for the possibility

---

[✧] Innovative Technology Solutions, Albuquerque, New Mexico

that there may be *no* penetrations in the lower head. If part or all of the lower head is covered by a water pool, a downward-facing boiling correlation [2] is used.

The "spreading" of decay heat by gamma-ray transport is now modeled, and its initial deposition is not limited to UO_2. An oxidizer allocation model has been added to better model the competition of various hot metallic surfaces for available steam and oxygen. Melting of the heat structures that define the thermal boundary for the COR package (typically the core shroud and representative upper internal structures) may now be modeled. The molten steel is added to core debris. Radiation between heat structures may also be treated.

The coupling between the COR package and thermalydraulics in the CVH and FL packages (referred to as the "dT/dz model") has been improved to better handle flow reversal situations. A blockage model has been added to allow more realistic treatment of the changing distribution of flow that will result from the formation and relocation of core debris. An ideal check valve model has been added to CVH/FL, as has an initialization option that should simplify establishment of steady operating conditions.

Treatment of lower plenum debris beds by the BH package is now applicable to PWRs. The modeling has been extended to treat oxidation of steel as well as Zircaloy in the debris bed, and the energy balance is now fully functional. Passive containment and core cooling models that were available only as part of the BH package in MELCOR 1.8.3 have been extracted as a new Condenser (CND) package, and may be used independently of BH.

In the realm of radionuclide modeling, the fission product scrubbing model has been upgraded to incorporate the SPARC90 code, and a model for predicting the chemisorption of Cesium to the surfaces of piping has been added. When the film tracking model in the Heat Structure model is activated, allowing water films to flow from one structure surface to another, deposited radionuclides (and their associated heat sources) may be transported from surface to surface with the water. The process is subject to the same solubility considerations as the transport of radionuclides to the control volume pool with draining films in older versions of MELCOR. An optional hygroscopic model that includes solubility, Kelvin, and noncontinuum effects is available for treatment of aerosol behavior. It is useful in the prediction of the enhanced depletion rates that are observed for hygroscopic aerosols.

SELECTED ASSESSMENT/VERIFICATION STUDIES

The following sections describe some of the more important details and results of recently performed assessment calculations with MELCOR 1.8.4. These assessments were selected to emphasize new model performance and improvements to existing models.

Fission Product Scrubbing in SPARC90

The aerosol (pool) scrubbing models in the RN Package were revised in MELCOR 1.8.4 to incorporate updated models from the stand-alone SPARC computer code. Specifically, clones of SPARC-90 models for bubble hydrodynamics and for various aerosol and iodine vapor deposition mechanisms (in water pools) were incorporated into MELCOR. Calculations were performed to evaluate the implementation of the updated pool scrubbing models against two independent series of experiments that measured pool DF as a function of several hydrodynamic and aerosol source parameters. Due to a lack of publicly available information regarding experimental measurements of fission product vapor removal in water pools, an assessment of the SPARC-90 iodine vapor removal models was not performed as part of the current MELCOR model assessment effort.

The technical approach to this assessment was to compare aerosol pool DFs calculated by MELCOR to data from the same experiments that were used to benchmark the stand-alone version of SPARC-90. Specifically, these data originated from:

- pool scrubbing experiments sponsored by the Electric Power Research Institute (EPRI) and performed at Battelle's Columbus Laboratories (BCL), and
- pool scrubbing tests performed as part of the Advanced Containment Experiments (ACE).

The specific experiments modeled with MELCOR were designed to evaluate the effectiveness of pool scrubbing under conditions in which the carrier gas enters a pool of water through a submerged, small orifice. The orifice size and pool conditions are similar to the individual holes of a T- or X-quencher at the terminus of a safety/relief valve tailpipe in a Boiling Water Reactor (BWR) suppression pool, or in a Pressurized Water Reactor (PWR) quench tank.

The experimental apparatus allowed several parameters to be varied from one case to another to measure pool DF over a broad range of conditions that might be expected during a severe accident, such as:

- injector submergence,
- carrier gas temperature and mass flow rate,
- steam mass fraction of the carrier gas,
- pool thermodynamic state (i.e., saturated vs. subcooled),
- aerosol source rate, and
- aerosol particle size (i.e., aerodynamic mass mean diameter - AMMD).

A comparison of MELCOR-calculated DFs to measurements for the EPRI/BCL aerosol pool scrubbing experiments and the ACE pool scrubbing tests is shown in Figure 1. In general, the DFs predicted by both codes were within a factor of 10 of measured values, and in most cases the DFs predicted were within a factor of 3 of measurements. Further, parallel calculations performed with the stand-alone SPARC-90 code demonstrated the DFs predicted by MELCOR and SPARC-90 to be generally consistent between the codes.

This assessment also generated several recommendations to code users when MELCOR's pool scrubbing models are being used. These are:

- First, aerosol particle size has a first-order effect on pool scrubbing DF. Therefore, users should be aware that MELCOR uses (as a default) an average aerosol size distribution for all aerosols in the problem. If users are interested in how different aerosols are transported within the system, and if these aerosols have significantly different size distributions, the user should consider representing these different aerosol classes with separate *components* in MELCOR. Each component has a unique size distribution based on the material represented by that component.

- Since the definition of aerosol size distribution is important, care should be taken to ensure that the distribution mesh is fine enough to adequately represent each distribution. MELCOR separates the aerosols into 5 discrete bins, called *sections,* as a default. This can be changed by user input. If the default distribution is enlarged for a calculation, the number of sections will likely need to be increased accordingly.

- Finally, aerosol density also has a first-order effect on pool scrubbing DF. Therefore, users should be aware that MELCOR applies a default aerosol density of 1000 kg/m^3 to all aerosols when performing transport (decontamination) calculations. This density may be inappropriate for reactor source term applications where heavier aerosols (such as CsI) are of importance.

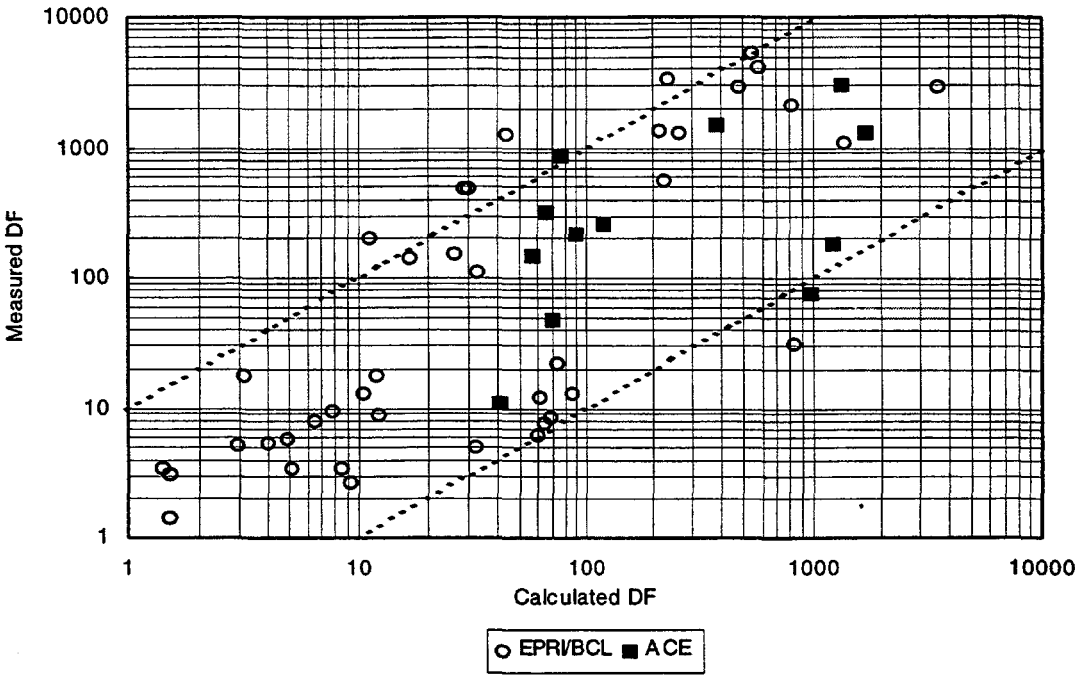

Figure 1. Summary of results - MELCOR-calculated vs. measured DF. (Note: Data within bands show agreement between calculated and measured DF within one order of magnitude.)

Hygroscopic Aerosol Behavior: AHMED[3]/VANAM M3[4] (ISP-37) Experiments

A model was added to MELCOR 1.8.4 to treat enhanced particle growth rate by water vapor condensation. Non-hygroscopic aerosol requires that the relative humidity be 100% in order for water vapor to condense on the particles. In contrast, hygroscopic aerosol, such as CsOH and CsI have the ability to condense water from moist air where the relative humidity is less than 100%. When this occurs, the particles will increase in size and mass, which subsequently leads to increased gravitational settling and depletion of the airborne concentrations. In general, the higher the relative humidity (RH) in a volume, the higher the rate of aerosol concentration decay. Thus, the hygroscopic effect has a relatively smaller effect for RH on the order of 30% or less, but greatly enhances condensation and particle growth for RH between 30 and 100%.

A hygroscopic aerosol model based on the Mason equation, and described by Prupracher and Klett [5], was implemented into MELCOR. The principal hygroscopic phenomena is often referred to as the solubility effect. The solubility effect addresses the consequence of water and aerosol mixing into a new, aqueous solution where the aqueous solution vapor pressure is lower than that of pure-water vapor pressure. Therefore, once mixed, the new aqueous particle will grow until the vapor pressure at the particle's immediate boundary reaches bulk gas pressure. The MELCOR model also includes the "Kelvin effect," a surface tension effect on the surface vapor pressure for very small particles, and correction terms for calculating water vapor transport to very small particles when the aerosol particle size is on the order of the mean free path of the water vapor molecules.

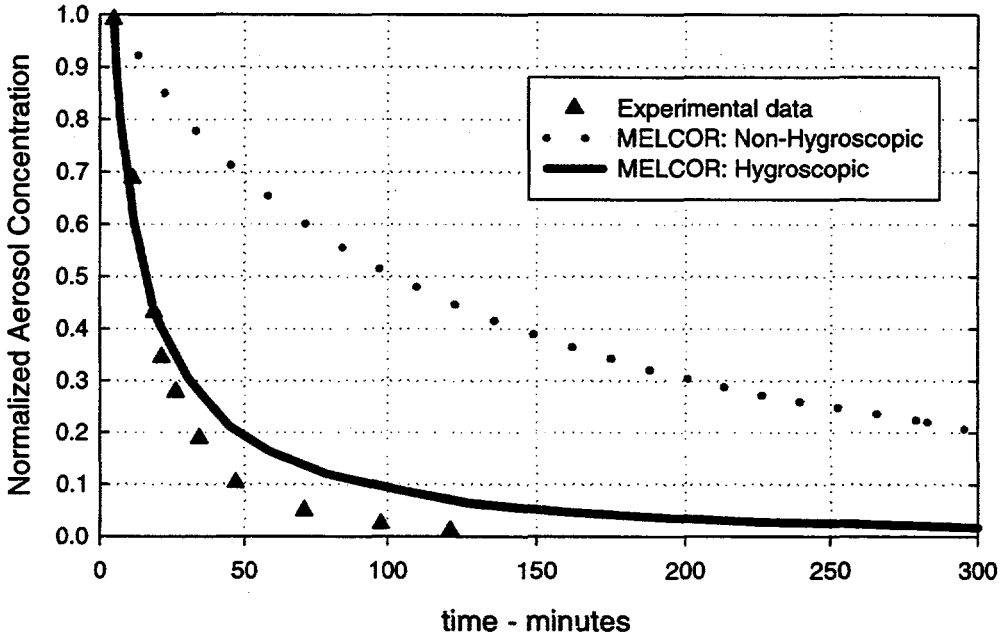

Figure 2. Comparison of AHMED NaOH concentration data for RH = 96% and hygroscopic and nonhygroscopic MELCOR.

Simulations of the VANAM M3 experiment (ISP37) and the AHMED experiments, both of which investigated the depletion behavior of hygroscopic aerosol, were conducted using the new MELCOR model. Predicted aerosol depletion behavior was compared to that measured in the experiments. In addition, comparisons to other hygroscopic codes, such as CONTAIN, MACRES, FIPLOC, IDRA, and NAUAHYGROS were made. Figure 2 shows the potential effectiveness of the hygroscopic effect on aerosol depletion for one of the AHMED tests. Neglecting the hygroscopic effects results in a significantly protracted aerosol depletion period, whereas including the effect results in much more rapid aerosol depletion. The predictions of the MELCOR hygroscopic model are seen to compare very well with the AHMED data. Figure 3 compares the ISP37 NaOH aerosol concentration as a function of time as predicted by MELCOR, various hygroscopic codes, and data for one of the several simulated containment compartments. As seen in this figure, the aerosol depletion behavior is reasonably captured by MELCOR and other codes. In conclusion, the code-to-data and code-to-code comparisons show that the new hygroscopic model captures (very well) experimentally observed hygroscopic aerosol phenomena and its performance is similar with other contemporary hygroscopic models.

Core Degradation: PHEBUS FPT-0, FPT-1 And CORA-13

Prior to the release of MELCOR 1.8.4, a number of deficiencies in the treatment of fuel degradation and hydrogen generation were identified as a result of both comparisons to fuel damage experiments and in analyses of plant scale core damage events. The general symptoms observed were lower than expected: peak

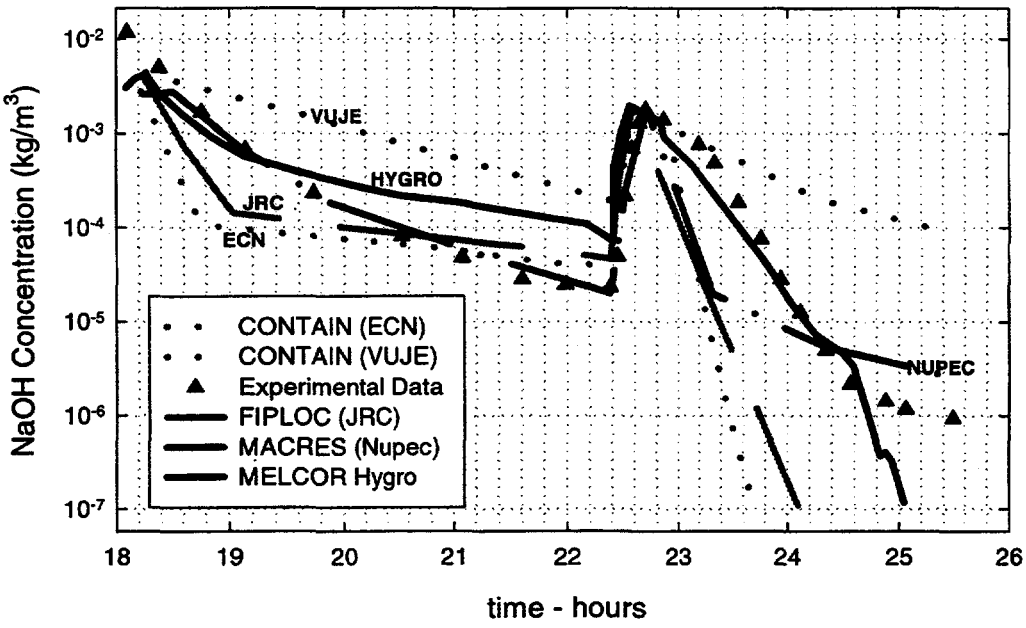

Figure 3 Comparison of ISP37 NaOH concentration between MELCOR, various hygroscopic codes, and data.

fuel temperatures, hydrogen generation, and fission product release. The observed tendencies were found in large part to be due to: 1) the lack of any retention of molten zircaloy cladding behind an outer oxide shell (oxidizing zircaloy relocated downward to cooler regions as soon as the melting point was attained thus terminating further chemical heat and hydrogen generation locally), and 2) the collapse of the UO_2 fuel rods when the metallic cladding melted. In general practice, both of these events occurred very near 2100 K, and because of the overall lower average fuel temperature, total fission product release was also lower than considered reasonable. In the MELCOR 1.8.4 code release, the fuel degradation modeling was improved to allow oxidizing molten zircaloy to remain in place behind an outer oxide shell until a user-adjustable temperature is reached. The default release temperature is 2400 K. Needless to say, the fuel rods are allowed to remain intact after the initial melting of the metallic portion of the cladding. Fuel rod collapse deferred until a different and higher user-specified temperature is attained. The default for the fuel rod collapse temperature is 2800 K, selected because of the eutectic which forms between UO_2 and ZrO_2 at that temperature. In order to judge the effectiveness of these core degradation modeling improvements, a number of assessment calculations were performed on available fuel damage experiments, including experiments from the Phebus project and CORA projects. Particular results from each analysis are described in the following sections.

Assessment of Core Degradation: PHEBUS FPT-0, FPT-1

PHEBUS FPT [6] is a series of in-pile fission product source term experiments conducted in the integral (PWR) test facility located in Cadarache, France. (The experimental program is jointly managed by

the Nuclear Safety and Protection Institute (IPSN) of the (French) Atomic Energy Commission (CEA), and the Joint Research Centre of the Commission of European Communities (CEC). The Phebus fuel bundle is approximately 1 m in height. Two Inconel spacer grids are located approximately ¼ and ¾ along the active fuel length. The fuel bundle is composed of 20 Zr-clad, UO_2 fuel rods in a rectangular pitch. A single Ag-In-Cd control rod is positioned in the center of the bundle. Surrounding the fuel bundle are several layers of dense insulation materials [primarily Zirconia (ZrO_2)] and an Inconel pressure tube. Two experiments from this project have been analyzed with MELCOR 1.8.4, test FPT-0, which used fresh fuel rods and test FPT-1, which used previously irradiated fuel rods. Of particular interest in the following assessments are the thermal response of the fuel to the nuclear and cladding oxidation heating, the amount of hydrogen generated during the oxidation transient, and the collapse of the fuel rod bundle.

Test FPT-0, the first of six planned source term experiments, was conducted on December 2, 1993. The primary objective of the test was to examine the release of fission products from lightly irradiated fuel and its subsequent transport and deposition throughout a simulated primary coolant system flow circuit.

Measurements from the thermocouples located in the test bundle are perhaps the most critical source of data for evaluating the calculated fuel response. Comparisons of measured and calculated bundle temperatures are shown in Figure 4. At all locations within the fuel bundle, the calculated temperature signature follows the qualitative trends observed in the data until material relocation occurs (indicated by the sharp decrease to 0 in calculated temperatures). In particular, the gradual rise in fuel temperature to ~1000°C following the first increase in core power (7,000 - 9,000 sec) is calculated with reasonable accuracy. Calculated values for the peak fuel temperature at both ~12,000 sec and ~15,000 sec are also in good agreement with measurements.

One significant improvement in the current calculation with MELCOR 1.8.4 over previous analyses is the fact that the fuel bundle remains until reaching a temperature near 2800 K, which compares reasonably well with the experimental measurements up to that point. Previous analyses with MELCOR 1.8.3 predicted fuel collapse at ~2100 K, and the high temperature escalation now attained was previously missed. The higher predicted temperatures and features of the heatup signature (now predicted correctly) are due both to the continued oxidation of molten zircaloy held in place by the oxide shell and by the retaining of intact rod geometry to temperatures in the neighborhood of 2800 K.

Figure 5 shows the predicted and measured integral hydrogen generated in the FPT-0 experiment. It must be pointed out that there were great difficulties encountered during the conduct of the experiment with the measurement of hydrogen. The data presented in Figure 5 indicates well the onset of the hydrogen generation, but the complete time signature of the hydrogen generation is suspect. It is known that the the instrument became saturated after a point and integral thereafter becomes "flat." The time at which significant oxidation begins is accurately calculated by MELCOR, and the total extent of bundle oxidation is within ~10% of the measure value[1]. The calculated rate of hydrogen production during the initial portion of the oxidation phase of the transient is also calculated to be in reasonable agreement with measurements. After approximately 12,000 seconds, however, the MELCOR calculation shows a significant decrease in the oxidation rate, resulting in a protracted period of hydrogen production. The total hydrogen generation predicted by MELCOR 1.8.4 is nearly double that predicted by MELCOR 1.8.3 and is very near the best estimates for the experimentally generated hydrogen.

A second assessment calculation was performed on the second experiment in the Phebus series, FPT-1. The FPT-1 experiment is very similar in configuration to FPT-0, the primary difference being the use of

---

[1] Note that the instrument measuring hydrogen generation became saturated when hydrogen production reached a level of 90 g. The actual amount of hydrogen generation is generally believed to be nearly 100 g.

irradiated fuel from the BR-3 reactor core in place of the fresh fuel used in FPT-0. There are other minor differences including the addition of a dense ThO_2 liner inserted between the bundle and the radial shroud, and changes in the circuit components. There were also some changes in steam flow rates and bundle power history. In general, however, the description given above for the FPT-0 experiment applies also to FPT-1.

An important difference in the fuel rod collapse was observed in the FPT-1 experiment in comparison with the FPT-0 experiment. In FPT-1, the fuel rods appeared to collapse at near 2500 K in contrast to a higher temperature observed in FPT-0. This is postulated to be due to irradiated fuel effects including irradiation-induced fuel pellet cracks and enhanced material interactions between molten zircaloy and the irradiated fuel material. In view of the experimental observations, the fuel collapse temperature threshold in MELCOR 1.8.4 was lowered from the default value of 2800 K to 2500 K. Doing so produced fuel bundle thermal signatures consistent with those observed in the experiment, as indicated in Figure 6.

Concerning hydrogen production, the generation rate signature predicted by MELCOR 1.8.4 was quite consistent with that measured in the experiment, and the total amount predicted by MELCOR was within 10% of the best estimate reported by the Phebus project.

Based on comparisons of the results of several additional MELCOR sensitivity calculations to experimental data, the following conclusions were drawn:

- The overall performance of MELCOR 1.8.4 was quite good in calculating key features and quantitative results of both the FPT-0 and the FPT-1 experiments. Temperature signatures for fuel, clad and the Ag-In-Cd control rod showed good agreement with data taken at several locations in the test bundle. The calculated quantity of hydrogen generated and magnitudes of fission product release from fuel also showed good agreement with data.
- Results of the current calculations suggest the revisions to the-COR Package models in the development of Version 1.8.4 made a significant improvement in calculated response of test FPT-0 over those from MELCOR 1.8.3. Fuel rods were calculated to remain intact for a sufficiently long period of time to attain peak temperatures very close to those measured in the experiment, and the total (cumulative) quantity of hydrogen generated was close to the measured value using current code default modeling options. For FPT-1, however it was necessary to reduce the default fuel rod failure temperature, nominally 2800 K, to 2500 K in order to reproduce the observed fuel relocation thermal signatures. This is believed to be a characteristic of irradiated fuel behavior.

Analysis of CORA-13 (ISP-31)

The CORA-13 test [7], which involved a bottom reflood quench phase was also analyzed with MELCOR 1.8.4. Previous MELCOR code versions 1.8.1 and 1.8.3 were also applied in the assessment exercise. In the MELCOR 1.8.4 calculations, the molten cladding release temperature (default=2400 K) was varied between 2400 K and 2750 K. The effect of activating the "eutectics" model was also investigated. The primary prediction quantity of interest was the total amount of hydrogen produced.

The emphasis of this study was on hydrogen mass generation and component temperatures. Figure 7 shows the hydrogen production rate predicted by the various code calculations and the experimentally measured hydrogen. Previous code versions showed a tendency to begin hydrogen generation early compared to the measured time of onset of hydrogen generation. The earlier MELCOR versions also predicted a termination of hydrogen production before the measured production rate reached its peak value. This was due both to the early onset of predicted hydrogen generation as well as to relocation of the oxidizing zircaloy. By the time that the reflood was initiated, the earlier code versions predicted that there was no zircaloy remaining in a hot enough location in the bundle to produce the quench-induce oxidation transient at ~4900 sec. The MELCOR 1.8.4 calculation showed improvements in both the total amount of hydrogen produced as well as

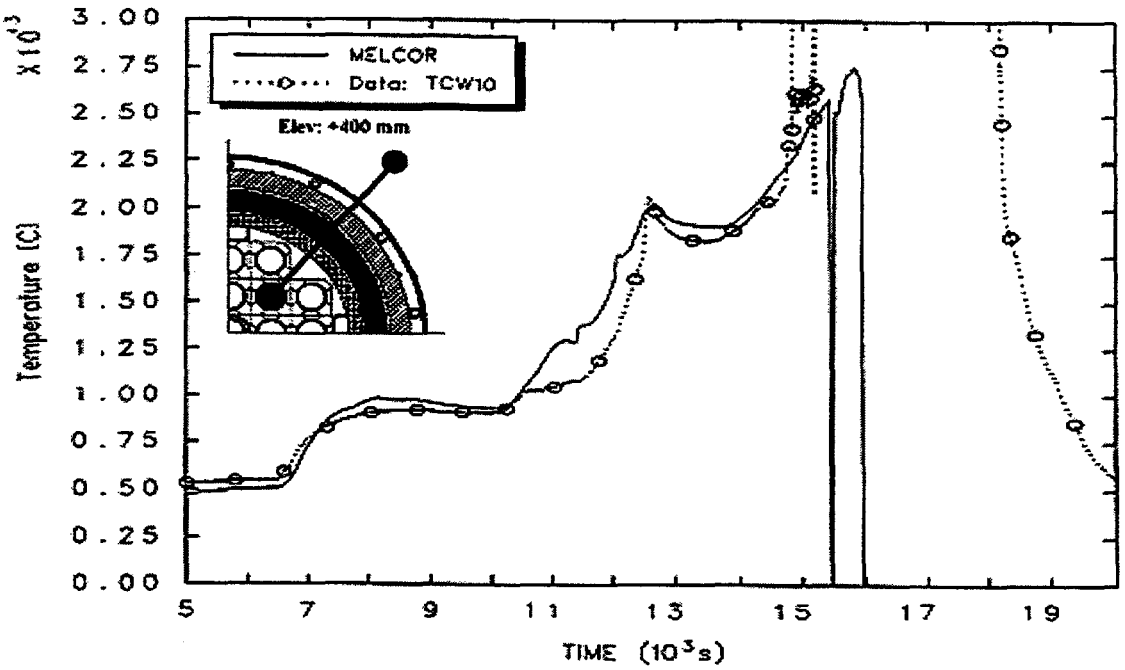

Figure 4. Comparison of calculated/measured fuel temperature [inner fuel rod: 262-420 mm above BAF].

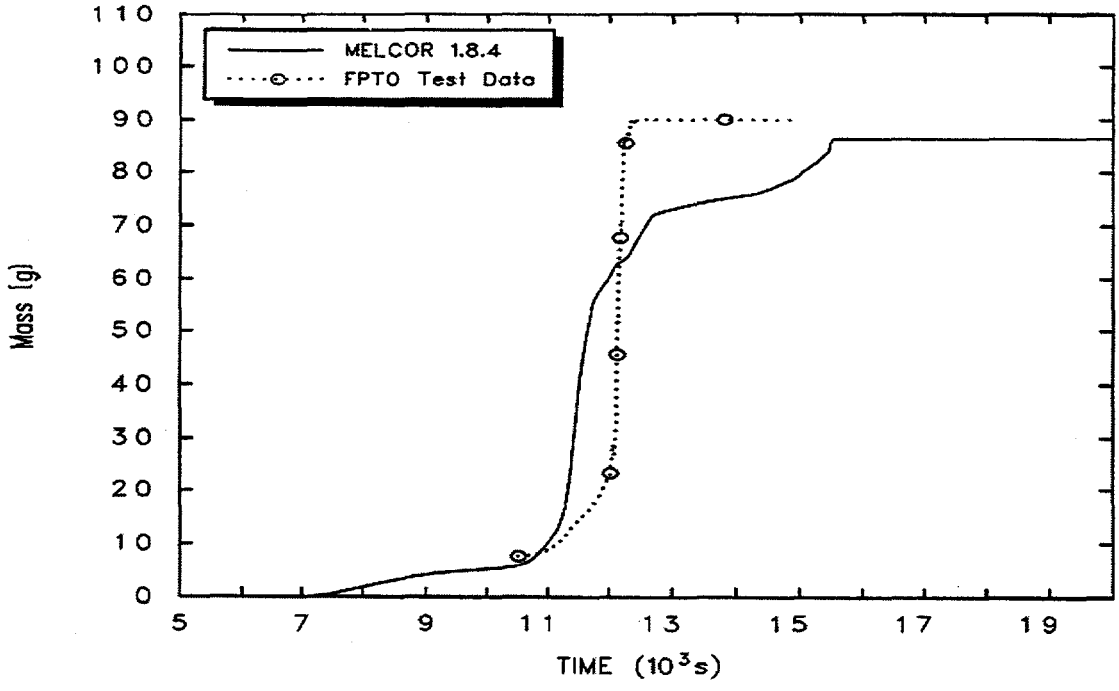

Figure 5. Total (cumulative) hydrogen generation during FPT-0.

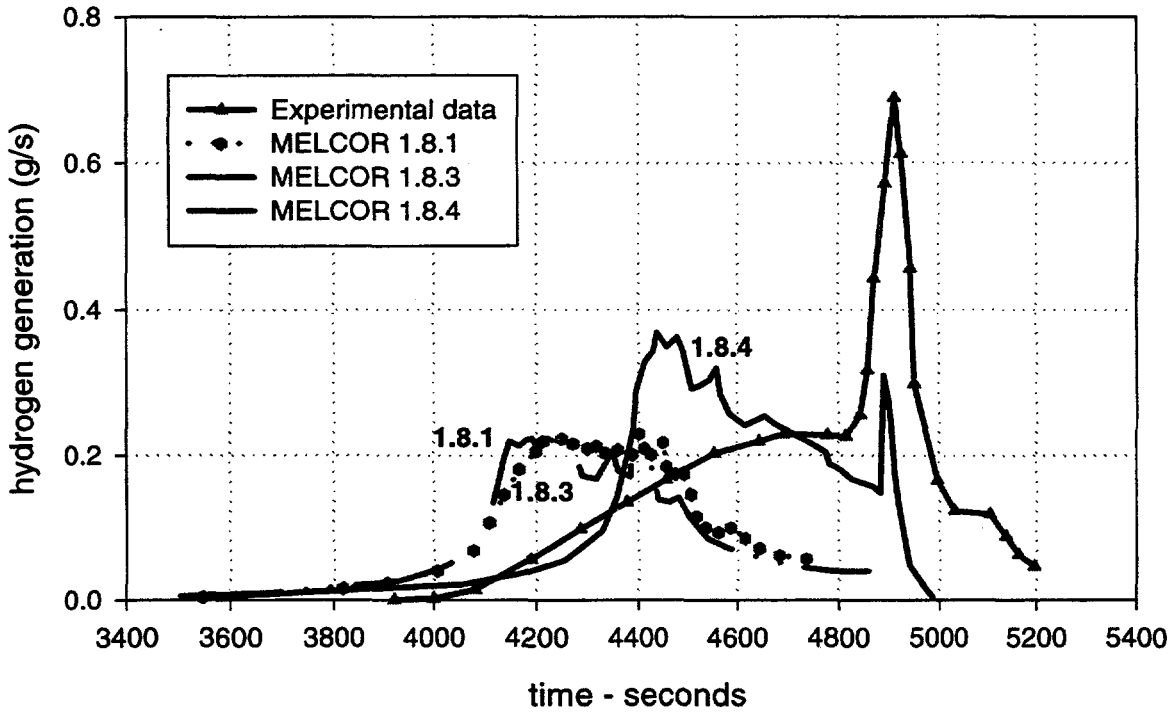

Figure 7. Comparison of data and MELCOR 1.8.1, 1.8.3, and 1.8.4 ISP31 hydrogen mass generation.

predicting a small oxidation transient to occur during the reflooding phase, however, as seen in the figure, the overall hydrogen generation signature does not match the measured signature particularly well. The cause for this difference has not yet been determined, and no problems of this sort were apparent with the Phebus calculations described previously. The MELCOR 1.8.4-predicted oxidation transient occurring during the

reflood phase indicates that the predicted bundle zircaloy spatial/temperature distribution is closer to the conditions of the actual CORA bundle than was predicted in previous code versions. The magnitude of the quench-induced hydrogen generation was not as large as measured. This is believed principally to be due to the lack of any modeling treatments for quench-induced cladding oxide fracturing. Improvements to the cladding oxidation modeling to account for these effects are currently planned.

FUTURE DEVELOPMENT PLANS

Even as MELCOR 1.8.4 was "frozen" for release, development on new models and improvements to existing models continued. Some of the development activities currently underway are described in the following section.

Core Spray and Reflood Modeling

Several fuel damage experiments conducted under the CORA program (involving a water reflooding period after severe fuel damage has occurred) have indicated that immediate cooldown and quenching of the overheated fuel does not occur. Instead, the sudden production of steam generation from the reflooding action produces a renewed oxidation transient in regions above the quench front where metallic zircaloy remains. This oxidation transient often produces the peak temperatures measured in the entirety of the test and can produce hydrogen in quantities nearly equal to the entire oxidation period prior to the reflood. The observed effects are believed to be due to a thermal shock induced fracturing of the outer cladding oxide shell which greatly facilitates the transport of steam to the unoxidized underlying metallic cladding. In light of these experimentally observed phenomena and in order to evaluate the full import of reflooding an overheated core in terms of additional hydrogen and heat generation on the subsequent character of an accident progression, improved models are currently under development to include these effects. Similar effects are expected for both core reflooding from the bottom, as well as top core spray reflooding, and it is planned to include treatments for both.

The planned core spray and reflood modeling will be capable of simulating quench front movement during top or bottom reflood, including treatments for clad oxide fracturing and accompanying enhanced hydrogen generation. There are two main classes of phenomena to be considered: hydrodynamic and heat transfer aspects, and clad mechanical and chemical effects. Briefly, the motion of the quench front in both top and bottom reflood is controlled by heat transfer to the cladding in a small region near the quench front. Countercurrent flow limitations can have an effect on top flooding at high flooding rates. The quench phenomena will be modeled in simplified fashion by using a parametric model to describe the quench front motion together with a countercurrent flow relation for top flooding. The quench model is a one- or two-dimensional heat transfer solution for the rewetting near the quench front, which has two or three parameters (depending on the model) that must be determined experimentally. Typically, there are two regions considered near the quench front: the dry, unwetted region below the quench front, and the boiling region directly behind the quench front. The effect of precursor cooling by droplets falling ahead of the quench front is generally unimportant and is ignored The proposed model for top flooding is a two parameter, two region model in which the wetside heat transfer coefficient and the sputtering temperature must be specified from experimental data for best accuracy.

Clad effects that have been noted in recent bottom flooding experiments (CORA and QUENCH) include transient oxidation due to splitting of the protective oxide layer on the clad and spalling of the oxide layer. Both effects occur due to thermal stress transients, and are likely to occur under top flooding conditions also. A parametric model of clad oxide layer is currently envisioned. The basic clad effect in reflood is the clad oxide cracking, caused by thermal transients, and the resulting burst of hydrogen and increased clad temperature from the increased oxidation. This effect can be modeled fairly simply as an increase in exposed clad surface area triggered by the quench or by an effective increase in the diffusion of steam through the fractured oxide shell as reflected in the oxidation correlation. Although there is only one clad node in the MELCOR clad model and hence no radial thermal gradient, sufficient information to trigger the cracking model can be obtained from the initial hot clad temperature, the quench front temperature and position, and the clad and clad oxide geometry and material properties. Experimental information from the QUENCH program will be used to establish appropriate parameters for the model.

Iodine Aqueous Chemistry

The possible release of iodine has always played a significant role in the regulation of nuclear reactors. In the past, it was specified (TID-14844) [8] that iodine would be released to the reactor containment as a gaseous species, and that one quarter of the initial core inventory would remain in the containment atmosphere. The iodine within the containment atmosphere would then be available to pass through containment leak paths to the environment and generate a dose and public consequence.

Research over the last 15 years has shown it to be more likely that most of the iodine will be released to the containment atmosphere as aerosol particles containing metal iodide such as CsI. The Revised Accident Source Term (NUREG-1465) [9] specifies that at least 95% of the iodine reaching the containment is in aerosol form. The containment will contain substantial quantities of water that can trap aerosol particles during severe accidents. For example, the condensation of steam formed during the core degradation processes will take place to a large extent within the containment. In addition, engineered safety systems such as sprays and suppression pools are effective mechanisms for scrubbing aerosol particles from the system and trapping them in the aqueous phase.

Trapping of most radionuclides in water, typically within a day, effectively removes them from further consideration in the analysis of the public consequences of reactor accidents. However, radioactive iodine is different. The removal processes are still effective, but there are important mechanisms that can regenerate gaseous forms of iodine that will release into the containment atmosphere from water pools. This will make iodine available for release to the environment for long times after the accident initiation.

The chemical reactions between iodine and water in this radioactive environment can lead to the formation of a variety of chemical forms of iodine, such as elemental iodine and volatile organic iodides. The formation of volatile forms of iodine in solution is dependent not only upon the dose rate to the aqueous phase but also on the temperature, the hydrogen ion concentration (conventionally expressed as pH), and the total iodine concentration. This process is followed by a partitioning of the iodine between the pool and atmosphere. It has been shown experimentally that large fractions of the iodine released from the reactor core can be expected to reside within the containment atmosphere in a volatile form when pH is not controlled to an alkalinity level greater than 7 [Soffer, 95]. It has also been observed that irradiation-induced release of acids from the wall surface coatings, cable insulation, and the containment air lowers the pH [10].

Currently, MELCOR considers iodine only as it is released from the fuel as I or CsI. A model is currently under development to allow many more iodine chemical species to be tracked within the containment atmosphere, pools, and sumps. The model will allow for a prediction of the partitioning of iodine species between pools and the atmosphere under radiation conditions inside the containment and a means to quantitatively predict the amount of volatile iodine that could be released from the containment. It will also include the possibility to manage the pH of water pools and sumps by addition of buffers in order to consider the benefits of maintaining alkaline sump conditions and reducing volatile iodine concentrations in the containment.

In the containment atmosphere, where gas phase behavior is important, the general aerosol and vapor behavior will continue to be treated by existing MELCOR models. These include the aerosol dynamics model, MAEROS. Additional phenomena that will be modeled are:

- radiolysis of the air and of cable insulation to generate nitric acid and hydrochloric acid, respectively, and
- reactions involving different paints on structural surfaces.

In the water pool, where liquid phase behavior is important, the new model will:

- determine the pool pH based upon cation hydrolysis, dissolved carbon dioxide, and the user controlled boric acid and phosphate buffering,
- include the effects of the acids introduced from the containment atmosphere due to radiolysis,
- consider the effects of methane and of the iron and control rod silver released by the accident scenario chosen, and
- determine the concentrations of volatile iodine species in the pool.

Transport of the new species across interfaces (atmosphere-to-pool and -to-water-film), with water films, and with flows between volumes will be treated in analogy with existing MELCOR models for aerosols and vapors. Binding of iodine in non-volatile form on surfaces will be treated in analogy with the existing chemisorption model.

Core Degradation and Materials Interactions Modeling Improvements

MELCOR was originally conceived as a PRA code that would use simplified—often parametric—models where possible, in the interests of reducing computer execution times. This was intended to facilitate the performance of large numbers of sensitivity studies. Over the past decade, however, actual applications of the code have tended to emphasize its capability to provide near-best-estimate predictions that include coupling of a wide variety of phenomena, typically in situations where severe core damage might occur.

As a result, modeling has been steadily upgraded in many areas. However, improvements in the core response (COR) package are now encountering limits imposed by the original simplifications in the representation of the core. We have already undertaken or anticipate undertaking several tasks that will require improving the underlying representation of a reactor core.

The material fields represented in MELCOR's COR package include intact components (fuel pellets, cladding, BWR canisters, and "other structures") and particulate debris (rubble) created when intact components lose their original geometry and collapse. A composition and an average temperature is tracked for each field in each cell of the COR package nodalization. There is currently only one "other structure" field that must be used—with variations of properties—to represent core support plates, control rods (in PWRs) or blades (in BWRs), and any and all other physical structures that an analyst chooses to model within the COR package. Only one such structure can be represented in any computational cell.

We are currently finishing a generalization that allows separate representation of two distinct types of other structures. One, with the capability to support other objects, will be used in the modeling core structures such as BWR control blades and guide tubes. The other, with no such capability, will be used to represent other structures without such support properties, such as PWR control rods. These may coexist in a single COR cell, and the characteristics of each may vary from cell to cell.

In addition to the main material fields, there is a tracking of "conglomerate debris": molten and/or refrozen materials that my reside on the surfaces of any of the intact components (with the exception of fuel pellets) and particulate debris. There are two essential simplifications in the current treatment: (1) such conglomerate is assumed to be in thermal equilibrium with the underlying component, so that no separate energy equation must be solved, and (2) all conglomerate associated with a component is treated as equivalent, making it unnecessary to distinguish that on the inside of the cladding or BWR canister from that on the outside.

The first simplification limits the ability of the candling model to accurately predict the distance that molten materials can candle before they refreeze. We are considering the possibility of including additional dynamic energy equations to better capture the freezing behavior. The second interferes with proper application of the existing materials interactions ("eutectics") models. In particular, interactions between

Zircaloy and UO_2 on the inside of the cladding cannot be properly separated from interactions with Inconel grid spacers and/or control materials on the outside of the cladding. A similar problem arises with differing interactions on the inside and outside of BWR canisters. We are considering the possibility of tracking more distinct conglomerate fields to correct this.

Finally, while the thermalhydraulic models can fully distinguish the channel and bypass regions (inside and outside of canisters) in a BWR, the COR package is currently unable to do so because it considers only a single particulate field in each COR cell. This deficiency will be corrected by the addition of a new material field to represent separately the particulate debris in the bypass region of a BWR..

REFERENCES

[1] Gauntt, R.O., R.K. Cole, et al., "MELCOR Computer Code Manuals,"NUREG/CR-6119, Rev.1, to be published, 1998.

[2] El-Genk, M.S. and Z. Guo, "Transient Critical Heat Flux for Inclined and Downward-Facing Flat Surfaces," ANS Proceedings, HTC-6 Volume 6, National Heat Transfer Conference, San Diego, August 9-12, 1992.

[3] Makynen, et al., "AHMED Tests on Hygroscopic and Inert Aerosol Behavior in LWR Containment Conditions," VTT Aerosol Technology Group Report No. 1/95, Finland, 1995.

[4] Firnhaber, M., et al., "International Standard Problem ISP-37," OECD/GD(97)16, GRS-137, 1996.

[5] Pruppacher, H. R. and J. D. Klett, "Microphysics of Clouds and Precipitation," D. Reidel Publishing Company.

[6] Krischer, W., and M.C. Rubinstein, The PHEBUS Fission Product Project, ISBN 1-85166-765-2, Elsevier Applied Science, New York, 1992.

[7] Hagen, S., et al., "Results of SFD Experiment CORA-13," KfK 5054, 1993.

[8] DiNunno, J.J., F.D. Anderson, and R.L. Waterfield, "Calculation of Distance Factors for Power and Test Reactor Sites," USAEC, TID-14844, 1962.

[9] Soffer, L., S.B. Burson, C.M. Ferrel, R.Y. Lee, J.N. Ridgely, "Accident Source Terms for Light Water Nuclear Power Plants," NUREG-1465, 1995.

[10] Beahm, E.C., R.A. Lorenz, and C.F. Weber, "Iodine Evolution and pH Control," NUREG/CR-5950, TI93-005714, 1992.

DYNAMIC BENCHMARKING PROGRAM FOR THE MAAP4 CODE

Robert E. Henry, Chan Y. Paik, Barbara J. Schlenger-Faber
Christopher E. Henry, Michael A. McCartney
Fauske & Associates, Inc.

Jason Chao
Electric Power Research Institute

ABSTRACT

Computer simulation of nuclear power plant response can be a full-scope control room simulator, an engineering simulator to represent the general behavior of the plant under normal and abnormal conditions, or the modeling of the plant response to conditions that would eventually lead to core damage. In any of these, the underlying foundation for their use in analyzing situations, training of vendor/utility personnel, etc. is how well they represent what has been known from industrial experience, large integral experiments and separate effects tests. Typically, simulation codes are benchmarked with some of these; the level of agreement necessary being dependent upon the ultimate use of the simulation tool. However, these analytical models are computer codes, and as a result, the capabilities are continually enhanced, errors are corrected, new situations are imposed on the code that are outside of the original design basis, etc. Consequently, there is a continual need to assure that the benchmarks with important transients are preserved as the computer code evolves. Retention of this benchmarking capability is essential to develop trust in the computer code.

Given the evolving world of computer codes, how is this retention of benchmarking capabilities accomplished? For the MAAP4 codes this capability is accomplished through a "dynamic benchmarking" feature embedded in the source code. In particular, a set of dynamic benchmarks are included in the source code and these are exercised every time the archive codes are upgraded and distributed to the MAAP users. Three different types of dynamic benchmarks are used:

- plant transients,
- large integral experiments, and
- separate effects tests.

Each of these is performed in a different manner. The first is accomplished by developing a parameter file for the plant modeled and an input deck to describe the sequence; i.e. the entire MAAP4 code is exercised. The pertinent plant data is included in the source code and the computer output includes a plot of the MAAP calculation and the plant data.

For the large integral experiments, a major part, but not all of the MAAP code is needed. These use an experiment specific benchmark routine that includes all of the information and boundary conditions for performing the calculation, as well as the information of which parts of MAAP are unnecessary and can be "bypassed".

Lastly, the separate effects tests only require a few MAAP routines. These are exercised through their own specific benchmark routine that includes the experiment specific information and boundary conditions. This benchmark routine calls the appropriate MAAP routines from the source code, performs the calculations, including integration where necessary and provide the comparison between the MAAP calculation and the experimental observations.

I. INTRODUCTION

Integral reactor safety computer codes include representations of numerous phenomena, each of which should be benchmarked with available experiments and plant experience. Previously, this has generally been performed at various stages in the code or module development, but not necessarily repeated for new versions/revisions. This means that the benchmark fidelity is potentially eroded as additional capabilities are added, errors corrected, etc. Therefore, it is increasingly important that the benchmarking for complex analytical tools be integrated into the code so the benchmarks are continually updated. Through this process, developers and users can continually examine the benchmarks to assure code capabilities are maintained. In particular, each officially released, archived version should be tested against the experimental database formed by major experiments and industrial experience. For these exercises to be repeated on a regular basis, it is necessary to integrate the information, including the experimental observations, directly into the integral code software. MAAP4 accomplishes this by creating three types of benchmarks (plant experience, integral experiments and separate effects tests) supported by the necessary documentation in the User's Manual with experimental specific benchmark routines integrated directly into the code.

II. THE MAAP4 APPROACH TO DYNAMIC BENCHMARKING

In MAAP4, the dynamic benchmarking capability is integrated into the source code. This includes the three types mentioned above with the plant experience exercises using the entire code and the other two being controlled through the executive subroutine BENCH. These are accomplished as follows:

- Plant Experience: A plant parameter file (plant geometry), is used with an input deck to represent operator actions and specific plant responses (such as scram) when the particular timing is known. With this, MAAP4 is exercised for the particular sequence and compared with the plant data. This "sequence definition" (input deck) and the transient plant data becomes part of the MAAP4 software and is incorporated into the test matrix to be examined for all versions/revisions.

- Integral Experiments Benchmarking: Tests like CORA and HDR exercise a significant part, but not all, of the MAAP code. The executive subroutine BENCH organizes the benchmarking activities and calls subroutine BENCH1 which contains the pertinent CORA and HDR experimental information. Figure 1 illustrates this organization of the benchmark specific routines. For example, the HDR benchmarks include a parameter file for the containment, the test injection history and the transient data for comparison with MAAP. Furthermore, some aspects of MAAP are not required, i.e. primary system (HDR). In this case, the unnecessary MAAP routines are bypassed and the remainder are used. Through this organization, those routines used for plant evaluations are tested directly as opposed to using a similar stand alone code that may not be current with the complete code. This benchmark is also included in the testing matrix.

- Separate Effects Tests: These exercises involve only limited parts of MAAP. Subroutine BENCH calls benchmark specific routines which in turn call the appropriate MAAP routines (Figure 1). Here again the MAAP routines are tested directly, but the testing is more limited than the entire MAAP code. These benchmarking activities are also included in the source code.

Such dynamic benchmarks should be performed using the uncertainty boundaries for the various model parameters. Typically, large integral computer codes that characterize the plant and containment response contain numerous individual models, some are influential and some are of minor importance. However, each model parameter should have a characterization of "optimistic" and "pessimistic" values for the individual parameters and these benchmarking exercises can be used to help determine these values. Furthermore, a technical basis should be developed and documented for these boundaries, i.e. what experiments or experiences have been used (benchmarked) to develop these boundaries. Of course, such evaluations should be current with the available experimental observations. "Optimistic" parameters represent uncertainty bounds for physical processes that would (a) slow the accident progression, (b) increase the rate of recovery of the damaged core and/or decrease the consequence of an accident. "Pessimistic" boundaries are those that would (a) increase the rate of the accident progression, (b) slow the recovery rate of a damaged core and/or increase the consequences of an accident. It is realized that some processes may be difficult to characterize in this light, thus some may need to be evaluated two different ways. However, these are typically processes not dominant in the accident progression.

III. RESULTS FOR THE PLANT TRANSIENT BENCHMARKS

Table 1 lists the plant transients currently being included as MAAP4 dynamic benchmarks. These include PWR and BWR designs as well as short transients, such as the Peach Bottom turbine trip tests and others which evolve over an extended interval, e.g. the Brown's Ferry fire

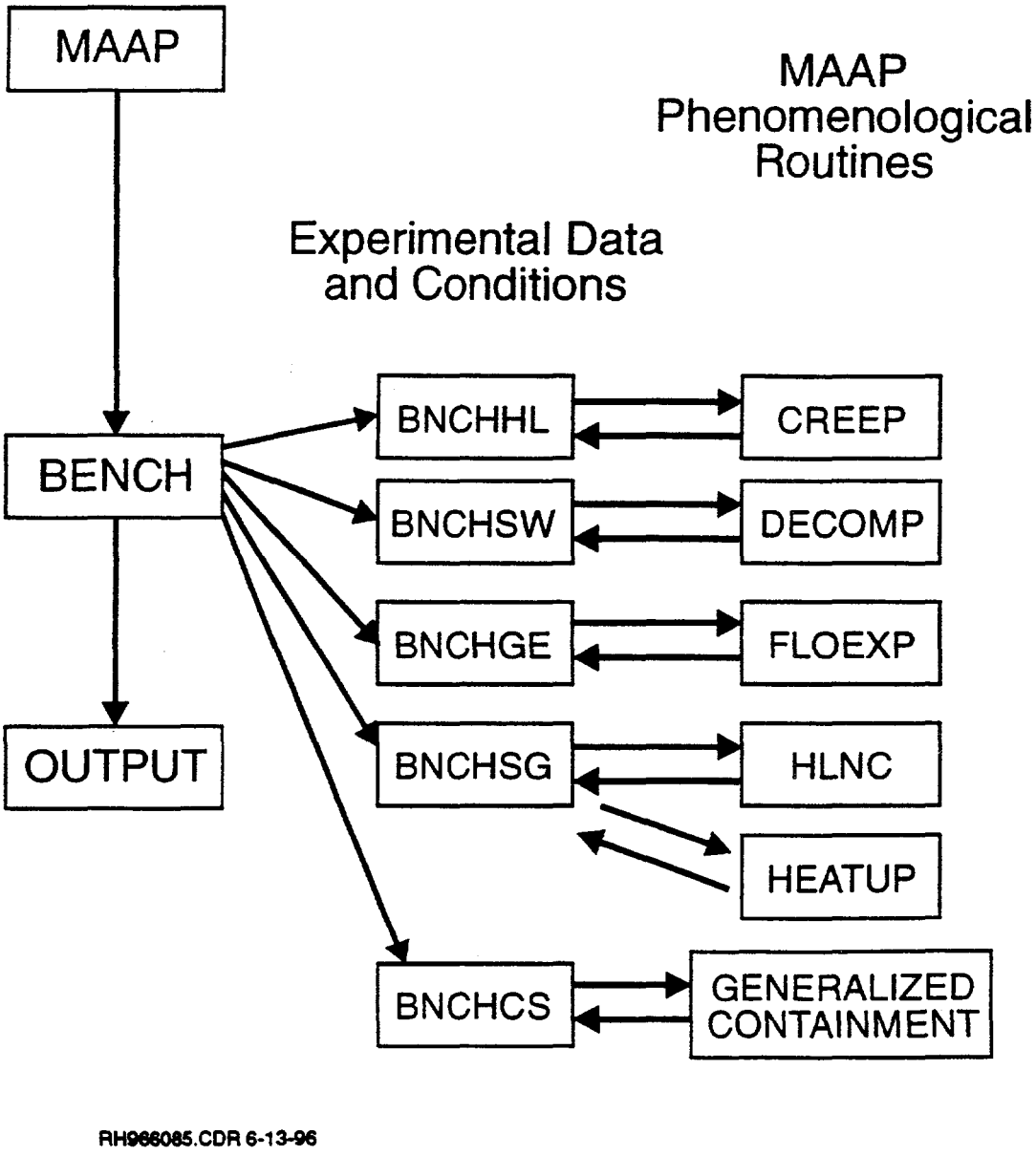

Figure 1 Strategy for incorporating separate effects tests in the MAAP4 code.

and the TMI-2 core damage accident. Since the TMI-2 benchmark has been recently published (Paik et al., 1995), we will focus on others to illustrate the MAAP4 approach.

Table 1
Plant Experience Benchmarks

- TMI-2 accident (PWR).
- Oyster Creek loss-of-feedwater (BWR).
- Crystal River loss-of-feedwater and stuck open PORV (PWR).
- Peach Bottom turbine trip tests (BWR).
- Tokai-2 turbine trip (BWR).
- Davis-Besse loss-of-feedwater (PWR).
- Brown's Ferry fire (BWR).

The Oyster Creek loss-of-feedwater event is an interesting example since this transient invokes the use of the two isolation condensers in this design. Hence, this provides a means of assessing both the RCS and the isolation condenser models in MAAP4. In this transient, feedwater was lost to the RPV and the operators initiated RPV heat removal using the A and B isolation condensers. The MAAP4 benchmark is performed using an Oyster Creek parameter file and the input deck (describing the operator actions), some of which are listed in Table 2. Actions such as activating the isolation condenser are straightforward in MAAP. Figure 2 shows the RPV pressure (2a) and water level (2b) during this transient and that the actions were effective, as well as the MAAP4 results corresponding with the measured response. This agreement is seen for those conditions in which the isolation condensers are not active, when a single unit is activated and when both A and B units are in service. As discussed previously, such benchmark analyses are performed with the "optimistic" and "pessimistic" bounds of the uncertainty parameters used for the physical models in MAAP, but these typically characterize the behavior after the core is uncovered. Since there is little difference between the two boundaries for these analyses, only best estimate values were used.

The Crystal River transient resulted from an instrument and control system electrical malfunction (Brown et al., 1981) causing the Integrated Control System (ICS) to stop feedwater to the steam generators. Eventually the reactor core was cooled by using high pressure injection, but the pressurizer Power Operator Relief Valve (PORV) opened prematurely and remained open. To assure that the core was adequately cooled, the operators continued to inject water to the RCS. The core was cooled down and stabilized as a result of this injection.

The Crystal River dynamic benchmark is performed using a modified (to represent Crystal River specific values) TMI parameter file with the operator actions characterized for the MAAP input deck, an example of which is shown in Table 3. As with the Oyster Creek input deck, the

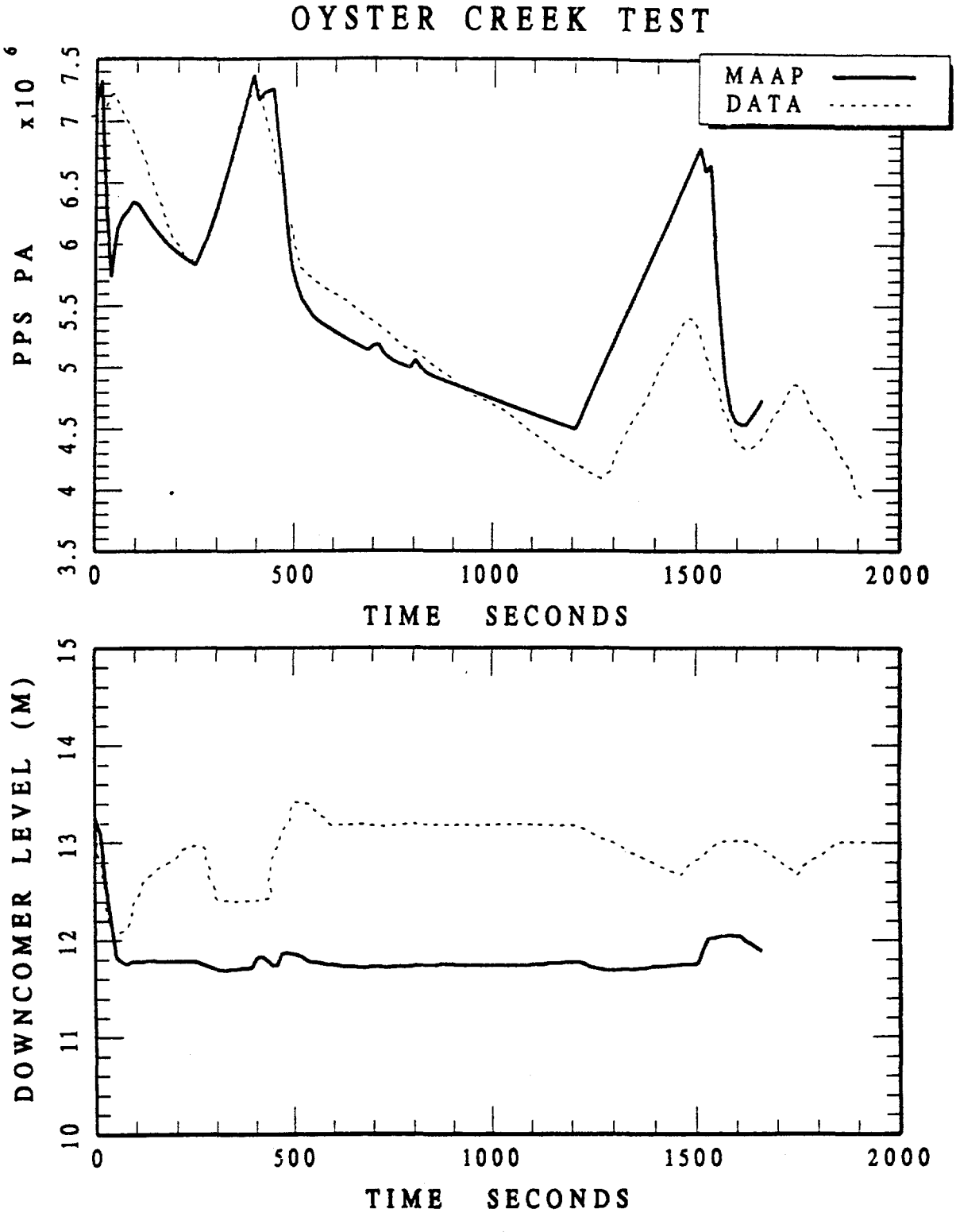

Figure 2 Transient pressure and downcomer water level for the Oyster Creek loss-of-feedwater event.

Table 2
Oyster Creek Loss-of-Feedwater Event

```
START TIME IS 0. SEC

END TIME IS 1910. SEC

INITIATORS
  REACTOR MAN SCRAMMED
END

IF TIM > 2.
  TURBINE STOP VALVE CLOSED
END

IF TIM > 13.
  FEEDWATER MAN OFF
  AJET = 0.05*AJET
END

IF TIME > 43.
  MSIVS LOCKED CLOSED
END

IF TIM > 76.              ! ISOLATION CONDENSER B STARTED
  AGO(3) = 0.041
END

IF TIM > 250.             ! B ISOLATION CONDENSER TURNED OFF
  AGO(3) = 0.0
END

IF TIM > 450.             ! BOTH ISOLATION CONDENSERS TURNED ON
  AGO(3) = 0.041
  AGO(2) = 0.041
END

IF TIM > 528.             ! B ISOLATION CONDENSER TURNED OFF
  AGO(3) = 0.0
END
```

Table 3
Crystal River Unit 3 Incident

```
START TIME IS 0. SEC
END TIME IS 800. SEC
PRINT INTERVAL IS 20.SEC

INITIATORS
END

IF TIM GE 10.
  UNBKN LOOP TURBINE DRIVEN AFW:  NOT MAN ON
  BKN LOOP TURBINE DRIVEN AFW:  NOT MAN ON
  MOTOR-DRIVEN AUX FEED WATER FORCED OFF
  PZR HTRS FORCED OFF
  ISTUCK(1)=1
  HPI FORCED OFF
  LPI FORCED OFF
END

IF TIM GE 15.
  WFWMX = 1.D0
END

IF TIM GE 34.
  KEEP MAIN FEED ON AT SCRAM
  MANUAL SCRAM
  S/G MSIV:  FORCED CLOSED
END

IF TIM GE 220.
  UNBKN S/G PORV OPENED MANUALLY
  HPI SWITCH NO FORCED OFF
  HPI SWITCH:  MAN ON
  MCP SWITCH OFF OR HI-VIBR TRIP
  WFWMX = 6.7D5          !NSAC/15
  TFW = 400.             !NSAC/15
  ZWCTLU = 0.01
  ZWCTLB = 30.
END
```

representations needed for the operator actions are straightforward and easily characterized by the MAAP4 input. Both the parameter changes to the TMI parameter file and the operator action characterizations are a permanent part of the MAAP4 source code. Figure 3a compares the MAAP4.0.2 calculated RCS pressure with the plant data, the depressurization resulting from the LOCA and injection and the subsequent repressurization because the pressurizer was filled with water. Figure 3b compares the measured hot leg temperature with the MAAP calculation for several of the temperatures including the core average temperature (TWCR) and the water temperature entering steam generators (TSGBHP). As shown, there is general agreement between the pressure and temperature responses for this dynamic transient.

Another plant benchmark is the Davis-Besse loss-of-feedwater event (NRC, 1985). In response to this event, the control room operators used a startup feedwater pump to restore secondary side cooling. For the MAAP4 benchmark, the TMI-2 parameter file is modified to represent the pertinent differences for the Davis-Besse design. Table 4 lists some of the MAAP4 characterization of the operator actions detailed in the report describing the event. As with the TMI-2 benchmark, the steam generator levels and pressure are input as boundary conditions. The subsequent RCS response is determined by the MAAP4 models. Given this approach, the resulting RCS pressure, temperature and pressurizer level are illustrated in Figure 4. As with the previous benchmark activities, this illustrates that the MAAP code represents the general behavior of the reactor coolant system and is in agreement with the measured values. Like the other dynamic benchmarks, the modifications to the TMI parameter file and the list of pertinent operator actions in Table 4 becomes a permanent part of the MAAP4 archived code such that this comparison can be repeated with subsequent code versions.

IV. INTEGRAL EXPERIMENT BENCHMARKS

Several large scale experiments (Table 5) which have been performed illustrate the integral response of certain aspects of the reactor/containment behavior during different plant transients. An excellent example of a large integral experiment are the large scale containment tests in the HDR facility (Wolf and Valencia, 1989, Valencia and Wolf, 1990). Different types of loss of coolant accidents were investigated, some having the steam discharge (blowdown) into the lower regions of the containment while others were configured with the discharge into the upper regions. As a result, this set of experiments provides benchmarks for integral computer codes with regard to significant containment phenomena such as stratification in the upper regions. For one experiment (E11.2), hydrogen and helium were injected to represent the conditions that could be experienced if the core were sufficiently overheated that the Zircaloy cladding was oxidized.

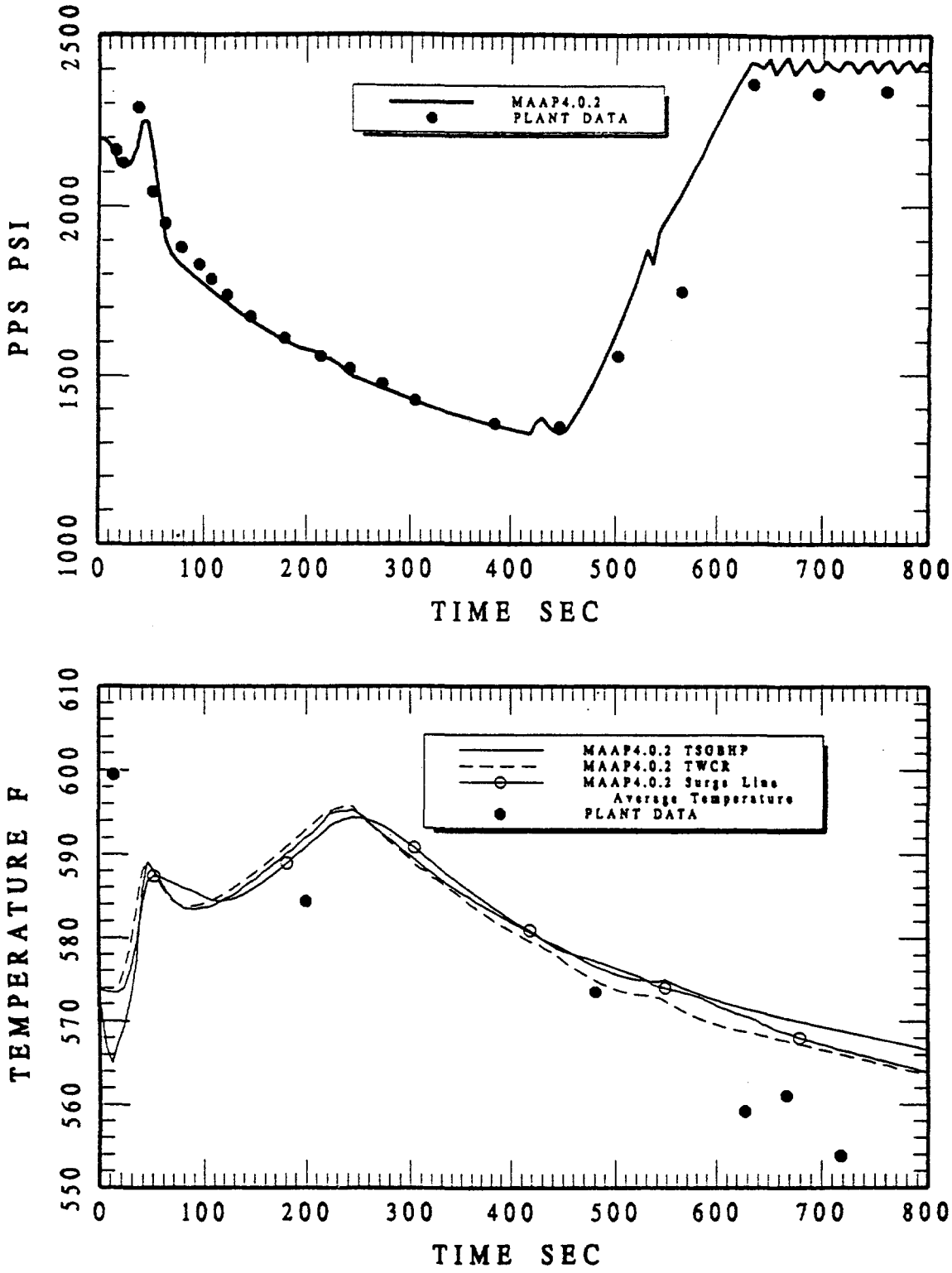

Figure 3 RCS pressure and hot leg temperature response for the Crystal River loss-of-feedwater event.

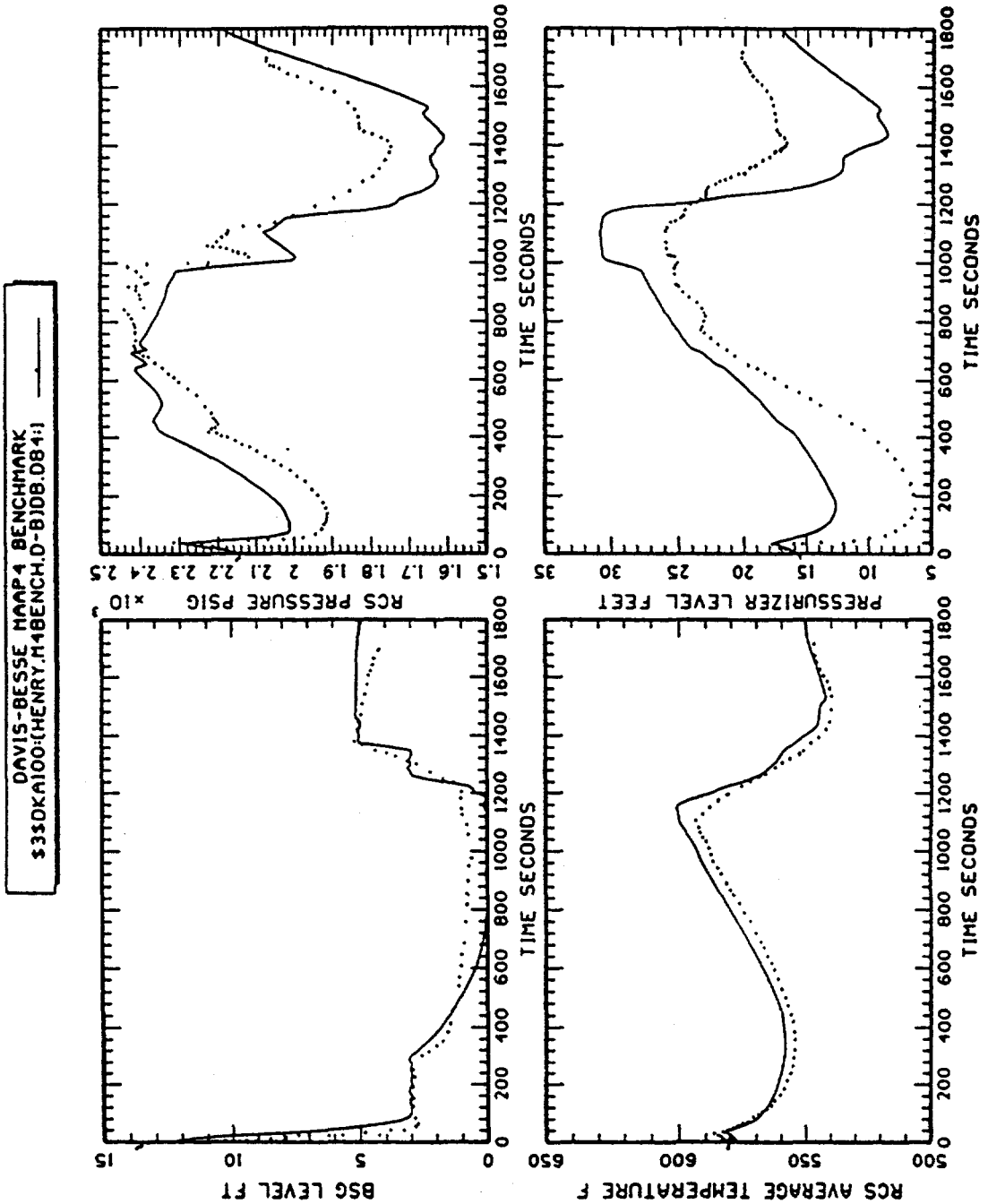

Figure 4 Davis-Besse loss-of-feedwater event (June 1985).

Table 4
Davis-Besse Loss-of-Feedwater Event

```
INITIATORS
  DONT SCRAM WHEN CHARGING PUMP ON
  PS MAKEUP ON
END

IF TIM GE 1.5 S                          !1:35:01
  QCR0 = 8.42E09                         !POWER RUNBACK INITIATED
END                                      !AVG POWER BETWEEN 1 AND 3 SECS

IF TIM GE 3. S                           !AVG POWER BETWEEN 3 AND 5 SECS
  QCR0 = 8.3E09
END

IF TIM GE 5. S                           !AVG POWER BETWEEN 5 AND 10 SECS
  QCR0 = 8.05E09
  WFWMX = 2.83E06
END

IF TIM GE 10. S                          !AVG POWER BETWEEN 10 AND 15 SECS
  QCR0 = 7.69E09
END

IF TIM GE 15. S                          !AVG POWER BETWEEN 15 AND 21 SECS
  QCR0 = 7.304E09
END

IF TIM GE 21. S                          !AVG POWER BETWEEN 21 AND 30 SECS
  QCR0 = 6.77E09
  PZR SPRAYS AUTOMATIC ON/OFF
  PZR SPR MAN ON
END
```

Table 4 (Continued)
Davis-Besse Loss-of-Feedwater Event

```
IF TIM GE 30. S                          !1:35:30
  KEEP MAIN FEED ON AT SCRAM
  CHARGING PUMP SWITCH:  MAN ON
  MANUAL SCRAM
  LETDOWN SWITCH OFF
  PS MAKEUP ON
  ZWPZMU = 21. FT
  ZDEADB = 0.1
  ZDEADU = 0.1
  ZWCTLB = 3.0 FT
  ZWCTLU = 2.5 FT
END

IF TIM GE 35. S
  S/G MSIV:  FORCED CLOSED
END

IF TIM GE 45. S                          !1:35:45
  PZR SPR AUTO
  PZR SPRAYS FORCES OFF
  TFW = 400. F
END

IF TIM GE 150. S
  TFW = 300. F
END

IF TIM GE 300. S                         !1:41:08 FEEDWATER LOST
  ZWCTLB = 1.5 FT
  ZWCTLU = 1.5 FT
  TFW = 200. F
END

IF TIM GE 420. S                         !1:42:00
  ZWCTLB = 0.0 FT
  ZWCTLU = 0.0 FT
  PZR SPRAYS AUTOMATIC ON/OFF
  PZR SPR MAN ON
```

Table 5 Integral Test Benchmarks
• HDR Tests • CSTF Tests • EPRI/Westinghouse Steam Generator Tests • Westinghouse Ice Condenser Tests

To perform this benchmark, a parameter file was developed to describe the HDR containment compartmentalization (Figure 5), the flow junctions between rooms, the heat sinks in each room, etc. (Lee et al., 1997). Parameter file information also included the steel dome, that was externally cooled (late in time) during the E11.2 experiment, and the concrete liner on the inside of the steel shell for the lower containment elevations. This low conductivity liner effectively insulates against energy transfer through the steel wall in the lower regions. Figure 6 illustrates the comparison of the MAAP calculation for the one day E11.2 transient, including the duration of the steam injection period (approximately 45,000 seconds), H_2/H_e injection for 30 minutes, steam injection period into lower elevation from 47,000 to about 57,000 seconds, and the response when the external spray was initiated. As illustrated, there is some difference between the actual pressure and that calculated by the MAAP4 code, yet the general transient behavior is well represented by the MAAP model. Figure 7a illustrates the measurements of hydrogen and helium in the containment upper dome, and 7b shows these measurements for the dead-end rooms approximately mid-height of the containment. MAAP4 calculates hydrogen stratification in the containment dome and also closely represents the concentration in other compartments. Moreover, it calculates the rapid increase and subsequent turnover (decrease) of hydrogen concentration in the upper dome when this region is cooled by the external spray. Consequently, this representation of the containment behavior, particularly that associated with the potential for stratification, is well represented by the MAAP4 code. To assure that this important modeling capability is maintained through subsequent versions, this containment nodalization and the injection histories associated with the various HDR tests are integrated into the MAAP4 dynamic benchmarking (source code). Therefore, this can be conveniently tested for future code versions. A similar strategy (input and experimental data files) is used for the ice condenser experiments at the CSTF facility, the EPRI/Westinghouse natural circulation experiments characterizing the core-to-upper plenum and steam generator flows and the Westinghouse experiments for the ice melting rate under Loss-of-Coolant Accident (LOCA) conditions.

V. SMALL SCALE SEPARATE EFFECTS BENCHMARKS

With the extensive list of phenomena represented in the integral code, there are numerous separate effects tests that can be used to benchmark individual models. Since these models typically only use a small number of MAAP routines, it is more convenient to create benchmark

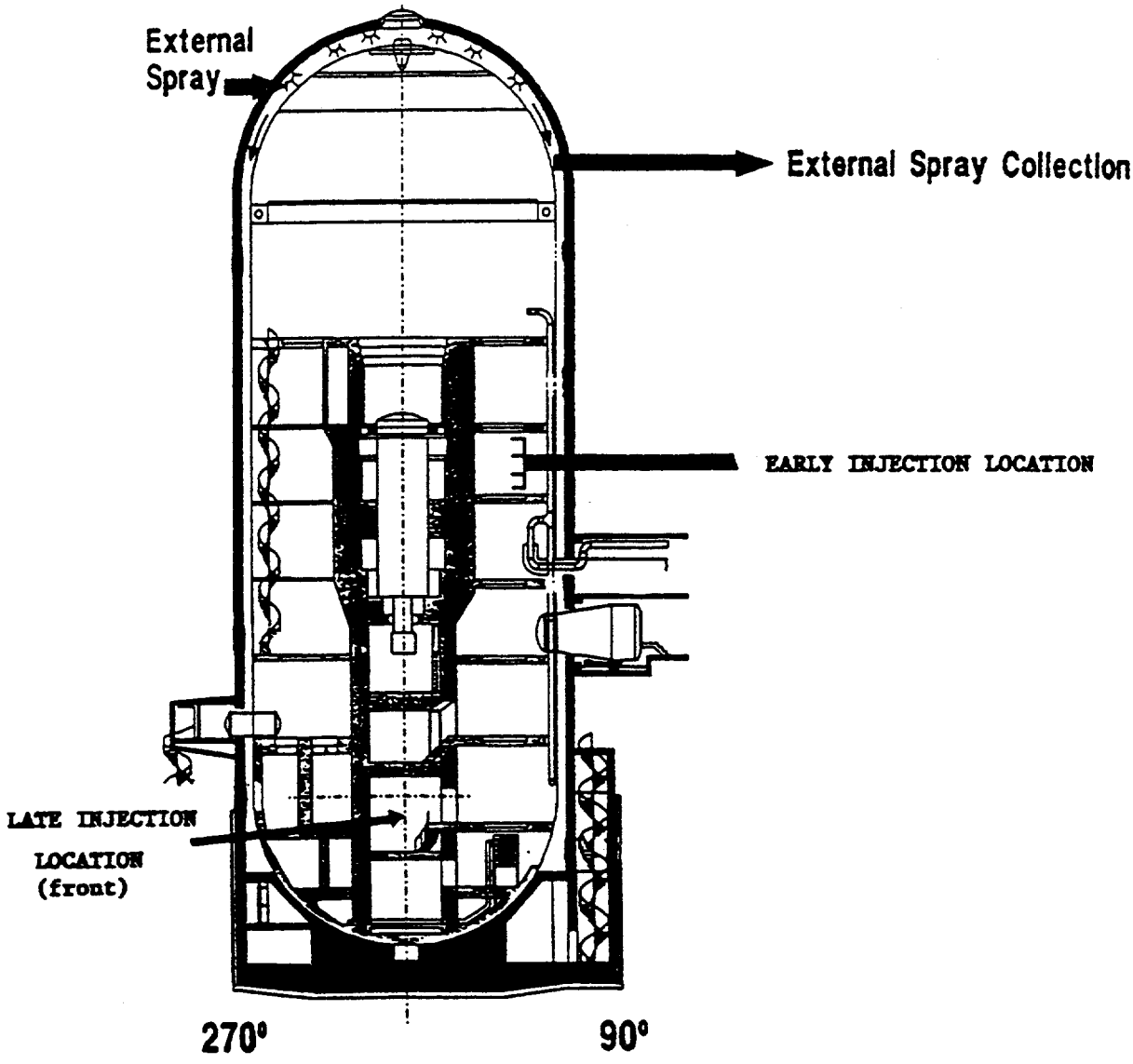

Figure 5 HDR facility with source locations for E11.2.

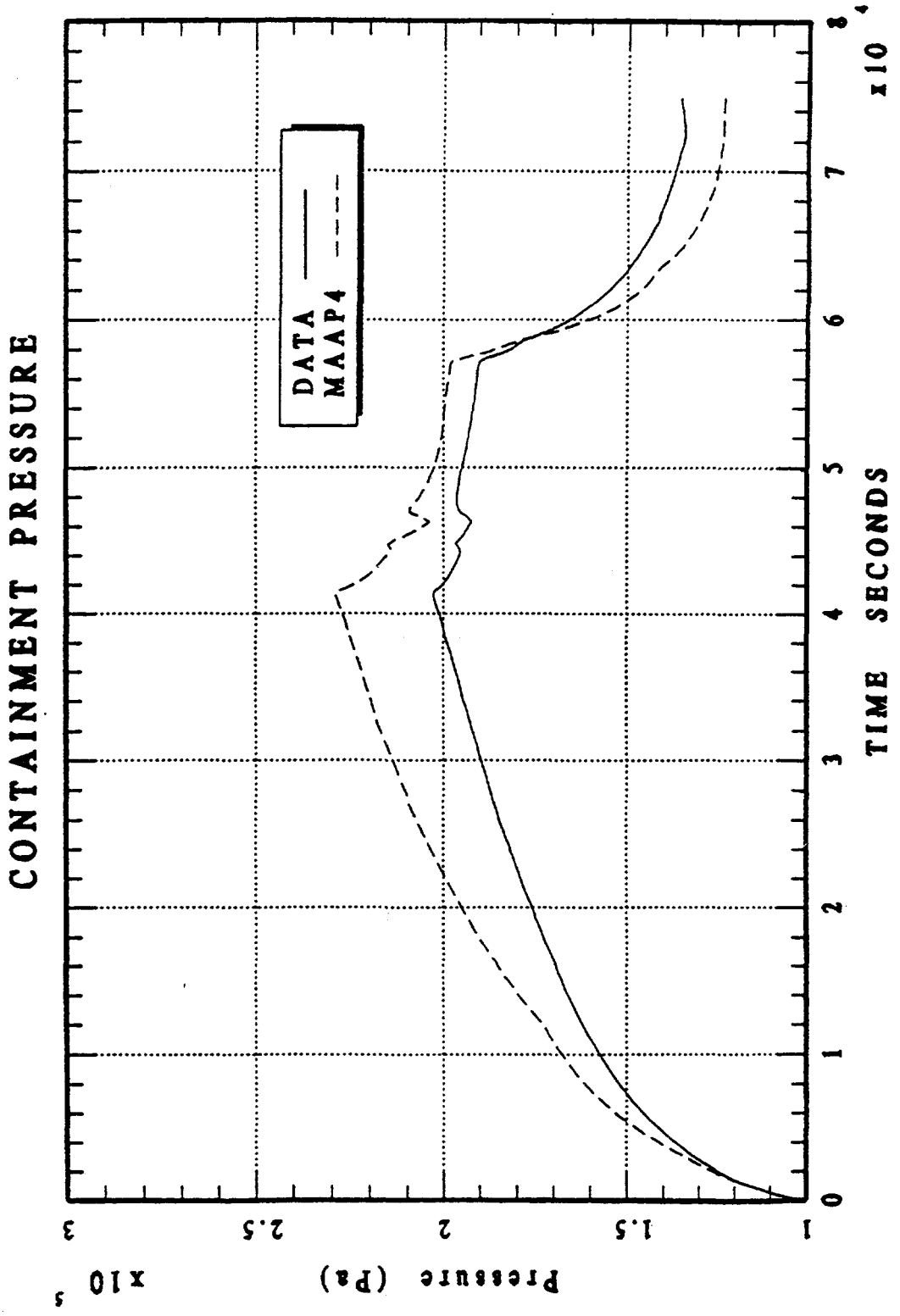

Figure 6 E11.2 containment pressure.

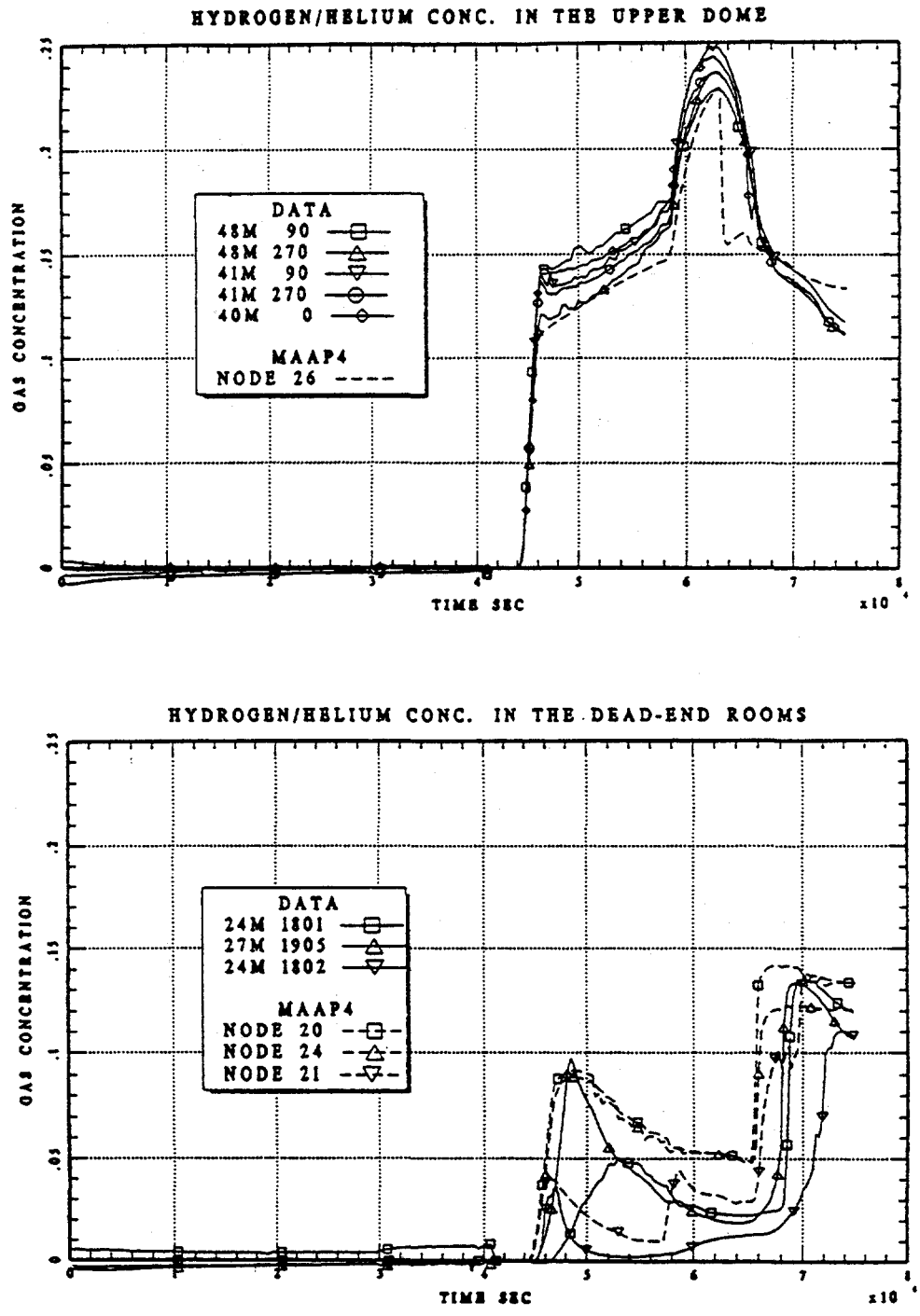

Figure 7 E11.2 hydrogen/helium concentrations in the upper dome (a) and dead-end rooms (b).

specific routines for each separate effects test. As illustrated in Figure 1, benchmark specific routine such as BENCHHL contains all the information for the hot leg creep rupture experiments performed by Maile, et al. (1990), and also carries out the benchmark calculation, including the integration of time dependent behavior while calling the MAAP specific routines, i.e. subroutine CREEP for this specific benchmark. As part of the experimental program, separate effects tests were performed to characterize the creep properties of the hot leg material. Figure 8 compares these properties with the TMI-2 vessel steel creep properties reported by Wolf et al. (1993). It is seen that the properties are almost identical. In this experiment, the hot leg was heated externally and had a significant temperature difference through the wall with the outside surface being the hottest. The time dependent inside and outside temperatures, as well as the internal pressure, are input as boundary conditions for the MAAP calculation. Furthermore, the experimental test apparatus was suspended freely in space, i.e. there were no axial supports. Hence, the total stress was a combination of hoop and longitudinal loadings. Therefore, the MAAP calculations are performed in two ways, the first uses only a hoop stress loading for the steel wall, while the second utilizes the vector addition of hoop and longitudinal stresses, which increases the total stress by 10%. Table 6 shows the results for these two approaches with the MAAP4 calculated failure times bracketing the experimental observation of about 1100 seconds. Thus, the MAAP4' model for evaluating material creep is consistent with the significant scale experiments performed using reactor grade steel. To assure that this calculational behavior is retained in the MAAP structure, this information is integrated into the MAAP software.

Table 6
Comparison of the MAAP4 Model for Creep Rupture With The Full Scale Experiment

Approach I

- Use the measured internal pressure.
- Use hoop stress only.
- Use measured material properties at 700°C.
- Use measured transient surface temperatures.
- MAAP4 calculates a failure time of 1225 secs compared to the observed 1100 secs.

Approach II

- Same as Approach I except that the longitudinal stress is added to the hoop stress as a vector addition. This increases the total stress by 10%.
- MAAP4 calculates a failure time of about 600 secs.

Conclusion: The MAAP4 model is as accurate as the material information given in the reference.

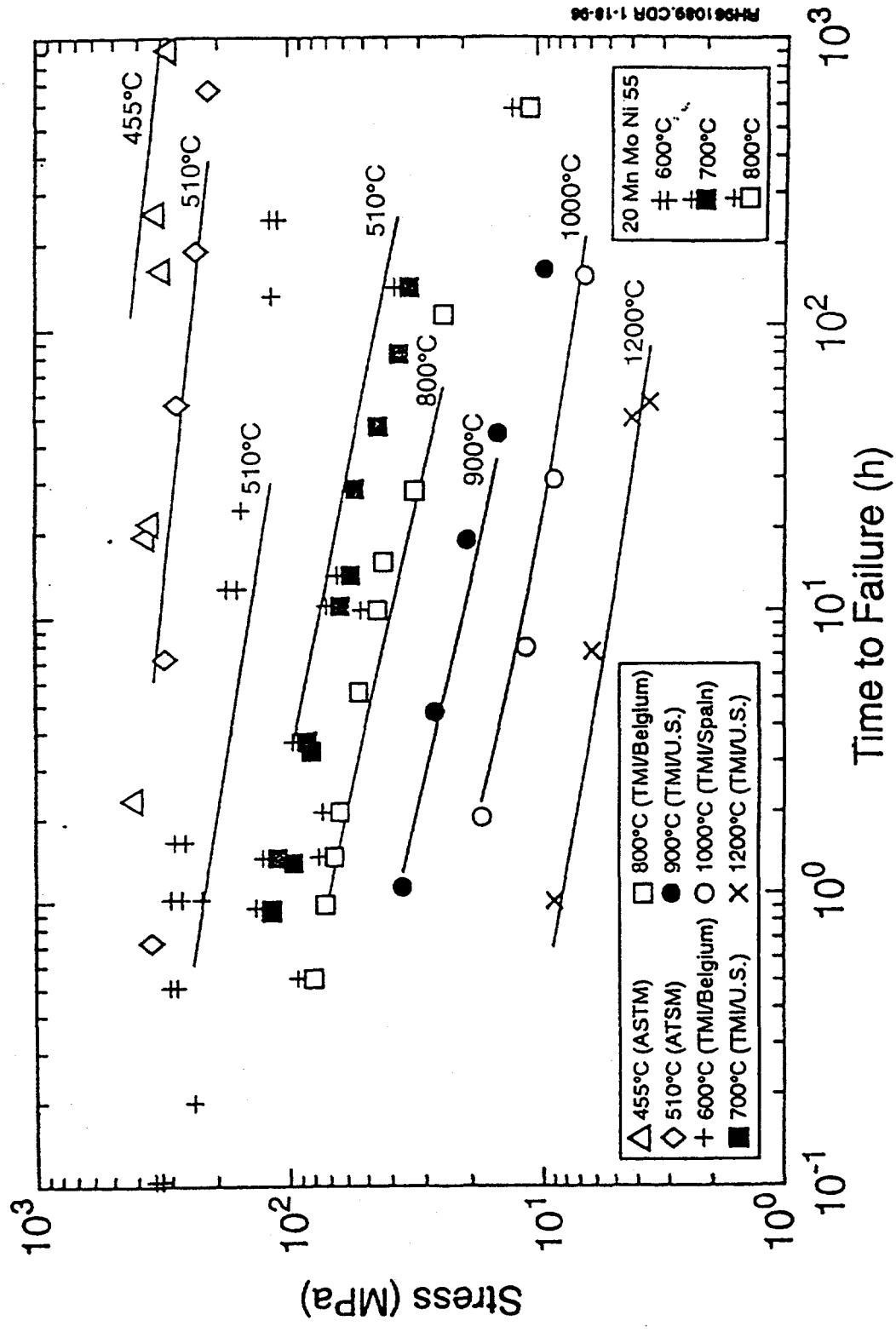

Figure 8 Comparison of TMI-2 vessel steel and 20 MnMoNi 55 for the material creep properties.

VI. CONCLUSIONS

Large integral codes are an important part of the analytical assessment for plant response to a variety of transients, including those potentially leading to severe accidents. As a result, such large computer codes model numerous phenomena having substantial interactions during the transients. Thus, there is a continual need to assess the credibility of individual models, and the combination of models, by testing these with the available experimental information. Furthermore, interactions between these physical phenomena need to be compared to the available large scale integral experiments as well as the plant transients experienced in the nuclear industry.

Because integral analyses are a key part of RCS and containment evaluations, it is essential that these benchmarking activities be repeated on a regular basis, with the most desirable situation being repetition each time a new version is released.

The only way these important benchmarks and their perspectives relative to phenomenological uncertainties can be maintained is to integrate the benchmarking information directly into the integral code software. The MAAP4 code has developed such an approach to cover the various types of benchmarks to be performed. The comparisons shown in this paper illustrate the capability of the MAAP4 code to track plant transients, important integral experiments and separate effects tests. With this approach, these comparisons and the knowledge base represented by the spectrum of large scale and small scale experiments will be maintained and expanded as the MAAP4 code usage continues and grows.

VII. REFERENCES

Brown, W., Caldwell, G., Chexal, B. and Layman, W., 1981, "Thermal Hydraulic Analysis of Crystal River Unit-2 Incident", Nuclear Safety Analysis Center Report NSAC-15.

Lee, S. J. et al., 1997, "Benchmark of the HDR E11.2 Containment Hydrogen Mixing Experiment Using the MAAP4 Code," 12th Proceedings of Nuclear Thermal Hydraulics, 1997 ANS Winter Meeting, Albuquerque, New Mexico, November 16-20, pp. 3-16.

Maile, K., Klenk, A., Obst, V. and Strum, D., 1990, "Load Carrying Behavior of the Primary System of PWRs for Loads Beyond the Design Limits", Nuclear Engineering and Design, Vol. 119, pp. 131-137.

Nuclear Regulatory Commission (NRC), 1985, "Loss of Main and Auxiliary Feedwater Event at the Davis-Besse Plant on June 9, 1985," NUREG-1154.

Paik, C. Y., Henry, R. E. and McCartney, M. A., 1995, "MAAP4.0 Benchmarking With the TMI-2 Experience", Proceedings of the Probabilistic Safety Assessment Methodology and Applications, PSA'95, Seoul, Korea, pp. 673-680.

Valencia, L. and Wolf, L., 1990, "Large-Scale HDR-Hydrogen Mixing Experiments Test Group E11", Paper Presented at the 18th Water Reactor Safety Information Meeting, Rockville, Maryland.

Wolf, L. and Valencia, L., 1989, "Hydrogen Mixing Experiments in the HDR-Facility", 17th Water Reactor Safety Meeting, Rockville, Maryland.

Wolf, J. R., et al., 1993, "TMI-2 Vessel Investigation Project Integration Report", NUREG/CR-6197 TMI V(93)EG10 EGG-2734.

CONTAIN 2.0 CODE RELEASE AND THE TRANSITION TO LICENSING*

K. K. Murata, J. Tills, R. O. Griffith and K. D. Bergeron**
Sandia National Laboratories, Albuquerque, NM

ABSTRACT

CONTAIN is a reactor accident simulation code developed by Sandia National Laboratories under US Nuclear Regulatory Commission (USNRC) sponsorship to provide integrated analysis of containment phenomena, including those related to nuclear reactor containment loads and radiological source terms. The recently released CONTAIN 2.0 code version represents a significant advance in CONTAIN modeling capabilities over the last major code release (CONTAIN 1.12V). The new modeling capabilities are discussed here. The principal motivation for many of the recent model improvements has been to allow CONTAIN to model the special features in advanced light water reactor (ALWR) designs. The work done in this area is also summarized. In addition to the ALWR work, the USNRC is currently engaged in an effort to qualify CONTAIN for more general use in licensing, with the intent of supplementing or possibly replacing traditional licensing codes. To qualify the CONTAIN code for licensing applications, studies utilizing CONTAIN 2.0 are in progress. A number of results from this effort are presented in this paper to illustrate the code capabilities. In particular, CONTAIN calculations of the NUPEC M-8-1 and ISP-23 experiments and CVTR test #3 are presented to illustrate (1) the ability of CONTAIN to model non-uniform gas density and/or temperature distributions, and (2) the relationship between such gas distributions and containment loads. CONTAIN and CONTEMPT predictions for a large-break loss-of-coolant accident scenario in the San Onofre plant are also compared.

1. INTRODUCTION

CONTAIN is a reactor accident simulation code developed by Sandia National Laboratories (SNL) under US Nuclear Regulatory Commission (USNRC) sponsorship to provide integrated analysis of containment phenomena. CONTAIN provides the analyst with the capability to predict nuclear reactor containment loads, radiological source terms, and associated phenomena

*This work was supported by the US Nuclear Regulatory Commission and was performed at Sandia National Laboratories. Sandia is a multiprogram laboratory operated by Sandia Corporation, a Lockheed Martin Company, for the United States Department of Energy under Contract DE-AC04-94AL85000.

**J. L. Tills and Associates, Albuquerque, NM

under accident conditions. The principal purpose of CONTAIN is to provide the USNRC with predictive containment analysis capabilities and to serve as a tool to provide technical information in support of regulatory decisions. The recently released CONTAIN 2.0 code version[1] represents a significant advance in CONTAIN modeling capabilities over the last major code release (CONTAIN 1.12V) in 1993. The principal motivation for many of the recent model improvements has been to allow CONTAIN to model the special features in advanced light water reactor (ALWR) designs. As a result, CONTAIN has been used successfully to model the Westinghouse AP600 containment, for several different types of loss-of-coolant accidents (LOCAs),[2] and to model many of the Westinghouse Large Scale Test (LST) 1/8-scale experiments.[3] CONTAIN has also been successfully used to model the passive safety features of the simplified boiling water reactor (SBWR) design from General Electric.[4]

In addition to the ALWR work, the USNRC is currently engaged in an effort to qualify CONTAIN for more general use in licensing, with the intent of supplementing or possibly replacing traditional licensing codes such as CONTEMPT[5] and COMPARE.[6] CONTAIN represents enhanced modeling capability and reflects the current status in our understanding of containment phenomena.

To qualify the CONTAIN code for licensing applications, a number of studies utilizing CONTAIN 2.0 are in progress. These studies are intended to (1) provide comparisons to previous design-basis-accident (DBA) licensing calculations performed with CONTEMPT and COMPARE, and (2) establish a methodology for use of CONTAIN in a manner consistent with the philosophy of conservatism taken in the USNRC's Standard Review Plan for containment analysis. At this point in time, a series of validation calculations involving DBA experiments has been completed; these include the early General Electric boiling water reactor (BWR) tests,[7] tests utilizing the Carolinas Virginia Tube Reactor (CVTR),[8] and two tests, International Standard Problem (ISP)-16 and ISP-23, in the German HDR facility.[9,10] Other validation calculations involving the NUPEC M-8-1 test[11] and the HDR E11.2 experiment[12] were also done to support the DBA analyses. Calculations of separate effects tests and comparisons to other codes have been performed to validate the CONTAIN approach to heat and mass transfer modeling under both natural and forced convective conditions. CONTAIN 2.0 has also been used to provide comparisons to CONTEMPT calculations for the San Onofre plant, a large dry pressurized water reactor (PWR), and the Grand Gulf plant, a Mark III BWR.

This paper provides a status report on the CONTAIN code qualification activities. In the next section, we provide background information on the code and discuss some of the differences between CONTAIN and traditional licensing codes. In Section 3, we summarize CONTAIN 2.0 calculations of NUPEC M-8-1, CVTR Test #3, and ISP-23 to illustrate (1) the ability of CONTAIN to model non-uniform gas density and/or temperature distributions under stratified conditions, and (2) the relationship between such gas distributions and containment loads. In Section 4, the differences between CONTAIN and CONTEMPT predictions for the San Onofre large break LOCA scenario are also discussed. Finally, Section 5 presents overall conclusions.

2. BACKGROUND INFORMATION

The CONTAIN code, up to and including the CONTAIN 2.0 release,[1] is a best-estimate, control volume code that is capable of handling a variety of fields in each cell, or control volume. These fields can include:

- gaseous atmosphere and any suspended water
- the water pool
- aerosols (including aerosolized water)
- gaseous and aerosolized fission products, and
- dispersed core debris fields from high pressure melt ejection.

Three methods are available for treating liquid coolant carried by the gas. The first or default method is to treat it as homogeneously dispersed, in which case the liquid is carried indefinitely with the gas unless it happens to evaporate. The second is to use the dropout option, in which case any liquid that forms is removed instantaneously to the pool or sump in the same control volume. The third method is intermediate between the other two: suspended water is represented as an aerosol component, in which case water aerosols are assumed to form by condensation and to have behavior governed by the CONTAIN aerosol dynamics models. The most important removal mechanism in the last case is typically gravitational settling.

Sweeping changes have recently been made in the ability of CONTAIN to handle the dynamics of water pools. In versions prior to CONTAIN 1.2, the pool was treated as an explicit field that was not coupled logically to the atmosphere dynamics. For example, the effects of submergence of gas flow paths and of atmosphere heat sinks were not considered, regardless of the degree of filling of the control volume by the pool. Beginning with CONTAIN 1.2 and including CONTAIN 2.0, the gas and water pool fields are treated on the same footing, and the submergence effects discussed above are taken into account. For flow paths, a simple pool-gas flow hierarchy has been implemented to allow sequential processes such as BWR vent clearing to be taken into account, and multiple vents such as those present in the Mark III may now be constructed of standard flow paths. Fully water-solid cells and pool stratification may also be treated in principle.

In addition to the above fields, any number of heat sinks may be modeled within a given control volume, and, if appropriate, the concrete basemat for the water pool may be modeled as well. The heat transfer from the atmosphere to these heat sinks is assumed to be governed by standard Nusselt correlations, and steam condensation on such sinks is assumed to be governed by Sherwood correlations of the same functional form as the Nusselt correlations, subject to appropriate substitutions for the dimensionless groups appearing in the Nusselt number. Such a correspondence can be established through boundary layer similarity arguments, customarily referred to as the heat and mass transfer analogy (HMTA).[13] While the basic HMTA treatment of heat transfer has not changed in CONTAIN 2.0, a number of heat transfer improvements have been made, including (1) incorporation of gas boundary layer composition effects in the Grashof number, (2) more accurate representation of gas boundary layer transport properties, (3) enhanced output for heat transfer processes, and (4) a number of user options for specifying the

Nusselt and Sherwood correlations used by the code and for combining the effects of forced and natural convection.

In contrast to the HMTA method used in CONTAIN, licensing codes typically use Uchida or Tagami/Uchida correlations for the total heat transfer coefficient under condensing conditions.[14,15] Unfortunately, such correlations are known not to scale properly away from the experimental conditions for which they were derived. For example, the Uchida correlation is assumed to depend only on the air/steam ratio. However, even under the saturated conditions of the experiments, this correlation should also depend strongly on other parameters such as the total pressure and the gas-wall temperature difference. Such limitations restrict the usefulness of such correlations to the narrow range of conditions under which they were derived or qualified. Because the HMTA method scales more correctly, it can be extrapolated over a broader range of conditions and is potentially more useful for licensing purposes. Recently, Peterson[16] has shown that the HMTA method gives good agreement with the Uchida data under the conditions of the experiments, and therefore the HMTA method is also consistent with the data.

Figure 1 gives a comparison of the total heat transfer coefficient between the HMTA method as calculated by CONTAIN and the Uchida correlation as implemented in CONTEMPT.[5] Good agreement is obtained for the conditions shown (i.e., a total pressure of 2 bars saturated and the gas-wall temperature differences shown). For lower total pressures or larger gas-wall temperature differences, the functional dependencies of the HMTA heat transfer rate on these quantities cause it to decrease or become more conservative relative to the Uchida correlation (which is independent of these quantities, as discussed above). For higher pressures or smaller gas-wall temperature differences, the converse is true: HMTA becomes less conservative relative to Uchida. Note that the heat transfer during a blowdown typically occurs over a range of pressures and gas-wall temperature differences. The heat transfer from the HMTA method on the average may be either conservative or nonconservative relative to the Uchida correlation, depending on the conditions.

Additional modeling capabilities in CONTAIN 2.0 include a new dynamic condensate film flow model for heat transfer structures, a new mass and energy conservation tracking scheme, and an improved equation of state for steam. Substantial improvements in the ability of the code to treat stable stratification have also been made through implementation of a hybrid formulation of gravitational heads.[17] This formulation, which has been subjected to extensive evaluation and assessment, allows substantially better predictions of stratified conditions than previous CONTAIN formulations, for stable stratification resulting from injection of buoyant steam or gas at an elevated location within a containment. The ability to predict such stratification could be important for DBA analysis, since conservative peak temperatures under highly stratified conditions cannot be predicted by a code that overmixes gas under such conditions, unless extremely conservative assumptions are made.

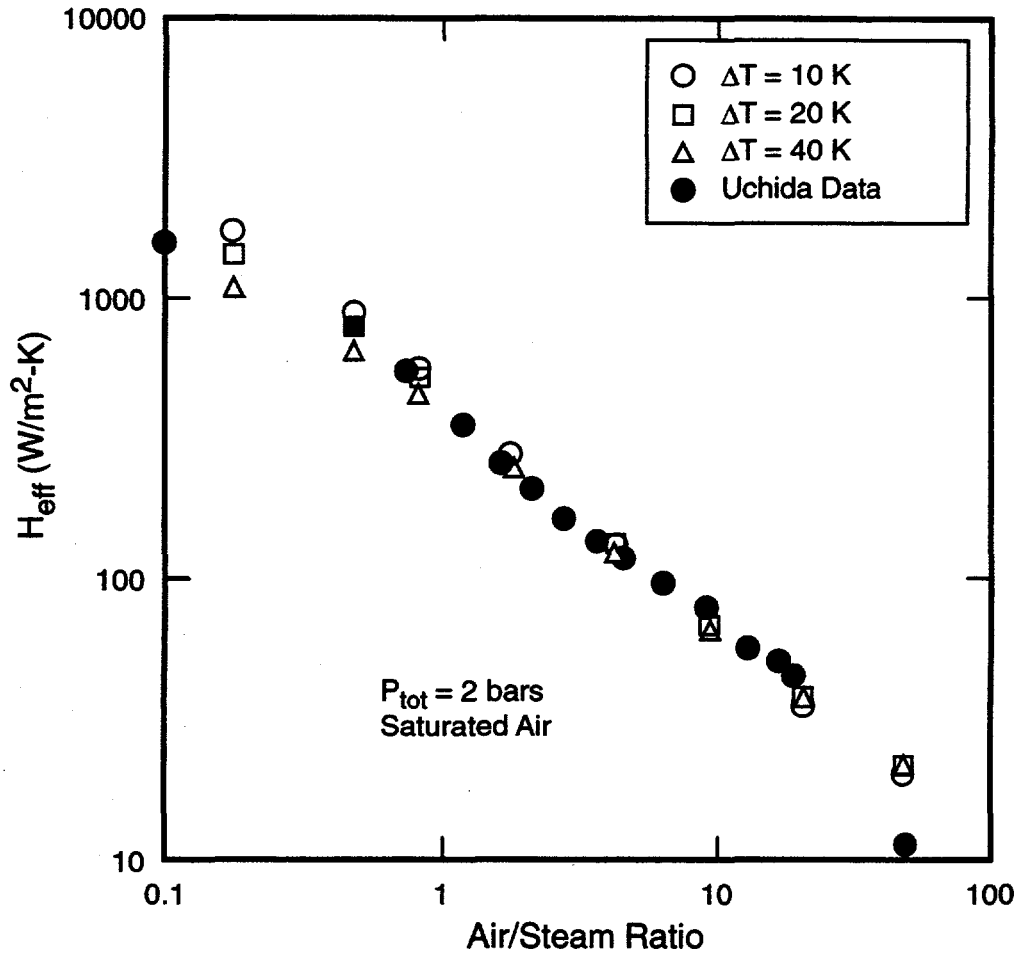

Figure 1. Comparison of the Total Heat Transfer Coefficient Calculated by CONTAIN and the Uchida Correlation, as Implemented in CONTEMPT, for a Total Pressure of P_{tot}=2 bars and Saturated Conditions

3. EXPERIMENT COMPARISONS

3.1 NUPEC Helium Mixing Test M-8-1

The NUPEC model containment was built to represent a 4-loop Pressurized Water Reactor (PWR) at 1/4 linear scale.[11] The NUPEC facility was constructed as a domed cylinder, approximately 10.8 m in diameter, 17.4 m high, and 1310 m^3 in volume. The facility contained 28 separate compartments of which only 25 were interconnected. Of the 25 compartments that were interconnected, however, the dome compartment constituted approximately 71% of the total containment volume.

A series of tests was performed in the NUPEC 1/4-scale model containment to investigate the thermal hydraulics of injecting helium and steam into a containment with and without the operation of water sprays. The tests simulated severe accident conditions in a nuclear power plant under simplified conditions in which helium (as a nonflammable substitute for hydrogen) and steam were released into a containment. The purpose of conducting the test series was to determine the thermal-hydraulic response and the mixing behavior of helium injected into the containment and to provide data for code verification.

Figure 2 shows the 35-cell nodalization used in the analysis, superimposed on a schematic of the facility. In this figure, the cells are denoted by the circled numbers, and the flow paths are denoted by the boxed numbers. The water storage tank, reactor vessel, and primary shield rooms (cells 26-28, respectively) were closed rooms and are not represented. The 35-cell nodalization basically uses one cell for each physical room except for the dome and the pressurizer room. To model gas circulation, the dome is subdivided into central and annular cells, and the pressurizer room is divided into three cells (cells 16, 22, and 35).

In test M-8-1, steam and helium were injected into the pressurizer room, and sprays were not involved. Because the pressurizer room was closed except for openings at the top, these openings determined the injection conditions into the remainder of the containment. The Froude number of this injection, based on jet diameter and velocity, was quite low. Based on the major flow path from the pressurizer room into the remainder of the containment the Froude number is estimated to have been 0.08. Thus, one would expect a stable stratification to form in the facility external to the pressurizer room, with the stratification interface located approximately at the openings at the top of the pressurizer room.

The gas pressure in the facility at the beginning of the experiment was approximately 101 kPa, and the structure and gas temperatures were at room temperature (approximately 280 K to 283 K). The helium and steam mass injection rates were constant at 0.027 kg/s and 0.33 kg/s, respectively, during the 30 minute injection period. It was assumed that helium and saturated steam were injected into the containment at 283 K and 381 K, respectively.

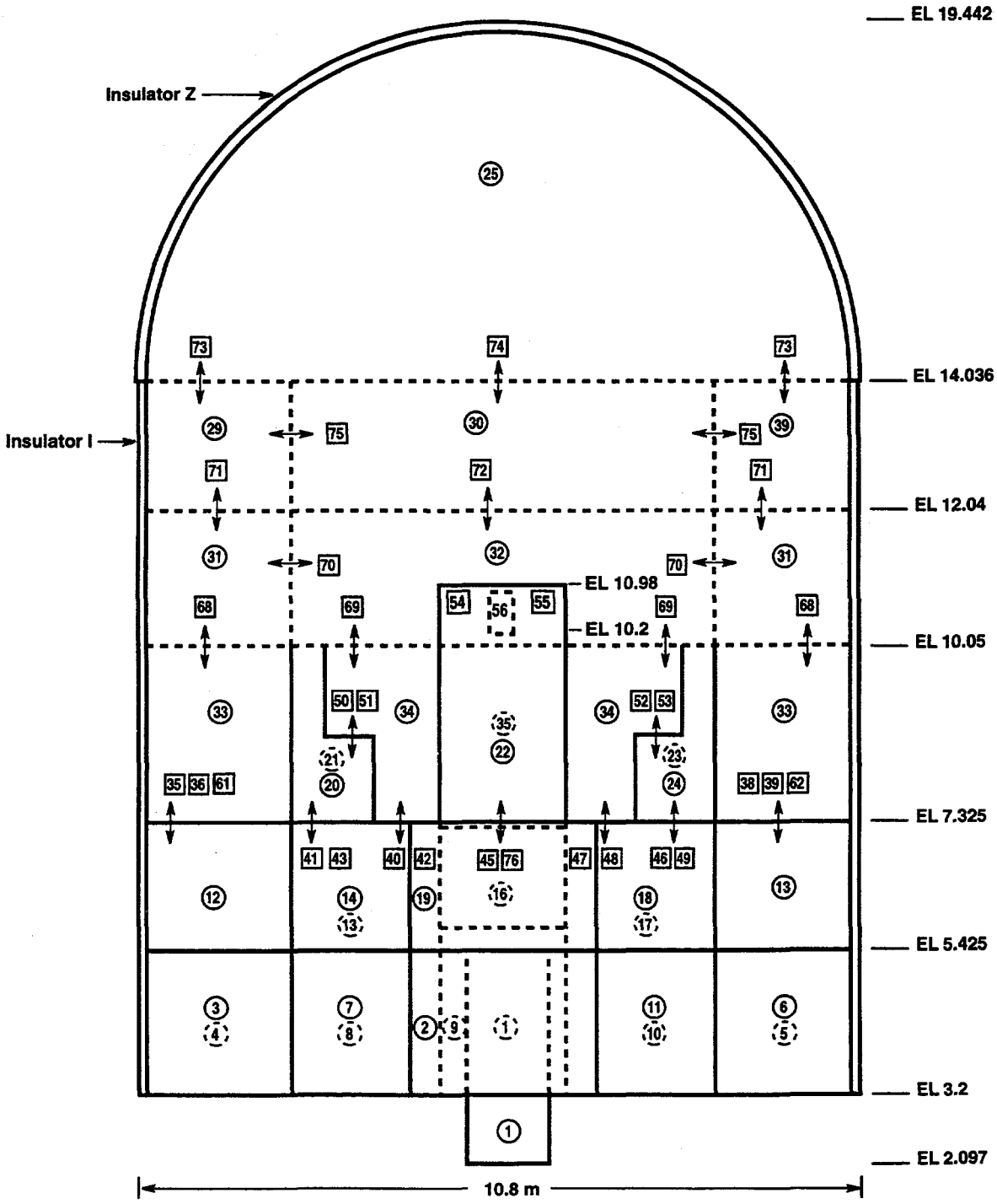

Figure 2. The CONTAIN 35-Cell Nodalization of the NUPEC 1/4-Scale Containment Model

Calculations with the hybrid gravitational head formulation have already been performed and reported in Reference 18 for a number of the NUPEC tests. More recently, the M-8-1 results were recalculated with CONTAIN 2.0. The predicted pressures from the hybrid and old gravitational head formulations are compared with the measured pressures in Figure 3. In Figure 4, the predicted gas temperatures from the hybrid formulation are compared to the measured gas temperatures at locations along a vertical axis through one of the steam generator towers. (The middle column of rooms referred to in this figure corresponds to the cells along this axis.) Good agreement is found between the predicted and measured pressures and temperatures; in addition the predicted peak pressure and temperature are shown to be conservative.

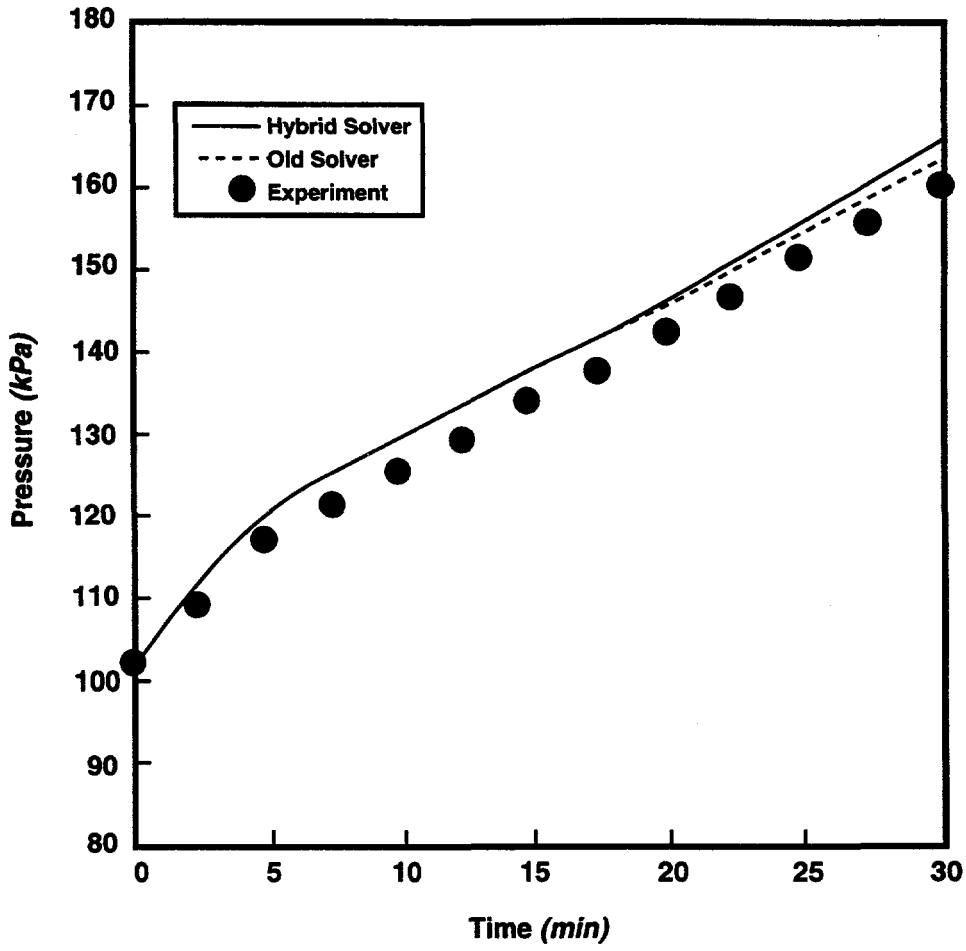

Figure 3. Predicted Pressures Compared to the Measured Pressures for the NUPEC M-8-1 Test

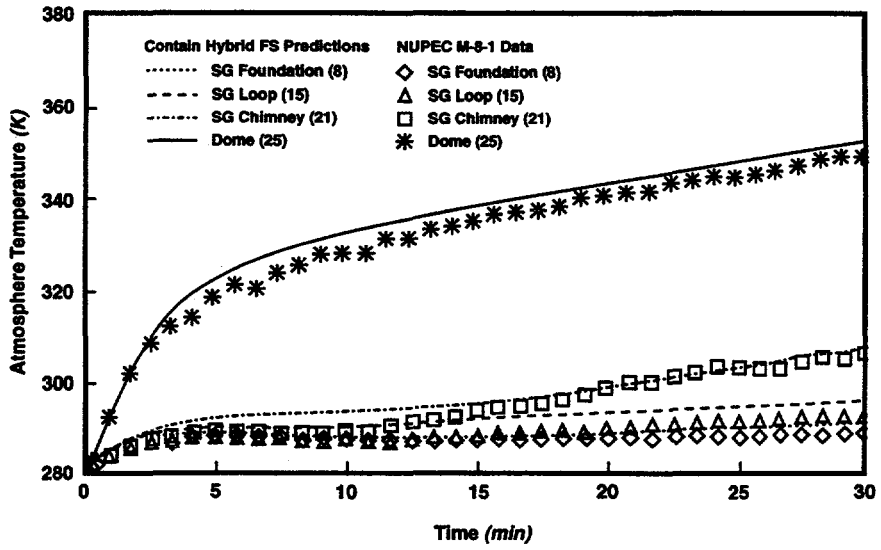

Figure 4. Predicted Gas Temperatures Using the Hybrid Formulation Compared to the Measured Temperatures for the NUPEC M-8-1 Test

With regard to the predicted stratification behavior, the differences between the hybrid and old formulations may be summarized through the predicted gas temperature profiles at the end of the 30-minute gas injection period. As shown in Figure 5, good agreement between the predicted and measured profiles is obtained with the hybrid formulation, but not the old formulation. The results from the latter clearly exhibit overmixing. It should also be noted that, in contrast to the hybrid formulation, the peak temperature is not conservatively predicted with the old formulation. With the hybrid formulation, good agreement is also found with the measured temperatures at other locations and with the measured helium concentrations.[17,18]

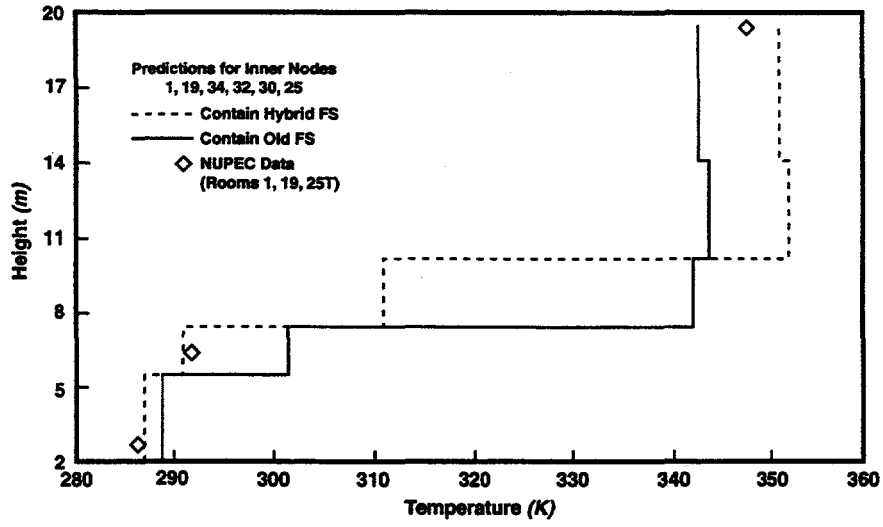

Figure 5. Predicted Temperature Profiles at the End of the Gas Injection Period Compared to the Measured Profile for the NUPEC M-8-1 Test

3.2 ISP-23

International Standard Problem (ISP)-23 (also known as test T31.5) was conducted in the German HDR facility.[10] This test was designed to represent a large-break LOCA, with the break occurring at mid-elevation in the containment, as shown in Figure 6. SNL was an original participant in this ISP, and a blind CONTAIN calculation was submitted in August 1988.[10] That submittal used a detailed nodalization of the HDR facility, as shown in Figure 7, with 33 cells to describe the containment within the steel shell representing its pressure boundary. Calculations using this 33-cell representation were recently redone with CONTAIN 2.0, and the results are shown in Figure 8. In the case labeled "No Forced Convection," the effects of forced convection on heat and mass transfer were ignored; in the case labeled "With Forced Convection," the degree of forced convection was estimated, and the forced convection velocities were specified through input. These two calculations utilized the aerosol method for treating suspended liquid water. In the case labeled "No Dropout," this water was treated in the default manner, as homogeneously dispersed liquid not subject to gravitational settling. Figure 9 shows local temperature comparisons at four elevations, ranging from -5 to 40 meters, in the "No Forced Convection" case. As indicated in this figure, the predicted temperature distribution within the containment and its time dependence agree reasonably well with the measured local temperatures, but the temperatures below the injection point at one elevation, namely at 5 m, are considerably overpredicted.

When steam is injected into the upper containment, one would expect the temperature rise in the lower containment to be partly the result of heating by compression, as the buoyant steam/air mixture in the upper containment expands and pressurizes the containment. Since this steam tends to be excluded from the lower containment because of its buoyancy, this compression would tend to produce superheated conditions in the lower containment. Overprediction of the lower containment temperatures may indicate that the superheating in the lower containment is suppressed by rainout of liquid into the lower containment and its concurrent evaporation, an effect that was not explored with respect to ISP-23, but was explored with respect to CVTR test #3 (see Section 3.3). The rainout conjectured here could arise either from liquid introduced during the blowdown or from entrainment of condensate films that have formed on heat sinks.

Another interesting feature of the ISP-23 calculation is the sub-compartment pressure differential between the break room and dome shown in Figure 10, for the "No Forced Convection" case. As shown in this figure, the peak pressure differential is slightly overpredicted by the code; however, the calculated pressure differential with the aerosol method of treating suspended liquid decreases rapidly enough that the prediction slightly underestimates the pressure differential at late times. As indicated by the no dropout case, this rapid drop-off may be an artifact. The difficulty is that the flow model neglects the inertial mass of the aerosolized water in calculating the flow rate, resulting in a flow rate out of the blowdown cell that is too high. A more realistic treatment of aerosol inertia would result in a pressure differential that lies somewhere between those of the two cases shown.

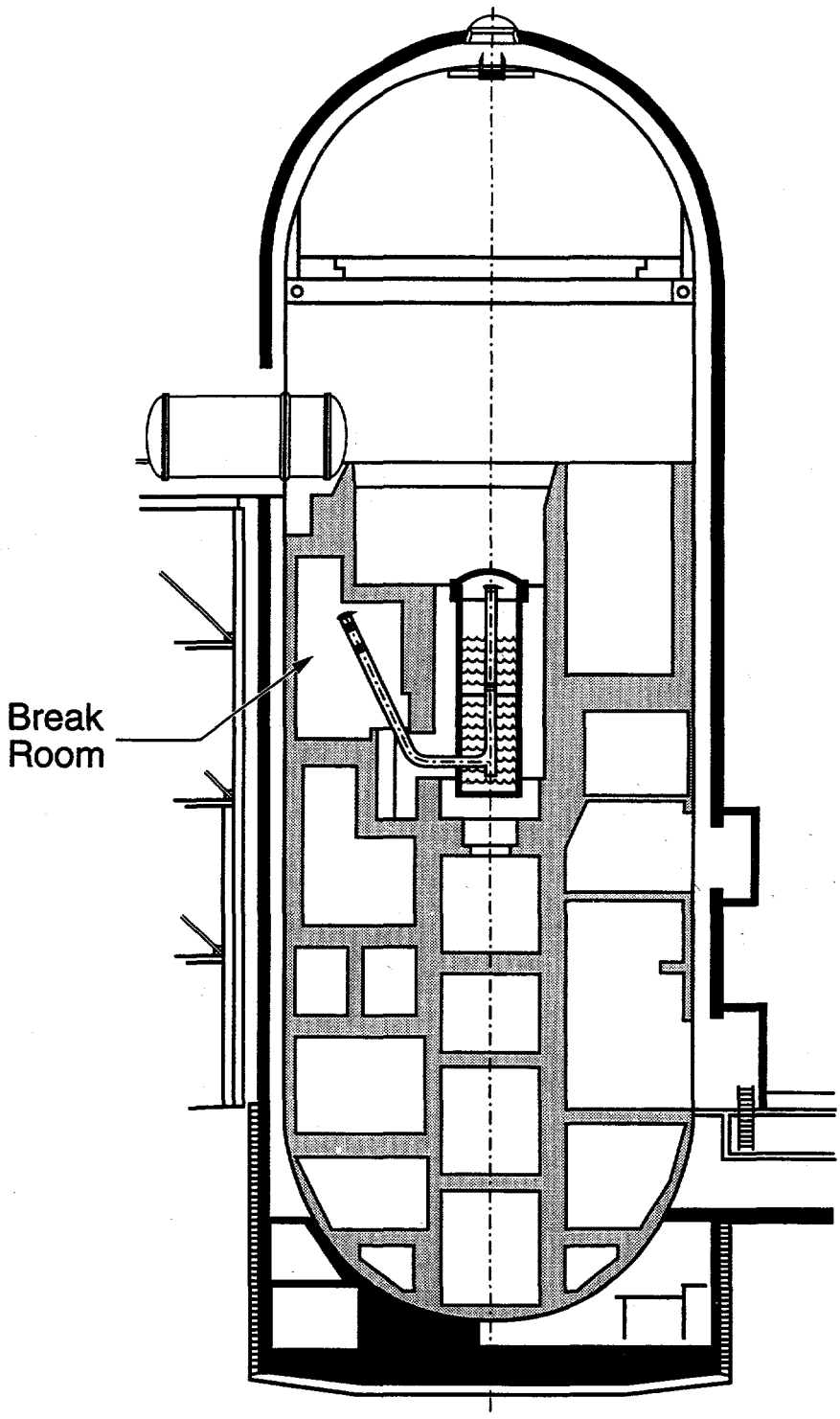

Figure 6. Layout of the HDR Facility, Showing the Blowdown Location Used for ISP-23

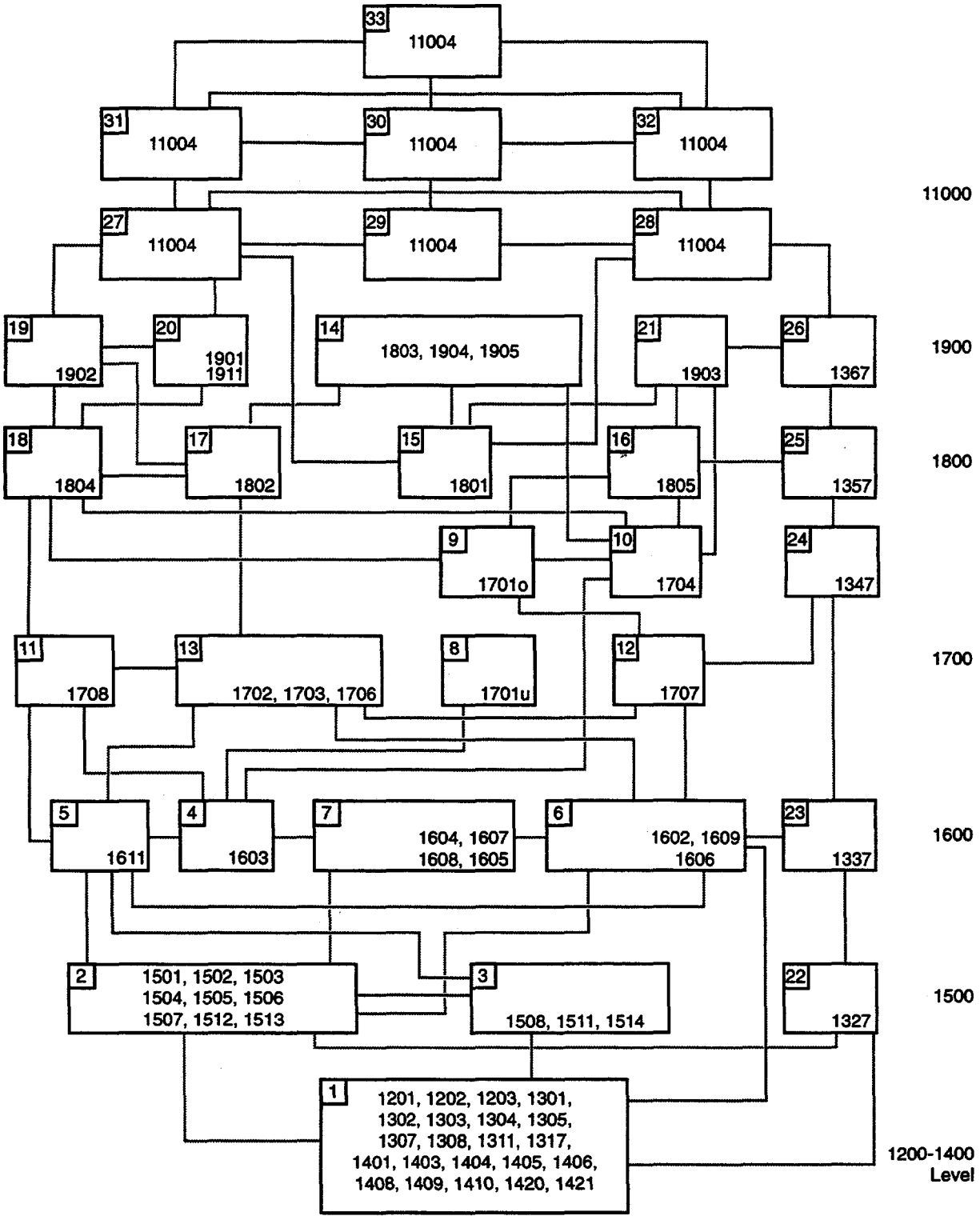

Figure 7. The 33-Cell Nodalization Used for ISP-23

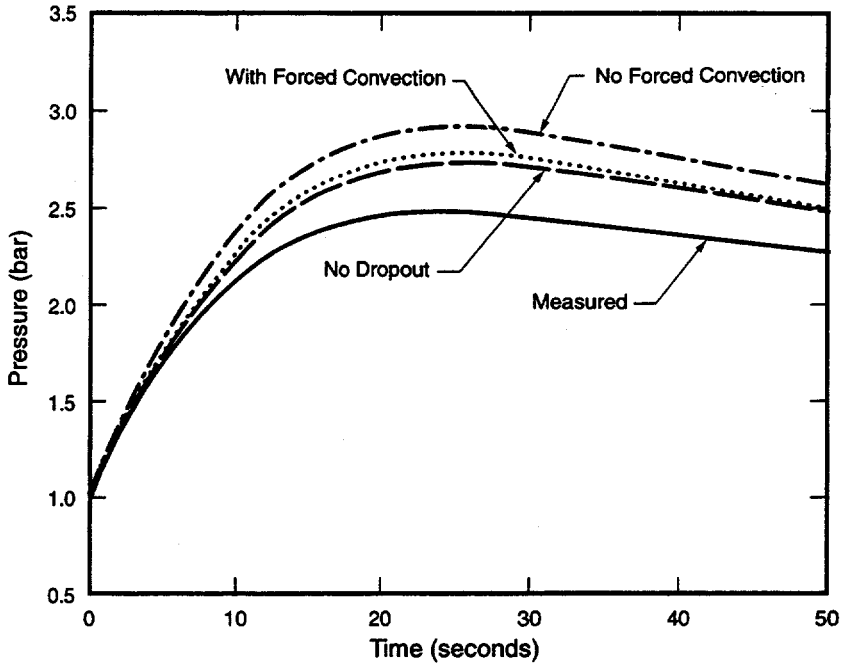

Figure 8. Various Pressure Predictions for ISP-23, Compared to Experiment

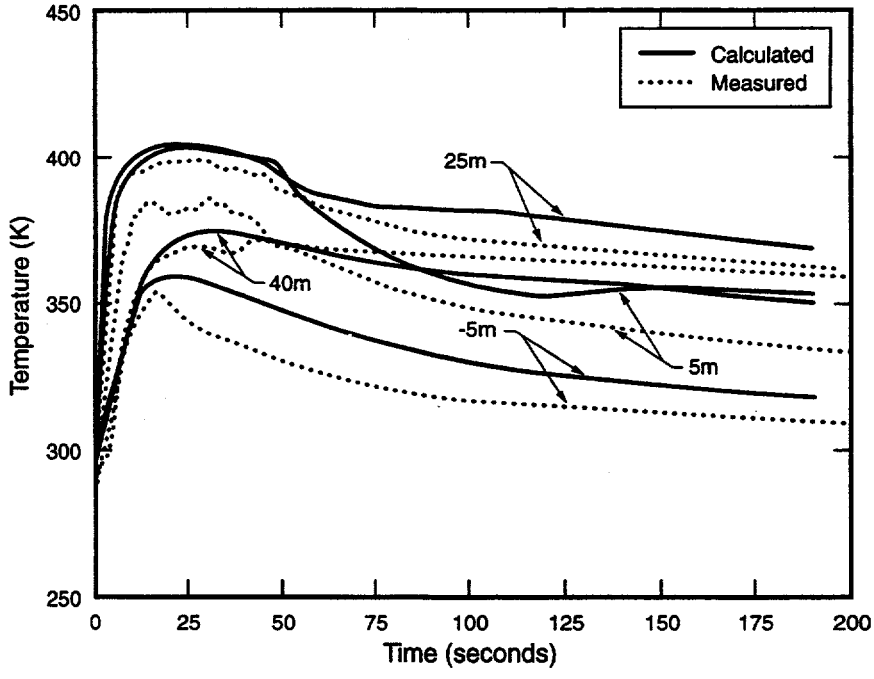

Figure 9. Predicted Gas Temperatures for ISP-23, Compared to Experiment

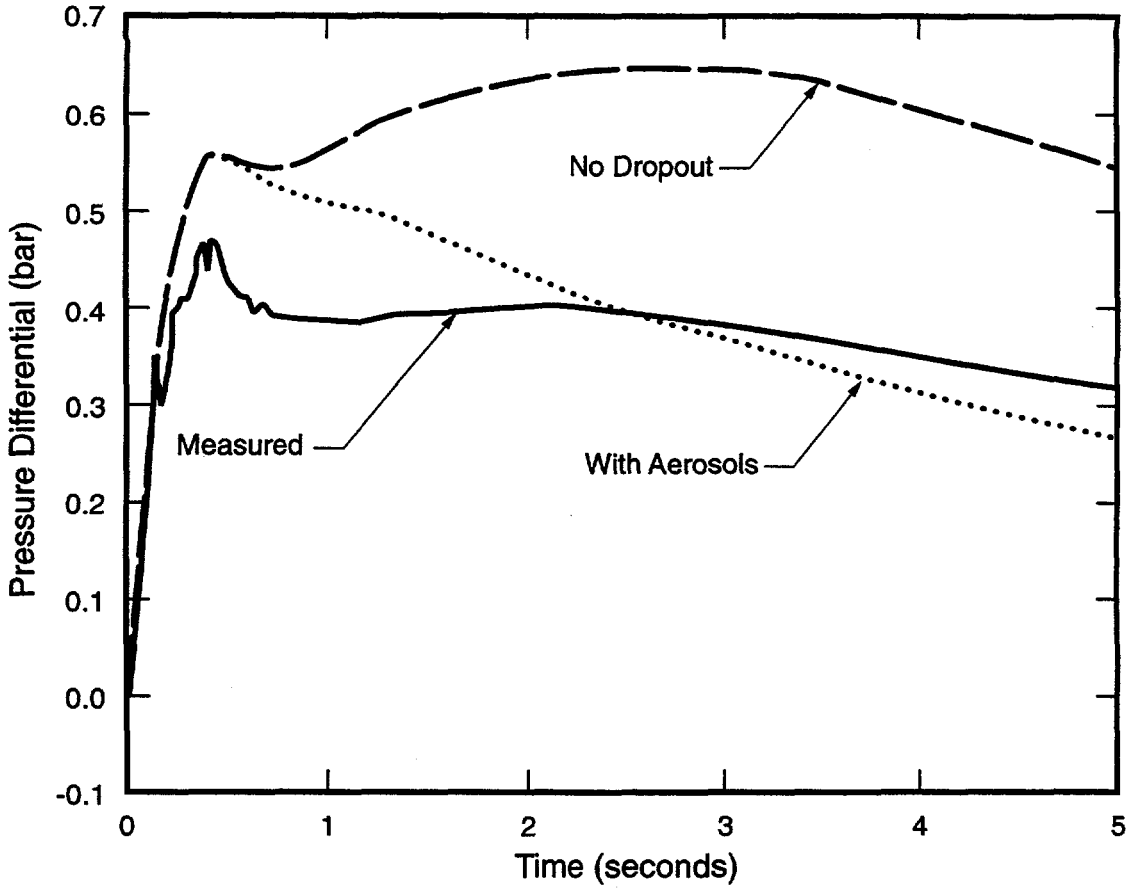

Figure 10. Predicted Sub-Compartment Pressure Differentials for ISP-23, Compared to Experiment

The pressure differential depends on other parameters such as loss coefficients that are difficult to determine accurately. However, with sufficient user guidance it should be possible to set flow parameters to assure conservative differentials. It should be noted that in the ISP-23 blind submittal, the CONTAIN predictions for sub-compartment pressures represented one of the best predictions from either control volume or fluid dynamics codes. The comparable agreement shown in Figure 10 is therefore as good as can be expected based on state-of-the-art code comparisons.

3.3 CVTR Test #3

CVTR test #3 is of particular interest because it has been used in the past for validating models in DBA codes.[19,20,21] In this test, steam was injected at a location just above the operating deck, and significant steam stratification was observed. Nevertheless, most containment analyses reported in the literature for this test have been performed using a single-cell representation of the containment. The CONTEMPT code was utilized for many of these analyses; therefore, the reported results also reflect specific limitations of CONTEMPT. Some of the more important modeling limitations common to past CVTR analyses include: (1) the use of the Uchida

correlation for determining condensation heat transfer, (2) the neglect of the air gap resistance for the containment shell, (3) the neglect of condensate film resistance and film flow, and (4) the neglect of paint resistance for structures. In addition to these heat and mass transfer modeling limitations, there are uncertainties involving the specification of heat sink areas, such as the miscellaneous steel and internal concrete wall areas.

The multi-cell CONTAIN model for CVTR uses the 19-cell nodalization shown in Figure 11. This model uses relatively fine nodes in the lower containment to help capture the motion of the steam stratification interface that formed between the upper and lower containment during the experiment. Note that this stratification interface, which formed initially at operating deck level (shown at 325 ft. in the figure), moved downward into the lower containment as a result of pressurization effects during the blowdown. Capturing the motion of this interface was found to be the most challenging numerical aspect of the calculations. The multi-cell CVTR model uses the CONTAIN 2.0 default forced convection option for the heat and mass transfer, with parameters set so that its effects are minimal. The heat sink input is based on "best-estimate" concrete areas as tabulated in the final report on the CVTR DBA tests[8] and on the upper bound estimate for exposed miscellaneous steel (this corresponds to 50% of the tabulated major-component steel area at 3/8 in. thickness).

Predicted pressures from two single-cell calculations and the multi-cell calculation are compared in Figure 12. The single-cell calculation labeled "No Misc. Steel" used the same input as the multi-cell calculation except for reduction to one cell, elimination of the miscellaneous steel heat sinks, and use of lower-bound concrete heat sink areas. This apparently results in a containment response similar to that from the CONTEMPT model used by other authors.[19,20] In particular, the peak pressure and peak temperature of 416 K predicted for this case are nearly identical to the results reported by Carbajo[19] for his case 5, which used a Uchida correlation with an assumed condensation efficiency of 0.92. The other single-cell calculation shown in Figure 12 used the same heat sinks as the multi-cell calculation. The predicted pressures from this single-cell calculation are considerably lower than the first and tend to follow closely the multi-cell predicted pressures during the blowdown period. However, during the relaxation period after the blowdown, when heat transfer to structures dominates the pressure response, the multi-cell calculation gives good agreement with the measured pressure relaxation rate, whereas the single-cell calculations tend to overpredict the pressure relaxation rate.

The gas temperature predictions from the single-cell models are shown in Figure 13. These should be compared to the predictions, shown in Figure 14, from the multi-cell calculation. During the blowdown, the predicted temperatures from the single-cell calculations are conservative with respect to the measured maximum temperatures, although obtaining this conservatism clearly requires the use of extremely conservative assumptions when highly stratified conditions are present. The predictions from the multi-cell calculation in Figure 14 indicate more clearly the degree of conservatism present with respect to the local temperatures. After the blowdown, the single-cell calculation is no longer conservative and underpredicts the maximum temperatures in the containment. In contrast, the predictions from the multi-cell calculation predict the relative temperature variation in the containment quite well at all times and give good agreement with the temperature distributions at late times.

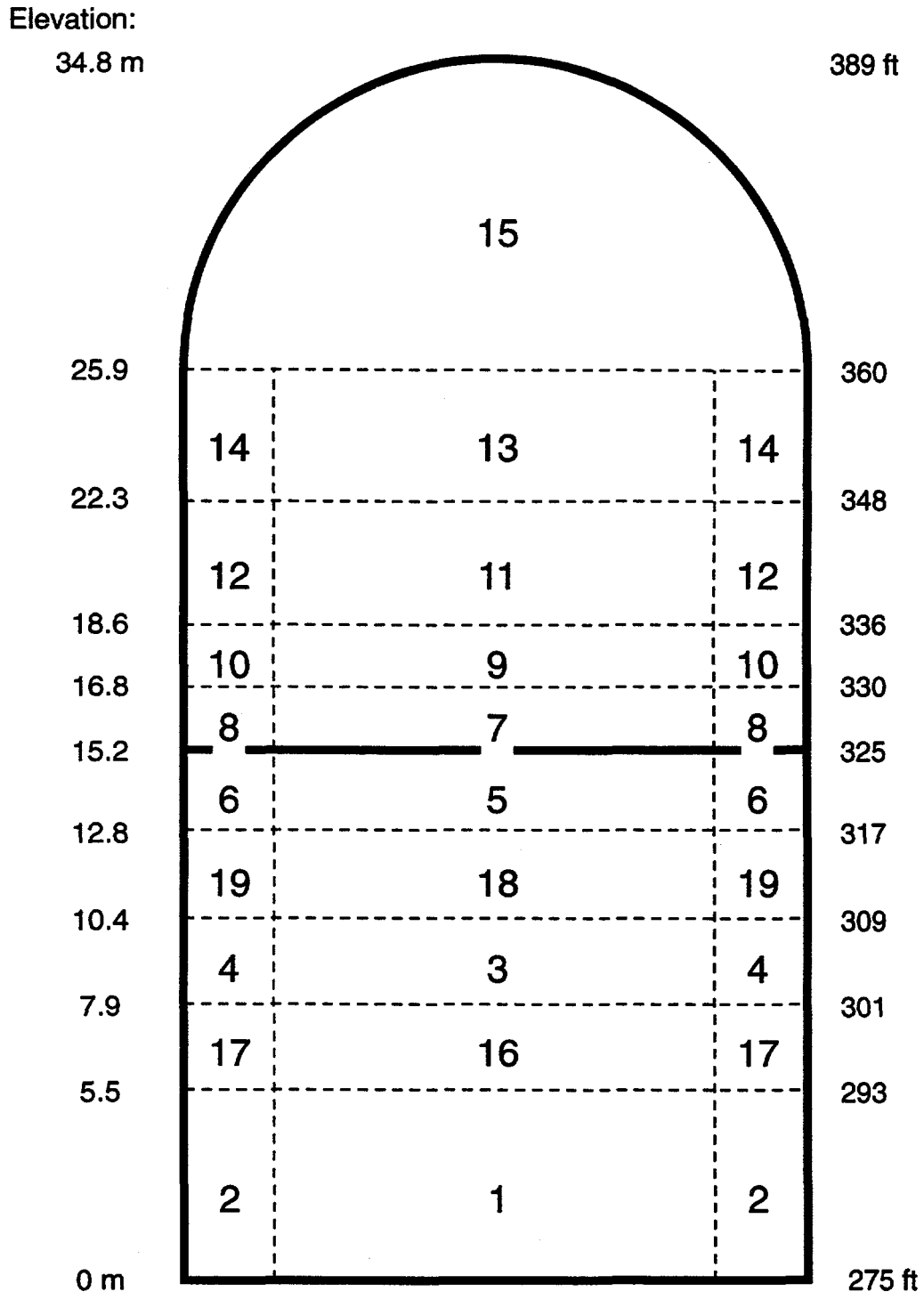

Figure 11. CVTR 19-Cell Nodalization

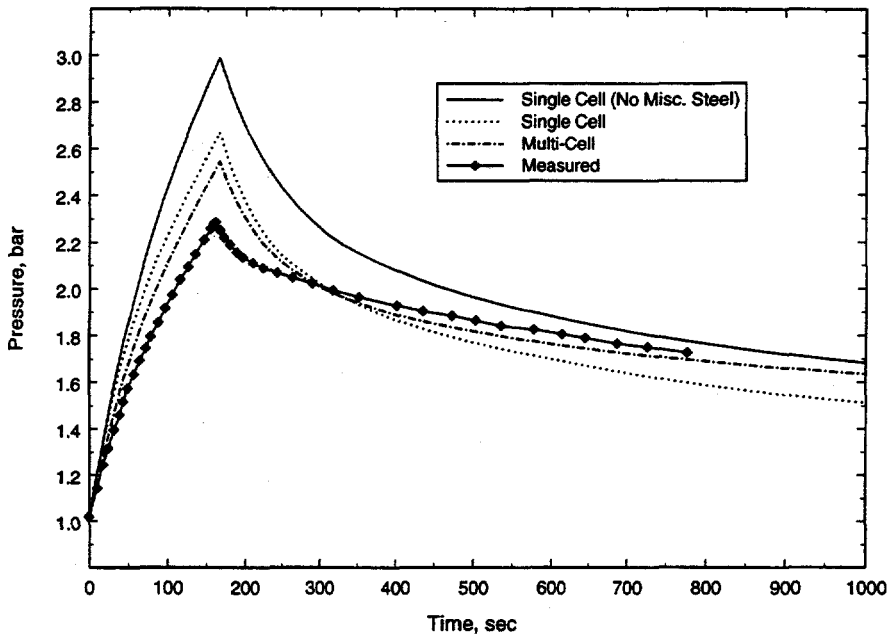

Figure 12. Predicted Pressures for CVTR Test #3 for Various Cases, Compared to Experiment

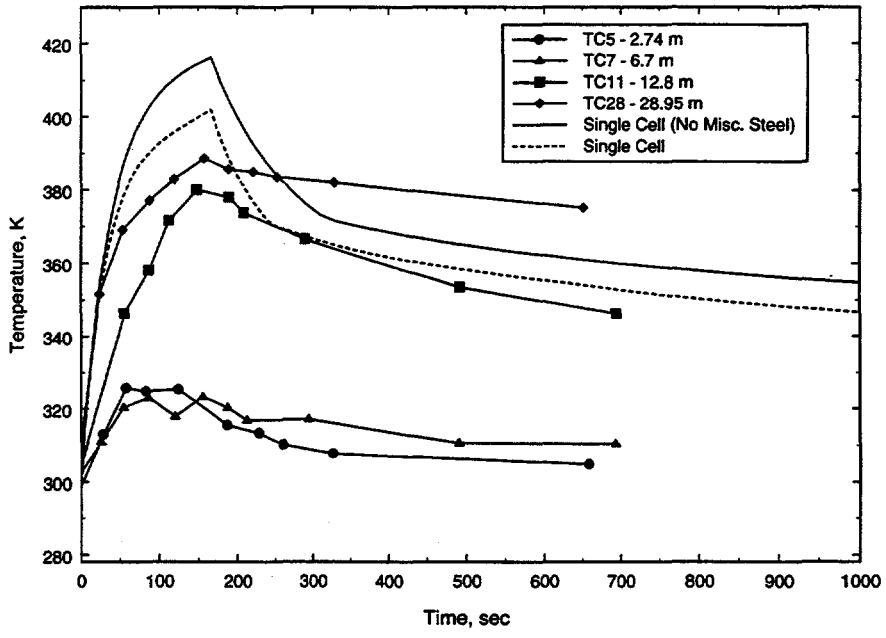

Figure 13. Single-Cell Temperature Predictions for CVTR Test #3, Compared to Experiment

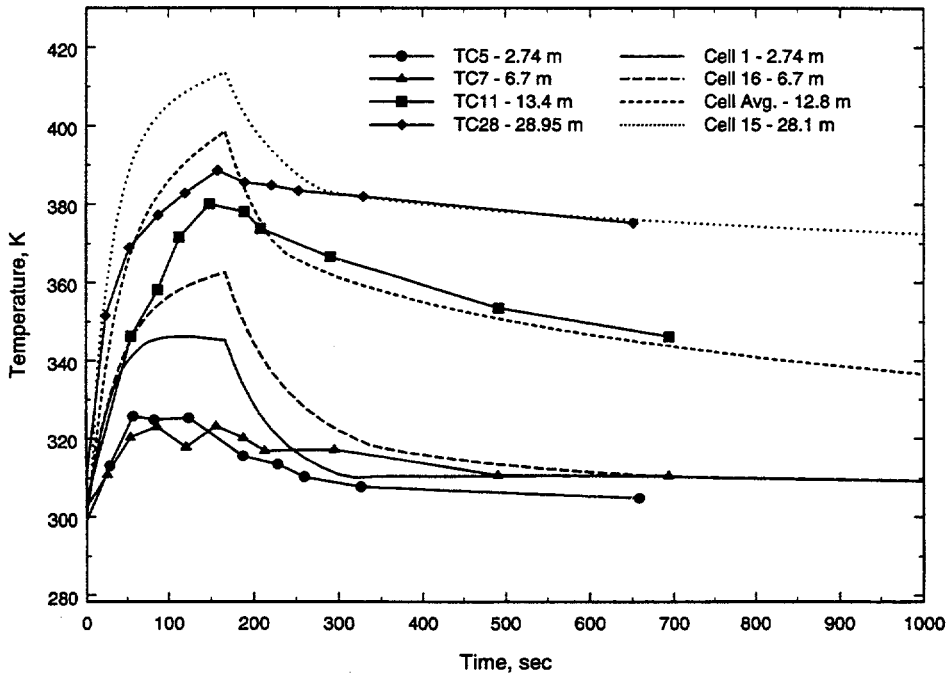

Figure 14. Multi-Cell Gas Temperature Predictions for CVTR Test #3, Compared to Experiment

In the results shown in Figure 14, the maximum calculated temperature corresponds to about 25 K of superheat, with the saturation temperature being approximately equal to the maximum measured temperature of 389 K. Likewise, in the lower regions of the containment the calculated maximum local temperatures correspond to approximately 20 K of superheat. The existence of such superheated conditions is clearly not supported by the data. To explore the uncertainties related to this superheat, sensitivity calculations were done with respect to forced convection effects, injected steam enthalpy, and rainout effects. Forced convection effects were introduced through flow boundary conditions that were imposed at the junctions between the annular cells 8, 10, and 12 of Figure 11 and the adjacent central cells, so as to match the observed forced convection velocities of 4.5 to 9 m/s along the containment wall during the blowdown.[8] Such flow boundary conditions result in long-range flow patterns that determine the forced convection conditions in the rest of the containment. This forced convection was found to affect primarily the pressure and upper containment temperatures: the discrepancy shown in Figure 12 between the predicted multi-cell and measured peak pressures was reduced by 1/2 and the discrepancy shown in Figure 14 between the predicted upper containment and measured peak temperatures was reduced by 1/3 by the effects of forced convection. A second sensitivity calculation indicated that, in the absence of forced convection, the discrepancy between the predicted and measured upper containment temperatures could be removed through a 2.8% reduction in the experimentally determined injected steam enthalpy of 2779.6 kJ/kg[8] used to obtain the results in Figures 12-14. This is comparable to the experimental uncertainty in the enthalpy, which was stated to be 2%.[8] It is, therefore, likely that a combination of forced convection effects and

enthalpy measurement errors can explain the discrepancies between the multi-cell calculation and the experiment with respect to the peak pressure and peak temperature. The lower containment temperatures, however, were not significantly altered in these sensitivity calculations. A third sensitivity calculation was therefore done to explore the rainout hypothesis advanced above with respect to ISP-23, and this calculation showed that small amounts of rainout could be quite effective in suppressing the lower containment superheat.

Finally, Figure 15 shows another quantity of interest with respect to DBAs, the fraction of the total heat transfer attributable to sensible heat transfer, as opposed to condensation or latent heat transfer. (This is sometimes referred to as the "revaporization" fraction. The "condensation efficiency" mentioned above corresponds to one minus this quantity.) Because of the difference in conditions between the upper and lower containment, this fraction was calculated separately for the two regions. The 8% revaporization fraction sometimes used in DBA calculations is in reasonable agreement with the upper containment prediction during the blowdown period.

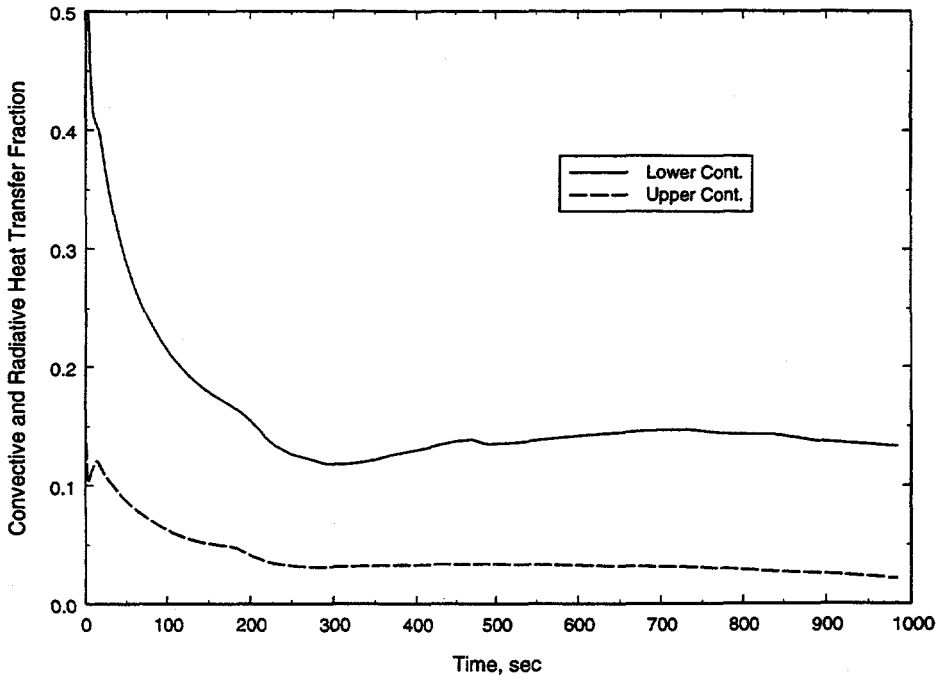

Figure 15. Sensible Heat Transfer Fraction Calculated for CVTR Test # 3

4. SAN ONOFRE PLANT CALCULATIONS

To illustrate how CONTAIN might perform in a conventional single-volume DBA analysis, comparisons between CONTAIN and CONTEMPT are presented in this section for a postulated large-break LOCA at the San Onofre plant. In this LOCA, fan coolers and sprays are assumed to be available. The CONTAIN and CONTEMPT modeling of this scenario were made to agree through CONTAIN input specifications, where possible. Such specifications eliminated uncertainties with regard to (1) concrete and steel properties, (2) paint thermal resistances, and (3) the treatment of suspended liquid water in the following comparisons. However, it should be noted that considerable differences still remain in the modeling. For example, in the CONTEMPT calculation, Tagami/Uchida heat transfer correlations for forced/natural convection were used; in the CONTAIN calculations, the HMTA model based on natural convection was used; in addition, the relatively small effect of forced convection was not taken into account in the results presented here.

As shown in Figure 16, CONTAIN predicts somewhat higher pressures than CONTEMPT for this scenario. The legend in this figure refers to the two options discussed in Section 2 for removing suspended liquid in CONTAIN, the dropout option similar to that used in CONTEMPT and the aerosol option. Figure 16 indicates that the effects on pressure from use of the aerosol option are approximately the same as those from the dropout option. The similarities during the initial pressure ramp are to be expected because the specific heat of liquid water is neglected once its mass is transferred to the aerosol field. Under condensing conditions, the water aerosols thus do not contribute thermally to the atmosphere, even if they remain suspended for some time.

Figure 17 shows various predictions for the gas temperature. As shown in this figure, and in contrast to the CONTEMPT prediction, the dropout option introduces a significant degree of superheat for this scenario, beginning at approximately 25 seconds. Note that fan coolers are assumed to actuate at 33 seconds and sprays at 55 seconds. Thus, the onset of superheat cannot be explained by the response to the latter. As shown in Figure 17, the tendency to superheat is reduced with the aerosol option, which retains more liquid in the atmosphere than the dropout option. Also, as shown in this figure, this tendency is further reduced by invoking the radiative heat transfer option, which allows additional heat to be transferred to heat sinks. The CONTAIN results with the aerosol option and radiative heat transfer are quite similar to the CONTEMPT results. However, since CONTEMPT treats suspended water in "drop-out" fashion similar to the CONTAIN option, and a comparison of heat transfer models[5] suggests that CONTEMPT should predict conditions that are more superheated than CONTAIN's prior to spray onset, the fact that the CONTEMPT calculations do not predict superheat is not understood.[†] Nevertheless, CONTAIN's pressures and temperatures are conservative relative to CONTEMPT's.

[†] After spray onset, the presence of superheat in the CONTAIN calculation indicates that the monodisperse spray droplets used in the CONTAIN spray model do not equilibrate with the atmosphere.

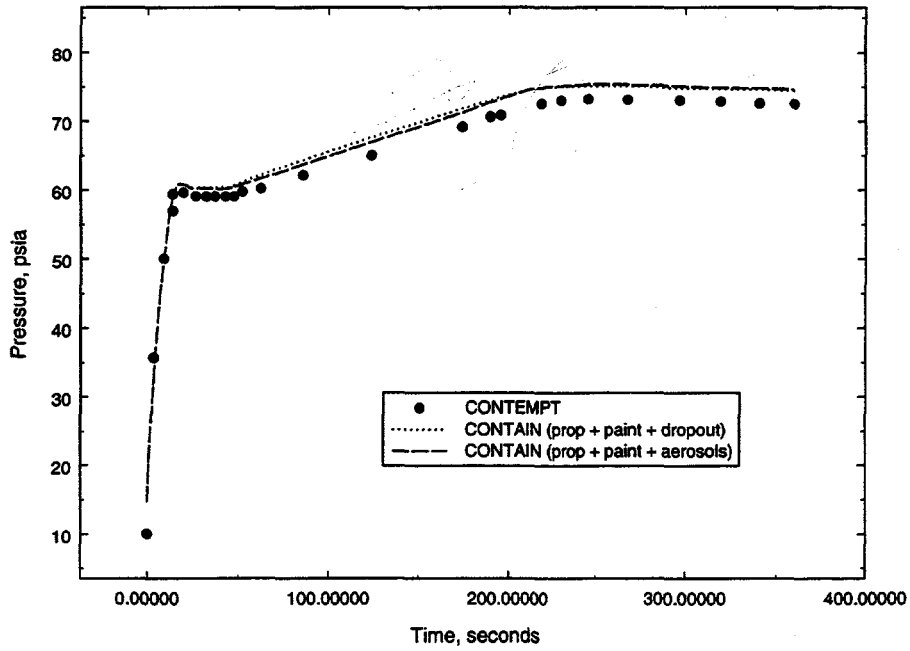

Figure 16. Comparison of CONTAIN and CONTEMPT Predicted Pressures for the San Onofre Large-Break LOCA

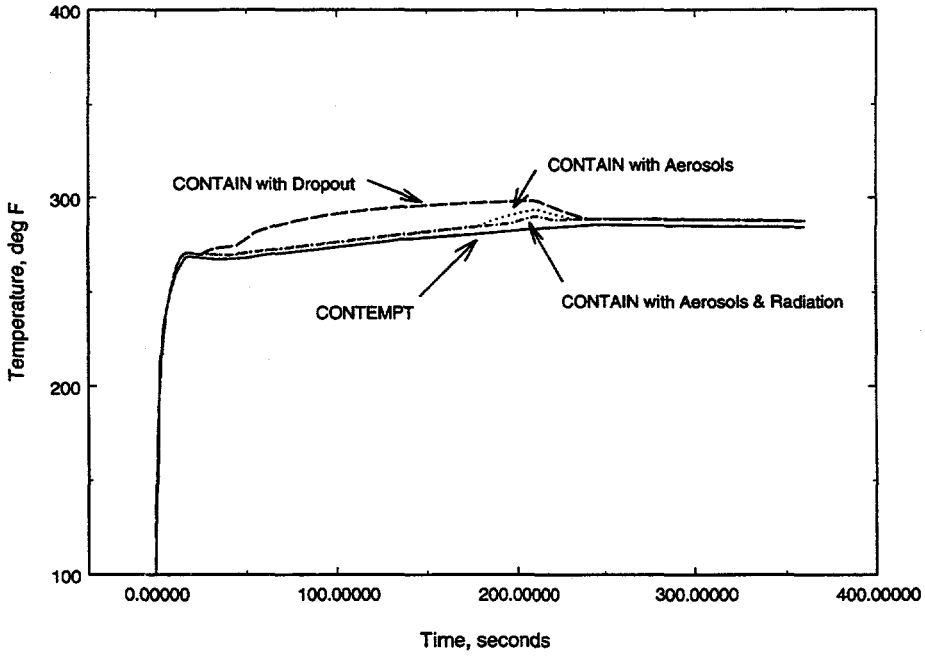

Figure 17. Comparison of CONTAIN and CONTEMPT Predicted Gas Temperatures for the San Onofre Large-Break LOCA

5. CONCLUSIONS

The new features of the CONTAIN 2.0 code release have been reviewed. In addition, work in progress to help qualify CONTAIN for more general use in licensing applications has been summarized. The work discussed here on PWR scenarios indicates that CONTAIN can predict conservative peak pressures and conservative peak temperatures, under well-mixed and highly stratified DBA conditions. These results also indicate that CONTAIN has potential for conservative prediction of subcompartment pressure differences, although further user guidance and perhaps model improvements in this area need to be developed.

REFERENCES

1. K. K. Murata et al., "Code Manual for CONTAIN 2.0: A Computer Code for Nuclear Reactor Containment Analysis," NUREG/CR-6533, SAND97-1735, Sandia National Laboratories, Albuquerque, NM, December 1997.

2. J. Tills, R. O. Griffith, K. K. Murata, and D. W. Stamps, "User Guidance on the CONTAIN Code for Advanced Light Water Reactors," SAND96-0947 (Proprietary), Sandia National Laboratories, Albuquerque, NM, 1996.

3. J. Tills, "Calculations and Analyses for the Large-Scale Passive Containment Cooling System (PCS) Tests," SAND96-1089 (Proprietary), Sandia National Laboratories, Albuquerque, NM, 1996.

4. J. Tills, K. K. Murata, and K. E. Washington, "PCCS Model Development for the SBWR Using the CONTAIN Code," presented at ARS '94 - International Topical Meeting on Advanced Reactor Safety, American Nuclear Society, Pittsburgh, PA, April 17-21, 1994.

5. D. W. Hargroves and L. J. Metcalf, "CONTEMPT-LT/028 — A Computer Program for Predicting Containment Pressure-Temperature Response to a Loss-of-Coolant Accident," NUREG/CR-0255, TREE-1279, Idaho National Engineering Laboratory, Idaho Falls, ID, 1979.

6. R. G. Gido, J. S. Gilbert, R. G. Lawton, and W.L. Jensen, "COMPARE MOD-1: A Code for the Transient Analysis of Volumes with Heat Sinks, Flowing Vents, and Doors," LA-7199-MS, Los Alamos National Laboratory, Los Alamos, NM, March 1978.

7. T. R. McIntyre, M. A. Ross, and L. L. Meyers, "Mark II Pressure Suppression Test Program Phase I Tests," NEDE-13442P-01 (Proprietary), General Electric Co., San Jose, CA, May 1976; L. L. Meyers, T. R. McIntyre, and R. J. Ernst, "Mark III Confirmatory Test Program Phase I - Large Scale Demonstration Tests: Test Series 5701-5703," NEDM-13377 (Proprietary), General Electric Co., San Jose, CA, October 1974.

8. R. C. Schmitt, G. E. Bingham, and J. A. Norberg, "Simulated Design Basis Accident Tests of the Carolinas Virginia Reactor Containment - Final Report," IN-1403, UC-80, Idaho Nuclear Corporation, National Reactor Testing Station, Idaho Falls, Idaho, December 1970.

9. M. Firnhaber, "ISP16: Rupture of a Steam Line Within the HDR-Containment Leading to an Early Two-Phase Flow — Results of the Post-Test Analysis," CSNI Report No. 112, Committee on the Safety of Nuclear Installations, OECD Nuclear Energy Agency, Paris, France, June 1985.

10. H. Karwat, "ISP23: Rupture of a Large Diameter Pipe Within the HDR Containment," CSNI Report No. 160, Vols. 1 and 2, Committee on the Safety of Nuclear Installations, OECD Nuclear Energy Agency, Paris, France, 1989.

11. "Final Comparison Report on ISP-35 NUPEC's Hydrogen Mixing and Distribution Test (Test M-7-1)," NEA/CSNI/R(94)29, Committee on the Safety of Nuclear Installations, OECD Nuclear Energy Agency, Paris, France, December 1994.

12. H. Karwat, "OECD-CSNI-ISP29, Distribution of Hydrogen Within the HDR-Containment Under Severe Accident Conditions – Final Comparison Report," OECD Committee on the Safety of Nuclear Installations, Paris, France, August 1992.

13. R. B. Bird, W. E. Stewart, and E. N. Lightfoot, *Transport Phenomena*, John Wiley and Sons, Inc., New York, 1960.

14. D. C. Slaughterbeck, "Review of Heat Transfer Coefficients for Condensing Steam in a Containment Building Following a Loss-of-Coolant Accident," IN-1338, Idaho Nuclear Corporation, National Reactor Testing Station, Idaho Falls, ID, September 1970.

15. H. Uchida et al., "Evaluation of Post Incident Cooling Systems of Light-Water Power Reactors," in *Proceedings of the Third International Conference on the Peaceful Uses of Atomic Energy, Held in Geneva, 31 August - 9 September, 1964*, 13, United Nations, New York, 1965.

16. P. F. Peterson, "Theoretical Basis for the Uchida Correlation for Condensation in Reactor Containments," *Nucl. Eng. and Design*, 162, pp. 301-306, 1996.

17. K. K. Murata, and D. W. Stamps, "Development and Assessment of the CONTAIN Hybrid Flow Solver," SAND96-2792, Sandia National Laboratories, Albuquerque, NM, November 1996.

18. D. W. Stamps, "CONTAIN Assessment of the NUPEC Mixing Experiments," SAND94-2880, Sandia National Laboratories, Albuquerque, NM, August 1995.

19. J. J. Carbajo, "Heat Transfer Coefficients Under LOCA Conditions in Containment Buildings," *Nucl. Engr. Design*, 65, pp. 369-386, 1981.

20. W. J. Krotiuk, and M. B. Rubin, "Condensing Heat Transfer Following a Loss-of-Coolant Accident," *Nucl. Tech.*, 37, pp. 118-128, February 1978.

21. E. Economos et al., "Condensation Heat Transfer Modelling for Containment Environmental Response Calculations - A Reappraisal for the Standard Review Plan - Main Report," Technical Report A-3719, Vol. 1, Department of Nuclear Energy, Brookhaven National Laboratory, Upton, NY, June 1987.

Status of VICTORIA: NRC Peer Review and Recent Code Applications*

N. E. Bixler
Sandia National Laboratories
Albuquerque, New Mexico 87185-0739

and J. H. Schaperow
Nuclear Regulatory Commission
Washington, DC 20555

ABSTRACT

VICTORIA is a mechanistic computer code designed to analyze fission product behavior within a nuclear reactor coolant system (RCS) during a severe accident. It provides detailed predictions of the release of radioactive and nonradioactive materials from the reactor core and transport and deposition of these materials within the RCS.

A summary of the results and recommendations of an independent peer review of VICTORIA by the U. S. Nuclear Regulatory Commission (NRC) is presented, along with recent applications of the code. The latter include analyses of a temperature-induced steam generator tube rupture sequence and post-test analyses of the Phebus FPT-1 test.

The next planned Phebus test, FPT-4, will focus on fission product releases from a rubble bed, especially those of the less-volatile elements, and on the speciation of the released elements. Pretest analyses using VICTORIA to estimate the magnitude and timing of releases are presented. The predicted release of uranium is a matter of particular importance because of concern about filter plugging during the test.

1.0. Introduction

Release of radionuclides into the atmosphere is the main concern in the event of a nuclear reactor accident. The consequences of a severe accident depend on the quantity, characteristics, and timing of the releases of radionuclides from the reactor coolant system (RCS) into the containment, and finally into the atmosphere. In a by-pass accident, releases by-pass the containment and go directly from the RCS into an auxiliary building or into the atmosphere. As a result, accurate determination of the quantity of fission products that are retained in the primary and secondary circuits and containment is paramount to the assessment of risk.

The physical processes that influence the quantity and timing of a release are complex. In order to predict the outcome of a nuclear accident, it is necessary to accurately model as many of the relevant physical processes as possible. VICTORIA [1] is a mechanistic computer code designed to model such processes so that the magnitude, speciation, physical properties, and timing of fission product releases can be predicted.

---

*This work was supported by the U.S. Nuclear Regulatory Commission and was performed at Sandia National Laboratories, which is a multiprogram laboratory operated by Sandia Corporation, a Lockheed Martin Company, for the U. S. Department of Energy under Contract DE-AC04-94AL85000.

VICTORIA does not predict thermal hydraulics, but requires such information as input. The heart of the code is in its mechanistic treatment of fission product release from fuel, chemistry, aerosol physics, transport, and decay heating. The coupled treatment of these phenomena make VICTORIA unique in its predictive capabilities.

The U.S. Nuclear Regulatory Commission (NRC) recently conducted a peer review to assess the code and documentation against a set of design objectives and targeted applications, and to make recommendations on how the code could be improved [2]. While the results of the review (completed in April 1997) confirm the overall adequacy of the VICTORIA code, the review committee made a number of recommendations for model improvements. These were ranked as findings and concerns. A plan for addressing these recommendations is discussed in Section 2. Some of these modifications have already been implemented.

The version of VICTORIA that was reviewed (version 1.0) is very similar to the current release (VICTORIA 92-01) but contains a few minor corrections and extensions. Versions used in this work are VICTORIA 1.1 and 1.2. The significant difference between versions 1.0 and 1.1 is that the latter was modified to optionally treat multiple condensed phases. In addition, VICTORIA 1.2 uses Blackburn's thermochemical model to represent oxidation and volatilization processes of the uranium fuel matrix.

Three applications of VICTORIA are discussed in Section 3. These are analyses of an induced steam generator tube rupture (ISGTR) sequence, the Phebus FPT-1 test, and the Phebus FPT-4 test, respectively. The FPT-1 test was conducted in Cadarache, France, in June 1996 and is a midscale, in-pile, integral test. The FPT-4 test will be conducted in 1999 and will use a preformed rubble bed rather than fuel rods. The FPT-1 test used spent fuel from the Belgian BR-3 reactor; whereas, the FPT-4 test will use spent fuel from a commercial Electricité de France (EDF) nuclear power plant. Section 4 provides a summary of the current status of VICTORIA development and recent applications of the code.

2.0. Peer Review Recommendations and Planned Response

The process followed by the peer review committee (PRC) was very similar to that of previous independent peer reviews of NRC codes. The starting point was a set of targeted applications and design objectives that was provided by the NRC. The targeted applications included (1) experimental simulation, (2) benchmarking of the MELCOR systems-level code, and (3) analysis of full-scale plant sequences. The first of these is necessary to validate and assess the models that make up the VICTORIA code. The third targeted application is necessary to achieve the second. Together they define the ultimate purpose of the code, namely, to be able to evaluate accident sequences and to apply lessons learned to other tools that are used for accident analysis and evaluation. The design objectives are very similar to ones used in previous peer reviews for the NRC.

The review was conducted in four steps: (1) a bottom-up review of the detailed models that comprise the VICTORIA code; (2) an evaluation of VICTORIA by running a series of calculations on a simple test problem; (3) a top-down review of the performance of the code on full-scale plant analyses performed by the developers; and (4) a review of the code manual and other code documentation. The results of each of these steps are described in the PRC report [2] and are ranked as findings, high-priority concerns, medium-priority concerns, and lower-priority concerns. Tables 1 through 4 list these findings and concerns and indicate when the item will be addressed by the code developers. All of the items in Tables 1 and 2, the

findings and high-priority concerns, will be addressed prior to the release of the next code version, which will be named VICTORIA 2.0. Some of the medium- and lower-priority concerns may also be addressed if time permits, as indicated in Tables 3 and 4.

2.1. Findings

The first three findings involve removing outdated and unused options from the code. The first recommendation in the findings is to remove the optional, highly mechanistic, fission product release models [3] because the mechanisms treated by these models are poorly understood. Furthermore, these models have not been used by any of the VICTORIA users. The second recommendation is to remove the option to model the chemistry of fission products in fuel grains. While there seems to be some controversy among the experts on whether chemical interactions between fission products and the UO_2 grain lattice are physical, the PRC is convinced that they are not. The code developers had previously abandoned the in-grain chemistry model on pragmatic grounds; validation studies against data from the Oak Ridge National Laboratory horizontal induction (HI) and vertical induction (VI) and the Sandia National Laboratories source term (ST) fission product release tests showed that the option to model fission product chemistry in the fuel pores, but not in the fuel grains, provides better agreement with the data [4]. The third recommendation is to remove an outdated option that allows the user to directly input mass and momentum boundary layer thicknesses. The existing option that is favored is to use standard correlations to determine the thicknesses of these layers.

Table 1. Findings

Finding No.	Description	Status
1	Remove optional fission-product release models	Done
2	Remove option to model chemistry in fuel grains	Done
3	Remove option to directly specify mass and momentum boundary layer thicknesses	Done
4	Make resuspension model optional	Done
5	Add warnings on time step and thermal-hydraulic input errors	In VICTORIA 2.0
6	Rewrite user's manual	In VICTORIA 2.0

The fourth finding involves making the aerosol resuspension model optional. This recommendation was made because in nearly all cases the aerosols that deposit are mixtures of liquid and solid phases; on the other hand, resuspension models are based on data for dry-dust aerosols [5]. The PRC also recommended that warnings be issued if the user specifies a time step that exceeds the Courant limit and when thermal-hydraulic inputs are not self-consistent. Finally, the PRC recommended that a new code manual be written to correspond to version 2.0, which will have a number of revisions since the previous version, VICTORIA 92-01. These last two modifications will be completed before VICTORIA 2.0 is released in mid-1998.

2.2. High-Priority Concerns

The PRC believes that three separate condensed phases will form rather than a single one, as modeled in previous versions of the code. More specifically, their recommendation is to model an oxidic phase, a metallic phase, and a third phase containing only cesium iodide. This recommendation has been implemented [6] and is demonstrated in the applications discussed later. They also recommend adding a model for fission product solubility in the fuel. Their second high-priority recommendation is that the sensitivity of results to "chemistry film" thickness be investigated and if the sensitivity is found to be unacceptable, that the numerical treatment be modified to eliminate these films. The "chemistry films" are currently used as a numerical device to allow chemical equilibrium to be calculated for fixed mass and fixed volume systems. The model for treating fission product solubilities in fuel has not been implemented and the effect of "chemistry films" has not been investigated, but these items will be completed before VICTORIA 2.0 is released.

Table 2. High-Priority Concerns

Concern No.	Description	Status
1a	Treat multiple condensed phases	Done
1b	Treat solubility of fission products in fuel	In VICTORIA 2.0
2	Investigate and, if necessary, remove "chemistry films"	In VICTORIA 2.0

2.3. Medium-Priority Concerns

Four medium-priority concerns were listed by the PRC. These items are expected to have a lesser impact on VICTORIA predictions than the findings and high-priority concerns. The first of the recommendations from the medium-priority concerns is to make a number of modifications to the thermochemical database. The second is to revise the treatment of uranium thermochemistry; the PRC preference is to implement Blackburn's method [7]. This has already been done for hyperstoichiometric fuel (UO_{2+x}, $x>0$) because of concern about potential uranium volatilization in the Phebus FPT-4 test. At this point, it is not certain whether this model will be extended to treat hypostoichiometric fuel ($x<0$) prior to the release of VICTORIA 2.0. The third medium-priority concern is in connection with boron carbide control blades and rods. Currently, the thermochemical database does not contain carbon and so cannot treat formation of carbonates of the fission products. The PRC recommended that the importance of carbon chemistry be investigated and, if necessary, that carbon species be added to the database before analyzing sequences in which boron carbide is present. The fourth medium-priority concern is connected with fission product release from fuel. The PRC recommended that appropriate values for grain diffusivities, interconnected porosities, and fuel permeabilities be investigated for a range of fuel burnups and levels of excess oxygen. They also recommend validating the pressure dependence of the VICTORIA release model. Responses to all of the medium-priority concerns, with the exception of revision of the fuel thermochemistry, are planned as future activities, i.e., following the release of VICTORIA 2.0.

Table 3. Medium-Priority Concerns

Concern No.	Description	Status
1	Modify Gibbs free-energy data	Future
2	Revise treatment of fuel thermochemistry	Done for x>0
3	Investigate and, if necessary, add carbon species	Future
4a	Additional investigation of values affecting fission product release from fuel	Future
4b	Validate pressure dependence of release model	Future

2.4. Lower-Priority Concerns

The PRC identified five lower-priority concerns and made the following recommendations. The first of these is to add uranic acid to the database. This may be done prior to release of VICTORIA 2.0 because it should take a relatively short time to implement. The second item is to add a diffusion-based cladding oxidation model as an option to the current Urbanic and Heidrick model [8]. This new model would be along the lines of a recent modification to SCDAP/RELAP5 (SR5) [9]. The third recommendation is to investigate and, if necessary, correct for the fact that thermal-hydraulic codes may not model changes in gas velocities caused by release of fission products from the core. The fourth recommendation is to update uranium oxidation and volatilization models based on Blackburn's model. Again, this has already been done for x>0. The final recommendation is to allow more user control over the fraction of decay heat that is deposited in fission product films and adjoining structures. All but the first and fourth of these items will be addressed after the release of VICTORIA 2.0.

Table 4. Lower-Priority Concerns in Independent Peer Review Report

Concern No.	Description	Status
1	Add uranic acid to database	In VICTORIA 2.0?
2	Add diffusion-based model for cladding oxidation and hydriding	Future
3	Investigate and, if necessary, correct gas velocity data	Future
4	Update fuel oxidation and volatilization models	Done for x>0
5	Make decay-heating model more flexible	Future

3.0. Recent Applications of VICTORIA

3.1. ISGTR Sequence in Surry Reactor Plant

SCDAP/RELAP5 [9] analyses were performed to evaluate the potential for an ISGTR during the early stages of a station blackout sequence [10]. Reference 10 documents 7 cases. Case 6 was chosen as the basis for this work. The specific characteristics of Case 6 are as follows: (1) the secondary side of loop C (the one with the pressurizer, hereafter denoted the faulted loop) depressurizes early in the sequence due to a stuck-open atmospheric dump valve (ADV) and (2) the primary remains at full system pressure even after the surge line and hot leg nozzle are predicted to fail by creep rupture. Table 5 shows the timing of major events, as predicted by SR5. Originally, the calculation was terminated at the point of pressurizer surge line failure; however, the actual thermal-hydraulic calculation used as the basis for this study was extended until reactor vessel lower head failure. VICTORIA 1.1 was used to analyze the release of fission products from the core and their transport through the primary circuit, secondary circuit, and out through the stuck-open ADV [11]. The objective of this calculation was to assess offsite releases for a regulatory initiative on steam generator tube integrity.

Table 5. Sequence of Events in ISGTR Sequence

Event	Time (s)
Station blackout initiates sequence	0
ADV sticks open on loop C	20
Onset of PORV cycling	1,960
Hot leg natural circulation of steam begins	9,090
Fuel rod oxidation begins	11,620
Surge line fails by creep rupture, but failure is ignored	13,730
Faulted loop (C) SG tube fails by creep rupture	14,960
Faulted loop hot leg nozzle melts, end of VICTORIA calculation	33,750

Figure 1 shows a schematic representation of the VICTORIA nodalization of the Surry reactor vessel and primary circuits. A total of 48 nodes are used to represent the domain. The unfaulted loops, A and B, are represented as a single loop since the thermal-hydraulic behavior in the two loops is almost identical. The faulted loop, C, which is the one with the pressurizer, is represented individually.

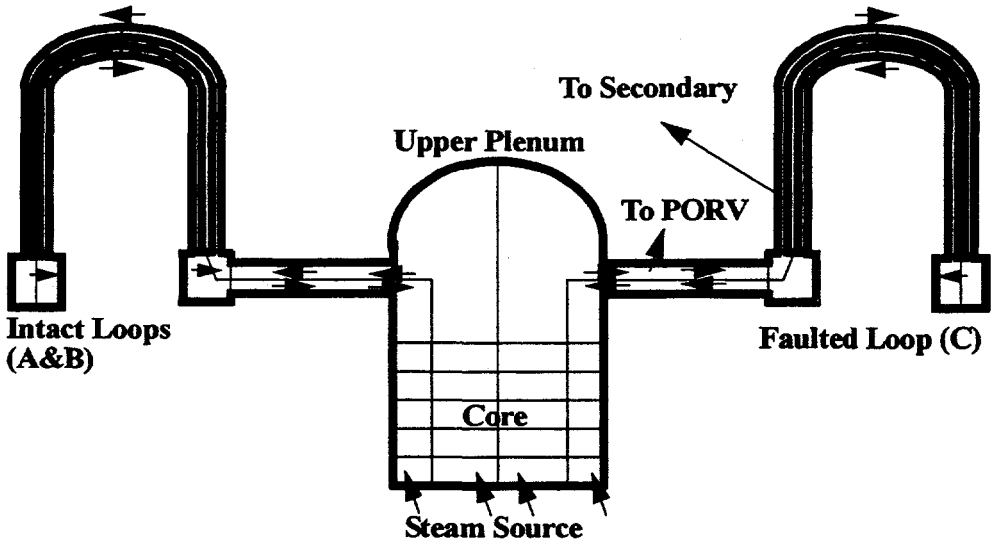

Figure 1. Schematic of the VICTORIA representation of the Surry reactor vessel and primary circuits.

During this sequence, periodic accumulator injection maintains a water level that fluctuates between the bottom of the core and about 40% of the height of the core. This water vaporizes, providing the source of steam to the core and primary circuits. Steam losses occur through the pressurizer and out through the pressure-operated relief valve (PORV) or through the broken steam generator tube, as indicated in Figure 1. The losses through the PORV and broken steam generator tube are distinct in time. Early losses occur through the PORV, which cycles until the steam generator tube rupture occurs. After that time, the system begins to depressurize and PORV cycling ceases.

Figure 2 shows the VICTORIA nodalization of the faulted secondary circuit. Four nodes represent this region: one for the steam separators, one for the steam dryers, and two for the long steam line. Coolant exiting from the primary flows into node 1; coolant exits from node 4 through the stuck-open ADV and into the environment.

Figure 3 shows the VICTORIA-predicted fission product release histories. Also shown in this figure is the peak core temperature history. Sudden reductions in the core temperature correspond to accumulator injections. By the end of the transient, peak core temperatures exceed 2700 K while the bottom 40% of the core is sufficiently cooled that little fission product release occurs from this region.

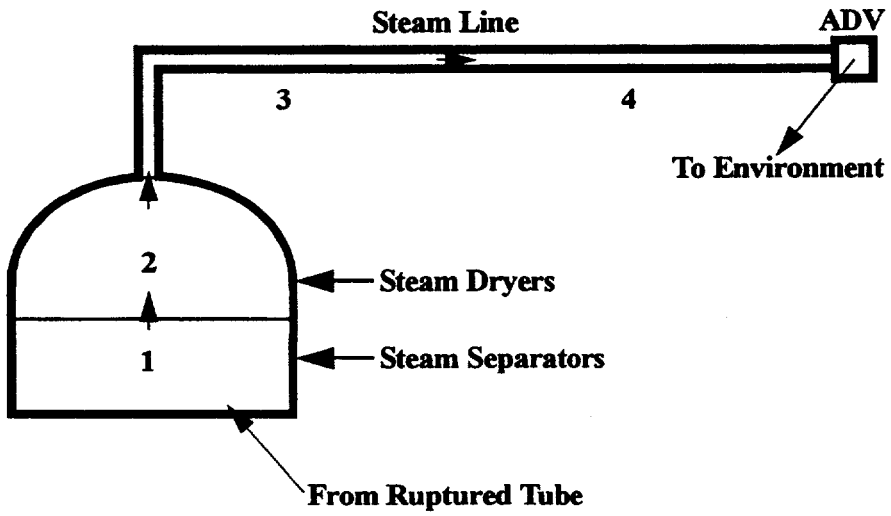

Figure 2. Schematic of the VICTORIA representation of the Surry faulted secondary circuit.

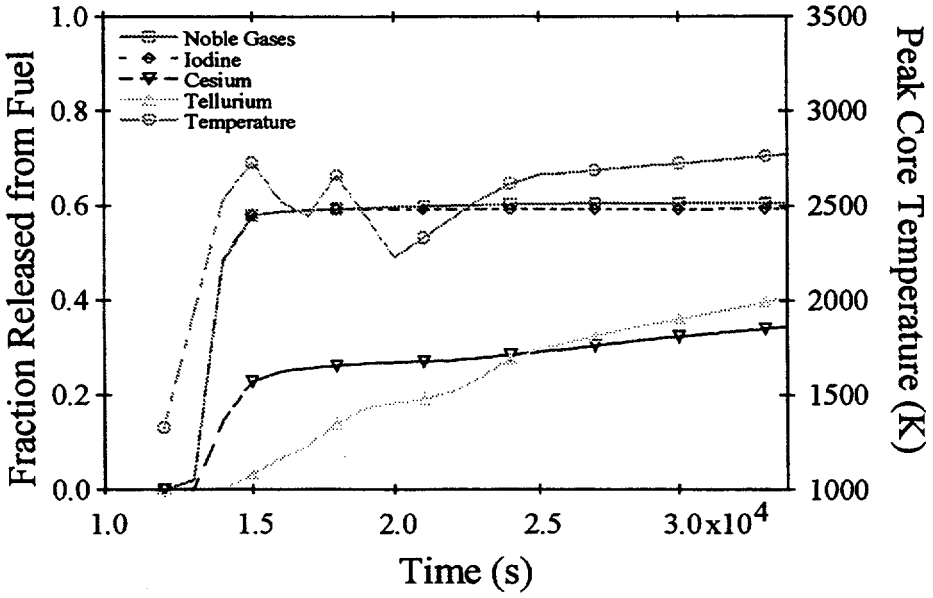

Figure 3. VICTORIA-predicted peak core temperature and fission product release histories from fuel for ISGTR sequence.

Fractional releases of the noble gases and iodine occur very early and ultimately reach 60%. Releases of these elements from the upper 60% of the core are nearly complete; releases from the bottom 40% of the core are minimal because of the lower temperatures there. Cesium and tellurium releases are

more protracted than those for the noble gases and iodine. Final release fractions for these elements are about 35% and 40%, respectively.

VICTORIA-predicted releases to the environment are shown in Figure 4. The noble gas releases to the environment are predicted to be only about 12%; the balance of the noble gases that are released from the core are predicted to exit the RCS through the PORV. Iodine release to the environment is predicted to be much higher, about 30%. This is because much of the iodine, in the form of cesium iodide, condenses onto the relatively cold structural surfaces. Later, as these surfaces heat up, the iodine revaporizes. Thus, even though noble gas and iodine fractional release histories from core are nearly identical, more iodine is released to the environment because it is retained within the RCS until after PORV cycling ceases. Cesium and tellurium are retained to a greater extent in the RCS than is iodine; their release fractions are predicted to be only about 8% and 12%, respectively. Other less volatile fission products are predicted to be released at even smaller fractions. Fission product release to the environment occurs over a 4- to 5-h interval.

Little retention of the volatile elements--iodine, cesium, and tellurium--is predicted to occur in the faulted secondary circuit. This is because temperatures throughout the secondary circuit exceed 1250 K by the end of the transient; at these temperatures, the more volatile species, such as cesium iodide, remain in the vapor phase and so cannot deposit. Primary circuit temperatures are even higher by the end of the transient, e.g., the hot leg nozzle on the faulted loop is predicted to exceed its melting point, which is more than 1700 K.

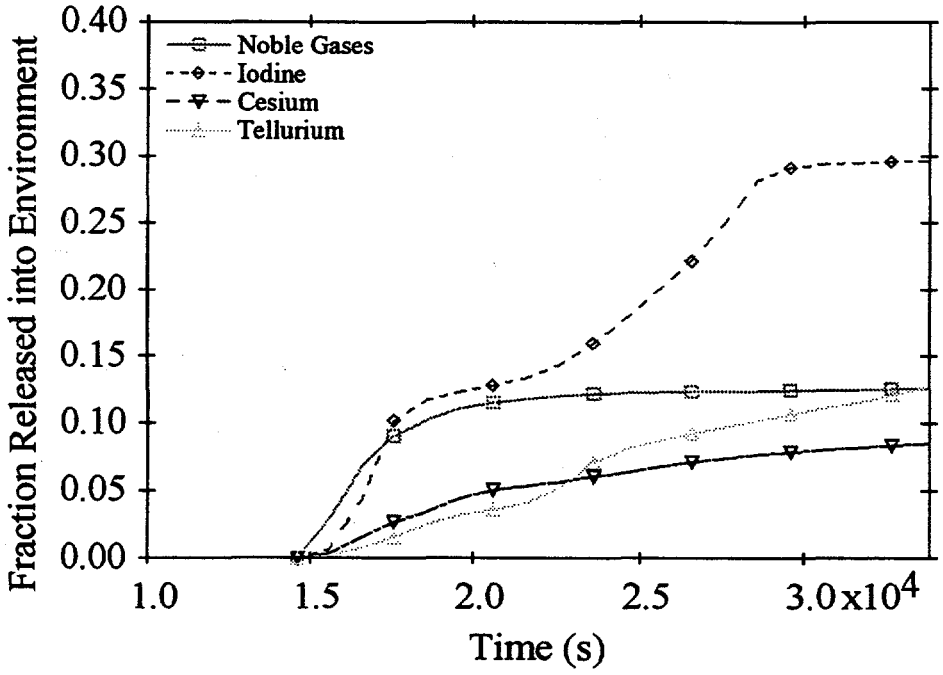

Figure 4. VICTORIA-predicted fission product releases to the environment for ISGTR sequence.

3.2. Phebus FPT-1 Test

Phebus is an experimental reactor located in Cadarache, France. A series of six tests, the FP series, is scheduled to be conducted there. The first test, FPT-0, was run in December 1993. The second test, FPT-1, was run in July 1996. The primary difference between FPT-0 and FPT-1 is that FPT-0 was a shakedown test using trace irradiated fuel while FPT-1 used spent fuel from the BR-3 reactor in Belgium.

The Phebus FP tests are integral in nature, i.e., they attempt to represent all of the processes that would take place during a severe nuclear accident. A schematic of the Phebus FP apparatus is shown in Figure 5. It consists of an in-pile fuel bundle containing 20 fuel rods and 1 control rod, all 1 m long, an upper plenum, a steam-generator tube, a containment vessel, and interconnecting pipework.

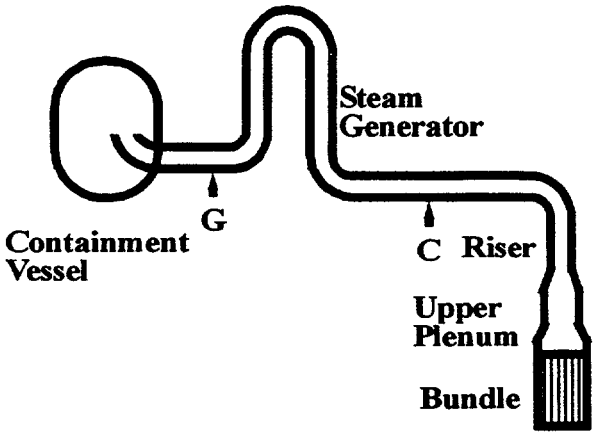

Figure 5. Schematic of the Phebus FPT-1 test configuration.

While the FPT-1 test was run about a year ago, data are just becoming available for fission product releases and deposition in the circuit. To the extent that data are available, they are compared with predictions. The primary purpose for the analyses presented here is to validate the VICTORIA code. Further comparisons will be made as more data become available.

VICTORIA [1] analyses of the Phebus FPT-1 test were performed for two regions [12]: (1) the fuel bundle, represented by ten nodes in two rings, and (2) the upper plenum and circuit leading to containment, represented by fourteen nodes in one ring. Figures 6 and 7 show the VICTORIA representations used for the FPT-1 fuel bundle and primary circuit, respectively. The reasons for subdividing the domain were as follows: (1) to reduce the CPU time required for the individual calculations; (2) to allow sensitivity studies to be conducted separately on the two subdomains; and (3) to allow different radial nodalizations for the two subdomains, i.e., two radial rings in the fuel bundle and one radial ring in the circuit.

Two options were employed to facilitate the analyses of FPT-1. The first of these was the boundary coupling option [13], which was used to couple the two-ring representation of the fuel bundle with the one-ring representation of the circuit. With this option, the mass flow rates of vapors and aerosols leaving the top of the fuel bundle were written as a data file; these values were then read, summed over the two rings, and used as vapor and aerosol sources in the first node of the single ring in the circuit analysis.

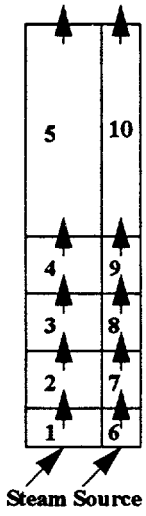

Figure 6. Schematic of the VICTORIA representation of the Phebus FPT-1 fuel bundle.

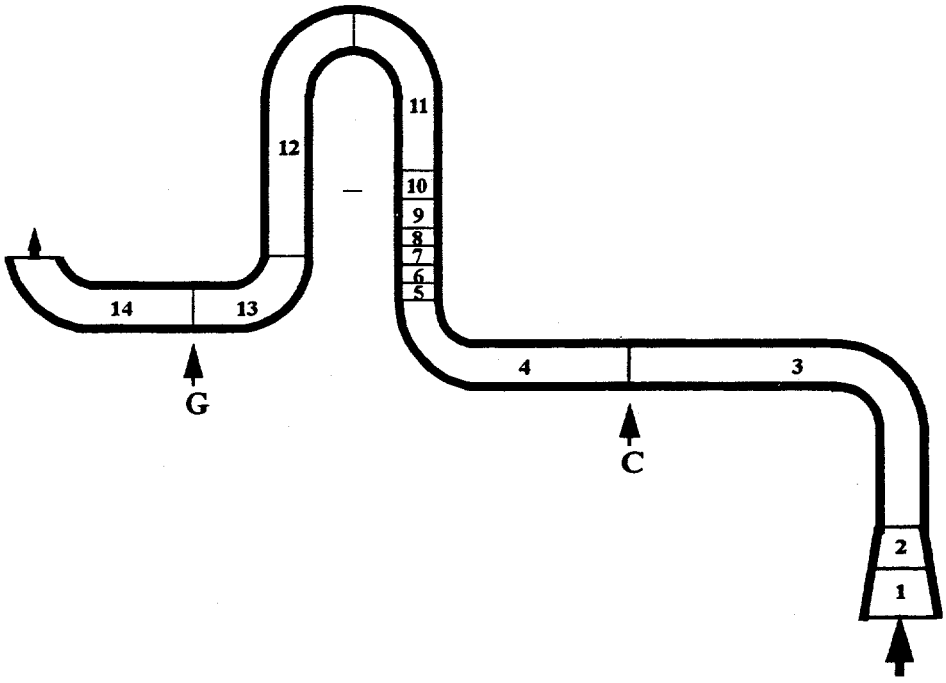

Figure 7. Schematic of the VICTORIA representation of the Phebus FPT-1 primary circuit.

In the second option, velocities for each node in the circuit were automatically calculated based on the mass source rates. Velocities in each node were calculated so that the flow of vapors out of each cell equaled the flow of vapors into it, i.e., there was no accumulation or depletion of vapor within a cell. The combination of these two techniques allows the analyst to perform the circuit calculation without any input of transient source or flow rate data.

Figure 8 compares bundle-release predictions using models for a single condensed phase and for three condensed phases with preliminary experimental data. No data are currently available for the noble gases, antimony, or strontium. For most of the fission products, the agreement between predictions and data is remarkable, regardless of the number of condensed phases modeled. Minor improvements in agreement with most of the data can be observed for the three condensed-phase treatment.

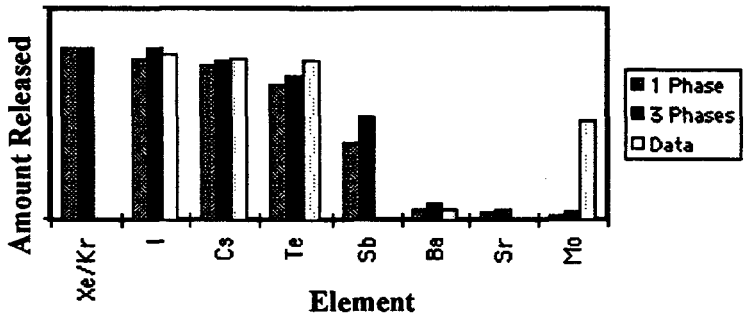

Figure 8. Comparisons of VICTORIA-predicted fission product bundle-release predictions using models for one- and three-condensed phases with preliminary experimental data.

A notable exception to this agreement is for molybdenum. While agreement for the three condensed-phase model is slightly better, releases are underpredicted by more than an order of magnitude for both cases. The reason for this discrepancy is not known at present, but bears further investigation. The most likely possibilities are that the preliminary data for molybdenum release are too high, thermochemical data for one or more molybdenum species are not well quantified, or a volatile molybdenum species is not included in the current VICTORIA thermochemical database. A weakness in the first of these possibilities is that similar molybdenum releases have been reported for the VERCORS test series [14].

Figures 9 and 10 show the effect of the number of condensed phases modeled on the predicted deposition pattern of iodine in the hot leg of the steam generator tube. Values are expressed as fractions of the initial bundle inventory.

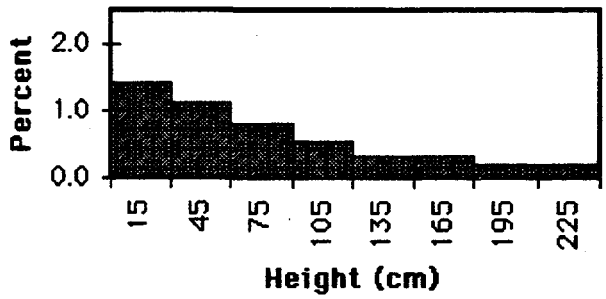

Figure 9. VICTORIA-predicted iodine deposition pattern in the steam generator tube hot leg for the one condensed-phase model.

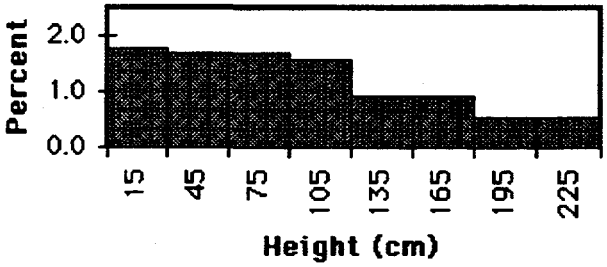

Figure 10. VICTORIA-predicted iodine deposition pattern in the steam generator tube hot leg for the three condensed-phase model.

While the deposition profiles are not dramatically different for the two cases shown in Figures 9 and 10, there are some important distinctions. Using the one condensed-phase model, iodine, which is primarily present as cesium iodide, begins to condense upstream of the steam generator tube. At the inlet to the tube, most of the cesium iodide is in the condensed phase, i.e., is an aerosol. The dominant mechanism for deposition of iodine in the steam generator tube is aerosol deposition by thermophoresis. In the prediction using the three condensed-phase model, iodine is again chiefly in the form of cesium iodide. However, most of the cesium iodide enters the steam generator tube as a vapor. This difference is because cesium iodide is treated as a pure phase in the three-phase model. Since cesium iodide enters the steam generator tube as a vapor, the dominant deposition mechanism is condensation onto the tube surface. The profile is flatter at the inlet of the steam generator in this case than for a single condensed phase because of the difference in deposition mechanisms. Predicted releases into containment are shown in Figure 11 using the three condensed-phase option. Values are in arbitrary units.

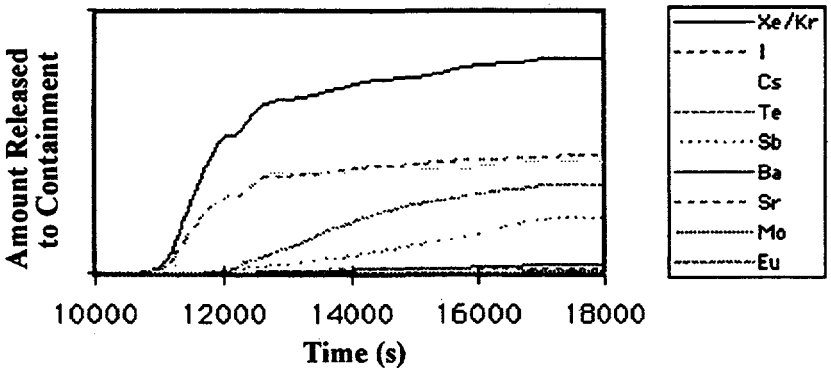

Figure 11. VICTORIA-predicted integral releases into containment for three condensed-phase model.

While deposition patterns and mechanisms are somewhat different for the two models, overall retention in the circuit is very similar. Predicted releases into containment for the single condensed-phase option are nearly the same as those shown in Figure 11 for most of the fission product elements. The largest difference is for iodine; about 30% more of the iodine inventory is predicted to be retained in the circuit using the single-phase option than using the three-phase option. When experimental data become available, they should be useful for determining which option better predicts overall deposition patterns in the FPT-1 circuit.

3.3. Phebus FPT-4 Test

Figure 12 shows a schematic of the Phebus FPT-4 test apparatus in the currently proposed, simplified configuration. The FPT-4 test is significantly different from the other tests in the Phebus FP series because it uses a preformed rubble bed rather than a bundle of fuel rods. Its purpose is primarily quantifying fission product release from a rubble bed rather than fission product behavior in the circuit, as in the other Phebus FP tests.

The rubble bed is to be composed of 80% fuel and 20% zirconia by mass. Because of safety considerations, the bottom third of the rubble bed is to be formed with depleted uranium; the top two-thirds is to be formed from three-cycle spent fuel from a commercial EDF nuclear power plant. A bank of filters, illustrated in Figure 12, is intended to capture fission products upstream of the 90° bend located at the top of the riser. These filters effectively prevent aerosol transport through the test circuit.

DEBRIS was used to provide the thermal-hydraulic data for VICTORIA [15]. (DEBRIS is a code developed at Sandia National Laboratories for the U.S. NRC to predict thermal-hydraulic behavior, including fuel melting and relocation, in a debris bed.) This calculation was done using the very fine nodalization shown in Figure 13. Overlaid on the DEBRIS nodalization is the coarser VICTORIA nodalization, shown by the thicker lines, which contains 16 nodes, 4 radial by 4 axial. The VICTORIA nodalization does not include the unenriched fuel region because temperatures reach only slightly more than 1000 K in this region, which is too low for fission product behavior or uranium volatilization to be important. Uranium volatilization is a primary concern for the FPT-4 test because of the potential for

clogging the filters in the filter bank. The current plan is to use 4 or 5 filters, each of which will be on-line during a portion of the transient.

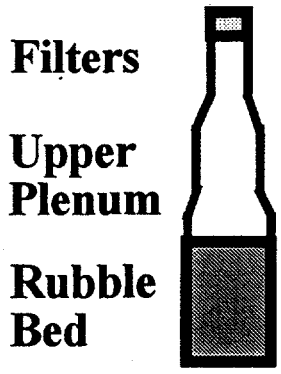

Figure 12. Schematic of the Phebus FPT-4 test configuration.

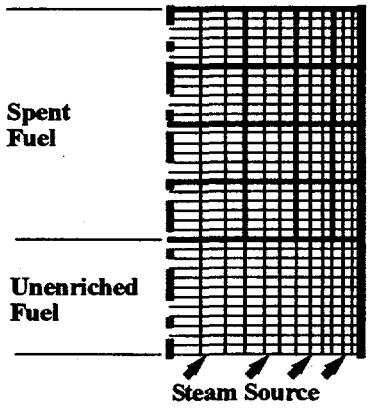

Figure 13. Schematic of the DEBRIS and VICTORIA representations of the Phebus FPT-4 test configuration.

A snapshot of the final debris bed configuration, as predicted by the DEBRIS code, is shown in Figure 14. The key features of the end state are a molten pool that penetrates down to about 15 cm above the depleted uranium zone, a large void region just above the molten pool, and a 2-cm-thick permeable crust above the void zone. DEBRIS predicts that the crust will survive the test, but this prediction is rather uncertain. If the crust collapses during the test, then a dense crust will form over the top of the molten pool. This would modify the thermal-hydraulic predictions and as a result the release predictions discussed below.

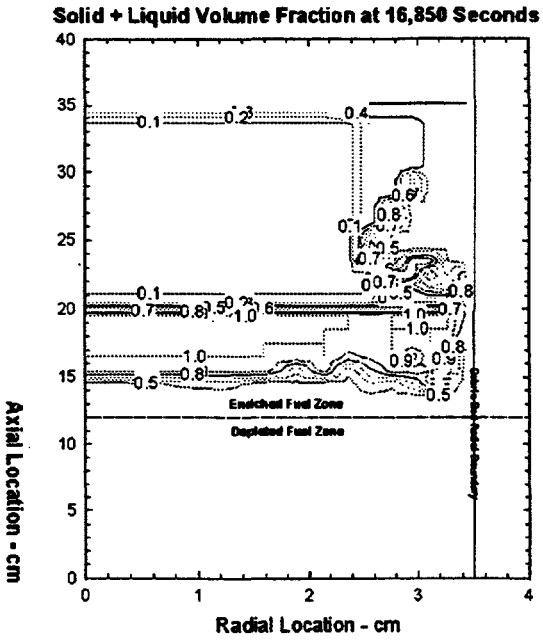

Figure 14. DEBRIS-predicted solid plus liquid volume fractions.

Figure 15 shows temperature and fission product release histories for the FPT-4 test. The temperature corresponds to the top centerline position of the debris bed. This represents the peak temperature in the debris bed through the plateau at 2700 K; after this time, the peak temperature is in the molten pool, which gradually moves downward to its final position, as shown in Figure 14. The small bump in the temperature history near the end of the transient shown in Figure 15 corresponds to a larger thermal ramp in the interior of the debris bed, where temperatures peak at over 3000 K.

Fission product fractional releases are shown in Figure 15 for barium, molybdenum, strontium, and ruthenium. Significant releases of these elements begin during the ramp leading to the 2700 K plateau shown in the figure and accelerate during the final ramp leading to melting. Significant release fractions of the less volatile fission products are predicted: about 60% for barium and about 30% for molybdenum and strontium. Release of ruthenium is predicted to be less than 1%. It is possible that the FPT-4 test will continue to 18,000 s if filter clogging is not a problem. If this is the case, releases will be even higher than those shown in Figure 15.

The VICTORIA-predicted integral uranium mass release history is shown in Figure 16. Up to the endpoint of this calculation at 16,800 s, about 115 g of uranium release are predicted. This corresponds to loss of about 130 g of UO_2. If the test is continued longer, uranium releases can be extrapolated since the release rate is nearly constant during the final plateau.

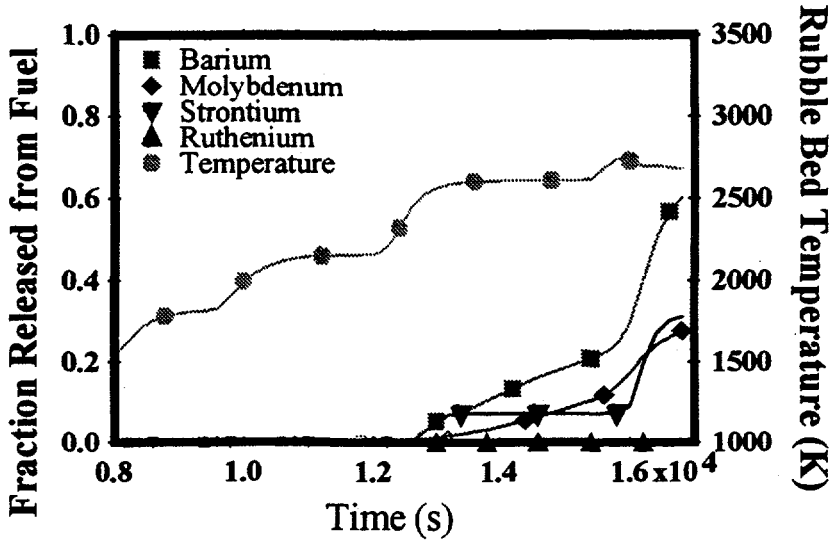

Figure 15. VICTORIA-predicted temperature and integral, fractional, fission-product release histories for Phebus FPT-4. Temperature is at the top centerline of the debris bed.

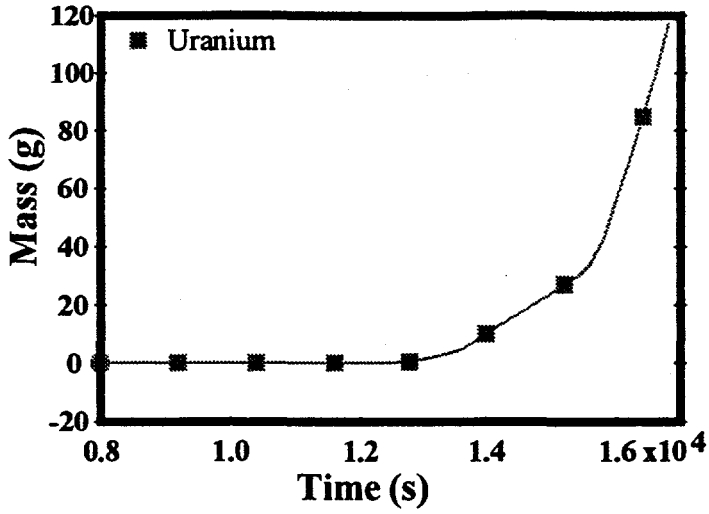

Figure 16. VICTORIA-predicted integral, uranium, mass release histories for Phebus FPT-4.

The predictions shown here are significant for the Phebus program in several ways. First of all, the release predictions indicate that FPT-4 should be a very useful test because releases of the less volatile, refractory elements are predicted to be much greater than for the other Phebus FP tests. The large predicted releases for FPT-4 are due to the high temperatures and to the direct contact between fuel particles and steam. Uranium release predictions are especially significant for the Phebus project because of concern about plugging the filters. The current work indicates that less than 150 g of UO_2 should be released at the

final time of the calculation, which is 16,800 s. At these levels, plugging should not be a significant problem. Other recent work has estimated higher releases of uranium. The greatest uncertainty in all of the uranium release estimates appears to be the choice of thermochemical data upon which vapor pressure curves are constructed. Finally, the timing estimates for uranium releases shown in Figure 16 should be useful for scheduling the opening and closing of the valves regulating flow through the filters during the test.

4.0. Summary

The recommendations in the recently completed independent peer review of the VICTORIA code are now being implemented. The plan is to address all of the highest priority recommendations before releasing the next code version, which will be named VICTORIA 2.0. The current schedule calls for this version to be released in the summer of 1998.

Recent work to support a regulatory initiative on the integrity of steam generator tubes has provided best estimates of releases to the environment. These predictions are for a temperature-induced steam generator tube rupture sequence using thermal-hydraulic data from SCDAP/RELAP5. The predictions are that about 30% of the iodine will be released to the environment if such an accident were to occur. About 12% of the cesium and tellurium would be released; releases of the other fission product elements would be less than 10%.

Comparisons between VICTORIA predictions and preliminary data from the Phebus FPT-1 test are remarkably good, with the single exception of molybdenum. Data for fission product deposition in the FPT-1 circuit, when they become available, should be useful for assessing the PRC recommendation to model three condensed phases rather than a single condensed phase, as in earlier versions of the VICTORIA code.

Pretest analyses of the Phebus FPT-4 test are being used to evaluate test protocol design and safety. VICTORIA predictions indicate that FPT-4 should be quite different than the other tests in the FP series because it uses a preformed rubble bed rather than fuel rods. Because of the direct contact between steam and fuel particles and because of the severe temperatures during this test, releases of the less volatile fission products, such as barium, strontium, and molybdenum, should be very high. Volatilization of uranium during this test is predicted to be low enough that filter plugging should not be a serious issue.

References

1. T. J. Heames, D. A. Williams, N. E. Bixler, A. J. Grimley, C. J. Wheatley, N. A. Johns, and M. D. Vine, P. Domagala, L. W. Dickson, C. A. Alexander, I. Osborn-Lee, S. Zawadzki, J. Rest, and H. S. Bond, "VICTORIA: A Mechanistic Model of Radionuclide Behavior in the Reactor Coolant System Under Severe Accident Conditions," Revision 1, SAND90-0756, NUREG/CR-5545, Sandia National Laboratories, Albuquerque, NM (1992).
2. V. Mubayi, J. A. Gieseke, D. R. Olander, and M. Schwarz, "VICTORIA Independent Peer Review," Technical Report W-6437 4-17-97, Brookhaven National Laboratory, Upton, NY (1997).
3. J. Rest and A. W. Cronenberg, "Modeling the Behavior of Xe, I, Cs, Te, Ba, and Sr in Solid and Liquefied Fuel During Severe Accidents," *J. of Nucl. Mat., 150*, 203-225 (1987).

4. N. E. Bixler and T. J. Heames, "VICTORIA-92-01 Validation Studies Against Data from the ORNL HI and VI, SNL ST, and CSNI ISP 34 (FALCON) Tests," SAND93-2301, Sandia National Laboratories, Albuquerque, NM, unpublished.
5. A. L. Wright, W. L. Pattison, and J. Y. King, "'SERIES -2' Aerosol Resuspension Test Data Summary Report," Oak Ridge National Laboratory, Oak Ridge, TN, unpublished.
6. N. E. Bixler, "An Approach for Modeling Three Condensed Phases with VICTORIA," Letter Report to the USNRC, Sandia National Laboratories, Albuquerque, NM (1997).
7. P. E. Blackburn, "Oxygen Pressures Over Fast Breeder Reactor Fuel I: A Model for $UO_{2\pm x}$," *J. Nuc. Mat. 46*, 244-252 (1973).
8. V. F. Urbanic and T. R. Heidrick, "High Temperature Oxidation of Zircaloy-2 and Zircaloy-4 in Steam," *J. Nuc. Mat. 75*, 251-261 (1978).
9. C. M. Allison, G. A. Berna, E. W. Coryell, K. L. Davis, D. T. Hagrman, J. K. Hohorst, R. R. Schultz, and L. J. Siefken, "SCDAP/RELAP5/MOD3.1 Code Manual Volume III: SCDAP/RELAP5 Users Guide and Input Manual," NUREG/CR-6150, EGG-2720, Idaho National Engineering Laboratory, Idaho Falls, ID (1993).
10. K. S. Quick and D. L. Knudson, "A SCDAP/RELAP5 Analysis of the Potential for Steam Generator Tube Rupture in Surry," Letter Report to the USNRC, Idaho National Engineering Laboratory, Idaho Falls, ID (1996).
11. N. E. Bixler, "VICTORIA Studies of Fission Product Release from an Induced Steam Generator Tube Rupture Sequence," Letter Report to the USNRC, Sandia National Laboratories, Albuquerque, NM (1997).
12. N. E. Bixler, "Analysis of Fission Product Behavior in the Phebus FPT-1 Test," Letter Report to the USNRC, Sandia National Laboratories, Albuquerque, NM (1997).
13. C. M. Erickson and N. E. Bixler, "Boundary Coupling with VICTORIA," Letter Report to the USNRC, Sandia National Laboratories, Albuquerque, NM (1994).
14. B. Andre, G. Ducros, J. P. Leveque, M. F. Osborne, R. A. Lorenz, and D. Marco, "Fission Product Releases at Severe Light Water Reactor Accident Conditions: ORNL/CEA Measurements Versus Calculations," *Nuc. Reactor Safety 114*, 23-50 (1996).
15. N. E. Bixler, "Pretest Analysis of Uranium Volatilization and Fission Product Release During the Phebus FPT-4 Rubble Bed Test," Letter Report to the USNRC, Sandia National Laboratories, Albuquerque, NM (1997).